PLASMODESMATA: RECENT PROGRESS AND NEW INSIGHTS

EDITED BY: Jung-Youn Lee, Tessa Maureen Burch-Smith and Manfred Heinlein

PUBLISHED IN: Frontiers in Plant Science

frontiers Research Topics

frontiers

ISSN 1664-8714
ISBN 978-2-88974-263-9
DOI 10.3389/978-2-88974-263-9

About Frontiers

Frontiers is more than just an open-access publisher of scholarly articles: it is a pioneering approach to the world of academia, radically improving the way scholarly research is managed. The grand vision of Frontiers is a world where all people have an equal opportunity to seek, share and generate knowledge. Frontiers provides immediate and permanent online open access to all its publications, but this alone is not enough to realize our grand goals.

Frontiers Journal Series

The Frontiers Journal Series is a multi-tier and interdisciplinary set of open-access, online journals, promising a paradigm shift from the current review, selection and dissemination processes in academic publishing. All Frontiers journals are driven by researchers for researchers; therefore, they constitute a service to the scholarly community. At the same time, the Frontiers Journal Series operates on a revolutionary invention, the tiered publishing system, initially addressing specific communities of scholars, and gradually climbing up to broader public understanding, thus serving the interests of the lay society, too.

Dedication to Quality

Each Frontiers article is a landmark of the highest quality, thanks to genuinely collaborative interactions between authors and review editors, who include some of the world's best academicians. Research must be certified by peers before entering a stream of knowledge that may eventually reach the public - and shape society; therefore, Frontiers only applies the most rigorous and unbiased reviews.
Frontiers revolutionizes research publishing by freely delivering the most outstanding research, evaluated with no bias from both the academic and social point of view. By applying the most advanced information technologies, Frontiers is catapulting scholarly publishing into a new generation.

What are Frontiers Research Topics?

Frontiers Research Topics are very popular trademarks of the Frontiers Journals Series: they are collections of at least ten articles, all centered on a particular subject. With their unique mix of varied contributions from Original Research to Review Articles, Frontiers Research Topics unify the most influential researchers, the latest key findings and historical advances in a hot research area! Find out more on how to host your own Frontiers Research Topic or contribute to one as an author by contacting the Frontiers Editorial Office: frontiersin.org/about/contact

PLASMODESMATA: RECENT PROGRESS AND NEW INSIGHTS

Topic Editors:
Jung-Youn Lee, University of Delaware, United States
Tessa Maureen Burch-Smith, The University of Tennessee, Knoxville, United States
Manfred Heinlein, Centre National de la Recherche Scientifique (CNRS), France

Citation: Lee, J.-Y., Burch-Smith, T. M., Heinlein, M., eds. (2022). Plasmodesmata: Recent Progress and New Insights. Lausanne: Frontiers Media SA. doi: 10.3389/978-2-88974-263-9

Table of Contents

frontiers in Plant Science

EDITORIAL
published: 24 March 2022
doi: 10.3389/fpls.2022.840821

Editorial: Plasmodesmata: Recent Progress and New Insights

Tessa Burch-Smith[1], *Manfred Heinlein*[2] *and Jung-Youn Lee*[3]*

[1] *Donald Danforth Plant Science Center, St. Louis, MO, United States,* [2] *Institut de Biologie Moléculaire des Plantes, CNRS, Université de Strasbourg, Strasbourg, France,* [3] *Department of Plant and Soil Sciences, Delaware Biotechnology Institute, University of Delaware, Newark, DE, United States*

Keywords: plasmodesmata, cell-to-cell movement, biotechnology, plant-pathogen interactions, symplasmic domains, cytoskeleton

Editorial on the Research Topic

Plasmodesmata: Recent Progress and New Insights

In this Frontiers Research Topic, readers will find a collection of research articles, mini-reviews, and opinion papers that focus on new findings and progress regarding plasmodesmata in the context of plant development and plant-pathogen interactions. Specifically, several reports present findings related to the targeted trafficking of endogenous and pathogen-derived proteins to or through plasmodesmata, or the role and regulation of plasmodesmata in defining symplasmic domains. The collection also includes articles that review progress with respect to cytoskeletal connections to basic plasmodesmal function or to interspecific plasmodesmata formed between hosts and their parasitic plants, or share perspectives on how plasmodesmal research may be relevant to addressing critical issues in producing resilient crops in the face of imminent challenges associated with climate change.

In higher plants, virtually all sister cells are connected to each other *via* the primary plasmodesmata formed at the division wall during cell division. However, as cells grow and differentiate, those plasmodesmata can undergo temporary closing or various structural modifications such as those that lead to the formation of secondary/modified plasmodesmata or to disconnection by severing or complete disintegration. These events sometimes lead to the symplasmic isolation of cells. Voitsekhovskaja et al. investigate how secondary plasmodesmata may differentially form depending on how they load sugar into the phloem, i.e., using an apoplastic or symplastic path. This study reveals that secondary plasmodesmata formation is enhanced in symplastic loaders, particularly at the cell walls joining epidermal cells and epidermal with mesophyll cells. In addition, comparative analysis of carbohydrate composition suggests that secondary plasmodesmata formed between the two cell layers are likely used to traffic photosynthetic assimilates. Collectively, these findings raise the intriguing possibility that the epidermis and mesophyll could together comprise a symplastic domain in symplastic loaders. Godel-Jedrychowska et al. investigate how symplamic domains are formed in zygotic and somatic embryos during their development. Their study suggests that although the symplasmic domains form similarly in both types of embryos, there are a few qualitative differences such as the timing of establishing domain boundaries and the size of molecules that can move between cells. Krause group addresses the functional specialization of secondary plasmodesmata

OPEN ACCESS

Edited by:
Sébastien Mongrand, CNRS - Université de Bordeaux, France

Reviewed by:
Patricia Zambryski, University of California, Berkeley, United States

***Correspondence:**
Jung-Youn Lee
jylee@udel.edu

Specialty section:
This article was submitted to Plant Cell Biology, a section of the journal Frontiers in Plant Science

Received: *21 December 2021*
Accepted: *28 February 2022*
Published: *24 March 2022*

Citation:
Burch-Smith T, Heinlein M and Lee J-Y (2022) Editorial: Plasmodesmata: Recent Progress and New Insights. Front. Plant Sci. 13:840821. doi: 10.3389/fpls.2022.840821

(Fischer et al.), examining what is known about interspecific plasmodesmata formed between parasitic plants and their plant hosts and provides cogent arguments for the value of parasitic plant-host systems in investigating various aspects of plasmodesmal formation and structure, and the establishment of symplastic domains.

Two reports describe findings about plasmodesmata in the context of plant development, one related to the role of cytokinin in plasmodesmal function and the other to transcription factor movement critical for xylem development. Various reports have shown that plant hormones, such as auxin, abscisic acid, gibberellin, and salicylic acid, regulate plasmodesmal status, and/or vice versa. Adding to the list of hormones linked to plasmodesmal function, Horner and Brunkard show that direct application of a cytokinin, *trans*-Zeatin, or virus-induced gene silencing of the components of the cytokinin signaling pathway both bring about changes in plasmodesmal permeability. The transcription factor AT-HOOK MOTIF NUCLEAR LOCALIZED PROTEIN(AHL)4 is a mobile member of a large protein family, which is necessary for the proper xylem differentiation in Arabidopsis. Using domain swapping between AHL4 and a non-mobile member, AHL1, followed by genetic analyses, Seo and Lee now show that a specific C-terminal domain in AHL4 determines the mobility of the protein, and that AHL4 mobility from the stele to the endodermis and xylem precursor cells is vital for xylem development.

Chritiaan van der Schoot and his team examine the relationship between lipid bodies and plasmodesmata in the shoot apical meristem in hybrid aspen and analyze the proteins associated with lipid bodies in dormant buds (Veerabagu et al.). Their findings indicate how lipid bodies may function as a putative delivery system for plasmodesmal proteins along the actin cytoskeleton to plasmodesmata. A mini review summarizes the association of actin with plasmodesmata (Diao and Huang) focusing on class I formins, actin-binding proteins involved in actin polymerization. Several class I formins localize to plasmodesmata including AtFH1 and AtFH2, which are required to maintain plasmodesmal permeability.

Reflecting recent interest in the role of plasmodesmata as the battleground against microbial intruders, more proteins encoded by various microbial pathogens are identified to target plasmodesmata. Kyaw Aung's team presents evidence showing that bacterial effector proteins can traffic between cells (Li et al.), adding to the previous findings from fungal and oomycete systems (Cheval and Faulkner, 2018; Iswanto et al., 2021). They show that the effector movement is restricted by accumulation of callose at plasmodesmata and that an effector targeted to the plasma membrane is more efficiently able to move between cells than a mutant version that does not associate with the plasma membrane. How plasma membrane association may facilitate the protein's intercellular movement and how broadly this putative mechanism may apply are interesting questions for future investigations. In addition, it would not be surprising if beneficial bacteria also deploy effectors to bring about potential non-cell-autonomous effects.

Notably, three research groups review and discuss potential applications of plasmodesmal research to improve crop health and yield. As the effects of global climate change become more pronounced in the coming years, there is no doubt that a variety of biotechnological approaches will be needed to enhance crop adaption. Along this line, Liu et al. succinctly summarize a large body of research on the ways pathogens may manipulate plasmodesmata to facilitate infection and how plants can deploy plasmodesmata-centered defenses to limit infection. Possible strategies of engineering plasmodesmata to enhance defense responses, for example by targeting callose metabolizing enzymes are also discussed. Iswanto et al. discuss plasmodesmal proteins involved in abiotic stress and in host-pathogen interactions as potential targets for gene editing using CRISPR/CAS9 technologies. The urgency to consider the importance of plasmodesmata research for crop improvement is furthermore underscored in the Perspective article from the Heinlein lab (Amari et al.). It highlights the potential impact of global warming on virus propagation in infected plants and agricultural productivity and collates work spanning decades that clearly indicates the increased susceptibility of plants to viral cell-to-cell movement at higher temperatures. Perhaps, the regulation of plasmodesmata may hold a promise as a new target for crop engineering and the time may be ripe for that exploration.

AUTHOR CONTRIBUTIONS

TB-S wrote the first draft of the editorial. J-YL revised the draft and added additional sections, and MH edited. All authors contributed to the conception and solicitation of this Research Topic.

FUNDING

This work was partially supported with funding provided by the National Science Foundation (MCB1820103 to J-YL and MCB 1846245 to TB-S) and the Agence Nationale de la Recherche (ANR-21-SUSC-0003-01 to MH).

ACKNOWLEDGMENTS

The editors would like to thank all the authors and reviewers for their participation and contribution to the Research Topic.

REFERENCES

Cheval, C., and Faulkner, C. (2018). Plasmodesmal regulation during plant-pathogen interactions. *New Phytol.* 217, 62–67. doi: 10.1111/nph.14857

Iswanto, A. B. B., Vu, M. H., Pike, S., Lee, J., Kang, H., Son, G. H., et al. (2021). Pathogen effectors: what do they do at plasmodesmata? *Mol. Plant Pathol.* 1–10. doi: 10.1111/mpp.13142

Conflict of Interest: The authors declare that the research was conducted in the absence of any commercial or financial relationships that could be construed as a potential conflict of interest.

Publisher's Note: All claims expressed in this article are solely those of the authors and do not necessarily represent those of their affiliated organizations, or those of the publisher, the editors and the reviewers. Any product that may be evaluated in this article, or claim that may be made by its manufacturer, is not guaranteed or endorsed by the publisher.

frontiers in Plant Science

MINI REVIEW
published: 15 February 2021
doi: 10.3389/fpls.2021.647123

An Update on the Role of the Actin Cytoskeleton in Plasmodesmata: A Focus on Formins

Min Diao[2] *and Shanjin Huang*[1]*

[1]Center for Plant Biology, School of Life Sciences, Tsinghua University, Beijing, China, [2]iHuman Institute, Shanghai Tech University, Shanghai, China

Cell-to-cell communication in plants is mediated by plasmodesmata (PD) whose permeability is tightly regulated during plant growth and development. The actin cytoskeleton has been implicated in regulating the permeability of PD, but the underlying mechanism remains largely unknown. Recent characterization of PD-localized formin proteins has shed light on the role and mechanism of action of actin in regulating PD-mediated intercellular trafficking. In this mini-review article, we will describe the progress in this area.

Keywords: intercellular trafficking, plasmodesmata, actin, actin-binding protein, formin

OPEN ACCESS

Edited by:
Jung-Youn Lee,
University of Delaware, United States

Reviewed by:
Viktor Zarsky,
Charles University, Czechia
Rosemary White,
Commonwealth Scientific and Industrial Research Organisation (CSIRO), Australia

***Correspondence:**
Shanjin Huang
sjhuang@tsinghua.edu.cn

Specialty section:
This article was submitted to Plant Cell Biology, a section of the journal Frontiers in Plant Science

Received: *29 December 2020*
Accepted: *26 January 2021*
Published: *15 February 2021*

Citation:
Diao M and Huang S (2021) An Update on the Role of the Actin Cytoskeleton in Plasmodesmata: A Focus on Formins. Front. Plant Sci. 12:647123. doi: 10.3389/fpls.2021.647123

INTRODUCTION

The growth and development of multicellular organisms requires intercellular communication. Intercellular communication in plants can be classified into symplasmic and apoplasmic pathways. For the symplasmic pathway, intercellular communication is achieved through complex channel-like structures embedded within the cell walls, called plasmodesmata (PD). The development of the PD structure enables the trafficking of molecules between adjacent plant cells, including some small molecules, such as ions, carbohydrates, and hormones, as well as some large molecules including RNAs, proteins, and viruses (Tilsner et al., 2016; Lee and Frank, 2018). As such, PD are involved in the regulation of plant growth and development and environmental adaptation including disease resistance (Cheval and Faulkner, 2018). The structure and function of PD must be tightly regulated throughout the life of a plant (Lee and Frank, 2018). Indeed, many factors have been shown to be involved in regulating the permeability of PD. For instance, the callose at the neck of PD is involved in the regulation of intercellular trafficking in plants. It was shown that callose deposition at PD will accelerate during virus infection in order to prevent the spread of viruses (Levy et al., 2007). In line with this finding, some viruses have movement proteins (MPs), which can mediate the degradation of callose to open up PD (Schoelz et al., 2011). In addition, consistent with the presence of actin cytoskeletal proteins in PD, the actin cytoskeleton has been implicated in the regulation of intercellular trafficking *via* PD (White and Barton, 2011; Pitzalis and Heinlein, 2017), but the underlying mechanism remains largely unexplored. In this mini-review, we are going to describe the recent progress made in this respect.

EVIDENCE SUPPORTING THE ROLE OF ACTIN IN REGULATING THE PERMEABILITY OF PD

Actin is a highly conserved 42 kDa protein, and it is very abundant in eukaryotes. Actin is involved in many cellular physiological processes in plants, including cell growth, cell division, cytokinesis, and various intracellular trafficking events. As such, actin plays a crucial role in plant growth and development (Szymanski and Staiger, 2018). Under optimal conditions, actin can assemble into filamentous structures, called actin filaments (F-actin) or microfilaments. Most actin-based functions are dictated by the spatial organization and dynamics of F-actin in cells. Within cells, actin is associated with many proteins, called actin-binding proteins (ABPs), which modulate the kinetics of actin assembly and disassembly as well as facilitating the formation of different actin structures (Wang et al., 2015). Characterization of the role and mechanism of action of ABPs promises to provide insights into the action of actin within different cellular physiological processes.

Experimental treatments with actin-based pharmacological agents showed that the actin cytoskeleton is involved in the regulation of intercellular communication *via* PD. It was shown that the transport efficiency through PD increases after microinjection of specific actin depolymerizers into tobacco mesophyll cells, whereas the transport efficiency decreases after microinjection of the microfilament stabilizer phalloidin into the cells (Ding et al., 1996; Su et al., 2010). In line with these findings, treatment with the myosin inhibitor 2,3-butanedione monoxime (BDM) reduces the neck width of PD (Radford and White, 1998). However, given that those drugs non-selectively target the actin cytoskeletal system within cells, it remains uncertain whether, and to what extent, the changes in structure and function of PD result from the alteration in the actin cytoskeletal system.

In addition to functioning in plant growth and development, PD are involved in defense against plant pathogens (Cheval and Faulkner, 2018). The important role of PD in virus infection is quite obvious, as viruses spread between cells using PD as the channels. Plant viruses encode MPs to mediate the intercellular transport of infectious genomes *via* PD. It was reported that MPs can mediate the degradation of callose to open up PD (Schoelz et al., 2011). Besides that, another interesting report showed that MPs open up PD *via* interacting with the actin cytoskeleton in PD. Specifically, it was shown that *Cucumber mosaic virus* (CMV) MP severs and caps actin filaments *in vitro* and its filament severing activity is required for its function in PD (Su et al., 2010). Accordingly, it was shown that pretreatment with the actin monomer sequestering reagent latrunculin A (LatA) to depolymerize actin filaments promotes the function of MP in opening up PD, whereas pretreatment with phalloidin to stabilize actin filaments has the opposite effect (Su et al., 2010). These studies imply that there might exist endogenous ABPs that are involved in regulating the permeability of PD *via* controlling actin dynamics in PD. However, due to the lack of techniques to directly visualize the actin cytoskeleton in PD, there is still a debate about whether filamentous actin exists in PD and, if so, how it is organized. This prevents us from understanding the function of the actin cytoskeleton in regulating cell-to-cell trafficking *via* PD. In this regard, development of technology enabling the visualization of the actin cytoskeleton in PD is extremely necessary. In addition, development of methods to specifically alter actin dynamics in PD might provide insights into the function and mechanism of action of actin in the regulation of PD function.

THE PRESENCE OF ACTIN AND ACTIN-BINDING PROTEINS IN PD

The involvement of the actin cytoskeleton in regulating the function of PD is also supported by data showing that actin and some ABPs associate with PD. The association of actin with PD was initially discovered by the immunogold labeling approach (**Table 1**; White et al., 1994; Blackman and Overall, 1998) using a monoclonal antibody against chicken gizzard actin. The association of actin with PD structures was further confirmed using fluorescent phalloidins or by immunofluorescence using an antibody against human actin (**Table 1**; Baluska et al., 2001, 2004).

Similarly, myosin was first discovered to associate with PD with immuno-EM using polyclonal antibodies against animal myosins (**Table 1**; Blackman and Overall, 1998; Radford and White, 1998), which recognize highly conserved motifs in the myosin head, as well as an antibody against the C-terminal tail of plant myosin VIII (**Table 1**; Reichelt et al., 1999). The association of myosins with PD was also verified by immunofluorescence analyses with the same antibodies (**Table 1**; Radford and White, 1998; Reichelt et al., 1999; Baluska et al., 2001, 2004). Subsequent analysis of myosin XI fused to different fluorescent proteins

TABLE 1 | Actin and its associated proteins identified in plasmodesmata (PD).

Cytoskeletal protein	Function	Reference(s)
Actin	Building blocks of the actin cytoskeleton	White et al., 1994; Ding et al., 1996; Blackman and Overall, 1998; Fernandez-Calvino et al., 2011
Myosin	Actin filament side binding; actin-based movement	Blackman and Overall, 1998; Radford and White, 1998; Reichelt et al., 1999; Volkmann et al., 2003; Wojtaszek et al., 2005; Golomb et al., 2008; Sattarzadeh et al., 2008; Fernandez-Calvino et al., 2011; Haraguchi et al., 2014
Tropomyosin	Actin filament side binding	Faulkner et al., 2009; Fernandez-Calvino et al., 2011
ARP2/3	Actin nucleation	Van Gestel et al., 2003
NET	Actin binding	Deeks et al., 2012
Formin	Barbed end capping, actin nucleation	Diao et al., 2018; Oulehlova et al., 2019
Profilin	Actin monomer binding	Fernandez-Calvino et al., 2011
ADF	Actin filament severing; actin monomer binding	Fernandez-Calvino et al., 2011
GSD1	Actin binding	Gui et al., 2014

showed no localization to PD (Reisen and Hanson, 2007). Interestingly, one GFP fusion with the IQ-tail zone of ATM1, a member of the *Arabidopsis* myosin VIII family, appears to localize to sites of ER attachment as well as pitfields when expressed in *Nicotiana benthamiana* leaves (Golomb et al., 2008).

In addition, it was shown that tropomyosin-like proteins localize to PD and cell plates using antibodies against mammalian tropomyosins (**Table 1**; Faulkner et al., 2009). Using the same approach, it was shown that actin-related protein 3 (Arp3) is localized in PD and multivesicular bodies (MVBs) in maize and tobacco (**Table 1**; Van Gestel et al., 2003). In addition, it was shown that a plant-specific ABP, network protein 1A (NET1A), is able to localize to PD (**Table 1**; Deeks et al., 2012). Another interesting report showed that grain setting defect1 (GSD1), a plant-specific remorin protein, is able to interact with actin (Gui et al., 2015) and can localize to PD (**Table 1**; Gui et al., 2014). The presence of ABPs in PD was also supported by data showing that profilin and ADF are present in the *Arabidopsis* plasmodesmal proteome (**Table 1**; Fernandez-Calvino et al., 2011). Certainly, direct cytological evidence is needed to confirm that these proteins are indeed localized to PD. Interestingly, recent characterization showed that several *Arabidopsis* and rice class I formins associate with PD (**Table 1**; Diao et al., 2018; Oulehlova et al., 2019). In summary, actin and some ABPs are able to associate with PD.

THE ROLE OF CLASS I FORMINS IN REGULATING THE PERMEABILITY OF PD

Formin (formin homology protein) nucleates actin assembly for the generation of linear actin bundles. The formin proteins contain the characteristic formin homology domain 1 (FH1) and FH2, which are capable of nucleating actin assembly from actin or actin-profilin complexes. The biochemical activities of plant formins have been characterized extensively *in vitro* and most of them are typical formins that nucleate actin assembly from actin or actin bound to profilin (van Gisbergen and Bezanilla, 2013). *In vitro* biochemical analysis revealed that some plant formins have evolved some unusual activities. For instance, AtFH1 was shown to be a nonprocessive actin polymerase, which can bundle actin filaments (Michelot et al., 2006). The formin proteins have been implicated in numerous actin-based cellular processes in plants, such as pollen germination (Lan et al., 2018; Liu et al., 2018), polarized pollen tube growth and root hair growth (Ye et al., 2009; Cheung et al., 2010; Huang et al., 2013; Lan et al., 2018), cell division (Li et al., 2010), cytokinesis (Ingouff et al., 2005), and cell expansion (Yang et al., 2011; Zhang et al., 2011), as well as defense (Favery et al., 2004). There are 21 formin genes in the *Arabidopsis* genome, and the encoded proteins can be divided into two classes (Blanchoin and Staiger, 2010). Specifically, there are 11 class I formins and 10 class II formins in *Arabidopsis*. Among them, Class I formins contain the characteristic transmembrane domain (TMD) at their N-terminus, which enable them to target to membranes (van Gisbergen and Bezanilla, 2013).

Interestingly, recent studies showed that several class I formins specifically localize to PD (Diao et al., 2018; Oulehlova et al., 2019) and they are involved in regulating the permeability of PD in *Arabidopsis* (Diao et al., 2018). It was shown that the class I formin AtFH2 localizes to PD in various tissues, and this function is dictated by its N-terminal TMD. Analysis of *atfh2* mutants showed that the permeability of PD is increased when compared to WT. As such, *atfh2* mutants are sensitive to virus infection. Strikingly, it was shown that a mutant AtFH2, which was deficient in interacting with actin filaments, failed to rescue the defective intercellular trafficking *via* PD in *atfh2* mutants. This suggests that the interaction of AtFH2 with the actin cytoskeleton is crucial for its function in PD. *In vitro* biochemical analysis showed that AtFH2 lacks actin nucleation activity but it caps the barbed end of actin filaments and stabilizes them against dilution-mediated depolymerization *in vitro* (Diao et al., 2018). This allows us to speculate that actin filaments become instable and/or the amount of actin filaments is reduced in PD in *atfh2* mutants. It is quite unusual that AtFH2 can cap the barbed end of actin filaments to prevent their elongation but fails to nucleate actin assembly *in vitro*. Certainly, it cannot be completely ruled out that AtFH2 is able to nucleate actin assembly after post-translational modification or by interacting with some partners *in vivo*. Nonetheless, the current *in vitro* biochemical data suggest that AtFH2 regulates actin dynamics only by binding to the barbed end of filamentous actin. To some extent, this supports the notion that actin filaments exist in PD. Certainly, uncovering the precise localization of AtFH2 in PD will further refine this hypothesis. However, we still do not know how to fit actin filaments into PD as the gap between the plasma membrane and the ER (called the cytoplasmic sleeve) within PD pores is less than 10 nm (Nicolas et al., 2017). It could be possible that actin filaments stay in cytoplasmic sleeve but twine around the ER within PD pores. In addition, Nicolas et al. (2017) also discovered a second PD morphotype (type I) that lacks a visible cytoplasmic sleeve but is capable of non-targeted movement of macromolecules, which indicates that the size of PD pores undergoes dynamic changes. Therefore, the space of cytoplasmic sleeve might increase substantially under certain condition that allows the fitting of actin filaments.

Interestingly, it was shown that several other class I formins are also able to target to PD. Specifically, the closest homolog of AtFH2, namely AtFH1, is also able to associate with PD (Diao et al., 2018; Oulehlova et al., 2019). AtFH1 functions redundantly with AtFH2 in regulating the permeability of PD (Diao et al., 2018). Strikingly, it was shown that several rice class I formins are also able to target to PD (Diao et al., 2018), suggesting that targeting of class I formins to PD is an evolutionarily conserved strategy in plants. An interesting but yet-to-be-answered question is how the TMD of the PD-localized class I formins have evolved to enable their targeting to PD. This function may be linked to the fact that the membrane of PD has a unique phospholipid composition (Grison et al., 2015). Certainly, it could be possible that the TMD of those class I formins might have additional functions besides the membrane anchoring. In support of this speculation, a very recent report showed that

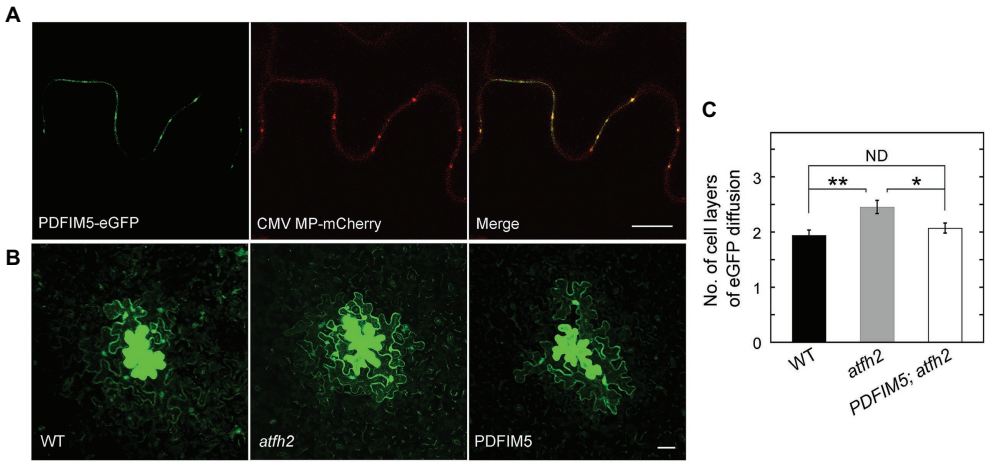

FIGURE 1 | Targeting of FIMBRIN 5 (FIM5) to PD Alleviates the PD Phenotype in *atfh2* Mutants. **(A)** Subcellular localization of PDFIM5-eGFP and *Cucumber mosaic virus* (CMV) movement protein (MP)-mCherry in epidermal pavement cells of *Nicotiana benthamiana* leaves. PDFIM5 was obtained by fusing the N-terminal fragment of AtFH2 ($AtFH2^{N282}$) with *Arabidopsis* FIMBRIN5 (Wu et al., 2010). PDFIM5 was further fused to eGFP (Diao et al., 2018). Plasmids encoding PDFIM5-eGFP and CMV MP-mCherry were introduced into *Agrobacterium tumefaciens* strain GV3101 and transiently expressed in *N. benthamiana* leaves by GV3101 injection. Bar = 10 μm. **(B)** Images of eGFP diffusion in leaf epidermal pavement cells of WT, *atfh2*, and *PDFIM5*; *atfh2* plants. PDFIM5 was constructed as in **(A)**. The PDFIM5 plasmid was introduced into *Agrobacterium tumefaciens* strain GV3101 and transformed into *atfh2* plants by the floral dip method. The PD permeability of WT, *atfh2*, and *atfh2* harboring PDFIM5 was assessed by the eGFP diffusion assay (Diao et al., 2019), and the images were collected by confocal microscopy. Bar = 10 μm. **(C)** Quantification of the number of cell layers with eGFP diffusion in *Arabidopsis* leaf epidermal pavement cells at 24 h after bombardment. *PDFIM5*; *atfh2* represents *atfh2* plants expressing PDFIM5. More than 30 cells were counted and the experiments were repeated at least three times. Error bars represent SE. $^{*}p < 0.05$ and $^{**}p < 0.01$ by Mann-Whitney U test. ND, no statistical difference.

TMD of *Arabidopsis thaliana* Plasmodesmata-located protein (PDLP) 5 is involved in the self-interaction of PDLP5 that is essential for PDLP5 to regulate cell-to-cell movement besides its role in membrane targeting (Wang et al., 2020).

As mentioned above, PD permeability is increased in *atfh2* mutants. Interestingly, targeting of *Arabidopsis* FIMBRIN 5 (FIM5) to PD alleviates the intercellular trafficking phenotype in *atfh2* mutants (**Figure 1**). This suggests that loss of AtFH2 causes instability of actin filaments and/or reduction in the amount of actin filaments in PD. These data actually support the previous notion that stabilization of actin filaments decreases the permeability of PD whereas destabilization of actin filaments increases it (Ding et al., 1996; Su et al., 2010). In summary, these data together suggest that the amount of actin filaments and/or the stability of actin filaments are crucial for the permeability of PD, and actin filaments in PD presumably act as the physical barrier to regulate the permeability of PD.

CONCLUSIONS AND PERSPECTIVES

Increasing evidence is showing that the actin cytoskeleton is involved in the regulation of intercellular transport through PD, whereas the molecular mechanism by which the actin cytoskeleton regulates the permeability of PD remains largely unexplored. Research in this area progresses slowly for at least two reasons. Firstly, researchers lack approaches to directly visualize the actin cytoskeleton in PD, because PD are tiny structures that are deeply embedded in the cell walls. Secondly, researchers lack approaches to specifically manipulate the function of the actin cytoskeleton in PD. Recent identification of PD-localized class I formins provides the possibility to manipulate the actin cytoskeleton in PD *via* regulating the function of those formins. Indeed, analysis of PD permeability in mutants lacking AtFH2 or AtFH1 and AtFH2, in combination with *in vitro* biochemical characterization of AtFH2, allows us to conclude that actin filaments might act as the physical barrier in controlling the permeability of PD. This is actually consistent with a previous assumption that actin filaments in PD might act as the filter in controlling PD permeability (Chen et al., 2010). However, the precise localization of AtFH2 in PD is currently unknown. Dissection of the AtFH2-mediated actin regulatory machinery in PD, for example, by searching for AtFH2-interacting proteins or screening for suppressors or enhancers of the *atfh2* mutant phenotype, might provide further insights into the function and regulation of the actin cytoskeleton in PD. In summary, recent characterizations of PD-localized class I formins have provided insights into the function and mechanism of action of actin in regulating the permeability of PD. However, it remains largely unknown how exactly the actin cytoskeleton regulates the structure and function of PD. This will be an exciting research avenue in the future.

AUTHOR CONTRIBUTIONS

All authors listed have made a substantial, direct and intellectual contribution to the work, and approved it for publication.

FUNDING

This work was supported by a grant from National Natural Science Foundation of China (31970180) and the funding from Beijing Advanced Innovation Center for Structural Biology.

ACKNOWLEDGMENTS

We thank the members of the Huang lab for helpful discussion on this review. We apologize to those whose work could not be cited due to space limitations.

REFERENCES

Baluska, F., Cvrckova, F., Kendrick-Jones, J., and Volkmann, D. (2001). Sink plasmodesmata as gateways for phloem unloading. Myosin VIII and calreticulin as molecular determinants of sink strength? *Plant Physiol.* 126, 39–46. doi: 10.1104/pp.126.1.39

Baluska, F., Samaj, J., Hlavacka, A., Kendrick-Jones, J., and Volkmann, D. (2004). Actin-dependent fluid-phase endocytosis in inner cortex cells of maize root apices. *J. Exp. Bot.* 55, 463–473. doi: 10.1093/jxb/erh042

Blackman, L. M., and Overall, R. L. (1998). Immunolocalisation of the cytoskeleton to plasmodesmata of *Chara corallina*. *Plant J.* 14, 733–741. doi: 10.1046/j.1365-313x.1998.00161.x

Blanchoin, L., and Staiger, C. J. (2010). Plant formins: diverse isoforms and unique molecular mechanism. *Biochim. Biophys. Acta* 1803, 201–206. doi: 10.1016/j.bbamcr.2008.09.015

Chen, C., Zhang, Y., Zhu, R., and Yuan, M. (2010). The actin cytoskeleton is involved in the regulation of the plasmodesmal size exclusion limit. *Plant Signal. Behav.* 5, 1663–1665. doi: 10.4161/psb.5.12.14018

Cheung, A. Y., Niroomand, S., Zou, Y., and Wu, H. M. (2010). A transmembrane formin nucleates subapical actin assembly and controls tip-focused growth in pollen tubes. *Proc. Natl. Acad. Sci. U. S. A.* 107, 16390–16395. doi: 10.1073/pnas.1008527107

Cheval, C., and Faulkner, C. (2018). Plasmodesmal regulation during plant-pathogen interactions. *New Phytol.* 217, 62–67. doi: 10.1111/nph.14857

Deeks, M. J., Calcutt, J. R., Ingle, E. K., Hawkins, T. J., Chapman, S., Richardson, A. C., et al. (2012). A superfamily of actin-binding proteins at the actin-membrane nexus of higher plants. *Curr. Biol.* 22, 1595–1600. doi: 10.1016/j.cub.2012.06.041

Diao, M., Ren, S., Wang, Q., Qian, L., Shen, J., Liu, Y., et al. (2018). *Arabidopsis* formin 2 regulates cell-to-cell trafficking by capping and stabilizing actin filaments at plasmodesmata. *Elife* 7:e36316. doi: 10.7554/eLife.36316

Diao, M., Wang, Q. N., and Huang, S. J. (2019). Quantitative plasmodesmata permeability assay for pavement cells of *Arabidopsis* leaves. *Bio-Protocol* 9:e3206. doi: 10.21769/BioProtoc.3206

Ding, B., Kwon, M. O., and Warnberg, L. (1996). Evidence that actin filaments are involved in controlling the permeability of plasmodesmata in tobacco mesophyll. *Plant J.* 10, 157–164. doi: 10.1046/j.1365-313X.1996.10010157.x

Faulkner, C. R., Blackman, L. M., Collings, D. A., Cordwell, S. J., and Overall, R. L. (2009). Anti-tropomyosin antibodies co-localise with actin microfilaments and label plasmodesmata. *Eur. J. Cell Biol.* 88, 357–369. doi: 10.1016/j.ejcb.2009.02.184

Favery, B., Chelysheva, L. A., Lebris, M., Jammes, F., Marmagne, A., De Almeida-Engler, J., et al. (2004). *Arabidopsis* formin AtFH6 is a plasma membrane-associated protein upregulated in giant cells induced by parasitic nematodes. *Plant Cell* 16, 2529–2540. doi: 10.1105/tpc.104.024372

Fernandez-Calvino, L., Faulkner, C., Walshaw, J., Saalbach, G., Bayer, E., Benitez-Alfonso, Y., et al. (2011). *Arabidopsis* plasmodesmal proteome. *PLoS One* 6:e18880. doi: 10.1371/journal.pone.0018880

Golomb, L., Abu-Abied, M., Belausov, E., and Sadot, E. (2008). Different subcellular localizations and functions of *Arabidopsis* myosin VIII. *BMC Plant Biol.* 8:3. doi: 10.1186/1471-2229-8-3

Grison, M. S., Brocard, L., Fouillen, L., Nicolas, W., Wewer, V., Dormann, P., et al. (2015). Specific membrane lipid composition is important for plasmodesmata function in *Arabidopsis*. *Plant Cell* 27, 1228–1250. doi: 10.1105/tpc.114.135731

Gui, J. S., Liu, C., Shen, J. H., and Li, L. G. (2014). Grain setting defect1, encoding a remorin protein, affects the grain setting in rice through regulating plasmodesmatal conductance. *Plant Physiol.* 166, 1463–1478. doi: 10.1104/pp.114.246769

Gui, J. S., Zheng, S., Shen, J. H., and Li, L. G. (2015). Grain setting defect1 (GSD1) function in rice depends on S-acylation and interacts with actin 1 (OsACT1) at its C-terminal. *Front. Plant Sci.* 6:804. doi: 10.3389/fpls.2015.00804

Haraguchi, T., Tominaga, M., Matsumoto, R., Sato, K., Nakano, A., Yamamoto, K., et al. (2014). Molecular characterization and subcellular localization of *Arabidopsis* class VIII myosin, ATM1. *J. Biol. Chem.* 289, 12343–12355. doi: 10.1074/jbc.M113.521716

Huang, J., Kim, C. M., Xuan, Y. H., Liu, J., Kim, T. H., Kim, B. K., et al. (2013). Formin homology 1 (OsFH1) regulates root-hair elongation in rice (*Oryza sativa*). *Planta* 237, 1227–1239. doi: 10.1007/s00425-013-1838-8

Ingouff, M., Fitz Gerald, J. N., Guerin, C., Robert, H., Sorensen, M. B., Van Damme, D., et al. (2005). Plant formin AtFH5 is an evolutionarily conserved actin nucleator involved in cytokinesis. *Nat. Cell Biol.* 7, 374–380. doi: 10.1038/ncb1238

Lan, Y., Liu, X., Fu, Y., and Huang, S. (2018). *Arabidopsis* class I formins control membrane-originated actin polymerization at pollen tube tips. *PLoS Genet.* 14:e1007789. doi: 10.1371/journal.pgen.1007789

Lee, J. Y., and Frank, M. (2018). Plasmodesmata in phloem: different gateways for different cargoes. *Curr. Opin. Plant Biol.* 43, 119–124. doi: 10.1016/j.pbi.2018.04.014

Levy, A., Erlanger, M., Rosenthal, M., and Epel, B. L. (2007). A plasmodesmata-associated beta-1,3-glucanase in *Arabidopsis*. *Plant J.* 49, 669–682. doi: 10.1111/j.1365-313X.2006.02986.x

Li, Y., Shen, Y., Cai, C., Zhong, C., Zhu, L., Yuan, M., et al. (2010). The type II *Arabidopsis* formin14 interacts with microtubules and microfilaments to regulate cell division. *Plant Cell* 22, 2710–2726. doi: 10.1105/tpc.110.075507

Liu, C., Zhang, Y., and Ren, H. (2018). Actin polymerization mediated by AtFH5 directs the polarity establishment and vesicle trafficking for pollen germination in *Arabidopsis*. *Mol. Plant* 11, 1389–1399. doi: 10.1016/j.molp.2018.09.004

Michelot, A., Derivery, E., Paterski-Boujemaa, R., Guerin, C., Huang, S., Parcy, F., et al. (2006). A novel mechanism for the formation of actin-filament bundles by a nonprocessive formin. *Curr. Biol.* 16, 1924–1930. doi: 10.1016/j.cub.2006.07.054

Nicolas, W. J., Grison, M. S., Trepout, S., Gaston, A., Fouche, M., Cordelieres, F. P., et al. (2017). Architecture and permeability of post-cytokinesis plasmodesmata lacking cytoplasmic sleeves. *Nat. Plants* 3:17082. doi: 10.1038/nplants.2017.82

Oulehlova, D., Kollarova, E., Cifrova, P., Pejchar, P., Zarsky, V., and Cvrckova, F. (2019). *Arabidopsis* class I formin FH1 relocates between membrane compartments during root cell ontogeny and associates with plasmodesmata. *Plant Cell Physiol.* 60, 1855–1870. doi: 10.1093/pcp/pcz102

Pitzalis, N., and Heinlein, M. (2017). The roles of membranes and associated cytoskeleton in plant virus replication and cell-to-cell movement. *J. Exp. Bot.* 69, 117–132. doi: 10.1093/jxb/erx334

Radford, J. E., and White, R. G. (1998). Localization of a myosin-like protein to plasmodesmata. *Plant J.* 14, 743–750. doi: 10.1046/j.1365-313x.1998.00162.x

Reichelt, S., Knight, A. E., Hodge, T. P., Baluska, F., Samaj, J., Volkmann, D., et al. (1999). Characterization of the unconventional myosin VIII in plant cells and its localization at the post-cytokinetic cell wall. *Plant J.* 19, 555–567. doi: 10.1046/j.1365-313X.1999.00553.x

Reisen, D., and Hanson, M. R. (2007). Association of six YFP-myosin XI-tail fusions with mobile plant cell organelles. *BMC Plant Biol.* 7:6. doi: 10.1186/1471-2229-7-6

Sattarzadeh, A., Franzen, R., and Schmelzer, E. (2008). The *Arabidopsis* class VIII myosin ATM2 is involved in endocytosis. *Cell Motil. Cytoskel.* 65, 457–468. doi: 10.1002/cm.20271

Schoelz, J. E., Harries, P. A., and Nelson, R. S. (2011). Intracellular transport of plant viruses: finding the door out of the cell. *Mol. Plant* 4, 813–831. doi: 10.1093/mp/ssr070

Su, S., Liu, Z., Chen, C., Zhang, Y., Wang, X., Zhu, L., et al. (2010). Cucumber mosaic virus movement protein severs actin filaments to increase the plasmodesmal size exclusion limit in tobacco. *Plant Cell* 22, 1373–1387. doi: 10.1105/tpc.108.064212

Szymanski, D., and Staiger, C. J. (2018). The actin cytoskeleton: functional arrays for cytoplasmic organization and cell shape control. *Plant Physiol.* 176, 106–118. doi: 10.1104/pp.17.01519

Tilsner, J., Nicolas, W., Rosado, A., and Bayer, E. M. (2016). Staying tight: plasmodesmal membrane contact sites and the control of cell-to-cell connectivity in plants. *Annu. Rev. Plant Biol.* 67, 337–364. doi: 10.1146/annurev-arplant-043015-111840

Van Gestel, K., Slegers, H., Von Witsch, M., Samaj, J., Baluska, F., and Verbelen, J. P. (2003). Immunological evidence for the presence of plant homologues of the actin- related protein Arp3 in tobacco and maize: subcellular localization to actin-enriched pit fields and emerging root hairs. *Protoplasma* 222, 45–52. doi: 10.1007/s00709-003-0004-8

van Gisbergen, P. A., and Bezanilla, M. (2013). Plant formins: membrane anchors for actin polymerization. *Trends Cell Biol.* 23, 227–233. doi: 10.1016/j.tcb.2012.12.001

Volkmann, D., Mori, T., Tirlapur, U. K., Konig, K., Fujiwara, T., Kendrick-Jones, J., et al. (2003). Unconventional myosins of the plant-specific class VIII: endocytosis, cytokinesis, plasmodesmata/pit-fields, and cell-to-cell coupling. *Cell Biol. Int.* 27, 289–291. doi: 10.1016/S1065-6995(02)00330-X

Wang, X., Luna, G. R., Arighi, C. N., and Lee, J. Y. (2020). An evolutionarily conserved motif is required for plasmodesmata-located protein 5 to regulate cell-to-cell movement. *Commun. Biol.* 3:291. doi: 10.1038/s42003-020-1007-0

Wang, J., Zhang, R., Chang, M., Qu, X., Diao, M., Zhang, M., et al. (2015). "Actin cytoskeleton" in *The plant sciences-cell biology*. *Vol. 20*. eds. S. Assmann and B. Liu (New York: Springer), 1–28.

White, R. G., Badelt, K., Overall, R. L., and Vesk, M. (1994). Actin associated with plasmodesmata. *Protoplasma* 180, 169–184. doi: 10.1007/BF01507853

White, R. G., and Barton, D. A. (2011). The cytoskeleton in plasmodesmata: a role in intercellular transport? *J. Exp. Bot.* 62, 5249–5266. doi: 10.1093/jxb/err227

Wojtaszek, P., Anielska-Mazur, A., Gabrys, H., Baluska, F., and Volkmann, D. (2005). Recruitment of myosin VIII towards plastid surfaces is root-cap specific and provides the evidence for actomyosin involvement in root osmosensing. *Funct. Plant Biol.* 32, 721–736. doi: 10.1071/FP05004

Wu, Y., Yan, J., Zhang, R., Qu, X., Ren, S., Chen, N., et al. (2010). *Arabidopsis* FIMBRIN5, an actin bundling factor, is required for pollen germination and pollen tube growth. *Plant Cell* 22, 3745–3763. doi: 10.1105/tpc.110.080283

Yang, W., Ren, S., Zhang, X., Gao, M., Ye, S., Qi, Y., et al. (2011). Bent uppermost internode1 encodes the class II formin FH5 crucial for actin organization and rice development. *Plant Cell* 23, 661–680. doi: 10.1105/tpc.110.081802

Ye, J., Zheng, Y., Yan, A., Chen, N., Wang, Z., Huang, S., et al. (2009). *Arabidopsis* formin3 directs the formation of actin cables and polarized growth in pollen tubes. *Plant Cell* 21, 3868–3884. doi: 10.1105/tpc.109.068700

Zhang, Z., Zhang, Y., Tan, H., Wang, Y., Li, G., Liang, W., et al. (2011). Rice morphology determinant encodes the type II formin FH5 and regulates rice morphogenesis. *Plant Cell* 23, 681–700. doi: 10.1105/tpc.110.081349

Conflict of Interest: The authors declare that the research was conducted in the absence of any commercial or financial relationships that could be construed as a potential conflict of interest.

frontiers in Plant Science

ORIGINAL RESEARCH
published: 22 March 2021
doi: 10.3389/fpls.2021.640277

Plasmodesmata-Dependent Intercellular Movement of Bacterial Effectors

*Zhongpeng Li, Haris Variz, Yani Chen, Su-Ling Liu and Kyaw Aung**

Department of Genetics, Development, and Cell Biology, Iowa State University, Ames, IA, United States

Pathogenic microorganisms deliver protein effectors into host cells to suppress host immune responses. Recent findings reveal that phytopathogens manipulate the function of plant cell-to-cell communication channels known as plasmodesmata (PD) to promote diseases. Several bacterial and filamentous pathogen effectors have been shown to regulate PD in their host cells. A few effectors of filamentous pathogens have been reported to move from the infected cells to neighboring plant cells through PD; however, it is unclear whether bacterial effectors can traffic through PD in plants. In this study, we determined the intercellular movement of *Pseudomonas syringae* pv. *tomato* (*Pst*) DC3000 effectors between adjoining plant cells in *Nicotiana benthamiana*. We observed that at least 16 *Pst* DC3000 effectors have the capacity to move from transformed cells to the surrounding plant cells. The movement of the effectors is largely dependent on their molecular weights. The expression of PD regulators, *Arabidopsis* PD-located protein PDLP5 and PDLP7, leads to PD closure and inhibits the PD-dependent movement of a bacterial effector in *N. benthamiana*. Similarly, a 22-amino acid peptide of bacterial flagellin (flg22) treatment induces PD closure and suppresses the movement of a bacterial effector in *N. benthamiana*. Among the mobile effectors, HopAF1 and HopA1 are localized to the plasma membrane (PM) in plant cells. Interestingly, the PM association of HopAF1 does not negatively affect the PD-dependent movement. Together, our findings demonstrate that bacterial effectors are able to move intercellularly through PD in plants.

Keywords: ***Pseudomonas syringae*, plasmodesmata-located protein, flg22, callose, *Nicotiana benthamiana***

OPEN ACCESS

Edited by:
Tessa Maureen Burch-Smith, The University of Tennessee, Knoxville, United States

Reviewed by:
Sergey Morozov, Lomonosov Moscow State University, Russia
Manfred Heinlein, Centre National de la Recherche Scientifique (CNRS), France

****Correspondence:***
Kyaw Aung
kaung@iastate.edu

Specialty section:
This article was submitted to Plant Cell Biology, a section of the journal Frontiers in Plant Science

Received: *11 December 2020*
Accepted: *01 March 2021*
Published: *22 March 2021*

Citation:
Li Z, Variz H, Chen Y, Liu S-L and Aung K (2021) Plasmodesmata-Dependent Intercellular Movement of Bacterial Effectors. Front. Plant Sci. 12:640277. doi: 10.3389/fpls.2021.640277

INTRODUCTION

Plasmodesmata (PD) are membrane-lined channels which physically connect adjoining plant cells. PD provide the symplastic pathway for the connected cells to exchange molecules directly (Lucas et al., 2009; Brunkard and Zambryski, 2017; Nicolas et al., 2017). The PD-dependent movement of hormones, sugars, proteins, and RNAs has been well documented (Kragler, 2013; Schulz, 2015; Kitagawa and Jackson, 2017; Reagan et al., 2018). In addition to their fundamental roles in plant growth and development, recent findings highlighted the crucial roles of PD in plant immunity (Cheval and Faulkner, 2018).

Plasmodesmata enable the continuity of the plasma membrane (PM) and endoplasmic reticulum (ER) and link the cytoplasm of adjoining plant cells. The space between the PM and ER membrane lining, known as cytoplasmic sleeve, allows the trafficking of molecules between the adjoining plant cells. The function of PD is largely defined by their aperture in permitting molecules to move across. The largest molecules that can traffic through the cytoplasmic sleeve are known as the size exclusion limit (SEL; Kim and Zambryski, 2005). Soluble green fluorescent proteins (1×sGFP; 27 kDa) can freely move between adjoining plant cells through PD, whereas the movement of 2×sGFP (54 kDa) and 3×sGFP (71 kDa) is largely inhibited between physically connected cells in *Arabidopsis* (Kim et al., 2005; Aung et al., 2020). Among different regulators, callose plays the most prominent role in regulating the PD function. Callose is a plant polysaccharide, which is deposited in the cell wall around the PM lining of PD. The accumulation and degradation of callose at PD allow plant cells to dynamically control the closing and opening of PD. Callose deposition at PD is positively correlated with PD closure. Callose synthase (CalS) and β-1,3-glucanase are involved in callose biosynthesis and degradation, respectively (De Storme and Geelen, 2014; Wu et al., 2018).

In addition to the enzymes directly involved in regulating callose homeosis at PD, plasmodesmata-located proteins (PDLPs) play critical roles in modulating the plasmodesmal function. PDLPs affect callose homeostasis at PD by an unknown mechanism. Ectopic expression of PDLP5 results in overaccumulation of callose, whereas a *pdlp5* knock-out mutant accumulates much less callose at PD compared to that of wild type in *Arabidopsis* (Lee et al., 2011). The expression of *PDLP5* transcripts is upregulated by *Pseudomonas syringae* pv. *maculicola* ES4326 infection (Lee et al., 2008, 2011). PDLP1 accumulates at the PM and haustorial interfaces during *Hyaloperonospora arabidopsidis* (*Hpa*) infection (Caillaud et al., 2014). The polar localization of PDLP1 at the haustorium leads to callose deposition at the interface (Caillaud et al., 2014). Despite the involvement of PDLP1 during *Hpa* infection, it is yet to establish whether the plasmodesmal immunity is involved. It has also been demonstrated that pathogen-associated molecular patterns (PAMPs), the fungal cell wall PAMP (chitin) or a 22-amino acid peptide of bacterial flagellin (flg22), are sufficient to trigger callose deposition at PD in *Arabidopsis* (Faulkner et al., 2013; Xu et al., 2017).

Recent findings began to reveal that pathogenic microbes utilize protein effectors to modulate the PD function in their hosts. Microbial effectors are known for altering plant cellular processes to suppress plant immunity (Cui et al., 2015; Buttner, 2016). The fungal pathogen *Fusarium oxysporum* effectors Avr2 and Six5 are localized to PD when transiently overexpressed in *Nicotiana benthamiana* (Cao et al., 2018). The two PD-localized effectors form heterodimer and regulate the plasmodesmal function to allow larger molecules to traffic through PD. The oomycete pathogen *Phytophthora brassicae* RxLR3 effector is localized to PD and physically associated with CalSs, CalS1, CalS2, and CalS3, when transiently overexpressed in *N. benthamiana*. RxLR3 expressed in *Arabidopsis* transgenic plants suppresses the function of the CalSs, inhibiting the callose accumulation at PD. In addition, transient overexpression of RxLR3 in *N. benthamiana* promotes the PD-dependent movement of fluorescent molecules between cells (Tomczynska et al., 2020). The bacterial pathogen *Pseudomonas syringae* pv. *tomato* DC3000 (*Pst* DC3000) delivers effector HopO1-1 to regulate the PD function. HopO1-1 expressed in *Arabidopsis* transgenic plants degrades PDLP5-YFP and PDLP7-YFP. In addition, *Pst* DC3000 promotes the degradation of PDLP7-HF in *Arabidopsis* in a HopO1-1-dependent manner during the infection (Aung et al., 2020). Together, the reports showed that pathogenic microbes use effectors to target different PD regulators.

Pseudomonas syringae pv. *tomato* DC3000 deploys 36 effectors into host cells through type III secretion system (Lindeberg et al., 2012; Wei et al., 2015). The regulation of PD by HopO1-1 prompted us to investigate whether *Pst* DC3000 effectors can move through PD. We determined the PD-dependent movements of *Pst* DC3000 effectors. We also explored whether PDLP5, PDLP7, and flg22 affect the PD-dependent movement of bacterial effectors between plant cells.

MATERIALS AND METHODS

Plant Growth Conditions

Nicotiana benthamiana plants were grown at 22°C with 50% humidity and irradiated with 120 μmol m^{-2} s^{-1} white light for 14 h per day.

Gene Cloning and Plasmid Construction

To generate effector fused to two tandem repeats of yellow fluorescent protein (YFP), the coding sequence of effectors and YFP without a stop codon was amplified from effector-YFP (Aung et al., 2020) and pGW2-YFP (Reumann et al., 2009), respectively. PCR products of effectors and YFP were fused together using an overlapping PCR method with Gateway-compatible primers as described previously (Aung et al., 2020). The stitched PCR fragments were cloned into pDONR 207 and a destination vector pGW2-YFP (Reumann et al., 2009) using a standard Gateway cloning system (Invitrogen). To construct $HopAF1^{G2A}$-YFP, the coding sequencing of $HopAF1^{G2A}$ was amplified from HopAF1-YFP using Gateway-compatible primers. A G to A mutation was introduced in the forward primer. The PCR product was cloned into pDONR 207 and then pGW2-YFP (Reumann et al., 2009). To construct a HF-mCherry construct, the coding sequence of mCherry was amplified from mCherry-pTA7002 (Fujioka et al., 2007) using Gateway-compatible primers. The PCR product was cloned into pDONR 207 and then pB7-HFN-stop (Lee et al., 2017). All primers used for cloning are listed in **Supplementary Table 1**.

Agrobacterium-Mediated Transient Expression for Subcellular Localization, Immunoblot Analysis, and PD-Dependent Movement Assay

Agrobacterium tumefaciens GV3101 harboring different expression constructs were cultured in a 30°C shaking incubator overnight.

The overnight cultures were adjusted to a desired bacterial density using sterilized ddH_2O. The bacterial solutions were infiltrated into the fourth leaves of 5-week-old *N. benthamiana* plants. For subcellular localization analysis, and immunoblot analysis a bacterial culture with an optical density of 0.1 (A_{600}) was used. *Nicotiana benthamiana* leaves were collected 2-days after infiltration for confocal imaging or immunoblot assays.

To establish an Agrobacterium-mediated protein movement assay, we followed the method previously described (Brunkard et al., 2015). *35S::His-Flag (HF)-YFP* or *35S::HopAF1-YFP* (Aung et al., 2020) was transformed into Agrobacterium harboring *35S::ER-CFP* (Nelson et al., 2007). The resulting Agrobacterium carrying two different plasmid DNAs were infiltrated into the fourth leaves of 5-week-old *N. benthamiana* at an optical density of 2×10^{-4} (A_{600}). The expression of the fusion proteins was detected 2 days post infection using confocal microscopy as described below. Plant cells expressing ER-CFP were designated as the transformed plant cells. The movement of HF-YFP or HopAF1-YFP was determined by the detection of YFP signals surrounding the transformed cells. About 76 and 52 images were captured from three biological replicates for HF-YFP and HopAF1-YFP, respectively. An independent Agrobacterium infiltration into different *N. benthamiana* plants was defined as a biological replicate. If YFP was only detected in the transformed cells, they were scored as 0. If YFP was detected in cells physically connecting the transformed cells, they were scored as 1. If YFP diffused beyond the first cell layer from the transformed cells, they were scored as ≥2. To compare the movement between YFP molecules, the numbers of surrounding plant cells to the transformed cells containing YFP signals were counted and analyzed.

To determine the SEL of *N. benthamiana*, the movement of 1×YFP, 2×YFP, and 3×YFP (Aung et al., 2020) was investigated as mentioned above. About 71, 94, and 81 images were captured from three biological replicates for 1×YFP, 2×YFP, and 3×YFP, respectively.

To determine the movement of effectors between plant cells, bacterial effector-YFP fusion proteins (Aung et al., 2020) were transiently expressed in *N. benthamiana* and examined as mentioned above. Plant cells with the strongest YFP signals were designated as the transformed plant cells. The movement of the effector fusion proteins was determined by the detection of YFP signals surrounding the transformed cells. More than 100 transformation events were imaged across at least three biological replicates for all effectors except AvrE-YFP. Around 48 images were collected for AvrE-YFP from three biological replicates.

To determine the effect of PDLP5 and PDLP7 on the movement of the bacterial effector HopAF1, the fourth leaves of 5-week-old *N. benthamiana* plants were infiltrated with mixtures of Agrobacterium harboring *35S::PDLP5-HF* (A_{600} 0.1), *35S::PDLP7-HF* (A_{600} 0.1), or *35S::HF-mCherry* (A_{600} 0.1) with *35S::HopAF1-YFP* (A_{600} 2×10^{-4}). The movement of HopAF1-YFP was determined by the detection of YFP signals surrounding the transformed cells as described above. The numbers of surrounding plant cells to the transformed cells containing YFP signals were counted and compared. More than 100 images collected from three biological replicates were analyzed.

To determine the effect of flg22 on the movement of a bacterial effector HopAF1, 0.1 μM of flg22 was infiltrated into fully expanded leaves of 5-week-old *N. benthamiana*. For a mock treatment, ddH_20 was infiltrated. Twenty-four hours after the treatment, Agrobacteria harboring *35S::HopAF1-YFP* were infiltrated into the mock- or flg22-treated leaves. More than 100 images collected from three biological replicates were analyzed.

Plasmodesmal Callose Staining Assay

The fourth leaf of *N. benthamiana* was infiltrated with ddH_2O (mock) or 0.1 μM of flg22 for 24 h. Aniline blue (0.01% in 1×PBS buffer, pH 7.4) was infiltrated into the treated area to image callose accumulation at PD as previously described (Xu et al., 2017). To determine the role of PDLP5 and PDLP7 in callose accumulation, Agrobacteria harboring *35S::PDLP5-HF*, *35S::PDLP7-HF*, and *35S::HF-YFP* (mock) were infiltrated into the fourth leaf of *N. benthamiana*. Aniline blue was infiltrated into the bacterial infected area 48 h post infection for imaging callose accumulation at PD as mentioned above. Plasmodesmal callose deposits were imaged using confocal microscopy 15 min after dye infiltration. Around 10 images were collected from each sample. Aniline blue stained callose was quantified using the Macro feature of FIJI for large scale data analysis. In brief, images were first converted from lsm to tif and then to eight-bit image files. RenyiEntropy white method was used to set Auto Threshold creating black and white images highlighting callose. Particle Analysis tool was used to outline each aniline blue-stained callose and ascribe a quantitative numerical value in μm^2. Exclusion setting of 0.10–20 μm^2 and a circularity of 0.30–1.00 were used to isolate callose excluding any non callose related fluorescence. About 10 images were collected from each treatment. Data from 10 images from an experiment were pooled and plotted as mentioned below.

FM4-64 staining

Around 50 μM of FM4-64 dye (Life Technologies) was infiltrated into the bacterial infected area of *N. benthamiana* leaves 48 h post infection for staining the PM. HopAF1-YFP, $HopAF1^{G2A}$-YFP, and FM4-64 signals were imaged using confocal microscopy 3 h after the dye infiltration.

Confocal Imaging

Zeiss Laser Scanning Microscopy 700 was used to image fluorescent signals. For subcellular localization and imaging aniline blue-stained callose, a small piece (~4 mm^2) of leaf tissues was mounted with water on a glass slide with the abaxial side facing upward. For imaging PD-dependent movement of fluorescent molecules, a larger piece (~1 cm^2) of leaf tissues was mounted with water on a glass slide with the abaxial side facing upward. Different fluorescent signals were excited with the following laser lines: callose (405 nm), YFP (488 nm), CFP (405 nm), and FM4-64 (555 nm). The signals were then collected using the following emission filters: callose (SP 555), YFP (SP 555), CFP (SP 555), and FM4-64 (SP 640).

Statistical Analysis

All presented experiments were performed at least three independent times. The pooling of data from different biological replicates for different experiments is indicated in each section. Violin box plots were created with an online software.[1]

Mann-Whitney *U* Test[2] was performed for testing statistical significance of differences.

Immunoblot Analyses

N. benthamiana leaves were frozen with liquid nitrogen and homogenized with 1600 miniG (SPEX). Protein extraction buffer [60 mM Tris-HCl (pH 8.8), 2% (v/v) glycerol, 0.13 mM EDTA (pH 8.0), and 1× protease inhibitor cocktail complete from Roche] was added to the homogenized tissues (100 µl/10 mg). The samples were vortexed for 30 s, heated at 70°C for 10 min, and centrifuged at 13,000 *g* for 5 min at room temperature. The supernatants were then transferred to new tubes. For SDS-PAGE analysis, 10 µl of the extract in 1x Laemmli sample buffer (Bio-Rad) was separated on 4–15% Mini-PROTEAN TGX precast protein gel (Bio-Rad). The separated proteins were transferred to a polyvinylidene fluoride membrane (Bio-Rad) using a Trans-Blot Turbo Transfer System RTA transfer kit following the manufacturer's instructions (Bio-Rad). The membrane was incubated in a blocking buffer [3% (v/v) BSA, 50 mM Tris base, 150 mM NaCl, 0.05% (v/v) Tween 20 (pH 8.0)] at room temperature for 1 h, then incubated overnight with an antibody prepared in the blocking buffer at 4°C overnight. The antibodies used are as follows: 1:20,000 anti-GFP (Abcam catalog No. ab290), 1:10,000 anti-cMyc (Abcam catalog No. ab9106), and 1:10,000 anti-Flag-HRP (Sigma-Aldrich catalog No. A8592). The probed membranes were washed three times with 1× TBST [50 mM Tris base, 150 mM NaCl, and 0.05% (v/v) Tween 20, pH 8.0] for 5 min before being incubated with a secondary antibody at room temperature for 1 h except for anti-Flag-HRP. The secondary antibodies used were 1:20,000 goat anti-rabbit IgG (Thermo Fisher Scientific catalog No. 31,460). Finally, the membranes were washed four times with 1× TBST for 10 min before the signals were visualized with SuperSignal West Dura Extended Duration Substrate (Pierce Biotechnology).

RESULTS

An Agrobacterium-Mediated Protein Movement Assay in *Nicotiana benthamiana*

The PD-dependent movement of fluorescent molecules has been previously established in *N. benthamiana* (Brunkard et al., 2015). To unambiguously locate Agrobacterium infected plant cells, we infiltrated Agrobacterium harboring two plasmids (*35S::ER-CFP and 35S::HF-YFP*) into *N. benthamiana* at an optical density of 2×10^{-4} (A_{600}), resulting in a few transformed cells per cm^2 of leaf surface. Free YFP molecules are able to move between cells through PD, whereas ER-CFP cannot move through PD from the transformed cells. Thus, the expression of ER-CFP can be used to locate the transformed plant cells. Using confocal microscopy, we observed transformation events on the epidermis of *N. benthamiana*, determined by the expression of ER-CFP. We imaged 76 transformation events from three biological repeats. We observed that the transformed plant cells always express the strongest YFP signals within a cluster of cells containing YFP. Plant cells containing weaker YFP signals surrounding the transformed cell are resulted from the PD-dependent movement of YFP (**Supplementary Figure 1A**). We thus concluded that the plant cells containing the strongest YFP signals could be used to identify the transformed plant cells using the experimental system. In addition, we tested the SEL of PD in *N. benthamiana* epidermis. It has been established that 1×YFP (~27 kDa) can effectively move through PD between *Arabidopsis* epidermal cells, whereas the movement of YFP concatemer 2×YFP (~54 kDa) was greatly inhibited. No movement of 3×YFP (~81 kDa) was observed in *Arabidopsis* (Aung et al., 2020). Using the Agrobacterium-mediated protein movement assay in *N. benthamiana*, we observed the PD-dependent movement of 1×YFP in all transformation events detected (**Supplementary Figure 1B**). Around 20% of the transformation events of 1×YFP led to the diffusion of two or more than two cell layers. 2×YFP and 3×YFP resulted in around 30 and 10% PD-dependent trafficking, respectively (**Supplementary Figure 1C**). More strikingly, 1×YFP diffused to an average of 5.5 cells, whereas the concatemers moved to less than one cell (**Supplementary Figure 1C**).

Bacterial Effectors Traffic Between Plant Cells

To determine whether effectors can move from the infected cells to the surrounding plant cells, we monitored the movement of YFP tagged *Pst* DC3000 effector (Aung et al., 2020). 29 *Pst* DC3000 effector-YFPs were transiently expressed in *N. benthamiana*. Transient expression of some effectors led to cell death (**Supplementary Table 2**), whereas the expression of a few effectors could not be detected. Although the expression of some effectors using higher Agrobacterium inoculum (A_{600} 0.1) leads to cell death, lower Agrobacterium inoculum (A_{600} 2×10^{-4}) allows us to detect the expression of the fusion proteins 2 days after infiltration. We selected 17 effectors to further investigate their movement between plant cells. Confocal images showed the expression of 16 effector-YFP fusion proteins in the epidermis *N. benthamiana* leaves (**Supplementary Figure 2**). It is noted that the expression of HopH1-YFP, HopN1-YFP, HopAO1-YFP, HopA1-YFP, and AvrE-YFP using a higher Agrobacterium inoculum (A_{600} 0.1) leads to cell death in *N. benthamiana*. Among the selected effectors, we observed the movement of 16 bacterial effectors between plant cells (**Figure 1A**). More than 50% of transformation events lead to the intercellular movement of HopK1-YFP, HopF2-YFP, HopH1-YFP, and HopAF1-YFP. Among them, HopAF1-YFP shows the most effective movement. More than 20% of transformation events result in the trafficking of HopAF1-YFP to two or more than

[1]https://huygens.science.uva.nl/PlotsOfData/

[2]https://www.socscistatistics.com/tests/mannwhitney/default2.aspx

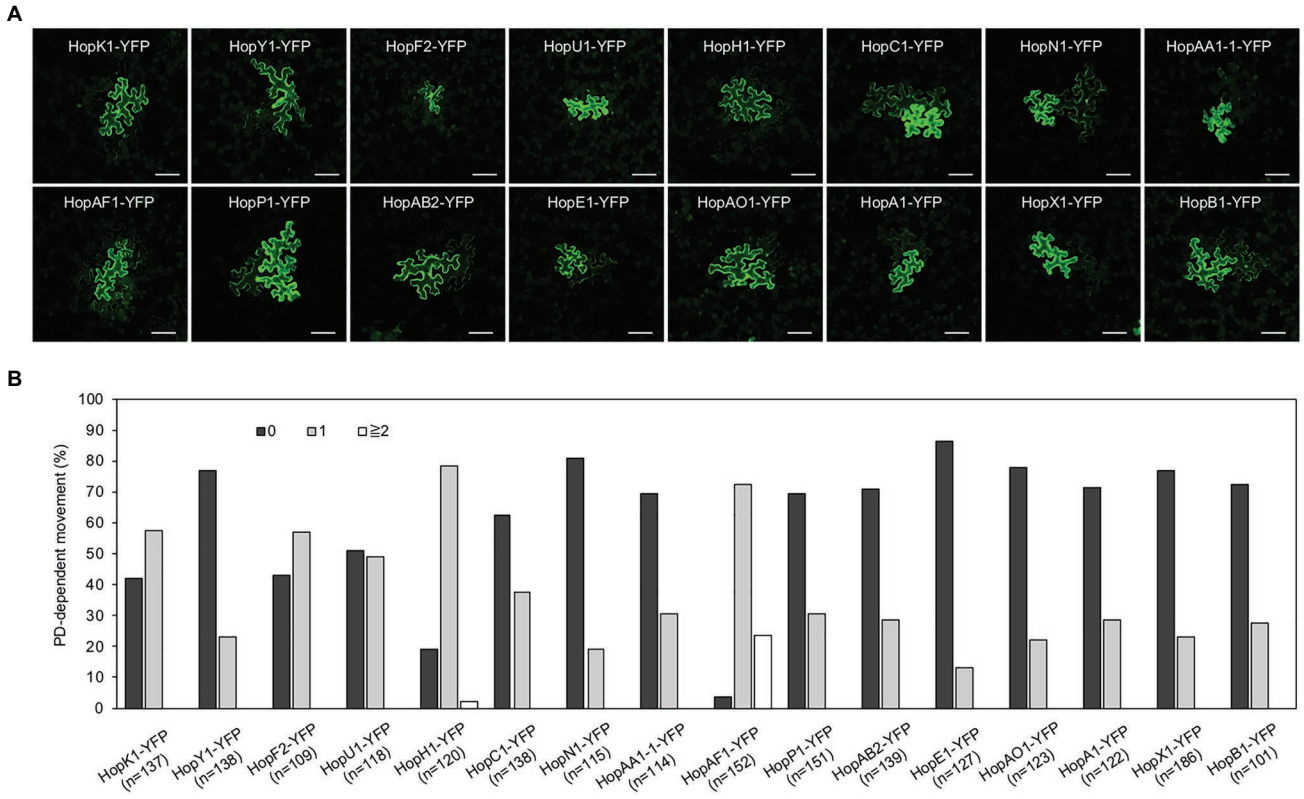

FIGURE 1 | The movement of bacterial effectors between plant cells. **(A)** Confocal images show the diffusion of effector-yellow fluorescent protein (YFP) fusion proteins. Images were taken from epidermis of *Nicotiana benthamiana* leaves. An agrobacterium-mediated protein movement assay was conducted to determine the movement of effector-YFP fusion proteins in plants. The transformed plant cell exhibits strong yellow fluorescent (YFP) signals. The movement of the fusion proteins is determined by the detection of YFP signals in cells surrounding the transformed cell. Scale bars = 100 μm. **(B)** Quantitative data show the percentage of transformation events resulting in no diffusion (0), one cell layer diffusion (1), and two or more than 2 cell layers diffusion (≧2). The data shown here are pooled from at least three biological replicates. The number of transformation events analyzed is indicated (n).

two cell layers from the transformed cells (**Figure 1B**). In addition, we also choose HopAF1-YFP to confirm the method in determining the transformed plant cells by locating cells with the strongest HopAF1-YFP signals. We observed a similar pattern as HF-YFP. The transformed cells expressing ER-CFP always contain the strongest HopAF1-YFP signals within a cluster of cells containing YFP signals (**Supplementary Figure 1A**). For the majority of mobile effectors, around 20–30% of transformed cells exhibit the movement beyond initially transformed cells (**Figure 1B**). We then conducted immunoblot analysis to confirm the expression of full-length fusion proteins. Total proteins were extracted from *N. benthamiana* leaves transiently expressing the effector fusion proteins. The expression of the fusion proteins was detected using a GFP antibody. As shown in **Supplementary Figure 3A**, we detected a major band for most effectors at a higher molecular weight, suggesting that fluorescence signals detected in **Figure 1A** are emitted from full-length effector fusion proteins. It is noted that most fusion proteins migrated slower than expected (**Supplementary Figure 3A**; **Supplementary Table 2**). It is postulated that the higher molecular weight of the effector fusion proteins than expected might be due to post translational modifications within plants cells or unknow reasons. Together, the findings suggest that bacterial effectors are able to move beyond initially transformed cells.

The Movement of Effectors Is Affected by Their Molecular Weights

Predicted molecular weights of most effector-YFP fusion proteins ranged between 50 and 80 kDa, whereas a few effectors like HopR1 and AvrE weight over 200 kDa (**Supplementary Table 2**). The majority of the mobile effector-YFPs shown in **Figure 1** weights below 70 kDa, expect HopAA1-1-YFP (77.6 kDa; **Supplementary Table 2**). Among the tested effectors, AvrE-YFP does not move from transformed cells to the neighboring cells (**Figures 2A,B**). As *AvrE-YFP* encodes a protein with the molecular weight of ~222 kDa, the large molecule weight might impede the PD-dependent movement of the effector.

As we hypothesized that effectors move intercellularly through PD, we next examined whether the molecular weights of the mobile effectors affects their movement. We thus constructed HopH1, HopC1, and HopAF1 with two tandem repeats of YFP, yielding HopH1-2×YFP, HopC1-2×YFP, and HopAF1-2×YFP. We first determined the molecular weights of the fusion proteins by transiently expressing them in *N. benthamiana*

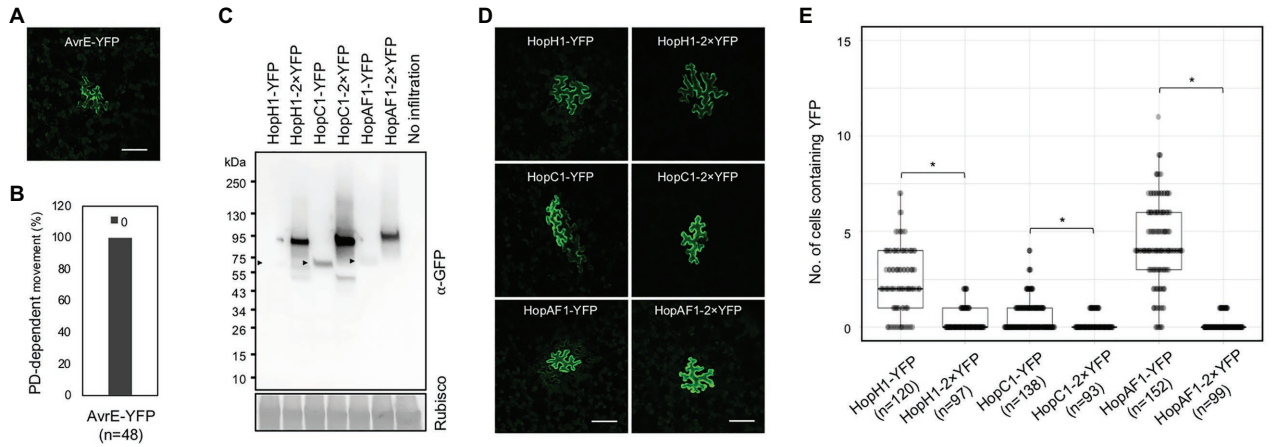

FIGURE 2 | The movement of effectors is largely affected by their sizes. **(A)** Confocal image shows the expression of AvrE-YFP. Scale bars = 100 μm. **(B)** Quantitative data show that AvrE-YFP cannot move through PD. 0: no diffusion. The number of transformation events analyzed is indicated (*n*). **(C)** Detection of full-length effector fusion proteins. Effector-YFPs and effector-2×YFPs were transiently expressed in *N. benthamiana*. The samples were then subjected to immunoblot analysis using an anti-GFP antibody. Rubisco is served as a loading control. Arrow heads indicate the expression of effector-YFPs. **(D)** Confocal images show the diffusion of effector-YFP fusion proteins. Images were taken from epidermis of *N. benthamiana* transiently expressing different fusion proteins. Scale bars = 100 μm. **(E)** Quantitative data present the plasmodesmata (PD)-dependent movement of effector-YFP fusion proteins. Mann-Whitney *U* Test was used to analyze the data. The *p*-value is <0.0001 for HopH1-YFP vs. HopH1-2×YFP, <0.00094 for HopC1-YFP and HopC1-2×YFP, and <0.00001 for HopAF1-YFP and HopAF1-2×YFP (*). The number of transformation events analyzed is indicated (*n*).

leaves using an Agrobacterium-mediated approach. We then detected the expression of the fusion proteins using a GFP antibody. Compared to 1×YFP fusion, 2×YFP fusion of the effectors increases the molecular weight by ~26 kDa (**Figure 2C**). To investigate the PD-dependent movement of 2×YFP fusion proteins, we determined the movement of HopH1-2×YFP, HopC1-2×YFP, and HopAF1-2×YFP in *N. benthamiana* leaves as mentioned above. Compared to the diffusion of 1×YFP fusion proteins, the movement of HopH1-2×YFP, HopC1-2×YFP, and HopAF1-2×YFP beyond initially transformed cells is drastically reduced (**Figures 2D,E**). Together, the findings support that the bacterial effectors move between plant cells through PD.

The Expression of PDLP5 and PDLP7 Suppresses the PD-Dependent Movement of HopAF1

Altered expression of PDLPs has been shown to impact the PD function. To further support that the intercellular movement of effectors depends on PD, we investigated whether the expression of PDLP affects the movement of bacterial effectors. PDLP5 has been shown to affect callose deposition at PD and alter the movements of GFP molecules between cells in *Arabidopsis*; however, it's unknown whether PDLPs regulates callose accumulation at PD when transiently expressed in *N. benthamiana*. To this end, we detected callose accumulation at PD in *N. benthamiana* after PDLP5 or PDLP7 was transiently expressed. PDLP5 and PDLP7 were selected due to their role in bacterial immunity (Lee et al., 2011; Aung et al., 2020). We first detected the expression of HF-YFP (mock), PDLP5-HF, and PDLP7-HF using immunoblot analysis (**Supplementary Figure 3B**). The leaf transiently expressing the fusion proteins was stained with aniline blue to detect callose accumulated at PD. Similar to *Arabidopsis* transgenic plants overexpressing PDLP5 (Lee et al., 2011), transient expression of *Arabidopsis* PDLP5 is sufficient to increase callose accumulation at PD compared to that of mock treatment (**Figures 3A–C**). While PDLP5 has been previously shown to regulate callose homeostasis, whether PDLP7 has similar roles in callose accumulation has not been determined. Here, we demonstrated that transient expression of *Arabidopsis* PDLP7 also leads to higher accumulation of callose at PD in *N. benthamiana* (**Figures 3A–C**). Together, the findings showed that transient overexpression of the PDLP5 and PDLP7 could increase the callose accumulation at PD in *N. benthamiana*.

Callose accumulation at PD is negatively associated with PD-dependent movement of molecules between plant cells (De Storme and Geelen, 2014; Amsbury et al., 2017; Wu et al., 2018). To further support that bacterial effectors move through PD, we investigated whether PDLP-mediated PD closure would suppress the movement of a bacterial effector HopAF1. Among the mobile effectors, HopAF1 was chosen in this assay because of its highest PD-dependent movement in plants (**Figure 1**). Relatively lower inoculum (A_{600} 2×10^{-4}) of Agrobacteria harboring *35S::HopAF1-YFP* was mixed with a higher inoculum (A_{600} 0.1) of Agrobacteria harboring *35S::HF-mCherry* (mock), *35S::PDLP5-HF*, or *35S::PDLP7-HF* and infiltrated into *N. benthamiana* leaves. The expression of the fusion proteins was determined using immunoblot analysis (**Supplementary Figure 3C**). The movement of HopAF1-YFP was determined 2 days after the Agrobacterium infiltration using confocal microscopy. As shown in **Figure 3D**, the expression of PDLP5 and PDLP7 drastically reduced the intercellular movement of HopAF1-YFP beyond the transformed cells. Together, the findings suggest that the expression of PDLP5

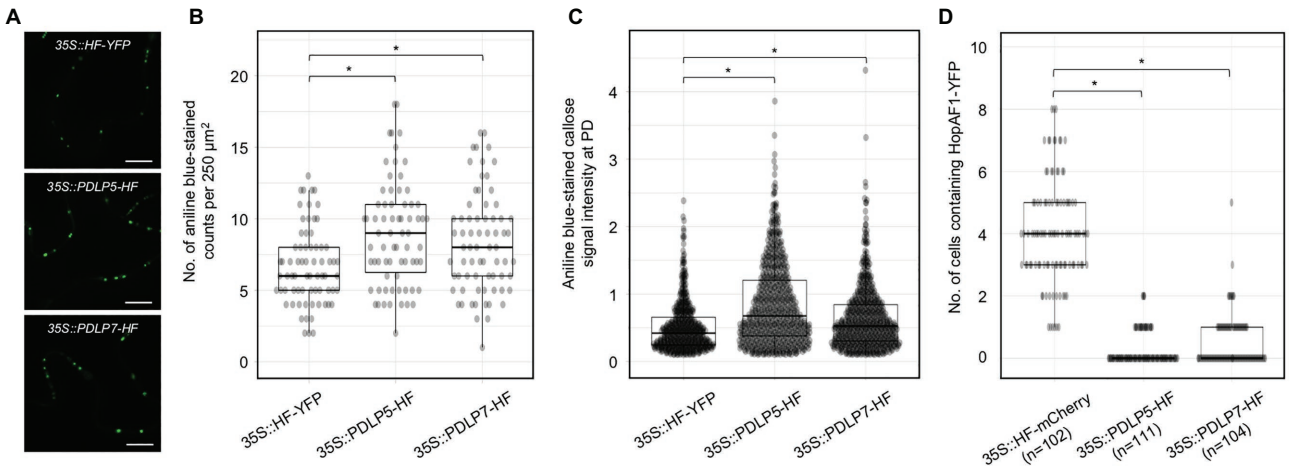

FIGURE 3 | Expression of PDLP5 and PDLP7 suppresses the PD-dependent movement of HopAF1. **(A)** Expression of plasmodesmata-located proteins (PDLPs) affects callose accumulation at PD. *N. benthamiana* leaves were infiltrated with Agrobacteria harboring *35S::HF-YFP*, *35S::PDLP5-HF*, and *35S::PDLP7-HF*. Infiltrated leaves were stained with 0.01% aniline blue and imaged with confocal microscopy. Scale bars = 10 µm. **(B)** Quantitative data present the number of aniline blue-stained callose at PD per 250 μm^2 of *N. benthamiana* epidermis. Mann-Whitney *U* Test was used to analyze the data. The *p*-value is <0.05 (*). **(C)** Quantitative data present the accumulation of callose at PD. Mann-Whitney *U* Test was used to analyze the data. The *p*-value is <0.0001 (*). **(D)** Quantitative data present the PD-dependent movement of HopAF1-YFP when co-expressed with *35S::HF-mCherry*, *35S::PDLP5-HF*, and *35S::PDLP7-HF*. Mann-Whitney *U* Test was used to analyze the data. The *p*-value is <0.00001 for both *35S::PDLP5-HF* and *35S::PDLP7-HF* (*). The number of transformation events analyzed is indicated (*n*).

and PDLP7 affects the PD-dependent movement of a bacterial effector.

flg22 Inhibits the Movement of a Bacterial Effector

In addition to PDLP expression, flg22 has been also reported to induce callose deposition at PD and reduce the PD-dependent molecular fluxes between cells in *Arabidopsis* (Faulkner et al., 2013; Xu et al., 2017). To determine the effect of flg22 on callose accumulation at PD in *N. benthamiana*, we treated a fully expended leaf of *N. benthamiana* with 0.1 µM flg22. Callose deposition at PD was examined 24 h after the infiltration. flg22-treated leaf, compared to mock-treated leaf (infiltrated with ddH_2O), exhibits higher accumulation of callose at PD (**Figures 4A,B**). We next determined whether flg22 treatment suppresses the movement of HopAF1 using an Agrobacterium-mediated protein movement assay mentioned above. The expression of HopAF1-YFP was detected using immunoblot analysis (**Supplementary Figure 3D**). In line with the callose accumulation at PD, flg22-treatment inhibits the PD-dependent movement of HopAF1 (**Figure 4C**).

PD-Dependent Movement of the PM-Associated HopAF1

Among the mobile effectors, HopAF1 and HopA1 are detected on the PM in plant cells (**Supplementary Figure 2**). The PM localization of HopA1 and HopAF1 has been previously reported (Toruno Calero, 2014; Washington et al., 2016). As HopAF1 contains a putative *N*-myristolation site (G2), we postulated that the PM association of HopAF1 is mediated through the protein lipidation. To determine the PM association of HopAF1 in an *N*-myristolation-dependent manner, we constructed a G2A mutant of HopAF1-YFP ($HopAF1^{G2A}$-YFP). Using the Agrobacterium-mediated transient expression approach, HopAF1-YFP and $HopAF1^{G2A}$-YFP were expressed in *N. benthamiana*. The expression of HopAF1-YFP and $HopAF1^{G2A}$-YFP was detected using a GFP antibody (**Supplementary Figure 3A**). To stain the PM, Agrobacterium-infected leaves were infiltrated with FM4-64 dye. HopAF1-YFP overlapped with the FM4-64 stained PM in *N. benthamiana*, confirming the PM association of HopAF1-YFP. As predicted, $HopAF1^{G2A}$-YFP was not associated with the PM. Instead, $HopAF1^{G2A}$-YFP was detected in the cytosol and nucleus (**Figure 5A**). The findings suggest that the PM association of HopAF1-YFP is mediated through the *N*-myristoylation at the N-terminal Glycine (G2).

We next determined the PD-dependent movement of $HopAF1^{G2A}$-YFP using the Agrobacterium-mediated protein movement assay in *N. benthamiana*. It was assumed that the PM association of molecules might negatively impact the PD-dependent movement. Surprisingly, the nucleocytoplasmic localized $HopAF1^{G2A}$-YFP is not as mobile as the PM associated HopAF1-YFP. Only around 30% of the transformation events of $HopAF1^{G2A}$-YFP led to the PD-dependent movement compared to HopAF1-YFP, in which all transformation events led to the PD-dependent movement (**Figures 5B–D**). The findings indicate that the PM association of HopAF1 does not negatively affect the PD-dependent movement of the protein.

DISCUSSION

The PD-dependent movement of fungal effectors (Khang et al., 2010) and an oomycete effector (Khang et al., 2010; Cao et al., 2018;

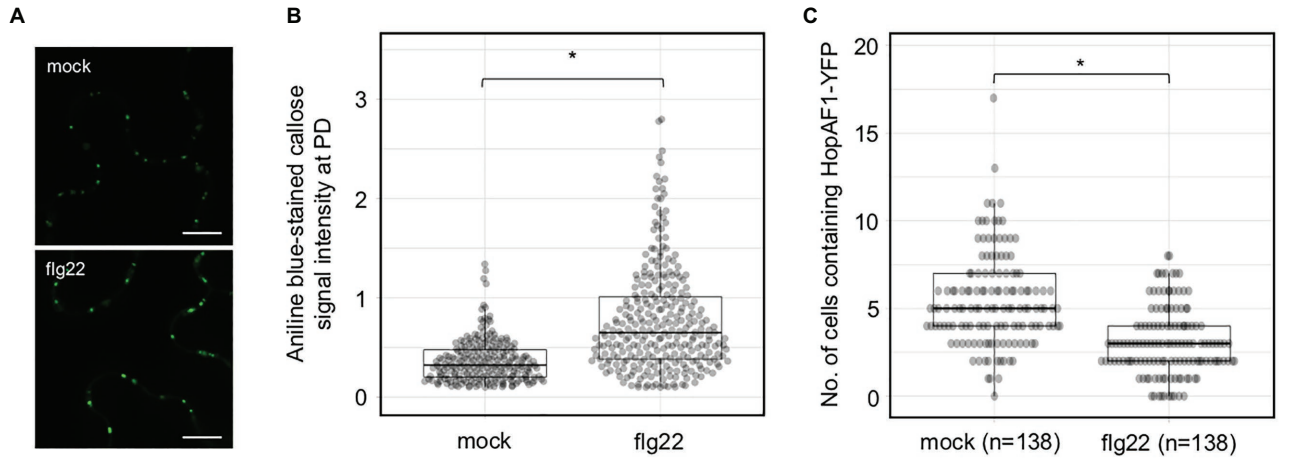

FIGURE 4 | Pattern-triggered immunity (PTI)-induced callose accumulation at PD reduces the movement of effectors. **(A)** Flagellin (flg22) induces callose accumulation at PD. *Nicotiana benthamiana* leaves were infiltrated with 0.1 μM of flg22 or ddH_2O (mock). Infiltrated leaves were stained with 0.01% aniline blue and imaged with confocal microscopy. Scale bars = 10 μm. **(B)** Quantitative data present the accumulation of callose at PD. Mann-Whitney *U* Test was used to analyze the data. The *p*-value is <0.00001 (*). **(C)** flg22 treatment suppresses the PD-dependent movement of HopAF1. *Nicotiana benthamiana* leaves were pretreated with 0.1 μM of flg22 or ddH_2O (mock) for 24 h. Agrobacteria harboring *35S::HopAF1-YFP* were later infiltrated into the pretreated leaves. The PD-dependent movement of HopAF1-YFP was examined 48 h post Agrobacterium infiltration using confocal microscopy. The data shown here were collected from four biological repeats. Mann-Whitney *U* Test was used to analyze the data. The *p*-value is <0.00001 (*). The number of transformation events analyzed is indicated (*n*).

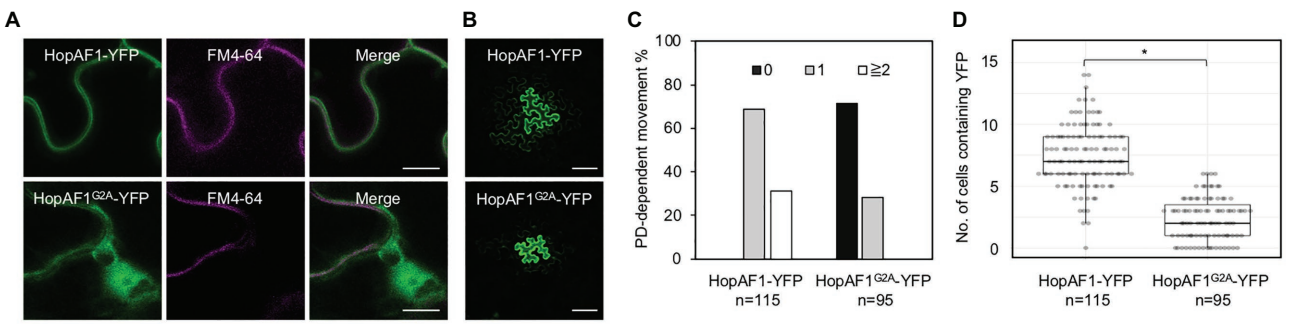

FIGURE 5 | The plasma membrane (PM) association of HopAF1 does not inhibit the PD-dependent movement. **(A)** *Nicotiana benthamiana* leaves transiently expressing HopAF1-YFP or HopAF1^{G2A}-YFP were stained with FM4–64 to label the PM. Confocal images show the PM localization of HopAF1-YFP and the nucleocytoplasmic localization of HopAF1^{G2A}-YFP. Scale bars = 10 μm. **(B)** Confocal images show the PD-dependent movement of HopAF1-YFP or HopAF1^{G2A}-YFP determined by an Agrobacterium-mediated protein movement assay. Images were taken from the epidermis of *N. benthamiana* leaves. The transformed plant cell exhibits strong YFP signals. The movement of the fusion proteins is determined by the detection of YFP signals in cells surrounding the transformed cell. Scale bars = 100 μm. **(C)** Quantitative data show the percentage of transformation events resulting in no diffusion (0), one cell layer diffusion (1), and two or more than two cell layers diffusion (≧2). The data shown here are pooled from at least three biological replicates. The number of transformation events analyzed is indicated (*n*). **(D)** Quantitative data present the numbers of surrounding plant cells to the transformed cells containing YFP signals. Mann-Whitney *U* Test was used to analyze the data. The *p*-value is <0.00001 (*). The number of transformation events analyzed is indicated (*n*).

Tomczynska et al., 2020) have been reported; however, it's unclear whether bacterial effectors move between plant cells or not. Empirical evidence from this work showed that at least 16 *Pst* DC3000 effectors move between plant cells through PD. We established that the movement of the effectors is dependent on PD from the following findings: (1) the effector-YFP fusion proteins can move from the transformed cells to the adjoining plant cells (**Figure 1**), (2) the movement of the effectors is largely dependent on their molecular weights (**Figure 2**), and (3) PDLP5-, PDLP7-, and flg22-induced callose accumulation at PD inhibits the movement of a bacterial effector HopAF1 (**Figures 3, 4**).

Although the movement of 16 effectors is reported here, it's plausible that more *Pst* DC3000 effectors are able to move between plants cells. The following reasons might account for the underestimation of the PD-dependent movement of bacterial effectors: (1) the YFP fusion of effectors increases their molecular weights and could suppress their PD-dependent movement, (2) transiently overexpressing individual effector induces cell death in *N. benthamiana* thus preventing the

visualization of the effectors, and (3) the expression level of some effectors is under the detectable threshold using confocal microscopy.

It is well established that the molecular weight of proteins affects their movement between plant cells through PD (Kim et al., 2005; Aung et al., 2020). In both *Arabidopsis* and *N. benthamiana*, the movement of 2×YFP and 3×YFP is greatly inhibited. Among the effectors we investigated, we did not observe the movement of AvrE-YFP (**Figures 2A,B**). The expression of DEX-His-AvrE was detected at ~250 kDa in *Arabidopsis* (Xin et al., 2015). Also, the tandem fusion of YFP to HopH1-YFP, HopC1-YFP, and HopAF1-YFP (yielding HopH1-2×YFP, HopC1-2×YFP, and HopAF1-2×YFP) drastically suppresses the PD-dependent movement (**Figures 2D,E**). The addition of another YFP increases the molecular weight of the fusion proteins by ~26 kDa (**Figure 2C**). It is also possible that the tandem fusion of YFP affects the tertiary structure of the fusion proteins, impeding the PD-dependent movement.

Many mobile effectors were detected both in the nucleus and cytoplasm (**Supplementary Figure 2**); however, we observed the PD-dependent movement of the PM-localized effectors, HopAF1 and HopA1. Interestingly, the PM-associated HopAF1 is the most mobile effector among the 16 effectors reported here (**Figure 1B**). A few *Pst* DC3000 effectors have been reported to associate with the PM of plant cells (Shan et al., 2000; Göhre et al., 2008; Xin et al., 2015; Washington et al., 2016; Aung et al., 2020), whereas none of *Pst* DC3000 effectors contains putative transmembrane domains. It was previous reported that mutations in putative sites for myristoylation (G2) and palmitoylation (C4) of HopAF1 (HopAF1^{G2AC4S}-cerulean-HA) abolishes the PM localization (Washington et al., 2016). Similar to HopO1-1 and AvrPto1 (Shan et al., 2000; Aung et al., 2020), the G2A mutation is sufficient to disrupt the PM association of HopAF1 (**Figure 5A**). Interestingly, the nucleocytoplasmic localized HopAF1^{G2A}-YFP is not as mobile as the wild-type HopAF1-YFP (**Figures 5B–D**). It is worth pursuing whether the PM association of effectors facilitates the PD-dependent movement of molecules along the PM lining the PD channel. Together, the findings suggest that the membrane association of effectors does not inhibit the PD-dependent movement. It is unclear whether mitochondrial, chloroplast, or the ER association of effectors affects the PD-dependent movement.

In *Arabidopsis*, the expression of PDLP5 is positively correlated with the accumulation of callose at PD (Lee et al., 2011). Here, we reported that the transient overexpression of *Arabidopsis* PDLP5 in *N. benthamiana* increases the accumulation of callose at PD (**Figures 3A,B**). The finding is supported by a recent report that the transient overexpression of PDLP5 suppresses the PD-dependent movement of mCherry (Wang et al., 2020). Similar to PDLP5, the transient expression of *Arabidopsis* PDLP7 also increases callose accumulation at PD in *N. benthamiana* (**Figures 3A,B**). Among different PDLP members, only the expression of PDLP5 transcripts and proteins is upregulated by bacterial infections and a defense hormone SA treatment (Lee et al., 2011). PDLP7 proteins are destabilized by *P. syringae* infection in a bacterial effector HopO1-1-dependent manner (Aung et al., 2020). Given that HopO1-1 physically associates with and destabilizes PDLP5 and PDLP7, the effector might target the PDLPs to suppress plasmodesmal immunity. The targeting of the PDLPs might play critical role in facilitating the PD-dependent movement of bacterial effectors from the infected cells to the adjoining non-infected cells through PD. In line with the notion, we observed that the transient overexpression of PDLP5 and PDLP7 significantly suppresses the PD-dependent movement of a highly mobile bacterial effector HopAF1.

Pathogen-associated molecular pattern-triggered callose accumulation at PD suggests that the plasmodesmal closure is a part of pattern-triggered immunity (PTI). PTI is considered the first line of plant immune responses during microbial infection (Boller and He, 2009). It is plausible that plants induce the plasmodesmal closure to limit the spread of microbial molecules from the infected cells to the surrounding plant cells. In line with the statement, flg22 treatment suppresses the PD-dependent movement of a bacterial effector HopAF1 (**Figure 4C**). It is postulated that the PTI-triggered callose accumulation at PD generally suppresses the PD-dependent movement of most effectors. Recent report showed that the expression of a bacterial effector HopO1-1 facilitates the PD-dependent movement of YFP molecules (Aung et al., 2020). As HopO1-1 targets and destabilizes PDLP5 and PDLP7, it is highly plausible that HopO1-1 functions to overcome the plasmodesmal immunity. We thus hypothesize that HopO1-1 might facilitate the PD-dependent movement of bacterial effectors to the surrounding plant cells. The hypothesis is supported by a recent report that the PD-dependent cell-to-cell movement of *F. oxysporum* effector Avr2-GFP requires Six5 (Cao et al., 2018). Further studies will reveal the role of HopO1-1 in modulating the PD-dependent movement of bacterial effectors.

Although the function of many *Pst* DC3000 effectors has been predicted according to their amino acid sequences, only a handful of them has been confirmed their activities *in planta* (**Supplementary Table 2**). As effector proteins are believed to be involved in suppressing plant immunity to benefit the microbes, the mobile effectors might play crucial roles in inhibiting non-cell-autonomous plant immunity. Successful suppression of both cell-autonomous and non-cell-autonomous plant immunity might be critical for pathogenic microbes to colonize and spread from the initial infection sites. Understanding the function of mobile effectors will allow us to better understand how pathogenic microbes regulate cellular processes in infected plant cells and the surrounding plant cells. This report also demonstrates that an Agrobacterium-mediated protein movement assay using *N. benthamiana* is a powerful experimental system to determine the PD-dependent movement of microbial effectors. The system has great potential in directly visualizing how the mobile effectors affect plant immune responses. Identification and characterization of robust plant immune response markers will allow us to investigate the functions of mobile effectors in modulating cell-autonomous and non-cell-autonomous immune responses *in planta*.

DATA AVAILABILITY STATEMENT

The original contributions presented in the study are included in the article/**Supplementary Material**; further inquiries can be directed to the corresponding author.

AUTHOR CONTRIBUTIONS

KA designed the research, conducted the experiments shown in **Figures 3D, 5A; Supplementary Figures 2**, **3**, and wrote the manuscript with input from all authors. ZL performed the experiments shown in **Figures 1, 2A,B, 5B–D**, and **Supplementary Figures 1**, **3A**. HV conducted the experiments shown in **Figures 3A–C, 4**. YC conducted the experiments shown in **Figures 2D,E**. S-LL contributed to **Figure 2C** and **Supplementary Figure 3**. All authors contributed to the article and approved the submitted version.

FUNDING

This work was supported by the National Institute of General Medical Sciences (R00GM115766) to KA.

ACKNOWLEDGMENTS

We would like to thank Dr. Sheng Yang He for his generosity. Most constructs used in this study were cloned by KA when he was a postdoc in the He laboratory at Michigan State University. We also would like to thank Tyler Weide for growing *N. benthaimana*.

SUPPLEMENTARY MATERIAL

The Supplementary Material for this article can be found online at: https://www.frontiersin.org/articles/10.3389/fpls.2021.640277/full#supplementary-material

REFERENCES

Amsbury, S., Kirk, P., and Benitez-Alfonso, Y. (2017). Emerging models on the regulation of intercellular transport by plasmodesmata-associated callose. *J. Exp. Bot.* 69, 105–115. doi: 10.1093/jxb/erx337

Aung, K., Kim, P., Li, Z., Joe, A., Kvitko, B., Alfano, J. R., et al. (2020). Pathogenic bacteria target plant plasmodesmata to colonize and invade surrounding tissues. *Plant Cell* 32, 595–611. doi: 10.1105/tpc.19.00707

Boller, T., and He, S. Y. (2009). Innate immunity in plants: an arms race between pattern recognition receptors in plants and effectors in microbial pathogens. *Science* 324, 742–744. doi: 10.1126/science.1171647

Brunkard, J. O., Burch-Smith, T. M., Runkel, A. M., and Zambryski, P. (2015). Investigating plasmodesmata genetics with virus-induced gene silencing and an agrobacterium-mediated GFP movement assay. *Methods Mol. Biol.* 1217, 185–198. doi: 10.1007/978-1-4939-1523-1_13

Brunkard, J. O., and Zambryski, P. C. (2017). Plasmodesmata enable multicellularity: new insights into their evolution, biogenesis, and functions in development and immunity. *Curr. Opin. Plant Biol.* 35, 76–83. doi: 10.1016/j.pbi.2016.11.007

Buttner, D. (2016). Behind the lines-actions of bacterial type III effector proteins in plant cells. *FEMS Microbiol. Rev.* 40, 894–937. doi: 10.1093/femsre/fuw026

Caillaud, M. C., Wirthmueller, L., Sklenar, J., Findlay, K., Piquerez, S. J., Jones, A. M., et al. (2014). The plasmodesmal protein PDLP1 localises to haustoria-associated membranes during downy mildew infection and regulates callose deposition. *PLoS Pathog.* 10:e1004496. doi: 10.1371/journal.ppat.1004496

Cao, L., Blekemolen, M. C., Tintor, N., Cornelissen, B. J. C., and Takken, F. L. W. (2018). The Fusarium oxysporum Avr2-Six5 effector pair alters plasmodesmatal exclusion selectivity to facilitate cell-to-cell movement of Avr2. *Mol. Plant* 11, 691–705. doi: 10.1016/j.molp.2018.02.011

Chavel, C., and Faulkner, C. (2018). Plasmodesmal regulation during plant-pathogen interactions. *New Phytol.* 217, 62–67. doi: 10.1111/nph.14857

Cui, H., Tsuda, K., and Parker, J. E. (2015). Effector-triggered immunity: from pathogen perception to robust defense. *Annu. Rev. Plant Biol.* 66, 487–511. doi: 10.1146/annurev-arplant-050213-040012

De Storme, N., and Geelen, D. (2014). Callose homeostasis at plasmodesmata: molecular regulators and developmental relevance. *Front. Plant Sci.* 5:138. doi: 10.3389/fpls.2014.00138

Faulkner, C., Petutschnig, E., Benitez-Alfonso, Y., Beck, M., Robatzek, S., Lipka, V., et al. (2013). LYM2-dependent chitin perception limits molecular flux via plasmodesmata. *Proc. Natl. Acad. Sci. U. S. A.* 110, 9166–9170. doi: 10.1073/pnas.1203458110

Fujioka, Y., Utsumi, M., Ohba, Y., and Watanabe, Y. (2007). Location of a possible miRNA processing site in SmD3/SmB nuclear bodies in *Arabidopsis*. *Plant Cell Physiol.* 48, 1243–1253. doi: 10.1093/pcp/pcm099

Göhre, V., Spallek, T., Häweker, H., Mersmann, S., Mentzel, T., Boller, T., et al. (2008). Plant pattern-recognition receptor FLS2 is directed for degradation by the bacterial ubiquitin ligase AvrPtoB. *Curr. Biol.* 18, 1824–1832. doi: 10.1016/j.cub.2008.10.063

Khang, C. H., Berruyer, R., Giraldo, M. C., Kankanala, P., Park, S. Y., Czymmek, K., et al. (2010). Translocation of magnaporthe oryzae effectors into rice cells and their subsequent cell-to-cell movement. *Plant Cell* 22, 1388–1403. doi: 10.1105/tpc.109.069666

Kim, I., Kobayashi, K., Cho, E., and Zambryski, P. C. (2005). Subdomains for transport via plasmodesmata corresponding to the apical-basal axis are established during Arabidopsis embryogenesis. *Proc. Natl. Acad. Sci. U. S. A.* 102, 11945–11950. doi: 10.1073/pnas.0505622102

Kim, I., and Zambryski, P. C. (2005). Cell-to-cell communication via plasmodesmata during Arabidopsis embryogenesis. *Curr. Opion. Plant Biol.* 599, 593–67. doi: 10.1016/j.pbi.2005.09.013

Kitagawa, M., and Jackson, D. (2017). Plasmodesmata-mediated cell-to-cell communication in the shoot apical meristem: how stem cells talk. *Plants* 6:12. doi: 10.3390/plants6010012

Kragler, F. (2013). Plasmodesmata: intercellular tunnels facilitating transport of macromolecules in plants. *Cell Tissue Res.* 352, 49–58. doi: 10.1007/s00441-012-1550-1

Lee, C. M., Adamchek, C., Feke, A., Nusinow, D. A., and Gendron, J. M. (2017). Mapping protein-protein interactions using affinity purification and mass spectrometry. *Methods Mol. Biol.* 1610, 231–249. doi: 10.1007/978-1-4939-7003-2_15

Lee, M. W., Jelenska, J., and Greenberg, J. T. (2008). Arabidopsis proteins important for modulating defense responses to *Pseudomonas syringae* that secrete HopW1-1. *Plant J.* 54, 452–465. doi: 10.1111/j.1365-313X.2008.03439.x

Lee, J. Y., Wang, X., Cui, W., Sager, R., Modla, S., Czymmek, K., et al. (2011). A plasmodesmata-localized protein mediates crosstalk between cell-to-cell communication and innate immunity in *Arabidopsis*. *Plant Cell* 23, 3353–3373. doi: 10.1105/tpc.111.087742

Lindeberg, M., Cunnac, S., and Collmer, A. (2012). *Pseudomonas syringae* type III effector repertoires: last words in endless arguments. *Trends Microbiol.* 20, 199–208. doi: 10.1016/j.tim.2012.01.003

Lucas, W. J., Ham, B. K., and Kim, J. Y. (2009). Plasmodesmata-bridging the gap between neighboring plant cells. *Trends Cell Biol.* 19, 495–503. doi: 10.1016/j.tcb.2009.07.003

Nelson, B. K., Cai, X., and Nebenfuhr, A. (2007). A multicolored set of in vivo organelle markers for co-localization studies in Arabidopsis and other plants. *Plant J.* 51, 1126–1136. doi: 10.1111/j.1365-313X.2007.03212.x

Nicolas, W. J., Grison, M. S., and Bayer, E. M. (2017). Shaping intercellular channels of plasmodesmata: the structure-to-function missing link. *J. Exp. Bot.* 69, 91–103. doi: 10.1093/jxb/erx225

Reagan, B. C., Ganusova, E. E., Fernandez, J. C., McCray, T. N., and Burch-Smith, T. M. (2018). RNA on the move: the plasmodesmata perspective. *Plant Sci.* 275, 1–10. doi: 10.1016/j.plantsci.2018.07.001

Reumann, S., Quan, S., Aung, K., Yang, P., Manandhar-Shrestha, K., Holbrook, D., et al. (2009). In-depth proteome analysis of Arabidopsis leaf peroxisomes combined with in vivo subcellular targeting verification indicates novel metabolic and regulatory functions of peroxisomes. *Plant Physiol.* 150, 125–143. doi: 10.1104/pp.109.137703

Schulz, A. (2015). Diffusion or bulk flow: how plasmodesmata facilitate pre-phloem transport of assimilates. *J. Plant Res.* 128, 49–61. doi: 10.1007/s10265-014-0676-5

Shan, L., Thara, V. K., Martin, G. B., and Tang, X. (2000). The pseudomonas AvrPto protein is differentially recognized by tomato and tobacco and is localized to the plant plasma membrane. *Plant Cell* 12, 2323–2338. doi: 10.1105/tpc.12.12.2323

Tomczynska, I., Stumpe, M., Doan, T. G., and Mauch, F. (2020). A Phytophthora effector protein promotes symplastic cell-to-cell trafficking by physical interaction with plasmodesmata-localised callose synthases. *New Phytol.* 227, 1467–1478. doi: 10.1111/nph.16653

Toruno Calero, T. Y. (2014). *Pseudomonas syringae* type III effectors: Targets and roles in plant immunity. ETD collection for University of Nebraska–Lincoln. AAI3667423.

Wang, X., Robles Luna, G., Arighi, C. N., and Lee, J. Y. (2020). An evolutionarily conserved motif is required for plasmodesmata-located protein 5 to regulate cell-to-cell movement. *Commun. Biol.* 3:291. doi: 10.1038/s42003-020-1007-0

Washington, E. J., Mukhtar, M. S., Finkel, O. M., Wan, L., Banfield, M. J., Kieber, J. J., et al. (2016). *Pseudomonas syringae* type III effector HopAF1 suppresses plant immunity by targeting methionine recycling to block ethylene induction. *Proc. Natl. Acad. Sci. U. S. A.* 113, E3577–E3586. doi: 10.1073/pnas.1606322113

Wei, H. L., Chakravarthy, S., Mathieu, J., Helmann, T. C., Stodghill, P., Swingle, B., et al. (2015). *Pseudomonas syringae* pv. Tomato DC3000 type III secretion effector polymutants reveal an interplay between HopAD1 and AvrPtoB. *Cell Host Microbe* 17, 752–762. doi: 10.1016/j.chom.2015.05.007

Wu, S. W., Kumar, R., Iswanto, A. B. B., and Kim, J. Y. (2018). Callose balancing at plasmodesmata. *J. Exp. Bot.* 69, 5325–5339. doi: 10.1093/jxb/ery317

Xin, X. F., Nomura, K., Ding, X., Chen, X., Wang, K., Aung, K., et al. (2015). *Pseudomonas syringae* effector avirulence protein E localizes to the host plasma membrane and down-regulates the expression of the nonrace-specific disease resistance1/harpin-induced1-like13 gene required for antibacterial immunity in *Arabidopsis*. *Plant Physiol.* 169, 793–802. doi: 10.1104/pp.15.00547

Xu, B., Cheval, C., Laohavisit, A., Hocking, B., Chiasson, D., Olsson, T. S. G., et al. (2017). A calmodulin-like protein regulates plasmodesmal closure during bacterial immune responses. *New Phytol.* 215, 77–84. doi: 10.1111/nph.14599

Conflict of Interest: The authors declare that the research was conducted in the absence of any commercial or financial relationships that could be construed as a potential conflict of interest.

frontiers in Plant Science

PERSPECTIVE
published: 31 March 2021
doi: 10.3389/fpls.2021.649768

Potential Impact of Global Warming on Virus Propagation in Infected Plants and Agricultural Productivity

*Khalid Amari†, Caiping Huang and Manfred Heinlein**

Institute of Plant Molecular Biology (IBMP), CNRS UPR 2357, Université de Strasbourg, Strasbourg, France

The increasing pace of global warming and climate instability will challenge the management of pests and diseases of cultivated plants. Several reports have shown that increases in environmental temperature can enhance the cell-to-cell and systemic propagation of viruses within their infected hosts. These observations suggest that earlier and longer periods of warmer weather may cause important changes in the interaction between viruses and their host's plants, thus posing risks of new viral diseases and outbreaks in agriculture and the wild. As viruses target plasmodesmata (PD) for cell-to-cell spread, these cell wall pores may play yet unknown roles in the temperature-sensitive regulation of intercellular communication and virus infection. Understanding the temperature-sensitive mechanisms in plant-virus interactions will provide important knowledge for protecting crops against diseases in a warmer climate.

Keywords: plant viruses, *Tobacco mosaic virus*, temperature, global warming, agriculture, plasmodesmata, tolerance

OPEN ACCESS

Edited by:
Giorgio Gambino, Institute for Sustainable Plant Protection, National Research Council (CNR), Italy

Reviewed by:
Ralf Georg Dietzgen, The University of Queensland, Australia
Bryce Falk, University of California, Davis, United States

***Correspondence:**
Manfred Heinlein
manfred.heinlein@ibmp-cnrs.unistra.fr

†Present address:
Khalid Amari, Julius Kühn Institute (JKI) – Federal Research Centre for Cultivated Plants, Institute for Biosafety in Plant Biotechnology, Quedlinburg, Germany

Specialty section:
This article was submitted to Plant Pathogen Interactions, a section of the journal Frontiers in Plant Science

Received: *27 January 2021*
Accepted: *03 March 2021*
Published: *31 March 2021*

Citation:
Amari K, Huang C and Heinlein M (2021) Potential Impact of Global Warming on Virus Propagation in Infected Plants and Agricultural Productivity. Front. Plant Sci. 12:649768. doi: 10.3389/fpls.2021.649768

INTRODUCTION

Viruses can cause major losses in crop yields and are the primary cause of emerging diseases in plants (Nicaise, 2014). As has been reviewed comprehensively, changes in temperature and other parameters of climate change (changes in rainfall patterns, wind, accumulation of greenhouse gases, and extreme weather events, to name a few) are expected to affect the geographic distribution of the viral hosts and vectors, and thus the epidemiology of viruses that depend on these hosts and vectors for propagation and inter-plant transmission (Canto et al., 2009; Jones and Barbetti, 2012). As global temperatures increase, poleward and higher altitude areas with currently colder weather likely assume a more temperate climate, whereas the regions with currently temperate climate become warmer and may assume a climate that is more typical for tropical zones. Thus, in response to global temperature increases, the viral hosts and vectors adapted to temperate climates are expected to spread with their viruses poleward and to higher altitudes where temperatures will then be temperate, whereas hosts and viral vectors in tropical regions will invade with their viruses the regions with a currently mild climate where temperatures may have increased toward values that are currently typical for tropical areas. In these newly invaded regions, virus hosts and vectors as well as their viruses may find conditions that are similar as in previous habitats, thus allowing them to interact as previously. From this point of view, a warmer climate is predicted to cause a global shift in the distribution of viruses along with their hosts and vectors. And, because this process may allow viruses to interact with their current hosts and vectors as previously, a strong global impact on virus propagation and virus-caused diseases in agriculture may not be expected. On the other hand, this view may be too simple. First, the new geographical locations

may allow viruses to find new hosts, which poses risks of new emerging diseases (Jones, 2020). Second and more important, plants tolerate broad ranges of temperatures (Parent and Tardieu, 2012; **Figure 1**), and most of them will likely not migrate, at least not immediately. For canola and potato, for example, the ranges of temperatures for growth with at least 50% of the maximum rate are from 15.0 to 29.6°C and from 21.6 to 37.3°C, respectively. For sunflower, which has a temperature optimum around 29°C, the range is from 17.3 to 38.3°C. The average high temperature currently reached in summer in London, Paris, or Berlin (23–25°C;[1]) is below the temperature optima for crops grown in the area such as wheat, barley, potato, maize, or sunflower (27.7, 26.6, 30.6, 30.8, and 29.3°C, respectively; Parent and Tardieu, 2012). Thus, there is room for temperature increases until these and other plants are forced to migrate. According to current climate change projections by the Intergovernmental Panel on Climate Change (IPCC), the global mean surface temperature change for the period 2016–2035 relative to 1986–2005 will likely be in the range of 0.3–0.7°C and, dependent on prediction scenarios, may reach 0.3–4.8°C at the end of the 21st century (2081–2100) (IPCC, 2014). These global changes in temperature are predicted to be accompanied by local weather extremes with heat waves and drought that cause significant yield losses (Bita and Gerats, 2013). However, except for plants currently growing in areas with conditions at their tolerance margins, these predicted changes in temperature will not cause an immediate global migration of all viruses and their hosts away from their current geographical zones. For most hosts and their viruses, expected movements to colder areas may occur only gradually, over long ranges of time. However, while these plants remain at their locations, warmer local temperatures will nevertheless already have immediate effects on the intracellular environment provided by these hosts to viruses, thus posing risks to agriculture.

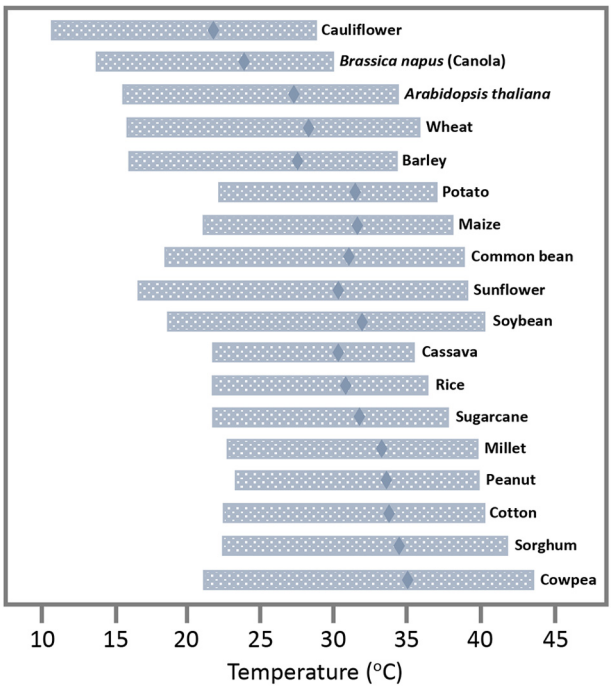

FIGURE 1 | Temperature tolerance range of plant and crop species. Temperature optimum at which plant development has its maximum rate (diamonds) and range of temperature for which the rate of development is at least 50% of its maximum (horizontal bars). Adapted from Parent and Tardieu (2012), with permission by the authors.

Temperature is a physical parameter that influences biochemical reactions and higher molecular structures, like DNA and proteins, and supramolecular components, like membranes and the elements of the cytoskeleton, through simple thermodynamic effects (Ruelland and Zachowski, 2010). Warmer temperature thereby causes increased membrane fluidity and cytoskeletal dynamics, which can enhance the propagation of plant viruses that generally depend on these cellular components for replication and spread within their hosts. Consistently, numerous studies demonstrated that the rate at which viruses replicate and move through the infected plant increases with temperature up to a certain temperature optimum, beyond which viral propagation decreases. For example, Lebeurier and Hirth (1966) demonstrated already more than 50 years ago in *Nicotiana tabacum* leaf disks that *Tobacco mosaic virus* (TMV) increases its multiplication with temperature and that replication is again lower only when temperature reaches 34–36°C. Later, with a green fluorescent protein (GFP)-tagged virus it was shown that the cell-to-cell spread in *N. benthamiana* plants was threefold stronger when the temperature was increased by 10 degrees (from 22 to 32°C) (Boyko et al., 2000a,b). Similarly, *Turnip mosaic virus* (TuMV) showed increased accumulation in Chinese cabbage when temperature was increased from 13 to 23–28°C (Chung et al., 2015) and a GFP-tagged version of this virus shows a twofold more efficient cell-to-cell (**Figures 2A,B**) and systemic (**Figures 2C,D**) spread in canola (*Brassica napus*) upon shifting the daytime temperature by only four degrees from 24 to 28°C. In Arabidopsis, TuMV was shown to accumulate to higher levels when kept at 25°C during the day and 15°C in the night as compared to colder temperatures with 15°C during the day and 5°C in the night (Honjo et al., 2020). Potato plants infected with *Potato virus Y* showed a dramatic increase in systemic infection when temperatures were increased from 23 to 28°C (Choi et al., 2017). *Barley yellow dwarf virus* (BYDV) showed strong increases in systemic movement in oat when the temperature was elevated from 15.5 to 21°C (Jensen, 1973) and infection of bean leaves with *Rothamsted tobacco necrosis virus* (RTNV) increased with rising temperature from 10 to 22°C (Harrison, 1956). The spread and replication of *Wheat streak mosaic virus* and disease development in Winter Wheat was shown to increase with temperature within the tested temperature range of 10–27°C (Wosula et al., 2017). Given that virus accumulation and disease symptoms are often correlated, these examples hint toward the imminent risk that earlier and longer periods of warmer weather will aggravate virus-induced diseases in crops in their current growing areas, thus endangering yields.

The risks imposed by global warming may not be limited to viruses in crops, however. It is often overlooked that viruses are

[1]https://www.weather-atlas.com/en/

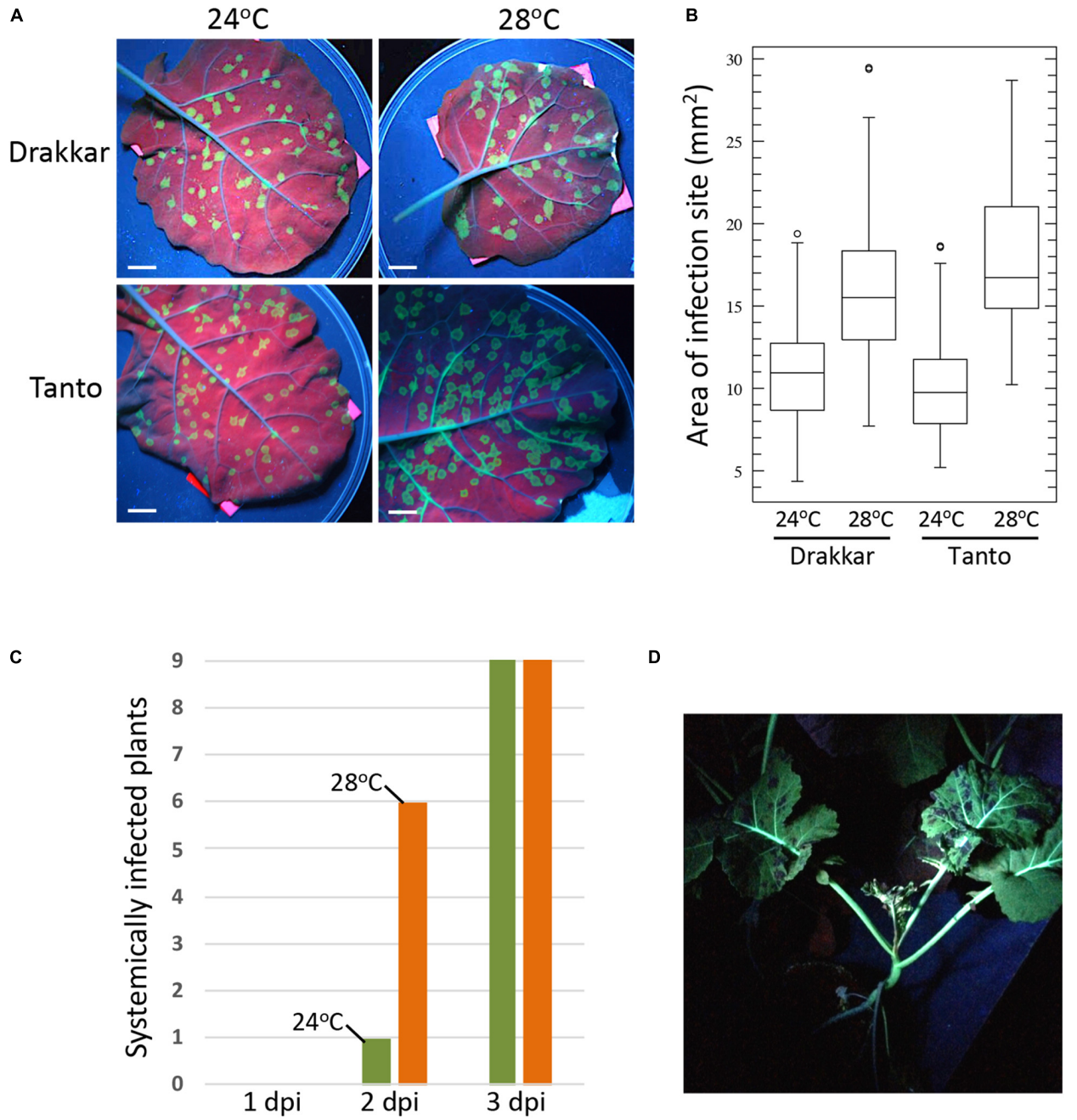

FIGURE 2 | Temperature effect on TuMV-GFP infection in *B. napus* cultivars Drakkar and Tanto. Plants were incubated at 20°C for 8 h (night) and 24°C for 16 h (day) until two leaf stage. Half of the plants were then transferred to 20°C for 8 h (night) and 28°C for 16 h (day). Plants were allowed to adjust for 2 days before inoculation. **(A)** Effect of temperature on viral cell-to-cell spread in inoculated leaves. Pictures were taken at 6 days post inoculation (6 dpi) under UV light. Scale bar, 1 cm. **(B)** Sizes of individual local infection sites at 6 dpi. Infection foci in leaves of five plants per condition were measured (Drakkar 24°C, $N = 117$; Drakkar 28°C, $N = 111$; Tanto 24°C, $N = 112$; Tanto 28°C, $N = 102$. The higher temperature causes a significant increase in the local cell-to-cell spread of infection in both Drakkar (ANOVA, $p = 4{,}3^{-21}$) and Tanto (ANOVA, $p = 2{,}5^{-37}$). **(C)** Systemic spread of TuMV-GFP in Drakkar is more efficient at 28°C (orange) than at 24°C (green). Inoculated leaves of nine plants at 24°C and of nine plants at 28°C were removed after 1, 2, or 3 dpi, followed by scoring the systemic leaves for GFP fluorescence (systemic infection) at 16 dpi. A control plant from which the inoculated leaf was not removed is shown in panel **(D)**. **(D)** TuMV-GFP-infected Drakkar plant showing systemic infection at 21 dpi. The picture was taken under UV light.

ubiquitous in the wild and play an important role in the evolution of life. Surveys have shown that 60–70% of plants grown in natural ecosystems are infected with viruses (Roossinck, 2015). Continuous host-virus co-evolution in natural habitats allows viruses to adapt to their hosts and maintain or even improve their fitness. Thus, plants in the wild are normally free of symptoms

despite infection by viruses. Although a significant virus load is sustained in such virus-tolerant plants, the plant growth, yield, or reproduction attributes are only minimally affected and visible symptoms are either absent or mild (Pagan and Garcia-Arenal, 2018; Paudel and Sanfacon, 2018). However, tolerance, thus the ability of the infected plant to reduce negative effects of the infection, is a complex and highly evolved trait that depends on a well-adjusted host-virus crosstalk (Kørner et al., 2018; Paudel and Sanfacon, 2018; Pitzalis et al., 2020) and contributes to host fitness through multiple molecular mechanisms (Pagan and Garcia-Arenal, 2018, 2020). Higher average temperatures, leading to a more favorable environment for virus replication and movement, may break the delicate equilibrium between plant viruses and their hosts and thereby lead to the outbreak of new diseases. Such temperature-related loss of tolerance in crops and wild species and the spreading of new diseases from natural reservoirs toward crops may have important consequences for agriculture.

As humanity faces increasing average annual temperatures, it is important to understand the temperature-sensitive mechanisms that determine the propagation and spread of viruses within their hosts. The underlying mechanisms can be of a diverse nature. Apart from increased membrane fluidity and cytoskeletal dynamics that likely accelerate the membrane- and cytoskeleton-associated processes involved in virus replication and transport, temperature may also affect the regulation of the intercellular communication channels in the plant cell walls (plasmodesmata). Plasmodesmata (PD) are important gates through which viruses must move their genomes to spread infection between cells, into the phloem, and finally throughout the plant. In accordance with their central function in intercellular communication, PD are equipped with receptor proteins and receptor protein kinases that form signaling hubs through which PD are enabled to orchestrate processes related to plant growth and development but also responses to pathogens and abiotic stresses (Lee, 2015; Stahl and Faulkner, 2016). A recent study highlights the ability of PD to recruit receptor-like kinases in response to osmotic stress (Grison et al., 2019). It seems feasible, therefore, that changes in temperature can lead to specific alterations in the composition and regulation of PD, which in turn likely affects virus spread from cell to cell. So far, there are only few studies addressing the specific effects of temperature on PD function. Studies in poplar revealed that temperature influences the expression of dormancy-related genes, including gibberellin-acid (GA)-inducible members of beta-1,3-glucanase family involved in the degradation of callose at the plasmodesmal dormancy sphincter complexes (Rinne et al., 2011, 2018). Effects of temperature on PD structure and conductivity were also observed in maize (Bilska and Sowinski, 2010). Recent progress made in the analysis of PD structure, composition, and regulation (Wu et al., 2018; Brault et al., 2019; Grison et al., 2019; Huang et al., 2019; Cheval et al., 2020; Iswanto et al., 2020; Liu et al., 2020) may facilitate future research in model systems such as *N. benthamiana* and Arabidopsis to reveal the impact of increasing temperature on PD proteins and membranes and whether such changes correlate with an altered flow of PD targeted and non-targeted macromolecules (e.g., GFP) through the pore.

Warmer temperature may facilitate virus spread also by altering the activity or turnover of the viral movement proteins (MPs), which may affect the interaction of viruses with PD. The mentioned increased efficiency of intercellular spread of TMV in *N. benthamiana* at higher temperature correlated with changes in the subcellular accumulation pattern of the virus-encoded, GFP-tagged MP (Boyko et al., 2000b). During infection the protein is expressed in distinct cortical endoplasmic reticulum (cortical ER)-associated replication complexes that are formed at sites of the cortical ER at which this membrane network intersects with cortical microtubules (Niehl et al., 2013). At the lower temperature (22°C) the MP tends to stay and over-accumulate in the replication complexes that can grow to large sizes over time (Padgett et al., 1996; Heinlein et al., 1998; Niehl et al., 2013; Heinlein, 2015). At the higher temperature (32°C), however, the MP accumulates along microtubules rather than in the replication complexes (Boyko et al., 2000b). The ability of MP to interact with microtubules is involved in virus movement and has been correlated with the formation and mobility of distinct MP-containing replication complexes during early stages of infection in cells at the infection front (Boyko et al., 2000a, 2007; Niehl et al., 2014). Accumulation of high amounts of MP along the length of microtubules, in contrast, is dispensable for movement and is rather linked to its degradation in cells having completed the movement process (Gillespie et al., 2002; Niehl et al., 2012). The degradation of MP is triggered by its accumulation in the ER and depends on CDC48, an ATP-driven machinery that controls ER homeostasis by extracting over-accumulating or misfolded proteins from the membrane (Niehl et al., 2012). These observations are important in the context of other findings indicating that ER-associated virus replication and viral protein accumulation cause ER stress (Park and Park, 2019) and can lead to PD closure (Guenoune-Gelbart et al., 2008), thereby causing resistance against virus movement. Thus, by enhancing the removal of over-accumulated MP from the ER, which thereby results in the accumulated binding of MP along microtubules and promotes MP degradation, warmer temperature may avoid ER stress and PD closure, thereby facilitating efficient virus movement. Because of its direct binding affinity for microtubules (Ashby et al., 2006), the extraction of accumulated MP from the ER leads to its alignment along microtubules, which is directly or indirectly supported by another microtubule-associated protein (Curin et al., 2007). It is noteworthy that the movement of the TMV-related Oilseed rape mosaic virus (ORMV, also known as Youcai mosaic virus or TMV-Cg) is associated with the formation of distinct MP-containing, replication complexes during early stages of infection just like in the case of TMV. However, unlike the MP of TMV, the MP of ORMV does not accumulate on the ER or along microtubules. Importantly, this MP allows faster virus movement than the MP of TMV (Niehl et al., 2014). These observations are consistent with the conclusion that the enhanced TMV movement at higher temperature is associated with specific MP activities and turnover conditions.

Warmer temperature could affect TMV movement also by increasing myosin motor activity, thus facilitating the myosin-driven transport of the virus and of MP along the ER-actin network to the PD (Hofmann et al., 2009; Amari et al., 2014).

Temperature may also alter the ability of MP to bind RNA and other proteins, or to gate the PD channel. Potentially, such alterations in MP activity could be mediated through changes in the post-translational phosphorylation of the protein (Trutnyeva et al., 2005).

However, warmer temperatures may affect virus cell-to-cell movement also more indirectly, for example, by causing changes in gene expression and alterations in the interactions of viruses with host defense responses. In plants carrying specific resistance (R) genes, warmer temperature may indeed provoke stronger infections since resistance genes against biotrophic and hemi-biotrophic microbes (viruses, bacteria, fungi) are often temperature-sensitive and are inactivated at elevated temperature (Wang et al., 2009). Thus, in several plant-virus interactions, hypersensitive resistance (HR) or HR-like responses are slower when the temperature is elevated by a few degrees from 21–22°C to 27–28°C, and are lost at temperatures above 30°C (Whitham et al., 1996; Wang et al., 2009). In addition to R-gene mediated resistance, plants control their viruses also through pattern-triggered immunity (PTI) (Kørner et al., 2013; Niehl et al., 2016; Teixeira et al., 2019; Amari and Niehl, 2020) and RNA silencing (Ding, 2010; Pumplin and Voinnet, 2013). Both defense pathways are activated by dsRNA produced during virus infection. PTI involves the activation of transcriptional signaling that confers broad-spectrum pathogen resistance. In contrast, RNA silencing uses 21–24 nts long small interfering RNAs (siRNAs) and 21 nts microRNAs (miRNAs) to direct sequence-specific cleavage or translational repression of viral and host RNAs through ARGONAUTE (AGO)-containing RNA silencing effector complexes. While antiviral PTI has only recently been discovered and its sensitivity to temperature in the context of virus infection remains to be studied, RNA silencing has been reported to be more active at higher temperature and shown to be correlated with reduced disease symptoms in infected tissues (Szittya et al., 2003). However, other reports argue against such correlations or even conclude that RNA silencing or its systemic signaling is inhibited at elevated temperature (Zhong et al., 2013). These contrasting findings show that we are far from understanding how temperature influences the interaction of viruses with host defense pathways and that further studies are needed.

As already highlighted, global warming comes along with various other impacts on humidity, drought, rainfall intensity and rainfall patterns, wind speed and direction, and greenhouse gas concentration. These parameters will result in altered crop cultivations systems and the range of cultivated species grown. This, in turn, will also influence the distribution of the viral insect vectors and plant hosts and, thereby, the distribution and evolution of virus species. However, while these long-term global consequences of climate change need to be studied, monitored, and modeled to improve disease management, changes in temperature have immediate effects on cellular mechanisms that are at the core of plant-virus interactions within each infected cell, irrespective of the region where the infected host is grown. This may aggravate diseases in natural and agricultural settings and damage yields and crop survival before temperatures will eventually exceed the host temperature tolerance ranges. To ensure agricultural yield, a concerted research effort is needed to understand the cellular mechanisms that determine disease tolerance in infected plants and to use this knowledge to adapt our crops toward temperature resilience and tolerance for viruses through dedicated breeding programs.

DATA AVAILABILITY STATEMENT

The original contributions presented in the study are included in the article/supplementary material, further inquiries can be directed to the corresponding author/s.

AUTHOR CONTRIBUTIONS

CH and MH wrote the manuscript. For **Figure 2**, MH conceived and designed the work. KA performed the acquisition and analysis of the data. All authors edited and approved the final version of the manuscript and agreed to be accountable for all aspects of the work.

FUNDING

Work shown in **Figure 2** was supported by funding from the Agence National de la Recherche (Grant ANR-13-KBBE-00 05-01) and by a Ph.D. fellowship from the Chinese Scholarship Foundation (CSC) to CH.

REFERENCES

Amari, K., Di Donato, M., Dolja, V. V., and Heinlein, M. (2014). Myosins VIII and XI play distinct roles in reproduction and transport of tobacco mosaic virus. *PLoS Pathog.* 10:e1004448. doi: 10.1371/journal.ppat.1004448

Amari, K., and Niehl, A. (2020). Nucleic acid-mediated PAMP-triggered immunity in plants. *Curr. Opin. Virol.* 42, 32–39. doi: 10.1016/j.coviro.2020.04.003

Ashby, J., Boutant, E., Seemanpillai, M., Groner, A., Sambade, A., Ritzenthaler, C., et al. (2006). Tobacco mosaic virus movement protein functions as a structural microtubule-associated protein. *J. Virol.* 80, 8329–8344. doi: 10.1128/JVI.00540-06

Bilska, A., and Sowinski, P. (2010). Closure of plasmodesmata in maize (Zea mays) at low temperature: a new mechanism for inhibition of photosynthesis. *Ann. Bot.* 106, 675–686. doi: 10.1093/aob/mcq169

Bita, C. E., and Gerats, T. (2013). Plant tolerance to high temperature in a changing environment: scientific fundamentals and production of heat stress-tolerant crops. *Front. Plant Sci.* 4:273. doi: 10.3389/fpls.2013.00273

Boyko, V., Ferralli, J., Ashby, J., Schellenbaum, P., and Heinlein, M. (2000a). Function of microtubules in intercellular transport of plant virus RNA. *Nat. Cell. Biol.* 2, 826–832. doi: 10.1038/35041072

Boyko, V., Ferralli, J., and Heinlein, M. (2000b). Cell-to-cell movement of TMV RNA is temperature-dependent and corresponds to the association of movement protein with microtubules. *Plant J.* 22, 315–325.

Boyko, V., Hu, Q., Seemanpillai, M., Ashby, J., and Heinlein, M. (2007). Validation of microtubule-associated tobacco mosaic virus RNA movement and involvement of microtubule-aligned particle trafficking. *Plant J.* 51, 589–603.

Brault, M. L., Petit, J. D., Immel, F., Nicolas, W. J., Glavier, M., Brocard, L., et al. (2019). Multiple C2 domains and transmembrane region proteins (MCTPs) tether membranes at plasmodesmata. *EMBO Rep.* 20, e47182. doi: 10.15252/embr.201847182

Canto, T., Aranda, M. A., and Fereres, A. (2009). Climate change effects on physiology and population processes of hosts and vectors that influence the spread of hemipteran-borne plant viruses. *Glob. Chang. Biol.* 15, 1884–1894.

Cheval, C., Samwald, S., Johnston, M. G., de Keijzer, J., Breakspear, A., Liu, X., et al. (2020). Chitin perception in plasmodesmata characterizes submembrane immune-signaling specificity in plants. *Proc. Natl. Acad. Sci. U. S. A.* 117, 9621–9629. doi: 10.1073/pnas.1907799117

Choi, K. S., Del Toro, F., Tenllado, F., Canto, T., and Chung, B. N. (2017). A model to explain temperature dependent systemic infection of potato plants by potato virus Y. *Plant Pathol. J.* 33, 206–211. doi: 10.5423/PPJ.NT.06.2016.0144

Chung, B. N., Choi, K. S., Ahn, J. J., Joa, J. H., Do, K. S., and Park, K.-S. (2015). Effects of temperature on systemic infection and symptom expression of turnip mosaic virus in Chinese cabbage (*Brassica campestris*). *Plant Pathol. J.* 31, 363–370.

Curin, M., Ojangu, E. L., Trutnyeva, K., Ilau, B., Truve, E., and Waigmann, E. (2007). MPB2C, a microtubule-associated plant factor, is required for microtubular accumulation of tobacco mosaic virus movement protein in plants. *Plant Physiol.* 143, 801–811.

Ding, S. W. (2010). RNA-based antiviral immunity. *Nat. Rev. Immunol.* 10, 632–644. doi: 10.1038/nri2824

Gillespie, T., Boevink, P., Haupt, S., Roberts, A. G., Toth, R., Vantine, T., et al. (2002). Functional analysis of a DNA shuffled movement protein reveals that microtubules are dispensable for the cell-to-cell movement of tobacco mosaic virus. *Plant Cell* 14, 1207–1222.

Grison, M. S., Kirk, P., Brault, M. L., Wu, X. N., Schulze, W. X., Benitez-Alfonso, Y., et al. (2019). Plasma membrane-associated receptor-like kinases relocalize to plasmodesmata in response to osmotic stress. *Plant Physiol.* 181, 142–160. doi: 10.1104/pp.19.00473

Guenoune-Gelbart, D., Elbaum, M., Sagi, G., Levy, A., and Epel, B. L. (2008). Tobacco mosaic virus (TMV) replicase and movement protein function synergistically in facilitating TMV spread by lateral diffusion in the plasmodesmal desmotubule of *Nicotiana benthamiana*. *Mol. Plant Microbe Interact.* 21, 335–345. doi: 10.1094/MPMI-21-3-0335

Harrison, B. D. (1956). Studies on the effect of temperature on virus multiplication in inoculated leaves. *Ann. Appl. Biol.* 44, 215–226.

Heinlein, M. (2015). Plant virus replication and movement. *Virology* 47, 657–671. doi: 10.1016/j.virol.2015.01.025

Heinlein, M., Padgett, H. S., Gens, J. S., Pickard, B. G., Casper, S. J., Epel, B. L., et al. (1998). Changing patterns of localization of the tobacco mosaic virus movement protein and replicase to the endoplasmic reticulum and microtubules during infection. *Plant Cell* 10, 1107–1120.

Hofmann, C., Niehl, A., Sambade, A., Steinmetz, A., and Heinlein, M. (2009). Inhibition of tobacco mosaic virus movement by expression of an actin-binding protein. *Plant Physiol.* 149, 1810–1823. doi: 10.1104/pp.108.133827

Honjo, M. N., Emura, N., Kawagoe, T., Sugisaka, J., Kamitani, M., Nagano, A. J., et al. (2020). Seasonality of interactions between a plant virus and its host during persistent infection in a natural environment. *ISME J.* 14, 506–518. doi: 10.1038/s41396-019-0519-4

Huang, D., Sun, Y., Ma, Z., Ke, M., Cui, Y., Chen, Z., et al. (2019). Salicylic acid-mediated plasmodesmal closure via Remorin-dependent lipid organization. *Proc. Natl. Acad. Sci. U. S. A.* 116, 21274–21284. doi: 10.1073/pnas.1911892116

IPCC (2014). *Climate Change 2014: Synthesis Report. Contribution of Working Groups I, II and III to the Fifth Assessment Report of the Intergovernmental Panel on Climate Change*. Geneva: IPCC.

Iswanto, A. B. B., Shon, J. C., Liu, K. H., Vu, M. H., Kumar, R., and Kim, J. Y. (2020). Sphingolipids modulate secretion of glycosylphosphatidylinositol-anchored plasmodesmata proteins and callose deposition. *Plant Physiol.* 184, 407–420. doi: 10.1104/pp.20.00401

Jensen, S. G. (1973). Systemic movement of barley yellow dwarf virus in small grains. *Phytopathology* 63, 854–856.

Jones, R. A. C. (2020). Disease pandemics and major epidemics arising from new encounters between indigenous viruses and introduced crops. *Viruses* 12:1388. doi: 10.3390/v12121388

Jones, R. A. C., and Barbetti, M. J. (2012). Influence of climate change on plant disease infections and epidemics caused by viruses and bacteria. *CAB Rev.* 7, 1–32.

Kørner, C. J., Klauser, D., Niehl, A., Dominguez-Ferreras, A., Chinchilla, D., Boller, T., et al. (2013). The immunity regulator BAK1 contributes to resistance against diverse RNA viruses. *Mol. Plant Microbe Interact.* 26, 1271–1280. doi: 10.1094/MPMI-06-13-0179-R

Kørner, C. J., Pitzalis, N., Peña, E. J., Erhardt, M., Vazquez, F., and Heinlein, M. (2018). Crosstalk between PTGS and TGS pathways in natural antiviral immunity and disease recovery. *Nat. Plants* 4, 157–164. doi: 10.1038/s41477-018-0117-x

Lebeurier, G., and Hirth, L. (1966). Effect of elevated temperatures on the development of two strains of tobacco mosaic virus. *Virology* 29, 385–395.

Lee, J. Y. (2015). Plasmodesmata: a signaling hub at the cellular boundary. *Curr. Opin. Plant Biol.* 27, 133–140. doi: 10.1016/j.pbi.2015.06.019

Liu, N. J., Zhang, T., Liu, Z. H., Chen, X., Guo, H. S., Ju, B. H., et al. (2020). Phytosphinganine affects plasmodesmata permeability via facilitating PDLP5-stimulated callose accumulation in Arabidopsis. *Mol. Plant* 13, 128–143. doi: 10.1016/j.molp.2019.10.013

Nicaise, V. (2014). Crop immunity against viruses: outcomes and future challenges. *Front. Plant Sci.* 5:660. doi: 10.3389/fpls.2014.00660

Niehl, A., Amari, K., Gereige, D., Brandner, K., Mély, Y., and Heinlein, M. (2012). Control of tobacco mosaic virus movement protein fate by CELL-DIVISION-CYCLE protein 48 (CDC48). *Plant Physiol.* 160, 2093–2108. doi: 10.1104/pp.112.207399

Niehl, A., Pasquier, A., Ferriol, I., Mely, Y., and Heinlein, M. (2014). Comparison of the oilseed rape mosaic virus and tobacco mosaic virus movement proteins (MP) reveals common and dissimilar MP functions for tobamovirus spread. *Virology* 45, 43–54. doi: 10.1016/j.virol.2014.03.007

Niehl, A., Pena, E. J., Amari, K., and Heinlein, M. (2013). Microtubules in viral replication and transport. *Plant J.* 75, 290–308. doi: 10.1111/tpj.12134

Niehl, A., Wyrsch, I., Boller, T., and Heinlein, M. (2016). Double-stranded RNAs induce a pattern-triggered immune signaling pathway in plants. *New Phytol.* 211, 1008–1019. doi: 10.1111/nph.13944

Padgett, H. S., Epel, B. L., Kahn, T. W., Heinlein, M., Watanabe, Y., and Beachy, R. N. (1996). Distribution of tobamovirus movement protein in infected cells and implications for cell-to-cell spread of infection. *Plant J.* 10, 1079–1088.

Pagan, I., and Garcia-Arenal, F. (2018). Tolerance to plant pathogens: theory and experimental evidence. *Int. J. Mol. Sci.* 19:810. doi: 10.3390/ijms19030810

Pagan, I., and Garcia-Arenal, F. (2020). Tolerance of plants to pathogens: a unifying view. *Annu. Rev. Phytopathol.* 58, 77–96. doi: 10.1146/annurev-phyto-010820-012749

Parent, B., and Tardieu, F. (2012). Temperature responses of developmental processes have not been affected by breeding in different ecological areas for 17 crop species. *New Phytol.* 194, 760–774. doi: 10.1111/j.1469-8137.2012.04086.x

Park, C. J., and Park, J. M. (2019). Endoplasmic reticulum plays a critical role in integrating signals generated by both biotic and abiotic stress in plants. *Front. Plant Sci.* 10:399. doi: 10.3389/fpls.2019.00399

Paudel, D. B., and Sanfacon, H. (2018). Exploring the diversity of mechanisms associated with plant tolerance to virus infection. *Front. Plant Sci.* 9:1575. doi: 10.3389/fpls.2018.01575

Pitzalis, N., Amari, K., Graindorge, S., Pflieger, D., Donaire, L., Wassenegger, M., et al. (2020). Turnip mosaic virus in oilseed rape activates networks of sRNA-mediated interactions between viral and host genomes. *Commun. Biol.* 3:702. doi: 10.1038/s42003-020-01425-y

Pumplin, N., and Voinnet, O. (2013). RNA silencing suppression by plant pathogens: defence, counter-defence and counter-counter-defence. *Nat. Rev. Microbiol.* 11, 745–760. doi: 10.1038/nrmicro3120

Rinne, P. L., Welling, A., Vahala, J., Ripel, L., Ruonala, R., Kangasjarvi, J., et al. (2011). Chilling of dormant buds hyperinduces FLOWERING LOCUS T and recruits GA-inducible 1,3-beta-glucanases to reopen signal conduits and release dormancy in Populus. *Plant Cell* 23, 130–146. doi: 10.1105/tpc.110.081307

Rinne, P. L. H., Paul, L. K., and van der Schoot, C. (2018). Decoupling photo- and thermoperiod by projected climate change perturbs bud development, dormancy establishment and vernalization in the model tree Populus. *BMC Plant Biol.* 18:220. doi: 10.1186/s12870-018-1432-0

Roossinck, M. J. (2015). Plants, viruses and the environment: ecology and mutualism. *Virology* 47, 271–277. doi: 10.1016/j.virol.2015.03.041

Ruelland, E., and Zachowski, A. (2010). How plants sense temperature. *Environ. Exp. Bot.* 69, 225–232.

Stahl, Y., and Faulkner, C. (2016). Receptor complex mediated regulation of symplastic traffic. *Trends Plant Sci.* 21, 450–459. doi: 10.1016/j.tplants.2015.11.002

Szittya, G., Silhavy, D., Molnar, A., Havelda, Z., Lovas, A., Lakatos, L., et al. (2003). Low temperature inhibits RNA silencing-mediated defence by the control of siRNA generation. *EMBO J.* 22, 633–640.

Teixeira, R. M., Ferreira, M. A., Raimundo, G. A. S., Loriato, V. A. P., Reis, P. A. B., and Fontes, E. P. B. (2019). Virus perception at the cell surface: revisiting the roles of receptor-like kinases as viral pattern recognition receptors. *Mol. Plant Pathol.* 20, 1196–1202. doi: 10.1111/mpp.12816

Trutnyeva, K., Bachmaier, R., and Waigmann, E. (2005). Mimicking carboxyterminal phosphorylation differentially effects subcellular distribution and cell-to-cell movement of tobacco mosaic virus movement protein. *Virology* 332, 563–577.

Wang, Y., Bao, Z., Zhu, Y., and Hua, J. (2009). Analysis of temperature modulation of plant defense against biotrophic microbes. *Mol. Plant Microbe Interact.* 22, 498–506. doi: 10.1094/MPMI-22-5-0498

Whitham, S., McCormick, S., and Baker, B. (1996). The N gene of tobacco confers resistance to tobacco mosaic virus in transgenic tomato. *Proc. Natl. Acad. Sci. U. S. A.* 93, 8776–8781.

Wosula, E. N., Tatineni, S., Wegulo, S. N., and Hein, G. L. (2017). Effect of temperature on wheat streak mosaic disease development in winter wheat. *Plant Dis.* 101, 324–330. doi: 10.1094/PDIS-07-16-1053-RE

Wu, S. W., Kumar, R., Iswanto, A. B. B., and Kim, J. Y. (2018). Callose balancing at plasmodesmata. *J. Exp. Bot.* 69, 5325–5339. doi: 10.1093/jxb/ery317

Zhong, S. H., Liu, J. Z., Jin, H., Lin, L., Li, Q., Chen, Y., et al. (2013). Warm temperatures induce transgenerational epigenetic release of RNA silencing by inhibiting siRNA biogenesis in Arabidopsis. *Proc. Natl. Acad. Sci. U. S. A.* 110, 9171–9176. doi: 10.1073/pnas.1219655110

Conflict of Interest: The authors declare that the research was conducted in the absence of any commercial or financial relationships that could be construed as a potential conflict of interest.

frontiers in Plant Science

PERSPECTIVE
published: 01 April 2021
doi: 10.3389/fpls.2021.641924

The Enigma of Interspecific Plasmodesmata: Insight From Parasitic Plants

Karsten Fischer[1], *Lena Anna-Maria Lachner*[1], *Stian Olsen*[1], *Maria Mulisch*[2] *and Kirsten Krause*[1]*

[1] Department of Arctic and Marine Biology, UiT The Arctic University of Norway, Tromsø, Norway, [2] Central Microscopy at the Biology Center, Christian-Albrechts-University, Kiel, Germany

Parasitic plants live in intimate physical connection with other plants serving as their hosts. These host plants provide the inorganic and organic compounds that the parasites need for their propagation. The uptake of the macromolecular compounds happens through symplasmic connections in the form of plasmodesmata. In contrast to regular plasmodesmata, which connect genetically identical cells of an individual plant, the plasmodesmata that connect the cells of host and parasite join separate individuals belonging to different species and are therefore termed "interspecific". The existence of such interspecific plasmodesmata was deduced either indirectly using molecular approaches or observed directly by ultrastructural analyses. Most of this evidence concerns shoot parasitic *Cuscuta* species and root parasitic Orobanchaceae, which can both infect a large range of phylogenetically distant hosts. The existence of an interspecific chimeric symplast is both striking and unique and, with exceptions being observed in closely related grafted plants, exist only in these parasitic relationships. Considering the recent technical advances and upcoming tools for analyzing parasitic plants, interspecific plasmodesmata in parasite/host connections are a promising system for studying secondary plasmodesmata. For open questions like how their formation is induced, how their positioning is controlled and if they are initiated by one or both bordering cells simultaneously, the parasite/host interface with two adjacent distinguishable genetic systems provides valuable advantages. We summarize here what is known about interspecific plasmodesmata between parasitic plants and their hosts and discuss the potential of the intriguing parasite/host system for deepening our insight into plasmodesmatal structure, function, and development.

Keywords: *Cuscuta*, feeding hyphae, haustorium, interspecific plasmodesmata, parasitic plants, secondary plasmodesmata, symplasm

OPEN ACCESS

Edited by:
Jung-Youn Lee,
University of Delaware, United States

Reviewed by:
Olga V. Voitsekhovskaja,
Komarov Botanical Institute (RAS), Russia
Koh Aoki,
Osaka Prefecture University, Japan
Michitaka Notaguchi,
Nagoya University, Japan
James H. Westwood,
Virginia Tech, United States

***Correspondence:**
Kirsten Krause
kirsten.krause@uit.no

Specialty section:
This article was submitted to Plant Cell Biology, a section of the journal Frontiers in Plant Science

Received: *15 December 2020*
Accepted: *09 March 2021*
Published: *01 April 2021*

Citation:
Fischer K, Lachner L-AM, Olsen S, Mulisch M and Krause K (2021) The Enigma of Interspecific Plasmodesmata: Insight From Parasitic Plants. Front. Plant Sci. 12:641924. doi: 10.3389/fpls.2021.641924

INTRODUCTION

Symplasmic domains are operational units which are formed by joining the protoplasts of cells by way of plasmodesmata (PD) that form complex structures across the plant cell walls (Ehlers and Kollmann, 2001) or by sieve pores that originate from PD (Kalmbach and Helariutta, 2019) but are limited to the sieve elements of the phloem. Based on when and where they originate, two different types of PD are distinguished: primary PD originate during cell division, while secondary PD are

formed across already existing cell walls. Despite their different origin, no structural differences can be discerned between them (Burch-Smith et al., 2011). Studies of secondary PD have, therefore, focused on non-division walls, which are of ontogenetically different origin and contain exclusively secondary PD (Ehlers and Kollmann, 2001). While this is a convenient system for structural analyses, a challenge that remains is to delineate the chain of molecular events that regulates secondary PD formation. To this end, the study of PD formed between genetically different plants promises a possibility to distinguish the molecular steps in each of the two cells that contribute to their establishment. Such interspecific PD (iPD) are by definition secondary as they are inserted in principle into existing cell walls of two unrelated individuals. Such a situation occurs either in graft unions (Kollmann and Glockmann, 1985, 1991) or at the interface between parasitic plant haustoria and the invaded tissue of their hosts (Dörr, 1969; Lee, 2009). While grafting is limited to closely related species of a few angiosperm families, some parasitic plants infect a wide range of distantly related host plant species encompassing both monocots and dicots (Westwood et al., 2010).

Parasitic plants, by definition, procure part or all of their nutrients from autotrophic plants, which serve as their hosts. Having initially evolved from fully photoautotrophic ancestors, they now occupy a narrow and specialized but apparently lucrative niche – given that the evolution of parasitic lineages has taken place many times independently within the angiosperms (Nickrent, 2020). The specialized lifestyle has led to various adaptations of which the invention of an infection organ, termed haustorium, was the primary key to their success (Yoshida et al., 2016). The term haustorium refers to the tissue of the parasite that develops endophytically within the infected host plant and is a morphological trait that is common to all parasitic plants (Smith et al., 2013). Unlike their fungal counterparts, parasitic plant haustoria are complex multicellular organs. With them, parasites can invade either the shoots (e.g., dodders, mistletoes) or the roots (e.g., broomrapes) of their hosts and withdraw either only water and inorganic nutrients through xylem connections (hemiparasites) or inorganic plus organic compounds via connections to host xylem, phloem, and parenchyma cells (holoparasites).

One parasitic plant genus that has been classified as a noxious weed in many countries is *Cuscuta* (dodder) (**Figure 1A**). *Cuscuta* species are destructive shoot parasites due to their broad host spectrum that includes annual plants and perennial shrubs and trees from most orders within the angiosperm lineage (Vogel et al., 2018). The endophytic haustorium of *Cuscuta* species protrudes from the center of a suction cup-like ring, the adhesive disk, which anchors the parasite to the host surface (Vaughn, 2002; Lee, 2007). At an early stage of infection, the haustorium penetrates the host plant surface by applying mechanical pressure and releasing cell wall degrading enzymes that weaken the host tissue cohesion (Vaughn, 2003; Johnsen et al., 2015). Following this initial invasion, the haustorium expands and grows through the cortex and often the sclerenchymal ring in search of the vascular tissue of the host. At the final stages of the infection, elongated cells (so-called searching and feeding hyphae) emerge from the tips and flanks of a haustorium (**Figure 1B**). The active feeding stage usually only lasts for a limited time, and the process of nutrient acquisition is taken over by younger haustoria as the parasite grows and finds new hosts.

The haustorial hyphae form physical and physiological bridges between host and parasite (**Figures 1C–E**) and facilitate the nutrient and water transfer. The hyphae appear to recognize which host cell type they approach, and they differentiate into a matching cell type (Vaughn, 2006). Thus, xylem vessels of the host, which are comprised of tube-like dead cells are intercepted by xylem-like (xylic) hyphae that re-direct water and minerals to the parasite (Christensen et al., 2003). On the other hand, amino acids, sugars, and other organic molecules in the phloem sap are channeled to the parasite through phloic hyphae that surround the host sieve elements (Dörr, 1972; Hibberd and Jeschke, 2001; Birschwilks et al., 2006; Vaughn, 2006). Hyphae connecting to parenchymal host cells show fewer morphological changes but are characterized by an electron-dense and organelle rich cytoplasm (Dörr, 1969). Chimeric cell walls and symplasmic connections between the different hyphae and the host tissue provide cohesion between the partners and it is tempting to also assume that they ensure the efficiency in nutrient uptake that the parasite depends on.

EVIDENCE FOR SYMPLASMIC CONNECTIONS BETWEEN HOLOPARASITIC PLANTS AND THEIR HOSTS

Although investigations of cytoplasmic contacts between parasitic plant haustoria and the infected host tissue are not exceptionally abundant, indirect and direct evidence for iPD at the host/parasite interface has accumulated over the past half century (**Table 1**).

Physiological and Molecular Evidence From the Genus *Cuscuta*

In contrast to mineral nutrients and small organic compounds that in plants take both apoplastic and symplastic transport routes (Offler et al., 2003; Zhang and Turgeon, 2018), macromolecules (proteins or nucleic acids) require symplasmic connections, either in the form of PD between neighboring cells or through sieve pores or sieve plates between sieve elements (Kalmbach and Helariutta, 2019). A nice demonstration of macromolecular transport between host plants and *Cuscuta* and, with it, unequivocal proof for a continuous and efficient connection between parasite and host vascular bundles was provided using the green fluorescent protein (GFP) (Haupt et al., 2001; Birschwilks et al., 2007). That the exchange of proteins in fact occurs at a large scale was recently shown through a proteomics approach (Liu et al., 2020). Several 100 host proteins were identified in *C. australis* growing on *A. thaliana* or soybean and, surprisingly, hundreds of *Cuscuta* proteins were found in the two host plants, indicating a massive bidirectional protein movement. Furthermore, mRNAs were found to move from host to parasite (Roney et al., 2007; David-Schwartz et al.,

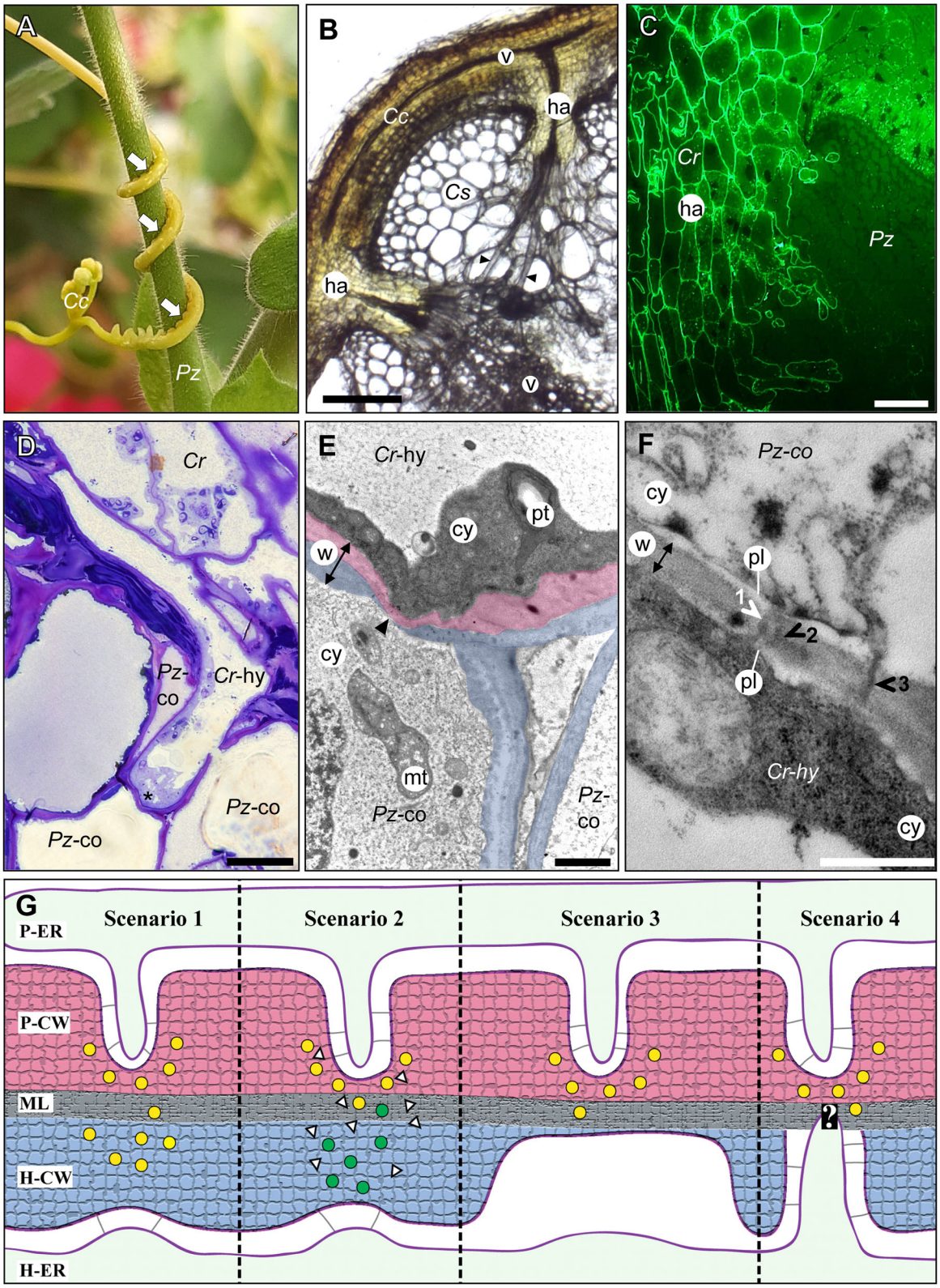

FIGURE 1 | The host/parasite feeding interface. **(A)** The yellow vine *C. campestris* (*Cc*) twines around its host *Pelargonium zonale* (Pz) making infection sites (arrows) where parasitic haustoria penetrate the host tissue. **(B)** Light micrograph of a transverse vibratome section of *C. campestris* (*Cc*) infecting *Cucumis sativus* (*Cs*)

(Continued)

FIGURE 1 | revealing the endophytic haustoria (ha) with their protruding hyphae (black arrowheads) that connect both plants' vascular elements (v). Scale bar: 300 μm. **(C)** Fluorograph of an immunolabeled microtome cross section of a parasite/host boundary. A monoclonal antibody (JIM8) against arabinogalactan proteins selectively labels *C. reflexa* (*Cr*) cell walls but not cell walls of the host *P. zonale* (*Pz*) and enables the precise identification of the haustorium (ha) interface. Scale bar: 100 μm. **(D)** Light micrograph of a toluidine blue-stained section showing a hypha (*Cr*-hy) of the parasite *C. reflexa* (*Cr*). The hypha has grown through one host cortex cell (*Pz*-co) and is in the process of penetrating another (site marked with an asterisk, *). Scale bar: 20 μm. **(E)** Electron micrograph of the hypha (*Cr*-hy) shown in **(D)** penetrating a host cortex cell (co). The thinned or ruptured host cell wall is marked with an arrowhead. Parasite (*Cr*) and host (*Pz*) cell walls are highlighted with red and blue shading, respectively. The cell wall (w, with double-sided arrow indicating its width), cytoplasm (cy), host cell mitochondrion (mt), and parasite plastid (pt) are labeled. Scale bar: 2 μm. **(F)** Electron micrograph of a cell wall (w) between a *C. reflexa* hypha (*Cr*-hy) and a penetrated *P. zonale* cortex cell (*Pz*-co). Three plasmodesmata (1, 2, and 3) are marked with arrowheads that are colored either white where they connect to both cells' plasmalemma (pl) and black where they appear to cross the wall only partially. PD 2 appears to be branched, while the others are seemingly unbranched PD. Scale bar: 0.5 μm. cy = cytoplasm. **(G)** Schematic illustration of four hypothetical scenarios (Scenarios 1–4) how PD formation at the parasite/host interface could be coordinated. Cell walls are shaded with red (parasite) and blue color (host) like in **(E)**. Cell wall enzymes secreted to thin/loosen the cell walls are represented by yellow (from parasite) or green (from host) dots. In Scenario 1, the parasite-secreted enzymes are moving across the middle lamellae (ML) to act on the host cell wall (H-CW). In Scenario 2, unknown signals (white triangles) from the parasite induce the release of host cell wall enzymes (green dots) to autodecompose their cell walls locally. In Scenario 3, the parasite cell wall enzymes are secreted in a location where the host wall is already thin [see situation at hyphal tips in **(E)**]. In Scenario 4, the parasite cell wall enzymes are secreted in a location where a pre-infection host PD is present. The white question mark indicates that this scenario is the most speculative because it assumes that the parasite is able to locate the host PD. The association of parasite ER (P-ER) and host ER (H-ER) with their respective plasma membranes is indicated by gray lines. The methods used to generate the microscopy images are described in the **Supplementary Materials** file.

2008; LeBlanc et al., 2013) and this happens at a genomic scale involving transcripts of thousands of genes (Kim et al., 2014). MicroRNAs are also shuttled from the parasite to the host to target host gene expression (Shahid et al., 2018; Johnson and Axtell, 2019). Last but not least, plant viruses have for 75 years been known to move between *Cuscuta* and its host plants (Bennett, 1944; Mikona and Jelkmann, 2010), a transmission also depending on PD. Collectively, these data point to a massive flow of substances in both directions that cannot be explained by apoplastic translocation alone but necessitates open symplasmic connections between *Cuscuta* and its hosts. There are to date no molecular studies that explain how this massive flow could be regulated or to what degree it is selective.

Ultrastructural Evidence From the Genera *Cuscuta* and *Orobanche*

Despite the molecular data discussed above, there is only limited ultrastructural evidence for symplasmic connections between parasite and host vascular tissues (**Table 1**). In the root parasitic genus *Orobanche* a connection between parasite and host via sieve elements has been convincingly shown for *O. crenata* connecting to *Vicia narbonensis* (Dörr and Kollmann, 1995) and for *O. cumana* parasitizing *Helianthus annuus* (Krupp et al., 2019). In both cases, interspecific sieve plates were observed. For the shoot parasite *Cuscuta*, in contrast, compelling evidence for sieve plates at the parasite/host border is still lacking. Claims regarding sieve pores between phloic hyphae of *Cuscuta japonica* and sieve elements of *Impatiens* (Lee, 2009) were not supported by visual evidence and have not been confirmed when the same host was infected with *Cuscuta pentagona* (Vaughn, 2003, 2006). However, several accounts of plasmodesmata between host parenchyma cells and *Cuscuta* searching hyphae have been published (**Table 1**). Such investigations revealing iPD have used five different *Cuscuta* species infecting an even larger range of different hosts from genera like *Pelargonium*, *Vicia, Impatiens, Nicotiana* or *Arabidopsis* (Dörr and Kollmann, 1995; Vaughn, 2003, 2006; Birschwilks et al., 2006, 2007). The reports differ with respect to the abundance of iPD and it was proposed that they may be relatively short-lived and present only in hyphae from the younger parts of the haustorium while they seem to degenerate later (Dörr, 1969; Vaughn, 2003). Both authors provided very detailed descriptions of the versatile iPD structures with unbranched and complex branched forms with visible desmotubules occurring side by side. Vaughn (2003) also described collars and fibrillar spokes radiating out from the desmotubule, suggesting that their ultrastructure could be very similar to that of PD that connect cells from the same organism. Later stages were observed to contain occlusions or appear to fuse and form hairpin loops running back to the same cell, but it should be kept in mind that the reports show 2-dimensional snapshots of a complex system and both the spatial and temporal dimensions have not been investigated. Therefore, caution should be exercised when interpreting findings of incomplete iPD (see **Figure 1F** and literature cited in **Table 1**). This notion, together with the still unexplained sustained transport activities, calls for higher temporal resolution of haustorial development and additional modern technologies in future studies of the host/parasite connections.

ESTABLISHMENT OF INTERSPECIFIC SECONDARY PD

iPD are a special case of secondary PD as they span the cells of different individuals, species and even higher order phylogenetic lineages. So far, very little is known about this type of PD.

Control of Secondary PD Formation

Some evidence suggests that PD do not develop from one side only, but that they are formed in a coordinated process by the two opposing cells (Kollmann and Glockmann, 1991; Ehlers and Kollmann, 2001). The process is believed to start with a local thinning of the cell wall on both sides followed by the trapping of ER cisternae which develop into plasmodesmal desmotubules, the fusion of the two plasma membranes and finally the reconstruction of the cell wall (Ehlers and Kollmann, 2001; Burch-Smith et al., 2011). If both cells contribute to the formation of complete secondary PD, some kind of communication across the cell borders is needed. Potential scenarios how this could

TABLE 1 | Summary of studies investigating cell-to-cell connections between parasitic plants and their hosts.

	Species		Host cell type		Interspecific symplasmic connection	Experimental method						References (chronologically sorted for each category)
	Parasite	Host	Parenchyma	Phloem		EM	IL[a]	FP[b]	FS[c]	RT[d]	V[e]	
Ultrastructural studies	*O. cumana*	*Helianthus annuus*		●	SP	●						Krupp et al., 2019
	C. japonica	*Impatiens balsaminea*		●	PD, SP	●						Lee, 2009
	C. reflexa	*Arabidopsis thaliana*	●		PD	●						Birschwilks et al., 2007
	C. platyloba	*Arabidopsis thaliana*	●		PD	●						Birschwilks et al., 2007
	C. odorata	*Arabidopsis thaliana*	●		PD	●						Birschwilks et al., 2007
	C. reflexa	*Vicia faba*	●		PD	●						Birschwilks et al., 2006
	C. platyloba	*Nicotiana tabacum*	●		PD	●						Birschwilks et al., 2006
	C. odorata	*Nicotiana tabacum*	●		PD	●						Birschwilks et al., 2006
	C. pentagona	*Impatiens balsaminea*	●		PD	●	●					Vaughn, 2006
	C. pentagona	*Impatiens sultanii*	●		PD	●	●					Vaughn, 2003
	O. crenata	*Vicia narbonensis L.*	●	●	PD, SP	●						Dörr and Kollmann, 1995
	C. odorata	*Pelargonium zonale*	●		PD	●						Dörr, 1969
Macromolecular transport	*P. ramosa*	*Brassica napus*		●	SP				●			Peron et al., 2016
	P. aegyptiaca	*Solanum lycopersicum*		●	SP		●	●	●			Ekawa and Aoki, 2017
	P. aegyptiaca	*Solanum lycopersicum*		●	SP			●				Aly et al., 2011
	C. reflexa	*Arabidopsis thaliana*		●	SP			●	●	●		Birschwilks et al., 2007
	C. odorata	*Arabidopsis thaliana*		●	SP			●	●	●		Birschwilks et al., 2007
	C. platyloba	*Arabidopsis thaliana*		●	SP			●	●	●		Birschwilks et al., 2007
	C. reflexa	*Vicia faba*		●	SP			●	●	●	●	Birschwilks et al., 2006
	C. odorata	*Nicotiana tabacum*		●	SP			●	●	●	●	Birschwilks et al., 2006
	C. platyloba	*Nicotiana tabacum*		●	SP			●	●	●	●	Birschwilks et al., 2006
	C. reflexa	*Nicotiana tabacum*		●	SP			●	●			Haupt et al., 2001

Ultrastructural studies provided direct evidence for the presence of interspecific symplasmic connections, while molecular studies provided indirect evidence for their existence based on macromolecular transport analysis. The main experimental approaches in each study (EM, electron microscopy; IL, immunolabeling; FP, fluorescent protein transport; FS, fluorescent stain; RT, radioactive tracer labeling; V, virus movement) are indicated. PD, plasmodesmata; SP, Sieve pores.

[a] *Callose antibody.*

[b] *AtSUC2-GFP, Tobacco mosaic virus movement protein-GFP, ER-targeted GFP.*

[c] *5,6-carboxyfluorescin diacetate (CFDA) for transport studies or aniline blue for callose staining.*

[d] *14C or 3H.*

[e] *potato virus Y isolate N.*

happen are depicted in **Figure 1G**. It should be noted that these are hypothetical alternatives and experimental insight regarding the regulation of secondary PD formation and the molecules involved in signaling is lacking. Whether PD initiation happens unilaterally by one cell in a given tissue or starts simultaneously in two neighboring cells, is also unresolved. While in the parasite/host system it is presumably the parasite that initiates PD formation as this connection appears to be vital for the parasite's survival, it is likewise still unclear how and how much the host contributes (**Figure 1G**).

Cell Wall Degradation and Rebuilding

Cell wall breakdown and rebuilding are thought to be important steps of secondary PD formation (Ehlers and Kollmann, 2001; Burch-Smith et al., 2011). In the case of intraspecific PD the two parts of the common cell wall and the enzymatic machinery for the cell wall remodeling are in principle identical. The cell walls of the host and parasite, on the other hand, do differ to some degree (Johnsen et al., 2015) (**Figure 1C**) and accordingly the enzymes involved in remodeling the cell walls are also expected to differ. It is well-known that during invasion of the host the parasite secretes a cocktail of enzymes which degrade the cell walls of the host but not their own (Nagar et al., 1984; Losner-Goshen et al., 1998; Olsen et al., 2016). Host cell walls abutting haustorial cells were observed to have a lower degree of pectin esterification than walls that were not in contact with the haustorium (Johnsen et al., 2015). Young hyphae were also often found to be surrounded by host cell walls that were stretched extremely thin [**Figures 1D,E** and Vaughn (2003)]. This provided evidence for extensive deconstruction and loosening of the host cell walls at the site of contact, but it remains speculative whether this thinning is mediated by host or parasite enzymes (see **Figure 1G**, scenarios 1 and 2). With cell wall degradation products being discussed as potential signaling molecules for cell wall integrity (Ferrari et al., 2013), the parasite's enzymes could tentatively contribute to the coordination of PD formation between parasite and host by inducing host enzyme secretion in corresponding places (**Figure 1G,** scenario 2). Alternatively, similar signals may help the parasite identify regions with thinned host walls and

induce PD formation in these regions (**Figure 1G**, scenarios 3 and 4).

iPD in Graft Unions

Besides parasitic/host interfaces, graft unions are sites where interspecific symplasmic connections can potentially be formed. Already Jeffree and Yeoman (1983) observed cell wall thinning and formation of plasmodesmata in opposing cells of autografted tomato (*Solanum lycopersicum*) plants. More pertinent, Kollmann and colleagues were able to show iPD in heterografts between different species (Kollmann et al., 1985) and different orders (Kollmann and Glockmann, 1985, 1991). Anatomically, both full and partial unbranched connections as well as complex branched PD were described, thus resembling closely what has been found at the parasite/host interface. Cell wall thinning seemed to precede the PD formation in the described cases. Using serial sections, Kollmann and Glockmann (1985) could show that apparently incomplete "half" iPD were in fact continuous structures connecting both adjacent cells. However, this seems to depend on the cell types that align with each other and "half PD" that end at the middle lamella were found where the alignment was not perfect (Kollmann et al., 1985). Diffusion through graft interface iPD was demonstrated using fluorescein in grafts between different Prunus species (Pina et al., 2009), demonstrating the functionality of these structures in transport.

PARASITIC PLANTS AS TOOLS FOR THE ANALYSIS OF SECONDARY PD

Secondary iPD at the host/parasite border are an excellent system to overcome limitations of current PD research for several reasons. First, the symplasmically connected partners have different genotypes, and form many more different combinations than grafting currently offers. This facilitates the identification of the origin of the genes and proteins involved in the establishment of secondary PD, which could finally answer the question whether the PD are initiated uni- or bilaterally. Moreover, the searching and feeding hyphae of the parasite can be faithfully distinguished based on their characteristic ultrastructure (Dörr, 1969, 1972; Vaughn, 2003, 2006) or on unique epitopes in their cell walls (Vaughn, 2003; Johnsen et al., 2015) (**Figure 1C**). Thus, the border between parasite and host tissues and thereby the location of heterospecific cell walls can be precisely mapped. The parasite/host system therefore allows detailed analyses of the roles that each of the two symplasmically connected cells have in this process. In contrast, in successful grafts the two partners are often very closely related, making such differentiation more challenging, if not impossible.

Second, quite many parasitic plants, including the well-researched *Orobanche* and *Cuscuta*, can infect many different hosts (Yoshida et al., 2016; Shimizu and Aoki, 2019). Their host range includes popular model plants like *A. thaliana,* tobacco or tomato and thus offers the opportunity to harness all molecular genetic tools developed for those. Among them, a plethora of transgenic and mutant lines (overexpressing lines, knock-out lines, introgression lines) are available and have already been used to dissect parasite/host interactions (Hegenauer et al., 2016; Krause et al., 2018). Classical transgenic technology, RNA interference (Mansoor et al., 2006) and genome editing technologies like CRISPR-Cas9 (Doudna and Charpentier, 2014) are available for many compatible hosts. Furthermore, whole genome sequences and large-scale transcriptomic datasets are available for hundreds if not soon thousands of plants (Wong et al., 2020). On the parasite side, the first genome sequences have been published for *Cuscuta* (Sun et al., 2018; Vogel et al., 2018). Although transgenic parasitic plants cannot yet be produced efficiently, recent progress gives reason to believe that genetic manipulation of these parasites will soon be a standard (Lachner et al., 2020).

With the development of new methodology for tracing symplasmic transport via non-invasive approaches and suitable biotracers, the origin and fate of enzymes and structural components and maybe even of signaling molecules might in the future be traceable or even manipulated unilaterally using interspecific interfaces in parasites, but also in grafts.

WHAT CAN WE LEARN ABOUT PD USING THE PARASITE/HOST SYSTEM?

The basic structure of primary and secondary PD is very similar (Brunkard and Zambryski, 2017; Sager and Lee, 2018). The ER membranes and the plasma membranes of the two cells are fused and span the PD to provide a symplasmic connection. However, it is unclear whether the fusion resembles well-described membrane fusion processes, e.g., those between vesicles and the plasma membrane, or whether it is completely different. In the parasite/host system the protein composition and most likely also the lipid composition of the membranes of the two cells are sufficiently different to be of benefit for more detailed analyses of the fusion process.

Proteins also contribute to the structure of PD (Sager and Lee, 2018). Although in the last decades many proteins localized in PD have been identified (Han et al., 2019), their physiological and molecular functions are mostly unknown. It is not even known if the proteins are contributed by one or both cells. The different genotypes of the host and parasite cells provide an optimal instrument to answer such developmental questions.

Transport through PD changes during the course of plant development and in response to stress, and is therefore tightly controlled through the size exclusion limit (SEL) or pore size, or by closure of the PD (Brunkard and Zambryski, 2017). Although some factors regulating transport through PD such as light, the circadian clock (Brunkard and Zambryski, 2019) or sugars (Brunkard et al., 2020) have been identified recently, there is limited knowledge about PD regulation at the physiological and molecular level. Only a few molecules regulating SEL have been characterized. Among them are virus movement proteins which increase SEL to allow movement of viruses in a process called gating. In the parasite/host system similar processes are assumed to take place and it is tempting to speculate that this is achieved by

"gating molecules" produced by the parasite to prevent closing of the PD by the host. Indeed, it has been proposed that the control of the common host/parasite symplast is the key characteristic of compatible interactions (Cheval and Faulkner, 2017), a claim that could be tested by investigating the iPD.

CONCLUSION

iPD established between parasitic plants and their hosts offer a unique perspective on symplasmic domains and secondary PD in general. They promise to be an advantageous system to address and answer open questions regarding their formation and regulation. In particular, the respective contribution of neighboring cells can be analyzed and discriminated. Considering that adequate molecular tools for the parasites are only now beginning to emerge, we will hopefully see many new pieces of valuable information generated in this highly contemporary field in the future.

DATA AVAILABILITY STATEMENT

The original contributions presented in the study are included in the article/**Supplementary Material**, further inquiries can be directed to the corresponding author.

AUTHOR CONTRIBUTIONS

All authors listed have made a substantial, direct and intellectual contribution to the work, and approved it for publication.

FUNDING

The authors' work on the parasite/host interface and host/parasite connections was financed by Tromsø Research Foundation (grant #16-TF-KK to KK).

ACKNOWLEDGMENTS

We are indebted to Anna Pielach (University of Gothenburg, Sweden) for providing the picture shown in **Figure 1C** and Marita Beese (Central Microscopy, Christian-Albrechts-University Kiel, Germany) for technical support. The JIM8 antibody was provided by Prof. Paul Knox, Universtity of Leeds, United Kingdom. Work on parasitic plants in the Krause group would not be possible without the invaluable help of the staff of the greenhouses at UiT The Arctic University of Norway, especially Leidulf Lund, and at CAU Kiel. Financially, the generous support of Tromsø Forskningsstiftelse (TFS) and the Department of Arctic and Marine Biology (AMB) is gratefully acknowledged. Prof. Karin Krupinska and the CAU Kiel are last but not least thanked for inviting the corresponding author as guest professor to Kiel for one semester, which enabled the collaboration between KK and MM.

SUPPLEMENTARY MATERIAL

The Supplementary Material for this article can be found online at: https://www.frontiersin.org/articles/10.3389/fpls.2021.641924/full#supplementary-material

REFERENCES

Aly, R., Hamamouch, N., Abu-Nassar, J., Wolf, S., Joel, D. M., Eizenberg, H., et al. (2011). Movement of protein and macromolecules between host plants and the parasitic weed *Phelipanche aegyptiaca* Pers. *Plant Cell Rep.* 30, 2233–2241. doi: 10.1007/s00299-011-1128-5

Bennett, C. W. (1944). Studies of dodder transmission of plant viruses. *Phytopathology* 34, 905–932.

Birschwilks, M., Haupt, S., Hofius, D., and Neumann, S. (2006). Transfer of phloem-mobile substances from the host plants to the holoparasite Cuscuta sp. *J. Exp. Bot.* 57, 911–921. doi: 10.1093/jxb/erj076

Birschwilks, M., Sauer, N., Scheel, D., and Neumann, S. (2007). *Arabidopsis thaliana* is a susceptible host plant for the holoparasite Cuscuta spec. *Planta* 226, 1231–1241. doi: 10.1007/s00425-007-0571-6

Brunkard, J. O., Xu, M., Scarpin, M. R., Chatterjee, S., Shemyakina, E. A., Goodman, H. M., et al. (2020). TOR dynamically regulates plant cell-cell transport. *Proc. Natl. Acad. Sci. U. S. A.* 117, 5049–5058. doi: 10.1073/pnas.1919196117

Brunkard, J. O., and Zambryski, P. (2019). Plant cell-cell transport via plasmodesmata is regulated by light and the circadian clock. *Plant Physiol.* 181, 1459–1467. doi: 10.1104/pp.19.00460

Brunkard, J. O., and Zambryski, P. C. (2017). Plasmodesmata enable multicellularity: new insights into their evolution, biogenesis, and functions in development and immunity. *Curr. Opin. Plant Biol.* 35, 76–83. doi: 10.1016/j.pbi.2016.11.007

Burch-Smith, T. M., Stonebloom, S., Xu, M., and Zambryski, P. C. (2011). Plasmodesmata during development: re-examination of the importance of primary, secondary, and branched plasmodesmata structure versus function. *Protoplasma* 248, 61–74. doi: 10.1007/s00709-010-0252-3

Cheval, C., and Faulkner, C. (2017). Plasmodesmal regulation during plant-pathogen interactions. *New Phytol.* 217, 62–67. doi: 10.1111/nph.14857

Christensen, N. M., Dörr, I., Hansen, M., van der Kooij, T. A. W., and Schulz, A. (2003). Development of Cuscuta species on a partially incompatible host: induction of xylem transfer cells. *Protoplasma* 220, 131–142. doi: 10.1007/s00709-002-0045-4

David-Schwartz, R., Runo, S., Townsley, B., Machuka, J., and Sinha, N. (2008). Long-distance transport of mRNA via parenchyma cells and phloem across the host-parasite junction in Cuscuta. *New Phytol.* 179, 1133–1141. doi: 10.1111/j.1469-8137.2008.02540.x

Dörr, I. (1969). Fine structure of intracellular growing Cuscuta-hyphae. *Protoplasma* 67, 123–137. doi: 10.1007/BF01248735

Dörr, I. (1972). Contact of Cuscuta-hyphae with sieve tubes of its host plants. *Protoplasma* 75, 167–184. doi: 10.1007/BF01279402

Dörr, I., and Kollmann, R. (1995). Symplasmic sieve element continuity between Orobanche and its host. *Bot. Acta* 108, 47–55. doi: 10.1111/j.1438-8677.1995.tb00830.x

Doudna, J. A., and Charpentier, E. (2014). The new frontier of genome engineering with CRISPR-Cas9. *Science* 346, 1077–1086. doi: 10.1126/science.1258096

Ehlers, K., and Kollmann, R. (2001). Primary and secondary plasmodesmata: structure, origin, and functioning. *Protoplasma* 216, 1–30. doi: 10.1007/BF02680127

Ekawa, M., and Aoki, K. (2017). Phloem-conducting cells in haustoria of the root-parasitic plant *Phelipanche aegyptiaca* retain nuclei and are not mature sieve elements. *Plants* 6:60. doi: 10.3390/plants6040060

Ferrari, S., Savatin, D. V., Sicilia, F., Gramegna, G., Cervone, F., and De Lorenzo, G. (2013). Oligogalacturonides: plant damage-associated molecular patterns and regulators of growth and development. *Front. Plant Sci.* 4:49. doi: 10.3389/fpls.2013.00049

Han, X., Huang, L. J., Feng, D., Jiang, W. H., Miu, W. Z., and Li, N. (2019). Plasmodesmata-related structural and functional proteins: the long sought-after secrets of a cytoplasmic channel in plant cell walls. *Int. J. Mol. Sci.* 20:2946. doi: 10.3390/ijms20122946

Haupt, S., Oparka, K. J., Sauer, N., and Neumann, S. (2001). Macromolecular trafficking between *Nicotiana tabacum* and the holoparasite *Cuscuta reflexa*. *J. Exp. Bot.* 52, 173–177. doi: 10.1093/jexbot/52.354.173

Hegenauer, V., Fürst, U., Kaiser, B., Smoker, M., Zipfel, C., Felix, G., et al. (2016). Detection of the plant parasite *Cuscuta reflexa* by a tomato cell surface receptor. *Science* 353, 478–481. doi: 10.1126/science.aaf3919

Hibberd, J. M., and Jeschke, W. D. (2001). Solute flux into parasitic plants. *J. Exp. Bot.* 52, 2043–2049. doi: 10.1093/jexbot/52.363.2043

Jeffree, C. E., and Yeoman, M. M. (1983). Development of intercellular connections between opposing cells in a graft union. *New Phytol.* 93, 491–509. doi: 10.1111/j.1469-8137.1983.tb02701.x

Johnsen, H. R., Striberny, B., Olsen, S., Vidal-Melgosa, S., Fangel, J. U., Willats, W. G. T., et al. (2015). Cell wall composition profiling of parasitic giant dodder (*Cuscuta reflexa*) and its hosts: a priori differences and induced changes. *New Phytol.* 207, 805–816. doi: 10.1111/nph.13378

Johnson, N. R., and Axtell, M. J. (2019). Small RNA warfare: exploring origins and function of trans-species microRNAs from the parasitic plant Cuscuta. *Curr. Opin. Plant Biol.* 50, 76–81. doi: 10.1016/j.pbi.2019.03.014

Kalmbach, L., and Helariutta, Y. (2019). Sieve plate pores in the phloem and the unknowns of their formation. *Plants* 8:25. doi: 10.3390/plants8020025

Kim, G., LeBlanc, M. L., Wafula, E. K., dePamphilis, C. W., and Westwood, J. H. (2014). Genomic-scale exchange of mRNA between a parasitic plant and its hosts. *Science* 345, 808–811. doi: 10.1126/science.1253122

Kollmann, R., and Glockmann, C. (1985). Studies on graft unions. I. Plasmodesmata between cells of plants belonging to different unrelated taxa. *Protoplasma* 124, 224–235. doi: 10.1007/BF01290774

Kollmann, R., and Glockmann, C. (1991). Studies on graft unions. III. On the mechanism of secondary formation of plasmodesmata at the graft interface. *Protoplasma* 165, 71–85. doi: 10.1007/BF01322278

Kollmann, R., Yang, S., and Glockmann, C. (1985). Studies on graft unions. II. Continuous and half plasmodesmata in different regions of the graft interface. *Protoplasma* 126, 19–29. doi: 10.1007/BF01287669

Krause, K., Johnsen, H. R., Pielach, A., Lund, L., Fischer, K., and Rose, J. K. C. (2018). Identification of tomato introgression lines with enhanced susceptibility or resistance to infection by parasitic giant dodder (*Cuscuta reflexa*). *Physiol. Plant.* 162, 205–218. doi: 10.1111/ppl.12660

Krupp, A., Heller, A., and Spring, O. (2019). Development of phloem connection between the parasitic plant *Orobanche cumana* and its host sunflower. *Protoplasma* 256, 1385–1397. doi: 10.1007/s00709-019-01393-z

Lachner, L. A. M., Galstyan, L., and Krause, K. (2020). A highly efficient protocol for transforming *Cuscuta reflexa* based on artificially induced infection sites. *Plant Direct* 4:254. doi: 10.1002/pld3.254

LeBlanc, M., Kim, G., Patel, B., Stromberg, V., and Westwood, J. (2013). Quantification of tomato and Arabidopsis mobile RNAs trafficking into the parasitic plant *Cuscuta pentagona*. *New Phytol.* 200, 1225–1233. doi: 10.1111/nph.12439

Lee, K. B. (2007). Structure and development of the upper haustorium in the parasitic flowering plant *Cuscuta japonica* (*Convolvulaceae*). *Am. J. Bot.* 94, 737–745. doi: 10.3732/ajb.94.5.737

Lee, K. B. (2009). Structure and development of the endophyte in the parasitic angiosperm *Cuscuta japonica*. *J. Plant Biol.* 52, 355–363. doi: 10.1007/s12374-009-9046-6

Liu, N., Shen, G., Xu, Y., Liu, H., Zhang, J., Li, S., et al. (2020). Extensive inter-plant protein transfer between Cuscuta parasites and their host plants. *Mol. Plant* 13, 573–585. doi: 10.1016/j.molp.2019.12.002

Losner-Goshen, D., Portnoy, V. H., Mayer, A. M., and Joel, D. M. (1998). Pectolytic activity by the haustorium of the parasitic plant *Orobanche* L. (Orobanchaceae) in host roots. *Ann. Bot.* 81, 319–326. doi: 10.1006/anbo.1997.0563

Mansoor, S., Amin, I., Hussain, M., Zafar, Y., and Briddon, R. W. (2006). Engineering novel traits in plants through RNA interference. *Trends Plant Sci.* 11, 559–565. doi: 10.1016/j.tplants.2006.09.010

Mikona, C., and Jelkmann, W. (2010). Replication of grapevine leafroll-associated virus-7 (GLRaV-7) by Cuscuta species and its transmission to herbaceous plants. *Plant Dis.* 94, 471–476. doi: 10.1094/PDIS-94-4-0471

Nagar, R., Singh, M., and Sanwal, G. G. (1984). Cell wall degrading enzymes in *Cuscuta reflexa* and its hosts. *J. Exp. Bot.* 35, 1104–1111. doi: 10.1093/jxb/35.8.1104

Nickrent, D. L. (2020). Parasitic angiosperms: how often and how many? *Taxon* 69, 5–27. doi: 10.1002/tax.12195

Offler, C. E., McCurdy, D. W., Patrick, J. W., and Talbot, M. J. (2003). Transfer cells: cells specialized for a special purpose. *Annu. Rev. Plant Biol.* 54, 431–454. doi: 10.1146/annurev.arplant.54.031902.134812

Olsen, S., Striberny, B., Hollmann, J., Schwacke, R., Popper, Z. A., and Krause, K. (2016). Getting ready for host invasion: elevated expression and action of xyloglucan endotransglucosylases/hydrolases in developing haustoria of the holoparasitic angiosperm Cuscuta. *J. Exp. Bot.* 67, 695–708. doi: 10.1093/jxb/erv482

Peron, T., Candat, A., Montiel, G., Veronesi, C., Macherel, D., Delavault, P., et al. (2016). New insights into phloem unloading and expression of sucrose transporters in vegetative sinks of the parasitic plant *Phelipanche ramosa* L. *Front. Plant Sci.* 7:2048. doi: 10.3389/fpls.2016.02048

Pina, A., Errea, P., Schulz, A., and Martens, H. J. (2009). Cell-to-cell transport through plasmodesmata in tree callus cultures. *Tree Physiol.* 29, 809–818. doi: 10.1093/treephys/tpp025

Roney, J. K., Khatibi, P. A., and Westwood, J. H. (2007). Cross-species translocation of mRNA from host plants into the parasitic plant dodder. *Plant Physiol.* 143, 1037–1043. doi: 10.1104/pp.106.088369

Sager, R. E., and Lee, J. Y. (2018). Plasmodesmata at a glance. *J. Cell Sci.* 131:e209346. doi: 10.1242/jcs.209346

Shahid, S., Kim, G., Johnson, N. R., Wafula, E., Wang, F., Coruh, C., et al. (2018). MicroRNAs from the parasitic plant *Cuscuta campestris* target host messenger RNAs. *Nature* 553, 82–85. doi: 10.1038/nature25027

Shimizu, K., and Aoki, K. (2019). Development of parasitic organs of a stem holoparasitic plant in genus *Cuscuta*. *Front. Plant Sci.* 10:1435. doi: 10.3389/fpls.2019.01435

Smith, J. D., Mescher, M. C., and De Moraes, C. M. (2013). Implications of bioactive solute transfer from hosts to parasitic plants. *Curr. Opin. Plant Biol.* 16, 464–472. doi: 10.1016/j.pbi.2013.06.016

Sun, G. L., Xu, Y. X., Liu, H., Sun, T., Zhang, J. X., Hettenhausen, C., et al. (2018). Large-scale gene losses underlie the genome evolution of parasitic plant *Cuscuta australis*. *Nat. Commun.* 9:2683. doi: 10.1038/s41467-018-04721-8

Vaughn, K. C. (2002). Attachment of the parasitic weed dodder to the host. *Protoplasma* 219, 227–237. doi: 10.1007/s007090200024

Vaughn, K. C. (2003). Dodder hyphae invade the host: a structural and immunocytochemical characterization. *Protoplasma* 220, 189–200. doi: 10.1007/s00709-002-0038-3

Vaughn, K. C. (2006). Conversion of the searching hyphae of dodder into xylic and phloic hyphae: a cytochemical and immunocytochemical investigation. *Int. J. Plant Sci.* 167, 1099–1114. doi: 10.1086/507872

Vogel, A., Schwacke, R., Denton, A. K., Usadel, B., Hollmann, J., Fischer, K., et al. (2018). Footprints of parasitism in the genome of the parasitic flowering plant *Cuscuta campestris*. *Nat. Commun.* 9:2515. doi: 10.1038/s41467-018-04344-z

Westwood, J. H., Yoder, J. I., Timko, M. P., and dePamphilis, C. W. (2010). The evolution of parasitism in plants. *Trends Plant Sci.* 15, 227–235. doi: 10.1016/j.tplants.2010.01.004

Wong, G. K., Soltis, D. E., Leebens-Mack, J., Wickett, N. J., Barker, M. S., Van de Peer, Y., et al. (2020). Sequencing and analyzing the transcriptomes of a thousand species across the tree of life for green plants. *Annu. Rev. Plant Biol.* 71, 741–765. doi: 10.1146/annurev-arplant-042916-041040

Yoshida, S., Cui, S. K., Ichihashi, Y., and Shirasu, K. (2016). The haustorium, a specialized invasive organ in parasitic plants. *Annu. Rev. Plant Biol.* 67, 643–667. doi: 10.1146/annurev-arplant-043015-111702

Zhang, C. K., and Turgeon, R. (2018). Mechanisms of phloem loading. *Curr. Opin. Plant Biol.* 43, 71–75. doi: 10.1016/j.pbi.2018.01.009

Conflict of Interest: The authors declare that the research was conducted in the absence of any commercial or financial relationships that could be construed as a potential conflict of interest.

frontiers in Plant Science

ORIGINAL RESEARCH
published: 06 April 2021
doi: 10.3389/fpls.2021.632078

Dissection of Functional Modules of AT-HOOK MOTIF NUCLEAR LOCALIZED PROTEIN 4 in the Development of the Root Xylem

Minji Seo[1] *and Ji-Young Lee*[1,2]*

[1] School of Biological Sciences, College of Natural Science, Seoul National University, Seoul, South Korea, [2] Plant Genomics and Breeding Institute, Seoul National University, Seoul, South Korea

Xylem development in the *Arabidopsis* root apical meristem requires a complex cross talk between plant hormone signaling and transcriptional factors (TFs). The key processes involve fine-tuning between neighboring cells, mediated *via* the intercellular movement of signaling molecules. As an example, we previously reported that AT-HOOK MOTIF NUCLEAR LOCALIZED PROTEIN (AHL) 4 (AHL4), a member of the 29 AT-hook family TFs in *Arabidopsis*, moves into xylem precursors from their neighbors to determine xylem differentiation. As part of the effort to understand the molecular functions of AHL4, we performed domain swapping analyses using AHL1 as a counterpart, finding that AHL4 has three functionally distinctive protein modules. The plant and prokaryotes conserved (PPC) domain of AHL4 acts as a mediator of protein–protein interactions with AHL members. The N-terminus of AHL4 is required for the regulation of xylem development likely *via* its unique DNA-binding activity. The C-terminus of AHL4 confers intercellular mobility. Our characterization of modules in the AHL4 protein will augment our understanding of the complexity of regulation and the evolution of intercellular mobility in AHL4 and its relatives.

Keywords: AT-HOOK MOTIF NUCLEAR LOCALIZED PROTEIN 4, intercellular movement, protein–protein interaction, xylem, root apical meristem (RAM)

OPEN ACCESS

Edited by:
Jung-Youn Lee,
University of Delaware, United States

Reviewed by:
Xingyun Qi,
Rutgers, The State University of New Jersey, United States
Steffen Vanneste,
Ghent University, Belgium

***Correspondence:**
Ji-Young Lee
jl924@snu.ac.kr

Specialty section:
This article was submitted to Plant Cell Biology, a section of the journal Frontiers in Plant Science

Received: *23 November 2020*
Accepted: *25 February 2021*
Published: *06 April 2021*

Citation:
Seo M and Lee J-Y (2021) Dissection of Functional Modules of AT-HOOK MOTIF NUCLEAR LOCALIZED PROTEIN 4 in the Development of the Root Xylem. Front. Plant Sci. 12:632078. doi: 10.3389/fpls.2021.632078

INTRODUCTION

The vascular system plays a key role in the transport and mechanical support processes in vascular plants. It is composed of two major tissues, the xylem and phloem, and undifferentiated stem cells between them. The organization of the vascular system is well defined in the *Arabidopsis* root apical meristem (**Figure 1A**). It is bisymmetrically organized with xylem vessels running through the center and two phloem poles located perpendicular to the xylem axis. On the xylem axis, protoxylem cells differentiate in the periphery and metaxylem cells differentiate in the center. Procambium cells, undifferentiated stem cells, occupy the region between the xylem and phloem (Mahonen et al., 2000). Five xylem vessels usually differentiate in a single row while neighboring procambium cells remain undifferentiated. This suggests the presence of a tight regulatory process that defines the xylem axis.

Given the importance of the vascular system in the success of plants in terrestrial environments, detailed molecular mechanisms underlying the development of this system have become available

in recent years (Vaughan-Hirsch et al., 2018; Chiang and Greb, 2019). Findings pertaining to the *Arabidopsis* root indicate that the processes generating xylem precursors and determining their cell fates and that differentiation require extensive interplay among transcription factors (TFs) and cell–cell signaling (Seo et al., 2020).

Several TFs provide positional information by directly moving between cells (Gallagher et al., 2014; Gundu et al., 2020). Among them, SHORTROOT (SHR) broadly impacts the specification and patterning of root tissues inside the epidermis and root cap (Benfey et al., 1993; Laurenzio et al., 1996; Helariutta et al., 2000; Sabatini et al., 2003; Carlsbecker et al., 2010). *SHR* is expressed in parts of the stele, e.g., the xylem precursors, procambium, and neighboring pericycle cells (Helariutta et al., 2000; Sena et al., 2004). Translated SHR protein moves into adjacent phloem pole and cell layers outside the stele, specifically the quiescent center (QC), cortex–endodermis initial (CEI), and endodermis (Nakajima et al., 2001). In the phloem pole, SHR induces asymmetric cell division for the formation of proto- and meta-phloem sieve elements (Kim et al., 2020). SHR moving outside of the stele maintains the QC, promotes asymmetric cell division in the CEI, specifies endodermis cell fate, and patterns xylem vessels. To regulate these processes, SHR induces the expression of *SCR* and BIRD family genes, including *JACKDAW* (*JKD*), *MAGPIE* (*MGP*), and *NUTCRACKER* (*NUC*) (Levesque et al., 2006; Moreno-Risueno et al., 2015), and then interacts with their proteins.

SHR, SCR, and one of the BIRD members form trimeric protein complexes which play a role in downstream gene expression (Gallagher et al., 2004; Cui et al., 2007; Welch et al., 2007; Long et al., 2015). SHR–SCR with either MGP or NUC promotes asymmetric cell division of the CEI to generate the cortex and endodermis layers (Welch et al., 2007; Long et al., 2015). This requires the activation of D-type cyclin in the CEI (Sozzani et al., 2010). Spatial restriction of D-type cyclin to the CEI is achieved *via* the competitive inhibitory binding of JDK to SHR–SCR (Long et al., 2015). A recent study of the structure of the SHR–SCR complex (Hirano et al., 2017) suggested that the α/β core subdomain of the SHR protein can specifically recognize BIRD proteins. Spatiotemporally coordinated interactions between BIRD proteins and SHR–SCR enable tissue patterning and cell division at the proper time and in the correct places (Moreno-Risueno et al., 2015; Long et al., 2017). Furthermore, this protein–protein interaction is critical for controlling the intercellular movement of SHR (Gallagher et al., 2004; Cui et al., 2007; Long et al., 2015). SHR–SCR–BIRD complexes target the nuclei, which blocks the movement of SHR to an adjacent cell layer.

Some mobile TFs are under the regulation of plant hormones. As the auxin gradient is established during embryogenesis, MONOPTEROS (MP) activates the expression of several downstream targets, including *TARGET OF MONOPTEROS 7* (*TMO7*) (Schlereth et al., 2010). TMO7, a small basic helix-loop-helix protein, moves into the hypophysis and promotes cell division of the hypophysis for QC formation (Lu et al., 2018). In postembryonic *Arabidopsis* roots, mutual inhibitory actions between auxin and cytokinin contribute to the bisymmetric organization of the xylem and phloem (Bishopp et al., 2011). Cytokinin on the phloem side promotes the expression of *PHLOEM EARLY DOF 1* (*PEAR1*) and its homologs. PEARs then move to neighboring procambial cells and there suppress the expression of HD-ZIP IIIs, which function as repressors of cell division (Miyashima et al., 2019). Our group previously reported that two AT-HOOK MOTIF NUCLEAR LOCALIZED PROTEIN (AHL) family members, AHL3 and AHL4, are also possible mobile outputs of cytokinin to regulate the xylem axis in the *Arabidopsis* root (Zhou et al., 2013). During this regulation process, the AHL4 protein interacts with AHL3. Because interaction and movement are frequently discovered as characteristics of mobile TFs involved in cell type patterning, dissecting these two aspects is important to understand the molecular mechanisms.

In *Arabidopsis*, there are 29 genes encoding AT-hook TF family members (Consortium, 2011; Zhao et al., 2014), which are classified into two major clades: clades A and B. Some AHLs in clade A are known to regulate plant growth and development processes, such as hypocotyl and petiole elongation, leaf senescence, and gibberellin synthesis (Matsushita et al., 2007; Street et al., 2008; Xiao et al., 2009; Favero et al., 2020). Based on the amino acid sequence alignment of AHL proteins, all AHL members contain two highly conserved motifs: the AT-hook motif and the plant and prokaryotes conserved (PPC) domain (Fujimoto et al., 2004). The AT-hook motif contains a conserved palindromic core with a sequence of three amino acids (Arg-Gly-Arg) that can bind to the minor groove of the AT-rich B form of DNA (Reeves and Nissen, 1990; Huth et al., 1997). The PPC domain is approximately 120 amino acids in length and is highly conserved among AHL proteins (Fujimoto et al., 2004; Lin et al., 2007). The PPC domain in AHL29 of clade A has been shown to be involved in the protein–protein interactions with other AHL members (Zhao et al., 2013).

To understand how AHL4 in clade B regulates xylem development, we defined the AHL4 full-length protein into three domains and investigated the molecular function of each domain. For the domain analyses, we chose AHL1 as a counterpart, which is relatively close to AHL4 in the phylogenetic tree but does not have intercellular mobility, and generated a series of chimeric proteins between AHL1 and AHL4. Multifaceted analyses of the behaviors of these chimeras enabled us to understand how each domain serves as a functional module of AHL4.

MATERIALS AND METHODS

Plant Material and Growth Condition

Arabidopsis thaliana ecotype Columbia-0 (Col-0) was used throughout this research. *ahl4* mutant (SALK_124619) was obtained from the ABRC in a previous study (Zhou et al., 2013). Seedlings for confocal imaging were germinated and grown vertically on the surface of the Murashige and Skoog (MS) solid medium supplemented with 1% sucrose. Before plating on the MS media, the seed surface was sterilized. Seeds on the MS media were stratified for 2 days at 4°C and then grown vertically in a

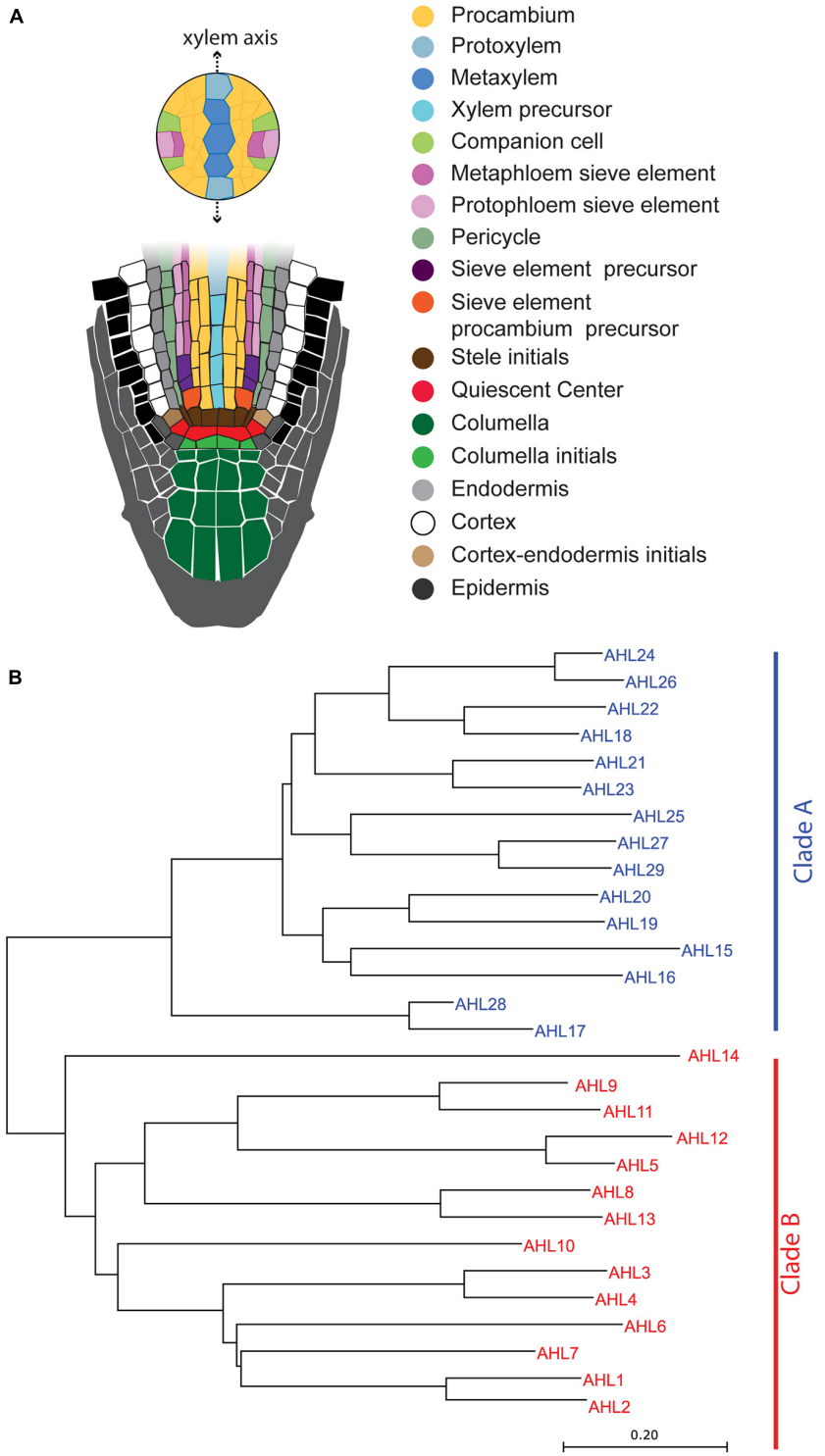

FIGURE 1 | Schematic illustration of the *Arabidopsis* root apical meristem and phylogenetic tree of AT-HOOK MOTIF NUCLEAR LOCALIZED PROTEINS (AHLs): **(A)** schematic illustration of the *Arabidopsis* root apical meristem. **(B)** Phylogenetic tree of AHL proteins in *Arabidopsis*. The evolutionary history was inferred using the neighbor-joining method (Saitou and Nei, 1987). The optimal tree with the sum of the branch length being 10.17264217 is shown. The tree is drawn to scale, with branch lengths in the units identical to those of the evolutionary distances used to infer the phylogenetic tree.

growth chamber that was constantly maintained at 22°C with a cycle of 16-h days and 8-h nights.

Inference of the Phylogeny of AT-Hook Family Transcription Factors

All AHL family protein sequences used in this report were downloaded from TAIR[1]. The full-length amino acid sequences were subsequently aligned with Clustal Omega[2] (Madeira et al., 2019). The phylogenetic relationship was analyzed using the MEGA X program (Kumar et al., 2018), with the neighbor-joining method (Saitou and Nei, 1987). The tree is drawn to scale, with branch lengths in the same units as those of the evolutionary distances used to infer the phylogenetic tree. The evolutionary distances were computed using the Poisson correction method (Zuckerkandl and Pauling, 1965) and are expressed here in units of the number of amino acid substitutions per site.

Cloning of the PPC Domain and AHL Protein Coding Sequences

All the *AHL* protein coding regions used in yeast two-hybrid assays, except for *AHL3* and *AHL4*, were amplified from the root cDNA of Col-0 using polymerase chain reactions (PCR). PPC domains of *AHL3* and *AHL4* coding regions were amplified from *AHL3* and *AHL4* cloned in pENTR221, respectively (Zhou et al., 2013). PCRs were performed using Phusion® High-Fidelity DNA Polymerase (New England Biolabs). Forward primers and reverse primers used in PCRs are indicated in **Supplementary Table 3**. Amplified DNAs from PCR were purified by HiGene™ Gel and PCR purification system (BIOFACT). Except for *AHL1*, other *AHL* genes were inserted into pENTR™/D-TOPO™ vector by pENTR/D-TOPO Cloning Kit (Invitrogen). The *AHL1* gene was cloned by BP Clonase reaction. The TOPO and BP reactions were proceeded following the manufacturer's instruction. The reaction mixture was transformed into *Escherichia coli* TOP10-competent cells and clones with expected cDNA inserts were identified. All the constructs were confirmed by Sanger sequencing.

AHL1 Promoter Cloning

Gateway technology (Invitrogen) was used for cloning the *AHL1* promoter. Two-step PCRs and the BP Clonase reaction were used to clone the upstream intergenic region of *AHL1* (*pAHL1*) into the pDONR P4_P1R vector. The primary PCR amplified the region encompassing the upstream and downstream sequences of *pAHL1* using the genomic DNA of Col-0 as a template. The primary PCR amplicant was used as a template for the second PCR to amplify *pAHL1* attached to attB sites. Phusion® High-Fidelity DNA Polymerase (New England Biolabs) was used for the PCRs. For primary PCR, promoter AHL1 _3kb_F and promoter AHL1_R primers were used, and for secondary (containing attB site) PCR, promoter AHL1_3kb_Sense and promoter AHL1_Antisense were used. Sequence information about the primers is presented in **Supplementary Table 3**. The BP cloning reaction and *E. coli* transformation were conducted following the manufacturer's instructions. The *AHL1* promoter clone was finally confirmed by Sanger sequencing.

AHL1–AHL4 Chimeric Protein Cloning

For the cloning of chimeric proteins, the Gibson method was used (Gibson et al., 2009; Gibson, 2011). A set of primers were designed by NEBuilder® [3]. The primers used in the PCRs are indicated in **Supplementary Table 3**. To clone AHL4-4-1, GB_AHL1_D3_F/GB_AHL1_D3_R (template: AHL1 CDS in p221) were used for insert fragment cloning and GB_p221_AHL4_D1D2_F/GB_p221_AHL4_D1D2_R (template: AHL4 CDS in p221) were used for vector fragment cloning. To clone AHL4-1-1, GB_AHL4 _D1_F/GB_AHL4_D1_R (template: AHL4 CDS in p221) were used for insert fragment cloning and GB_p221_AHL1 _D2D3_F/GB_p221_AHL1_D2D3_R (template: AHL1 CDS in p221) were used for vector fragment cloning. To clone AHL1-1-4, GB_AHL4_D3_F/GB_AHL4_D3_R (template: AHL4 CDS in p221) were used for insert fragment cloning and GB_p221_AHL1_D1D2_F/GB_p221_AHL1_D1D2_R (template: AHL1 CDS in p221) were used for vector fragment cloning. To clone AHL1-4-4, GB_AHL1_D1_F/GB _AHL1_D1_R (template: AHL1 CDS in p221) were used for insert fragment cloning and GB_p221 _AHL4_D2D3_F/GB_p221_AHL4_D2D3_R (template: AHL4 CDS in p221) were used for vector fragment cloning. Then, 4 μl of purified insert, 1 μl of purified vector, and 5 μl 2 × Gibson Assembly Master Mix (New England Biolabs)® were mixed and incubated at 50°C for 1 h. The reaction mixture was subsequently transformed into *E. coli* DH5a (dam$^+$ strain), and the cloned plasmids from *E. coli* were purified and screened to select the predicted chimera. All the chimera constructs were confirmed by Sanger sequencing.

Cloning Transcriptional and Translational GFP Fusion Constructs

To generate transcriptional and translational GFP fusion constructs, Multisite Gateway LR cloning was used. Promoters were cloned into the pDONR P4_P1R vector. CDS for translational fusion without a stop codon was cloned into the pDONR221 vector. Free GFP and erGFP cloned into pDONR P2R_P3 were used (Lee et al., 2006). Then, *pAHL1*:erGFP, *pAHL1*:AHL1-GFP, *pSHR*:AHL1-GFP, *pSHR*:AHL4-GFP, *pSHR*:AHL4-4-1-GFP, *pSHR*:AHL4-1-1-GFP, *pSHR*:AHL1-1-4-GFP, *pSHR*:AHL1-4-4-GFP, *pWOL:AHL1*-GFP, and *pWOL*:AHL4-GFP were constructed into dpGreen-BarT (Lee et al., 2006) by means of an LR Clonase™ II Plus enzyme reaction (Invitrogen). *pAHL4*:erGFP and *pAHL4*:AHL4-GFP transgenic plants were generated in a previous study (Zhou et al., 2013).

Floral Dipping and Transgenic Selection

All constructs in dpGreen-BarT were transformed into *Agrobacterium tumefaciens* GV3101 with pSOUP and were transformed into either the wild type or *ahl4* by the floral

[1]https://www.arabidopsis.org

[2]https://www.ebi.ac.uk/Tools/msa/clustalo

[3]http://nebuilder.neb.com

dipping method (Clough and Bent, 1998). Every transgenic line containing a target transgene was selected with a 2,000-fold diluted Basta (Bayer Crop Science) solution on soil or 10 μg/ml of glufosinate ammonium (Fluka) on MS media.

Yeast Vector Cloning

Each of the AHL3, AHL4, and PPC domains of AHL3 and AHL4 in pENTR221 was cloned into both pDEST22, a prey vector for fusion with the GAL4 activation domain, and pDEST32, a bait vector for fusion with GAL4 DNA-binding domain, using Gateway LR recombination. Other AHLs and AHL1–AHL4 chimeras, AHL4-4-1, AHL4-1-1, AHL1-1-4, and AHL1-4-4, in pENTR221 were cloned into pDEST22. For LR reaction, 3 μl of each donor plasmid, 1 μl of pDEST22 or pDEST32, and 1 μl of LR II clonase were mixed and incubated for 1 h at room temperature. Then, the reaction mixture was transformed into *E. coli* TOP10-competent cells and screened for clones with expected cDNA inserts. All the constructs were confirmed by Sanger sequencing.

Yeast Two-Hybrid Assay

A ProQuest two-hybrid system (Invitrogen) was used for the yeast two-hybrid analysis. All of the procedures were performed according to the manufacturer's standard protocol. Recombinant hybrid proteins were tested for self-activation. Plasmids between the pDEST32 and the pDEST22 vector were used as negative control. Plasmid DNA pairs between pEXP32-Krev1 and pEXP22-RalGDS were used as controls for positive interactions. To judge the protein–protein interaction, the 3-amino-1,2,4-triazole (3-AT) assay method was used. For the 3-AT assay, each yeast transformant was placed into 1.5 ml of SD^{2-} (Leu^-/Trp^-) liquid media. After incubation for 2 days at 30°C, the OD_{600} value was measured using a biophotometer spectrometer (Eppendorf). Next, every yeast culture was diluted to an OD_{600} value of 0.1 by adding pure SD^{2-} (Leu^-/Trp^-) media. These diluted transformants were dropped onto SD^{2-} (Leu^-/Trp^-) media, SD^{3-} ($Leu^-/Trp^-/His^-$) media, SD^{3-} ($Leu^-/Trp^-/His^-$) media with 10 mM 3-AT, SD^{3-} ($Leu^-/Trp^-/His^-$) media with 20 mM 3-AT, and SD^{3-} ($Leu^-/Trp^-/His^-$) media with 40 mM 3-AT. These yeast droplets on the selection media were incubated at 30°C for 2 days.

Vibratome Sectioning of Roots for Confocal Microscopy

For *Arabidopsis* xylem pattern phenotyping, 5 DAT (days after transfer to growth chamber from stratification) seedlings were used. Five to six seedlings overlaid straight on a MS plate were pulled together and then dipped into 4% low-melting temperature SeaPlaque® Agarose (Lonza), which was melted in 1 × PBS buffer (pH 7.5). Next, the seedlings in the 4% agarose solution were placed in disposable base molds (30 mm × 24 mm × 5 mm). The solidified agarose was cut into a block and sectioned using a vibratome (Leica VT1000S), resulting in thicknesses in the range of 100–120 μm. For observation of the cell boundaries under a confocal microscope, each slice was stained with 10 μg/ml of a Calcofluor white M2R (Sigma-Aldrich) solution.

Confocal Microscopy

To visualize the GFP protein, 5 DAT seedlings were stained with 10 μg/ml of a propidium iodide (PI) solution (Life Technologies) for 2 min and imaged with a confocal microscope. Subsequently, a 500 × PI solution (5 mg/ml) was prepared and diluted with a 1 × PI solution in water before staining. Images were taken on a Carl Zeiss LSM700 and a Leica TCS SP8 confocal microscope with an argon-ion laser (488 nm excitation and 509 nm emission for GFP; 493 nm excitation and 636 nm emission for PI; 349 nm excitation and 420 nm emission for Calcofluor white M2R).

Statistical Analysis

All statistical analyses were performed using RStudio v.1.4.1103. A non-parametric chi-square test of goodness of fit was conducted to determine the *p*-value of each dataset. Bar graphs were generated by GraphPad Prism v.8.4.0 (Motulsky and Christopoulos, 2004).

RESULTS

The PPC Domain of AHL4 Mediates Protein–Protein Interaction

A total of 29 AHL proteins in *Arabidopsis* can be classified into two major clades, clade A and clade B (**Figure 1B**), as defined by Zhao et al. (2014). These clades are supported by major differences in amino acid sequences of the PPC domains of the AHLs. Clade A has a type of PPC domain which starts with Leu-Arg-Ser-His, and clade B has another type of PPC domain which starts with Phe-Thr-Pro-His (Zhao et al., 2014). The PPC domain of the AHL proteins in clade A was found to mediate the protein–protein interaction (Zhao et al., 2013). However, the PPC domain sequences between clade A and clade B are quite different; therefore, it remains unknown as to whether the PPC domain of clade B also serves to mediate the interaction between AHL proteins.

AHL3 and AHL4 are clade B AHLs. To define the role of the PPC domain in the clade B AHLs, we cloned the PPC domains of AHL3 and AHL4 into yeast expression vectors and then analyzed the interactions between the AHL3/4 proteins and the cloned PPC domains. A series of 3-AT was used to prevent autoactivation by the bait. We found that the PPC domains of AHL3 and AHL4 interact well with full-length AHL3/AHL4 proteins (**Figure 2A**). The criterion of protein–protein interaction was whether a yeast colony appeared on the $SD3^-$ media with 20 mM of 3-AT. We extended these assays to other 14 AHL members, finding that the PPC domain of AHL4 does not interact with that of the AHL in clade A, whereas it does interact with AHLs belonging to the same subclade as AHL4, except for AHL2 (**Figure 2B**). These data suggest that the PPC domain in the AHL4 protein functions as a key mediator of protein–protein interactions to form homomeric or heteromeric proteins

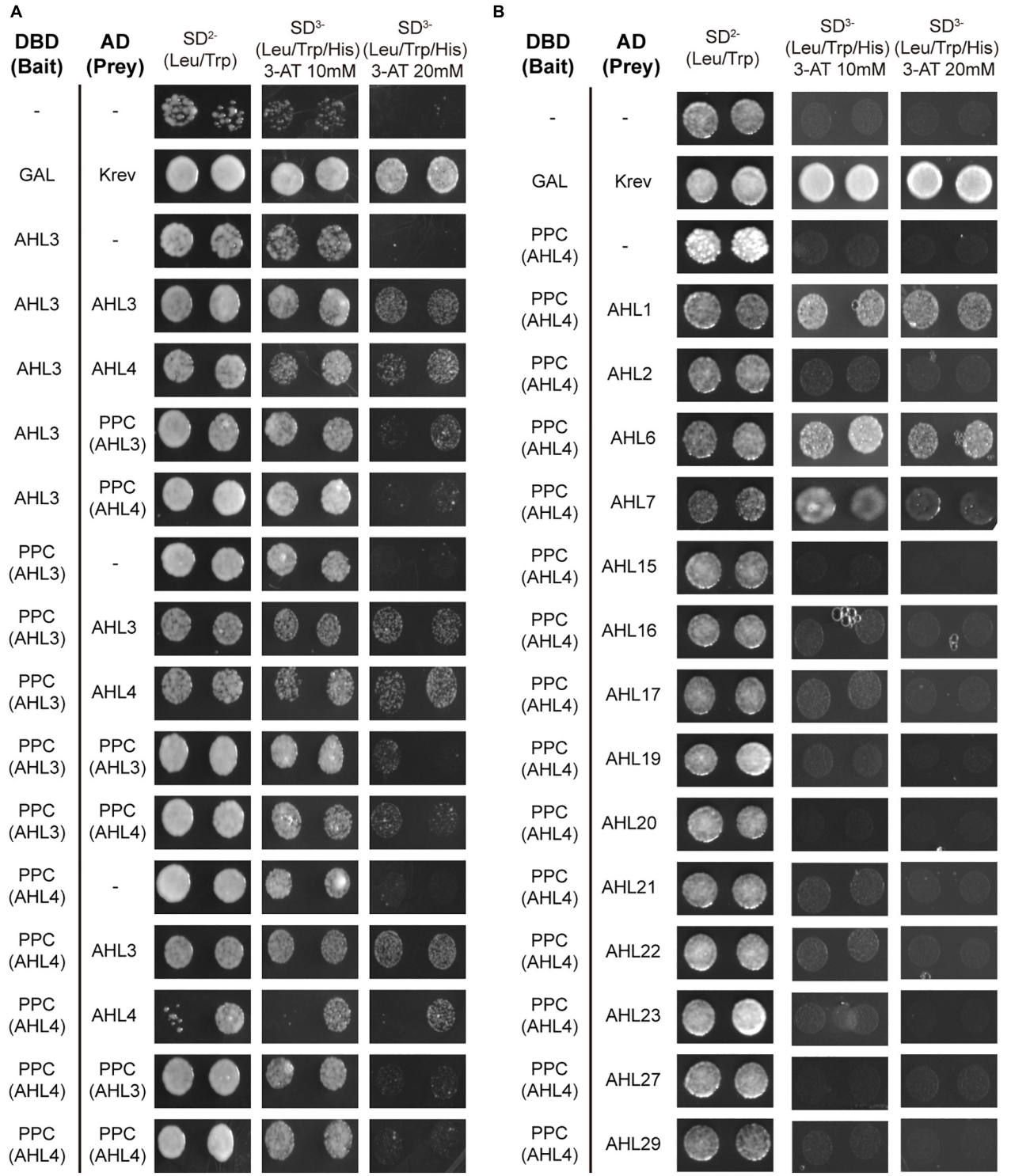

FIGURE 2 | Plant and prokaryotes conserved (PPC) domain of AHL4 mediates protein–protein interaction specific to clade B AHLs. **(A)** Analysis of the PPC domain of AHL3 and AHL4 in the protein–protein interactions using yeast two-hybrid assays. **(B)** Analysis of the PPC domain of AHL4 during interactions with other AHLs using a yeast two-hybrid assay. Left column, a pair of interactors; upper row, series of selection media. DBD (bait), DNA-binding domain; AD (prey), activation domain.

and that it provides specificity to interact with AHL proteins in the same clade.

AHL1 and AHL4 Show Differences in Spatial Expression Patterns and Intercellular Mobility Levels

In the phylogenetic analysis, AHL3 and AHL4 belong to the subclade that includes AHL1, AHL2, AHL6, and AHL7 (**Figure 1B**). While *AHL3*, *AHL4*, and *AHL6* showed enriched expression levels in the xylem precursor in *Arabidopsis* roots, *AHL1*, *AHL2*, and *AHL7* showed broad expression levels in multiple cell types (**Supplementary Figure 1**; Zhang et al., 2019). For further analyses of AHL4 protein domains, we selected AHL1 and compared its behavior with that of AHL4.

First, we aimed to define the transcriptional domain of *AHL1* and the intercellular mobility of AHL1 proteins in the root meristem. To this end, we cloned the 3,265-bp-long upstream intergenic region of *AHL1* (*pAHL1*) and attached the endoplasmic reticulum-targeted green fluorescence protein (erGFP). This construct, *pAHL1:erGFP*, which we call transcriptional fusion, was introduced into wild type Col-0. We also made translational fusion lines in Col-0 which express the AHL1 protein fused with a free GFP driven by *pAHL1*. In our confocal microscopy observations, the GFP signal of the *AHL1* transcriptional fusion lines was very low, making it challenging for us to discern the cell layers with GFP expression from those with autofluorescence (**Supplementary Figures 2A,B**). Nevertheless, the GFP signal was higher in the epidermis and stele region than in the cortex and endodermis (**Supplementary Figure 2B**). The GFP intensity in the translational fusion lines was much higher than that in the transcriptional fusion lines (**Supplementary Figure 2C**). Due to the major difference in the GFP intensity levels between the transcriptional and translational fusion lines, we could not determine the intercellular mobility of AHL1. We compared the *AHL1* expression patterns with those in *AHL4* transcriptional (**Supplementary Figure 2D**) and translational fusion lines (**Supplementary Figure 2E**). The spatial expression of *AHL4* transcriptional fusion was restricted to the subset of the stele, while AHL4 translational fusion GFP was broadly found in the stele, consistent with a previous report (Zhou et al., 2013).

The intercellular mobility of AHL1 was unclear when it was examined with its own promoter. Thus, we employed the promoter of *SHR*, which is well defined. We expressed erGFP under the *SHR* promoter (*pSHR:erGFP* in the Col-0) as a non-mobile control (**Figure 3A**) (Gallagher et al., 2004) and compared its expression domains with those of GFP translationally fused with AHL1 and AHL4 in each case. The expression levels of these proteins were imaged in five to seven individuals of at least five independent T2 lines. *pSHR:erGFP* started GFP expression broadly right above the QC and then became restricted to the xylem and procambium (**Figure 3A**). We observed AHL4-GFP throughout the stele and endodermis in all five transgenic lines analyzed (**Figure 3B**). However, the expression of AHL1-GFP was found only in the stele cells and not in the endodermis (**Figure 3C**). Z-stack images of each transgenic line were consistent with the longitudinal images (**Figures 3D–F**). We also noted that the expression level of the AHL1 protein was remarkably lower than that of the AHL4 protein. Nevertheless, our results collectively indicate that AHL1 is not mobile between cells, in contrast to AHL4. To reconfirm this finding, we also checked the expression patterns of GFP fused to either AHL1 or AHL4 under the *WOODEN LEG* (*WOL*) promoter (**Figures 3G–J**) (Mahonen et al., 2000). Consistent with AHL4/AHL1-GFP driven by the *SHR* promoter, AHL4-GFP expressed under the *WOL* promoter expanded its domain to the endodermis, while AHL1-GFP did not (**Figures 3G–J**).

Design of Chimeric Proteins Between AHL4 and AHL1 to Identify Functional Modules

Proteins consist of modules (domains) with distinctive structural/functional features (Lin et al., 2005, 2007). AHL members are defined by a highly conserved PPC domain in the middle and one or two DNA-binding AT-hook domains in the N-terminus. To determine the functional modules of AHL4, its amino acid sequence was compared with AHL1, which does not have intercellular mobility. The amino acid alignment showed three distinctive regions separated by a PPC domain in the middle (**Figure 4A**). In the alignment, the N-terminus and C-terminus regions separated by the PPC domain are dissimilar between AHL1 and AHL4; however, there is a well-conserved AT-hook motif located in the N-terminus region. In our search for a nuclear localization signal (NLS) in the AHL1 and AHL4 protein sequences using the NLS Mapper (Kosugi et al., 2009), one NLS in the C-terminus of AHL1, two in the N-terminus of AHL4, and one in the C-terminus of AHL4 were detected (**Figure 4A**). To characterize the functional modules of AHL4, we divided the AHL1 and AHL4 protein sequences into three domains: N-terminus, PPC domain, and C-terminus. Then, we designed four chimeric proteins, each of which had partial sequences from both the AHL1 and AHL4 proteins by means of Gibson cloning (**Figure 4B**). The first of these, AHL4-4-1, had the AHL4 N-terminus, the AHL4 PPC domain, and the AHL1 C-terminus. The second, AHL4-1-1, had the AHL4 N-terminus, AHL1 PPC domain, and AHL1 C-terminus. The third, AHL1-1-4, had the AHL1 N-terminus, AHL1 PPC domain, and AHL4 C-terminus. The last domain, AHL1-4-4, had the AHL1 N-terminus, AHL4 PPC domain, and AHL4 C-terminus.

It was previously shown that the interaction between AHL4 and AHL3 proteins affects the intercellular movement of the AHL4 protein (Zhou et al., 2013). Accordingly, we examined whether four chimeric proteins still interact with the AHL3 protein as one indication of the maintenance of functional integrity. To do this, we cloned the chimeric proteins and AHL3 into yeast expression vectors and analyzed the interactions between each of the chimeric proteins and AHL3 using a yeast two-hybrid assay (**Supplementary Figure 3**). It was found that AHL1 and all four chimeric proteins interact with the AHL3 protein. Therefore, creating chimeric proteins did not affect the protein–protein interaction capacity.

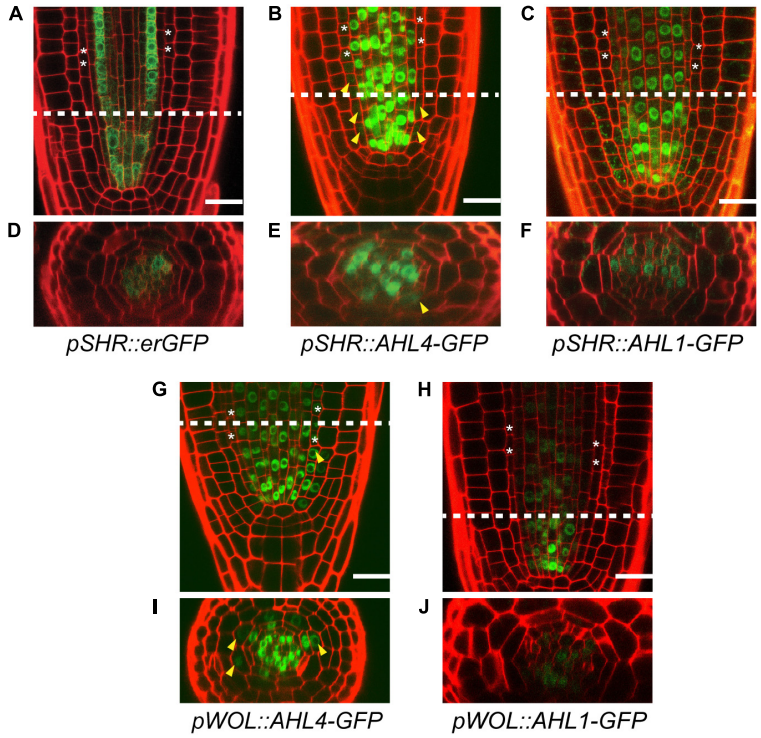

FIGURE 3 | Comparison of the intercellular movements of AHL1 and AHL4 under the *SHR* and *WOL* promoters. Longitudinal views of root apical meristems expressing *pSHR:erGFP* **(A)**, *pSHR:AHL4-GFP* **(B)**, and *pSHR:AHL1-GFP* **(C)**. **(D–F)** Cross-sectional images of the dashed-line positions of panels **(A–C)**. Longitudinal views of root apical meristems expressing *pWOL:AHL4-GFP* **(G)** and *pWOL:AHL1-GFP* **(H)**. **(I,J)** Cross-sectional images on the dashed-line positions of panels **(G,H)**. White asterisks, endodermis; yellow arrowheads, GFP moved to the endodermis; scale bars = 20 μm.

C-Terminus Domain of AHL4 Confers Intercellular Mobility

After confirming that all chimeric proteins from AHL1 and AHL4 interacted with the AHL3 protein (**Supplementary Figure 3**), we generated transgenic lines expressing each of the chimeric proteins to study their cell-to-cell mobility characteristics. We introduced the following constructs, *pSHR:AHL4-4-1-GFP*, *pSHR:AHL4-1-1-GFP*, *pSHR:AHL1-1-4-GFP*, and *pSHR:AHL1-4-4-GFP*, into the wild type Col-0 background. Then, we observed the localization of GFP proteins in T2 seedling roots of each transgenic line under a confocal microscope. For AHL4-4-1-GFP (**Figures 4C–E**) and AHL4-1-1-GFP (**Figures 4F–H**), GFP was restricted to the stele. In contrast, AHL1-1-4-GFP (**Figures 4I–K**) and AHL1-4-4-GFP (**Figures 4L–N**) were observed outside of the stele.

The N-Terminus Domain of AHL4 Is Required for the Regulation of Xylem Development

Next, we investigated whether any of these four chimeric proteins can complement the *ahl4* mutant phenotype. In a previous paper, we reported that the *ahl4* mutant shows a higher frequency of the extra-xylem phenotype than the wild type; however, this report lacked a quantitative analysis (Zhou et al., 2013).

To analyze the xylem phenotype in a quantitative manner, we cross-sectioned the root differentiation zone of wild type *Arabidopsis* seedlings using a vibratome, stained the sections with Calcofluor white, and then imaged them under a confocal microscope (**Figures 5A–D**). Based on this quantitative phenotyping, we categorized xylem organizations into four types. We considered large cells with thickened cell walls as differentiated xylem vessels. The first type is defined as "normal" because it is the most abundant phenotype in the wild type with two protoxylem cells on both ends of the xylem axis and three metaxylem cells in the center (**Figure 5A**). The second type is defined as "4 xylem cells," having only four xylem cells on the xylem axis even after the xylem cell wall thickening process (**Figure 5B**). The third phenotype is "6 xylem cells in a row," having an extra xylem cell along the xylem axis (**Figure 5C**). The last phenotype is called "extra-xylem," having a differentiated extra protoxylem or metaxylem cell present outside the single row of xylem cells (**Figure 5D**). To ensure that the aforementioned types of xylem organization in the root differentiation zone are consistent with the organizations of the xylem precursors in the root meristem, we analyzed the GFP expression levels of typical molecular marker lines in the root meristem (**Supplementary Figure 4**). These are *pTMO5:erGFP* to denote the xylem axis (Lee et al., 2006), *pARR5:erGFP* for procambium cells (Lee et al., 2006), and *pAHP6:erGFP* for protoxylem cell and two neighboring pericycle cells (Mahonen et al., 2006). This molecular marker

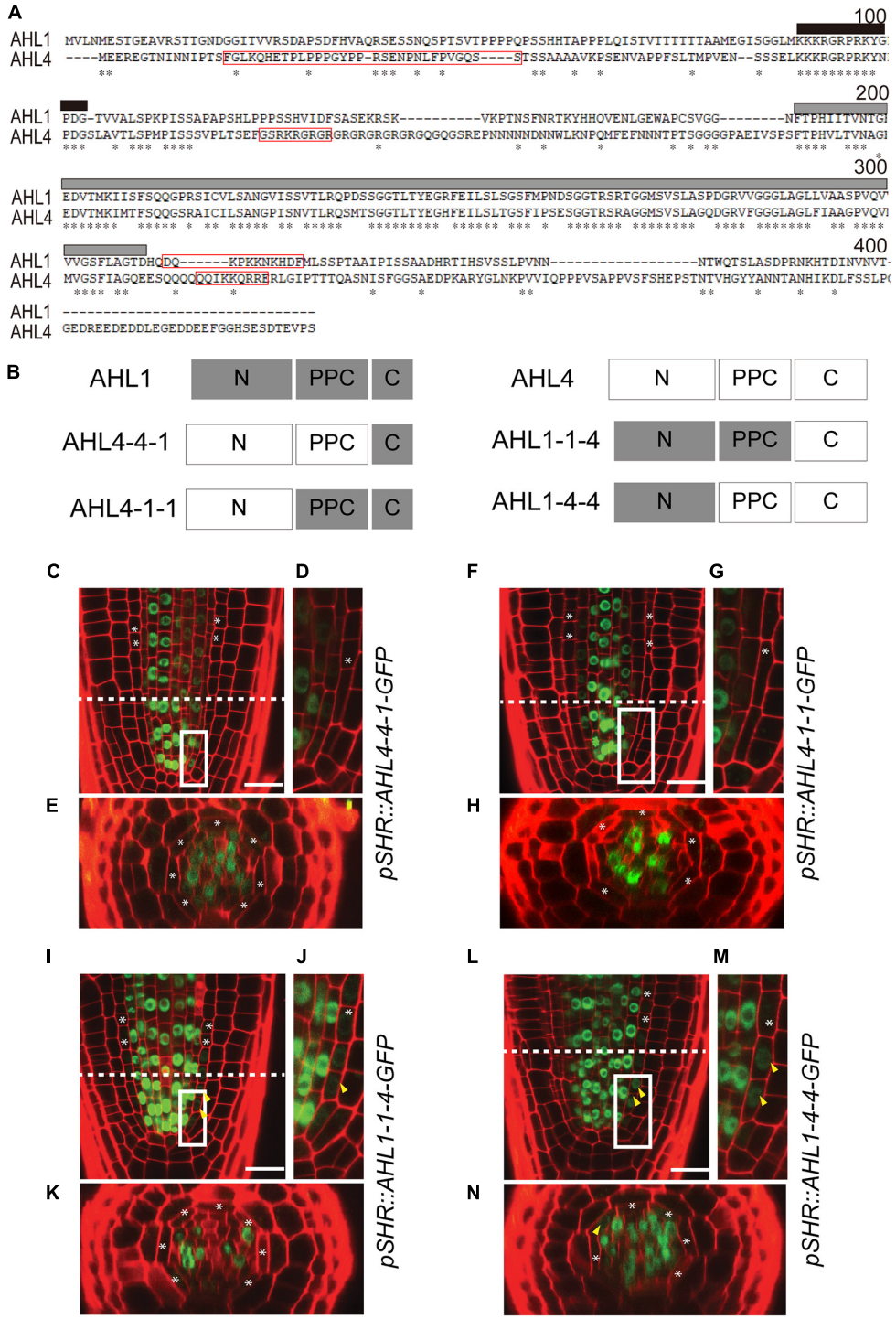

FIGURE 4 | Intercellular movement of AHL1–AHL4 chimeric proteins: **(A)** Amino acid sequence alignment of AHL1 and AHL4 using the AlignX program (Lu and Moriyama, 2004). Asterisks, identical amino acids; red box; NLS sequence; black box, AT-hook motif; gray box, PPC domain. **(B)** Schematic illustration of four chimeric proteins between AHL1 and AHL4. Dark gray box, domain from the AHL1 protein; white box outlined in the light gray, domain from the AHL4 protein. **(C–N)** Confocal microscopy of roots expressing chimeric proteins in the wild type Col-0. **(C–E)** *pSHR:AHL4-4-1-GFP*, **(F–H)** *pSHR:AHL4-1-1-GFP*, **(I–K)** *pSHR:AHL1-1-4-GFP*, and **(L–N)** *pSHR:AHL1-4-4-GFP*. **(D,G,J,M)** Magnified images of regions outlined in white in panels **(C,F,I,L)**. **(E,H,K,N)** Cross-sectional images of the dashed-line positions of panels **(C,F,I,L)**. White asterisks, endodermis; yellow arrowheads, GFP moved into the endodermis; scale bar = 20 μm.

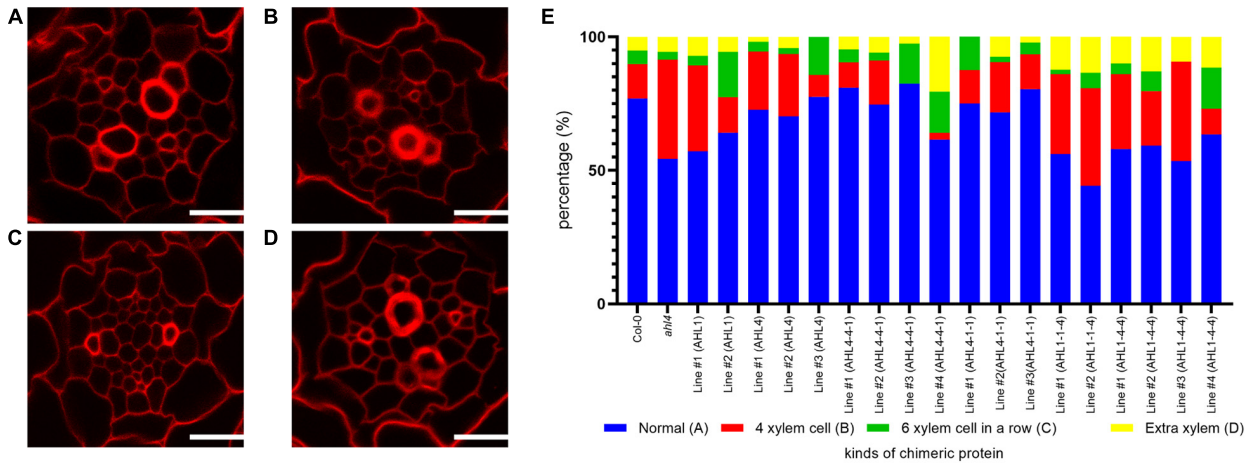

FIGURE 5 | Xylem phenotype recovery by chimeric proteins that are expressed in the stele of the *ahl4* mutant: **(A–D)** Four typical phenotypes of xylem arrangements categorized in the root. Normal phenotype **(A)**, "four xylem cells" phenotype **(B)**, "six xylem cells in a row" phenotype **(C)**, and "extra-xylem" phenotype **(D)**. Scale bars = 20 μm. **(E)** Distribution of the xylem phenotypes of the wild type, *ahl4*, and *ahl4* expressing each chimeric protein, as categorized in **(A–D)**. n = 39∼85. All of the detailed scoring data are presented in **Supplementary Table 1**.

analysis suggested that the xylem phenotype can be divided into four classes, consistent with our classification of four xylem cell phenotypes based on cell wall thickening in the differentiation zone.

In our analyses of 39 wild type Col-0 individuals, 77% showed the "normal" xylem type and 23% showed variant xylem types. When we analyzed 66 individuals of the *ahl4* mutant, we found a reduction of the "normal" type to 54% and an increase of variant types. Next, we analyzed *ahl4* introduced with chimeric proteins expressed under the *SHR* promoter. Because the *SHR* promoter drives transcription in the xylem precursor, procambium, and neighboring pericycle, it can cover the region into which the AHL4 protein moves to function. We thus used the same constructs used for the analysis of intercellular mobility to analyze the complementation of the *ahl4* phenotype.

Before checking whether chimeric proteins can rescue *ahl4* or not, we analyzed the cases of *pSHR:AHL4-GFP; ahl4* and *pSHR:AHL1-GFP; ahl4*. In the AHL4 case, we noted the recovery of the xylem phenotype to "normal" in three independent transgenic lines. The percentage of "normal" increases from 54 to 73% on average. On the other hand, in the AHL1 case, we noted that there is no meaningful change in the ratio of the xylem phenotype (two individual lines, 54 and 60%) (**Figure 5E**). Because AHL1 cannot recover the *ahl4* mutant phenotype, we conclude that the molecular function of AHL1 differs from that of AHL4.

In the analysis of transgenic plants with four different chimeric proteins, we determined the rescue of the xylem phenotype based on whether the frequencies of the "normal" phenotype are recovered to those of the wild type and the *pSHR:AHL4-GFP; ahl4* transgenic lines, which are between 73 and 77% (**Figure 5E**). We also performed chi-square test-based goodness-of-fit analyses between distributions of xylem types of transgenic lines and the reference genotypes (**Supplementary Table 1**). Under this criterion, we found that the recovery of the xylem phenotype was to "normal" in three out of four independent transgenic lines expressing *pSHR:AHL4-4-1-GFP; ahl4* (two lines with the xylem distribution similar to the wild type; p value of goodness-of-fit test > 0.5) and all three lines expressing *pSHR:AHL4-1-1-GFP; ahl4*. In contrast, two independent transgenic lines with *pSHR:AHL1-1-4-GFP; ahl4* (50% of the normal phenotype on average; p-values of goodness-of-fit test < 0.5) and four independent transgenic lines with *pSHR:AHL1-4-4-GFP; ahl4* (59% of the normal phenotype on average; p-values of goodness-of-fit test < 0.5) did not show a rescue of *ahl4* xylem phenotype. These data indicate that the chimeric proteins containing the AHL4 N-terminus can complement the *ahl4* xylem phenotype. In this context, the N-terminus of AHL4 is important for the specific functions of AHL4 during the xylem development process.

Intercellular Movement of AHL4 to the Xylem Axis Is Required for Its Regulation of Xylem Development

To reconfirm the importance of the N-terminus of AHL4 in the xylem development process, we analyzed the GFP expression levels and the xylem phenotype of the *ahl4* mutant introduced with *AHL4-4-1-GFP*, *AHL1-1-4-GFP*, or *AHL1-4-4-GFP* under the *AHL4* promoter. Given that the C-terminus of AHL4 confers intercellular mobility (**Figure 4**), we expected that the immobile AHL4-4-1-GFP protein would only be in the procambium area, while GFP fused to AHL1-1-4 or AHL1-4-4 would be mobile and would be found broadly in the stele. Consistent with our prediction, confocal microscopy indicated that AHL4-4-1-GFP was in the stele but excluded from the xylem axis (**Figures 6A,D**), while AHL1-1-4-GFP and AHL1-4-4-GFP were found throughout the stele (**Figures 6B,C,E,F**). The intercellular mobility of AHL1-1-4 and AHL1-4-4 appeared to be more extensive than that of AHL4 because the GFP fusion of the former two expanded not only throughout

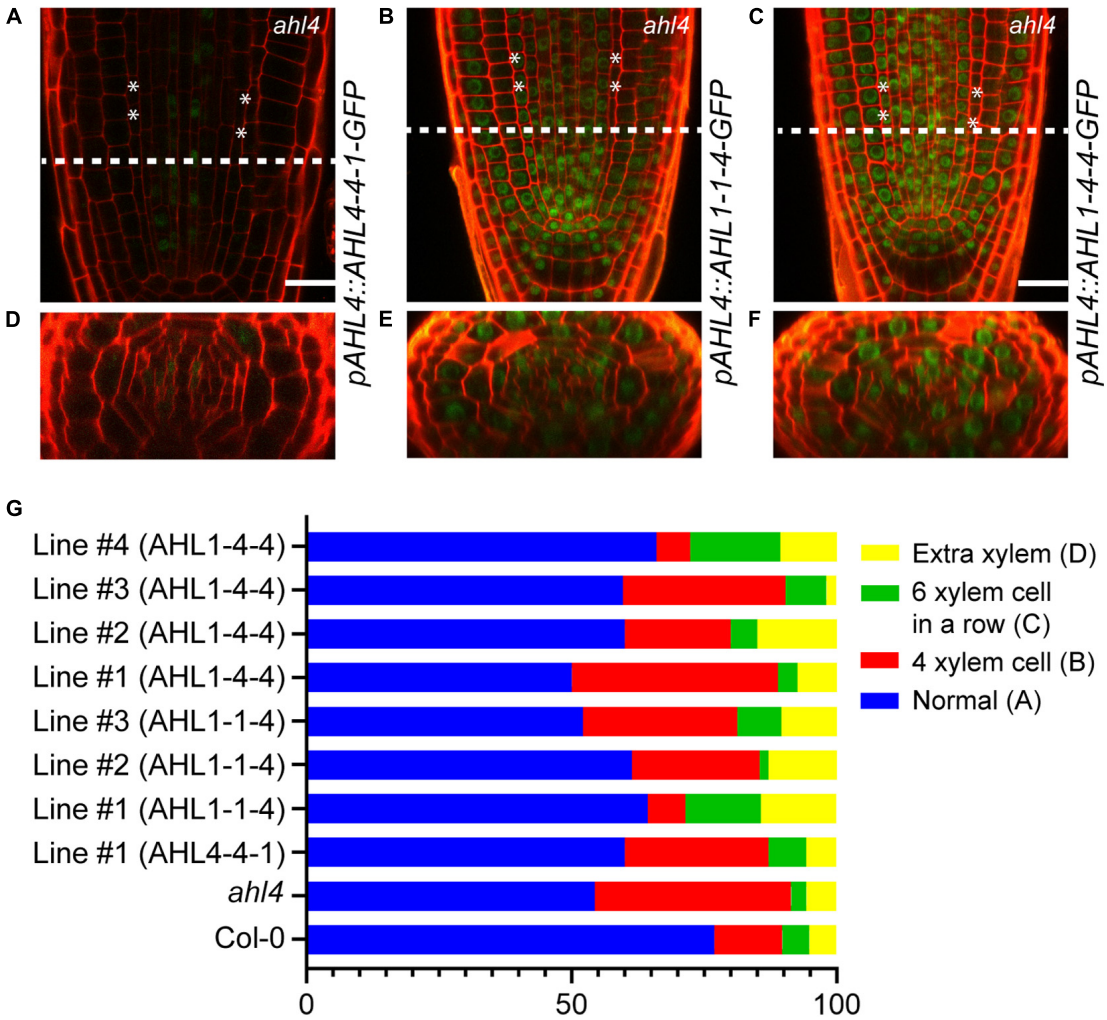

FIGURE 6 | Xylem phenotype rescue of the *ahl4* mutant by chimeric proteins expressed under the *AHL4* promoter. Longitudinal views of root apical meristems expressing *pAHL4:AHL4-4-1-GFP* **(A)**, *pAHL4:AHL1-1-4-GFP* **(B)**, and *pAHL4:AHL1-4-4-GFP* **(C)**. **(D–F)** Cross-sectional images of the dashed-line positions of panels **(A–C)**. Scale bars = 20 μm. **(G)** Distribution of xylem phenotypes of the wild type, *ahl4*, and *ahl4* expressing *pAHL4:AHL4-4-1-GFP*, *pAHL4:AHL1-1-4-GFP*, and *pAHL4:AHL1-4-4-GFP*. Xylem phenotype categorization is identical to that in **Figures 5A–D**. *n* = 27∼70. All detailed scoring data are presented in **Supplementary Table 2**.

the stele but also to the ground tissue, epidermis, quiescent center, and root cap.

Subsequently, we analyzed whether those chimeric proteins could recover the xylem phenotype in *ahl4*. Based on complementation analyses of chimeric proteins expressed under the *SHR* promoter (**Figure 5E**), AHL4-4-1 expressed under the *AHL4* promoter was predicted not to recover the *ahl4* phenotype because it cannot move into xylem precursor cells even though it has a functional domain in the N-terminus. AHL1-1-4 and AHL1-4-4 were also predicted not to rescue the *ahl4* phenotype because these two proteins do not have functional domains in the N-terminus even though they move into the xylem precursors. As predicted, one independent line expressing *pAHL4:AHL4-4-1-GFP; ahl4* showed only 60% of the "normal" phenotype. Three independent lines expressing *pAHL4:AHL1-1-4-GFP; ahl4* showed only 59% of the "normal" phenotype. Likewise, four independent lines expressing *pAHL4:AHL1-4-4-GFP* showed 59% of the "normal" phenotype (**Figure 6G** and **Supplementary Table 2**).

DISCUSSION

In this study, we characterized the functional domains of AHL4, one of the 29 AHLs in *Arabidopsis*. AHLs are largely classified into two clades, clades A and B, based on the amino acid sequences of the PPC domain. The PPC domain in clade A has been characterized as a mediator of the protein–protein interactions between AHL members in clade A (Zhao et al., 2013). In the N-terminus region outside the PPC domain, there are one or two AT-hook motifs, a condition required for DNA binding (Fujimoto et al., 2004). Other than the AT-hook motif, the

N-terminus and C-terminus regions outside of the PPC domain are highly variable among AHLs.

AHL4 belongs to clade B and has one AT-hook motif. Our group reported that AHL4 controls xylem development in the root meristem by moving from the procambium to the xylem precursor (Zhou et al., 2013). However, how the functions of AHL4 are differentiated from those of other AHLs remains elusive. To address this, we divided the AHL4 protein into three domains and investigated the function of each domain. First, we isolated the PPC domains of AHL3 and AHL4 and examined their interactions with AHL3 and AHL4 as well as other AHLs (**Figure 2**). Our yeast two-hybrid assays suggest that the PPC domains alone can interact with the AHL3 or AHL4 protein (**Figure 2A**). Thus, like the PPC domain in clade A, the PPC domain in clade B appears to mediate the protein–protein interactions among AHLs. Moreover, we found that the PPC domain of AHL4 does not interact with the AHLs in clade A, whereas it does interact with AHL1, AHL6, and AHL7 in clade B (**Figure 2B**). This finding indicates that the PPC domain of AHL4 confers the specificity of interactions exclusively with the AHLs in clade B. Interestingly, the PPC domain of AHL4 does not interact with the AHL2 protein despite that AHL2 belongs to clade B.

Next, we constructed chimeric proteins while employing AHL1, which is closely related to AHL4 in the phylogeny but does not have intercellular mobility. Analyses of the chimeric proteins between AHL1 and AHL4 provided important clues related to the definitions of the functions of each domain in AHL4. Visual inspections of *pSHR:AHL4-4-1-GFP* and *pSHR:AHL4-1-1-GFP* indicated that these two types of chimeric proteins do not move from the stele to the endodermis (**Figures 4C–H**). In contrast, our analysis of *pSHR:AHL1-1-4-GFP* and *pSHR:AHL1-4-4-GFP* indicated the movement of GFP-fused proteins from the stele to endodermis cells (**Figures 4I–N**). Moreover, a visual inspection supported our contention that the movement of GFP fused to AHL1-4-4 is more pronounced than that of AHL1-1-4 (**Figures 4I–N**). These data indicate that the AHL4 C-terminus domain is responsible for the intercellular mobility of AHL4. Because GFP with the AHL4 C-terminus exhibited different frequencies of movement depending on the origin of the attached PPC domain, the PPC domain appears to be capable of influencing the efficiency of intercellular movements. A previous study reported that NLS in the C-terminus and a hydrophobic end part of the PPC domain are required for the nuclear localization of AHL1 (Fujimoto et al., 2004). AHL4 also possesses predicted NLS in the C-terminus domain (**Figure 4A**), and all the chimeric proteins we examined, including AHL1-1-4, are nuclear localized. In that context, NLS in the C-terminus domain of AHL4 also seems to play a key role for nuclear localization.

This leads to the question of how the development of the xylem is regulated by AHL4. The N-terminus domain of AHL4 contains an AT-hook domain, which is known to be involved in DNA-binding activity (Reeves and Nissen, 1990; Huth et al., 1997). The AHL1 protein expressed under the *SHR* promoter could not rescue *ahl4*'s xylem phenotype. However, when the chimeric protein had the AHL4 N-terminus and others derived from AHL1, it could complement the *ahl4* phenotype if the protein was expressed in the xylem precursors in the root meristem (*pSHR:AHL4-1-1-GFP*; **Figure 5E**). This complementation did not occur when the chimeric protein could not move into the xylem precursors (*pAHL4:AHL4-4-1-GFP*; **Figure 6**). These findings collectively indicate that the N-terminus of AHL4 contains AHL4-specific DNA-binding domains and that this DNA binding likely occurs in xylem precursors.

To consolidate these findings further, we expressed GFP-tagged AHL1-1-4 and AHL1-4-4 under the *AHL4* promoter in the *ahl4* mutant background. Consistent with the proposal that the C-terminus of AHL4 confers intercellular mobility, their expression levels expanded to outside of the stele region as well as to the xylem precursors. The degree of domain expansion of these chimeric proteins appeared to be more extensive than that of the intact AHL4 protein. Considering that both chimeric proteins interact with AHL3, as does AHL4, this phenomenon is unlikely due to the enhanced protein mobility caused by the lack of protein–protein interaction. Despite the presence of AHL1-1-4 and AHL1-4-4 proteins in xylem precursors (**Figures 6B,C,E,F**), these two chimeras failed to complement the *ahl4* xylem phenotype (**Figure 6G**), highlighting the importance of the AHL4 N-terminus for the AHL4-specific regulation of xylem development.

AHL4 can interact with AHL3 and likely other AHLs in the same clades *via* the PPC domain. Thus, AHL4 may regulate xylem development as a protein complex with other AHLs. Based on a structural analysis of the PPC domain, AHLs are predicted to form heterotrimers (Fujimoto et al., 2004). In such a case, deciphering the structure and components of an AHL complex would be important to understand how it functions. Furthermore, the interaction between the AHL complex and a non-AHL protein appears to be crucial for downstream regulation. For example, AHL22 binds to and recruits a subset of histone deacetylase (HDAC) enzymes to regulate flowering times (Yun et al., 2012). AHL27 and AHL29 interact with TCP4 and TCP13 to regulate hypocotyl elongation (Zhao et al., 2013). In the clade B case, it has been reported that AHL10 directly interacts with highly ABA-induced1 (HAI1), a protein phosphatase that functions in response to drought stress (Wong et al., 2019).

CONCLUSION

We found that the molecular functions of AHL4 for xylem development, protein–protein interaction, and intercellular mobility are achieved *via* its N-terminus, middle PPC domain, and C-terminus. These findings indicate that AHL4 (and possibly others, too) is composed of modules, each of which has its unique function. Whether and how such a modular composition of AHL4 and related AT-hook members contribute to their evolution as positional signals for xylem development, and diversification in vascular plants (Zhao et al., 2014), would be interesting topics for further studies.

SUMMARY STATEMENT

This article reports how the modular organization of the AHL4 protein, an AT-hook family transcription factor in *Arabidopsis*, contributes to its function as an intercellular signal during the root xylem development process.

DATA AVAILABILITY STATEMENT

The original contributions presented in the study are publicly available. This data can be found here: sequence data from this article can be found in the GenBank/EMBL data libraries under the following accession numbers: AHL1 (AT4G12080), AHL2 (AT4G22770), AHL3 (AT4G25320), AHL4 (AT5G51590), AHL6 (AT5G62260), AHL7 (AT4G00200), AHL15 (AT3G55560), AHL16 (AT2G42940), AHL17 (AT5G49700), AHL19 (AT3G04570), AHL20 (AT4G14465), AHL21 (AT2G35270), AHL22 (AT2G45430), AHL23 (AT4G17800), AHL27 (AT1G20900), and AHL29 (AT1G76500).

AUTHOR CONTRIBUTIONS

J-YL and MS: conceptualization, validation, investigation, resources, writing—original draft, and writing—review and editing. MS: methodology, software, formal analysis, and visualization. J-YL: supervision, project administration, and funding acquisition. Both authors: contributed to the article and approved the submitted version.

FUNDING

This work was supported by the National Research Foundation of Korea (NRF-2021R1A2C3006061 and 2018R1A5A1023599) grants to J-YL. MS was supported by the Brain Korea 21 Plus Program, the WooDuk Foundation, and Fellowship for Fundamental Academic Fields at Seoul National University.

ACKNOWLEDGMENTS

We thank Jihyun Choi for the help with the cloning of the *AHL1* promoter and Drs. Nam V. Hoang and Muhammad Kamran for commenting on the manuscript. We also thank the members of the Lee lab for assisting in the experiments at various stages.

SUPPLEMENTARY MATERIAL

The Supplementary Material for this article can be found online at: https://www.frontiersin.org/articles/10.3389/fpls.2021.632078/full#supplementary-material

Supplementary Figure 1 | Expression patterns of AHL1, AHL2, AHL3, AHL4, AHL6, and AHL7 in representative cell types of Arabidopsis roots. Relative expression patterns of AHL1, AHL2, AHL3, AHL4, AHL6, and AHL7 in the cell-type-specific expression data. Expression values were row-normalized to visualize relative expression patterns along cell types.

Supplementary Figure 2 | Comparison of expression domains and intercellular movements of AHL1 and AHL4 in the root apical meristem. **(A–E)** Transcriptional and translational GFP expressions of *AHL1* and *AHL4*. **(A)** Wild type non-transgenic root, **(B)** pAHL1:erGFP, **(C)** *p*AHL1:AHL1-GFP, **(D)** *p*AHL4:erGFP, and **(E)** *p*AHL4:AHL4-GFP. Scale bar 20μm.

Supplementary Figure 3 | Interaction between AHL3 and four types of AHL1-AHL4 chimeric proteins. The result of a 3-AT assay of the interaction between *AHL3* and AHL1-4 chimeric proteins is shown. Left column, a pair of interactors; upper row, a series of selection media. DBD (bait), DNA binding domain; AD (prey), Activation domain.

Supplementary Figure 4 | Cell-type-specific molecular marker expression levels in four types of xylem organization: **(A–C)** Expressions of TMO5 **(A)**, ARR5 **(B)**, and AHP6 **(C)** of the 'normal' type. **(D–F)** Expressions of TMO5 **(D)**, ARR5 **(E)**, and AHP6 **(F)** of the 'four xylem cell' type. **(G–I)** Expressions of TMO5 **(G)**, ARR5 **(H)**, and AHP6 **(I)** of the 'six xylem cell in a row' type. **(J–L)** Expressions of TMO5 **(J)**, ARR5 **(K)**, and AHP6 **(L)** of the 'extra-xylem' type. Xylem phenotype categorization is identical to that in **Figures 5A–D**. Yellow arrowhead, xylem axis.

Supplementary Table 1 | Xylem phenotype scoring of ahl4 introduced with four chimeric proteins under the SHR promoter and statistical analyse.

Supplementary Table 2 | Xylem phenotype scoring of ahl4 introduced with four chimeric proteins under the AHL4 promoter and statistical analyses.

Supplementary Table 3 | List of primers used in this study.

REFERENCES

Benfey, P. N., Linstead, P. J., Roberts, K., Schiefelbein, J. W., Hauser, M.-T., and Aeschbacher, R. A. (1993). Root development in *Arabidopsis* four mutants with dramatically altered root morphogenesis. *Development* 119, 57–70.

Bishopp, A., Help, H., El-Showk, S., Weijers, D., Scheres, B., Friml, J., et al. (2011). A mutually inhibitory interaction between auxin and cytokinin specifies vascular pattern in roots. *Curr. Biol.* 21, 917–926. doi: 10.1016/j.cub.2011.04.017

Carlsbecker, A., Lee, J. Y., Roberts, C. J., Dettmer, J., Lehesranta, S., Zhou, J., et al. (2010). Cell signalling by microRNA165/6 directs gene dose-dependent root cell fate. *Nature* 465, 316–321. doi: 10.1038/nature08977

Chiang, M. H., and Greb, T. (2019). How to organize bidirectional tissue production? *Curr. Opin. Plant Biol.* 51, 15–21. doi: 10.1016/j.pbi.2019.03.003

Clough, S. J., and Bent, A. F. (1998). Floral dip: a simplified method for *Agrobacterium*-mediated transformation of *Arabidopsis thaliana*. *Plant J.* 16, 735–743. doi: 10.1046/j.1365-313x.1998.00343.x

Consortium, A. I. M. (2011). Evidence for network evolution in an *Arabidopsis* interactome map. *Science* 333, 601–607. doi: 10.1126/science.1203877

Cui, H., Levesque, M. P., Vernoux, T., Jung, J. W., Paquette, A. J., Gallagher, K. L., et al. (2007). An evolutionarily conserved mechanism delimiting shr movement defines a single layer of endodermis in plants. *Science* 316, 421–425. doi: 10.1126/science.1139531

Favero, D. S., Kawamura, A., Shibata, M., Takebayashi, A., Jung, J. H., Suzuki, T., et al. (2020). AT-hook transcription factors restrict petiole growth by antagonizing PIFs. *Curr. Biol.* 30, 1454–1466. doi: 10.1016/j.cub.2020.02.017

Fujimoto, S., Matsunaga, S., Yonemura, M., Uchiyama, S., Azuma, T., and Fukui, K. (2004). Identification of a novel plant MAR DNA binding protein localized on chromosomal surfaces. *Plant Mol. Biol.* 56, 225–239. doi: 10.1007/s11103-004-3249-5

Gallagher, K. L., Paquette, A. J., Nakajima, K., and Benfey, P. N. (2004). Mechanisms regulating SHORT-ROOT intercellular movement. *Curr. Biol.* 14, 1847–1851. doi: 10.1016/j.cub.2004.09.081

Gallagher, K. L., Sozzani, R., and Lee, C. M. (2014). Intercellular protein movement: deciphering the language of development. *Annu. Rev. Cell Dev. Biol.* 30, 207–233. doi: 10.1146/annurev-cellbio-100913-012915

Gibson, D. G. (2011). "Chapter 15 Enzymatic Assembly of Overlapping DNA Fragments," in *Methods Enzymol*, ed. C. Voigt (Cambridge, MA: Academic Press), 349–361.

Gibson, D. G., Young, L., Chuang, R.-Y., Venter, J. C., Hutchison, C. A., and Smith, H. O. (2009). Enzymatic assembly of DNA molecules up to several hundred kilobases. *Nat. Methods* 6, 343–345. doi: 10.1038/nmeth.1318

Gundu, S., Tabassum, N., and Blilou, I. (2020). Moving with purpose and direction: transcription factor movement and cell fate determination revisited. *Curr. Opin. Plant Biol.* 57, 124–132.

Helariutta, Y., Fukaki, H., Wysocka-Diller, J., Nakajima, K., Jung, J., Sena, G., et al. (2000). The SHORT-ROOT gene controls radial patterning of the *Arabidopsis* root through radial signaling. *Cell* 101, 555–567. doi: 10.1016/s0092-8674(00)80865-x

Hirano, Y., Nakagawa, M., Suyama, T., Murase, K., Shirakawa, M., Takayama, S., et al. (2017). Structure of the SHR–SCR heterodimer bound to the BIRD/IDD transcriptional factor JKD. *Nat. Plants* 3:17010. doi: 10.1038/nplants.2017.10

Huth, J. R., Bewley, C. A., Nissen, M. S., Evans, J. N. S., Reeves, R., Gronenborn, A. M., et al. (1997). The solution structure of an HMG-I(Y)–DNA complex defines a new architectural minor groove binding motif. *Nat. Struct. Biol.* 4, 657–665. doi: 10.1038/nsb0897-657

Kim, H., Zhou, J., Kumar, D., Jang, G., Ryu, K. H., Sebastian, J., et al. (2020). SHORTROOT-mediated intercellular signals coordinate phloem development in *Arabidopsis* roots. *Plant Cell* 32, 1519–1535. doi: 10.1105/tpc.19.00455

Kosugi, S., Hasebe, M., Tomita, M., and Yanagawa, H. (2009). Systematic identification of cell cycle-dependent yeast nucleocytoplasmic shuttling proteins by prediction of composite motifs. *Proc. Natl. Acad. Sci. U.S.A.* 106, 10171–10176. doi: 10.1073/pnas.0900604106

Kumar, S., Stecher, G., Li, M., Knyaz, C., and Tamura, K. (2018). MEGA X: molecular evolutionary genetics analysis across computing platforms. *Mol. Biol. Evol.* 35, 1547–1549. doi: 10.1093/molbev/msy096

Laurenzio, L. D., Wysocka-Diller, J., Malamy, J. E., Pysh, L., Helariutta, Y., Freshour, G., et al. (1996). The SCARECROW gene regulates an asymmetric cell division that is essential for generating the radial organization of the *Arabidopsis* root. *Cell* 86, 423–433. doi: 10.1016/s0092-8674(00)80115-4

Lee, J. Y., Colinas, J., Wang, J. Y., Mace, D., Ohler, U., and Benfey, P. N. (2006). Transcriptional and posttranscriptional regulation of transcription factor expression in *Arabidopsis* roots. *Proc. Natl. Acad. Sci. U.S.A.* 103, 6055–6060. doi: 10.1073/pnas.0510607103

Levesque, M. P., Vernoux, T., Busch, W., Cui, H., Wang, J. Y., Blilou, I., et al. (2006). Whole-genome analysis of the SHORT-ROOT developmental pathway in *Arabidopsis*. *PLoS Biol.* 4:e143. doi: 10.1371/journal.pbio.0040143

Lin, L., Nakano, H., Nakamura, S., Uchiyama, S., Fujimoto, S., Matsunaga, S., et al. (2007). Crystal structure of *Pyrococcus horikoshii* PPC protein at 1.60 A resolution. *Proteins* 67, 505–507. doi: 10.1002/prot.21270

Lin, L., Nakano, H., Uchiyama, S., Fujimoto, S., Matsunaga, S., Nakamura, S., et al. (2005). Crystallization and preliminary X-ray crystallographic analysis of a conserved domain in plants and prokaryotes from *Pyrococcus horikoshii* OT3. *Acta Crystallogr. Sect. F Struct. Biol. Cryst. Commun.* 61, 414–416. doi: 10.1107/S1744309105007815

Long, Y., Smet, W., Cruz-Ramírez, A., Castelijns, B., de Jonge, W., Mähönen, A. P., et al. (2015). *Arabidopsis* BIRD zinc finger proteins jointly stabilize tissue boundaries by confining the cell fate regulator SHORT-ROOT and contributing to fate specification. *Plant Cell* 27, 1185–1199. doi: 10.1105/tpc.114.132407

Long, Y., Stahl, Y., Weidtkamp-Peters, S., Postma, M., Zhou, W., Goedhart, J., et al. (2017). In vivo FRET–FLIM reveals cell-type-specific protein interactions in *Arabidopsis* roots. *Nature* 548, 97–102. doi: 10.1038/nature23317

Lu, G., and Moriyama, E. N. (2004). Vector NTI, a balanced all-in-one sequence analysis suite. *Brief. Bioinform.* 5, 378–388. doi: 10.1093/bib/5.4.378

Lu, K.-J., De Rybel, B., van Mourik, H., and Weijers, D. (2018). Regulation of intercellular TARGET OF MONOPTEROS 7 protein transport in the *Arabidopsis* root. *Development* 145:dev152892. doi: 10.1242/dev.152892

Madeira, F., Park, Y. M., Lee, J., Buso, N., Gur, T., Madhusoodanan, N., et al. (2019). The EMBL-EBI search and sequence analysis tools APIs in 2019. *Nucleic Acids Res.* 47, W636–W641. doi: 10.1093/nar/gkz268

Mahonen, A. P., Bishopp, A., Higuchi, M., Nieminen, K. M., Kinoshita, K., Tormakangas, K., et al. (2006). Cytokinin signaling and its inhibitor AHP6 regulate cell fate during vascular development. *Science* 311, 94–98. doi: 10.1126/science.1118875

Mahonen, A. P., Bonke, M., Kauppinen, L., Riikonen, M., Benfey, P. N., and Helariutta, Y. (2000). A novel two-component hybrid molecule regulates vascular morphogenesis of the *Arabidopsis* root. *Genes Dev.* 14, 2938–2943. doi: 10.1101/gad.189200

Matsushita, A., Furumoto, T., Ishida, S., and Takahashi, Y. (2007). AGF1, an AT-hook protein, is necessary for the negative feedback of AtGA3ox1 encoding GA 3-oxidase. *Plant Physiol.* 143, 1152–1162. doi: 10.1104/pp.106.093542

Miyashima, S., Roszak, P., Sevilem, I., Toyokura, K., Blob, B., Heo, J.-O., et al. (2019). Mobile PEAR transcription factors integrate positional cues to prime cambial growth. *Nature* 565, 490–494. doi: 10.1038/s41586-018-0839-y

Moreno-Risueno, M. A., Sozzani, R., Yardımcı, G. G., Petricka, J. J., Vernoux, T., Blilou, I., et al. (2015). Transcriptional control of tissue formation throughout root development. *Science* 350, 426–430. doi: 10.1126/science.aad1171

Motulsky, H., and Christopoulos, A. (2004). *Fitting Models to Biological Data using Linear and Nonlinear Regression: A Practical Guide to Curve Fitting*. New York: Oxford University Press.

Nakajima, K., Sena, G., Nawy, T., and Benfey, P. N. (2001). Intercellular movement of the putative transcription factor SHR in root patterning. *Nature* 413, 307–311. doi: 10.1038/35095061

Reeves, R., and Nissen, M. S. (1990). The A.T-DNA-binding domain of mammalian high mobility group I chromosomal proteins. A novel peptide motif for recognizing DNA structure. *J. Biol. Chem.* 265, 8573–8582.

Sabatini, S., Heidstra, R., Wildwater, M., and Scheres, B. (2003). SCARECROW is involved in positioning the stem cell niche in the *Arabidopsis* root meristem. *Genes Dev.* 17, 354–358. doi: 10.1101/gad.252503

Saitou, N., and Nei, M. (1987). The neighbor-joining method: a new method for reconstructing phylogenetic trees. *Mol. Biol. Evol.* 4, 406–425. doi: 10.1093/oxfordjournals.molbev.a040454

Schlereth, A., Moller, B., Liu, W., Kientz, M., Flipse, J., Rademacher, E. H., et al. (2010). MONOPTEROS controls embryonic root initiation by regulating a mobile transcription factor. *Nature* 464, 913–916. doi: 10.1038/nature08836

Sena, G., Jung, J. W., and Benfey, P. N. (2004). A broad competence to respond to SHORT ROOT revealed by tissue-specific ectopic expression. *Development* 131, 2817–2826. doi: 10.1242/dev.01144

Seo, M., Kim, H., and Lee, J.-Y. (2020). Information on the move: vascular tissue development in space and time during postembryonic root growth. *Curr. Opin. Plant Biol.* 57, 110–117. doi: 10.1016/j.pbi.2020.08.002

Sozzani, R., Cui, H., Moreno-Risueno, M. A., Busch, W., Van Norman, J. M., Vernoux, T., et al. (2010). Spatiotemporal regulation of cell-cycle genes by SHORTROOT links patterning and growth. *Nature* 466, 128–132. doi: 10.1038/nature09143

Street, I. H., Shah, P. K., Smith, A. M., Avery, N., and Neff, M. M. (2008). The AT-hook-containing proteins SOB3/AHL29 and ESC/AHL27 are negative modulators of hypocotyl growth in Arabidopsis. *Plant J.* 54, 1–14. doi: 10.1111/j.1365-313X.2007.03393.x

Vaughan-Hirsch, J., Goodall, B., and Bishopp, A. (2018). North, East, South, West: mapping vascular tissues onto the *Arabidopsis* root. *Curr. Opin. Plant Biol.* 41, 16–22. doi: 10.1016/j.pbi.2017.07.011

Welch, D., Hassan, H., Blilou, I., Immink, R., Heidstra, R., and Scheres, B. (2007). *Arabidopsis* JACKDAW and MAGPIE zinc finger proteins delimit asymmetric cell division and stabilize tissue boundaries by restricting SHORT-ROOT action. *Genes Dev.* 21, 2196–2204. doi: 10.1101/gad.440307

Wong, M. M., Bhaskara, G. B., Wen, T. N., Lin, W. D., Nguyen, T. T., Chong, G. L., et al. (2019). Phosphoproteomics of *Arabidopsis* highly ABA-induced1 identifies AT-hook-like10 phosphorylation required for stress growth regulation. *Proc. Natl. Acad. Sci. U.S.A.* 116, 2354–2363.

Xiao, C., Chen, F., Yu, X., Lin, C., and Fu, Y.-F. (2009). Over-expression of an AT-hook gene, AHL22, delays flowering and inhibits the elongation of hypocotyl in *Arbidopsis thaliana*. *Plant Mol. Biol.* 71, 39–50. doi: 10.1007/s11103-009-9507-9

Yun, J., Kim, Y.-S., Jung, J.-H., Seo, P. J., and Park, C.-M. (2012). The AT-hook motif-containing protein AHL22 regulates flowering initiation by modifying FLOWERING LOCUS T chromatin in *Arabidopsis*. *J. Biol. Chem.* 287, 15307–15316. doi: 10.1074/jbc.M111.318477

Zhang, J., Eswaran, G., Alonso-Serra, J., Kucukoglu, M., Xiang, J., Yang, W., et al. (2019). Transcriptional regulatory framework for vascular cambium development in *Arabidopsis* roots. *Nat. Plants* 5, 1033–1042. doi: 10.1038/s41477-019-0522-9

Zhao, J., Favero, D. S., Peng, H., and Neff, M. M. (2013). *Arabidopsis thaliana* AHL family modulates hypocotyl growth redundantly by interacting with each other via the PPC/DUF296 domain. *Proc. Natl. Acad. Sci. U.S.A.* 110, E4688–E4697. doi: 10.1073/pnas.1219277110

Zhao, J., Favero, D. S., Qiu, J., Roalson, E. H., and Neff, M. M. (2014). Insights into the evolution and diversification of the AT-hook motif nuclear localized gene family in land plants. *BMC Plant Biol.* 14:266. doi: 10.1186/s12870-014-0266-7

Zhou, J., Wang, X., Lee, J. Y., and Lee, J. Y. (2013). Cell-to-cell movement of two interacting AT-hook factors in *Arabidopsis* root vascular tissue patterning. *Plant Cell* 25, 187–201. doi: 10.1105/tpc.112.102210

Zuckerkandl, E., and Pauling, L. (1965). "Evolutionary divergence and convergence in proteins," in *Evolving Genes and Proteins*, eds V. Bryson and H. J. Vogel (New York: Academic Press), 97–166.

Conflict of Interest: The authors declare that the research was conducted in the absence of any commercial or financial relationships that could be construed as a potential conflict of interest.

frontiers in Plant Science

ORIGINAL RESEARCH
published: 28 May 2021
doi: 10.3389/fpls.2021.649806

Similarities and Differences in the GFP Movement in the Zygotic and Somatic Embryos of Arabidopsis

Kamila Godel-Jędrychowska, Katarzyna Kulińska-Łukaszek and Ewa Kurczyńska**

Institute of Biology, Biotechnology and Environmental Protection, Faculty of Natural Sciences, The University of Silesia in Katowice, Katowice, Poland

Intercellular signaling during embryo patterning is not well understood and the role of symplasmic communication has been poorly considered. The correlation between the symplasmic domains and the development of the embryo organs/tissues during zygotic embryogenesis has only been described for a few examples, including Arabidopsis. How this process occurs during the development of somatic embryos (SEs) is still unknown. The aim of these studies was to answer the question: do SEs have a restriction in symplasmic transport depending on the developmental stage that is similar to their zygotic counterparts? The studies included an analysis of the GFP distribution pattern as expressed under diverse promoters in zygotic embryos (ZEs) and SEs. The results of the GFP distribution in the ZEs and SEs showed that 1/the symplasmic domains between the embryo organs and tissues in the SEs was similar to those in the ZEs and 2/the restriction in symplasmic transport in the SEs was correlated with the developmental stage and was similar to the one in their zygotic counterparts, however, with the spatio-temporal differences and different PDs SEL value between these two types of embryos.

Keywords: GFP, plasmodesmata, somatic embryo, symplasmic domain, tissue formation, zygotic embryo

OPEN ACCESS

Edited by:
Jung-Youn Lee, University of Delaware, United States

Reviewed by:
Rosemary White, Commonwealth Scientific and Industrial Research Organisation (CSIRO), Australia
Célia Baroux, University of Zurich, Switzerland
Jae-Yean Kim, Gyeongsang National University, South Korea

****Correspondence:***
Kamila Godel-Jędrychowska
kamila.godel-jedrychowska@us.edu.pl
orcid.org/0000-0002-0136-2746
Ewa Kurczyńska
ewa.kurczynska@us.edu.pl
orcid.org/0000-0003-0772-8961

Specialty section:
This article was submitted to Plant Cell Biology, a section of the journal Frontiers in Plant Science

Received: *05 January 2021*
Accepted: *03 May 2021*
Published: *28 May 2021*

Citation:
Godel-Jędrychowska K, Kulińska-Łukaszek K and Kurczyńska E (2021) Similarities and Differences in the GFP Movement in the Zygotic and Somatic Embryos of Arabidopsis. Front. Plant Sci. 12:649806. doi: 10.3389/fpls.2021.649806

INTRODUCTION

Intercellular communication and the spatio-temporal regulation of gene expression are global mechanisms that control development. Plants have developed a unique structure, plasmodesmata (PDs), for intercellular communication in which each plant cell can form direct conduits to its neighbors, thus creating domains of cells that share common components. PDs are active channels that control the movement of the factors that regulate plant development (Heinlein, 2002; Sevilem et al., 2015; Otero et al., 2016; Sager and Lee, 2018 and literature therein).

The presence/absence and permeability of PDs lead to the formation of symplasmic domains, e.g., specialized groups of cells that become isolated either due to the absence of PDs or the downregulation of the cytoplasmic flux on the border of the domain (Bayer and Salmon, 2013; Kitagawa and Jackson, 2017 and literature therein). Such transient symplasmic domains may participate in the coordination of plant growth and development (Sager and Lee, 2014).

Why a symplasmic communication survey during plant development is important? What makes PDs an element of the supracellular information exchange system? By identifying which cells and tissues communicate through PDs, it is possible to determine when and where the signaling is related to the developmental processes. Signaling molecules, transcription factors and mRNA

can travel through PDs and are thought to influence the developmental processes (Tilsner et al., 2016; Kehr and Kragler, 2018 and literature therein).

Embryogenesis, during which the zygote follows a defined cell division pattern and differentiation to form the mature embryo, is a crucial developmental process in the lives of flowering plants (Schrick and Laux, 2001; Park and Harada, 2008; Smertenko and Bozkhov, 2014 and literature therein). During embryo development, the basic body pattern is established and therefore, understanding the mechanisms that regulate this stage is important because they affect further growth. The details of ZEs development at the morpho-histological and molecular levels have been well described (Capron et al., 2009; Tvorogova and Lutova, 2018). Because the present studies concern an analysis of symplasmic communication/isolation in SE, specifically its correlation with morphogenesis and histogenesis, the differences in the morphology and histology between the ZEs and SEs will be briefly described. The morphological and histological abnormalities in SEs compared to their zygotic counterparts are manifested by an increased number of ground promeristem layers (Levi and Sink, 1991; Mordhorst et al., 1998; Kurczyńska et al., 2007; Jariteh et al., 2015), an abnormal patterning of the root apical meristem (Bassuner et al., 2007), fused cotyledons of the SEs and fused SEs with changes in the cell patterning (Luo and Koop, 1997; Pescador et al., 2008), differences in the embryo size (Tereso et al., 2007; Jin et al., 2014) and malformations of the SEs (Etienne et al., 2013). If the pattern formation is correlated with the determination of organs/tissues during embryogenesis, the question of how symplasmic communication occurs in these embryos arises.

What is known about symplasmic communication during ZEs and SEs development? An analysis of the zygotic embryogenesis of *Capsella bursa-pastoris* (Schulz and Jensen, 1968) and *Torenia fourieri* (Han et al., 2000) showed changes in symplasmic communication from the beginning of ZEs development. Patricia Zambryski's team conducted fundamental research for determining the correlation between the symplasmic tracer movement and ZE development. It was proven that in *Arabidopsis thaliana*, cell-to-cell communication *via* the PDs conveys positional information that is critical for establishing the axial body pattern during embryogenesis (Kim et al., 2002, 2005b; Burch-Smith and Zambryski, 2010; Burch-Smith et al., 2011). Ruth Stadler's team conducted another set of studies on Arabidopsis seeds and ZEs. They demonstrated that the establishment of symplasmic domains coincides with the differentiation of specific cells/tissues (Stadler et al., 2005). Changes in symplasmic communication during zygotic embryogenesis were also observed in *Sedum acre* (Wróbel-Marek et al., 2017).

Data concerning the involvement of symplasmic communication/isolation during the development of SEs are scarce. There is much more information about symplasmic communication in explants during the induction phase of embryogenesis than during SEs development (Dubois et al., 1991; Canhoto et al., 1996; Puigderrajols et al., 2001; Verdeil et al., 2001; Grimault et al., 2007; Reis et al., 2008; Godel-Jedrychowska et al., 2020). Because elucidating the patterning mechanisms in embryogenesis requires understanding intercellular communication, a good knowledge of the establishment of the symplasmic domain in embryos of different origins is required. Therefore, the aim of the presented study was to analyze symplasmic communication in the SEs in order to determine whether the symplasmic domains that form in SEs correspond to the developing tissue and organs that is similar to their zygotic counterparts.

MATERIALS AND METHODS

Plant Material and Culture Conditions

The *STM:ER-GFP, STM:1XsGFP, STM:2XsGFP,* and *STM:3XsGFP* transgenic lines were described in Kim et al. (2005a). The *AtGL2:tmGFP9, AtGL2:GFP, AtSUC3:tmGFP9,* and *AtSUC3:GFP*

TABLE 1 | Characteristics and comparison of the zygotic and somatic embryos.

	Similarities/differences	
	Zygotic embryo	**Somatic embryo**
Embryo size	Globular < 100 μm Heart 100 μm Torpedo 300 μm Cotyledonary 700 μm	Globular 100–150 μm Heart 160–250 μm Torpedo 260–400 μm Cotyledonary 410–1000 μm
Morphology	SAM. two cotyledons, radicle.	SAM. sometimes more than two cotyledons, radicle.
Histology	Normal arrangement of tissues in term of the number of cell layers in tissues; protodermis, ground promeristem, provascular tissue.	Tissue arrangement similar to zygotic counterparts, but number of cells within tissue sometimes changed; tissues often built with more layers than zygotic counterparts; protodermis, ground promeristem, provascular tissue.
Symplasmic domains	Relevant to embryo organs and tissues.	Relevant to embryo organs and tissues.
SEL	Between embryo organs; longitudinal arrangement Globular 81 kDa Heart 51 kDa Torpedo 51 kDa Cotyledonary 27 kDa Between embryo tissues; radial arrangement – centripetal Globular 27 kDa Heart 27 kDa Torpedo 27 kDa Cotyledonary 27 kDa Between embryo tissues; radial arrangement – centrifugal Globular 27 kDa Heart 27 kDa Torpedo 27 kDa[2,3] Cotyledonary 27 kDa	Between embryo organs; longitudinal arrangement Globular 27 kDa Heart 27 kDa Torpedo < 27 kDa Cotyledonary < 27 kDa Between embryo tissues; radial arrangement – centripetal Globular 27 kDa Heart 27 kDa Torpedo 27 kDa* Cotyledonary 27 kDa* Between embryo tissues; radial arrangement – centrifugal Globular 27 kDa Heart 27 kDa[1] Torpedo 27 kDa*[2,3] Cotyledonary 27 kDa[1,2]

**Indicates that the exchange of the GFP occurred only between the hypocotyl tissues; [1]only in the provascular tissue; [2]in the protodermis and [3]in the ground promeristem.*

TABLE 2 | Comparison between the ZEs and SEs domains that emerged during development in *Arabidopsis thaliana STM:1XsGFP, STM:2XsGFP,* and *STM:3XsGFP* lines.

	1XsGFP						2XsGFP						3xXsGFP					
Embryo type	**ZEs**			**SEs**			**ZEs**			**SEs**			**ZEs**			**SEs**		
Domain	**Globular**			**Globular**			**Globular**			**Globular**			**Globular**			**Globular**		
% globular embryos	**100% (*n* = 18)**			**100% (*n* = 12)**			**100% (*n* = 14)**			**No activity detected (*n* = 15)**			**100% (*n* = 14)**			**No activity detected (*n* = 15)**		
Comment	No domain was distinguished up to 27 kDa			No domain was distinguished up to 27 kDa			No domain was distinguished up to 54 Da			Not applicable			No domain was distinguished up to 81 kDa			Not applicable		
Domain	Apical	Central	Basal	Apical	Central	Basal	Apical	Central	Basal	Apical	Central	Basal	Apical	Central	Basal	Apical	Central	Basal
% heart embryos	**100% (*n* = 18)**	**100% (*n* = 15)**	**100% (*n* = 17)**	**75% (*n* = 8)**	**96% (*n* = 12)**	**75% (*n* = 10)**	**100% (*n* = 15)**	**100% (*n* = 10)**	**100% (*n* = 19)**	**100% (*n* = 7)**	**100% (*n* = 10)**	**100% (*n* = 7)**	**100% (*n* = 14)**	**100% (*n* = 14)**	**100% (*n* = 15)**	**2% (*n* = 12)**	**86% (*n* = 8)**	**76% (*n* = 12)**
Comment	No domain was distinguished up to 27 kDa			Three domains: (1) cotyledon node; (2) hypocotyl: (3) root			No domain was distinguished up to 54 kDa			Three domains: (1) cotyledon node; (2) hypocotyl: (3) root			Three domains: (1) cotyledon node; (2) hypocotyl: (3) root			Two domains: (1) cotyledon node; (2) Hypocotyl/root		
% torpedo embryos	**100% (*n* = 15)**	**100% (*n* = 15)**	**100% (*n* = 18)**	**83% (*n* = 18)**	**86% (*n* = 15)**	**100% (*n* = 15)**	**100% (*n* = 19)**	**100% (*n* = 19)**	**100% (*n* = 18)**	**100% (*n* = 13)**	**75% (*n* = 13)**	**100% (*n* = 17)**	**100% (*n* = 15)**	**100% (*n* = 15)**	**100% (*n* = 13)**	**88% (*n* = 8)**	**79% (*n* = 8)**	**90% (*n* = 15)**
Comment	No domain was distinguished up to 27 kDa			Three domains: (1) cotyledon node; (2) hypocotyl: (3) root			Three domains: (1) cotyledon node; (2) hypocotyl: (3) root			Three domains: (1) cotyledon node; (2) Hypocotyl: (3) root			Three domains: (1) cotyledon node; (2) hypocotyl: (3) root			Three domains: (1) cotyledon node; (2) hypocotyl: (3) root		
% cotyledonary embryos	**100% (*n* = 14)**	**100% (*n* = 14)**	**100% (*n* = 16)**	**33% (*n* = 9)**	**85% (*n* = 13)**	**95% (*n* = 11)**	**100% (*n* = 12)**	**100% (*n* = 13)**	**100% (*n* = 19)**	**98% (*n* = 20)**	**96% (*n* = 21)**	**100% (*n* = 21)**	**100% (*n* = 13)**	**100% (*n* = 17)**	**100% (*n* = 15)**	**96% (*n* = 21)**	**100% (*n* = 22)**	**96% (*n* = 21)**
Comment	No domain was distinguished up to 27 kDa			Three domains: (1) cotyledon node; (2) hypocotyl: (3) root			Three domains: (1) cotyledon node; (2) hypocotyl: (3) root			Three domains: (1) cotyledon node; (2) hypocotyl: (3) root			Three domains: (1) cotyledon node; (2) hypocotyl: (3) root			Three domains: (1) cotyledon node; (2) hypocotyl: (3) root		

% – the percentage of embryos that enable GFP movement to the number of embryos tested (according to Kim et al., 2002; Wróbel-Marek et al., 2017). A large% value (bold%) indicates that movement was possible in this stage of embryo.

transgenic lines were described in Stadler et al. (2005) and PDBG2OE [PD-located beta 1,3 glucanases that is tagged internally with mCitrine was described in Benitez-Alfonso et al. (2013)]. The seeds of all of the lines were sown into pots with garden soil and vermiculite mixed at a 1:1 volume ratio. The plants were grown under controlled conditions at a temperature of 20–23°C under a 16 h photoperiod with a light intensity of 40 $\mu mol/m^{-2}s^{-1}$ and relative humidity of 60–70%. After 6–8 weeks, siliques with immature zygotic embryos (IZEs) were collected (Gaj, 2001), surface-sterilized for 20 min in a 20% sodium hypochlorite solution and rinsed three times in sterile water. The IZEs were isolated from the seeds in sterile dishes in water using preparation needles under a stereomicroscope. 10–15 IZEs (explants) were grown on a Phytagel solidified (Sigma, Poland; 3.6 g L-1) E5 medium (Sigma, Poland; Gamborg et al., 1968), which had been supplemented with 1.1 mg/ml 2,4-dichlorophenoxyacetic acid (2,4-D, Sigma-Aldrich) and 20 g L^{-1} sucrose (pH 5.8). The embryo culture was conducted at 21°C under a 16h photoperiod at a light intensity of 20 $\mu mol/m^{-2}s^{-1}$ for up to 21 days. Next, SEs at various stages of development were collected. The analyses were repeated three times. The pictures on the plates show the figures that illustrate the representative results for each variant/replication. For the analyses of the ZEs, 45–71 embryos were tested for each line and the number of examined embryos ranged from 18 in the heart stage to 28 in the torpedo stage per one repetition. For the SEs, the total number of embryos that was analyzed was 65 on average and for each developmental stage, it was about 20 per one repetition. The data in the tables are from the documented and collected images that were taken during the study (a range of "n" = the number of embryos per line/stage; **Tables 1–4**).

Histochemical Staining

For the histological analyses, the samples were fixed in a solution of 2.5% (w/v) glutaraldehyde (GA) in a phosphate buffer (pH = 7.0) for 12 h at 4°C. Then, they were embedded in Steedman's wax as was described in Sala et al. (2019). The sections (5–7 μm thick) were cut using a HYRAX M40 rotary microtome (Zeiss, Oberkochen, Germany) and collected on microscopic slides that were covered with Haupt's adhesive (according to Barlow and Kurczyńska, 2007). The sections were stained using the periodic acid-Schiff (PAS) reactions and toluidine blue (TBO, Sigma-Aldrich) staining (0.1% water solution of TBO for 5 min).

Microscopic Observation

In order to analyze the GFP distribution within the ZEs and SEs, serial optical sections of the embryos were obtained using a confocal laser scanning microscope (CLSM; system FLUO-view 1000; Olympus). The GFP was excited using a multi-Argon Laser (laser power 100 mV; Melles Griot BV; Max. 150 mW) at a 488 nm wavelength and an emission at 500–530 nm. Targeted embryos at each stage of development were studied with an objective lens at different magnifications (UPlanFLN 10x-0.30 numerical aperture, UPlanFLN 20x-0.50 numerical aperture, UPlanFLN 40x-1.35 numerical aperture). Observations were also made using an Olympus BX42 epifluorescence microscope equipped with an Olympus XC50 digital camera and software

TABLE 3 | Comparison of the movement frequency of the GFP in the SEs and ZEs of the *Arabidopsis thaliana AtGL2:GFP* transgenic line.

Stage of development	Part of embryo/ embryo type	Protoderm		Ground promeristem		Provascular tissue	
		ZEs	SEs	ZEs	SEs	ZEs	SEs
Heart	**Apical**	**100%(17*/17**)**	0%(0*/10**)	**100%(18*/18**)**	80%(15*/21**)	**100%(18*/18**)**	0%(0*/10**)
	Central	**100%(18*/18**)**	**100%(10*/10**)**	**100%(18*/18**)**	**90%(9*/10**)**	**100%(18*/18**)**	0%(0*/10**)
	Basal	**100%(18*/18**)**	**100%(10*/10**)**	**100%(18*/18**)**	**90%(9*/10**)**	**100%(18*/18**)**	0%(0*/10**)
Torpedo	**Apical**	**100%(25*/25**)**	**95%(18*/19**)**	**96%(22*/23**)**	**94%(16*/17**)**	**96%(24*/25**)**	**80%(16*/20**)**
	Central	**100%(25*/25**)**	**95%(20*/21**)**	**95%(20*/21**)**	**94%(16*/17**)**	**95%(20*/21**)**	**96%(21*/22**)**
	Basal	**100%(25*/25**)**	0%(20*/20**)	**95%(18*/19**)**	5%(1*/20**)	**96%(22*/23**)**	10%(2*/20**)
Cotyledonary	**Apical**	0%(19*/19**)	**93%(15*/16**)**	0%(19*/19**)	0%(17*/17**)	0%(19*/19**)	0%(17*/17**)
	Central	**100%(19*/19**)**	**100%(17*/17**)**	0%(19*/19**)	0%(17*/17**)	0%(19*/19**)	0%(17*/17**)
	Basal	**100%(19*/19**)**	0%**(17*/17**)**	0%(19*/19**)	0%(17*/17**)	0%(19*/19**)	0%(17*/17**)

**Number of embryos that enabled the movement of GFP; when the analyzed area (apical/central/basal) was filled with GFP above 80%.*
***Number of embryos tested. The GFP distribution was analyzed in the radial direction and along the apical-basal axis from the areas of the promoter activity. A large% value (**bold%**) indicates that movement was possible in this direction.*

TABLE 4 | Comparison of the movement frequency of the GFP in ZEs and SEs of the *Arabidopsis thaliana AtSUC3:GFP* transgenic line.

Stage of development	Part of embryo/ embryo type	Protoderm		Ground promeristem		Provascular tissue	
		ZEs	SEs	ZEs	SEs	ZEs	SEs
Heart	**Apical**	**100%(17*/17**)**	0%(19*/19**)	**100%(17*/17**)**	0%(19*/19**)	**100%(17*/17**)**	0%(19*/19**)
	Central	**100%(17*/17**)**	**75%(14*/19**)**	**100%(17*/17**)**	0%(19*/19**)	**100%(17*/17**)**	0%(19*/19**)
	Basal	**100%(17*/17**)**	**95%(19*/20**)**	**100%(17*/17**)**	**95%(19*/20**)**	**95%(18*/20**)**	**95%(18*/20**)**
Torpedo	**Apical**	0%(15*/15**)	**95%(18*/19**)**	0%(15*/15**)	0%(19*/19**)	0%(15*/15**)	0%(20*/20**)
	Central	**100%(15*/15**)**	**96%(21*/22**)**	**100%(15*/15**)**	**80%(16*/20**)**	**100%(15*/15**)**	0%(20*/20**)
	Basal	**100%(15*/15**)**	**100%(22*/22**)**	**100%(15*/15**)**	**95%(19*/20**)**	**100%(15*/15**)**	0%(20*/20**)
Cotyledonary	**Apical**	0%(18*/18**)	**90%(18*/20**)**	0%(18*/18**)	0%(19*/19**)	**89%(16*/18**)**	0%(19*/19**)
	Central	0%(18*/18**)	**96%(19*/20**)**	0%(18*/18**)	0%(19*/19**)	0%(18*/18**)	0%(19*/19**)
	Basal	**100%(18*/18**)**	5%(1*/20**)	**100%(18*/18**)**	0%(19*/19**)	**100%(18*/18**)**	0%(19*/19**)

**Number of embryos that enabled the movement of GFP; when the analyzed area (apical/central/basal) was filled with GFP in about 80%.*
***Number of embryos tested. The GFP distribution was analyzed in the radial direction and along the apical-basal axis from the areas of the promoter activity. A large% value (**bold%**) indicates that movement was possible in this direction.*

(Nikon, Tokyo, Japan). The GFP was excited at a maximum wavelength of 490 nm [Nikon Plan Fluor 10x objective lens (0.30 numerical aperture); 20x (0.5 numerical aperture); and 40x (0.75 numerical aperture)]. The histological images were acquired with a Nikon Eclipse Ni-U microscope equipped with a Nikon Digital DS-Fi1-U3 camera and software (Nikon, Tokyo, Japan).

Image Processing

Maximum intensity projections (**Figures 1B–D**,D inset,J inset,K–O,O inset,P, 2D,D inset,F,H,M,O,P, 3B,C,C inset,E,E inset,F,I,I inset,L,L inset, 4E,E inset,F,I,K,L, 5) were created from at least 20 optical sections using FLUOVIEW (Olympus 1.6) and/or ImageJ software. The brightness and contrast of the images that were used for the figure panels were adjusted in Corel Draw X10.

Classification of the SE Stages

Spherical-shape embryos with an easily distinguishable protodermis and a diameter of about 100 μm were called globular. Heart-shaped, rod-like, or triangular shaped embryos with the cotyledon primordia and size (long axis) between 150 and 250 μm were called the heart. Embryos 250–400 μm long with distinguishable cotyledons were classified as torpedo. The length of the embryos in the cotyledonary stage was greater than 400 μm with a maximum of about 1000 μm (**Table 1**).

RESULTS

Symplasmic Communication Between the Embryo Organs

To compare the symplasmic communication between the embryo organs (along the apical-basal axis) in the *Arabidopsis thaliana* SEs with ZEs, GFP variants of different molecular sizes that were under the control of the *SHOOT MERISTEMLESS* (*STM*) gene promoter were used. In order to trace the mobility of the molecules of 27 kDa (1XsGFP), 54 kDa (2XsGFP), and 81 kDa (3XsGFP), they were compared with the GFP that had been retained in the endoplasmic reticulum (ER-GFP). The analyses concerned: 1/determining the promoter activity sites and 2/determining the distribution of the 1Xs, 2Xs, and 3Xs

mobile GFP molecules (sGFP) at various stages of the ZEs and SEs embryo development. The *STM* gene promoter in the ZEs was active in the globular stage (**Figure 1A**). In the heart (**Figure 1B**) stage, the gene promoter activity was detected in the shoot apical meristem (SAM) and cells in nearest vicinity. At the torpedo stage (**Figure 1C**), the area of promoter activity was detected in the cotyledon node and the ectopic expression of promoter activity was observed in some of the cells of the hypocotyl (to facilitate the description of the individual areas of embryos, especially SEs, the following terms were used: apical – comprising the SAM, cotyledon node and cotyledons; central – comprising the hypocotyl and basal – comprising the root pole). In the cotyledonary stage, the *STM* promoter activity was observed in the SAM and in the basal part of the hypocotyl (**Figure 1D** and inset).

In the SEs in the early globular stage, no *STM* promoter activity was observed (**Figure 1E**) and this activity appeared in the embryos in the late globular stage (**Figure 1E** inset). In the heart stage, promoter activity was detected in the SAM and in the hypocotyl (**Figure 1F**). In the torpedo stage (**Figure 1G**), the activity of the *STM* promoter was observed in the cells of the emerging SAM (cotyledon node), the hypocotyl and the basal part of the embryo. In the embryos in the cotyledonary stage, a double distribution pattern of the promoter activity was observed: in the SAM cells (**Figure 1H** inset) and in the basal part of the hypocotyl (**Figure 1H**). To summarize, the *STM* promoter activity in the heart stage SEs was not only found in the SAM but also in the hypocotyl cells and from the torpedo stage was similar to that described for the ZEs.

The distribution pattern of 3XsGFP, which is expressed under the *STM* promoter in different developmental stages of ZEs and SEs, was also compared. In the globular ZEs, 3XsGFP was distributed almost uniformly in the entire embryo (**Figure 1I**). In the heart stage embryos, the GFP did not move from the sites of its expression or only moved into the cells in its nearest vicinity (**Figure 1J**). In the torpedo stage, the GFP distribution pattern in the SAM was similar to the one that was observed for the heart stage, but additionally, the GFP was detected in the basal part of the hypocotyl (**Figure 1K**). In the cotyledonary stage, the 3XsGFP was detected in the SAM and the basal part of the hypocotyl (**Figure 1L**). In the globular stage of the SEs, no fluorescence of the 3XsGFP was detected (**Figure 1M**). In the heart stage, the GFP was detected in the hypocotyl and basal part of the embryo corresponding to novel subdomain(**Figure 1N** and **Table 2**). In the torpedo (**Figure 1O**) and cotyledonary (**Figure 1P**) stages, the 3XsGFP was present only in the embryo areas that corresponded to the sites of promoter activity. The results suggest that for molecules up to 81 kDa in the ZEs and SEs, three symplasmic domains were present from the torpedo stage (**Table 2**).

The distribution pattern of the 1XsGFP and 2XsGFP was analyzed in both embryo types (**Figure 2**). The distribution of the 1XsGFP at different stages of the ZEs development showed that all of the domain boundaries permitted the passage of the 1XsGFP to spread from the *STM* expression site (**Figures 2A–D**). In the SEs in the globular stage, the GFP was detected in the entire embryo (**Figure 2E**). In the heart stage, the 1XsGFP was present in the entire embryo except for several layers of the cells at the distal parts of the cotyledons and the basal part of the embryo (**Figure 2F**). This restricted movement of the 1XsGFP in the SEs (**Figure 2F**) might indicate that novel subdomain boundaries must be established for the movement of the 1XsGFP from the *STM* expression site in the direction toward the distal part of the cotyledons. In the torpedo stage, the 1XsGFP was observed in the hypocotyl and the cotyledon node (**Figure 2G**). The cotyledonary stage was characterized by the presence of the 1XsGFP only in the SAM, the basal part of hypocotyl and the root (**Figure 2H** and inset). These results indicate that in SEs, restrictions in symplasmic transport for molecules up to 27 kDa began in the heart stage of embryo development and from the torpedo stage led to the formation of the three symplasmic domains (apical, central and basal, that corresponded to the somatic embryo organs (cotyledon, hypocotyl and root). To summarize: (1) the distribution pattern of the GFP in the ZEs indicates that all of the domain boundaries permitted the passage of molecules up to 27 kDa in all of the developmental stages; for SEs, the distribution pattern of the 1XsGFP indicates the presence of the symplasmic domains and subdomains from the heart stage, and therefore, the domain boundaries had been established earlier than in ZEs; (2) a globular SEs and ZE are a single symplasmic domain in which the SEL of the PDs is at least 27 kDa; (3) in the heart stage SE, the SEL of the PDs between the symplasmic domains is equal to 27 kDa; (4) in the torpedo stage SE, there are three symplasmic domains: a cotyledon and a root meristem domain with the SEL of the PDs equal to or less than 27 kDa and a hypocotyl domain with the PDs SEL on the boundaries that are equal to or more than 27 kDa and (5) in the cotyledonary stage, three symplasmic domain are present (**Table 2**).

An analysis of the 2XsGFP distribution in the ZEs showed that up to the heart stage, the 2XsGFP was observed throughout the entire embryo (**Figures 2I,J**). In the torpedo stage, the presence of the 2XsGFP was observed only in the hypocotyl (**Figure 2K**). This indicates a restriction in the GFP movement into the cotyledons and the basal part of embryos at this stage of development. In the cotyledonary stage, the 2XsGFP was detected in the basal part of the hypocotyl and the SAM (**Figure 2L**). In the globular stage SEs, no fluorescence of the 2XsGFP was detected (**Figure 2M**). In the heart stage, the 2XsGFP was observed in groups of irregularly distributed cells in the hypocotyl (**Figure 2N**). In the SEs in the torpedo stage, the 2XsGFP was detected only in the SAM and root pole (**Figure 2O**). In the the cotyledonary stage SEs, the 2XsGFP was detected in the cotyledon node cells and in the basal part of the embryo (**Figure 2P**). To summarize: (1) restrictions in the movement of molecules up to 54 kDa began to occur in the torpedo stage of the ZEs; (2) the 2XsGFP did not move within the SEs to the same extent as it did in the ZEs; (3) the globular ZEs, which comprise one domain as the distribution pattern of 3XsGFP compared with that of ER-GFP, indicate that all of the PD can traffic molecules of at least 81 kDa; (4) in the heart stage, the 2XsGFP appeared to spread into the SE cotyledons from the hypocotyl expression zone (see the ER-GFP pattern in SE); (5) the distribution pattern of the 2XsGFP in the SEs seemed to be more restricted than in the 3XsGFP; (6) the distribution of the 2XsGFP in the torpedo SEs was observed only within the hypocotyl and there was little to no expression in the root pole and (7) in the

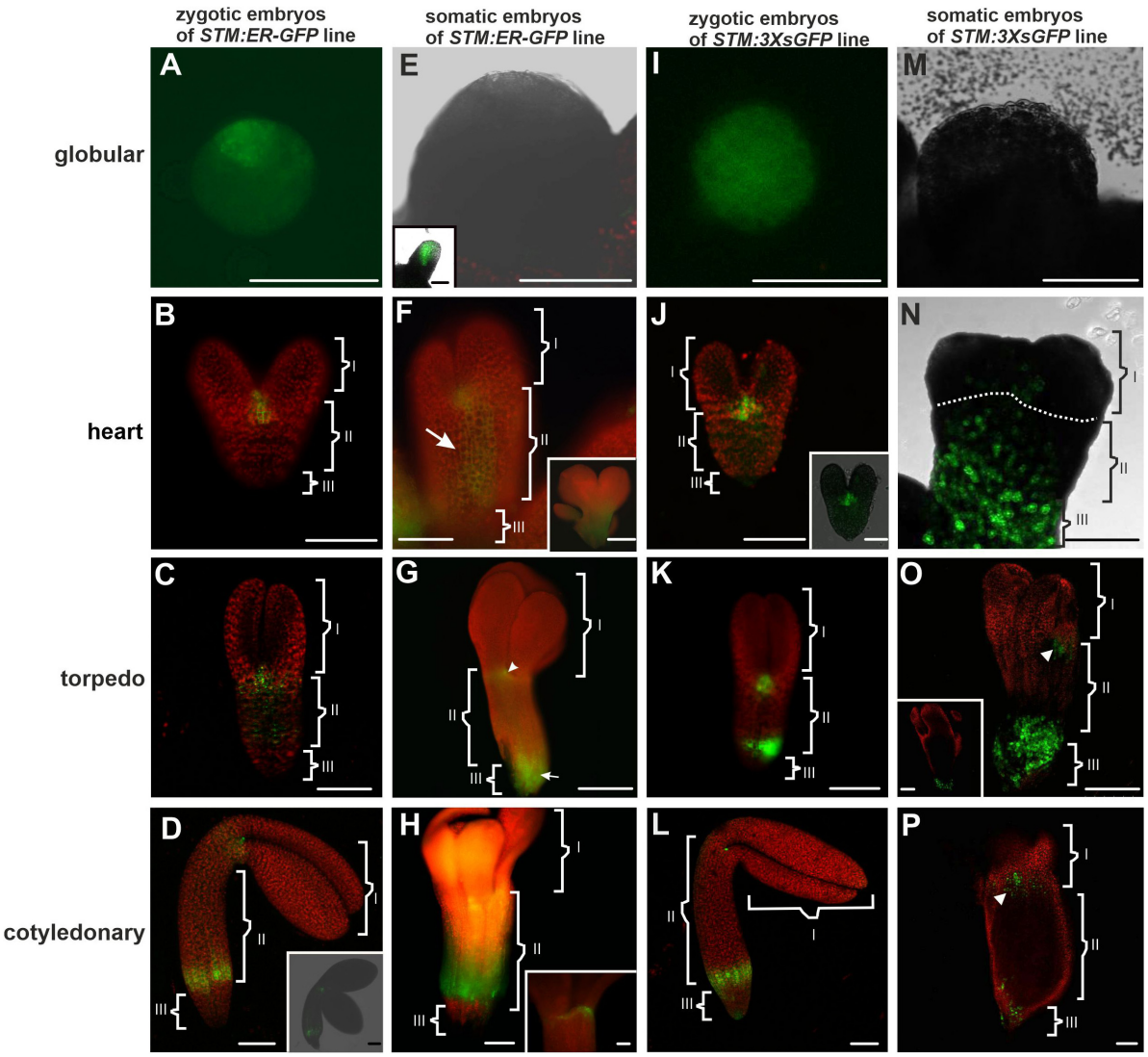

FIGURE 1 | *STM:ER-GFP* promoter activity and localization of the 3XsGFP in the ZEs and SEs. Promoter activity in the **(A)** globular; **(B)** heart, **(C)** torpedo, and **(D)** cotyledonary stages of ZEs. **(D inset)** The optical section of the ZE (from CLSM). **(E)** Globular SE without any visible promoter activity. **(E inset)** Advanced stage of the globular SE with a promoter activity. **(F and F inset)** Heart and **(G)** torpedo stages of the SE. **(H)** Cotyledonary stage of the SE. **(H inset)** The SAM in an embryo in the cotyledonary stage. **(I)** Globular and **(J)** heart stages of the ZEs with the fluorescence of the 3XsGFP. **(J inset)** Optical section through the heart embryo. **(K)** Torpedo and **(L)** cotyledonary stages of the ZE – green fluorescence indicates the presence of the 3XsGFP. **(M)** In the globular SE, the 3XsGFP was not detected. **(N)** Heart and **(O)** torpedo stages of the SE. **(O inset)** The optical section through the basal part of the SE embryo in the torpedo stage. **(P)** Cotyledonary stage of the SE – green fluorescence indicates the presence of the 3XsGFP [arrowheads on **(O,P)** indicate the area with the GFP in the identified SAM area]. The embryo was divided into three parts **I** – apical, **II** – central and **III** – basal. **A,F,F inset,G,H,H inset** – Images from the epifluorescence microscope; **B–D,D inset,J inset,K–O,O inset,P** – images from CLSM. Scale bars; **A,C,D,D inset E,E inset,F,F inset,G–O,O inset**, $P = 100$ μm; **B,J,J inset,H inset** = 50 μm.

SE, the 2XsGFP and 3XsGFP did not spread from the location of their expression, unlike in the ZEs.

Symplasmic Communication Between the Embryo Tissues

The sites of the *AtGL2* promoter activity (*Arabidopsis thaliana GLABRA 2*) were analyzed using the transgenic lines *AtGL2:tmGFP*. The distribution pattern of the GFP molecule between the protodermis and underlying tissues was determined using the *AtGL2:GFP* transgenic line (*AtGL2* promoter/*GFP*; in the *AtGL2:tmGFP* transgenic line, the GFP was fused to the C-terminus of the transmembrane helicase of the AtSTP9 monosaccharide transporter; Stadler et al., 2005).

The *tmGFP* expression site in the ZEs and SEs indicated that the *AtGL2* promoter was inactive in the globular stage (not shown). It was activated in the heart stage and was expressed in the protodermal cells of the hypocotyl (**Figure 3A**). These sites of promoter activity persisted in the successive stages of the development of the ZEs and, in some cases, the fluorescence of tmGFP also occurred in the proximal part of the cotyledons

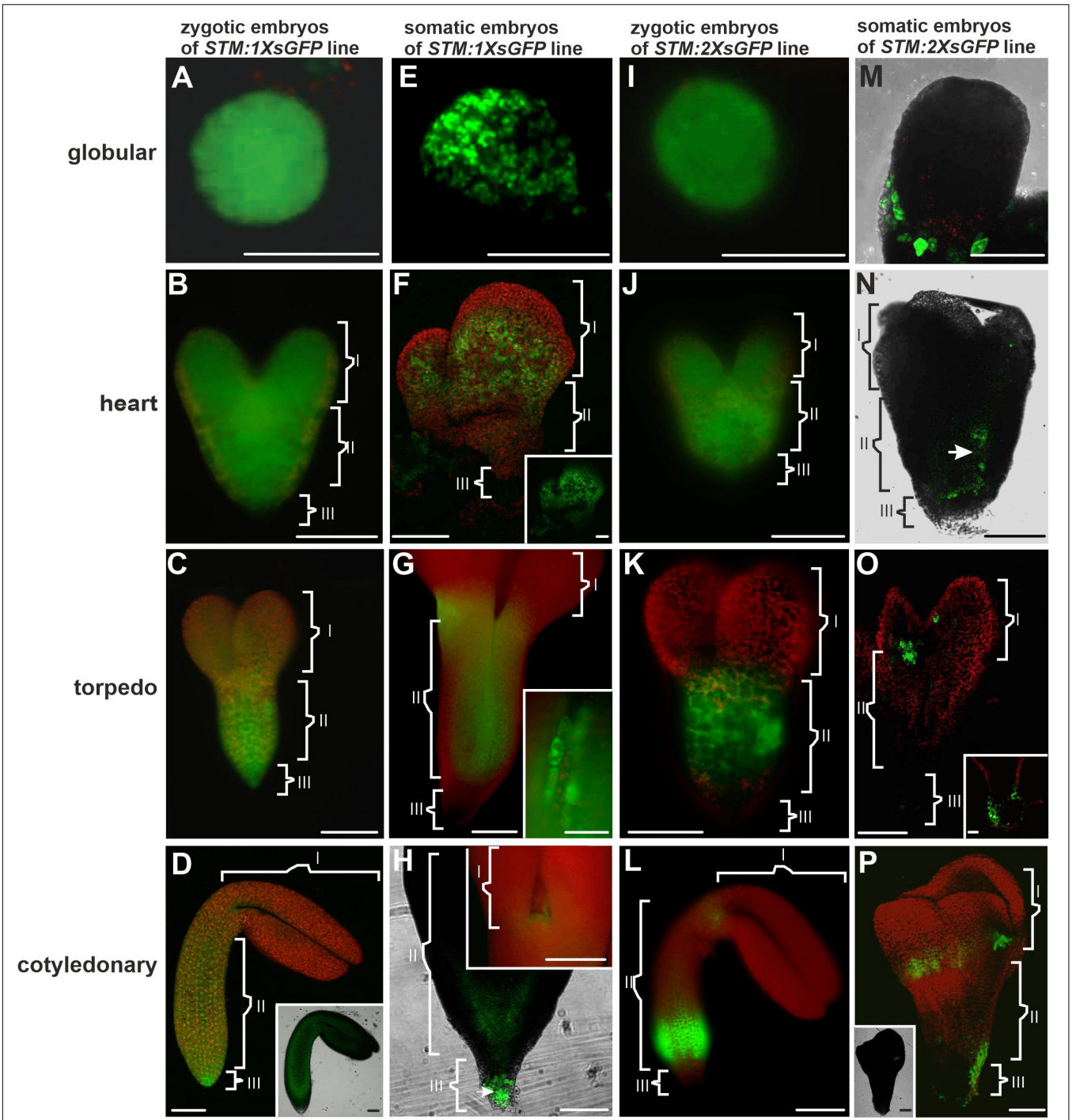

FIGURE 2 | Distribution pattern of the 1XsGFP and 2XsGFP in the ZEs and SEs. Distribution of the 1XsGFP was observed in the entire ZEs at all of the developmental stages: **(A)** globular, **(B)** heart, **(C)** torpedo, and **(D)** cotyledonary. **(D inset)** The optical section (CLSM; only GFP channel) shows the 1XsGFP presence in the entire embryo. **(E)** Globular and **(F)** heart stages of the SE with the fluorescence of the 1XsGFP. **(F inset)** The GFP channel. **(G)** Torpedo stage of the SE. **(G inset)** The intracellular localization of the GFP. **(H)** Embryo in the cotyledonary stage. **(H inset)** The SAM in the embryo in the cotyledonary stage (green fluorescence indicates the presence of the 1XsGFP). **(I)** Globular, **(J)** heart, **(K)** torpedo, and **(L)** cotyledonary stage of the ZEs (green fluorescence indicates the presence of the 2XsGFP). **(M)** In the globular SE, the 2XsGFP was not detected. **(N)** Heart and **(O)** torpedo SE. **(O inset)** Basal part of the torpedo SE. **(P)** Cotyledonary stage of the SE (green fluorescence indicates the presence of the 2XsGFP). **(P inset)** Optical section through the SE in the cotyledonary stage with fluorescence visible in the SAM cells. (**I, II,** and **III** – description is the same as for **Figure 1**). **A–C,E,G,H inset,I–L** – images from the epifluorescence microscope; **D,D inset, F,H,M,O,P,P inset** – images from the CLSM. Scale bars; **A,C,D,D inset,E–G,H inset,I,K–O,O inset,P,P inset** = 100 μm; **B,J,H** = 50 μm; **G inset** = 10 μm.

(**Figure 3B**). There was a characteristic pattern in the distribution of the fluorescence of the tmGFP in the hypocotyl in the torpedo stage (**Figure 3B** inset), which was quite pronounced in the cotyledonary stage (**Figure 3C** and inset). The protodermal cells in which the tmGFP was expressed formed files along the long embryo axis and alternated with the cells that did not express the tmGFP. The *AtGL2* promoter was only active in the protodermal cells (**Figures 3B,C** and insets).

In the SEs, promoter activity was mainly observed in the heart stage embryo's basal parts (**Figure 3D**). In the torpedo stage, the fluorescence of the tmGFP was mainly observed in the hypocotyl and also in a punctate pattern within the protodermal cells of the cotyledons (**Figure 3E**). Within the hypocotyl, the *tmGFP*-expressing cells formed irregular files along the organ's long axis, which alternated with the tmGFP-negative cell files (**Figure 3E** and inset). The expression of the *tmGFP* in the cotyledonary SEs was detected in the hypocotyl and cotyledons (**Figure 3F**). Similar to the ZEs, the *AtGL2* promoter was active only in the protodermal cells of the SEs (**Figures 3E** inset,F inset). The results indicate that there are similarities in the sites of the *AtGL2* promoter activity in the SEs and ZEs, but that in the SEs, the expression pattern of the *tmGFP* in the hypocotyl was quite irregular and was also visible in the cotyledons (**Table 3**).

An analysis of the GFP distribution in the ZEs of the *AtGL2:GFP* line showed that in the heart stage, the GFP was detected throughout the entire embryo in both the protodermis and in the underlying cell layers (**Figure 3G**). A similar distribution of the GFP was observed for the

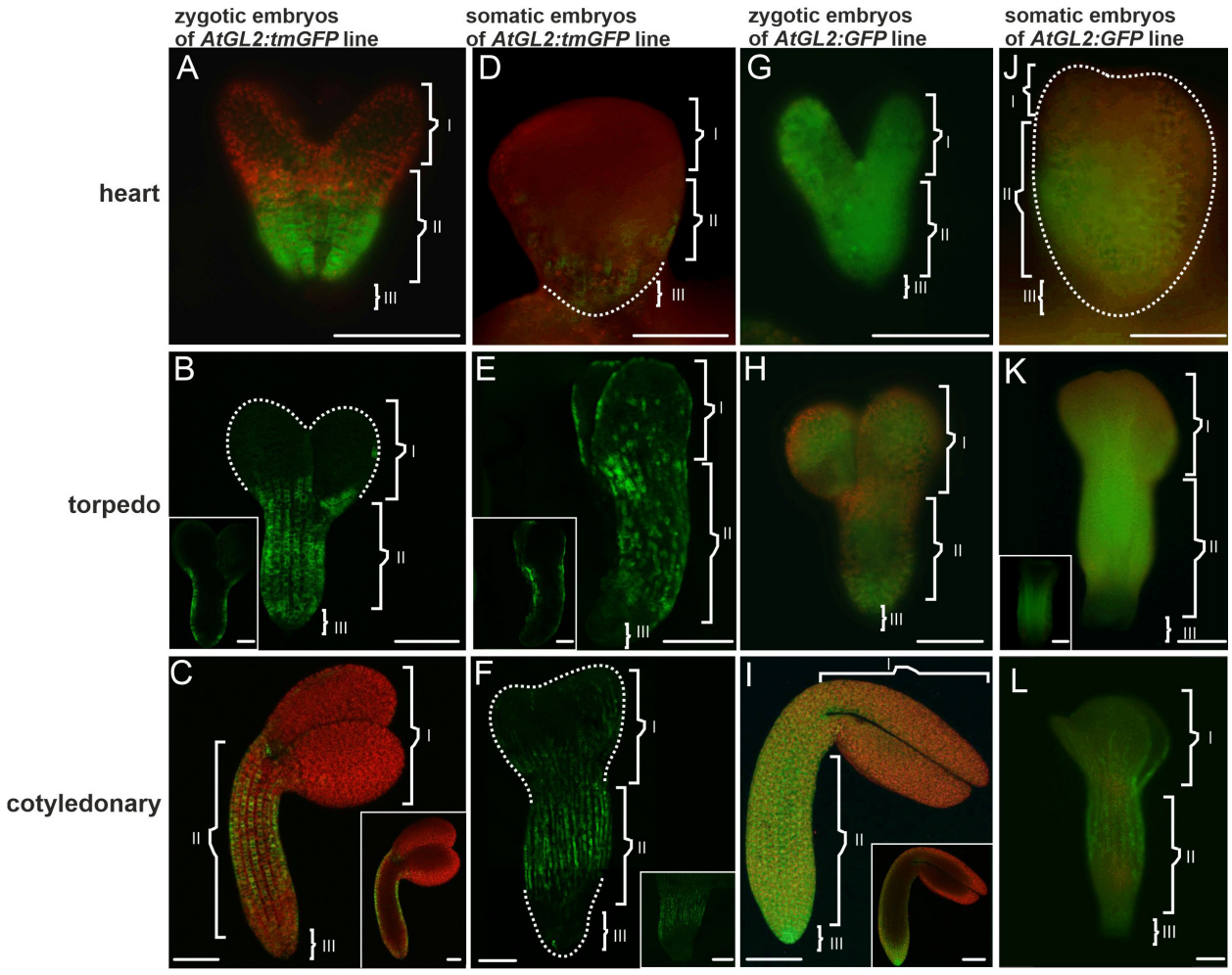

FIGURE 3 | The *AtGL2* promoter activity and GFP distribution pattern in the ZEs and SEs. **(A)** *AtGL2* promoter activity in the ZE in the heart stage, **(B)** in the torpedo and **(C)** cotyledonary stages. **(B,C insets)** An optical section. **(D)** Heart stage of the SE – fluorescence in the central and basal part of the embryo. **(E)** The torpedo stage – promoter activity is present in the protodermal cell of the entire embryo. **(E inset)** An optical section showing the fluorescence in the protodermal cells. **(F)** Cotyledonary stage with fluorescence in the protodermal cells of the hypocotyl and cotyledons. The GFP distribution in the **(G)** heart, **(H)** torpedo, and **(I)** cotyledonary stages of the ZE embryos. **(I inset)** An optical section. The GFP in the **(J)** heart and **(K)** torpedo stages of the SE. **(K inset)** Hand-cut section through the SE – fluorescence in the provascular tissue. **(L)** Cotyledonary stage of the SE. Dotted lines indicate the embryo surface. (**I, II,** and **III** – description is the same as for **Figure 1**). **A,D,G,H,J,K,K inset** – images from the epifluorescence microscope; **B,C,C inset,E,E inset,F,I,I inset,L,L inset** – images from the CLSM. Scale bars = 100 μm.

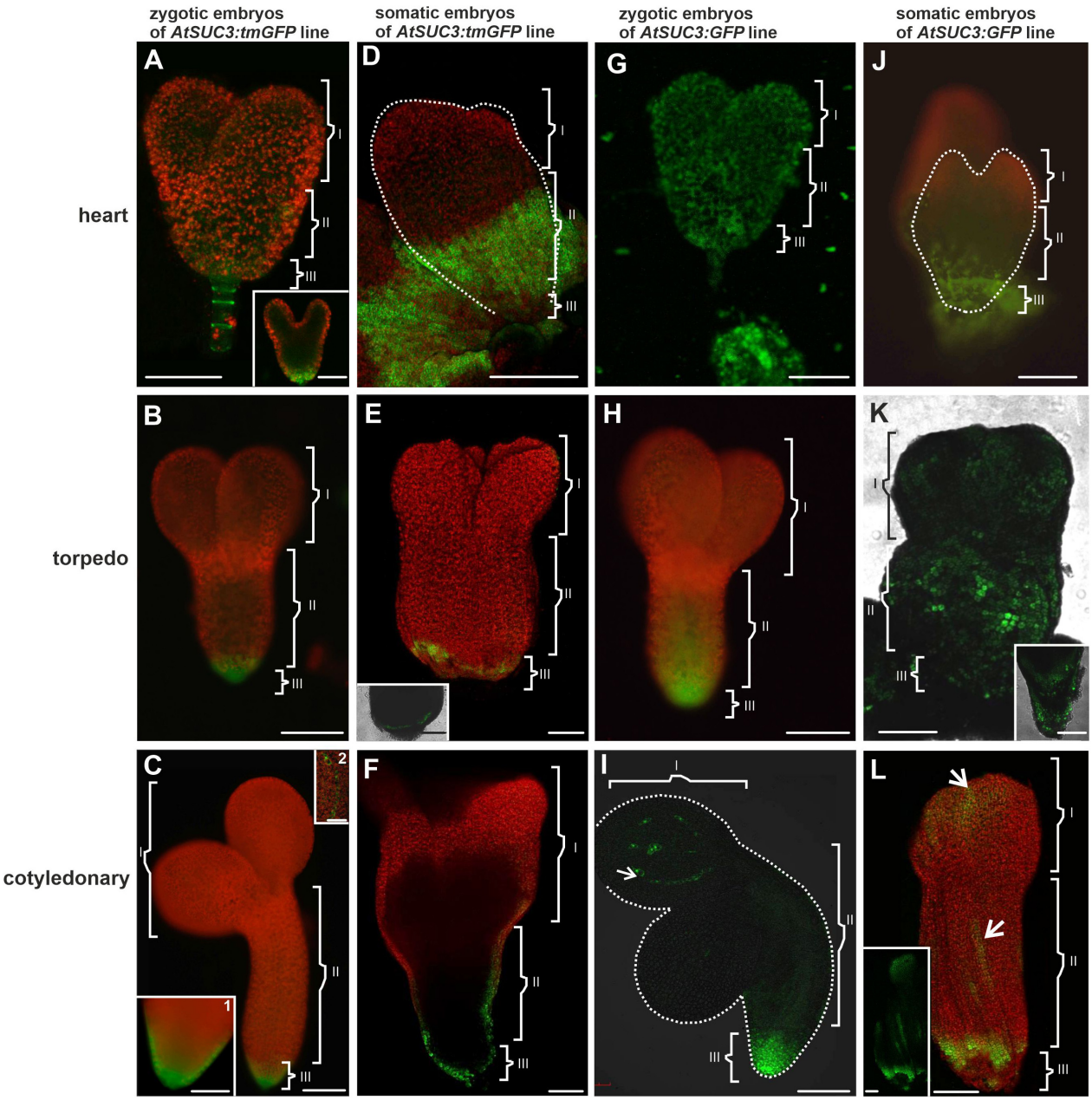

FIGURE 4 | The *AtSUC3* promoter activity and GFP distribution in the ZEs and SEs. The *AtSUC3* promoter was active in the ZE **(A)** in the heart, **(B)** torpedo, and **(C)** cotyledonary stages. In SE: **(D)** in the heart, **(E)** torpedo, and **(F)** cotyledonary stages, the promoter activity was in the central and basal parts of the embryo. The GFP distribution in **(G)** the heart, **(H)** torpedo, and **(I)** cotyledonary stages of the ZE. GFP in **(J)** the heart, **(K)** torpedo, and **(L)** cotyledonary stages of the SE embryos. **(K inset)** An optical section through the basal part of the hypocotyl. **(L inset)** – confocal image showed that the GFP fluorescence was only in the protodermal cells. Dotted lines indicate the embryo surface. (**I, II,** and **III** – description is the same as for **Figure 1**). **A–C,C insets,D,G,H,J** – images from the epifluorescence microscope; **E,E inset,F,I,K,L** – images from the CLSM. Scale bars: **A,A inset G** – 50 μm; **B,C,C inset 1,D–F,H,I–K,K inset,L,L inset** = 100 μm

embryos in the torpedo stage (**Figure 3H**). In the cotyledonary stage, the GFP fluorescence was only observed in the protodermal cells (**Figure 3I** and inset). To summarize, the GFP moves until (including) torpedo stage, within the entire embryo from the protodermis to the underlying tissues, thus indicating that the movement of molecules of 27 kDa through the PDs in centripetal direction was possible. In the cotyledonary stage, the protodermis is a symplasmic domain for molecules up to 27 kDa.

An analysis of the GFP distribution in the SEs of the *AtGL2*:*GFP* line, the GFP was not detected in the globular stage (not shown). In the heart stage, the GFP fluorescence was visible throughout the embryo's hypocotyl and embryo basal parts (**Figure 3J**). In the torpedo stage, the GFP fluorescence was

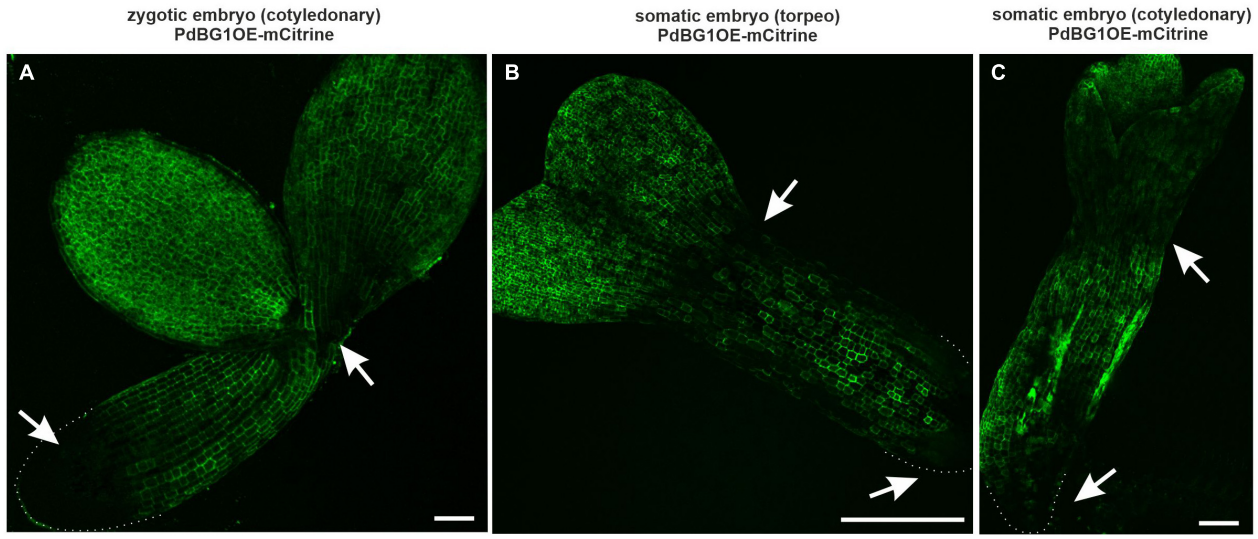

FIGURE 5 | PDGB1 distribution in ZEs and SEs. **(A)** ZE in the cotyledonary stage. **(B)** SE in torpedo and **(C)** in cotyledonary stage. Arrows indicated the areas with lower PDGB1. Dotted lines indicate the embryo root surface. All images are from CLSM. Scale bars; **(A)** = 50 μm; **(B,C)** = 100 μm.

observed in the hypocotyl protodermis and in the underlying cell layers (**Figure 3K** inset) as well as in the apical part of the embryo (**Figure 3K**). In the embryos in the cotyledonary stage, the GFP fluorescence was observed in the hypocotyl and in the proximal and middle parts of the cotyledons. The GFP was not detected in the underlying cell layers (**Figure 3L** and **Table 3**). The results indicate that there were restrictions in the symplasmic movement of the GFP between the protodermal cells in the cotyledonary stage in both the SEs and ZEs.

The transgenic lines *AtSUC3:tmGFP* and *AtSUC3:GFP* (Arabidopsis *Suc-transporter3 AtSUC3* gene promoter) were used to design these constructs (Stadler et al., 2005). Using the *AtSUC3:tmGFP* line, the sites of the *AtSUC3* promoter activity in the ZEs were examined first. The analysis showed that in the early stages of embryogenesis, the *AtSUC3* promoter was active in the suspensor and the hypophysis (**Figure 4A**). In the torpedo stage, the promoter activity was observed in all of the cells in the basal part of the embryo (**Figure 4B**) and in the cotyledonary stage, it was visible in the columella cells and the root cap peripheral cells (**Figure 4C**, inset 1) as well as in the cotyledon provascular tissue (**Figure 4C**, inset 2).

In the SEs, the *AtSUC3* promoter was inactive in the globular stage (not shown). In the heart stage, the promoter activity was observed in the cells of the middle (hypocotyl) and basal (the root pole) parts of the embryo (**Figure 4D**). The area of the tmGFP-derived fluorescence at this stage covered a significant part of the embryo. In the torpedo stage, the tmGFP was expressed only in the cells in the basal part of the embryo (**Figure 4E** and inset). The expression of the tmGFP in the SEs in the cotyledonary stage was detected in the cells of the root and in the basal part of the hypocotyl (**Figure 4F**). The results indicate that the sites of the *AtSUC3* promoter activity in the SEs and ZEs are similar and include the embryonic root surface cells; however, in the SEs, especially in the heart stage, the number of cells expressing the *tmGFP* was greater.

The GFP in the ZEs of the *AtSUC3:GFP* line in the heart stage was detected in the cells of the entire embryo (**Figure 4G**). In the torpedo stage, the GFP fluorescence was observed in the basal and central parts of the embryo, where it was present in the protodermal cells, ground promeristem and provascular tissue (**Figure 4H**). In the cotyledonary stage, the GFP fluorescence was observed in the basal part of the embryo and in discontinuous cell files (representing the provascular tissue) within the cotyledon (**Figure 4I**). The results indicate that in the cotyledonary stage of the ZEs, symplasmic isolation occurs between the embryo root and the other embryo organs and between the cells of the provascular tissue and ground promeristem (**Table 4**).

The presence of the GFP in the SEs of *AtSUC3:GFP* in the heart stage was detected in the central and basal parts of the embryo (**Figure 4J**). In the torpedo stage (**Figure 4K**), the GFP fluorescence was seen in the protodermal cells of the entire embryo and in the ground promeristem cells in the basal part of the hypocotyl (**Figure 4K** and inset). In the cotyledonary stage, the GFP fluorescence was observed throughout the protodermal cells of the hypocotyl and cotyledons but the distribution pattern was patchy (**Figure 4L** and **Table 4**).

The PdBG1OE-mCitrine line (PdBG1 – a Callose-Degrading Enzyme in PDs; Benitez-Alfonso et al., 2013) was used to determine the involvement of callose in the formation of the symplasmic domains during embryogenesis. This enzyme is directly involved in degrading the β-1,3 glucans and indirectly in modifying the callose deposition in the PDs. The PdBG1 tagged with mCitrine shows areas with a higher enzyme activity that corresponds to less callose deposition (Benitez-Alfonso et al., 2013). Present studies were performed on ZEs in the cotyledonary stage and SEs in the torpedo and cotyledonary stages, for which the symplasmic domains were determined and described above.

In the ZEs, the area without the PdBG1 was detected in the basal part of the embryos, which might indicate that there is a higher level of callose compared to the other embryo parts (**Figure 5A**). In the SEs in torpedo and cotyledonary stages, the areas without the PDBG1 were localized in the cotyledon node and at the boundary between the hypocotyl and the root pole, that is, in the areas that corresponded to the distinguished symplasmic domains (**Figures 5B,C**).

Histology of the SE in the Different Developmental Stages

The studies on symplasmic communication in the SEs were accompanied by a histological analysis to define the histology of the SEs. The SE developmental stages were globular (**Supplementary Figure 1A** and inset), heart (**Supplementary Figure 1B**), torpedo (**Supplementary Figure 1C**), and cotyledonary (**Supplementary Figure 1D**). The embryos had a more or less spherical shape in the globular stage with an easily distinguishable protodermis (**Supplementary Figure 1A**). Embryos in the heart stage had cotyledon primordia, ground promeristem and provascular tissue (**Supplementary Figure 1B** and inset). The histological structure of the embryos in the torpedo stage was similar to that of the embryos in the heart stage (**Supplementary Figure 1C**). The SAM was rarely convex and was usually flat (**Supplementary Figure 1C** and inset). In the cotyledonary stage, the SEs had well-developed cotyledons, hypocotyl and embryonic root and protodermis, provascular tissue and a ground promeristem (**Supplementary Figures 1D,E**). The SEs quite often had more than two cotyledons (not shown), fused hypocotyls and roots (**Supplementary Figures 1F,H**) or had a malformed hypocotyl (**Supplementary Figure 1G**). The provascular tissue ran from the root meristem along the hypocotyl, then branched and passed into the cotyledons (**Supplementary Figure 1E**). The abnormalities in tissue arrangement and cytological features of the cells that comprised the tissues were distinct from the cotyledonary stage. The most pronounced malformations were detected in the ground promeristem and provascular strands (**Supplementary Figures 1F–H**). The files of the ground promeristem cells were not aligned (**Supplementary Figure 1D** inset) and in many of the SEs were composed of more cell layers than in their zygotic counterparts (**Supplementary Figures 1C–H** for comparison, a ZE is shown as an inset in **Supplementary Figure 1G**). The provascular tissue was well visible and like the ground promeristem was composed of more cell files than their zygotic counterparts (**Supplementary Figures 1F,H** and **Table 4**).

DISCUSSION

The establishment of the body pattern during embryogenesis, both zygotic and somatic, is under the control of auxin signaling and differential gene expression (Smertenko and Bozkhov, 2014; Horstman et al., 2017; Fehér, 2019; Tian et al., 2020 and literature therein). Increasing evidence had indicated that symplasmic communication is also involved in the control of embryogenesis (Xu et al., 2012; Brunkard et al., 2015; Choudhary et al., 2020; Godel-Jedrychowska et al., 2020 and literature therein) as well as postembryonic development (Sorkin and Nusinow, 2021; Sager et al., 2021 and literature therein). In the present study, the distribution pattern of the GFP within the SEs and ZEs at different developmental stages was studied to determine the spatio-temporal localization of the symplasmic domains that accompany the establishment of the embryo organs and tissues.

The results of the GFP distribution in the ZEs and SEs showed that: (1) in the SEs, the symplasmic domains for molecules up to 27 kDa can be distinguished from the heart stage; (2) in the ZEs, the symplasmic domains were established from the torpedo stage for molecules up to 54 kDa; (3) the symplasmic domains between the embryo tissues in the SEs is similar to the one in the ZEs; (4) a key difference between the ZEs and SEs is that in the SE, there is no expression of the STM in the globular stage, which might indicate that the apical-basal polarity is not established at this stage and (5) a restriction in symplasmic transport in the SEs and ZEs is correlated with the developmental stages (**Figure 6**).

Symplasmic Domains and Embryo organ Development

During embryogenesis, along the apical-basal axis, the SAM, cotyledons, hypocotyl and radicula are determined and in the radial direction, the protodermis, ground promeristem and provascular tissues are established (Laux et al., 2004). Achieving such an organization requires cell specification in an integrated manner (Laux et al., 2004; Radoeva et al., 2019 and literature therein). The involvement of symplasmic communication/restriction in embryogenesis was first described for development in Arabidopsis ZEs. Studies using the GFP as a mobile fluorescent protein have shown that the symplasmic domains accompany the development of the embryo organs and are established by the mid-torpedo stage with the PDs SEL of 54 kDa at the organ boundaries (Kim et al., 2005a,b). Similar symplasmic domains were detected in the Arabidopsis SEs, but these subdomains appeared in the heart stage and the PDs SEL at their boundaries was determined to be 27 kDa (**Figure 6**). Regardless of the identified differences, the results support the hypothesis that restrictions in symplasmic communication was correlated with embryo development and the idea that postulates the participation of the PDs as control "points" for the movement of signals during embryogenesis (Otero et al., 2016; Sager and Lee, 2018 and literature therein). The question then arises of whether the identified differences between the ZEs and SEs are developmentally significant. It seems not because the correlation between the emerging domains and the developing embryo organs is clear, and therefore, from a qualitative point of view, there are no differences between the SEs and ZEs in terms of the correlation between the embryo development and the formation of the symplasmic domains. The reason that the limitations in symplasmic communication appear earlier in the SEs than in the ZEs is unknown. It can be presumed that they arise from the morphological heterogeneity (a greater number of cotyledons, the malformation of the SAM and RAM in SEs in comparisons to the ZEs) between the SEs and ZEs that have been described

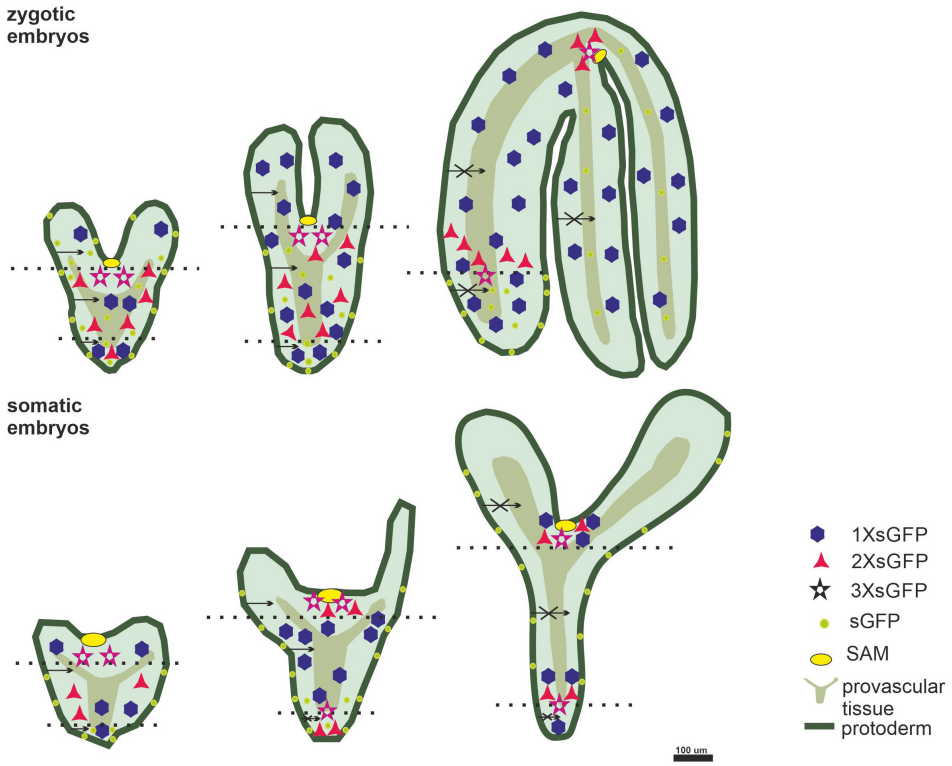

FIGURE 6 | The symplasmic domains identified in the longitudinal direction (between the embryo organs; dotted lines indicate the embryo parts; apical central; basal). In the radial direction – between the embryo tissues; dark green – protodermis; light green – ground promeristem; olive – provascular tissue; octagon – 1XsGFP; triangle – 2XsGFP; star – 3XsGFP; yellow circle – SAM; greenish circle – GFP expressed under *pSUC3*; arrows – the movement in the direction indicated by the arrowhead; a crossed arrows indicates no movement in the direction indicated by the arrowhead.

in many species (Dodeman et al., 1997; Mordhorst et al., 1998; Pullman et al., 2003; Etienne et al., 2013; Jariteh et al., 2015) and that was observed in the present study. Such heterogeneity may be the result of disturbances in the spatio-temporal establishment of the apical-basal and radial polarity of the SEs. The detected differences could also have resulted from the diverse capacity of the PDs to transport molecules in these two types of embryos. The GFP movement is (generally) a passive, diffusion-driven transport. Such transport is a function (among others) of the area of passage, the length of the PDs, the wall effects and the electrochemical potential differences between adjacent cells (Liarzi and Epel, 2005; Dashevskaya et al., 2008). It cannot be ruled out that these parameters are different in the ZEs and SEs, at least in the early stages of development. The the shape of the PDs can also influence the GFP movement between organs/tissues (Dashevskaya et al., 2008; Amsbury et al., 2018 and literature therein). Thus, in future studies, the cell wall thickness and the the shape of the PDs in the SEs must also be evaluated.

Radial Pattering of Embryo and Symplasmic Domains

The results showed that using two transgenic lines, it was possible to trace the GFP distribution pattern between the embryo tissues during embryogenesis. The epidermis has been shown to become symplasmically isolated from the underlying shoot/embryo tissues for tracer dyes and several transcription factors and the reasons for this have previously been discussed (e.g., Roberts and Oparka, 2003; van Bel, 2018). The symplasmic communication between the protodermis and underlying tissues in the ZEs occurred freely in the heart and torpedo stages, thus indicating that these embryos were a single symplasmic domain (Stadler et al., 2005). The results for the SEs were similar to those that were obtained for their zygotic counterparts. In the cotyledonary stage, the protodermis was a distinct symplasmic domain in the ZE and SE, thus indicating that the protodermis, at least for molecules equal to or greater than 27 kDa, was isolated from the underlying tissues. Why is it important to isolate the protodermis as a separate symplasmic domain? Perhaps, this covering tissue must be specified because in the post-embryonic development, it differentiates into several different cell types, but whether this is the only reason is unknown.

Studies on the ZEs of Arabidopsis showed that the embryos in the heart stage that had been derived from the *AtSUC3* promoter/*GFP* plants were a single symplasmic domain (Stadler et al., 2005). In the torpedo stage, only the hypocotyl was a single domain, but in the fully developed embryos, there was restricted movement between the embryo tissues (Stadler et al., 2005). It appeared that in the SEs, the symplasmic domain occurred

earlier in the temporal sense but that it was similar to their zygotic counterparts in qualitative sense (**Figure 6**).

PD SEL Changes and Embryogenesis

The PDs SEL is regulated during development (Sager and Lee, 2018; Petit et al., 2020 and literature therein) and can be changed by callose deposition (Benitez-Alfonso et al., 2013; Wu et al., 2018; Li et al., 2020 and literature therein). Callose turnover in the PDs plays a key role in different developmental processes (Benitez-Alfonso et al., 2013 and literature therein), including embryogenesis (Du et al., 2020). The reason for the difference in the PDs SEL between the ZEs and SEs is not known. Because the PDs SEL is associated with callose deposition, it seems reasonable to look at this mechanism for an explanation of the detected difference. Results describing the symplasmic communication between the embryonic and non-embryonic areas of an Arabidopsis explant indicated that callose deposition at the PDs is a prerequisite for changing the cell fate (Godel-Jedrychowska et al., 2020). The present results using the PdBG1OE-mCitrine line indicate that callose degradation was lower on the boundaries of the distinguished symplasmic domains along the apical-basal axis. These results support the role of the PDBG1 in callose deposition in the PD and indicate that the establishment of symplasmic domains is important for embryogenesis independent of the origin of an embryo.

CONCLUSION

Despite the detected differences in the the spatio-temporal diversity in the formation of the symplasmic domains, there was a clear correlation between the identified domains and the embryo development independent of origin of an embryo (**Figure 6**). This may indicate that symplasmic communication, which is based on the restrictions of the symplasmic transport of signals, is a mechanism that is involved in regulating embryogenesis.

DATA AVAILABILITY STATEMENT

The raw data supporting the conclusions of this article will be made available by the authors, without undue reservation.

AUTHOR CONTRIBUTIONS

KK-Ł, KG-J, and EK designed the experiments. KK-Ł and KG-J performed the experiments and analyzed the data. EK and KG-J wrote the manuscript. All the authors provided feedback on the manuscript.

FUNDING

This research was supported as a part of the statutory activities of the Institute of Biology, Biotechnology and Environmental Protection, Faculty of Natural Sciences, University of Silesia.

ACKNOWLEDGMENTS

The authors are very grateful to Patrycja Zambryski (Department of Plant and Microbial Biology, University of California, Berkeley, CA, United States; (https://vcresearch.berkeley.edu/faculty/patricia-zambryski) for providing the Col-0 transgenic line that carries the *STM:ER-GFP, STM:1XsGFP, STM:2XsGFP,* and *STM:3XsGFP*; Ruth Stadler (Molekulare Pflanzenphysiologie, Universität Erlangen-Nürnberg, Erlangen, Germany) for providing the *Arabidopsis thaliana* transgenic lines *AtGL2:tmGFP9, AtGL2:GFP, AtSUC3:tmGFP9,* and *AtSUC3:GFP,* and Yoselin Benitez-Alfonso for (Centre for Plant Sciences, School of Biology, University of Leeds, Leeds, United Kingdom) for providing the *PdBG1OE*-mCitrine line. Because of space constraints, not all of the relevant studies could be cited. The authors are grateful to the reviewers for their valuable comments and Michele Simmons, native English speaker, for editing our manuscript.

SUPPLEMENTARY MATERIAL

The Supplementary Material for this article can be found online at: https://www.frontiersin.org/articles/10.3389/fpls.2021.649806/full#supplementary-material

Supplementary Figure 1 | Histology of the somatic embryos in the different stages of development. **(A)** Somatic embryos in the globular stage (arrow on inset points to the protodermis), **(B,B inset)** heart stage, **(C)** torpedo stage (arrows point to the SAM), **(D,E)** cotyledonary stage. (**D inset**) intercellular spaces between the ground promeristem cells. **(F)** Somatic embryos fused along the root and hypocotyl axis. (**F inset**) vessels on a single cross-section; the appearance of these vessels indicates that the provascular tissue meanders in the embryo. **(G)** A somatic embryo with a malformed hypocotyl. **(G inset)** longitudinal section through the ZE (for comparison to the SE). **(H)** Somatic embryos fused in the hypocotyl part. Staining: 0.05% TBO. Scale bars: **(A)** – 50 μm; **(A inset)** – 20 μm; **(B,C,G inset)** – 100 μm; **(B inset,F inset)** – 50 μm; **(C inset,D inset)** – 30 μm; **(D–H)** – 200 μm.

REFERENCES

Amsbury, S., Kirk, P., and Benitez-Alfonso, Y. (2018). Emerging models on the regulation of intercellular transport by plasmodesmata-associated callose. *J. Exp. Bot.* 69, 105–115. doi: 10.1093/jxb/erx337

Barlow, P. W., and Kurczyńska, E. U. (2007). The anatomy of the chi-chi of *Ginkgo biloba* suggests a mode of elongation growth that is an alternative to growth driven by an apical meristem. *J. Plant. Res.* 120, 269–280. doi: 10.1007/s10265-006-0050-3

Bassuner, B. M., Lam, R., Lukowitz, W., and Yeung, E. C. (2007). Auxin and root initiation in somatic embryos of Arabidopsis. *Plant Cell Rep.* 26, 1–11. doi: 10.1007/s00299-006-0207-5

Bayer, E. M. F., and Salmon, M. S. (2013). Dissecting plasmodesmata molecular composition by mass spectrometry-based proteomics. *Front. Plant Sci.* 3:307. doi: 10.3389/fpls.2012.00307

Benitez-Alfonso, Y., Faulkner, C., Pendle, A., Miyashima, S., Helariutta, Y., and Maule, A. (2013). Symplastic intercellular connectivity regulates lateral root patterning. *Dev. Cell* 26, 136–147. doi: 10.1016/j.devcel.2013.06.010

Brunkard, J. O., Runkel, A. M., and Zambryski, P. C. (2015). The cytosol must flow: intercellular transport through plasmodesmata. *Curr. Opin. Cell Biol.* 35, 13–20. doi: 10.1016/j.ceb.2015.03.003

Burch-Smith, T. M., Stonebloom, S., Xu, M., and Zambryski, P. C. (2011). Plasmodesmata during development: re-examination of the importance of primary, secondary and branched plasmodesmata structure versus function. *Protoplasma* 248, 61–74. doi: 10.1007/s00709-010-0252-3

Burch-Smith, T. M., and Zambryski, P. C. (2010). Loss of increased size exclusion limit (ISE)1 or ISE2 increases the formation of secondary plasmodesmata. *Curr. Biol.* 20, 989–993. doi: 10.1016/j.cub.2010.03.064

Canhoto, J. M., Mesquita, J. F., and Cruz, G. S. (1996). Ultrastructural changes in cotyledons of *pineapple guava (Myrtaceae*) during somatic embryogenesis. *Ann. Bot.* 78, 513–521. doi: 10.1006/anbo.1996.0149

Capron, A., Chatfield, S., Provart, N., and Berleth, T. (2009). Embryogenesis: pattern formation from a single cell. *Arabidopsis Book/Am. Soc. Plant Biol.* 7:e0126. doi: 10.1199/tab.0126

Choudhary, A., Kumar, A., Kaur, N., and Paula, A. (2020). Plasmodesmata the nano bridges in plant cell: are the answer for all the developmental processes? *Russian J. Plant Physiol.* 67, 785–796. doi: 10.1134/s1021443720050039

Dashevskaya, S., Kopito, R. B., Friedman, R., Elbaum, M., and Epel, B. L. (2008). Diffusion of anionic and neutral GFP derivatives through plasmodesmata in epidermal cells of *Nicotiana benthamiana*. *Protoplasma* 234:13. doi: 10.1007/s00709-008-0014-7

Dodeman, V. L., Ducreux, G., and Kreis, M. (1997). Zygotic embryogenesis versus somatic embryogenesis. *J. Exp. Bot.* 48, 1493–1509. doi: 10.1093/jexbot/48.313.1493

Du, B., Zhang, Q., Cao, Q., Xing, Y., Qin, L., and Fang, K. (2020). Changes of cell wall components during embryogenesis of Castanea mollissima. *J. Plant Res.* 133, 257–270. doi: 10.1007/s10265-020-01170-7

Dubois, T., Guedira, M., Dubois, J., and Vasseur, J. (1991). Direct somatic embryogenesis in leaves of *Cichorium*. *Protoplasma* 162, 120–127.

Etienne, A., Génard, M., Bancel, D., Benoit, S., and Bugaud, C. (2013). A model approach revealed the relationship between banana pulp acidity and composition during growth and post-harvest ripening. *Sci. Hortic.* 162, 125–134. doi: 10.1016/j.scienta.2013.08.011

Fehér, A. (2019). Callus, dedifferentiation, totipotency, somatic embryogenesis: what these terms mean in the era of molecular plant biology? *Front. Plant Sci.* 10:536. doi: 10.3389/fpls.2019.00536

Gaj, M. D. (2001). Direct somatic embryogenesis as a rapid and efficient system for in vitro regeneration of *Arabidopsis thaliana*. *Plant Cell Tiss. Org.* 64, 39–46.

Gamborg, O. L., Miller, R., and Ojima, K. (1968). Nutrient requirements of suspension cultures of soybean root cells. *Exp. Cell Res.* 50, 151–158. doi: 10.1016/0014-4827(68)90403-5

Godel-Jedrychowska, K., Kulinska-Lukaszek, K., Horstman, A., Soriano, M., Li, M., Malota, K., et al. (2020). Symplasmic isolation marks cell fate changes during somatic embryogenesis. *J. Exp. Bot.* 71, 2612–2628. doi: 10.1093/jxb/eraa041

Grimault, V., Helleboid, S., Vasseur, J., and Hilbert, J. L. (2007). Co-Localization of ß-1, 3-glucanases and callose during somatic embryogenesis in *Cichorium*. *Plant Signal. Behav.* 2, 455–461. doi: 10.4161/psb.2.6.4715

Han, Y. Z., Huang, B. Q., Zee, S. Y., and Yuan, M. (2000). Symplastic communication between the central cell and the egg apparatus cells in the embryo sac of *Torenia fournieri Lind*. before and during fertilization. *Planta*. 211, 158–162. doi: 10.1007/s004250000289

Heinlein, M. (2002). Plasmodesmata: dynamic regulation and role in macromolecular cell-to-cell signaling. *Curr. Opin. Plant Biol.* 5, 543–552. doi: 10.1016/s1369-5266(02)00295-9

Horstman, A., Bremer, M., and Boutilier, K. (2017). A transcriptional view on somatic embryogenesis. *Regeneration* 4, 201–216. doi: 10.1002/reg2.91

Jariteh, M., Ebrahimzadeh, H., Niknam, V., Mirmasoumi, M., and Vahdati, K. (2015). Developmental changes of protein, proline and some antioxidant enzymes activities in somatic and zygotic embryos of *Persian walnut (Juglans regia* L.). *Plant Cell Tiss. Org.* 122, 101–115. doi: 10.1007/s11240-015-0753-z

Jin, F., Hu, L., Yuan, D., Xu, J., Gao, W., He, L., et al. (2014). Comparative transcriptome analysis between somatic embryos (SE s) and zygotic embryos in cotton: evidence for stress response functions in SE development. *Plant Biotechnol. J.* 12, 161–173. doi: 10.1111/pbi.12123

Kehr, J., and Kragler, F. (2018). Long distance RNA movement. *New Phytol.* 218, 29–40. doi: 10.1111/nph.15025

Kim, I., Hempel, F. D., Sha, K., Pfluger, J., and Zambryski, P. C. (2002). Identification of a developmental transition in plasmodesmatal function during embryogenesis in *Arabidopsis thaliana*. *Development* 129, 1261–1272. doi: 10.1242/dev.129.5.1261

Kim, I., Kobayashi, K., Cho, E., and Zambryski, P. C. (2005b). Subdomains for transport via plasmodesmata corresponding to the apical–basal axis are established during Arabidopsis embryogenesis. *Proc. Natl. Acad. Sci. U.S.A.* 102, 11945–11950. doi: 10.1073/pnas.0505622102

Kim, I., Cho, E., Crawford, K., Hempel, F. D., and Zambryski, P. C. (2005a). Cell-to-cell movement of GFP during embryogenesis and early seedling development in Arabidopsis. *Proc. Natl. Acad. Sci. U.S.A.* 102, 2227–2231. doi: 10.1073/pnas.0409193102

Kitagawa, M., and Jackson, D. (2017). Plasmodesmata-mediated cell-to-cell communication in the shoot apical meristem: how stem cells talk. *Plants* 6:12. doi: 10.3390/plants6010012

Kurczyńska, E. U., Gaj, M. D., Ujczak, A., and Mazur, E. (2007). Histological analysis of direct somatic embryogenesis in *Arabidopsis thaliana (L.)* Heynh. *Planta* 226, 619–628. doi: 10.1007/s00425-007-0510-6

Laux, T., Würschum, T., and Breuninger, H. (2004). Genetic regulation of embryonic pattern formation. *Plant Cell* 16, S190–S202.

Levi, A., and Sink, K. C. (1991). Somatic embryogenesis in asparagus: the role of explants and growth regulators. *Plant Cell Rep.* 10, 71–75.

Li, Z. P., Paterlini, A., Glavier, M., and Bayer, E. M. (2020). Intercellular trafficking via plasmodesmata: molecular layers of complexity. *Cell. Mol. Life Sci.* 78, 799–816. doi: 10.1007/s00018-020-03622-8

Liarzi, O., and Epel, B. L. (2005). Development of a quantitative tool for measuring changes in the coefficient of conductivity of plasmodesmata induced by developmental, biotic and abiotic signals. *Protoplasma* 225, 67–76. doi: 10.1007/s00709-004-0079-x

Luo, Y., and Koop, H. U. (1997). Somatic embryogenesis in cultured immature zygotic embryos and leaf protoplasts of *Arabidopsis thaliana* ecotypes. *Planta* 202, 387–396. doi: 10.1007/s004250050141

Mordhorst, A. P., Voerman, K. J., Hartog, M. V., Meijer, E. A., van Went, J., Koornneef, M., et al. (1998). Somatic embryogenesis in *Arabidopsis thaliana* is facilitated by mutations in genes repressing meristematic cell divisions. *Genetics* 149, 549–563. doi: 10.1093/genetics/149.2.549

Otero, S., Helariutta, Y., and Benitez-Alfonso, Y. (2016). Symplastic communication in organ formation and tissue patterning. *Curr. Opin. Plant Biol.* 29, 21–28. doi: 10.1016/j.pbi.2015.10.007

Park, S., and Harada, J. J. (2008). Arabidopsis embryogenesis. *Methods Mol Biol.* 427, 3–16. doi: 10.1007/978-1-59745-273-1_1

Pescador, R., Kerbauy, G. B., Viviani, D., and Kraus, J. E. (2008). Anomalous somatic embryos in Acca sellowiana (O. Berg) Burret (Myrtaceae). *Braz. J. Bot.* 31, 155–164.

Petit, J. D., Li, Z. P., Nicolas, W. J., Grison, M. S., and Bayer, E. M. (2020). Dare to change, the dynamics behind plasmodesmata-mediated cell-to-cell communication. *Curr. Opin. Plant Biol.* 53, 80–89. doi: 10.1016/j.pbi.2019.10.009

Puigderrajols, P., Mir, G., and Molinas, M. (2001). Ultrastructure of early secondary embryogenesis by multicellular and unicellular pathways in cork oak (*Quercus suber* L.). *Ann. Bot.* 87, 179–189. doi: 10.1006/anbo.2000.1317

Pullman, G. S., Zhang, Y., and Phan, B. H. (2003). Brassinolide improves embryogenic tissue initiation in conifers and rice. *Plant Cell Rep.* 22, 96–104. doi: 10.1007/s00299-003-0674-x

Radoeva, T., Vaddepalli, P., Zhang, Z., and Weijers, D. (2019). Evolution, initiation and diversity in early plant embryogenesis. *Dev. Cell* 50, 533–543. doi: 10.1016/j.devcel.2019.07.011

Reis, E., Batista, M. T., and Canhoto, J. M. (2008). Effect and analysis of phenolic compounds during somatic embryogenesis induction in *Feijoa sellowiana* Berg. *Protoplasma* 232, 193–202. doi: 10.1007/s00709-008-0290-2

Roberts, A. G., and Oparka, K. J. (2003). Plasmodesmata and the control of symplastic transport. *Plant. Cell Environ.* 26, 103–124. doi: 10.1046/j.1365-3040.2003.00950.x

Sager, R., Bennett, M., and Lee, J.-Y. (2021). A tale of two domains pushing lateral roots. *Trends Plant Sci.* doi: 10.1016/j.tplants.2021.01.006. [Epub ahead of print].

Sager, R., and Lee, J. Y. (2014). Plasmodesmata in integrated cell signalling: insights from development and environmental signals and stresses. *J. Exp. Bot.* 65, 6337–6358. doi: 10.1093/jxb/eru365

Sager, R. E., and Lee, J. Y. (2018). Plasmodesmata at a glance. *J. Cell Sci.* 131:jcs209346.

Sala, K., Karcz, J., Rypień, A., and Kurczyńska, E. U. (2019). Unmethyl-esterified homogalacturonan and extensins seal Arabidopsis graft union. *BMC Plant Biol.* 19:151. doi: 10.1186/s12870-019-1748-4

Schrick, K., and Laux, T. (2001). "Zygotic embryogenesis: developmental genetics," in *Current Trends in the Embryology of Angiosperms*, eds S. S. Bhojwani and W. Y. Soh (Dordrecht: Springer), 249–277. doi: 10.1007/978-94-017-1203-3_11

Schulz, R., and Jensen, W. A. (1968). Capsella embryogenesis: the egg, zygote and young embryo. *Am. J. Bot.* 55, 807–819. doi: 10.2307/2440969

Sevilem, I., Yadav, S. R., and Helariutta, Y. (2015). "Plasmodesmata: channels for intercellular signaling during plant growth and development," in *Plasmodesmata*, ed. M. Heinlein (New York, NY: Humana Press), 3–24. doi: 10.1007/978-1-4939-1523-1_1

Smertenko, A., and Bozkhov, P. V. (2014). Somatic embryogenesis: life and death processes during apical–basal patterning. *J. Exp. Bot.* 65, 1343–1360. doi: 10.1093/jxb/eru005

Sorkin, M. L., and Nusinow, D. A. (2021). Time will tell: intercellular communication in the plant clock. *Trends Plant Sci.* doi: 10.1016/j.tplants.2020.12.009. [Epub ahead of print].

Stadler, R., Lauterbach, C., and Sauer, N. (2005). Cell-to-cell movement of green fluorescent protein reveals post-phloem transport in the outer integument and identifies symplastic domains in Arabidopsis seeds and embryos. *Plant Physiol.* 139, 701–712. doi: 10.1104/pp.105.065607

Tereso, S., Zoglauer, K., Milhinhos, A., Miguel, C., and Oliveira, M. M. (2007). Zygotic and somatic embryo morphogenesis in *Pinus pinaster*: comparative histological and histochemical study. *Tree Physiol.* 27, 661–669. doi: 10.1093/treephys/27.5.661

Tian, R., Paul, P., Joshi, S., and Perry, S. E. (2020). Genetic activity during early plant embryogenesis. *Biochemi. J.* 477, 3743–3767. doi: 10.1042/bcj20190161

Tilsner, J., Nicolas, W., Rosado, A., and Bayer, E. M. (2016). Staying tight: plasmodesmal membrane contact sites and the control of cell-to-cell connectivity in plants. *Annu. Rev. Plant Biol.* 67, 337–364. doi: 10.1146/annurev-arplant-043015-111840

Tvorogova, V. E., and Lutova, L. A. (2018). Genetic regulation of zygotic embryogenesis in angiosperm plants. *Russ. J. Plant Physiol.* 65, 1–14. doi: 10.1134/s1021443718010107

van Bel, A. J. (2018). "Plasmodesmata: a history of conceptual surprises," in *Concepts in Cell Biology-History and Evolution*, eds F. Baluška and V. P. Sahi (Cham: Springer), 221–270. doi: 10.1007/978-3-319-69944-8_11

Verdeil, J. L., Hocher, V., Huet, C., Grosdemange, F., Escoute, J., Ferrière, N., et al. (2001). Ultrastructural changes in coconut calli associated with the acquisition of embryogenic competence. *Ann. Bot.* 88, 9–18. doi: 10.1006/anbo.2001.1408

Wróbel-Marek, J., Kurczyńska, E., Płachno, B. J., and Kozieradzka-Kiszkurno, M. (2017). Identification of symplasmic domains in the embryo and seed of *Sedum acre* L.(*Crassulaceae*). *Planta* 245, 491–505. doi: 10.1007/s00425-016-2619-y

Wu, S. W., Kumar, R., Iswanto, A. B. B., and Kim, J. Y. (2018). Callose balancing at plasmodesmata. *J. Exp. Bot.* 69, 5325–5339.

Xu, M., Cho, E., Burch-Smith, T. M., and Zambryski, P. C. (2012). Plasmodesmata formation and cell-to-cell transport are reduced in decreased size exclusion limit 1 during embryogenesis in Arabidopsis. *Proc. Natl. Acad. Sci. U.S.A.* 109, 5098–5103. doi: 10.1073/pnas.1202919109

Conflict of Interest: The authors declare that the research was conducted in the absence of any commercial or financial relationships that could be construed as a potential conflict of interest.

frontiers in Plant Science

ORIGINAL RESEARCH
published: 31 May 2021
doi: 10.3389/fpls.2021.674128

Cytokinins Stimulate Plasmodesmatal Transport in Leaves

Wilson Horner[1,2,3] *and Jacob O. Brunkard*[1,2,3]*

[1]*Department of Plant and Microbial Biology, University of California, Berkeley, Berkeley, CA, United States,* [2]*Plant Gene Expression Center, USDA Agricultural Research Service, Albany, CA, United States,* [3]*Laboratory of Genetics, University of Wisconsin – Madison, Madison, WI, United States*

Plant cells are connected by plasmodesmata (PD), nanoscopic channels in cell walls that allow diverse cytosolic molecules to move between neighboring cells. PD transport is tightly coordinated with physiology and development, although the range of signaling pathways that influence PD transport has not been comprehensively defined. Several plant hormones, including salicylic acid (SA) and auxin, are known to regulate PD transport, but the effects of other hormones have not been established. In this study, we provide evidence that cytokinins promote PD transport in leaves. Using a green fluorescent protein (GFP) movement assay in the epidermis of *Nicotiana benthamiana*, we have shown that PD transport significantly increases when leaves are supplied with exogenous cytokinins at physiologically relevant concentrations or when a positive regulator of cytokinin responses, *ARABIDOPSIS HISTIDINE PHOSPHOTRANSFER PROTEIN 5 (AHP5)*, is overexpressed. We then demonstrated that silencing cytokinin receptors, *ARABIDOPSIS HISTIDINE KINASE 3 (AHK3)* or *AHK4* or overexpressing a negative regulator of cytokinin signaling, *AAHP6*, significantly decreases PD transport. These results are supported by transcriptomic analysis of mutants with increased PD transport (*ise1–4*), which show signs of enhanced cytokinin signaling. We concluded that cytokinins contribute to dynamic changes in PD transport in plants, which will have implications in several aspects of plant biology, including meristem patterning and development, regulation of the sink-to-source transition, and phytohormone crosstalk.

Keywords: plasmodesmata, cytokinin, *AHP6*, *AHP5*, *AHK4*, *AHK3*, cell–cell signaling, phytohormones

OPEN ACCESS

Edited by:
Tessa Maureen Burch-Smith, The University of Tennessee, Knoxville, United States

Reviewed by:
Rosemary White, Commonwealth Scientific and Industrial Research Organisation (CSIRO), Australia
Kirsten Krause, Arctic University of Norway, Norway

***Correspondence:**
Jacob O. Brunkard
brunkard@wisc.edu

Specialty section:
This article was submitted to Plant Cell Biology, a section of the journal Frontiers in Plant Science

Received: *28 February 2021*
Accepted: *28 April 2021*
Published: *31 May 2021*

Citation:
Horner W and Brunkard JO (2021) Cytokinins Stimulate Plasmodesmatal Transport in Leaves. Front. Plant Sci. 12:674128. doi: 10.3389/fpls.2021.674128

INTRODUCTION

Plasmodesmata (PD) are narrow, membrane-lined channels in plant cell walls that connect the cytosols of neighboring cells (Brunkard and Zambryski, 2017; Faulkner, 2018; Azim and Burch-Smith, 2020). Diverse cytosolic molecules move through PD, including metabolites, small RNAs, proteins up to ~80 kDa, and viruses. The size of molecules that can move through PD and the rate of trafficking through PD varies considerably during plant development and in response to physiological cues. However, little is known about how PD transport is regulated at the molecular level. To discover genetic pathways that coordinate PD transport, the Zambryski lab conducted forward genetic screens for mutants with increased or decreased PD transport at the mid-torpedo stage of *Arabidopsis embryogenesis*

(Kim et al., 2002; Xu et al., 2012). These screens led to the discovery and characterization of five mutants so far: four with increased PD trafficking (*ise1–ise4*; Kobayashi et al., 2007; Stonebloom et al., 2009; Burch-Smith and Zambryski, 2010; Burch-Smith et al., 2011; Brunkard et al., 2020) and one with decreased PD trafficking (*dse1*; Xu et al., 2012).

To identify pathways that could contribute to the increased PD transport phenotype observed in *ise* mutants, we took a comparative transcriptomic approach. Previously, we used this approach to discover that chloroplast retrograde signaling (Burch-Smith et al., 2011; Burch-Smith and Zambryski, 2012; Brunkard et al., 2013) and target of rapamycin (TOR) signaling (Brunkard et al., 2020) coordinate PD transport in embryos and leaves. One of the most strongly repressed genes in both *ise1* and *ise2* embryos is *ARABIDOPSIS HISTIDINE PHOSPHOTRANSFER PROTEIN 6* (*AHP6*; Burch-Smith et al., 2011). *AHP6* is expressed during wild-type embryogenesis from the heart stage through the torpedo stage; later in development, *AHP6* is most strongly expressed in inflorescence and root meristems (Bishopp et al., 2011; Besnard et al., 2014). In both *ise1* and *ise2*, *AHP6* expression is reduced by >20-fold at the mid-torpedo stage of development compared to wild-type plants, one of the most strongly repressed genes in these transcriptomes (Burch-Smith et al., 2011).

ARABIDOPSIS HISTIDINE PHOSPHOTRANSFER PROTEIN 6 is a member of the *AHP* family (Hutchison et al., 2006; Mähönen et al., 2006), which is composed of histidine phosphotransfer proteins that mediate responses to a phytohormone, cytokinin, *via* a two-component system (Hwang and Sheen, 2001). Briefly, cytokinins directly bind to and stimulate a family of histidine kinases (*ARABIDOPSIS HISTIDINE KINASE (AHK) 2*, *AHK3*, and *AHK4*) that phosphorylate AHPs, which then transfer phosphorylation and thus activate *ARABIDOPSIS RESPONSE REGULATORs (ARRs)*, a large family of diverse transcription factors (Müller and Sheen, 2007). Cytokinins regulate diverse developmental and physiological processes, with especially important roles in cell fate and proliferation (Amasino, 2005; Hwang et al., 2012; Wybouw and De Rybel, 2019). *AHP6* is unique in this pathway because it is a pseudo-histidine phosphotransfer protein with a mutation in the conserved histidine residue that prevents it from relaying the phosphorylation to response regulators (Mähönen et al., 2006). Instead of facilitating cytokinin signaling, *AHP6* interferes with the phosphorelay and attenuates cytokinin responses. Detailed studies of *AHP6* have revealed that it is transcriptionally induced by another phytohormone, auxin, which often antagonizes cytokinin signaling (Bishopp et al., 2011). After transcription and translation, the small (17.9 kDa) cytosolic *AHP6* protein freely moves to neighbor cells *via* PD, effectively establishing an inhibitory field that limits cytokinin responses and thereby locally enhances the formation of auxin maxima (Bishopp et al., 2011; Besnard et al., 2014). In meristems, the mobile *AHP6* signal helps to define boundaries and establish robust developmental patterning (Besnard et al., 2014). In embryos, *AHP6* is expressed primarily in cotyledons and differentiating vasculature (Bishopp et al., 2011), but given the small size of *AHP6*, we suspect that the *AHP6* protein may spread to an even larger domain when it is briefly transcriptionally induced during the heart-to-torpedo stages.

Phytohormones can play crucial roles in regulating PD transport during plant development and physiological responses to biotic and abiotic stresses (Lee, 2014; Brunkard et al., 2015b). For example, salicylic acid (SA) triggers membrane remodeling and callose deposition in the cell wall surrounding PD, limiting PD trafficking in response to pathogen infection (Lee et al., 2011; Wang et al., 2013; Lim et al., 2016; Huang et al., 2019). Auxin also stimulates callose deposition in the cell wall surrounding PD, restricting PD transport during developmental transitions, such as lateral root formation (Benitez-Alfonso et al., 2009; Han et al., 2014). Little is known about the connections between other phytohormones and PD, although there is evidence that other hormones can at least conditionally regulate PD trafficking. For example, abscisic acid promotes dormancy in *Populus* buds during winter, in part by decreasing PD transport to isolate buds from growth signals (Tylewicz et al., 2018); gibberellins antagonize abscisic acid signaling and can therefore impact PD transport, at least in this context (Singh et al., 2019). Cytokinins can stimulate PD formation in some circumstances (Ormenese et al., 2006), but it is not known whether cytokinins dynamically impact PD transport in plant cells. In this study, using an established model system for functional studies of PD transport, the leaf epidermis of *Nicotiana benthamiana*, we directly tested how the cytokinin signaling network affects PD transport.

MATERIALS AND METHODS

Plant Growth Conditions

For *trans*-Zeatin application experiments, *N. benthamiana* (accession Nb-1) plants were grown in a greenhouse at 22°C and in 16-h daylengths for 4 weeks prior to infiltration. For transient overexpression experiments, growth conditions were identical, but plants were grown for 4 or 5 weeks before infiltration, depending on the size of the plant. For virus-induced gene silencing (VIGS) experiments, plants were grown in autoclaved soil and in isolation from other plants to prevent the presence of pathogens and pests at 22°C and in 16-h daylengths for 3 weeks prior to silencing. All plants used in the VIGS experiments were photographed prior to infiltration to assess phenotypic differences among *AHK3*-, *AHK4*-, and mock β-glucuronidase (*GUS*)-silenced plants and validate effective silencing with *PHYTOENE DESATURASE* (*PDS*)-silenced plants. As previously described (Brunkard et al., 2015a), plants that have effectively silenced *PDS* exhibit photobleached leaves.

Cloning Silencing Triggers

Silencing triggers were cloned as previously described (Brunkard et al., 2015a). Briefly, RNA was isolated from *N. benthamiana*, Nb-1, with the Spectrum Plant Total RNA kit (Sigma-Aldrich, St. Louis, MO, United States), treating RNA with on-column DNase I digestion (New England Biolabs, Ipswich, MA, United States). Complementary DNA (cDNA) was synthesized from

isolated RNA using random hexamers and SuperScript III reverse transcriptase (Fisher Scientific, Waltham, MA, United States). Silencing triggers were amplified with Phusion DNA polymerase (New England Biolabs). Triggers and the TRV2 plasmid pYL156 were digested with XbaI and XhoI (New England Biolabs) and ligated with Promega T4 DNA ligase (Fisher Scientific). Ligations were transformed into XL1-Blue *Escherichia coli*, were mini-prepped (New England Biolabs, Ipswich, MA, United States), and were Sanger sequenced to confirm insertion sequences. The *AHK4* trigger was cloned with oligonucleotides 5'-gat TCT AGA AAC TAT GGA GGA ACG GG-3' and 5'-gat ctc GAG GTT TCA TTA TCA CCG C-3' to silence the two *AHK4* homologues, *Niben101Scf08855g02013* and *Niben101g09260g03002*. The *AHK3* trigger was cloned with oligonucleotides 5'-cat TCT AGA TGT GAC ACA ACA AGA TTA TGT C-3' and 5'-gat ctC GAG CAA TAG AAG GAC CAA C-3' to silence the two *AHK3* homologues, *Niben10103911g05013* and *Niben101Scf02711g00003*.

Cloning AHP Overexpression Constructs

As with the silencing triggers, *AHP5* and *AHP6* were amplified with Phusion DNA polymerase (New England Biolabs) from *N. benthamiana* cDNA that was synthesized as above. *AHP5* was cloned using oligonucleotides 5'-aattacaggcctcccgggacc ATGAACACCATCGTCGTT-3' and 5'-TTCGCTTCCTGAccc CTAATTTATATCCACTTGAGGAATT-3', while *AHP6* was cloned using oligonucleotides 5'-aattacaggcctcccgggacc ATGTTGGGGTTGGGTGTG-3' and 5'-TTCGCTTCCTGAccc CTACATTGGATATCTGACTCCTGC-3'. All oligonucleotides contained 15 bp of homology compatible with the SmaI digestion site of binary vectors containing a CaMV 35S promoter, TMV Omega enhancer sequence, and CaMV 35S terminator for transient gene expression. The plasmid was digested with SmaI, and both genes were treated with T5 DNA exonuclease (New England Biolabs) as previously described (Xia et al., 2019). These reactions were used to transform chemically competent DH10B *E. coli*, were mini-prepped, and were Sanger sequenced to confirm insertion sequences.

Agroinfiltration

Agrobacterium tumefaciens strain, GV3101, was grown overnight in a lysogeny broth medium at 28°C, 250 rpm, with kanamycin, gentamicin, and rifampicin (each at 50 mg ml^{-1}). Cultures were centrifuged at ×700 *g* for 10 min and then resuspended in an infiltration medium [10 mM $MgCl_2$, 10 mM 2-(N-morpholino) ethanesulfonic acid (MES), and 200 μM acetosyringone, pH 5.6, adjusted with KOH] to OD_{600nm} = 1.0. Agrobacteria were then left to induce virulence at room temperature for 2–4 h with gentle shaking prior to infiltration. Immediately before infiltrating, cultures were then further diluted in infiltration media to $OD_{600nm} = 10^{-5}$ for green fluorescent protein (GFP) movement assays or OD_{600nm} = 0.1 for overexpression. Cultures were left at OD_{600nm} = 1.0 for VIGS, as previously described (Brunkard et al., 2015a).

Briefly, for VIGS experiments, the first two true leaves of *N. benthamiana* plants were infiltrated with equal induced inocula of *A. tumefaciens* carrying the previously described binary vectors: pYL192 (which expresses the TRV1 subgenome) and pYL156 (which expresses the TRV2 subgenome with silencing triggers). A TRV2-*GUS* trigger was used as a negative control for VIGS, and a TRV2-*NbPDS* trigger was used as a positive control for VIGS. About 14 days after infiltration of the VIGS inocula, the fourth leaf of each plant was infiltrated with an induced inoculum containing the $35S_{PRO}$:*GFP* binary vector diluted to $OD_{600nm} = 10^{-5}$. Each plant was left under normal growing conditions (22°C and 16-h daylengths) for 48 h prior to GFP movement assays (described below).

For overexpression experiments, the fourth leaf from 4-to-5-week-old *N. benthamiana* plants was infiltrated with an induced inoculum containing the $35S_{PRO}$:*GFP* binary vector diluted to $OD_{600nm} = 10^{-5}$ and the transient overexpression vector diluted to OD_{600nm} = 0.1, with an empty transient overexpression plasmid used as a negative control. These plants were left under normal growing conditions (22°C and 16-h daylengths) for 72 h prior to GFP movement assays (described below).

Trans-Zeatin Infiltration

A 1 mM stock solution of *trans*-Zeatin (Cayman Chemical Company) in DMSO was diluted to several concentrations (1.0 nM, 10 nM, and 100 nM) in infiltration media, with the infiltration media containing no *trans*-Zeatin used as a negative control. The $35S_{PRO}$:*GFP* binary vector was then diluted to $OD_{600nm} = 10^{-5}$ in these solutions and infiltrated into the fourth leaf from 4-week-old *N. benthamiana* plants, as above. These plants were left under normal growing conditions (22°C and 16-h daylengths) for 48 h prior to GFP movement assays (described below).

Assaying PD Transport With GFP Transformation

Plasmodesmata movement assays were performed using the fourth leaf from either 4-week-old (for *trans*-Zeatin treatment experiments) or 4-to-5-week-old (for VIGS and overexpression experiments) *N. benthamiana* plants. GFP movement assays were conducted as previously described (Brunkard et al., 2015a; **Figure 1**), observing GFP movement in only the proximal 25% of the leaf. Briefly, leaves were infiltrated with very low inocula of *Agrobacterium* ($OD_{600nm} < 10^{-4}$) carrying a binary vector to transform cells to express GFP under the CaMV 35S promoter. Only a handful of individual, isolated cells are transformed by the low inocula of *Agrobacterium*. About 48 h after agroinfiltration, the genetically transformed cells show bright GFP fluorescence and are surrounded by "rings" of cells with lower fluorescence, indicating that GFP has moved into these cells *via* PD. In this study, we report the greatest distance, in numbers of cells, that GFP has spread.

In all experiments, leaves that were previously infiltrated with the $35S_{PRO}$:*GFP* vector were infiltrated with water immediately prior to harvesting. For VIGS experiments, leaves were harvested from plants infiltrated with media containing the $35S_{PRO}$:*GFP* vector 48 h after infiltration. For *trans*-Zeatin experiments, leaves were similarly harvested from plants infiltrated with media containing *trans*-Zeatin and the $35S_{PRO}$:*GFP* vector 48 h after infiltration. For overexpression experiments,

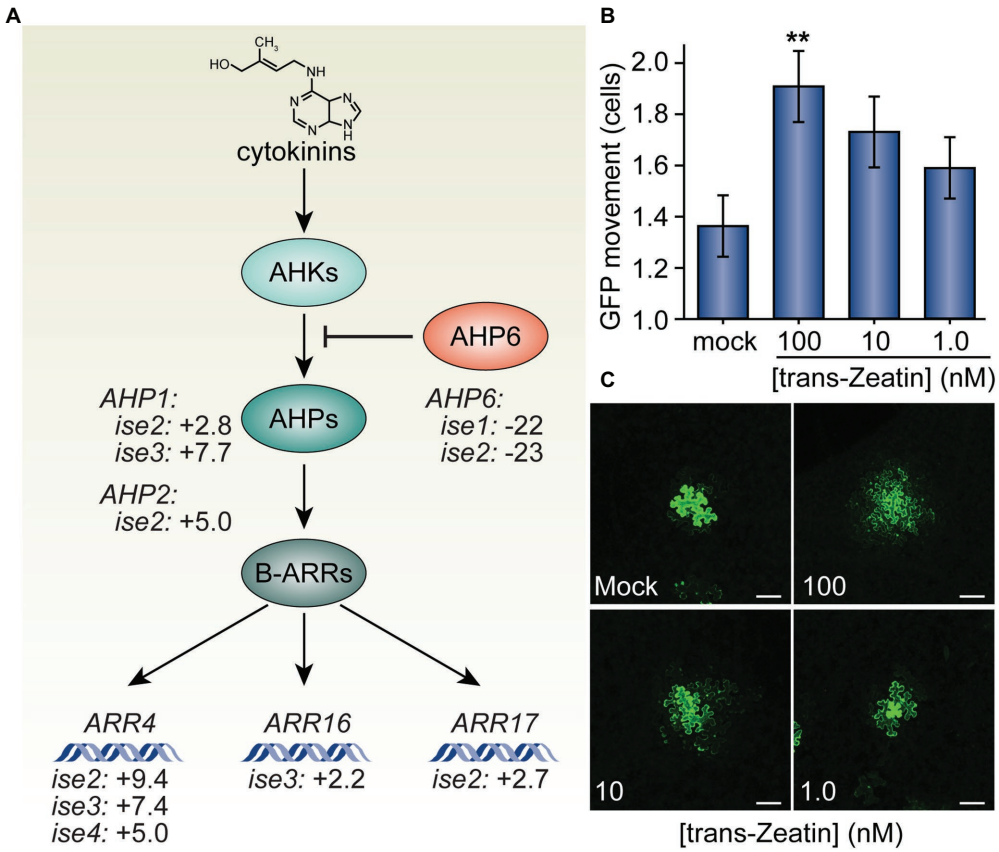

FIGURE 1 | *Trans*-Zeatin (cytokinin) stimulates plasmodesmata (PD)-mediated green fluorescent protein (GFP) movement in *Nicotiana benthamiana* leaves. **(A)** Cytokinins (e.g., *trans*-Zeatin, whose structure is shown) stimulate the cytokinin receptors, *ARABIDOPSIS HISTIDINE KINASES* (*AHK*s, light teal), to phosphorylate *ARABIDOPSIS HISTIDINE PHOSPHOTRANSFER PROTEINS* (*AHP*s, teal), which transfer phosphorylation to B-class *ARABIDOPSIS RESPONSE REGULATORS* (*ARR*s, dark teal), which then promote transcription of cytokinin response genes, including the A-type *ARR* genes, *ARR4*, *ARR16*, and *ARR17*. *AHP6* (orange) acts as a decoy *AHP*, preventing phosphorylation of *AHP*s and thus antagonizing cytokinin signaling. Transcriptomic analysis of four mutants with increased PD trafficking, *ise1* through *ise4*, revealed the induction of *AHP* genes that promote cytokinin signaling, induction of A-type *ARR* genes that indicate elevated cytokinin responses, and repression of the *AHP6* gene that inhibits cytokinin signal transduction (Burch-Smith et al., 2011; Brunkard et al., 2020). Fold-changes in mRNA levels of these genes are indicated. **(B)** Infiltration of 100 nM solutions of *trans*-Zeatin significantly increased PD transport ($n = 53$, $^{**}p < 0.01$; error bars indicate SEM). 10 or 1.0 nM *trans*-Zeatin somewhat increased PD transport, but not to statistically significant thresholds ($n = 51$ or $n = 56$, respectively). **(C)** Representative confocal images of transformed *N. benthamiana* cells for different treatments of the *trans*-Zeatin show the range of GFP movement from transformed cells. In mock-treated leaves, GFP rarely moved 1–2 cells beyond the transformed cell. After applying *trans*-Zeatin, GFP movement tended to increase, often moving to three cells or more beyond the transformed cell in leaves treated with 100 nM *trans*-Zeatin. The fourth leaf from 4-week-old *N. benthamiana* plants was used for each experiment; white scale bars = 100 μm.

leaves were harvested from plants infiltrated with media containing the $35S_{PRO}$:*GFP* vector 72 h after infiltration. For all conditions, small sections were cut from each infiltrated leaf (~1 × 2 cm), mounted abaxial side up on microscope slides, and imaged (as shown in "Microscopy" below).

For each experiment, at least 5, and as many as 24, plants were assayed for each condition per replicate, and each experiment was replicated three times, resulting in each experiment being conducted in at least 70 plants. GFP movement from 1 to 5 randomly selected transformed cells per plant was observed, depending on how many transformed cells were found in the section used for microscopy. The movement was scored by counting the distance in rings of cells to which GFP had moved from the originally transformed cell (e.g., no movement was scored as zero, since GFP remained only in the transformed cell; movement into one or all cells immediately touching the originally transformed cell but none beyond was scored as one; and so on). The total number of cells containing GFP was also counted for each sample.

Microscopy

GFP was observed in the epidermis of *N. benthamiana* leaves using a Leica DM6 CS confocal laser scanning microscope, with settings as described by Brunkard et al. (2015a). To ensure no artifacts were introduced during microscopy, identical settings (such as laser strength, gain, emission filters, and aperture) were used in all experiments, and samples were imaged in randomized order to avoid any bias during experimentation. All movement assays were scored by both authors to ensure reproducibility.

Quantification and Statistical Analysis

Movement assay results are presented as the average movement of GFP and SEM. Differences in GFP movement between two given conditions were compared using unpaired heteroscedastic Student's *t*-tests in Excel, with $p < 0.05$ being considered significantly different.

RESULTS

Based on the previous finding that the cytokinin signaling inhibitor, *AHP6*, is severely transcriptionally repressed in *ise1* and *ise2* (Burch-Smith et al., 2011), we explored whether the transcriptomes of *ise* mutants reveal any clear changes in the gene expression that could reflect enhanced cytokinin signaling, which would support the hypothesis that cytokinin signaling could contribute to the *ise* phenotype. Indeed, *ise2* shows several additional signatures of elevated cytokinin signaling, including a 9-fold increase in the messenger RNA (mRNA) level of a standard transcriptional reporter for cytokinin responses, *ARR4* (*ARABIDOPSIS RESPONSE REGULATOR 4*), and >3-fold induction of cytokinin phosphorelay proteins, *AHP1* and *AHP2*, that promote cytokinin responses. The cytokinin response reporter gene, *ARR4*, is also induced >5-fold in both *ise3* and *ise4*, suggesting that elevated cytokinin signaling could be a common feature of *ise* mutants.

Cytokinin Can Stimulate PD Movement in Leaves

Given the evidence of enhanced cytokinin signaling and increased PD transport in the *ise* mutants, we next tested whether exogenous application of cytokinin is sufficient to increase PD transport. To this end, we infiltrated leaves of 4-week-old *N. benthamiana* plants with infiltration media containing a low inoculum of *Agrobacterium* ($OD_{600nm} < 10^{-4}$) carrying a $35S_{PRO}$:*GFP* binary vector and a range of concentrations (1.0, 10, or 100 nM) of the cytokinin *trans*-Zeatin (Letham and Miller, 1965). Infiltration media with no *trans*-Zeatin was used as a negative control. About 48 h post-infiltration, we excised sections of infiltrated leaves, imaged GFP foci with confocal microscopy, and statistically analyzed the results to quantitatively assess GFP movement. The final results are expressed as the maximal distance that GFP had spread from the transformed cell into neighboring cells.

We found that higher concentrations of *trans*-Zeatin correspondingly increased the movement of GFP in leaves (**Figure 1**). On average, GFP moved 1.36 ± 0.12 cells from the transformed cell in the presence of no exogenous *trans*-Zeatin. With the addition of 100 nM of *trans*-Zeatin, GFP moved 1.91 ± 0.14 cells from the transformed cell; when compared with results from the control, we found that this difference is statistically significant ($n = 53$, $p < 0.01$). Even with smaller concentrations of *trans*-Zeatin application, GFP movement also apparently increased, though to proportionately smaller degrees (1.73 ± 0.14 cells with 10 nM of *trans*-Zeatin, 1.59 ± 0.12 cells with 1.0 nM of *trans*-Zeatin). Overall, these results demonstrate that cytokinins promote PD movement.

Silencing Expression of Cytokinin Receptor Genes Reduces PD Transport

Following these results, we took a genetic approach and tested whether silencing the expression of genes directly involved in cytokinin sensing would result in lowered PD movement. Using VIGS, we silenced *AHK3* and *AHK4*, which encode cytokinin receptors that initiate the cytokinin-*AHK-AHP-ARR* signal transduction pathway in plant cells. We used a TRV2-*GUS* trigger as a negative control for silencing and a TRV2-*NbPDS* trigger as a positive control for silencing. After plants were infiltrated with the VIGS constructs, we allowed 2 weeks for silencing to establish before infiltrating leaves on each plant with the same $35S_{PRO}$:*GFP* construct used in other experiments. Immediately prior to this, we took photographs of each plant to document phenotypic differences among conditions. We observed no obvious morphological or physiological differences between mock silenced and *AHK*-silenced plants, so we experimented in the same manner as above for the *trans*-Zeatin experiments.

In both *AHK3*- and *AHK4*-silenced plants, we observed a significant decrease in GFP movement relative to the *GUS* mock treatment (**Figure 2**). Whereas GFP moved 1.61 ± 0.07 cells from the transformed cell in mock-silenced (TRV-GUS) plants, GFP movement in *AHK3*-silenced plants was reduced to 1.31 ± 0.07 cells and to 1.35 ± 0.06 cells in *AHK4*-silenced plants. We found that both results were statistically significant ($n = 124$, $p < 0.01$; $n = 133$, $p < 0.01$). These findings further bolstered the hypothesis that the regulation of PD transport is intimately linked to the cytokinin signaling pathway.

AHP5 and *AHP6* Antagonistically Regulate PD Transport in Leaves

Given the findings regarding the influence of upstream members of the cytokinin signaling pathway on GFP movement, we asked whether overexpressing proteins downstream of *AHK*s in the cytokinin signaling pathway would alter PD transport. To test this hypothesis, we cloned *AHP5* and *AHP6* into binary vectors for transient expression in *N. benthamiana* leaves. Agrobacteria carrying $35S_{PRO}$:*AHP5* or $35S_{PRO}$:*AHP6* were then co-infiltrated with $35S_{PRO}$:*GFP* into *N. benthamiana* leaves.

When compared to control plants infiltrated with empty vector, we found that leaves overexpressing *AHP5* exhibited significantly increased levels of PD transport, whereas leaves overexpressing *AHP6* exhibited significantly decreased levels of PD transport (**Figure 3**). In leaves agroinfiltrated with empty vector, GFP moved 1.58 ± 0.07 cells from the transformed cell vs. 2.13 ± 0.07 for plants overexpressing *AHP5* and 1.38 ± 0.06 for plants overexpressing *AHP6*. The change in GFP movement was significant for both *AHP5*-overexpressing plants ($n = 141$, $p < 0.001$) and *AHP6*-overexpressing plants ($n = 161$, $p < 0.05$) relative to control plants. Together, these results indicate that manipulating the expression of different

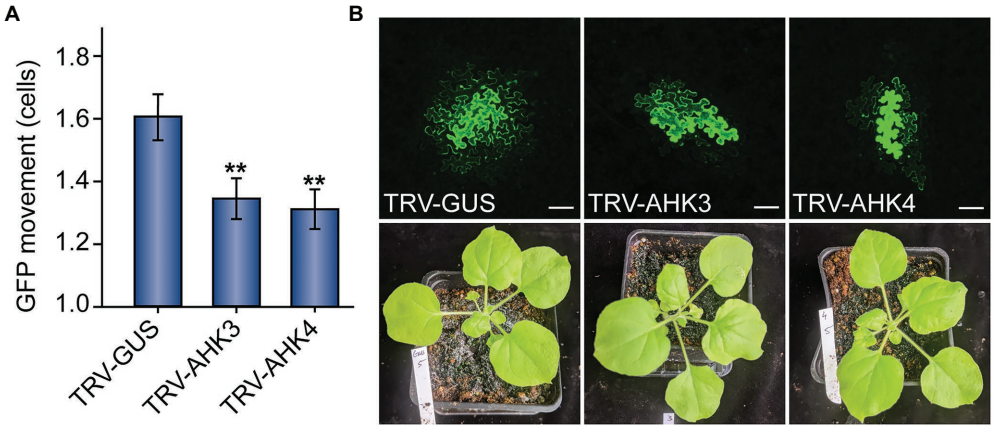

FIGURE 2 | Virus-induced gene silencing (VIGS) of cytokinin receptor expression reduces PD-mediated GFP movement in *N. benthamiana* leaves. **(A)** Compared to control TRV-GUS plants, GFP movement from transformed cells was significantly lowered in plants where the cytokinin receptors *AHK3* or *AHK4* were silenced (n = 124, $^{**}p < 0.01$; or n = 133, $^{**}p < 0.01$; respectively; error bars indicate SEM). **(B)** Representative confocal images of transformed *N. benthamiana* cells and examples of 5-week-old VIGS-treated plants indicate that GFP movement was reduced in *AHK3* and *AHK4*-silenced plants, but there were no obvious phenotypic effects on the plants themselves. In mock-treated TRV-GUS plants, GFP typically moved 1–3 cells beyond the transformed cell; in *AHK3* and *AHK4*-silenced plants, GFP movement rarely exceeded two cells. The fourth leaf from 5-week-old *N. benthamiana* plants was used for each experiment; white scale bars = 100 μm.

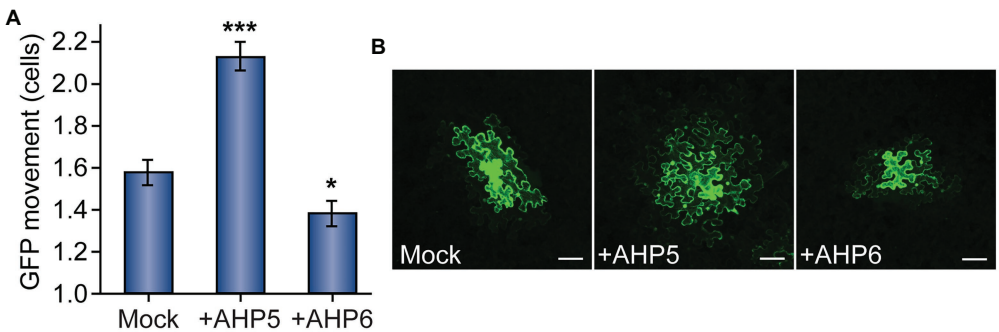

FIGURE 3 | Cytokinin phosphorelay proteins *AHP5* and *AHP6* regulate PD transport. **(A)** Compared to mock-infiltrated plants, GFP movement from transformed cells significantly increased in leaves overexpressing *AHP5* (n = 141, $^{***}p < 0.001$; error bars indicate SEM). Overexpressing the negative regulator of cytokinin signaling, *AHP6*, had the opposite effect, decreasing PD transport in leaves (n = 161, $^{*}p < 0.05$; error bars indicate SEM). **(B)** Representative confocal images of transformed *N. benthamiana* cells demonstrate the difference in GFP movement between conditions. GFP moved 1–3 cells beyond the transformed cell in mock-treated leaves. In leaves overexpressing *AHP5*, GFP regularly moved more than two cells and often as many as four cells from the transformed cell. In leaves overexpressing *AHP6*, GFP movement was confined to one, or sometimes two, cell(s) beyond the transformed cell. The fourth leaf from 4-to-5-week-old *N. benthamiana* plants was used for each experiment; white scale bars = 100 μm.

members of the cytokinin signaling pathway phosphorelay chain directly impacts the rate of PD transport.

DISCUSSION

In this study, we provide evidence that cytokinins can stimulate intercellular trafficking through PD in plants. We demonstrated that manipulating the cytokinin signaling pathway produces consistent observable effects on GFP movement in the leaf epidermal tissue. Directly infiltrating cytokinins increased the rate of GFP movement, as did overexpression of the gene encoding a phosphotransfer protein, *AHP5*, that promotes cytokinin responses. Conversely, overexpressing *AHP6*, which encodes a protein that lacks the phosphotransfer capability of *AHP5* and thus suppresses cytokinin responses, or silencing *AHK3* or *AHK4*, which encodes two cytokinin receptors, decreased PD-mediated GFP movement. Given the transcriptomic signs that cytokinin signaling is enhanced in *ise* mutants, it is plausible that increased cytokinin levels contribute to the elevated PD transport observed in *ise* embryos.

Previous studies in non-model systems demonstrated that cytokinin treatment can induce the *de novo* formation of PD in cell walls (Ormenese et al., 2006), but this is the only direct experimental evidence that cytokinin signaling affects PD trafficking. Cytokinins can now be added to the growing list of physiological and developmental cues that dynamically regulate PD transport, including auxin, SA, abscisic acid, light,

and the circadian clock, metabolic status, and oxidative stress, among others. Admittedly, in this report, we have not determined how cytokinins promote trafficking through PD. The best-defined mechanisms that mediate changes in PD trafficking are the reversible hyperaccumulation of callose in the cell wall surrounding PD, which is believed to occlude the PD channel and prevent trafficking, or *de novo* PD biogenesis, which is consistently correlated with increased PD transport. We hypothesize that cytokinins could act through multiple mechanisms to alter PD transport. For example, cytokinin could stimulate rapid *de novo* PD biogenesis, which will require further investigation in the future. We should note that there are more PD in the cell walls of *ise1* and *ise2* embryos; if cytokinin indeed does stimulate the formation of new PD in cell walls, the additional PD in *ise1*/*ise2* embryos could correlate with the induction of transcriptional responses to cytokinin in these mutants.

Although a relationship between cytokinin levels and PD transport in leaves has not been previously explored, cytokinin is known to impact sink-source relations in plants (Peleg et al., 2011; Kieber and Schaller, 2014). As young leaves develop, they transition from rapidly-growing "sinks" that import sugars to mature "sources" that export sugars for long-distance transport *via* the phloem (Turgeon, 2010). PD transport rapidly decreases during the sink-to-source transition, which is thought to contribute to the sink-to-source transition by limiting the diffusive backflow of sugars from the phloem into the exporting source leaf (Roberts et al., 1997, 2001; Imlau et al., 1999; Brunkard, 2020; Brunkard et al., 2020). Genetic and physiological experiments have shown that cytokinins increase so-called "sink strength" in leaves, the rate of sugar import into growing leaves. For example, tobacco transformed to overexpress cytokinin oxidases, which degrade cytokinins and thus reduce cytokinin signaling, decreased the concentrations of glucose, fructose, and sucrose by as much as 10-fold in sink leaves without comparably affecting the sugar concentrations in source leaves (Werner et al., 2008). While the defect in sink strength is likely due to multiple pathways impacted by cytokinin signaling, we speculate that PD transport could be limited in cytokinin-deficient plants, effectively reducing the rate of phloem import to sink leaves.

Plasmodesmata transport dynamics are especially crucial for patterning in the shoot apical meristem (SAM; Rinne and Van der Schoot, 1998; Gisel et al., 1999; Kitagawa and Jackson, 2019). Multiple transcription factors that determine whether SAM cells proliferate, differentiate, or remain quiescent readily move between cells *via* PD, including the homeobox proteins Knotted1 (Kn1, sometimes called SHOOT MERISTEMLESS or STM in *Arabidopsis*; Lucas et al., 1995) and WUSCHEL (WUS; Yadav et al., 2011). The hormones that specify cell fate in the meristem, especially cytokinin and auxin, which act antagonistically to regulate meristem size and organ initiation, can also move through PD (Kitagawa and Jackson, 2019). Kn1 and WUS maintain stem cell fates in the meristem partly by stimulating cytokinin biosynthesis; the cytokinins then move through PD to neighboring cells, presumably forming a concentration gradient. In contrast, as auxin maxima form, auxin response factors drive the expression of *AHP6* to locally prevent cytokinin signal transduction (Besnard et al., 2014). Like the transcription factors and hormones, *AHP6* also moves through PD, creating a zone of cells that are "immune" to the WUS-Kn1-promoted cytokinin biosynthesis (Besnard et al., 2014). The discovery that supplying cells with cytokinin is sufficient to increase PD transport suggests that cytokinin-PD signaling should be considered in models of cell–cell communication at the SAM. Given the intricate balance of molecules, ranging from metabolites and hormones to transcription factors and small RNAs, that move through PD in the SAM, we expect that reevaluation of SAM dynamics in light of cytokinin-PD signaling could open exciting new avenues for future research.

DATA AVAILABILITY STATEMENT

The original contributions presented in the study are included in the article/supplementary material, further inquiries can be directed to the corresponding author.

AUTHOR CONTRIBUTIONS

WH and JB designed the project, analyzed the data, and wrote the manuscript. WH performed the experiments. JB initiated and supervised the project. All authors contributed to the article and approved the submitted version.

FUNDING

This study was supported by NIH grant DP5-OD023072 to JB.

ACKNOWLEDGMENTS

We acknowledge De Wood and Tina Williams (USDA Agricultural Research Service) for microscopy support and Pat Zambryski and John Zupan for early guidance on this project.

REFERENCES

Amasino, R. (2005). 1955: Kinetin arrives. The 50th anniversary of a new plant hormone. *Plant Physiol.* 138, 1177–1184. doi: 10.1104/pp.104.900160

Azim, M. F., and Burch-Smith, T. M. (2020). Organelles-nucleus-plasmodesmata signaling (ONPS): an update on its roles in plant physiology, metabolism and stress responses. *Curr. Opin. Plant Biol.* 58, 48–59. doi: 10.1016/j.pbi.2020.09.005

Benitez-Alfonso, Y., Cilia, M., San Roman, A., Thomas, C., Maule, A., Hearn, S., et al. (2009). Control of *Arabidopsis* meristem development by thioredoxin-dependent regulation of intercellular transport. *Proc. Natl. Acad. Sci. U. S. A.* 106, 3615–3620. doi: 10.1073/pnas.0808717106

Besnard, F., Refahi, Y., Morin, V., Marteaux, B., Brunoud, G., Chambrier, P., et al. (2014). Cytokinin signalling inhibitory fields provide robustness to phyllotaxis. *Nature* 505, 417–421. doi: 10.1038/nature12791

Bishopp, A., Help, H., El-Showk, S., Weijers, D., Scheres, B., Friml, J., et al. (2011). A mutually inhibitory interaction between auxin and cytokinin specifies vascular pattern in roots. *Curr. Biol.* 21, 917–926. doi: 10.1016/j.cub.2011.04.017

Brunkard, J. O. (2020). Exaptive evolution of target of rapamycin signaling in multicellular eukaryotes. *Dev. Cell* 54, 142–155. doi: 10.1016/j.devcel.2020.06.022

Brunkard, J. O., Burch-Smith, T. M., Runkel, A. M., and Zambryski, P. C. (2015a). Investigating plasmodesmata genetics with virus-induced gene silencing and an agrobacterium-mediated GFP movement assay. *Methods Mol. Biol.* 1217, 185–198. doi: 10.1007/978-1-4939-1523-1_13

Brunkard, J. O., Runkel, A. M., and Zambryski, P. C. (2013). Plasmodesmata dynamics are coordinated by intracellular signaling pathways. *Curr. Opin. Plant Biol.* 16, 614–620. doi: 10.1016/j.pbi.2013.07.007

Brunkard, J. O., Runkel, A. M., and Zambryski, P. C. (2015b). The cytosol must flow: intercellular transport through plasmodesmata. *Curr. Opin. Cell Biol.* 35, 13–20. doi: 10.1016/j.ceb.2015.03.003

Brunkard, J. O., Xu, M., Regina Scarpin, M., Chatterjee, S., Shemyakina, E. A., Goodman, H. M., et al. (2020). TOR dynamically regulates plant cell-cell transport. *Proc. Natl. Acad. Sci. U. S. A.* 117, 5049–5058. doi: 10.1073/pnas.1919196117

Brunkard, J. O., and Zambryski, P. C. (2017). Plasmodesmata enable multicellularity: new insights into their evolution, biogenesis, and functions in development and immunity. *Curr. Opin. Plant Biol.* 35, 76–83. doi: 10.1016/j.pbi.2016.11.007

Burch-Smith, T. M., Brunkard, J. O., Choi, Y. G., and Zambryski, P. C. (2011). Organelle-nucleus cross-talk regulates plant intercellular communication via plasmodesmata. *Proc. Natl. Acad. Sci. U. S. A.* 108, E1451–E1460. doi: 10.1073/pnas.1117226108

Burch-Smith, T. M., and Zambryski, P. C. (2010). Loss of increased size exclusion limit (ise)1 or ise2 increases the formation of secondary plasmodesmata. *Curr. Biol.* 20, 989–993. doi: 10.1016/j.cub.2010.03.064

Burch-Smith, T. M., and Zambryski, P. C. (2012). Plasmodesmata paradigm shift: regulation from without versus within. *Annu. Rev. Plant Biol.* 63, 239–260. doi: 10.1146/annurev-arplant-042811-105453

Faulkner, C. (2018). Plasmodesmata and the symplast. *Curr. Biol.* 28, R1374–R1378. doi: 10.1016/j.cub.2018.11.004

Gisel, A., Barella, S., Hempel, F. D., and Zambryski, P. C. (1999). Temporal and spatial regulation of symplastic trafficking during development in *Arabidopsis thaliana* apices. *Development* 126, 1879–1889. doi: 10.1242/dev.126.9.1879

Han, X., Hyun, T. K., Zhang, M., Kumar, R., Koh, E. ji, Kang, B. H., et al (2014). Auxin-callose-mediated plasmodesmal gating is essential for tropic auxin gradient formation and signaling. *Dev. Cell* 28, 132–146. doi: 10.1016/j.devcel.2013.12.008

Huang, D., Sun, Y., Ma, Z., Ke, M., Cui, Y., Chen, Z., et al. (2019). Salicylic acid-mediated plasmodesmal closure via remorin-dependent lipid organization. *Proc. Natl. Acad. Sci. U. S. A.* 116, 21274–21284. doi: 10.1073/pnas.1911892116

Hutchison, C. E., Li, J., Argueso, C., Gonzalez, M., Lee, E., Lewis, M. W., et al. (2006). The *Arabidopsis* histidine phosphotransfer proteins are redundant positive regulators of cytokinin signaling. *Plant Cell* 18, 3073–3087. doi: 10.1105/tpc.106.045674

Hwang, I., and Sheen, J. (2001). Two-component circuitry in *Arabidopsis* cytokinin signal transduction. *Nature* 413, 383–389. doi: 10.1038/35096500

Hwang, I., Sheen, J., and Müller, B. (2012). Cytokinin signaling networks. *Annu. Rev. Plant Biol.* 63, 353–380. doi: 10.1146/annurev-arplant-042811-105503

Imlau, A., Truernit, E., and Sauer, N. (1999). Cell-to-cell and long-distance trafficking of the green fluorescent protein in the phloem and symplastic unloading of the protein into sink tissues. *Plant Cell* 11, 309–322. doi: 10.1105/tpc.11.3.309

Kieber, J. J., and Schaller, G. E. (2014). Cytokinins. *Arabidopsis Book* 12:e0168. doi: 10.1199/tab. 0168

Kim, I., Hempel, F. D., Sha, K., Pfluger, J., and Zambryski, P. C. (2002). Identification of a developmental transition in plasmodesmatal function during embryogenesis in *Arabidopsis thaliana*. *Development* 129, 1261–1272. doi: 10.1242/dev.129.5.1261

Kitagawa, M., and Jackson, D. (2019). Control of meristem size. *Annu. Rev. Plant Biol.* 70, 269–291. doi: 10.1146/annurev-arplant-042817-040549

Kobayashi, K., Otegui, M. S., Krishnakumar, S., Mindrinos, M., and Zambryski, P. (2007). Increased size exclusion limit2 encodes a putative DEVH box RNA helicase involved in plasmodesmata function during Arabidopsis embryogenesis. *Plant Cell* 19, 1885–1897. doi: 10.1105/tpc.106.045666

Lee, J. Y. (2014). New and old roles of plasmodesmata in immunity and parallels to tunneling nanotubes. *Plant Sci.* 221–222, 13–20. doi: 10.1016/j.plantsci.2014.01.006

Lee, J. Y., Wang, X., Cui, W., Sager, R., Modla, S., Czymmek, K., et al. (2011). A plasmodesmata-localized protein mediates crosstalk between cell-to-cell communication and innate immunity in *Arabidopsis*. *Plant Cell* 23, 3353–3373. doi: 10.1105/tpc.111.087742

Letham, D. S., and Miller, C. O. (1965). Identity of kinetin-like factors from Zea mays. *Plant Cell Physiol.* 6, 355–359. doi: 10.1093/oxfordjournals.pcp.a079106

Lim, G. H., Shine, M. B., De Lorenzo, L., Yu, K., Cui, W., Navarre, D., et al. (2016). Plasmodesmata localizing proteins regulate transport and signaling during systemic acquired immunity in plants. *Cell Host Microbe* 19, 541–549. doi: 10.1016/j.chom.2016.03.006

Lucas, W. J., Bouché-Pillon, S., Jackson, D. P., Nguyen, L., Baker, L., Ding, B., et al. (1995). Selective trafficking of KNOTTED1 homeodomain protein and its mRNA through plasmodesmata. *Science* 270, 1980–1983. doi: 10.1126/science.270.5244.1980

Mähönen, A. P., Bishopp, A., Higuchi, M., Nieminen, K. M., Kinoshita, K., Törmäkangas, K., et al. (2006). Cytokinin signaling and its inhibitor AHP6 regulate cell fate during vascular development. *Science* 311, 94–98. doi: 10.1126/science.1118875

Müller, B., and Sheen, J. (2007). Arabidopsis cytokinin signaling pathway. *Sci. STKE* 2007:cm5. doi: 10.1126/stke.4072007cm5

Ormenese, S., Bernier, G., and Périlleux, C. (2006). Cytokinin application to the shoot apical meristem of *Sinapis alba* enhances secondary plasmodesmata formation. *Planta* 224, 1481–1484. doi: 10.1007/s00425-006-0317-x

Peleg, Z., Reguera, M., Tumimbang, E., Walia, H., and Blumwald, E. (2011). Cytokinin-mediated source/sink modifications improve drought tolerance and increase grain yield in rice under water-stress. *Plant Biotechnol. J.* 9, 747–758. doi: 10.1111/j.1467-7652.2010.00584.x

Rinne, P. L. H., and Van der Schoot, C. (1998). Symplasmic fields in the tunica of the shoot apical meristem coordinate morphogenetic events. *Development* 125, 1477–1485. doi: 10.1242/dev.125.8.1477

Roberts, I. M., Boevink, P., Roberts, A. G., Sauer, N., Reichel, C., and Oparka, K. J. (2001). Dynamic changes in the frequency and architecture of plasmodesmata during the sink-source transition in tobacco leaves. *Protoplasma* 218, 31–44. doi: 10.1007/BF01288358

Roberts, A. G., Santa Cruz, S., Roberts, I. M., Prior, D. A. M., Turgeon, R., and Oparka, K. J. (1997). Phloem unloading in sink leaves of nicotiana benthamiana: comparison of a fluorescent solute with a fluorescent virus. *Plant Cell* 9, 1381–1396. doi: 10.2307/3870389

Singh, R. K., Miskolczi, P., Maurya, J. P., and Bhalerao, R. P. (2019). A tree ortholog of SHORT VEGETATIVE PHASE floral repressor mediates photoperiodic control of bud dormancy. *Curr. Biol.* 29, 128–133.e2. doi: 10.1016/j.cub.2018.11.006

Stonebloom, S., Burch-Smith, T., Kim, I., Meinke, D., Mindrinos, M., and Zambryski, P. (2009). Loss of the plant DEAD-box protein ISE1 leads to defective mitochondria and increased cell-to-cell transport via plasmodesmata. *Proc. Natl. Acad. Sci. U. S. A.* 106, 17229–17234. doi: 10.1073/pnas.0909229106

Turgeon, R. (2010). The role of phloem loading reconsidered. *Plant Physiol.* 152, 1817–1823. doi: 10.1104/pp.110.153023

Tylewicz, S., Petterle, A., Marttila, S., Miskolczi, P., Azeez, A., Singh, R. K., et al. (2018). Photoperiodic control of seasonal growth is mediated by ABA acting on cell-cell communication. *Science* 360, 212–215. doi: 10.1126/science.aan8576

Wang, X., Sager, R., Cui, W., Zhang, C., Lu, H., and Lee, J. Y. (2013). Salicylic acid regulates plasmodesmata closure during innate immune responses in *Arabidopsis*. *Plant Cell* 25, 2315–2329. doi: 10.1105/tpc.113.110676

Werner, T., Holst, K., Pörs, Y., Guivarc'h, A., Mustroph, A., Chriqui, D., et al. (2008). Cytokinin deficiency causes distinct changes of sink and source parameters in tobacco shoots and roots. *J. Exp. Bot.* 59, 2659–2672. doi: 10.1093/jxb/ern134

Wybouw, B., and De Rybel, B. (2019). Cytokinin – a developing story. *Trends Plant Sci.* 24, 177–185. doi: 10.1016/j.tplants.2018.10.012

Xia, Y., Li, K., Li, J., Wang, T., Gu, L., and Xun, L. (2019). T5 exonuclease-dependent assembly offers a low-cost method for efficient cloning and site-directed mutagenesis. *Nucleic Acids Res.* 47:e15. doi: 10.1093/nar/gky1169

Xu, M., Cho, E., Burch-Smith, T. M., and Zambryski, P. C. (2012). Plasmodesmata formation and cell-to-cell transport are reduced in decreased size exclusion limit 1 during embryogenesis in *Arabidopsis*. *Proc. Natl. Acad. Sci. U. S. A.* 109, 5098–5103. doi: 10.1073/pnas.1202919109

Yadav, R. K., Perales, M., Gruel, J., Girke, T., Jönsson, H., and Venugopala Reddy, G. (2011). WUSCHEL protein movement mediates stem cell homeostasis in the *Arabidopsis* shoot apex. *Genes Dev.* 25, 2025–2030. doi: 10.1101/gad.17258511

Conflict of Interest: The authors declare that the research was conducted in the absence of any commercial or financial relationships that could be construed as a potential conflict of interest.

frontiers in Plant Science

REVIEW
published: 02 June 2021
doi: 10.3389/fpls.2021.679140

Genome Editing for Plasmodesmal Biology

Arya Bagus Boedi Iswanto[1†], Rahul Mahadev Shelake[1†], Minh Huy Vu[1], Jae-Yean Kim[1,2] and Sang Hee Kim[1,2*]*

[1] *Division of Applied Life Sciences (BK21 Four Program), Plant Molecular Biology and Biotechnology Research Center, Gyeongsang National University, Jinju, South Korea,* [2] *Division of Applied Life Sciences, Gyeongsang National University, Jinju, South Korea*

Plasmodesmata (PD) are cytoplasmic canals that facilitate intercellular communication and molecular exchange between adjacent plant cells. PD-associated proteins are considered as one of the foremost factors in regulating PD function that is critical for plant development and stress responses. Although its potential to be used for crop engineering is enormous, our understanding of PD biology was relatively limited to model plants, demanding further studies in crop systems. Recently developed genome editing techniques such as Clustered Regularly Interspaced Short Palindromic Repeats/CRISPR associate protein (CRISPR/Cas) might confer powerful approaches to dissect the molecular function of PD components and to engineer elite crops. Here, we assess several aspects of PD functioning to underline and highlight the potential applications of CRISPR/Cas that provide new insight into PD biology and crop improvement.

Keywords: plasmodesmata, CRISPR/Cas, genome editing, plant stress, crop engineering

OPEN ACCESS

Edited by:
Tessa Maureen Burch-Smith, The University of Tennessee, Knoxville, United States

Reviewed by:
Kuan-Ju Lu, National Chung Hsing University, Taiwan
Alexander Schulz, University of Copenhagen, Denmark

***Correspondence:**
Sang Hee Kim
sangheekim@gnu.ac.kr
Jae-Yean Kim
kimjy@gnu.ac.kr

[†]These authors have contributed equally to this work and share first authorship

Specialty section:
This article was submitted to Plant Cell Biology, a section of the journal Frontiers in Plant Science

Received: *11 March 2021*
Accepted: *10 May 2021*
Published: *02 June 2021*

Citation:
Iswanto ABB, Shelake RM, Vu MH, Kim J-Y and Kim SH (2021) Genome Editing for Plasmodesmal Biology. Front. Plant Sci. 12:679140. doi: 10.3389/fpls.2021.679140

Abbreviations: ACLSV, *Apple chlorotic leaf spot virus*; ACMV, *African cassava mosaic virus*; ADV, *Alfalfa dwarf virus*; ANK1, *Ankyrin 1*; BAM, BARELY ANY MERISTEM; BBWV-2, *broad bean wilt virus 2*; BDMV, *Bean dwarf mosaic virus*; BG, β-1,3-glucanase; BMV, *Brome mosaic virus*; BNYVV, *Beet necrotic yellow vein virus*; BSMV, *Barley stripe mosaic virus*; BYV, *Beet yellows virus*; CaCV, *Capsicum chlorosis virus*; CaLCuV, *Cabbage leaf curl virus*; CalS, callose synthase; CaML, calmodulin; CaMV, *Cauliflower mosaic virus*; CCYV, *Cucurbit chlorotic yellows virus*; CMV, *Cucumber mosaic virus*; CP, capsid protein; CPMV, *Cowpea mosaic virus*; CPsV, *Citrus psorosis virus*; CRISPR, clustered regularly interspaced short palindromic repeats; CRK2, cys-rich receptor-like kinase 2; CTV, *Citrus tristeza virus*; CWMV, *Chinese wheat mosaic virus*; DHyPRP1, double hybrid proline-rich protein; DSB, double-strand break; ER, endoplasmic reticulum; EXPA1, expansin 1; GFLV, *Grapevine fanleaf virus*; GM, genetically modified; GSD1, grain setting defect 1; GVA, *Grapevine virus A*; GVB, *Grapevine virus B*; HDR, homology-directed repair; HIPP26, heavy metal-associated isoprenylated plant protein 26; HR-GT, homologous recombination-based gene targeting; IMK2, inflorescence meristem kinase 2; LIYV, *Lettuce infectious yellows virus*; LNYV, *Lettuce necrotic yellows virus*; LYM2, Lysin motif domain-containing glycosylphosphatidylinositol-anchored protein 2; MAPK, mitogen-activated protein kinase; MiLBVV, *Mirafiori lettuce big-vein virus*; MNSV, *Melon necrotic spot virus*; MP, movement protein; MSV, *Maize streak virus*; NHEJ, non-homologous end joining; NPBT, new plant breeding technologies; OLV-2, *Olive latent virus 2*; PAM, protospacer adjacent motif; PATL, Patellin; PD, plasmodesmata; PDLP, plasmodesmata-located protein; PeVYV, *Pepper vein yellows virus*; PLRV, *Potato leafroll virus*; PLS, PD localization signal; PM, plasma membrane; PMTV, *Potato mop-top pomovirus*; PPV, *Plum pox virus*; PepRSV, *Pepper ringspot virus*; PVX, *Potato virus x*; PVY, *Potato virus y*; PWL, Pathogenicity toward Weeping Lovegrass; QSK1, Qian Shou Kinase 1; RBSDV, *Rice black-streaked dwarf virus*; RCMV, *Red clover mottle virus*; REM, Remorin; RGP2, reversibly glycosylated polypeptide 2; RGSV, *Rice grassy stunt virus*; RLBV, *Raspberry leaf blotch emaravirus*; RLK, receptor-like kinase; RLP, receptor-like protein; RNAi, RNA interference; ROS, reactive oxygen species; RP, replication protein; RSV, *Rice stripe virus*; RTYV, *Rice transitory yellowing virus*; SA, salicylic acid; SEL, size exclusion limit; sgRNA, scaffold-fused gRNA; siRNA, small interfering RNA; SP, structural protein; SYTA, SYNAPTOTAGMIN A; TBSV, *Tomato bushy stunt virus*; TGB, triple gene block; TMV, *Tobacco mosaic virus*; TSWV, *Tomato spotted wilt virus*; TuMV, *Turnip mosaic virus*; TVCV, *Turnip vein-clearing virus*; TYLCF, *Tomato yellow leaf curl virus*; TYLCV, *Tomato yellow leaf curl virus*; VSR, viral suppressors of RNA.

INTRODUCTION

The discovery of plasmodesmata (PD) in 1885 by Edward Tangl has revolutionized the field of plant science. PD functions as one of the vital controllers in plant growth and development (Wu et al., 2018; Vu et al., 2020). Briefly, PD are symplasmic (cytoplasm-to-cytoplasm) nanochannels between adjacent cells, approximately 50-60 nm in size. Structurally, a plasmodesma (the singular form of PD) consists of a cytoplasmic sleeve and a desmotubule (Bell and Oparka, 2011). The space between plasmalemma connecting the cytosol of adjacent cells is the cytoplasmic sleeve. Tubes of appressed endoplasmic reticulum (ER) connecting two adjacent cells are termed desmotubules. As symplasmic tunnels, PD provide pathways for transport of a range of molecules from cell-to-cell, including sugars, ions, proteins, and other essential nutrients, as well as different types of RNA molecules (Wu and Gallagher, 2012; Sager and Lee, 2018; Li et al., 2020b). Cell-to-cell movement of molecules through PD is thought to be dependent on a PD-size exclusion limit (PD-SEL), which involves several aspects, such as PD permeability, PD morphology, PD-associated proteins, and their functions (Sager and Lee, 2018). SEL is determined by the size of the largest molecules that can diffuse through PD. PD-SEL regulates the effectiveness of intracellular communication, which is required for plants to fine-tune their biological and developmental processes under various environmental circumstances (Wu et al., 2018). PD permeability is highly dynamic. The up-and-down modes of PD permeability are controlled by callose, a polysaccharide formed by callose (or β-1,3-glucan) synthase (CalS) enzymes and degraded by glucanase (BG) proteins (Zavaliev et al., 2011; Wu et al., 2018). Callose degradation increases the PD-SEL, whereas callose deposits reduce the PD-SEL. Moreover, PD morphology is considered an essential factor in intercellular transport and can range from simple, twinned or funnel to more complex forms (Oparka et al., 1999; Roberts et al., 2001; Faulkner et al., 2008; Nicolas et al., 2017; Ross-Elliott et al., 2017; Sager and Lee, 2018; Dorokhov et al., 2019).

As plasma membrane (PM)-lined channels, PD-PMs are occupied by unique membrane domains named lipid rafts, sterols- and sphingolipid-enriched microdomains. Lipid rafts provide attractive places for PD-receptor-like proteins (PD-RLPs) and PD-receptor-like kinases (PD-RLKs) to perceive signaling molecules in response to prevailing environmental stimuli (Iswanto and Kim, 2017; Iswanto et al., 2020; Vu et al., 2020). As a gatekeeper of cell trafficking, dynamic PD structure permits the cell-to-cell movement of endogenous molecules and acts as a channel for spreading disease-causing factors. Genome sequencing and proteome analyses are expanding the database of putative or partially characterized PD-related proteins from different plant species (Fernandez-Calvino et al., 2011; Kraner et al., 2017; Leijon et al., 2018). Also, some genes encoding PD-related proteins are redundant in sequence and function. In this regard, to characterize the functions of redundant genes, recent techniques such as genome editing serve as an ideal tool for generating knockout mutants, inducing randomized mutagenesis of the targeted region, or modulating transcriptional regulation.

The most popular genome-editing tool is CRISPR (clustered regularly interspaced short palindromic repeats)/Cas (CRISPR associated) for engineering plants at the DNA and RNA levels (Shelake et al., 2019a; Pramanik et al., 2021). CRISPR/Cas technology has been widely optimized for various applications in several plant species. Such applications include knockout generation, DNA insertion, DNA deletion, gene replacement, chromosome rearrangement, nucleic acid imaging, precise nucleotide substitution, epigenetic modification, pathogen detection, transcription regulation, and more. In this article, we highlight the role of PD-SEL (including PD-associated proteins) in response to multiple external stimuli. We also summarize the characterization of viral/fungal/bacterial proteins targeted at PD, along with potential genome editing tools, strategies, and techniques to understand the basics and improve agronomic traits through PD-SEL engineering.

PD PROTEINS INVOLVED IN ABIOTIC STRESS RESPONSES

The characteristics of callose deposition in response to abiotic stresses (such as osmotic, drought, cold, heat, metal stress) have been reviewed in recent literature (Sager and Lee, 2014). Several reports have highlighted the factors that regulate callose accumulation, thereby conferring enhanced abiotic stress resistance. However, the mechanisms that connect callose-mediated cell-to-cell signaling to the perception of abiotic cues are elusive. This section highlights the PD-associated proteins that positively or negatively control PD-callose under abiotic stresses.

In Arabidopsis, callose deposition in response to salt (NaCl) stress was first characterized by Wrzaczek's group. It has been reported that the receptor-like kinase (RLK), Cys-rich receptor-like kinase 2 (CRK2), can positively regulate the salt stress-dependent pathway in Arabidopsis (Hunter et al., 2019). CRK2-overexpressing lines showed an enhanced germination rate and root length under high salinity conditions. They also found that CRK2 relocalizes to PD after 15 min of mannitol treatment or 30 min of 150 mM NaCl treatment. Furthermore, CRK2 regulates callose deposition under salt-stress conditions by interacting with CalS1. They also highlighted that the CalS1 played an important role in PD permeability during salt stress. *cals1* mutant plants showed impairment in callose accumulation and germination deficiency under high NaCl treatment, which indicated that the phenotype of *cals1* was similar to the *crk2* mutant. The exact mechanism of salt-stress tolerance mediated by CRK2 relocalization (from PM to PD) and callose deposition is not clear because the CRK2-overexpression plants showed enhanced PD callose deposition and reduced PD permeability even without salt stress. Therefore, it can be hypothesized that CRK2 is implicated not only in callose-dependent salt-stress tolerance but may also be involved in plant growth and development irrespective of salt-stress conditions. In the same year, another study demonstrated that Qian Shou kinase 1 (QSK1) and inflorescence meristem kinase 2 (IMK2), a different class of RLKs, relocalize from the PM to PD in response to salt stress (Grison et al., 2019). The

mechanism of callose-mediated salt stress tolerance depends on QSK1 phosphorylation but not on sterol or sphingolipid membrane composition. Interestingly, QKS1 and IMK2 rapidly modulate its localization from PM to PD within 1–4 min post-treatment of 400 mM mannitol and 100 mM NaCl. QSK1 is involved in callose deposition, the PD transportation pathway, lateral root density control, and root development. QSK1 overexpression displays an increased lateral root number and a slightly delayed lateral root formation compared to wild-type and mutant. It was also suggested that the relationship between callose accumulation and tolerance phenotypes observed with QSK1 overexpression was unclear.

Some metals were reported to trigger PD-associated proteins. Calreticulin is a highly conserved Ca^{2+}-sequestering protein that typically resides within the ER lumen, especially in maize and *Medicago truncatula* (Baluska et al., 1999; Sujkowska-Rybkowska and Znojek, 2018). Under Aluminum stress, calreticulin protein in *M. truncatula* mycorrhizal roots was induced and colocalized with Ca^{2+} at the interface of fungal structures and in the periphery of the infected cortex cells (Sujkowska-Rybkowska and Znojek, 2018). Microscopic observations suggested that this colocalization might be required for the calcium mobilization that controls fungal accommodation inside the cortical cells and arbuscular development under Al stress conditions. However, the interaction of calreticulin and Ca^{2+} at PD needs further characterization. Interestingly, calmodulin (CaML) proteins have been found to reside at PD during flg22 treatment in Arabidopsis, which raises the possibility of CaML and calreticulin involvement in stress response (Xu et al., 2017; Wu et al., 2018). Similarly, treatment with subtoxic levels of copper and iron can severely inhibit primary root growth and interfere with the cell-to-cell movement of green fluorescence protein (GFP) (O'Lexy et al., 2018). Iron and copper alter PD permeability in roots via the regulation of callose synthases (CalS5, CalS12) and β-1,3-glucanases (BG_ppap, β-1,3-glucanase-putative; BG6, β-1,3-glucanase 6), respectively.

Wound stress results in alteration of callose accumulation via CalS1 and CalS8 (Cui and Lee, 2016). Aniline blue staining and Drop-ANd-See assay revealed no accumulation of PD callose in mutant leaves lacking CalS1/8 compared with wild-type after wounding. Genetically, CalS8 regulates PD permeability independently with PD-located protein 5 (PDLP5) upon wounding-induced reactive oxygen species (ROS) stress, while CalS1 requires PDLP5 in salicylic-dependent plasmodesmal response. Notably, CalS1 and CalS8 are suggested to localize along with the PM and PD. It remains to deciphered how CalS1 and CalS8 overexpression control PD permeability to enhance plant defense during biotic stresses. Abiotic stresses like heat and light trigger multi-layer signaling pathways that produce systemic acquired acclimation in plants. For example, a recent study reported the involvement of PD proteins (PDLP1 and 5) in propagating systemic ROS-signal waves in response to high light stress in Arabidopsis by altering the PD pore size (Fichman et al., 2021). Further studies into the role of PD-associated proteins in regulating the relay of different systemic signals triggered by various stresses may uncover novel mechanisms of plant protection. The list of PD-associated proteins involved in abiotic stresses is summarized in **Table 1**. Overall, examining the dynamic relocalization of PD-associated proteins from PM-to-PD and their role in long-distance signaling during abiotic stresses will help to understand new dimensions of PD biology.

PD PROTEINS INVOLVED IN BIOTIC STRESS RESPONSES

Several living organisms, specifically fungi, bacteria, yeast, nematodes, insects, arachnids, and weeds, interact with plants. These plant interactions with other species could be beneficial (mutualism), useful to another partner only (commensalism), or harmful to a partner (parasitism). When viruses, fungi, or bacteria attack the plants, it often causes disease due to their virulence activities. In many cases, invasion by pathogens causes plant growth retardation and significant losses in crop quality and productivity. To protect from pathogens, host plants have evolved diverse barricades and remarkable immune machinery for pathogen recognition and the activation of defense signaling modes (Jones and Dangl, 2006; Nguyen et al., 2021). However, some viral, fungal, and bacterial pathogens target PD to mediate intercellular spread in host plant cells.

VIRUS-PD PROTEIN INTERACTIONS

Viruses are neither "living" nor "non-living" and depend on host organisms to replicate and propagate, such as animals, bacteria, fungi, and plants. When viruses invade host plants, they form three major types of proteins, replication proteins (RPs), structural proteins (SPs), and movement proteins (MPs) which are classified based on their functions. RP is crucial for nucleic acid production; SP forms the outer protein shell and other units in the virions, whereas MP is employed to facilitate virus spread between host plant cells (Lefeuvre et al., 2019). The first study on plant viruses began in the 1890s; an infectious virus causing leaf spots in tobacco was characterized, *Tobacco mosaic virus* (TMV). TMV was the first virus of any host ever to be identified. So far, hundreds of plant viruses have been identified, almost all of which are infectious viruses of crop plants (Roossinck, 2010). Ten important plants viruses were ranked based on the scientific and economic importance, including TMV, *Tomato spotted wilt virus* (TSWV), *Tomato yellow leaf curl virus* (TYLCF), *Cucumber mosaic virus* (CMV), *Potato virus y* (PVY), *Cauliflower mosaic virus* (CaMV), *African cassava mosaic virus* (ACMV), *Plum pox virus* (PPV), *Brome mosaic virus* (BMV), and *Potato virus x* (PVX) (Scholthof et al., 2011). Plant viruses are transmitted from one plant to another by different modes such as seeds or pollen, vectors, grafting, or mechanical wounds (Hipper et al., 2013). Upon entry into the plant cell, viral components replicate and move from cell to cell through PD or are transported to long-distant organs through the vascular system. Plant viruses have evolved mechanisms of cell-to-cell movement, which involves the MP to facilitate intercellular trafficking of the plant viruses to and through the PD (Heinlein, 2015). Strikingly, some plant viruses encode multiple MPs, epitomized by triple gene block

(TGB) proteins. Each TGB protein is involved in different stages of virus replication and cell-to-cell movement. In addition to MPs, some viral movement machinery requires additional virus-encoded proteins to deliver the viral genome. For instance, PVX also requires capsid protein (CP), whereas some potyviruses which do not encode MP require cylindrical inclusion protein for their cell-to-cell and long-distance dissemination (Carrington et al., 1998; Tilsner et al., 2013; Kumar et al., 2015). Many MP and other virus-encoded proteins are targeted to be localized at intercellular host regions such as the chloroplast, vesicles, ER, Golgi apparatus, nucleus, PM, and PD apertures. The list of plant virus-encoded proteins-targeted PD is summarized in **Table 2**.

Since many plant virus-encoded proteins localize to PD, it has been assumed that these symplasmic channels play a pivotal role in the viral spread. Plant viruses have evolved in several ways to achieve virulence and pathogenicity. However, PD-SEL is considered one of the main factors limiting the spread of virus infection (Kumar et al., 2015). The PD-SEL is highly linked to the callose accumulation at the edges of PD; therefore, the regulation of CalSs or BGs are depicted as the central signaling pathways to maintain intercellular trafficking via PD (Wu et al., 2018). It has been reported that increased callose accumulation at PD through the suppression of class I BG (GLU I, β-1,3-glucanase) inhibits intercellular movement of TMV, PVX, CMV in the tobacco plants. In contrast, increased PD flux by class III BG (GLU III) overexpression dilates the spread of potato virus Y^{NTN} (PVY^{NTN}) in the potato plants (Iglesias et al., 2000; Bucher et al., 2001; Dobnik et al., 2013), see **Table 2**. The alteration of callose-mediated PD-SEL upon virus infection also involves the physical interaction between PD-associated proteins and virus-encoded proteins. A cytoplasmic receptor ankyrin repeat-containing protein 1 (ANK1) from *Nicotiana tabacum* recruited and interacted directly with TMV MP at PD, resulting in callose attenuation, subsequently enhancing the cell-to-cell movement of TMV MP (Ueki et al., 2010). In addition to PD-associated proteins, PDLP1 interacts with 2B MP from *Grapevine fanleaf virus* (GFLV) at PD, and a *pdlp1/2/3* triple mutant leads to reduced intercellular movement of GFLV (Amari et al., 2010). Besides PDLP1, PDLP5 may also be essential for the movement of other viral proteins. It has been reported that PDLP5 regulates PD permeability in a callose-dependent manner, and reduced callose accumulation in the *pdlp5* mutant exhibits increased cell-to-cell movement of TMV MP30 (Cui and Lee, 2016). However, it remains unknown whether PDLP1 regulates the cell-to-cell movement of GFLV through a callose-dependent manner, and it has not yet been explicitly verified whether PDLP5 physically interacts with TMV MP30.

In addition to PD-associated proteins, a plant-specific lipid microdomain and PD protein, *Solanum tuberosum* Remorin 1.3 (*St*REM1.3), physically interacts with PVX TGB1 protein (Raffaele et al., 2009). The overexpression of *StREM1.3* significantly inhibits the cell-to-cell movement of PVX TGB1, TMV MP30 as well as PVY Hc-Pro (Raffaele et al., 2009; Perraki et al., 2014). Another study on plant REM has shown that *Nicotiana benthamiana REM1* (*NbREM1*) is a negative regulator of the intercellular movement of *Rice stripe virus* (RSV) through the *S*-acylation suppression process (Fu et al., 2018). Although a PVX TGB2 protein interacts indirectly with a BG protein (Fridborg et al., 2003) and grain setting defect 1 (GSD1) (Gui et al., 2015), a REM protein identified from *Oryza sativa* interacts directly with OsACT1 at PD in controlling PD permeability (Gui et al., 2014). Most recent studies on plant REM indicate that the restriction of PVX spread occurs in a REM-induced callose accumulation-dependent manner and may involve the activation of salicylic acid (SA) signaling (Perraki et al., 2018; Huang et al., 2019). Overall, REM proteins from different plant species were reported to be implicated in callose deposition at PD, a key mechanism in plant development and stress responses. Therefore, REM interaction with viral components could be targeted by genome editing or transgenic technology for imparting viral-stress tolerance depending on the negative or positive effect on the viral spread, respectively.

In structure, PD represents membrane-lined canals that provide a suitable compartment for plant receptors to perceive diverse environment-related stimuli. Some of the plant receptors are predominantly localized or recruited at PD in response to

TABLE 1 | PD-associated proteins and their involvements in response to abiotic stress.

No	Plant species	PD-associated protein	Gene ID	Abiotic stimuli	References
(1)	*A. thaliana*	CRK2 (cys-rich receptor-like kinase 2)	AT1G70520	Salinity	Hunter et al., 2019
(2)	*A. thaliana*	QSK1 (Qian Shou kinase 1)	AT3G02880	Salinity and osmotic	Grison et al., 2019
		IMK2 (inflorescence meristem kinase 2)	AT3G51740		
(3)	*M. truncatula*	Calreticulin	MTR_7g080370 calreticulin	Aluminum	Sujkowska-Rybkowska and Znojek, 2018
(4)	*A. thaliana*	CalS5 (callose synthase 5)	AT2G13680	Heavy metals (iron, copper, zinc, and cadmium)	O'Lexy et al., 2018
		CalS12 (callose synthase 12)	AT4G03550		
		BG_PPAP (β-1,3-glucanase_putative)	AT5G42100		
		BG6 (β-1,3-endoglucanase)	AT4G16260		
(5)	*A. thaliana*	CalS1 (callose synthase 1)	AT1G05570	Wounding	Cui and Lee, 2016
		CalS8 (callose synthase 8)	AT3G14570		
(6)	*A. thaliana*	PDLP1 (plasmodesmata-located protein 1)	AT5G43980	High light	Fichman et al., 2021
		PDLP5 (plasmodesmata-located protein 5)	AT1G70690		

TABLE 2 | List of plants virus/bacterial/fungal-encoded proteins-targeted PD.

No.	Pathogen	Protein name	Subcellular localization	Host plant/characterized from	References
(1)	*Red clover mottle virus* (RCMV)	43-kDa	PD	Cowpea (*Vigna unguiculata*)	Shanks et al., 1989
(2)	*Tobacco mosaic virus* (TMV)	30-kDa MP	PD	Tobacco	Wolf et al., 1989
(3)	*Cowpea mosaic virus* (CPMV)	48-kDa	PD	Cowpea (*Vigna unguiculata*)	Wellink et al., 1993
(4)	*Maize streak virus* (MSV)	PV1	PD	Maize (*Zea mays* L.)	Dickinson et al., 1996
(5)	*Potato leafroll virus* (PLRV)	pr17-kDa	PD	Potato (*Solanum tuberosum* L.)	Schmitz et al., 1997
(6)	*Cucumber mosaic virus* (CMV)	3a MP	PD	Cucumber (*Cucumis sativus*)/*Nicotiana clevelandii*	Blackman et al., 1998
(7)	*Olive latent virus 2* (OLV-2)	36K	PD, cell walls, and cytoplasm	*N. benthamiana* and *N. tabacum*	Grieco et al., 1999
(8)	*Beet necrotic yellow vein virus* (BNYVV)	P42 MP	PD	*Chenopodium quinoa*	Erhardt et al., 2000
(9)	*Beet yellows virus* (BYV)	Hsp70h	PD	*Chenopodium quinoa*/*N. benthamiana*	Avisar et al., 2008
(10)	*Brome mosaic virus* (BMV)	3a MP	PD	*N. benthamiana*	Kaido et al., 2007
(11)	*Lettuce infectious yellows virus* (LIYV)	36-kDa (P26)	PD	Lettuce/*N. tabacum*	Stewart et al., 2009
(12)	*Turnip mosaic virus* (TuMV)	P3N-PIPO	PD	Turnip/*N. benthamiana*	Wei et al., 2010; Chai et al., 2020
(13)	*Turnip mosaic virus* (TuMV)	$6K_2$	vesicle, PM, and PD	Turnip/*N. benthamiana*	Grangeon et al., 2013
(14)	*Potato mop-top pomovirus* (PMTV)	TGB3	ER, PD	*N. benthamiana*	Tilsner et al., 2010
(15)	*Bean dwarf mosaic virus* (BDMV)	BDMV-MP	PD	*N. benthamiana*	Zhou et al., 2011
(16)	*Rice stripe virus* (RSV)	NSvc4	PD	*Oryza sativa* L./*N. benthamiana*	Yuan et al., 2011; Xu and Zhou, 2012
(17)	*Rice grassy stunt virus* (RGSV)	pC6	cell wall, PD	*N. benthamiana*	Hiraguri et al., 2011; Sui et al., 2018
(18)	*Broad bean wilt virus 2* (BBWV-2)	VP37	PD	*Chenopodium quinoa*	Liu et al., 2011
(19)	*Rice transitory yellowing virus* (RTYV)	P3	Nucleus and PD	*Oryza sativa* L./*N. benthamiana*	Hiraguri et al., 2012
(20)	*Grapevine virus A* (GVA)/*grape virus B* (GVB)	p31/p36	PD	*Vitris vinifera* L./*N. benthamiana*	Haviv et al., 2012
(21)	*Rice black-streaked dwarf virus* (RBSDV)	P7-1	Nucleus, cytoplasm, and PD	*Oryza sativa* L., *Zea mays* L., *Hordeum vulgare* L., *Triticum aestivum* L./*N. benthamiana*	Sun et al., 2013
(22)	*Raspberry leaf blotch emaravirus* (RLBV)	P4	PM and PD	*Rubus*/*N. benthamiana*	McGavin et al., 2012; Yu et al., 2013
(23)	*Chinese wheat mosaic virus* (CWMV)	37K	PD and ER	*Triricum,* cereal plants worldwide/*N. benthamiana*	Andika et al., 2013
(24)	*Citrus psorosis virus* (V)	54K	PD	Citrus/*N. benthamiana*	Robles Luna et al., 2013
(25)	*Mirafiori lettuce big-vein virus* (MiLBVV)	54K	PD	Lettuce/*N. benthamiana*	Robles Luna et al., 2013
(26)	*Apple chlorotic leaf spot virus* (ACLSV)	50 kDa	cytoplasm and PD	Apple/*N. occidentalis*	Yoshikawa et al., 1999
(27)	*Cauliflower mosaic virus* (CaMV)	P6	PD	*N. benthamiana*	Rodriguez et al., 2014
(28)	*Pepper ringspot virus* (PepRSV)	P29	PD	*Capsicum* sp./*N. benthamiana*	Rodrigues et al., 2015
(29)	*Turnip vein-clearing virus* (TVCV)	P30	PD	Turnip/*N. benthamiana*	Mann et al., 2016
(30)	*Lettuce necrotic yellows virus* (LNYV)	P3	PD	Lettuce/*N. benthamiana*	Mann et al., 2016
(31)	*Alfalfa dwarf virus* (ADV)	P3	PD	Lucerne or alfalfa (*Medicago sativa* L.)/*N. benthamiana*	Mann et al., 2016
(32)	*Melon necrotic spot virus* (MNSV)	DGBp2	PD	Melon (*Cucumis melo* L.)/*N. benthamiana*	Genoves et al., 2011; Navarro and Pallas, 2017

(Continued)

TABLE 2 | Continued

No.	Pathogen	Protein name	Subcellular localization	Host plant/characterized from	References
(33)	*Melon necrotic spot virus* (MNSV)	p7B	ER, Golgi apparatus, and PD	Melon (*Cucumis melo* L.)/*N. benthamiana*	Genoves et al., 2011
(34)	*Capsicum chlorosis virus* (CaCV)	NSm	Cell periphery and PD	*Capsicum annuum* L. and *Solanum lycopersicum* L./*N. benthamiana*	Widana Gamage and Dietzgen, 2017
(35)	*Citrus tristeza virus* (CTV)	P23	Nucleolus, cajal bodies and PD	Citrus/*N. benthamiana*	Ruiz-Ruiz et al., 2018
(36)	*Cucurbit chlorotic yellows virus* (CCYV)	P4.9	Nucleus, cytoplasm, and PD	Cucumber (*Cucumis sativus* L.) and melon (*Cucumis melo* L.)/*N. benthamiana*	Wei et al., 2019
(37)	*Pepper vein yellows virus* (PeVYV)	P4	PD	*Capsicum* sp./*N. benthamiana*	Li et al., 2020a
(38)	*Barley stripe mosaic virus* (BSMV)	γb	Chloroplast, ER, actin filaments, and PD	Barley (*Hordeum vulgare* L.)/*N. benthamiana*	Jiang et al., 2020
(39)	*Grapevine fanleaf virus* (GFLV)	2B	PD	*Vitis vinifera* L./*N. benthamiana*	Amari et al., 2010
(40)	*Fusarium oxysporum* f. sp. *lycopersici*	Avr2 and Six5 (interaction)	PD	Tomato (*Solanum lycopersicum* L.)/*N. benthamiana*	Cao et al., 2018
(41)	*Melampsora larici-populina*	MLP37347	PD	Genus Populus/*A. thaliana*	Germain et al., 2018
(42)	*Phytophthora brassicae*	RxLR3	PD	*Brassica oleracea* L. and *Brassica sinensis* L./*N. benthamiana* and *A. thaliana*	Tomczynska et al., 2020
(43)	*Pseudomonas syringae* pv. *tomato (Pst)* DC3000	HopO1-1	PM and PD	Tomato (*Solanum lycopersicum* L.)/*N. benthamiana* and *A. thaliana*	Aung et al., 2020

abiotic and biotic stresses (Vu et al., 2020). In the case of viral infection, host plants have evolved an antiviral defense mechanism, namely RNA interference (RNAi) mediated by small interfering RNA (siRNA) (Borges and Martienssen, 2015). This RNAi moves from cell to cell through PD to overcome virus infectivity (Smith et al., 2007). However, viruses also develop viral suppressors of RNA silencing (VSR) to target multiple parts of the RNAi machinery (Csorba et al., 2015). In the recent study of virus-related PD-RLKs, BARELY ANY MERISTEM 1 and 2 (BAM1 and BAM2) are essential for the cell-to-cell movement of RNAi whereby they interact with C4 protein from TYLCV (Rosas-Diaz et al., 2018) and the viral silencing suppressor P19 from *Tomato bushy stunt virus* (TBSV) at PD (Garnelo Gomicronmez et al., 2021). However, the role of BAM1 and BAM2 in callose-mediated PD closure is still elusive. In addition to PD-PM protein, SYNAPTOTAGMIN A (SYTA)- an ER-PM contact site protein- can be recruited at PD to facilitate the cell-to-cell movement of *Turnip vein-clearing virus* (TVCV) MP (Levy et al., 2015). SYTA also interacts with the TMV MP and PD localization signal (PLS) of TMV MP and other virus-encoded proteins from *Cabbage leaf curl virus* (CaLCuV). The suppression of *SYTA* leads to reduced cell-to-cell movement of TMV MP, inhibited the systemic spread of CaLCuV, *Turnip mosaic virus* (TuMV), and TVCV, and disrupted PD targeting of TMV PLS (Lewis and Lazarowitz, 2010; Uchiyama et al., 2014; Yuan et al., 2016; Yuan et al., 2018). However, it remains unknown whether SYTA-mediated viral movement occurs in a callose-mediated PD closure-dependent manner or not. A recent study highlighted the importance of phosphorylatable amino acid residues of CMV MP in symptom development and PD localization (Sáray et al., 2021). Investigating such new aspects will shed light on virus-plant host interactions in detail and provide potential clues toward designing novel crop protection strategies in the future.

FUNGAL/BACTERIAL-PD PROTEIN INTERACTIONS

Like pathogenic viruses, plant pathogenic fungi and bacteria cause different diseases that hinder crop quality and productivity. The following plant pathogenic fungi and bacteria have been listed based on their scientific and economic importance. The list of pathogenic fungi includes *Magnaporthe oryzae*, *Botrytis cinerea*, *Puccinia* spp., *Fusarium graminearum*, *Fusarium oxysporum*, *Blumeria graminis*, *Mycosphaerella graminicola*, *Colletotrichum* spp., *Ustilago maydis,* and *Melampsora lini* (Dean et al., 2012). The list of pathogenic bacteria includes *Pseudomonas syringae* pathovars, *Ralstonia solanacearum*, *Agrobacterium tumefaciens*, *Xanthomonas oryzae* pv. *oryzae*, *Xanthomonas campestris* pathovars, *Xanthomonas axonopodis* pathovars, *Erwinia amylovora*, *Xylella fastidiosa*, *Dickeya* (*dadantii* and *solani*), *Pectobacterium carotovorum,* and *Pectobacterium atrosepticum* (Mansfield et al., 2012). Like viruses, pathogenic fungi and bacteria have also evolved sophisticated machinery to invade their host plants. The most common approach for invasion among pathogenic fungi and bacteria is to deploy various effector proteins that can target and modulate PD channels, thus activating various processes in host plants (Lee and Lu, 2011). A hemibiotrophic rice blast fungus *M. oryzae* utilizes invasive hyphae to exploit PD channels (Kankanala et al., 2007) and spread to neighboring cells through PD to expand its vicinity, possibly by delivering an effector Pathogenicity toward Weeping Lovegrass (PWL2) protein (Khang et al., 2010).

In addition to *M. oryzae*, the effectiveness of fungal growth from one cell to a neighboring cell is mainly controlled by the attenuation of callose deposition at PD in which a single fungal mitogen-activated protein kinase (MAPK), PmK1, is involved (Sakulkoo et al., 2018). *Melampsora larici-populina* causes rust disease and severe problems in the genus Populus plants and other family *Salicaceae* plants. *M. larici-populina* is grouped into biographic plant-parasites that secrete an assortment of effectors to determine host cell colonization. A recent study indicates that one of the effectors from *M. larici-populina,* MLP37347, is located at PD (Germain et al., 2018). Even though MLP37347 is targeted to PD, there is no unequivocal evidence showing that MLP37347 effector regulates PD function during *M. larici-populina* infection. It will be interesting to explore the role of the MLP37347 effector in correlation with PD biology. Other effectors from *F. oxysporum*, Avr2 and Six5, have been reported to interact at PD. This interaction is required to manipulate PD apertures, allowing Avr2 to move from one cell to neighboring cells. The presence of Six5 is required for Avr2 cell-to-cell movement through PD, whereas without Avr2, the Six5 effector alone is not sufficient to alter PD permeability. This experiment indicates that to trigger PD opening upon *F. oxysporum* infection, the interaction between Avr2 and Six5 effectors in host cells is required (Cao et al., 2018).

To manipulate the immunity and physiology of host plants, pathogenic fungi and bacteria not only secrete effectors but also target them into PD aperture or other host interiors. Like viruses, it can be assumed that some fungi or bacteria effectors target PD and interact directly with PD-associated proteins to regulate symplasmic continuity. Recently, two pathogen effectors, RxLR3 from *Phytophthora brassicae* and HopO1-1 from *P. syringae*, were reported to localize at PD and interact with PD proteins (Aung et al., 2020; Tomczynska et al., 2020). RxLR3 targets CalS1, CalS2, and CalS3 to control symplasmic trafficking through callose turnover at PD (Tomczynska et al., 2020). Unlike the RxLR3 effector, HopO1-1 physically associates with other PD proteins, such as PDLP5 and PDLP7, to hamper their stability (**Table 3**). The destabilization of PDLP5 and PDLP7 proteins upon HopO1-1 infection leads to enhanced symplasmic conductivity (Aung et al., 2020). It has been shown that PDLP5 is involved in the immune response upon bacterial infection through maintaining callose accumulation at PD (Lee et al., 2011; Cui and Lee, 2016). Furthermore, the mechanism of HopO1-1-enhanced PD permeability seems to be PDLP5/PDLP7-regulated callose accumulation-dependent. In addition to HopO1-1, recent studies reported that several effectors from *P. syringae* not only localized at PD, but they also moved symplastically between the cells through these channels (Kang et al., 2021; Li et al., 2021). It was also suggested that the intercellular movement of effectors is PD permeability dependent manner (Li et al., 2021). However, the molecular linkage between the intercellular movement of effectors and PD regulation is still poorly understood.

GENOME EDITING TOOLS

Recent advancements in genome engineering tools based on CRISPR/Cas systems have opened new doors to fine-tune the plant genome at all layers of the central dogma (Pramanik et al., 2021). Another major advantage of CRISPR-based tools is the ability to customize a strategy to precisely edit the redundant genes or simultaneously edit multiple homologs (Wang et al., 2019; Hong et al., 2020). CRISPR-based tools have been employed in the editing of PD-related genes in recent times (Rosas-Diaz et al., 2018), but their real potential is yet to be explored for manipulating PD biology. In the following sections, we present and discuss the CRISPR/Cas tools and their future applications to

TABLE 3 | PD-associated proteins and their interactions with virus/fungal/bacterial proteins.

No	Plant species	PD-associated protein	Gene ID	(Virus/fungal/bacterial) protein	References
(1)	*A. thaliana*	CalS3/GSL12	AT5G13000	(*Phytophthora brassicae*) RxLR3	Tomczynska et al., 2020
(2)	*A. thaliana*	PDLP5	AT1G70690	(*Pst* DC3000) HopO1-1	Aung et al., 2020
(3)	*A. thaliana*	PDLP7	AT5G37660	(*Pst* DC3000) HopO1-1	Aung et al., 2020
(4)	*A. thaliana*	BAM1	AT5G65700	(TYLCV) C4	Rosas-Diaz et al., 2018
(5)	*A. thaliana*	BAM1	AT5G65700	(TBSV), P19	Garnelo Gomicronmez et al., 2021
(6)	*A. thaliana*	BAM2	AT3G49670	(TYLCV) C4	Rosas-Diaz et al., 2018
(7)	*A. thaliana*	BAM2	AT3G49670	(TBSV) P19	Garnelo Gomicronmez et al., 2021
(8)	*Solanum tuberosum*	StREM1.3	NP_001274989/102577743	(PVX) TGBp1	Raffaele et al., 2009; Perraki et al., 2014
(9)	*A. thaliana*	PDLP1	AT5G43980	(GFLV) 2B	Amari et al., 2010
(10)	*A. thaliana*	Calreticulin	AT1G09210	(TMV) MP30	Chen et al., 2005
(11)	*A. thaliana*	SYTA	AT2G20990	(TMV) 30K, (CaLCuV) MP, (TVCV) MP, and (SqLCV) MP	Lewis and Lazarowitz, 2010; Uchiyama et al., 2014; Levy et al., 2015; Yuan et al., 2016, 2018

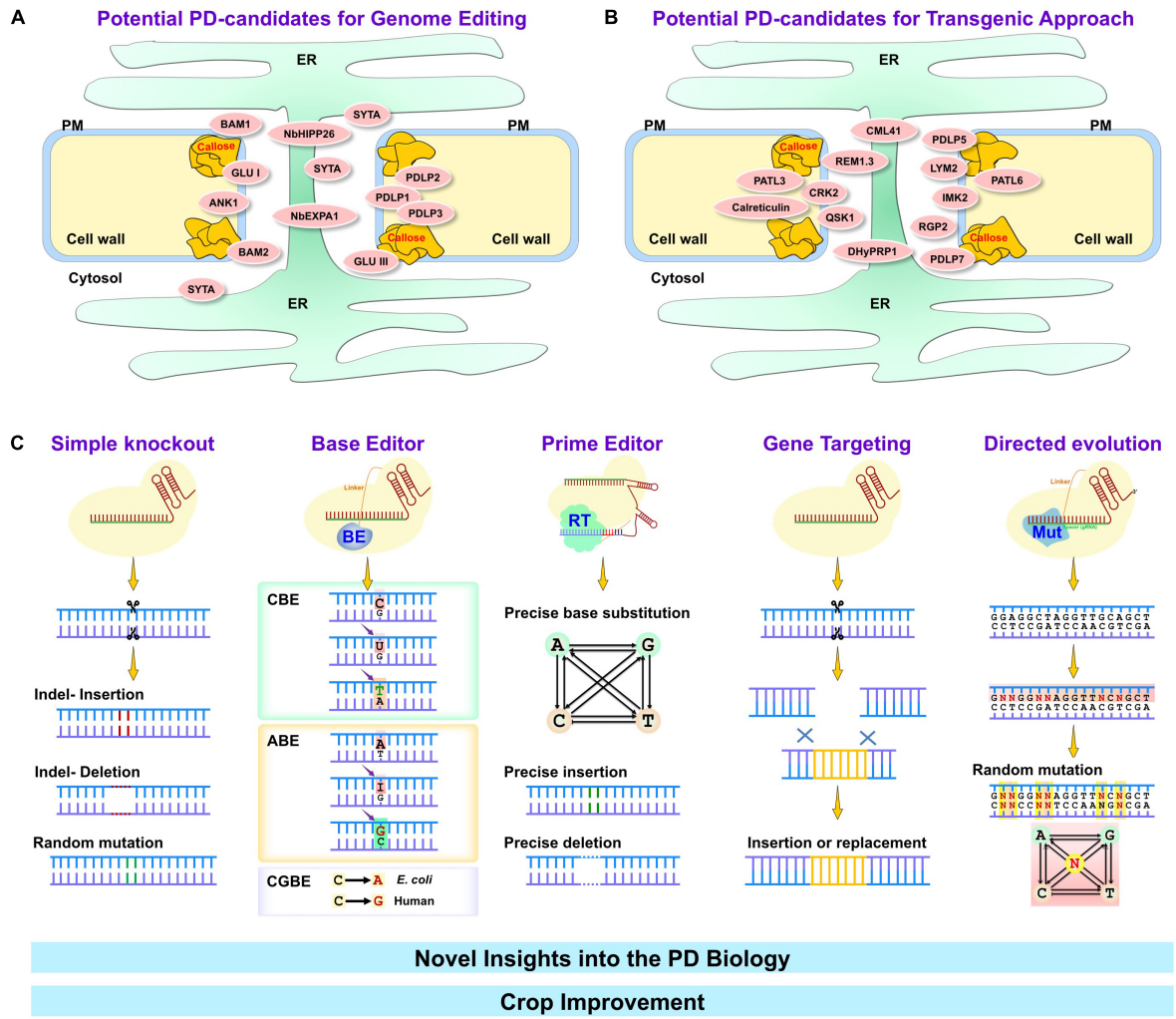

FIGURE 1 | Major genome editing techniques for crop improvement through plasmodesmal engineering. Many PD-associated proteins are involved in a variety of environmental stresses (abiotic and biotic stresses). Depending on the impact on stress mechanism, particular PD-associated proteins can be classified as negative **(A)** or positive **(B)** regulators. PD-associated proteins that negatively regulate stress tolerance in plants (summarized in panel **A**) can be targeted using genome editing tools such as simple knockout by CRISPR/Cas, base editor, prime editor, gene targeting and directed evolution tools **(C)**. On the other hand, PD-associated proteins that positively regulate stress tolerance in plants (summarized in panel **B**) may provide the easiest way to overexpress them by transgenic approach. Targeting PD-associated proteins by genome editing or transgenically possess potential avenues to improve crop quality and productivity. ER, Endoplasmic reticulum; PM, plasma membrane; BAM1 and 2, barely any meristem 1 and 2; GLU I and III, β-1,3-glucanase class I and III; ANK1, ankyrin repeat-containing protein; SYTA, Synaptotagmin A; NbHIPP26, *Nicotiana benthamiana* heavy metal-associated isoprenylated plant protein; NbEXPA1, *N. benthamiana* α-expansin 1; PDLP1, 2, 3, 5, and 7, Plasmodesmata-located protein 1, 2, 3, 5, and 7; PATL3 and 6, patellin 3 and 6; CML41, calmodulin-like protein 41; REM1.3, Remorin 1.3; CRK2, Cys-rich receptor-like kinase 2; QSK1, Qian Shou kinase 1; DHyPRP1, double hybrid proline-rich protein 1; LYM2, lysin motif domain-containing glycosylphosphatidylinositol-anchored protein 2; IMK2, inflorescence meristem kinase 2; RGP2, reversibly glycosylated polypeptide 2.

investigate fundamental aspects of PD biology or PD engineering for stress management strategies.

The first report demonstrating the potential of CRISPR/Cas components for genome editing was published in 2012 (Jinek et al., 2012). Since then, tremendous progress has been made in developing novel CRISPR-based tools (**Figure 1**). The primary CRISPR/Cas tool consists of two components comprising a nuclease enzyme (Cas) and a programmable RNA guide (gRNA) complementary to the target DNA. Cas enzyme bound with scaffold-fused gRNA (sgRNA) recognizes the target site followed by a short recognition motif called protospacer adjacent motif (PAM). The protein-RNA-DNA complex formation leads to the generation of DNA double-strand breaks (DSBs) at desired sites in the complex genome, and endogenous DNA repair pathways make precise or error-prone DNA modifications. The Cas9 and Cas12a (Cpf1) are the most commonly applied Cas enzymes for mutant creation in different organisms (Shelake et al., 2019b). Various Cas variants and orthologs have been characterized to maximize the editing scope and different PAM specificities. Simultaneous targeting of multiple loci in the genome is a significant advantage of CRISPR-based tools compared to other genome engineering methods.

The use of CRISPR/Cas in homologous recombination-based gene targeting (HR-GT) has demonstrated the potential to improve gene-targeting efficiency through precise DSB induction if a donor template is provided to promote the homology-directed repair (HDR) pathway (Capdeville et al., 2021). The HDR-based GT mostly occurs in dividing cells and desired HR-GT products are often mixed with additional indels (insertions/deletions) due to preferred non-homologous end joining (NHEJ). To address this issue, partial catalyzed (nickase, D10A, or H840A) or fully deactivated (dead D10A together with H840A) Cas9 nuclease is engineered for delivering the effector molecules to the target locus for many applications beyond simple DSB-mediated knockout generation (Adli, 2018). Primary tools based on the fusion of effector molecules with nCas9 or dCas9 include base editors that introduce base substitutions without the need for HDR, DSBs, or donor templates (Komor et al., 2016; Gaudelli et al., 2017). A recent addition to the CRISPR toolbox is the prime editor, which needs a template (Anzalone et al., 2019). Although the prime editor tool can introduce customized changes (small insertions or deletions, all 12 base substitutions) at the targeted genomic locus, optimization for plant use is desirable in the near future. Several *in silico* and *in vivo* protocols are being devised for target site selection, validation of gRNAs, appropriate choice of CRISPR tool for the desired application, and suitable delivery strategies depending on the species (Huang et al., 2021). Overall, several features like simple design, high precision, efficiency, lower cost, choice of versatile tools, and a broad range of targeting in the genome have enabled the wider adoption of CRISPR/Cas technology for various purposes in plants.

Genome Editing of PD-Related Genes

Despite the discovery of PD in the nineteenth century, precise knowledge about PD structure and function is still elusive. Although PD operating mode remains challenging to understand, applications of contemporary techniques are revealing their novel facets. Broadly, CRISPR-based technologies can be applied in PD research with bidirectional aims. The first direction is the understanding of PD biology, and secondly, targeting PD-related proteins for the development of stress-tolerant crops. The choice of the CRISPR tool predominantly depends on the possible outcome. As discussed earlier, CRISPR tools may produce a variety of genetic modifications- for example, simple knockout, base substitution, precise insertion/deletion/replacement, strong/weak allele generation, epigenetic modulation, transcriptional regulation, and chromosomal rearrangements (Shelake et al., 2019a). We describe the potential of CRISPR tools for exploiting plasmodesmal biology in two parts: understanding the basics of PD functioning and their modulation for stress management.

Genome Editing for Understanding PD Biology and Crop Improvement

The PD interactome can be roughly divided into three parts depending on their direct or indirect role in PD formation and functioning. Group 1 consists of the actual players that form the PD structure itself; the second group involves the molecules that regulate the PD SEL. The third group contains the molecules trafficking through PD. The interplay between the molecules from these three groups is crucial not only to plant physiology and development but also to plant stress responses and environmental signals (Azim and Burch-Smith, 2020). On the one hand, long-distance trafficking of soluble molecules and defense signals occurs through PD. On the other hand, pathogens also hijack the PD cell-to-cell movement machinery to spread from infected to non-infected plant parts. Therefore, the PD-PM interface is at the forefront of the battle between pathogens and plant defense molecules.

Considerably, several studies have uncovered different facets of PD-mediated spread of viruses and plant defense signaling molecules such as siRNAs. For example, the C4 protein of TYLCV primarily interacts with proteins implicated in plant defense, ubiquitination, and translation from host tomato plants (Kim et al., 2016). Recent reports showed that the RLK homologs (BAM1 and BAM2) act as a positive regulator of siRNA spread through PD (Rosas-Diaz et al., 2018). CRISPR-mediated double knockout mutants (*bam1 bam2*) were generated, confirming the redundant role of BAM1 and BAM2 in promoting the cell-to-cell spread of RNAi. Also, this study suggested the C4 interaction halts the BAM1/2 function and eventually the spread of RNA silencing. In the follow-up study, another viral protein, P19 from TBSV, was demonstrated to interact with BAM1/2 in a similar fashion like C4, indicating that BAM1 and BAM2 are good candidates for CRISPR targeting of C4/P19-interacting domains to develop geminiviral-resistant plants (Garnelo Gomicronmez et al., 2021). Overall, CRISPR-mediated genome editing of PD-related genes is valuable to explore their function and provides attractive potential candidates from the PD interactome to edit and develop biotic and abiotic stress tolerance (**Table 4**).

The symbiotic interaction between host plant-PD and nitrogen-fixing microbes is another research area that needs to be explored. Recent work has shed some light on the molecular dialog between the host plant and associated microbes confirming that PD regulation is a key early event for establishing the symbiotic legume plant-microbe association (Gaudioso-Pedraza et al., 2018). The PD-localized β-1,3-glucanase from *Medicago truncatula* MtBG2 promoted the symplasmic connectivity, thereby facilitating the nodule formation. The increased PD permeability (Complainville et al., 2003) or higher number of PD pores (Schubert et al., 2013) substantially increased nodule number in *M. truncatula* and *Casuarina glauca*, respectively. Also, some tetraspanin proteins like TET3 from Arabidopsis (Fernandez-Calvino et al., 2011), PvTET3, and PvTET6 from the common bean were reported to be localized at the PD-PM interface during nodule formation with rhizobia (Jimenez-Jimenez et al., 2019), suggesting their direct role in symplasmic interaction through PD regulation and cellular trafficking. Thus, the use of CRISPR tools in altering PD may help to promote the positive interaction of symbiotic association of nitrogen-fixing microbes and host plants.

The new set of plant breeding techniques, collectively known as new plant breeding technologies (NPBT), includes the concept of grafting wild-type onto genetically modified

TABLE 4 | Genetic engineering strategies for modulating PD-associated proteins.

No	Gene name	Gene ID	Reported study		Proposed genetic engineering technique		Purpose	References
			KO/KD	OE	CRISPR/Cas9	OE		
(1)	*BAM1*	AT5G65700	Inhibits RNAi movement	Promotes RNAi movement	o (modifying C4/P19-interacting domain)	o	Biotic stress tolerance (TYLCV, TBSV)	Rosas-Diaz et al., 2018; Garnelo Gomicronmez et al., 2021
(2)	*BAM2*	AT3G49670	Inhibits RNAi movement	nd	o (modifying C4/P19-interacting domain)	o	Biotic stress tolerance (TYLCV, TBSV)	Rosas-Diaz et al., 2018; Garnelo Gomicronmez et al., 2021
(3)	*CRK2*	AT1G70520	S	R	x	o	Abiotic stress tolerance (salinity)	Hunter et al., 2019
(4)	*IMK2*	AT3G51740	nd	R	x	o	Abiotic stress tolerance (salinity and drought)	Grison et al., 2019
(5)	*QSK1*	AT3G02880	S	R	x	o	Abiotic stress tolerance (salinity and drought)	Grison et al., 2019
(6)	*PDLP1,2,3*	AT5G43980, AT1G04520 and AT2G33330	R	nd	o	x	Biotic stress tolerance (GFLV)	Amari et al., 2010
((7)	*PDLP5*	AT1G70690	S	R	x	o	Biotic stress tolerance (*Pst* DC3000, *Psm* ES4326, TMV and CMV)	Lee et al., 2011; Lim et al., 2016; Aung et al., 2020
(8)	*PDLP7*	AT5G37660	S	nd	x	o	Biotic stress tolerance (*Pst* DC3000 and *Psm* ES4326)	Aung et al., 2020
(9)	*LYM2*	AT2G17120	S	nd	x	o	Biotic stress tolerance (*Botrytis cinerea*)	Faulkner et al., 2013
(10)	*GLU I*	–	R	S	o	x	Biotic stress tolerance (TMV, PVX and CMV)	Iglesias et al., 2000; Bucher et al., 2001
(11)	*StREM1.3*	NP_001274989/102577743	S	R	x	o	Biotic stress tolerance (PVX)	Raffaele et al., 2009; Perraki et al., 2014
(12)	*RGP2*	AT5G15650	nd	R	x	o	Biotic stress tolerance (TMV)	Zavaliev et al., 2010
(13)	*ANK1* and *ANK2*	AAK18619/AAN63819	R	S	o	x	Biotic stress tolerance (TMV)	Ueki et al., 2010
(14)	*GLU III*	KC437380	nd	S	o	x	Biotic stress tolerance (*potato virus* Y^{NTN})	Dobnik et al., 2013
(15)	*DHyPRP1*	AT4G22470	S	R	x	o	Biotic stress tolerance (*Pst* DC3000 and *Botrytis cinerea*)	Li et al., 2014

(Continued)

TABLE 4 | Continued

No	Gene name	Gene ID	Reported study		Proposed genetic engineering technique		Purpose	References
			KO/KD	OE	CRISPR/Cas9	OE		
(16)	*CML41*	AT3G50770	S	R	x	o	Biotic stress tolerance (*Pst* DC3000)	Xu et al., 2017
(17)	*NbEXPA1*	NbS00007680g0013.1	nd	S	o	x	Biotic stress tolerance (TuMV)	Park et al., 2017
(18)	*NbHIPP26*	Niben101Scf02621g04026.1	R	nd	o	x	Biotic stress tolerance (PMTV)	Cowan et al., 2018
(19)	*PATL3* and *PATL6*	AT1G72160 and AT3G51670	S	R	x	o	Biotic stress tolerance (*alfalfa mosaic virus,* AMV)	Peiro et al., 2014
(20)	*Calreticulin*	AT1G09210	nd	R	x	o	Biotic stress tolerance (TMV)	Chen et al., 2005
(21)	*SYTA*	AT2G20990	R	nd	o	x	Biotic stress tolerance (TMV, CaLCuV, TVCV and SqLCV)	Lewis and Lazarowitz, 2010; Uchiyama et al., 2014; Yuan et al., 2018

KO, knock out; KD, knock down; OE, overexpression; S, susceptible; R, resistant; nd, not determined; O, modification expected for the positive effect.

(GM) rootstock (Langner et al., 2018). The proper combination of scion and rootstock is advantageous to develop improved crop traits. The bi-directional interaction between rootstock and scion involves exchanging all three major macromolecules (DNA, RNA, and protein) through the PD. A recent report showed that even the genomes could transfer horizontally via organelle travel during the remodeling of PD and vascular connection at the root-scion junction (Hertle et al., 2021). Previous reports have successfully used transgenic rootstocks to transfer transgene-mediated traits to the wild-type scion parts- for example, the development of CMV resistance in tomato (Bai et al., 2016), Pierce's disease resistance in grape (Dandekar et al., 2019), PPV resistance in plum (Sidorova et al., 2021), and increased nitrogen levels in walnut overexpressing an ammonium transporter gene (Liu et al., 2021). In such studies, engineering of PD trafficking and the use of transgene-free CRISPR techniques to attain desired traits would be highly desirable because the non-transgenic genome editing approach may easily avoid the GM issues and related-regulatory hurdles.

CONCLUSION AND PERSPECTIVE

PD-mediated symplasmic transport permits cell-to-cell communication in multicellular plants, regulating the harmonized physiological growth and development during environmental stresses. Even though the dynamic nature of PD allows surprisingly high intercellular transport of molecules, PD plasticity makes it challenging to establish the regulatory mechanisms of PD functioning. In this regard, advanced techniques like genome editing and high-resolution microscopy are promising to solve the mysteries around PD structure and function. The primary goal of crop improvement is to design climate-resilient varieties with superior traits. The crucial role of the PD interactome in plant defense is now well-known. The use of genome editing in PD engineering has a vast potential to improve molecule transport for higher nutrition quality for human health, to protect plants against biotic and abiotic stresses, to design improved symbiotic interactions for plant nutrition, and to enhance grafting-based strategies for crop improvement.

AUTHOR CONTRIBUTIONS

ABBI and RMS designed the manuscript structure. ABBI, RMS, and MHV wrote the manuscript. J-YK and SHK designed the manuscript structure and edited the manuscript. All authors contributed to the article and approved the submitted version.

FUNDING

This work was supported by the National Research Foundation of Korea (the Bio & Medical Technology Development Program 2020M3A9I4038352 and Priority Research Centers Program 2020R1A6A1A03044344), and a grant from the New breeding technologies development Program (Project No. PJ01483601), Rural Development Administration, South Korea.

REFERENCES

Adli, M. (2018). The CRISPR tool kit for genome editing and beyond. *Nat. Commun.* 9:1911.

Amari, K., Boutant, E., Hofmann, C., Schmitt-Keichinger, C., Fernandez-Calvino, L., Didier, P., et al. (2010). A family of plasmodesmal proteins with receptor-like properties for plant viral movement proteins. *PLoS Pathog* 6:e1001119. doi: 10.1371/journal.ppat.1001119

Andika, I. B., Zheng, S., Tan, Z., Sun, L., Kondo, H., Zhou, X., et al. (2013). Endoplasmic reticulum export and vesicle formation of the movement protein of Chinese wheat mosaic virus are regulated by two transmembrane domains and depend on the secretory pathway. *Virology* 435, 493–503. doi: 10.1016/j.virol.2012.10.024

Anzalone, A. V., Randolph, P. B., Davis, J. R., Sousa, A. A., Koblan, L. W., Levy, J. M., et al. (2019). Search-and-replace genome editing without double-strand breaks or donor DNA. *Nature* 576, 149–157. doi: 10.1038/s41586-019-1711-4

Aung, K., Kim, P., Li, Z., Joe, A., Kvitko, B., Alfano, J. R., et al. (2020). Pathogenic bacteria target plant plasmodesmata to colonize and invade surrounding tissues. *Plant Cell* 32, 595–611. doi: 10.1105/tpc.19.00707

Avisar, D., Prokhnevsky, A. I., and Dolja, V. V. (2008). Class VIII myosins are required for plasmodesmatal localization of a closterovirus Hsp70 homolog. *J. Virol.* 82, 2836–2843. doi: 10.1128/jvi.02246-07

Azim, M. F., and Burch-Smith, T. M. (2020). Organelles-nucleus-plasmodesmata signaling (ONPS): an update on its roles in plant physiology, metabolism and stress responses. *Curr. Opin. Plant Biol.* 58, 48–59. doi: 10.1016/j.pbi.2020.09.005

Bai, M., Chen, W.-T., Xie, B.-Y., and Yang, G.-S. (2016). A novel strategy to enhance resistance to Cucumber mosaic virus in tomato by grafting to transgenic rootstocks. *J. Int. Agriculture* 15, 2040–2048. doi: 10.1016/s2095-3119(16)61330-8

Baluska, F., Samaj, J., Napier, R., and Volkmann, D. (1999). Maize calreticulin localizes preferentially to plasmodesmata in root apex. *Plant J.* 19, 481–488. doi: 10.1046/j.1365-313x.1999.00530.x

Bell, K., and Oparka, K. (2011). Imaging plasmodesmata. *Protoplasma* 248, 9–25. doi: 10.1007/s00709-010-0233-6

Blackman, L. M., Boevink, P., Cruz, S. S., Palukaitis, P., and Oparka, K. J. (1998). The movement protein of cucumber mosaic virus traffics into sieve elements in minor veins of nicotiana clevelandii. *Plant Cell* 10, 525–538. doi: 10.2307/3870730

Borges, F., and Martienssen, R. A. (2015). The expanding world of small RNAs in plants. *Nat. Rev. Mol. Cell Biol.* 16, 727–741. doi: 10.1038/nrm4085

Bucher, G. L., Tarina, C., Heinlein, M., Di Serio, F., Meins, F. Jr., et al. (2001). Local expression of enzymatically active class I beta-1, 3-glucanase enhances symptoms of TMV infection in tobacco. *Plant J.* 28, 361–369. doi: 10.1046/j.1365-313x.2001.01181.x

Cao, L., Blekemolen, M. C., Tintor, N., Cornelissen, B. J. C., and Takken, F. L. W. (2018). The *Fusarium oxysporum* Avr2-Six5 effector pair alters plasmodesmatal exclusion selectivity to facilitate cell-to-cell movement of Avr2. *Mol. Plant* 11, 691–705. doi: 10.1016/j.molp.2018.02.011

Capdeville, N., Merker, L., Schindele, P., and Puchta, H. (2021). Sophisticated CRISPR/Cas tools for fine-tuning plant performance. *J. Plant Physiol.* 257:153332. doi: 10.1016/j.jplph.2020.153332

Carrington, J. C., Jensen, P. E., and Schaad, M. C. (1998). Genetic evidence for an essential role for potyvirus CI protein in cell-to-cell movement. *Plant J.* 14, 393–400. doi: 10.1046/j.1365-313x.1998.00120.x

Chai, M., Wu, X., Liu, J., Fang, Y., Luan, Y., Cui, X., et al. (2020). P3N-PIPO interacts with P3 via the shared N-Terminal domain to recruit viral replication vesicles for cell-to-cell movement. *J. Virol.* 94:e01898-19.

Chen, M. H., Tian, G. W., Gafni, Y., and Citovsky, V. (2005). Effects of calreticulin on viral cell-to-cell movement. *Plant Physiol.* 138, 1866–1876. doi: 10.1104/pp.105.064386

Complainville, A., Brocard, L., Roberts, I., Dax, E., Sever, N., Sauer, N., et al. (2003). Nodule initiation involves the creation of a new symplasmic field in specific root cells of medicago species. *Plant Cell* 15, 2778–2791. doi: 10.1105/tpc.017020

Cowan, G. H., Roberts, A. G., Jones, S., Kumar, P., Kalyandurg, P. B., Gil, J. F., et al. (2018). Potato mop-top virus co-opts the stress sensor HIPP26 for long-distance movement. *Plant Physiol.* 176, 2052–2070. doi: 10.1104/pp.17.01698

Csorba, T., Kontra, L., and Burgyan, J. (2015). viral silencing suppressors: tools forged to fine-tune host-pathogen coexistence. *Virology* 47, 85–103. doi: 10.1016/j.virol.2015.02.028

Cui, W., and Lee, J. Y. (2016). Arabidopsis callose synthases CalS1/8 regulate plasmodesmal permeability during stress. *Nat. Plants* 2:16034.

Dandekar, A. M., Jacobson, A., Ibanez, A. M., Gouran, H., Dolan, D. L., Aguero, C. B., et al. (2019). Trans-Graft protection against pierce's disease mediated by transgenic grapevine rootstocks. *Front. Plant Sci.* 10:84. doi: 10.3389/fpls.2019.00084

Dean, R., Van Kan, J. A., Pretorius, Z. A., Hammond-Kosack, K. E., Di Pietro, A., Spanu, P. D., et al. (2012). The top 10 fungal pathogens in molecular plant pathology. *Mol. Plant Pathol.* 13, 414–430. doi: 10.1111/j.1364-3703.2011.00783.x

Dickinson, V. J., Halder, J., and Woolston, C. J. (1996). The product of maize streak virus ORF V1 is associated with secondary plasmodesmata and is first detected with the onset of viral lesions. *Virology* 220, 51–59. doi: 10.1006/viro.1996.0285

Dobnik, D., Baebler, S., Kogovsek, P., Pompe-Novak, M., Stebih, D., Panter, G., et al. (2013). beta-1,3-glucanase class III promotes spread of PVY(NTN) and improves in planta protein production. *Plant Biotechnol. Rep.* 7, 547–555. doi: 10.1007/s11816-013-0300-5

Dorokhov, Y. L., Ershova, N. M., Sheshukova, E. V., and Komarova, T. V. (2019). Plasmodesmata conductivity regulation: a mechanistic model. *Plants (Basel)* 8:595. doi: 10.3390/plants8120595

Erhardt, M., Morant, M., Ritzenthaler, C., Stussi-Garaud, C., Guilley, H., Richards, K., et al. (2000). P42 movement protein of beet necrotic yellow vein virus is targeted by the movement proteins P13 and P15 to punctate bodies associated with plasmodesmata. *Mol. Plant Microbe Interact.* 13, 520–528. doi: 10.1094/mpmi.2000.13.5.520

Faulkner, C., Akman, O. E., Bell, K., Jeffree, C., and Oparka, K. (2008). Peeking into pit fields: a multiple twinning model of secondary plasmodesmata formation in tobacco. *Plant Cell* 20, 1504–1518. doi: 10.1105/tpc.107.056903

Faulkner, C., Petutschnig, E., Benitez-Alfonso, Y., Beck, M., Robatzek, S., Lipka, V., et al. (2013). LYM2-dependent chitin perception limits molecular flux via plasmodesmata. *Proc. Natl. Acad. Sci. U S A.* 110, 9166–9170. doi: 10.1073/pnas.1203458110

Fernandez-Calvino, L., Faulkner, C., Walshaw, J., Saalbach, G., Bayer, E., Benitez-Alfonso, Y., et al. (2011). Arabidopsis plasmodesmal proteome. *PLoS One* 6:e18880. doi: 10.1371/journal.pone.0018880

Fichman, Y., Myers, R. J., Grant, D. G., and Mittler, R. (2021). Plasmodesmata-localized proteins and ROS orchestrate light-induced rapid systemic signaling in *Arabidopsis*. *Sci. Signal.* 14:eabf0322. doi: 10.1126/scisignal.abf0322

Fridborg, I., Grainger, J., Page, A., Coleman, M., Findlay, K., and Angell, S. (2003). TIP, a novel host factor linking callose degradation with the cell-to-cell movement of Potato virus X. *Mol. Plant Microbe Interact.* 16, 132–140. doi: 10.1094/mpmi.2003.16.2.132

Fu, S., Xu, Y., Li, C., Li, Y., Wu, J., and Zhou, X. (2018). Rice stripe virus interferes with S-acylation of remorin and induces its autophagic degradation to facilitate virus infection. *Mol. Plant* 11, 269–287. doi: 10.1016/j.molp.2017.11.011

Garnelo Gomicronmez, B., Rosas-Diaz, T., Shi, C., Fan, P., Zhang, D., Rufian, J. S., et al. (2021). The viral silencing suppressor P19 interacts with the receptor-like kinases BAM1 and BAM2 and suppresses the cell-to-cell movement of RNA silencing independently of its ability to bind sRNA. *New Phytol.* 229, 1840–1843. doi: 10.1111/nph.16981

Gaudelli, N. M., Komor, A. C., Rees, H. A., Packer, M. S., Badran, A. H., Bryson, D. I., et al. (2017). Programmable base editing of A·T to G·C in genomic DNA without DNA cleavage. *Nature* 551, 464–471. doi: 10.1038/nature24644

Gaudioso-Pedraza, R., Beck, M., Frances, L., Kirk, P., Ripodas, C., Niebel, A., et al. (2018). Callose-Regulated symplastic communication coordinates symbiotic root nodule development. *Curr. Biol.* 28:e3566.

Genoves, A., Pallas, V., and Navarro, J. A. (2011). Contribution of topology determinants of a viral movement protein to its membrane association, intracellular traffic, and viral cell-to-cell movement. *J. Virol.* 85, 7797–7809. doi: 10.1128/jvi.02465-10

Germain, H., Joly, D. L., Mireault, C., Plourde, M. B., Letanneur, C., Stewart, D., et al. (2018). Infection assays in *Arabidopsis* reveal candidate effectors from the poplar rust fungus that promote susceptibility to bacteria and oomycete pathogens. *Mol. Plant Pathol.* 19, 191–200. doi: 10.1111/mpp.12514

Grangeon, R., Jiang, J., Wan, J., Agbeci, M., Zheng, H., and Laliberte, J. F. (2013). 6K2-induced vesicles can move cell to cell during turnip mosaic virus infection. *Front. Microbiol.* 4:351. doi: 10.3389/fmicb.2013.00351

Grieco, F., Castellano, M. A., Di Sansebastiano, G. P., Maggipinto, G., Neuhaus, J. M., and Martelli, G. P. (1999). Subcellular localization and in vivo identification of the putative movement protein of olive latent virus 2. *J. Gen. Virol.* 80(Pt 5), 1103–1109. doi: 10.1099/0022-1317-80-5-1103

Grison, M. S., Kirk, P., Brault, M. L., Wu, X. N., Schulze, W. X., Benitez-Alfonso, Y., et al. (2019). Plasma membrane-associated receptor-like kinases relocalize to plasmodesmata in response to osmotic stress. *Plant Physiol.* 181, 142–160. doi: 10.1104/pp.19.00473

Gui, J., Liu, C., Shen, J., and Li, L. (2014). Grain setting defect1, encoding a remorin protein, affects the grain setting in rice through regulating plasmodesmatal conductance. *Plant Physiol.* 166, 1463–1478. doi: 10.1104/pp.114.246769

Gui, J., Zheng, S., Shen, J., and Li, L. (2015). Grain setting defect1 (GSD1) function in rice depends on S-acylation and interacts with actin 1 (OsACT1) at its C-terminal. *Front. Plant Sci.* 6:804. doi: 10.3389/fpls.2015.00804

Haviv, S., Moskovitz, Y., and Mawassi, M. (2012). The ORF3-encoded proteins of vitiviruses GVA and GVB induce tubule-like and punctate structures during virus infection and localize to the plasmodesmata. *Virus Res.* 163, 291–301. doi: 10.1016/j.virusres.2011.10.015

Heinlein, M. (2015). Plant virus replication and movement. *Virology* 479-480, 657–671. doi: 10.1016/j.virol.2015.01.025

Hertle, A. P., Haberl, B., and Bock, R. (2021). Horizontal genome transfer by cell-to-cell travel of whole organelles. *Sci. Adv.* 7:eabd8215. doi: 10.1126/sciadv.abd8215

Hipper, C., Brault, V., Ziegler-Graff, V., and Revers, F. (2013). Viral and cellular factors involved in phloem transport of plant viruses. *Front. Plant Sci.* 4:154. doi: 10.3389/fpls.2013.00154

Hiraguri, A., Hibino, H., Hayashi, T., Netsu, O., Shimizu, T., Uehara-Ichiki, T., et al. (2012). The movement protein encoded by gene 3 of rice transitory yellowing virus is associated with virus particles. *J. Gen. Virol.* 93, 2290–2298. doi: 10.1099/vir.0.044420-0

Hiraguri, A., Netsu, O., Shimizu, T., Uehara-Ichiki, T., Omura, T., Sasaki, N., et al. (2011). The nonstructural protein pC6 of rice grassy stunt virus trans-complements the cell-to-cell spread of a movement-defective tomato mosaic virus. *Arch. Virol.* 156, 911–916. doi: 10.1007/s00705-011-0939-6

Hong, W. J., Kim, Y. J., Kim, E. J., Kumar Nalini, Chandran, A., Moon, S., et al. (2020). CAFRI-Rice: CRISPR applicable functional redundancy inspector to accelerate functional genomics in rice. *Plant J.* 104, 532–545. doi: 10.1111/tpj.14926

Huang, D., Sun, Y., Ma, Z., Ke, M., Cui, Y., Chen, Z., et al. (2019). Salicylic acid-mediated plasmodesmal closure via Remorin-dependent lipid organization. *Proc. Natl. Acad. Sci. U S A.* 116, 21274–21284. doi: 10.1073/pnas.1911892116

Huang, T. P., Newby, G. A., and Liu, D. R. (2021). Precision genome editing using cytosine and adenine base editors in mammalian cells. *Nat. Protoc.* 16, 1089–1128. doi: 10.1038/s41596-020-00450-9

Hunter, K., Kimura, S., Rokka, A., Tran, H. C., Toyota, M., Kukkonen, J. P., et al. (2019). CRK2 enhances salt tolerance by regulating callose deposition in connection with PLDalpha1. *Plant Physiol.* 180, 2004–2021. doi: 10.1104/pp.19.00560

Iglesias, V. A., Meins, F., and Jr. (2000). Movement of plant viruses is delayed in a beta-1,3-glucanase-deficient mutant showing a reduced plasmodesmatal size exclusion limit and enhanced callose deposition. *Plant J.* 21, 157–166. doi: 10.1046/j.1365-313x.2000.00658.x

Iswanto, A. B., and Kim, J. Y. (2017). Lipid raft, regulator of plasmodesmal callose homeostasis. *Plants (Basel)* 6:15. doi: 10.3390/plants6020015

Iswanto, A. B. B., Shon, J. C., Liu, K. H., Vu, M. H., Kumar, R., and Kim, J. Y. (2020). Sphingolipids modulate secretion of glycosylphosphatidylinositol-anchored plasmodesmata proteins and callose deposition. *Plant Physiol.* 184, 407–420. doi: 10.1104/pp.20.00401

Jiang, Z., Zhang, K., Li, Z., Li, Z., Yang, M., Jin, X., et al. (2020). The barley stripe mosaic virus gammab protein promotes viral cell-to-cell movement by enhancing ATPase-mediated assembly of ribonucleoprotein movement complexes. *PLoS Pathog* 16:e1008709. doi: 10.1371/journal.ppat.1008709

Jimenez-Jimenez, S., Santana, O., Lara-Rojas, F., Arthikala, M. K., Armada, E., Hashimoto, K., et al. (2019). Differential tetraspanin genes expression and subcellular localization during mutualistic interactions in *Phaseolus vulgaris*. *PLoS One* 14:e0219765. doi: 10.1371/journal.pone.0219765

Jinek, M., Chylinski, K., Fonfara, I., Hauer, M., Doudna, J. A., and Charpentier, E. (2012). A programmable dual-RNA-guided DNA endonuclease in adaptive bacterial immunity. *Science* 337, 816–821. doi: 10.1126/science.1225829

Jones, J. D., and Dangl, J. L. (2006). The plant immune system. *Nature* 444, 323–329.

Kaido, M., Inoue, Y., Takeda, Y., Sugiyama, K., Takeda, A., Mori, M., et al. (2007). Downregulation of the NbNACa1 gene encoding a movement-protein-interacting protein reduces cell-to-cell movement of Brome mosaic virus in *Nicotiana benthamiana*. *Mol. Plant Microbe Interact.* 20, 671–681. doi: 10.1094/mpmi-20-6-0671

Kang, H., Nguyen, Q.-M., Iswanto, A. B. B., Hong, J. C., Bhattacharjee, S., Gassmann, W., et al. (2021). Nuclear localization of HopA1Pss61 is required for effector-triggered immunity. *Plants* 10:888. doi: 10.3390/plants10050888

Kankanala, P., Czymmek, K., and Valent, B. (2007). Roles for rice membrane dynamics and plasmodesmata during biotrophic invasion by the blast fungus. *Plant Cell* 19, 706–724. doi: 10.1105/tpc.106.046300

Khang, C. H., Berruyer, R., Giraldo, M. C., Kankanala, P., Park, S. Y., Czymmek, K., et al. (2010). Translocation of Magnaporthe oryzae effectors into rice cells and their subsequent cell-to-cell movement. *Plant Cell* 22, 1388–1403. doi: 10.1105/tpc.109.069666

Kim, N., Kim, J., Bang, B., Kim, I., Lee, H. H., Park, J., et al. (2016). Comparative analyses of tomato yellow leaf curl virus C4 Protein-Interacting host proteins in healthy and infected tomato tissues. *Plant Pathol. J.* 32, 377–387. doi: 10.5423/ppj.ft.08.2016.0165

Komor, A. C., Kim, Y. B., Packer, M. S., Zuris, J. A., and Liu, D. R. (2016). Programmable editing of a target base in genomic DNA without double-stranded DNA cleavage. *Nature* 533, 420–424. doi: 10.1038/nature17946

Kraner, M. E., Muller, C., and Sonnewald, U. (2017). Comparative proteomic profiling of the choline transporter-like1 (CHER1) mutant provides insights into plasmodesmata composition of fully developed *Arabidopsis thaliana* leaves. *Plant J.* 92, 696–709. doi: 10.1111/tpj.13702

Kumar, D., Kumar, R., Hyun, T. K., and Kim, J. Y. (2015). Cell-to-cell movement of viruses via plasmodesmata. *J. Plant Res.* 128, 37–47. doi: 10.1007/s10265-014-0683-6

Langner, T., Kamoun, S., and Belhaj, K. (2018). CRISPR crops: plant genome editing toward disease resistance. *Annu. Rev. Phytopathol.* 56, 479–512. doi: 10.1146/annurev-phyto-080417-050158

Lee, J. Y., and Lu, H. (2011). Plasmodesmata: the battleground against intruders. *Trends Plant Sci.* 16, 201–210. doi: 10.1016/j.tplants.2011.01.004

Lee, J. Y., Wang, X., Cui, W., Sager, R., Modla, S., Czymmek, K., et al. (2011). A plasmodesmata-localized protein mediates crosstalk between cell-to-cell communication and innate immunity in *Arabidopsis*. *Plant Cell* 23, 3353–3373. doi: 10.1105/tpc.111.087742

Lefeuvre, P., Martin, D. P., Elena, S. F., Shepherd, D. N., Roumagnac, P., and Varsani, A. (2019). Evolution and ecology of plant viruses. *Nat. Rev. Microbiol.* 17, 632–644.

Leijon, F., Melzer, M., Zhou, Q., Srivastava, V., and Bulone, V. (2018). Proteomic analysis of plasmodesmata from populus cell suspension cultures in relation with callose biosynthesis. *Front. Plant Sci.* 9:1681. doi: 10.3389/fpls.2018.01681

Levy, A., Zheng, J. Y., and Lazarowitz, S. G. (2015). Synaptotagmin SYTA forms ER-plasma membrane junctions that are recruited to plasmodesmata for plant virus movement. *Curr. Biol.* 25, 2018–2025. doi: 10.1016/j.cub.2015.06.015

Lewis, J. D., and Lazarowitz, S. G. (2010). *Arabidopsis synaptotagmin* SYTA regulates endocytosis and virus movement protein cell-to-cell transport. *Proc. Natl. Acad. Sci. U S A.* 107, 2491–2496. doi: 10.1073/pnas.0909080107

Li, B. C., Zhang, C., Chai, Q. X., Han, Y. Y., Wang, X. Y., Liu, M. X., et al. (2014). Plasmalemma localisation of DOUBLE HYBRID PROLINE-RICH PROTEIN 1 and its function in systemic acquired resistance of *Arabidopsis thaliana*. *Funct. Plant Biol.* 41, 768–779. doi: 10.1071/fp13314

Li, S., Su, X., Luo, X., Zhang, Y., Zhang, D., Du, J., et al. (2020a). First evidence showing that Pepper vein yellows virus P4 protein is a movement protein. *BMC Microbiol.* 20:72. doi: 10.1186/s12866-020-01758-y

Li, Z. P., Paterlini, A., Glavier, M., and Bayer, E. M. (2020b). Intercellular trafficking via plasmodesmata: molecular layers of complexity. *Cell Mol. Life Sci.* 78, 799–816. doi: 10.1007/s00018-020-03622-8

Li, Z., Variz, H., Chen, Y., Liu, S.-L., and Aung, K. (2021). Plasmodesmata-dependent intercellular movement of bacterial effectors. *Front. Plant Sci.* 12:640277. doi: 10.3389/fpls.2021.640277

Lim, G. H., Shine, M. B., De Lorenzo, L., Yu, K., Cui, W., Navarre, D., et al. (2016). Plasmodesmata localizing proteins regulate transport and signaling during systemic acquired immunity in plants. *Cell Host Microbe* 19, 541–549. doi: 10.1016/j.chom.2016.03.006

Liu, C., Ye, L., Lang, G., Zhang, C., Hong, J., and Zhou, X. (2011). The VP37 protein of Broad bean wilt virus 2 induces tubule-like structures in both plant and insect cells. *Virus Res.* 155, 42–47. doi: 10.1016/j.virusres.2010.08.013

Liu, H.-J., Zhang, J.-Q., Hu, H.-K., Huang, Y.-J., Xv, C.-M., Hu, Y.-Y., et al. (2021). Overexpression of JrAMT2 in walnut (*Juglans regia* L.) rootstock enhances nitrogen level in grafted wild-type walnut scions. *Sci. Horticulturae* 280:109928. doi: 10.1016/j.scienta.2021.109928

Mann, K. S., Bejerman, N., Johnson, K. N., and Dietzgen, R. G. (2016). Cytorhabdovirus P3 genes encode 30K-like cell-to-cell movement proteins. *Virology* 489, 20–33. doi: 10.1016/j.virol.2015.11.028

Mansfield, J., Genin, S., Magori, S., Citovsky, V., Sriariyanum, M., Ronald, P., et al. (2012). Top 10 plant pathogenic bacteria in molecular plant pathology. *Mol. Plant Pathol.* 13, 614–629. doi: 10.1111/j.1364-3703.2012.00804.x

McGavin, W. J., Mitchell, C., Cock, P. J. A., Wright, K. M., and Macfarlane, S. A. (2012). Raspberry leaf blotch virus, a putative new member of the genus Emaravirus, encodes a novel genomic RNA. *J. Gen. Virol.* 93, 430–437. doi: 10.1099/vir.0.037937-0

Navarro, J. A., and Pallas, V. (2017). An update on the intracellular and intercellular trafficking of carmoviruses. *Front. Plant Sci.* 8:1801. doi: 10.3389/fpls.2017.01801

Nguyen, Q.-M., Iswanto, A. B. B., Son, G. H., and Kim, S. H. (2021). Recent advances in effector-triggered immunity in plants: new pieces in the puzzle create a different paradigm. *Int. J. Mol. Sci.* 22:4709. doi: 10.3390/ijms22094709

Nicolas, W. J., Grison, M. S., Trepout, S., Gaston, A., Fouche, M., Cordelieres, F. P., et al. (2017). Architecture and permeability of post-cytokinesis plasmodesmata lacking cytoplasmic sleeves. *Nat. Plants* 3:17082.

O'Lexy, R., Kasai, K., Clark, N., Fujiwara, T., Sozzani, R., and Gallagher, K. L. (2018). Exposure to heavy metal stress triggers changes in plasmodesmatal permeability via deposition and breakdown of callose. *J. Exp. Bot.* 69, 3715–3728. doi: 10.1093/jxb/ery171

Oparka, K. J., Roberts, A. G., Boevink, P., Santa Cruz, S., Roberts, I., Pradel, K. S., et al. (1999). Simple, but not branched, plasmodesmata allow the nonspecific trafficking of proteins in developing tobacco leaves. *Cell* 97, 743–754. doi: 10.1016/s0092-8674(00)80786-2

Park, S. H., Li, F., Renaud, J., Shen, W., Li, Y., Guo, L., et al. (2017). NbEXPA1, an alpha-expansin, is plasmodesmata-specific and a novel host factor for potyviral infection. *Plant J.* 92, 846–861. doi: 10.1111/tpj.13723

Peiro, A., Izquierdo-Garcia, A. C., Sanchez-Navarro, J. A., Pallas, V., Mulet, J. M., and Aparicio, F. (2014). Patellins 3 and 6, two members of the plant patellin family, interact with the movement protein of Alfalfa mosaic virus and interfere with viral movement. *Mol. Plant Pathol.* 15, 881–891. doi: 10.1111/mpp.12146

Perraki, A., Binaghi, M., Mecchia, M. A., Gronnier, J., German-Retana, S., Mongrand, S., et al. (2014). StRemorin1.3 hampers Potato virus X TGBp1 ability to increase plasmodesmata permeability, but does not interfere with its silencing suppressor activity. *FEBS Lett.* 588, 1699–1705. doi: 10.1016/j.febslet.2014.03.014

Perraki, A., Gronnier, J., Gouguet, P., Boudsocq, M., Deroubaix, A. F., Simon, V., et al. (2018). REM1.3's phospho-status defines its plasma membrane nanodomain organization and activity in restricting PVX cell-to-cell movement. *PLoS Pathog* 14:e1007378. doi: 10.1371/journal.ppat.1007378

Pramanik, D., Shelake, R. M., Kim, M. J., and Kim, J. Y. (2021). CRISPR-Mediated engineering across the central dogma in plant biology for basic research and crop improvement. *Mol. Plant* 14, 127–150. doi: 10.1016/j.molp.2020.11.002

Raffaele, S., Bayer, E., Lafarge, D., Cluzet, S., German Retana, S., Boubekeur, T., et al. (2009). Remorin, a solanaceae protein resident in membrane rafts and plasmodesmata, impairs potato virus X movement. *Plant Cell* 21, 1541–1555. doi: 10.1105/tpc.108.064279

Roberts, I. M., Boevink, P., Roberts, A. G., Sauer, N., Reichel, C., and Oparka, K. J. (2001). Dynamic changes in the frequency and architecture of plasmodesmata during the sink-source transition in tobacco leaves. *Protoplasma* 218, 31–44. doi: 10.1007/bf01288358

Robles Luna, G., Pena, E. J., Borniego, M. B., Heinlein, M., and Garcia, M. L. (2013). Ophioviruses CPsV and MiLBVV movement protein is encoded in RNA 2 and interacts with the coat protein. *Virology* 441, 152–161. doi: 10.1016/j.virol.2013.03.019

Rodrigues, K. B., Orilio, A. F., Blawid, R., Melo, F. L., and Nagata, T. (2015). Subcellular localization of p29, a putative movement protein of pepper ringspot virus. *Arch. Virol.* 160, 359–364. doi: 10.1007/s00705-014-2237-6

Rodriguez, A., Angel, C. A., Lutz, L., Leisner, S. M., Nelson, R. S., and Schoelz, J. E. (2014). Association of the P6 protein of *Cauliflower mosaic* virus with plasmodesmata and plasmodesmal proteins. *Plant Physiol.* 166, 1345–1358. doi: 10.1104/pp.114.249250

Roossinck, M. J. (2010). Lifestyles of plant viruses. *Philos. Trans. R. Soc. Lond. B Biol. Sci.* 365, 1899–1905. doi: 10.1098/rstb.2010.0057

Rosas-Diaz, T., Zhang, D., Fan, P., Wang, L., Ding, X., Jiang, Y., et al. (2018). A virus-targeted plant receptor-like kinase promotes cell-to-cell spread of RNAi. *Proc. Natl. Acad. Sci. U S A.* 115, 1388–1393. doi: 10.1073/pnas.1715556115

Ross-Elliott, T. J., Jensen, K. H., Haaning, K. S., Wager, B. M., Knoblauch, J., Howell, A. H., et al. (2017). Phloem unloading in *Arabidopsis* roots is convective and regulated by the phloem-pole pericycle. *eLife* 6:e24125.

Ruiz-Ruiz, S., Spano, R., Navarro, L., Moreno, P., Pena, L., and Flores, R. (2018). Citrus tristeza virus co-opts glyceraldehyde 3-phosphate dehydrogenase for its infectious cycle by interacting with the viral-encoded protein p23. *Plant Mol. Biol.* 98, 363–373. doi: 10.1007/s11103-018-0783-0

Sager, R., and Lee, J. Y. (2014). Plasmodesmata in integrated cell signalling: insights from development and environmental signals and stresses. *J. Exp. Bot.* 65, 6337–6358. doi: 10.1093/jxb/eru365

Sager, R. E., and Lee, J. Y. (2018). Plasmodesmata at a glance. *J. Cell Sci.* 131:jcs209346.

Sakulkoo, W., Oses-Ruiz, M., Oliveira Garcia, E., Soanes, D. M., Littlejohn, G. R., Hacker, C., et al. (2018). A single fungal MAP kinase controls plant cell-to-cell invasion by the rice blast fungus. *Science* 359, 1399–1403. doi: 10.1126/science.aaq0892

Sáray, R., Fábián, A., Palkovics, L., and Salánki, K. (2021). The 28 Ser amino acid of Cucumber mosaic virus movement protein has a role in symptom formation and plasmodesmata localization. *Viruses* 13:222. doi: 10.3390/v13020222

Schmitz, J., Stussi-Garaud, C., Tacke, E., Prufer, D., Rohde, W., and Rohfritsch, O. (1997). In situ localization of the putative movement protein (pr17) from potato leafroll luteovirus (PLRV) in infected and transgenic potato plants. *Virology* 235, 311–322. doi: 10.1006/viro.1997.8679

Scholthof, K. B., Adkins, S., Czosnek, H., Palukaitis, P., Jacquot, E., Hohn, T., et al. (2011). Top 10 plant viruses in molecular plant pathology. *Mol. Plant Pathol.* 12, 938–954. doi: 10.1111/j.1364-3703.2011.00752.x

Schubert, M., Koteyeva, N. K., Zdyb, A., Santos, P., Voitsekhovskaja, O. V., Demchenko, K. N., et al. (2013). Lignification of cell walls of infected cells in *Casuarina glauca* nodules that depend on symplastic sugar supply is accompanied by reduction of plasmodesmata number and narrowing of plasmodesmata. *Physiol. Plant.* 147, 524–540. doi: 10.1111/j.1399-3054.2012.01685.x

Shanks, M., Tomenius, K., Clapham, D., Huskisson, N. S., Barker, P. J., Wilson, I. G., et al. (1989). Identification and subcellular localization of a putative cell-to-cell transport protein from red clover mottle virus. *Virology* 173, 400–407. doi: 10.1016/0042-6822(89)90552-7

Shelake, R. M., Pramanik, D., and Kim, J.-Y. (2019a). Evolution of plant mutagenesis tools: a shifting paradigm from random to targeted genome editing. *Plant Biotechnol. Rep.* 13, 423–445. doi: 10.1007/s11816-019-00562-z

Shelake, R. M., Pramanik, D., and Kim, J. Y. (2019b). Exploration of plant-microbe interactions for sustainable agriculture in CRISPR Era. *Microorganisms* 7:269. doi: 10.3390/microorganisms7080269

Sidorova, T., Miroshnichenko, D., Kirov, I., Pushin, A., and Dolgov, S. (2021). Effect of grafting on viral resistance of non-transgenic plum scion combined with transgenic PPV-Resistant rootstock. *Front. Plant Sci.* 12:621954. doi: 10.3389/fpls.2021.621954

Smith, L. M., Pontes, O., Searle, I., Yelina, N., Yousafzai, F. K., Herr, A. J., et al. (2007). An SNF2 protein associated with nuclear RNA silencing and the spread of a silencing signal between cells in *Arabidopsis*. *Plant Cell* 19, 1507–1521. doi: 10.1105/tpc.107.051540

Stewart, L. R., Medina, V., Sudarshana, M. R., and Falk, B. W. (2009). Lettuce infectious yellows virus-encoded P26 induces plasmalemma deposit cytopathology. *Virology* 388, 212–220. doi: 10.1016/j.virol.2009.03.016

Sui, X., Liu, X., Lin, W., Wu, Z., and Yang, L. (2018). Targeting of rice grassy stunt virus pc6 protein to plasmodesmata requires the ER-to-Golgi secretory pathway and an actin-myosin VIII motility system. *Arch. Virol.* 163, 1317–1323. doi: 10.1007/s00705-018-3726-9

Sujkowska-Rybkowska, M., and Znojek, E. (2018). Localization of calreticulin and calcium ions in mycorrhizal roots of *Medicago truncatula* in response to aluminum stress. *J. Plant Physiol.* 229, 22–31. doi: 10.1016/j.jplph.2018.05.014

Sun, Z., Zhang, S., Xie, L., Zhu, Q., Tan, Z., Bian, J., et al. (2013). The secretory pathway and the actomyosin motility system are required for plasmodesmatal localization of the P7-1 of rice black-streaked dwarf virus. *Arch. Virol.* 158, 1055–1064. doi: 10.1007/s00705-012-1585-3

Tilsner, J., Cowan, G. H., Roberts, A. G., Chapman, S. N., Ziegler, A., Savenkov, E., et al. (2010). Plasmodesmal targeting and intercellular movement of potato mop-top pomovirus is mediated by a membrane anchored tyrosine-based motif on the lumenal side of the endoplasmic reticulum and the C-terminal transmembrane domain in the TGB3 movement protein. *Virology* 402, 41–51. doi: 10.1016/j.virol.2010.03.008

Tilsner, J., Linnik, O., Louveaux, M., Roberts, I. M., Chapman, S. N., and Oparka, K. J. (2013). Replication and trafficking of a plant virus are coupled at the entrances of plasmodesmata. *J. Cell Biol.* 201, 981–995. doi: 10.1083/jcb.201304003

Tomczynska, I., Stumpe, M., Doan, T. G., and Mauch, F. (2020). A Phytophthora effector protein promotes symplastic cell-to-cell trafficking by physical interaction with plasmodesmata-localised callose synthases. *New Phytol.* 227, 1467–1478. doi: 10.1111/nph.16653

Uchiyama, A., Shimada-Beltran, H., Levy, A., Zheng, J. Y., Javia, P. A., and Lazarowitz, S. G. (2014). The Arabidopsis synaptotagmin SYTA regulates the cell-to-cell movement of diverse plant viruses. *Front. Plant Sci.* 5:584. doi: 10.3389/fpls.2014.00584

Ueki, S., Spektor, R., Natale, D. M., and Citovsky, V. (2010). ANK, a host cytoplasmic receptor for the Tobacco mosaic virus cell-to-cell movement protein, facilitates intercellular transport through plasmodesmata. *PLoS Pathog* 6:e1001201. doi: 10.1371/journal.ppat.1001201

Vu, M. H., Iswanto, A. B. B., Lee, J., and Kim, J. Y. (2020). The role of plasmodesmata-associated receptor in plant development and environmental response. *Plants (Basel)* 9:216.

Wang, W., Pan, Q., Tian, B., He, F., Chen, Y., Bai, G., et al. (2019). Gene editing of the wheat homologs of TONNEAU1-recruiting motif encoding gene affects grain shape and weight in wheat. *Plant J.* 100, 251–264. doi: 10.1111/tpj.14440

Wei, T., Zhang, C., Hong, J., Xiong, R., Kasschau, K. D., Zhou, X., et al. (2010). Formation of complexes at plasmodesmata for potyvirus intercellular movement is mediated by the viral protein P3N-PIPO. *PLoS Pathog* 6:e1000962. doi: 10.1371/journal.ppat.1000962

Wei, Y., Shi, Y., Han, X., Chen, S., Li, H., Chen, L., et al. (2019). Identification of cucurbit chlorotic yellows virus P4.9 as a possible movement protein. *Virol. J.* 16:82.

Wellink, J., Van Lent, J. W., Verver, J., Sijen, T., Goldbach, R. W., and Van Kammen, A. (1993). The cowpea mosaic virus M RNA-encoded 48-kilodalton protein is responsible for induction of tubular structures in protoplasts. *J. Virol.* 67, 3660–3664. doi: 10.1128/jvi.67.6.3660-3664.1993

Widana Gamage, S. M. K., and Dietzgen, R. G. (2017). Intracellular localization, interactions and functions of capsicum chlorosis virus proteins. *Front. Microbiol.* 8:612. doi: 10.3389/fmicb.2017.00612

Wolf, S., Deom, C. M., Beachy, R. N., and Lucas, W. J. (1989). Movement protein of tobacco mosaic virus modifies plasmodesmatal size exclusion limit. *Science* 246, 377–379. doi: 10.1126/science.246.4928.377

Wu, S., and Gallagher, K. L. (2012). Transcription factors on the move. *Curr. Opin. Plant Biol.* 15, 645–651. doi: 10.1016/j.pbi.2012.09.010

Wu, S. W., Kumar, R., Iswanto, A. B. B., and Kim, J. Y. (2018). Callose balancing at plasmodesmata. *J. Exp. Bot.* 69, 5325–5339.

Xu, B., Cheval, C., Laohavisit, A., Hocking, B., Chiasson, D., Olsson, T. S. G., et al. (2017). A calmodulin-like protein regulates plasmodesmal closure during bacterial immune responses. *New Phytol.* 215, 77–84. doi: 10.1111/nph.14599

Xu, Y., and Zhou, X. (2012). Role of rice stripe virus NSvc4 in cell-to-cell movement and symptom development in *Nicotiana benthamiana*. *Front. Plant Sci.* 3:269. doi: 10.3389/fpls.2012.00269

Yoshikawa, N., Oogake, S., Terada, M., Miyabayashi, S., Ikeda, Y., Takahashi, T., et al. (1999). Apple chlorotic leaf spot virus 50 kDa protein is targeted to plasmodesmata and accumulates in sieve elements in transgenic plant leaves. *Arch. Virol.* 144, 2475–2483. doi: 10.1007/s007050050660

Yu, C., Karlin, D. G., Lu, Y., Wright, K., Chen, J., and Macfarlane, S. (2013). Experimental and bioinformatic evidence that raspberry leaf blotch emaravirus P4 is a movement protein of the 30K superfamily. *J. Gen. Virol.* 94, 2117–2128. doi: 10.1099/vir.0.053256-0

Yuan, C., Lazarowitz, S. G., and Citovsky, V. (2016). Identification of a functional plasmodesmal localization signal in a plant viral Cell-To-Cell-Movement protein. *mBio* 7:e02052-15.

Yuan, C., Lazarowitz, S. G., and Citovsky, V. (2018). The plasmodesmal localization signal of TMV MP is recognized by plant synaptotagmin SYTA. *mBio* 9:e01314-18.

Yuan, Z., Chen, H., Chen, Q., Omura, T., Xie, L., Wu, Z., et al. (2011). The early secretory pathway and an actin-myosin VIII motility system are required for plasmodesmatal localization of the NSvc4 protein of Rice stripe virus. *Virus Res.* 159, 62–68. doi: 10.1016/j.virusres.2011.04.023

Zavaliev, R., Sagi, G., Gera, A., and Epel, B. L. (2010). The constitutive expression of *Arabidopsis* plasmodesmal-associated class 1 reversibly glycosylated polypeptide impairs plant development and virus spread. *J. Exp. Bot.* 61, 131–142. doi: 10.1093/jxb/erp301

Zavaliev, R., Ueki, S., Epel, B. L., and Citovsky, V. (2011). Biology of callose (beta-1,3-glucan) turnover at plasmodesmata. *Protoplasma* 248, 117–130. doi: 10.1007/s00709-010-0247-0

Zhou, Y., Rojas, M. R., Park, M. R., Seo, Y. S., Lucas, W. J., and Gilbertson, R. L. (2011). Histone H3 interacts and colocalizes with the nuclear shuttle protein and the movement protein of a geminivirus. *J. Virol.* 85, 11821–11832. doi: 10.1128/jvi.00082-11

Conflict of Interest: The authors declare that the research was conducted in the absence of any commercial or financial relationships that could be construed as a potential conflict of interest.

frontiers in Plant Science

REVIEW
published: 03 June 2021
doi: 10.3389/fpls.2021.644870

Plasmodesmata-Involved Battle Against Pathogens and Potential Strategies for Strengthening Hosts

Jie Liu[1], *Lin Zhang*[2] *and Dawei Yan*[1]*

[1] State Key Laboratory of Crop Stress Adaptation and Improvement, School of Life Sciences, Henan University, Kaifeng, China, [2] Joint International Research Laboratory of Agriculture and Agri-Product Safety of the Ministry of Education, Yangzhou University, Yangzhou, China

Plasmodesmata (PD) are membrane-lined pores that connect adjacent cells to mediate symplastic communication in plants. These intercellular channels enable cell-to-cell trafficking of various molecules essential for plant development and stress responses, but they can also be utilized by pathogens to facilitate their infection of hosts. Some pathogens or their effectors are able to spread through the PD by modifying their permeability. Yet plants have developed various corresponding defense mechanisms, including the regulation of PD to impede the spread of invading pathogens. In this review, we aim to illuminate the various roles of PD in the interactions between pathogens and plants during the infection process. We summarize the pathogenic infections involving PD and how the PD could be modified by pathogens or hosts. Furthermore, we propose several hypothesized and promising strategies for enhancing the disease resistance of host plants by the appropriate modulation of callose deposition and plasmodesmal permeability based on current knowledge.

Keywords: plasmodesmata, plant pathogens, disease resistance, callose, callose synthase, cell-to-cell movement

OPEN ACCESS

Edited by:
Jung-Youn Lee,
University of Delaware, United States

Reviewed by:
Zhonglin Mou,
University of Florida, United States
Sabine Dagmar Zimmermann,
Délégation Languedoc Roussillon (CNRS), France

***Correspondence:**
Dawei Yan
ydw2019@henu.edu.cn

Specialty section:
This article was submitted to Plant Pathogen Interactions, a section of the journal Frontiers in Plant Science

Received: *22 December 2020*
Accepted: *28 April 2021*
Published: *03 June 2021*

Citation:
Liu J, Zhang L and Yan D (2021) Plasmodesmata-Involved Battle Against Pathogens and Potential Strategies for Strengthening Hosts. Front. Plant Sci. 12:644870. doi: 10.3389/fpls.2021.644870

INTRODUCTION

Throughout their life span, plants are constantly challenged by pathogens, namely fungi, bacteria, and viruses (Jones and Dangl, 2006). It is well-known that plant cells can respond to pathogens autonomously. Plants recognize microbe-associated molecular patterns (MAMPs) via pattern recognition receptors (PRRs) on the cell membrane, which initiates a series of signaling events and activates pattern-triggered immunity (PTI; Ranf, 2017; Saijo et al., 2018). Some pathogens, however, can produce effectors capable of inhibiting PTI to overcome the host immune system (Grant et al., 2006; Le Fevre et al., 2015; Toruno et al., 2016). A second defense response, which is activated by recognizing pathogenic effectors with corresponding nucleotide-binding leucine-rich repeat (NLR) proteins of hosts, is called effector-triggered immunity (ETI; Cui et al., 2015). Recently, the PTI and ETI systems were found to share common elements and to interact with each other (Ngou et al., 2021; Yuan et al., 2021). Besides the cell-autonomous immunity within infected regions, uninfected host cells could also establish immune responses in what is known as systemic acquired resistance (SAR; Klessig et al., 2018). To gain SAR, signaling molecules must move from infected cells to distal uninfected tissues (Wendehenne et al., 2014; Singh et al., 2017). Further, SAR confers an immune "memory" in hosts enabling them to activate defense responses more quickly and effectively when exposed to another pathogen attack (Conrath, 2006; Ramirez-Prado et al., 2018; Hake and Romeis, 2019; Guerra et al., 2020).

Plant cells have evolved unique cell-wall-spanning structures, termed PD, that link neighboring cells for their symplastic communication (Epel, 1994; Lucas et al., 2009). The typical PD are composed of plasma membrane (PM), cytoplasmic sleeve, and desmotubule derived from the endoplasmic reticulum (ER) (Zambryski and Crawford, 2000; Zambryski, 2008). Various key PD-localized proteins and lipids have been identified, including actin, receptor-like kinases, glycosylphosphatidylinositol-anchor proteins, remorins, sphingolipids, and sterols (Fernandez-Calvino et al., 2011). By controlling the intercellular exchange of both micromolecules and macromolecules, PD are functionally critical during the development of plants and in their responses to abiotic and biotic stresses (Maule, 2008; Lee and Lu, 2011; Lee et al., 2011; Han et al., 2014; Lee, 2014; Sager and Lee, 2014; Cui and Lee, 2016; Wu et al., 2016; Reagan et al., 2018; Miyashima et al., 2019; Yan and Liu, 2020). The aperture of the PD pore, which determines the size exclusion limit (SEL), is a major determinant of PD permeability (Lucas and Lee, 2004; Peters et al., 2021). This PD aperture is dynamically controlled by the deposition and degradation of callose within the cell walls near the neck of PD (Amsbury et al., 2017; Wu et al., 2018). Callose synthases (CalSs) and β-1,3 glucanases (BGs) govern the production and degradation of callose, respectively, fulfilling crucial roles in various developmental and physiological processes of plants (Chen and Kim, 2009; Zavaliev et al., 2011). PD-LOCALIZED PROTEINS (PDLPs) and PLASMODESMATA CALLOSE-BINDING PROTEINS (PDCBs) are two key protein families that positively regulate the dynamics of callose accumulation at PD (Simpson et al., 2009; Lee et al., 2011). Apart from callose, the architecture of PD also affects their conductivity and functioning. In this respect, PD may be classified as type I or II according to the status of the cytoplasmic sleeve between the PM and desmotubule. Compared with type II, the structure of type I PD lacks a visible cytoplasmic sleeve and internal tethers (Nicolas et al., 2017). Loss of function of the *PHLOEM UNLOADING MODULATOR* gene results in the lack of type II PD, whereas enhances PD permeability, fosters phloem unloading, and accelerates root elongation (Yan et al., 2019).

Beyond the key roles in plant development, the PD can participate in plant-pathogen interactions (Faulkner et al., 2013; Wang et al., 2013; Brunkard and Zambryski, 2017; Cheval and Faulkner, 2018). Specifically, PD facilitate the intercellular transport of mobile signal molecules, such as azelaic acid and glycerol-3-phosphate, needed for the establishment of SAR (Singh et al., 2017). Yet many pathogens and effectors can also spread in a cell-to-cell manner via PD to hasten the infection (Lent et al., 1991; Waigmann et al., 1994; Benitez-Alfonso et al., 2010; Cao et al., 2018). Currently, it remains an open question how plants modulate the timing of PD closure and the movement of SAR signals and pathogenic effectors to achieve the defense response. We speculate the apoplastic trafficking of immune molecules might provide an alternative way to impede the spread of pathogens or effectors in the case of blocked PD (Lim et al., 2016b; Singh et al., 2017). Further study of PD in the battle between plants and pathogens is gaining interest and becoming important. Here, we summarize the studied mobile pathogens and effectors, the recognition between pathogens and PD, and the antagonistic regulation of PD by plants and pathogens. Finally, we propose several hypothesized strategies to assist hosts in their battle against pathogens via the appropriate modulation of PD.

PATHOGENS EXPLOIT PD TO FACILITATE HOST INFECTIONS

Through the PD, the cell-to-cell movement of a variety of molecules is possible. But based on this intercellular connection, phytopathogens have evolved mechanisms that take advantage of PD as gateways to facilitate their host infections (**Figure 1**). To do this, pathogens encode their own proteins and recruit or interact with the host proteins to target and modify the PD, either directly or indirectly (**Table 1**).

Viral Spread Through PD

Plant viruses are biotrophic pathogens that utilize the transcriptional machinery of hosts to replicate and propagate with them. To overcome the cell wall barrier, viruses may exploit the PD to engage in cell-to-cell movement and thereby systemically spread throughout the host plants. Viruses encode movement proteins (MPs) to target to and dilate PD (Heinlein and Epel, 2004; Waigmann et al., 2004; Lucas, 2006). For example, a plasmodesmal localization signal sequence in *tobacco mosaic virus* (TMV) and *sugar canemosaic virus* MPs was found necessary and sufficient for PD localization (Yuan et al., 2016; Cheng et al., 2017). Viruses harbor different transport strategies based on differing MP numbers (Epel, 2009). TMV encodes only a single MP, which binds to its RNA and increase the SEL of PD in the form of ribonucleoprotein complexes (Wolf et al., 1989; Brill et al., 2000; Asurmendi et al., 2004; Peña and Heinlein, 2012). In *cowpea mosaic virus*, *grapevine fanleaf virus*, and *cauliflower mosaic virus*, the MPs reorganize and expand the PD pores by forming a movement tubule (Thomas and Maule, 1995; Laporte et al., 2003; Pouwels et al., 2004). *Carnation mottled virus* encodes two small MPs (DGBp1 and DGBp2) by the double-gene block module (Epel, 2009; Hull, 2014). An early model was proposed, in which DGBp2 interacts with DGBp1:vRNA and drives the transportation of this ternary complex to PD via the endomembrane system. This model is not perfect, however, because of some inconsistencies and the mechanism of *carmovirus* movement is believed to be more complicated (Navarro et al., 2019). The triple gene block module encodes three MPs termed TGBp1, TGBp2, and TGBp3; the TGBp2 and TGBp3 are ER membrane-associated proteins and they form both homologous and heterologous complexes (Morozov and Solovyev, 2003; Lim et al., 2008). Binding of TGBp2/TGBp3 to TGBp1:vRNA allows for the targeting of vRNA to PD and its cell-to-cell spread in the host (Epel, 2009). *Beet yellows virus* (BYV) assembles five MPs to facilitate its intercellular movement, including four viral components-an Hsp70h, a 64kDa protein, and two capsid proteins-and a none-structural 6-kDa hydrophobic protein (Alzhanova et al., 2000). The Hsp70h autonomously targets to PD and its ATPase activity drives the intercellular translocation of BYV (Dolja, 2003; Avisar et al., 2008).

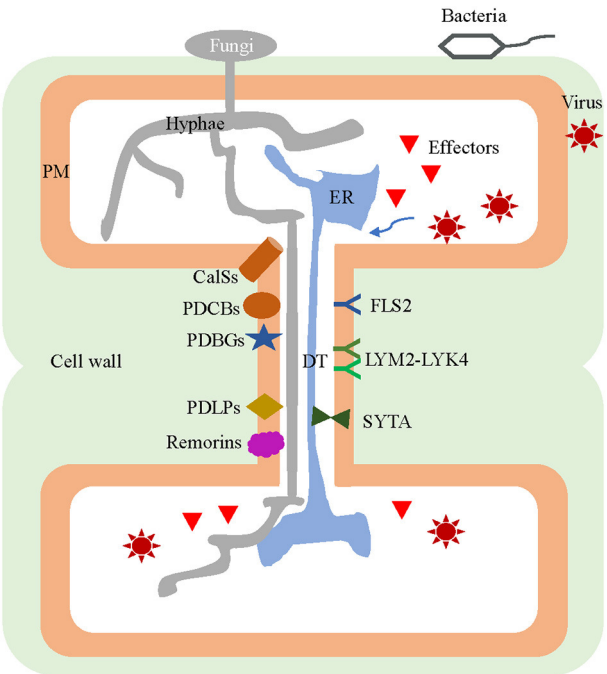

FIGURE 1 | Plasmodesmal components involved in both pathogen infection of plants and host defense responses. Virions, effectors of fungi and bacteria, as well as the fungal hyphae are transported from infected cells to the neighboring healthy cells through the plasmodesmata (PD). Many PD-localized components are jointly exploited by both pathogens and host plants, for use in their interaction during an infection. The pathogens inhibit callose synthesis by inactivating CalSs, suppressing *PDCBs*, destabilizing PDLPs, and/or recruiting PDBGs to assist in their intercellular movement. Viruses can interact with SYTA by relying on MP to remodel the PD. Conversely, PD harbor specific plasmodesmal PM-located receptors of LYM2-LYK4 complex and FLS2 for perception of fungal elicitor chitin and bacterial flagellin, respectively. During infection, some *CalS* and *PDLP* genes can be induced so as to promote callose accumulation and PD closure. The remorins in the membrane microdomains of plasmodesmal PM interact with MP and impede the movement of the virus among host cells. PD, plasmodesmata; DT, desmotubule; CalS, callose synthase; PDCB, PLASMODESMATA CALLOSE-BINDING PROTEIN; PDLP, PD-LOCALIZED PROTEIN; PDBG, plasmodesmal-localized β-1,3 glucanase; SYTA, synaptotagmin A; MP, movement protein; PM, plasma membrane; LYM2, LYSM-CONTAINING GPI-ANCHORED PROTEIN 2; LYK4, LysM-CONTAINING RECEPTOR-LIKE KINASE 4; FLS2, FLAGELLIN SENSING.

As mentioned before, some plant viruses reorganize the inner structure of PD to produce a movement tubule while passing through it (Thomas and Maule, 1995; Laporte et al., 2003; Pouwels et al., 2004). In this process, MPs are assembled into tubular structures by interacting with the host PDLPs, and this replaces the PD desmotubule to leave only a simple PM-lined tunnel remaining, which aids the viral transport (Amari et al., 2010). The *pdlp1/2/3* triple mutant showed a significant reduction of tubule formation along with diminished local and systemic spread of infection, indicating the important roles of PDLPs (Amari et al., 2010). The cytoskeletons, which are involved in the physical formation and structural operation of PD, are also the modification targets of certain viruses (Liu et al., 2005; Prokhnevsky et al., 2005; Wright et al., 2007; Avisar et al., 2008). One study proved that the MPs of *Cucumber mosaic virus* and TMV are able to sever F-actin, weakening the integrity of PD, thereby allowing larger molecules to pass (Su et al., 2010).

Callose around the PD plays a critical role in regulating their permeability and symplastic communication (Amsbury et al., 2017; Wu et al., 2018). Decreasing this callose was shown to result in an enhanced viral infection (Bucher et al., 2001; Li et al., 2012), whereas increasing callose in the β-1,3-glucanase-deficient and *atbg pap* mutants slowed the spread of the virus (Iglesias and Meins, 2000; Zavaliev et al., 2013). Nevertheless, viruses can facilitate their intercellular movement in hosts by limiting the synthesis of callose and promoting its degradation at PD. For example, *potato virus Y* is capable of inducing the activity of a class I β-1,3-glucanase and suppressing callose accumulation in a strain-nonspecific manner, which may explain why some viruses are still able to spread in resistant-genotype hosts (Chowdhury et al., 2020).

PD is a compelling type of membrane contact site, perhaps best illustrated by the specialization of the ER and the PM at the sites of cell-to-cell junctions (Tilsner et al., 2016). The desmotubule and PM together provide a cytoplasmic conduit for intercellular transport (Roberts and Oparka, 2003; Brunkard et al., 2015). Plant synaptotagmin A (SYTA), a membrane protein, can be recruited to form ER-PM contact sites adjacent to the PD. But viral MPs can interact with SYTA to remodel these contact sites to alter PD and aid viral movement (Lewis and Lazarowitz, 2010; Uchiyama et al., 2014; Levy et al., 2015; Pitzalis and Heinlein, 2017). Recently, the multiple C2 domains and transmembrane region protein family were reported to act as ER-PM tethers specifically at PD (Brault et al., 2019). Further studies need to clearly elucidate the role of the ER-PM membrane in PD functioning and identify more PD tethering machineries that participate in the interactions between pathogens and plants.

Chloroplasts are the organelle responsible for not only the generation of small molecules and secondary metabolites important for plant defense, but also the origination of signals in response to developmental and environmental cues (Ganusova and Burch-Smith, 2019). Nevertheless, particular plant viral proteins can interact with chloroplast proteins to impair the defense of hosts and facilitate the infection of virus (Zhao et al., 2016; Bhattacharyya and Chakraborty, 2018). During Potato virus X (PVX) infection, the viral p25 protein interacts with the chloroplast protein ferredoxin 1 (FD1) to reduce its mRNA and protein levels, resulting in a dramatic decrease of PD callose accumulation that is probably associated with the reduction in phytohormones abscisic acid (ABA) and salicylic acid (SA) (Yang et al., 2020). Arabidopsis *INCREASED SIZE EXCLUSION LIMIT* (*ISE*) *2* encodes a chloroplast DEAH RNA helicase, whose mutation increases the branched PD formation and intercellular trafficking (Kobayashi et al., 2007). The *ISE2* expression can be induced by the infection of TMV or *turnip mosaic virus* in *Nicotiana benthamiana*. However, *ISE2*-overexpressing plants are more susceptible to viral infection, without any influence on callose deposition (Ganusova et al., 2017). These findings imply a still, as of yet unknown mechanism of *ISE2*-mediated chloroplast-nucleus signaling in the interactions between PD and viruses.

TABLE 1 | Viral, fungal, and bacterial pathogens and the effectors that move cell-to-cell through the plasmodesmata of attacked plants.

	Pathogens	MPs/Effectors	Function	References
Virus	Tobacco mosaic virus (TMV)	MP30	MPs bind viral RNAs and increase the SEL of PD in the form of ribonucleoprotein complexes.	Wolf et al., 1989; Brill et al., 2000; Peña and Heinlein, 2012; Pitzalis and Heinlein, 2017
	Carnation mottled carmovirus (CarMV)	P7 and P9		Vilar et al., 2002
	Turnip crinkle virus (TCV)	P8 and P9		Hacker et al., 1992; Li et al., 1998
	Melon necrotic spot virus (MNSV)	P7A and P7B	MPs bind viral RNAs and transit through PD in the form of ribonucleoprotein complexes. TGBp1 of PVX and TGBp2 and TGBp3 of PVX and PMTV increase the PD SEL Tamai and Meshi, 2001; Howard et al., 2004; Haupt et al., 2005	Genoves et al., 2006
	Pelargonium flower break virus (PFBV)	P7 and P12		Martinez-Turino and Hernandez, 2011
	Potato virus X (PVX)	TGB: TGBp1, TGBp2 and TGBp3		Tilsner et al., 2013
	Bamboo mosaic virus (BaMV)			Chou et al., 2013
	Barley stripe mosaic virus (BSMV)			Lim et al., 2008;
	Poasemi latent virus (PSLV)			Shemyakina et al., 2011
	Potato mop-top virus (PMTV)			Zamyatnin et al., 2004
	Beet yellows virus (BYV)	Hsp70h, 64kDa protein, two capsid proteins, and 6-kDa hydrophobic protein		Alzhanova et al., 2000; Dolja, 2003; Avisar et al., 2008
	Tobacco etch virus	Capsid protein (CP)	The CP is required for cell-to-cell and long-distance movement of virus.	Dolja et al., 1995
	Cowpea mosaic virus (CPMV)	MP 58K and 48K	MPs form movement tubles to replace PD desmotubule.	Pouwels et al., 2004; Ritzenthaler and Hofmann, 2007
	Grapevine fanleaf virus (GFLV)	MP 2B		Laporte et al., 2003; Amari et al., 2010
	Cauliflower mosaic virus (CaMV)	MP P1		Thomas and Maule, 1995
	Broad bean wilt virus 2	MP VP37		Xie et al., 2016
	Turnip mosaic virus (TuMV)	6K2 protein	6K2 induces vesicle formation for intercellular movement through PD.	Grangeon et al., 2013
Viroids	Potato spindle tuber viroid (PSTVd)	/	11 RNA loop motifs are critical for cell-to-cell mvement.	Ding et al., 1997; Zhong et al., 2008
Fungi	Magnaporthe oryzae (M. oryzae)	/	IH seek for the pit fields, followed by crossing the PD channels into adjacent cells with constricted hyphae.	Kankanala et al., 2007
		BSA3	BSA3 locates near PD.	Mosquera et al., 2009
		PWL2 and BAS1	PWL2 and BAS1were delivered into the cytoplasm of rice cells by biotrophic interfacial complex (BIC), and finally into neighboring cells via PD.	Khang et al., 2010
	Melampsora larici-populina	AvrL567	AvrL567 accumulates at PD.	Germain et al., 2018
	Ustilago maydis	Cmu1	Cmu1 could likely spread to the neighboring cells through PD and repress SA biosynthesis in host plants.	Djamei et al., 2011

(Continued)

TABLE 1 | Continued

	Pathogens	MPs/Effectors	Function	References
	Phytophthora brassicae	RxLR3	RxLR3 reduce the callose deposition around PD by interacting with and inhibiting CalS1, CalS2, and CalS3	Tomczynska et al., 2020
	Fusarium graminearum	Fusaoctaxin A	Fusaoctaxin A inhibit expression of *PDCB-like* genes and *CalS* genes.	Jia et al., 2019
	Fusarium oxysporum	Avr2 and Six5	Avr2-Six5 effector pair alters plasmodesmatal conductivity to facilitate intercellular movement of Avr2.	Cao et al., 2018
Bacteria	Candidatus Liberibacter asiaticus (CLas)	/	CLas move through sieve pores, and cause callose overproduction and sieve-pore plugging in phloem.	Koh et al., 2012; Achor et al., 2020
	Pseudomonas syringae pv. tomato (Pst) DC3000	HopO1-1	HopO1-1 targets to PD and destabilizes PDLP7 and PLDP5.	Aung et al., 2020
	Pseudomonas syringae pv. tomato (Pst) DC3000	HopK1, HopY1, HopF2, HopU1, HopH1, HopC1, HopN1, HopAA1, HopAF1, HopP1, HopAB2, HopE1, HopAO1, HopA1, HopX1, HopB1	Hop effectors move from infected cells to neighboring cells through PD.	Li et al., 2020

Viroids are the smallest known pathogenic agents, consisting only of circular single-stranded RNAs that replicate autonomously and traffic themselves systemically throughout their hosts via the vascular tissue phloem (Flores et al., 2005). Viroids differ from viruses in having unique structural, functional, and evolutionary properties (Flores et al., 2005). Work by Ding et al. (1997) demonstrated that *potato spindle tuber viroid* (PSTVd) can move rapidly from the initially injected mesophyll cells which are interconnected by PD into neighboring cells, whereas it was retained in mature guard cells lacking PD connections. The PSTVd consists of 27 RNA loop motifs flanked by short helices, of which 11 loops were identified as critical for its intercellular movement (Zhong et al., 2008). A small RNA from the virulence-modulating region of PSTVd can suppress the expression of tomato *CalS11-like* and *CalS12-like* genes, pointing to a hypothesized mechanism of viroid movement through PD (Adkar-Purushothama et al., 2015). More mechanisms underpinning the regulation of viroid intercellular trafficking by RNA motifs and cellular factors are reviewed by Takeda and Ding (2009).

Fungal Infection by Invasive Hyphae (IH) and Effectors

Perhaps the best example of how a fungal pathogen can spread through PD is the study of the hemibiotrophic rice blast fungus, *Magnaporthe oryzae* (M. oryzae; Kankanala et al., 2007; Sakulkoo et al., 2018). By means of the enormous turgor pressure generated by their appressoria, *M. oryzae* breaches the outer cell surface and produces special hyphae named the penetration peg (Howard and Valent, 1996). When entering the epidermal cell lumen, this penetration peg expands to form primary hyphae, which differentiate into bulbous invasive hyphae (IH; Heath et al., 1990). These IH are encased in a plant-derived extra-invasive hyphal membrane outside their cell wall. Then, the bulbous IH seek out pit fields composed of PD clusters in the cell wall, after which they crossing the PD channels into adjacent cells using constricted hyphae (Kankanala et al., 2007). Callose occlusions around the PD were found absent only during the early stages (24–27 h post-inoculation) of invasion in the first rice cell; hence, over this period the PD stayed open, indicating the fungus is able to suppress the callose deposition at pit fields in the host at a specific time before invading the neighboring cells (Sakulkoo et al., 2018). Consistent with this key role of PD, another investigation revealed the failure of IH to move into mature guard cells from neighboring cells due to the degeneration of PD (Kankanala et al., 2007).

Furthermore, the mobile effectors PATHOGENICITY TOWARD WEEPING LOVEGRASS (PWL2) and BIOTROPHY-ASSOCIATED SECRETED (BAS1) produced by *M. oryzae* can move in a cell-to-cell fashion to facilitate host infection (Khang et al., 2010). Both PWL2 and BAS1 are released by IH into the cytoplasm of rice cells by a biotrophic interfacial complex, and move into non-invaded neighboring cells via PD before the spread of IH, which was presumed to better prepare the host cells for the following invasion of IH (Khang et al., 2010). Pmk1, a single fungal mitogen-activated protein kinase, regulates the

expression of secreted fungal effectors that inhibit ROS (reactive oxygen species) generation and callose deposition at the PD in rice (Sakulkoo et al., 2018). Accordingly, inhibiting Pmk1 prevents *M. oryzae* from infecting adjacent plant cells, leaving it trapped in the present cell, yet without affecting the biotrophic interfacial complex structure and hyphae morphology (Sakulkoo et al., 2018). These findings indicate the importance of PD for the cell-to-cell invasion of rice cells by *M. oryzae* during the infection process.

The RxLR3 effector produced by *Phytophthora brassicae* can interact with and inhibit CalS1, CalS2, and CalS3, to reduce the callose deposition around PD, so as to promote symplastic trafficking (Tomczynska et al., 2020). In wheat, three *PDCB-like* genes and seven *CalS* genes are suppressed by the virulence factor Fusaoctaxin A during *Fusarium graminearum* infection, which suggests this pathogen may interfere with normal callose accumulation and disrupt the PD status of host plants (Jia et al., 2019). The effectors Avr2 and Six5 secreted by *F. oxysporum* interact at the PD during its infection of tomato; however, Avr2 only moves cell-to-cell in the presence of Six5, while Six5 alone does not alter plasmodesmal conductivity (Cao et al., 2018). Generally, however, the consensus PD-targeting signal peptides of such pathogen effectors have yet to be identified.

Bacterial Infection With Symplastic Trafficking

Presently, the cell-to-cell spread of bacteria has been mostly reported to occur in the sieve tubes of phloem tissues. *Candidatus* Liberibacter asiaticus (CLas) is a phloem-inhabiting bacterium that causes a destructive disease of citrus trees called Huanglongbing (HLB), which is achieved by its spread via sap flow in the phloem throughout the host plants (Bove, 2006). The cells of CLas adhere to the plasma membrane of those phloem cells positioned specifically adjacent to the sieve pores, and the ensuing morphology changes there enable its movement (Achor et al., 2020). Although we know HLB-infected phloem cells undergo callose accumulation and sieve-pore plugging (Koh et al., 2012; Achor et al., 2020), there is still no evidence showing CLas passing through PD between cells in other plant tissues. The interaction between CLas and phloem cells evidently needs more careful investigation. Usually, bacterial pathogens do not cross the cell wall, probably because their suitable habitat is mostly limited to the apoplastic spaces between plant cells, unlike viruses and fungi which spread intercellularly during local and systemic infections (reviewed by Lee and Lu, 2011). Still, bacteria can release specific effector molecules into plant cells not unlike fungi do, which then move through the PD to spread intercellularly in the host (Li et al., 2020; **Figure 1**). Only a few effectors have been studied to date. A notable example is the effector protein HopO1-1 of *Pseudomonas syringae* pv. *tomato* (*Pst*) DC3000, a putative mono-ADP-ribosyltransferase. The amino acids in position 41 to 283 (C-terminal end residue) of HopO1-1 are required for its localization to PD (Aung et al., 2020). Once there, HopO1-1 enhances the PD-dependent intercellular molecular flux by destabilizing the PDLP7 and PLDP5 proteins of hosts without affecting their transcript levels (Aung et al., 2020). Further, Li et al. (2020) recently proved that the movement of 16 Hop effectors of *Pst* DC3000 move from transformed cells into neighboring cells through PD depends on their molecular weights. Among them, HopAF1 was characterized by the highest PD-dependent movement, which can nonetheless be inhibited by callose overproduction (Li et al., 2020). This study provided robust evidence that the effectors of bacteria, like fungi, may possess an intercellular mobile ability. It would seem those mobile effectors exploit different mechanisms when interacting with the host during its infection, a topic that warrants further investigation.

UTILIZATION OF PD BY HOSTS FOR DEFENSE

In plant-pathogen interactions, plants have evolved two protein families to recognize pathogens: PM-anchored PRR receptors for PAMPs and intracellular NLR receptors for pathogens effectors (reviewed by Dodds and Rathjen, 2010). The lysin motif (LysM) domain-containing protein CHITIN ELICTOR BINDING PROTEIN (CEBiP) and the receptor-like kinases FLAGELLIN SENSING (FLS2) respectively recognize chitin and flagellin (Kaku et al., 2006; Shimizu et al., 2010; Bücherl et al., 2017). The plasmodesmal PM that is enriched with particular proteins and lipids will integrate extracellular signals differently from the other remaining PM. Increasing numbers of receptors and kinases have been shown to be active in or recruited to plasmodesmal PM (Stahl et al., 2013; Grison et al., 2019; Hunter et al., 2019). A PD-located receptor, LYSM-CONTAINING GPI-ANCHORED PROTEIN 2 (LYM2)/ CEBiP, responds to chitin and signaling, thereby reducing the molecular flux through PD (Faulkner et al., 2013). A receptor complex called LYM2-LYSIN MOTIF-CONTAINING RECEPTOR-LIKE KINASE 4 (LYK 4) (**Table 3**) found localized at plasmodesmal PM is utilized for plant defense in response to fungal chitin (Cheval et al., 2020). Downstream chitin signaling triggers the phosphorylation of the NADPH oxidase RESPIRATORY BURST OXIDASE HOMOLOG PROTEIN D via a calcium-dependent protein kinase, leading to callose deposition and eventual PD closure. Intriguingly, FLS2 was observed in the vicinity of PD and mediates flg22-triggered changes of PD-mediated trafficking (Faulkner et al., 2013). This phenomenon suggests FLS2 may have an unconsidered role in recognizing flagellin at PD. More receptors at the plasmodesmal PM await discovery.

Being more than simply passive conduits for trafficking, PD also act as hubs capable of integrating multiple signals from the plant development and defense pathways. How do plants protect themselves from pathogens invasion relying on PD? The underlying molecular mechanisms have been elucidated by a few studies. Callose deposition at PD was proven able to restrict infection by pathogen (Cheval and Faulkner, 2018; Wu et al., 2018), suggesting one potential mechanism. The expression levels of *CalS1*, *5*, *9*, *10* and *12* genes were stimulated by *Hyaloperonospora* infection and a SA treatment, whereas the induction of *CalS1* and *CalS12* was significantly repressed in the *npr1* mutant, thus implying a NPR1-dependent regulation

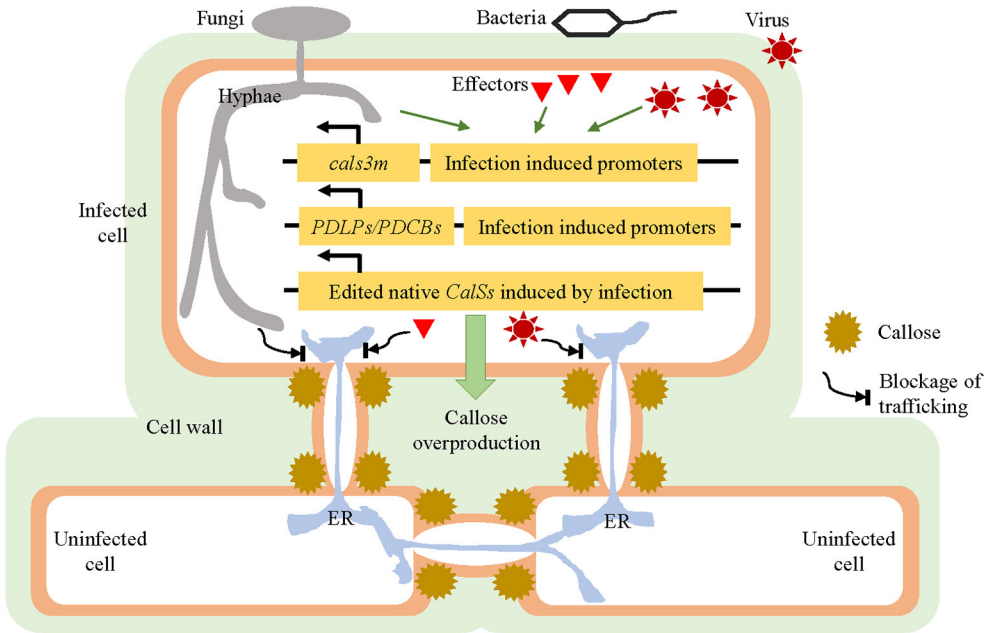

FIGURE 2 | Strategies for improving the disease resistance of hosts by modulating their plasmodesmata (PD). Under normal plant growing conditions, the *cals3m*, *PDLPs/PDCBs*, and edited *CalSs* genes are expressed at a relatively low level, without affecting the plants' ordinary development. Once a pathogen attack is detected, the expression of *cals3m*, *PDLPs/PDCBs*, and edited *CalSs* could be induced quickly and strongly, resulting in prompt callose overproduction around the PD and PD closure; this is followed by imposing a blockage of connections between the primary invaded cells and neighboring uninfected cells, which should also stop the intercellular trafficking of pathogens or effectors. These hypothesized approaches are supposed to slow down the spread of pathogens and thus enhance the disease resistance of host plants. PD, plasmodesmata; CalS, callose synthase; PDLP, PD-Localized Protein; PDCB, Plasmodesmata Callose-Binding Protein.

(Dong et al., 2008). In the *cals1* mutant, callose at the PD is not affected by either an SA treatment or *Pseudomonas* infection (Cui and Lee, 2016), which suggests CalS1 is essential for SA-mediated callose deposition. The *pdlp1/2/3* triple mutant is more susceptible to the downy mildew pathogen *Hyaloperonospora arabidopsidis*, whereas *PDLP1* overexpression increases callose deposition around the haustoria and enhances plant resistance (Caillaud et al., 2014). PDLP5, localized at the central region of PD, plays a positive role in conferring an enhanced innate immunity of host plants against bacterial pathogens in a SA-dependent manner, by modulating PD callose deposition (Lee et al., 2011; Wang et al., 2013). Enrichment of t18:0-based sphingolipids were found to facilitate the recruitment of PDLP5 proteins to PD, which consequently led to reduced PD conductivity and enhanced resistance to the fungal-wilt pathogen *Verticillium dahlia* and the bacterium *Pst* DC3000 (Liu et al., 2020). Remorins are plant-specific proteins found especially in PM microdomains (Raffaele et al., 2009). Applying SA to plants can trigger a remorin-dependent reorganization of lipid raft nanodomains at PD, thereby modifying the inner structure of PD to impede viral spreading in hosts (Huang et al., 2019). Further, remorins can physically interact with TGBp1, a MP of PVX, to impede the cell-to-cell spread of PVX in tomato leaves (Raffaele et al., 2009).

The number and architecture of PD vary among different cell types and plant developmental stages, which enables the dynamic changes of symplastic transport (Ormenese et al., 2000; Ehlers and Kollmann, 2001; Burch-Smith et al., 2011). During the floral transition of the shoot apical meristem in *Sinapis alba*, for example, the PD frequency increased substantially (Ormenese et al., 2000). While sink leaf cells may contain simple PD in excess of 90%, in stark contrast the source leaf cells mainly contain highly branched PD in *Arabidopsis thaliana*. Correspondingly, the PD in sink cells permit the transport of relatively large molecules, whereas tissues composed of source cells predominantly show a decline in their transport ability (Oparka et al., 1999). *Tomato yellow leaf curl virus* infection leads to an increased number of PD in susceptible tomato plants (Reuveni et al., 2015). Similarly, in *Casuarina glauca* nodules there are fewer PD, perhaps because of the cell enlargement combined with a failed secondary PD formation (Schubert et al., 2013). One study proved ABA negatively regulates PD permeability via callose induction, leading to restricted viral cell-to-cell spreading (Alazem and Lin, 2017). Another study showed treating plants with ABA can modify the number, width, and frequency of their PD (Kitagawa et al., 2019). Collectively, these findings indicate that host plants may reduce and modulate the density and architecture of PD to better defend against invading pathogens. Further investigation is arguably needed to explore in depth the functional PD regulators involved.

STRATEGIES FOR IMPROVING DISEASE RESISTANCE OF HOSTS BY MODULATING PD

Overall, it is evident that PD can be employed as a weapon, by both pathogens and their hosts, who may compete for control

TABLE 2 | Experimentally studied Host proteins/lipids that can regulate the plasmodesmata for plant defense.

Proteins/lipids	Function	References
LYM2-LYK4	PD located LYM2-LYK4 recognize the chitin and trigger downstream signaling to reduce the molecular flux through PD.	Faulkner et al., 2013; Cheval et al., 2020
FLS2	FLS2 is observed in the vicinity of PD and mediates flg22-triggered changes of PD-mediated trafficking.	Faulkner et al., 2013
RBOHD	RBOHD produce ROS that induces PD closure in the signaling cascade of LYM2-LYK4.	Cheval et al., 2020
CalS1	Callose deposition	Dong et al., 2008; Cui and Lee, 2016
CalS12	Callose deposition	Dong et al., 2008
PDLP1	Callose deposition	Caillaud et al., 2014
PDLP5	Callose deposition	Lee et al., 2011; Wang et al., 2013
Calreticulin	Calreticulin interact directly with TMV MP and interferes with targeting of TMV MP to delay cell-to-cell movement of the virus.	Chen et al., 2005
Remorins	Remorins interact with MP TGBp1 of PVX and impairs PVX movement.	Raffaele et al., 2009
	Remorins narrow the PD channels to impede virus spreading depended on SA signaling.	Huang et al., 2019
Sphingolipids	Sphingolipids recruited PDLP5 proteins to PD, which consequently results in the decreased PD conductivity.	Liu et al., 2020

TABLE 3 | Abbreviation list.

Abbreviation	Full name
ABA	Abscisic acid
A. thaliana	*Arabidopsis thaliana*
BG	β-1,3 glucanase
PD	Plasmodesmata
CalS	Callose synthase
CEBiP	CHITIN ELICTOR BINDING PROTEIN
DGB	Double gene block
ER	Endoplasmic reticulum
ETI	Effector-triggered immunity
FLS2	FLAGELLIN SENSING
HLB	Huanglongbing
IH	Invasive hyphae
ISE	INCREASED SIZE EXCLUSION LIMIT
LysM	Lysin motif
LYM2	LYSM-CONTAINING GPI-ANCHORED PROTEIN 2
LYK4	LysM-CONTAINING RECEPTOR-LIKE KINASE 4
MAMPs	Microbe-associated molecular patterns
MP	Movement protein
NLR	Nucleotide-binding leucine-rich repeat
PDBG	Plasmodesmal-lacalized β-1,3 glucanase
PDCB	PLASMODESMATA CALLOSE-BINDING PROTEIN
PDLP	PD-LOCALIZED PROTEIN
PM	Plasma membrane
PRRs	Pattern recognition receptors
PSTVd	Potato spindle tuber viroid
PTI	Pattern-triggered immunity
PVX	Potato virus X
SA	Salicylic acid
SAR	Systemic acquired resistance
SEL	Size exclusion limit
SYTA	Synaptotagmin A
TGB	Triple gene block
TMV	Tobacco mosaic virus

of key PD sites. Although PD confer benefits to both pathogenic infections and their host defense responses (**Tables 1**, **2**), we can try to impede the invasion of one or more pathogens by developing corresponding strategies capable of modifying the PD of the host accordingly. Due to the possible trade-off in functioning between the closure of PD and symplastic transmission of immune signals (Lim et al., 2016b), these strategies must feature quick and effective regulation of PD conductivity spatiotemporally. The prompt and timely induction of PD closure in hosts suffering pathogen attacks are thus speculated to block the trafficking of pathogens, effectors, and toxic molecules from the primary invaded cells into adjacent cells, as well as the needed nutrient import into invaded cells for pathogen growth (Lee et al., 2011; Zavaliev et al., 2011); this might weaken the necessity of systemic immune signal transport. Based on previous findings, we propose three promising hypothesized approaches to spatiotemporally induce callose overproduction and PD closure after pathogen invasion, which would be worth trying to improve plant resistance against enemies (**Figure 2**).

Inducible Callose Overproduction by *icals3m* System

Vatén et al. (2011) developed a system, named *icals3m*, which blocks PD-mediated trafficking by inducing the overproduction of callose surrounding PD in a cell-specific manner. The *icals3m* system has been widely applied to the studies of intercellular trafficking of proteins and small RNAs in biological processes. For example, the symplastic movements of the transcription factor SHORT-ROOT and microRNA165 between the stele and the endodermis were confirmed by the study in plants expressing *pCRE1::icals3m* and *p6xUAS::icals3m* (Vatén et al., 2011). The *cals3m* was also used to investigate cell-cell connectivity between pericycle cells, founder cells, and the neighboring tissues during lateral root formation and patterning in *Arabidopsis thaliana* (Benitez-Alfonso et al., 2013). In the shoot apical meristem, *cals3m* expression could lead to abnormal development and differentiation due to limited movement of WUSCHEL (Daum et al., 2014). Inducible blocking of symplastic signaling going in and out of endodermis by *cals3m* disrupts the coordinated growth and development of roots, which includes an increase of cell layers and the misspecification of stele cells (Wu et al., 2016).

The *icals3m* system provides a wonderful tool for spatially and temporally modulating the aperture of PD. The strategy is to introduce the *icals3m* under the control of pathogen infection-induced promoters into the hosts. Therefore, PD trafficking should get blocked, due to ectopic callose synthesis, once pathogens invade the host cells. The best situation would be that where the attacking pathogens are trapped in primary infected cells without any further spread. In such a case, the usual trafficking of immune signals might not be required even they are also affected. The following three important points likely merit consideration as prerequisites for this approach. First, the promoters must be induced only by pathogen invasion, so they remain inactive or active at very low levels under normal conditions. Otherwise, the callose produced by *cals3m* might interfere with the usual growth and development of host plants. Second, the promoters must respond to the pathogen invasion as soon as possible, preferably prior to the start of its spread into the second plant cell. Third, the induced activities of the promoters must be high enough to yield sufficient callose to constrict the PD. It is known that plant defense responses vary within the same host and among differing ones against different pathogens, so the screening, analysis, and testing for appropriate promoters are crucial steps.

Inducible Callose Overproduction Utilizing the PDLPs/PDCBs

PDLPs and PDCBs are well known for being positive regulators of callose production. Compared to wild-type plants, overexpression of *PDLP5* restricts the movement of the symplastic tracers CFDA and GFP and some MPs, and conversely the reduction of PDLP5 leads to increased intercellular trafficking (Lee et al., 2011). These findings indicate that changes in *PDLP5* expression were sufficient to regulate both basal PD permeability and MP movement. Similarly, overexpression of *PDLP1* decreased the efficiency of protein diffusion through PD (Thomas et al., 2008). Furthermore, the overexpression of both *PDLP1* and *PDLP5* enhanced plant resistance against pathogens revealing a positive relationship between the levels of PDLPs and plant resistance (Lee et al., 2011; Caillaud et al., 2014). The PDCBs are located at the outer neck region of PD, and greater expression of PDCB1 can lead to increased callose deposition and reduced cell-to-cell trafficking (Simpson et al., 2009). Therefore, we speculate that a timely increase in the expression of PDLPs or PDCBs, or both, could make same contribution to plant defense as *cals3m*. The same selective promoters mentioned above in *icals3m* system may be applied to drive the expression of *PDLPs* and *PDCBs* to increase the callose deposition at the initially infected cells during the onset of infection, thereby preventing pathogens from continuing to invade uninfected tissues. However, a study showed that PDLP5-overexpressing plants are still susceptibility to *turnip crinkle virus* (Lim et al., 2016a), probably due to the ability of virus to alter the aperture of PD (Singh et al., 2017). It is hoped that our approach will prove useful for helping to augment plant resistance to some pathogens to a certain extent. It cannot be expected to inhibit all possible pathogen infections facing host plants due to their different and unknown pathogenic mechanisms.

Gene Editing of Native Callose Synthases in Hosts

Vatén et al. (2011) identified three allelic semidominant *A. thaliana* mutants called *cals3-1d*, *-2d*, and *-3d*, which showed aberrant unloading patterns due to the blockage of PD. The *cals3-1d*, *cals3-2d*, and *cals3-3d* mutations lead to non-synonymous amino acid changes of R84K, R1926K, and P189L, respectively. By combining the two mutations of R84K and R1926K together, the enzymatic activity of encoded callose synthase (cals3m) is increased by 10 to 50% (Vatén et al., 2011). In brief, such mutations in *CALS3* can foster the increased production of callose and reduced aperture of PD that together impair cell-to-cell trafficking activity. This raises an intriguing hypothesis: the introduction of same-site mutations of *cals3m* into other native CalS genes that are quickly and dramatically induced by pathogen attacks, may function similarly as *cals3m*, precluding the introduction of an exogenous gene resource. CRISPR technology is a suitable choice for gene editing (Zaynab et al., 2020). For instance, it was reported that the expression levels of *CalS1* and *CalS12* were highly induced in response to biotic stresses (Dong et al., 2008; Cui and Lee, 2016). Through sequence alignments, we found that both 84R and 1926R of CalS3 are conserved in CalS1 and CalS12 (**Supplementary Figure 1**), suggesting the feasibility of generating *cals1m* and *cals12m* similarly. However, a pre-test for screening those modifications that do not interfere with the normal functioning of plants in the absence of pathogens is still necessary. When pathogens attack, these improved CalS proteins are then functioning at high efficiency.

FUTURE PERSPECTIVES

Over the last few decades, findings have increasingly emerged which are helpful for addressing how pathogens modify the PD structure and permeability to facilitate their intercellular movement and how plants manipulate PD to impede pathogenic infections. It is known that various PD-localized components are involved in the interactions between pathogens and plants, but many questions about mechanistic differences in how PD are regulated remain unanswered. For example, is there any conserved molecular mechanism conferring symplastic mobility to various pathogens? How do some pathogens or effectors overcome the blockage of PD by callose, and why do others fail to? How do plants manage themselves to gain control over the modification of PD when competing for this with pathogens during an infection? Previously, high-resolution electron microscopy and genetic approaches have greatly advanced our understanding of PD structure and function. Methodological improvements in the isolation and purification of PD may be helpful for identifying new PD components and examining their modifications that occur during interactions between pathogens and plants. PD regulation by pathogens and plants could provide us with a new perspective for the genetic improvement of plant disease resistance.

AUTHOR CONTRIBUTIONS

JL, LZ, and DY wrote the manuscript. DY and JL designed the figures. All authors contributed to the article and approved the submitted version.

FUNDING

This work was supported by the National Natural Science Foundation of China (32070192), the Program of Introducing Talents of Discipline to Universities (111 Project, D16014), and the Scientific Research Foundation for Advanced Talents of Henan University.

SUPPLEMENTARY MATERIAL

The Supplementary Material for this article can be found online at: https://www.frontiersin.org/articles/10.3389/fpls.2021.644870/full#supplementary-material

Supplementary Figure 1 | Sequence alignments of callose synthase proteins in *A. thaliana*. Protein sequences from AtCalS1 (NP_563743.2), AtCalS2 (Q9SL03.3), AtCalS3 (Q9LXT9.3), AtCalS4 (Q9LTG5.2), AtCalS5 (Q3B724.1), AtCalS6 (Q9LYS6.2), AtCalS7 (NP_172136.2), AtCalS8 (Q9LUD7.2), AtCalS9 (Q9SFU6.2), AtCalS10 (ACV04899.1), AtCalS11 (Q9S9U0.1), and AtCalS12 (Q9ZT82.1). The red boxes and asterisks denote those amino acids mutated in *cals3m* which are conserved in CalS1 and CalS12.

REFERENCES

Achor, D., Welker, S., Ben-Mahmoud, S., Wang, C., Folimonova, S. T., Dutt, M., et al. (2020). Dynamics of *candidatus* liberibacter asiaticus movement and sieve-pore plugging in citrus sink cells. *Plant Physiol*. 182, 882–891. doi: 10.1104/pp.19.01391

Adkar-Purushothama, C. R., Brosseau, C., Giguere, T., Sano, T., Moffett, P., and Perreault, J. P. (2015). Small RNA derived from the virulence modulating region of the potato spindle tuber viroid silences callose synthase genes of tomato plants. *Plant Cell* 27, 2178–2194. doi: 10.1105/tpc.15.00523

Alazem, M., and Lin, N. S. (2017). Antiviral roles of abscisic acid in plants. *Front. Plant Sci*. 8:1760. doi: 10.3389/fpls.2017.01760

Alzhanova, D. V., Hagiwara, Y., Peremyslov, V. V., and Dolja, V. V. (2000). Genetic analysis of the cell-to-cell movement of beet yellows closterovirus. *Virology* 268, 192–200. doi: 10.1006/viro.1999.0155

Amari, K., Boutant, E., Hofmann, C., Schmitt-Keichinger, C., Fernandez-Calvino, L., Didier, P., et al. (2010). A family of plasmodesmal proteins with receptor-like properties for plant viral movement proteins. *PLoS Pathog.* 6:e1001119. doi: 10.1371/journal.ppat.1001119

Amsbury, S., Kirk, P., and Benitez-Alfonso, Y. (2017). Emerging models on the regulation of intercellular transport by plasmodesmata-associated callose. *J. Exp. Bot*. 69, 105–115. doi: 10.1093/jxb/erx337

Asurmendi, S. R. H., Berg, J. C. K., and Beachy, R.N. (2004). Coat protein regulates formation of replication complexes during tobacco mosaic virus infection. *Proc. Natl. Acad. Sci. U.S.A*. 101, 1415–1420. doi: 10.1073/pnas.0307778101

Aung, K., Kim, P., Li, Z., Joe, A., Kvitko, B., Alfano, J. R., et al. (2020). Pathogenic bacteria target plant plasmodesmata to colonize and invade surrounding tissues. *Plant Cell* 32, 595–611. doi: 10.1105/tpc.19.00707

Avisar, D., Prokhnevsky, A. I., and Dolja, V. V. (2008). Class VIII myosins are required for plasmodesmatal localization of a closterovirus Hsp70 homolog. *J. Virol*. 82, 2836–2843. doi: 10.1128/JVI.02246-07

Benitez-Alfonso, Y., Faulkner, C., Pendle, A., Miyashima, S., Helariutta, Y., and Maule, A. (2013). Symplastic intercellular connectivity regulates lateral root patterning. *Dev. Cell* 26, 136–147. doi: 10.1016/j.devcel.2013.06.010

Benitez-Alfonso, Y., Faulkner, C., Ritzenthaler, C., and Maule, A. J. (2010). Plasmodesmata: gateways to local and systemic virus infection. *Mol. Plant Microbe Interact*. 23, 1403–1412. doi: 10.1094/MPMI-05-10-0116

Bhattacharyya, D., and Chakraborty, S. (2018). Chloroplast: the Trojan in plant-virus interaction. *Mol. Plant Pathol*. 19, 504–518. doi: 10.1111/mpp.12533

Bove, J. M. (2006). Huanglongbing: A destructive, newly-emerging, century-old disease of citrus. *J. Plant Pathol*. 88, 7–37. doi: 10.4454/jpp.v88i1.828

Brault, M. L., Petit, J. D., Immel, F., Nicolas, W. J., Glavier, M., Brocard, L., et al. (2019). Multiple C2 domains and transmembrane region proteins (MCTPs) tether membranes at plasmodesmata. *EMBO Rep*. 20:e47182. doi: 10.15252/embr.201847182

Brill, L. M., Nunn, R. S., Kahn, T. W., Yeager, M., and Beachy, R. N. (2000). Recombinant tobacco mosaic virus movement protein is an RNA-binding, α-helical membrane protein. *Proc. Natl. Acad. Sci. U.S.A*. 87, 7112–7117. doi: 10.1073/pnas.130187897

Brunkard, J. O., Runkel, A. M., and Zambryski, P. C. (2015). The cytosol must flow: intercellular transport through plasmodesmata. *Curr. Opin. Cell Biol*. 35, 13–20. doi: 10.1016/j.ceb.2015.03.003

Brunkard, J. O., and Zambryski, P. C. (2017). Plasmodesmata enable multicellularity: new insights into their evolution, biogenesis, and functions in development and immunity. *Curr. Opin. Plant Biol*. 35, 76–83. doi: 10.1016/j.pbi.2016.11.007

Bucher, G. L., Tarina, C., Heinlein, M., Serio, F. D., Fred Meins, J., and Iglesias, V. A. (2001). Local expression of enzymatically active class I β-1, 3-glucanase enhances symptoms of TMV infection in tobacco. *Plant J.* 28, 361–369. doi: 10.1046/j.1365-313X.2001.01181.x

Bücherl, C. A., Jarsch, I. K., Schudoma, C., Segonzac, C., Mbengue, M., Robatzek, S., et al. (2017). Plant immune and growth receptors share common signalling components but localise to distinct plasma membrane nanodomains. *Elife* 6:e25114. doi: 10.7554/eLife.25114.028

Burch-Smith, T. M., Stonebloom, S., Xu, M., and Zambryski, P. C. (2011). Plasmodesmata during development: re-examination of the importance of primary, secondary, and branched plasmodesmata structure versus function. *Protoplasma* 248, 61–74. doi: 10.1007/s00709-010-0252-3

Caillaud, M. C., Wirthmueller, L., Sklenar, J., Findlay, K., Piquerez, S. J., Jones, A. M., et al. (2014). The plasmodesmal protein PDLP1 localises to haustoria-associated membranes during downy mildew infection and regulates callose deposition. *PLoS Pathog.* 10:e1004496. doi: 10.1371/journal.ppat.1004496

Cao, L., Blekemolen, M. C., Tintor, N., Cornelissen, B. J. C., and Takken, F. L. W. (2018). The fusarium oxysporum avr2-six5 effector pair alters plasmodesmatal exclusion selectivity to facilitate cell-to-cell movement of avr2. *Mol. Plant* 11, 691–705. doi: 10.1016/j.molp.2018.02.011

Chen, M. H., Tian, G. W., Gafni, Y., and Citovsky, V. (2005) Effects of Calreticulin on Viral Cell-to-Cell Movement. *Plant Physiol*. 183, 1866–1876. doi: 10.1104/pp.105.064386

Chen, X. Y., and Kim, J. Y. (2009). Callose synthesis in higher plants. *Plant Signal Behav*. 4, 489–492. doi: 10.4161/psb.4.6.8359

Cheng, G., Dong, M., Xu, Q., Peng, L., Yang, Z., Wei, T., et al. (2017). Dissecting the molecular mechanism of the subcellular localization and cell-to-cell movement of the sugarcane mosaic virus P3N-PIPO. *Sci. Rep*. 7:9868. doi: 10.1038/s41598-017-10497-6

Cheval, C., and Faulkner, C. (2018). Plasmodesmal regulation during plant-pathogen interactions. *New Phytol*. 217, 62–67. doi: 10.1111/nph.14857

Cheval, C., Samwald, S., Johnston, M. G., De Keijzer, J., Breakspear, A., Liu, X., et al. (2020). Chitin perception in plasmodesmata characterizes submembrane immune-signaling specificity in plants. *Proc. Natl. Acad. Sci. U.S.A*. 117, 9621–9629. doi: 10.1073/pnas.1907799117

Chou, Y. L., Hung, Y. J., Tseng, Y. H., Hsu, H. T., Yang, J. Y., Wung, C. H., et al. (2013). The stable association of virion with the triple-gene-block protein 3-based complex of Bamboo mosaic virus. *PLoS Pathog.* 9:e1003405. doi: 10.1371/journal.ppat.1003405

Chowdhury, R. N., Lasky, D., Karki, H., Zhang, Z., Goyer, A., Halterman, D., et al. (2020). HCPro suppression of callose deposition contributes to strain-specific resistance against potato virus Y. *Phytopathology* 110, 164–173. doi: 10.1094/PHYTO-07-19-0229-FI

Conrath, U. (2006). Systemic acquired resistance. *Plant Signal Behav*. 1, 179–184. doi: 10.4161/psb.1.4.3221

Cui, H., Tsuda, K., and Parker, J. E. (2015). Effector-triggered immunity: from pathogen perception to robust defense. *Annu. Rev. Plant Biol.* 66, 487–511. doi: 10.1146/annurev-arplant-050213-040012

Cui, W., and Lee, J.-Y. (2016). *Arabidopsis* callose synthases CalS1/8 regulate plasmodesmal permeability during stress. *Nat. Plants* 2:16034. doi: 10.1038/nplants.2016.34

Daum, G., Medzihradszky, A., Suzaki, T., and Lohmann, J. U. (2014). A mechanistic framework for noncell autonomous stem cell induction in Arabidopsis. *Proc. Natl. Acad. Sci. U.S.A.* 111, 14619–14624. doi: 10.1073/pnas.1406446111

Ding, B., Kwon, M.-O., Hammond, R., and Owens, R. (1997). Cell-to-cell movement of potato spindle tuber viroid. *Plant J.* 12, 931–936. doi: 10.1046/j.1365-313X.1997.12040931.x

Djamei, A., Schipper, K., Rabe, F., Ghosh, A., Vincon, V., Kahnt, J., et al. (2011). Metabolic priming by a secreted fungal effector. *Nature* 478, 395–398. doi: 10.1038/nature10454

Dodds, P. N., and Rathjen, J. P. (2010). Plant immunity: towards an integrated view of plant-pathogen interactions. *Nat. Rev. Genet.* 11, 539–548. doi: 10.1038/nrg2812

Dolja, V. V. (2003). *Beet yellows virus*: the importance of being different. *Mol. Plant Pathol.* 4, 91–98. doi: 10.1046/j.1364-3703.2003.00154.x

Dolja, V. V., Haldeman-Cahill, R., Montgomery, A. E., Vandenbosch, K. A., and Carrington, J. C. (1995). Capsid protein determinants involved in cell-to-cell and long distance movement of tobacco etch potyvirus. *Virology* 206, 1007–1016. doi: 10.1006/viro.1995.1023

Dong, X., Hong, Z., Chatterjee, J., Kim, S., and Verma, D. P. S. (2008). Expression of callose synthase genes and its connection with *Npr1* signaling pathway during pathogen infection. *Planta* 229, 87–98. doi: 10.1007/s00425-008-0812-3

Ehlers, K., and Kollmann, R. (2001). Primary and secondary plasmodesmata: structure, origin, and functioning. *Protoplasma* 216, 1–30. doi: 10.1007/BF02680127

Epel, B. L. (1994). Plasmodesmata: composition, structure and trafficking. *Plant Mol. Biol.* 26, 1343–1356. doi: 10.1007/BF00016479

Epel, B. L. (2009). Plant viruses spread by diffusion on ER-associated movement-protein-rafts through plasmodesmata gated by viral induced host beta-1,3-glucanases. *Semin. Cell Dev. Biol.* 20, 1074–1081. doi: 10.1016/j.semcdb.2009.05.010

Faulkner, C., Petutschnig, E., Benitez-Alfonso, Y., Beck, M., Robatzek, S., Lipka, V., et al. (2013). LYM2-dependent chitin perception limits molecular flux via plasmodesmata. *Proc. Natl. Acad. Sci. U.S.A.* 110, 9166–9170. doi: 10.1073/pnas.1203458110

Fernandez-Calvino, L., Faulkner, C., Walshaw, J., Saalbach, G., Bayer, E., Benitez-Alfonso, Y., et al. (2011). Arabidopsis plasmodesmal proteome. *PLoS ONE* 6:e18880. doi: 10.1371/journal.pone.0018880

Flores, R., Hernández, C., Martínez de Alba, A. E., Daròs, J.-A., and Di Serio, F. (2005). Viroids and viroid-host interactions. *Annu. Rev. Phytopathol.* 43, 117–139. doi: 10.1146/annurev.phyto.43.040204.140243

Ganusova, E. E., and Burch-Smith, T. M. (2019). Review: Plant-pathogen interactions through the plasmodesma prism. *Plant Sci.* 279, 70–80. doi: 10.1016/j.plantsci.2018.05.017

Ganusova, E. E., Rice, J. H., Carlew, T., S., Patei, A., Perrodin-Njoku, E., et al. (2017). Altered expression of chloroplast protein affects the outcome of virus and nematode infection. *Mol. Plant Microbe In* 30, 478–488. doi: 10.1094/MPMI-02-17-0031-R

Genoves, A., Navarro, J. A., and Pallas, V. (2006). Functional analysis of the five melon necrotic spot virus genome-encoded proteins. *J. Gen. Virol.* 87, 2371–2380. doi: 10.1099/vir.0.81793-0

Germain, H., Joly, D. L., Mireault, C., Plourde, M. B., Letanneur, C., Stewart, D., et al. (2018). Infection assays in *Arabidopsis* reveal candidate effectors from the poplar rust fungus that promote susceptibility to bacteria and oomycete pathogens. *Mol. Plant Pathol.* 18, 191–200. doi: 10.1111/mpp.12514

Grangeon, R., Jiang, J., Wan, J., Agbeci, M., Zheng, H., and Lalibert,é, J. F. (2013). 6K2-induced vesicles can move cell to cell during turnip mosaic virus infection. *Front. Microbiol.* 4:351. doi: 10.3389/fmicb.2013.00351

Grant, S. R., Fisher, E. J., Chang, J. H., Mole, B. M., and Dangl, J. L. (2006). Subterfuge and manipulation: type III effector proteins of phytopathogenic bacteria. *Annu. Rev. Microbiol.* 60, 425–449. doi: 10.1146/annurev.micro.60.080805.142251

Grison, M. S., Kirk, P., Brault, M. L., Wu, X. N., Schulze, W. X., Benitez-Alfonso, Y., et al. (2019). Plasma membrane-associated receptor-like kinases relocalize to plasmodesmata in response to osmotic stress. *Plant Physiol.* 181, 142–160. doi: 10.1104/pp.19.00473

Guerra, T., Schilling, S., Hake, K., Gorzolka, K., Sylvester, F.-P., Conrads, B., et al. (2020). Calcium-dependent protein kinase 5 links calcium signaling with N-hydroxy-L-pipecolic acid- and SARD1-dependent immune memory in systemic acquired resistance. *N. Phytol.* 225, 310–325. doi: 10.1111/nph.16147

Hacker, D. L., Petty, I. T., Wei, N., and Morris, T. J. (1992). Turnipcrinkle virus genes required for RNA replication and virus movement. *Virology* 186, 1–8. doi: 10.1016/0042-6822(92)90055-T

Hake, K., and Romeis, T. (2019). Protein kinase-mediated signalling in priming: Immune signal initiation, propagation, and establishment of long-term pathogen resistance in plants. *Plant Cell Environ.* 42, 904–917. doi: 10.1111/pce.13429

Han, X., Kumar, D., Chen, H., Wu, S., and Kim, J. Y. (2014). Transcription factor-mediated cell-to-cell signalling in plants. *J. Exp. Bot.* 65, 1737–1749. doi: 10.1093/jxb/ert422

Haupt, S., Cowan, G. H., Ziegler, A., Roberts, A. G., Oparka, K. J., and Torrance, L. (2005). Two plant-viral movement proteins traffic in the endocytic recycling pathway. *Plant Cell* 17, 164–181. doi: 10.1105/tpc.104.027821

Heath, M. C., Valent, B., Howard, R. J., and Chumley, F. G. (1990). Interactions of two strains of *Magnaporthe grisea* with rice, goosegrass, and weeping lovegrass. *Can. J. Bot.* 68, 1627–1637. doi: 10.1139/b90-209

Heinlein, M., and Epel, B. L. (2004). Macromolecular transport and signaling through plasmodesmata. *Int. Rev. Cytol.* 235, 93–164. doi: 10.1016/S0074-7696(04)35003-5

Howard, A. R., Heppler, M. L., Ju, H. J., Krishnamurthy, K., Payton, M. E., and Verchot-Lubicz, J. (2004). Potato virus X TGBp1 induces plasmodesmata gating and moves between cells in several host species whereas CP moves only in *N. benthamiana* leaves. *Virology* 328, 185–197. doi: 10.1016/j.virol.2004.06.039

Howard, R. J., and Valent, B. (1996). Breaking and entering: host penetration by the fungal rice blast pathogen *Magnaporthe grisea*. *Annu. Rev. Microbiol.* 50, 491–512. doi: 10.1146/annurev.micro.50.1.491

Huang, D., Sun, Y., Ma, Z., Ke, M., Cui, Y., Chen, Z., et al. (2019). Salicylic acid-mediated plasmodesmal closure via remorin-dependent lipid organization. *Proc. Natl. Acad. Sci. U.S.A.* 1176, 21274–21284. doi: 10.1073/pnas.1911892116

Hull, R. (2014). "Plant to plant movement," in *Plant Virology*, fifth edition, ed. Hull, R (Boston, Academic Press), 669–751. doi: 10.1016/B978-0-12-384871-0.00012-1

Hunter, K., Kimura, S., Rokka, A., Tran, H. C., Toyota, M., Kukkonen, J. P., et al. (2019). CRK2 enhances salt tolerance by regulating callose deposition in connection with PLDα1. *Plant Physiol.* 180, 2004–2021. doi: 10.1104/pp.19.00560

Iglesias, V. A., and Meins, M. Jr. (2000). Movement of plant viruses is delayed in β-1,3-glucanase-deficient mutant showing a reduced plasmodesmatal sizeexclusion limit and enhanced callose deposition. *Plant J.* 21, 157–166. doi: 10.1046/j.1365-313x.2000.00658.x

Jia, L. J., Tang, H. Y., Wang, W. Q., Yuan, T. L., Wei, W. Q., Pang, B., et al. (2019). A linear nonribosomal octapeptide from Fusarium graminearum facilitates cell-to-cell invasion of wheat. *Nat. Commun.* 10:922. doi: 10.1038/s41467-019-08726-9

Jones, J. D. J., and Dangl, J. L. (2006). The plant immune system. *Nature* 444, 323–329. doi: 10.1038/nature05286

Kaku, H., Nishizawa, Y., Ishii-Minami, N., Akimoto-Tomiyama, C., Dohmae, N., Takio, K., et al. (2006). Plant cells recognize chitin fragments for defense signaling through a plasma membrane receptor. *Proc. Natl. Acad. Sci. U.S.A.* 103, 11086–11091. doi: 10.1073/pnas.0508882103

Kankanala, P., Czymmek, K., and Valent, B. (2007). Roles for rice membrane dynamics and plasmodesmata during biotrophic invasion by the blast fungus. *Plant Cell* 19, 706–724. doi: 10.1105/tpc.106.046300

Khang, C. H., Berruyer, R., Giraldo, M. C., Kankanala, P., Park, S.-Y., Czymmek, K., et al. (2010). Translocation of Magnaporthe oryzae effectors into rice cells and their subsequent cell-to-cell movement. *Plant Cell* 22, 1388–1403. doi: 10.1105/tpc.109.069666

Kitagawa, M., Tomoi, T., Fukushima, T., Sakata, Y., Sato, M., Toyooka, K., et al. (2019). Abscisic acid acts as a regulator of molecular trafficking through plasmodesmata in the moss *Physcomitrella patens*. *Plant Cell Physiol*. 60, 738–751. doi: 10.1093/pcp/pcy249

Klessig, D. F., Choi, H. W., and Dempsey, D. A. (2018). Systemic acquired resistance and salicylic acid: past, present, and future. *Mol. Plant Microbe Interact*. 31, 871–888. doi: 10.1094/MPMI-03-18-0067-CR

Kobayashi, K., Otegui, M. S., Krishnakumar, S., Mindrinos, M., and Zambryski, P. (2007). INCREASED SIZE EXCLUSION LIMIT2 Encodes a putative DEVH box RNA helicase involved in plasmodesmata function during Arabidopsis embryogenesis. *Plant Cell* 19, 1885–1897. doi: 10.1105/tpc.106.045666

Koh, E.-J., Zhou, L., Williams, D. S., Park, J., Ding, N., Duan, Y.-P., et al. (2012). Callose deposition in the phloem plasmodesmata and inhibition of phloem transport in citrus leaves infected with "*Candidatus Liberibacterasiaticus*". *Protoplasma* 249, 687–697. doi: 10.1007/s00709-011-0312-3

Laporte, C., Vetter, G., Loudes, A. M., Robinson, D. G., Hillmer, S., Stussi-Garaud, C., et al. (2003). Involvement of the secretory pathway and the cytoskeleton in intracellular targeting and tubule assembly of Grapevine fanleaf virus movement protein in tobacco BY-2 cells. *Plant Cell* 15, 2058–2075. doi: 10.1105/tpc.013896

Le Fevre, R., Evangelisti, E., Rey, T., and Schornack, S. (2015). Modulation of host cell biology by plant pathogenic microbes. *Annu. Rev. Cell Dev. Biol.* 31, 201–229. doi: 10.1146/annurev-cellbio-102314-112502

Lee, J. Y. (2014). New and old roles of plasmodesmata in immunity and parallels to tunneling nanotubes. *Plant Sci.* 221-222, 13–20. doi: 10.1016/j.plantsci.2014.01.006

Lee, J. Y., and Lu, H. (2011). Plasmodesmata: the battleground against intruders. *Trends Plant Sci.* 16, 201–210. doi: 10.1016/j.tplants.2011.01.004

Lee, J. Y., Wang, X., Cui, W., Sager, R., Modla, S., Czymmek, K., et al. (2011). A plasmodesmata-localized protein mediates crosstalk between cell-to-cell communication and innate immunity in *Arabidopsis*. *Plant Cell* 23, 3353–3373. doi: 10.1105/tpc.111.087742

Lent, J. V., Storms, M., van der Meer, F., Weilink, J., and Goldbach, R. (1991). Tubular structures involved in movement of cowpea mosaic virus are also formed in infected cowpea protoplasts. *J. General Virol.* 72, 2615–2623. doi: 10.1099/0022-1317-72-11-2615

Levy, A., Zheng, J. Y., and Lazarowitz, S. G. (2015). Synaptotagmin SYTA forms ER-plasma membrane junctions that are recruited to plasmodesmata for plant virus movement. *Curr. Biol.* 25, 2018–2025. doi: 10.1016/j.cub.2015.06.015

Lewis, J. D., and Lazarowitz, S. G. (2010). *Arabidopsis* synaptotagmin SYTA regulates endocytosis and virus movement protein cell-to-cell transport. *Proc. Natl. Acad. Sci. U.S.A.* 107, 2491–2496. doi: 10.1073/pnas.0909080107

Li, W., Zhao, Y., Liu, C., Yao, G., Wu, S., Hou, C., et al. (2012). Callose deposition at plasmodesmata is a critical factor in restricting the cell-to-cell movement of *Soybean mosaic* virus. *Plant ell Rep*. 31, 905–916. doi: 10.1007/s00299-011-1211-y

Li, W. Z., Qu, F., and Morris, T. J. (1998). Cell-to-cell movement of turnip crinkle virus is controlled by two small open reading frames that function in trans. *Virology* 244, 405–416. doi: 10.1006/viro.1998.9125

Li, Z., Variz, H., Chen, Y., Liu, S., and Aung., K. (2020). Plasmodesmata-dependent intercellular movement of bacterial effectors. *BioRxiv*. doi: 10.1101/2020.12.10.420240

Lim, G., Kachroo, A., and Kachroo, P. (2016a). Role of plasmodesmata and plasmodesmata localizing proteins in systemic immunity. *Plant Signal Behav*. 11:e1219829. doi: 10.1080/15592324.2016.1219829

Lim, G., Shine, M. B., de Lorenzo, L., Yu, K., Cui, W., Navarre, D., et al. (2016b). Plasmodesmata localizing proteins regulate transport and signaling during systemic acquired immunity in plants. *Cell Host Microbe* 19, 541–549. doi: 10.1016/j.chom.2016.03.006

Lim, H. S., Bragg, J. N., Ganesan, U., Lawrence, D. M., Yu, J., Isogai, M., et al. (2008). Triple gene block protein interactions involved in movement of *Barley stripe mosaic virus*. *J. Virol.* 82, 4991–5006. doi: 10.1128/JVI.02586-07

Liu, J. Z., Blancaflor, E. B., and Nelson, R. S. (2005). The tobacco mosaic virus 126-kilodalton protein, a constituent of the virus replication complex, alone or within the complex aligns with and traffics along microfilaments. *Plant Physiol.* 138, 1853–1865. doi: 10.1104/pp.105.065722

Liu, N., Zhang, T., Liu, Z., Chen, X., Guo, H., Ju, B., et al. (2020). Phytosphinganine affects plasmodesmata permeability via facilitating PDLP5-stimulated callose accumulation in Arabidopsis. *Mol. Plant* 13, 128–143. doi: 10.1016/j.molp.2019.10.013

Lucas, W. J. (2006). Plant viral movement proteins: agents for cell-to-cell trafficking of viral genomes. *Virology* 344, 169–184. doi: 10.1016/j.virol.2005.09.026

Lucas, W. J., Ham, B. K., and Kim, J. Y. (2009). Plasmodesmata-bridging the gap between neighboring plant cells. *Trends Cell Biol.* 19, 495–503. doi: 10.1016/j.tcb.2009.07.003

Lucas, W. J., and Lee, J. Y. (2004). Plasmodesmata as a supracellular control network in plants. *Nat. Rev. Mol. Cell Biol.* 5, 712–726. doi: 10.1038/nrm1470

Martinez-Turino, S., and Hernandez, C. (2011). A membrane-associated movement protein of Pelargonium flower break virus shows RNA-binding activity and contains a biologically relevant leucine zipper-like motif. *Virology* 413, 310–319. doi: 10.1016/j.virol.2011.03.001

Maule, A. J. (2008). Plasmodesmata: structure, function and biogenesis. *Curr. Opin. Plant Biol.* 11, 680–686. doi: 10.1016/j.pbi.2008.08.002

Miyashima, S., Roszak, P., Sevilem, I., Toyokura, K., Blob, B., Heo, J. O., et al. (2019). Mobile PEAR transcription factors integrate positional cues to prime cambial growth. *Nature* 565, 490–494. doi: 10.1038/s41586-018-0839-y

Morozov, S. Y., and Solovyev, A. G. (2003). Triple gene block: modular design of a multifunctional machine for plant virus movement. *J. Gen. Virol.* 84, 1351–1366. doi: 10.1099/vir.0.18922-0

Mosquera, G., Giraldo, M. C., Khang, C. H., Coughlan, S., and Valent, B. (2009). Interaction transcriptome analysis identifies *Magnaporthe oryzae* BAS1-4 as Biotrophy-associated secreted proteins in rice blast disease. *Plant Cell* 21, 1273–1290. doi: 10.1105/tpc.107.055228

Navarro, J. A., Sanchez-Navarro, J. A., and Pallas, V. (2019). Key checkpoints in the movement of plant viruses through the host. *Adv. Virus Res.* 104, 1–64. doi: 10.1016/bs.aivir.2019.05.001

Ngou, B. P. M., Ahn, H., Ding, P., and Jones, J. D. G. (2021). Mutual potentiation of plant immunity by cell-surface and intracellular receptors. *Nature.* 592, 110–115. doi: 10.1038/s41586-021-03315-7

Nicolas, W. J., Grison, M. S., Trépout, S., Gaston, A., Fouch,é, M., Cordelières, F. P., et al. (2017). Architecture and permeability of post-cytokinesis plasmodesmata lacking cytoplasmic sleeves. *Nat. Plants* 3:17082. doi: 10.1038/nplants.2017.82

Oparka, K. J., Roberts, A. G., Boevink, P., Cruz, S. S., Roberts, I., Pradel, K. S., et al. (1999). Simple, but not branched, plasmodesmata allow the nonspecific trafficking of proteins in developing tobacco leaves. *Cell* 97, 743–754. doi: 10.1016/S0092-8674(00)80786-2

Ormenese, S., Havelange, A., Deltour, R., and Bernier, G. (2000). The frequency of plasmodesmata increases early in the whole shoot apical meristem of *Sinapis alba* L. during foral transition. *Planta* 211, 370–375. doi: 10.1007/s004250000294

Peña, E. J., and Heinlein, M. (2012). RNA transport during TMV cell-to-cell movement. *Front. Plant Sci.* 3:193. doi: 10.3389/fpls.2012.00193

Peters, W. S., Jensen, K. H., Stone, H. A., and Knoblauch, M. (2021). Plasmodesmata and the problems with size: interpreting the confusion. *J. Plant Physiol.* 257:153341. doi: 10.1016/j.jplph.2020.153341

Pitzalis, N., and Heinlein, M. (2017). The roles of membranes and associated cytoskeleton in plant virus replication and cell-to-cell movement. *J. Exp. Bot.* 69, 117–132. doi: 10.1093/jxb/erx334

Pouwels, J., Van Der Velden, T., Willemse, J., Borst, J. W., Van Lent, J., Bisseling, T., et al. (2004). Studies on the origin and structure of tubules made by the movement protein of Cowpea mosaic virus. *J. Gen. Virol.* 85, 3787–3796. doi: 10.1099/vir.0.80497-0

Prokhnevsky, A. I., Peremyslov, V. V., and Dolja, V. V. (2005). Actin cytoskeleton is involved in targeting of a viral Hsp70 homolog to the cell periphery. *J. Virol.* 79, 14421–14428. doi: 10.1128/JVI.79.22.14421-14428.2005

Raffaele, S., Bayer, E., Lafarge, D., Cluzet, S., Retana, S. G., Boubekeur, T., et al. (2009). Remorin, a solanaceae protein resident in membrane rafts and plasmodesmata, impairs *potato virus X* movement. *Plant Cell* 21, 1541–1555. doi: 10.1105/tpc.108.064279

Ramirez-Prado, J. S., Abulfaraj, A. A., Rayapuram, N., Benhamed, M., and Hirt, H. (2018). Plant immunity: from signalings to epigenetic control of defense. *Trends Plant Sci.* 23, 833–844. doi: 10.1016/j.tplants.2018.06.004

Ranf, S. (2017). Sensing of molecular patterns through cell surface immune receptors. *Curr. Opin. Plant Biol.* 38, 68–77. doi: 10.1016/j.pbi.2017.04.011

Reagan, B. C., Ganusova, E. E., Fernandez, J. C., Mccray, T. N., and Burch-Smith, T. M. (2018). RNA on the move: the plasmodesmata perspective. *Plant Sci.* 275, 1–10. doi: 10.1016/j.plantsci.2018.07.001

Reuveni, M., Debbi, A., Kutsher, Y., Gelbart, D., Zemach, H., Belausov, E., et al. (2015). *Tomato yellow leaf curl virus* effects on chloroplast biogenesis and cellular structure. *Physiol. Mol. Plant Pathol.* 92, 51–58. doi: 10.1016/j.pmpp.2015.08.001

Ritzenthaler, C., and Hofmann, C. (2007). "Tubule-guided movement of plant viruses," in *Viral Transport in Plants*. Berlin: Springer Berlin Heidelberg 63–83. doi: 10.1007/7089_2006_105

Roberts, A. G., and Oparka, K. J. (2003). Plasmodesmata and the control of symplastic transport. *Plant Cell Environment* 26, 103–124. doi: 10.1046/j.1365-3040.2003.00950.x

Sager, R., and Lee, J.-Y. (2014). Plasmodesmata in integrated cell signalling insights from development and environmental signals and stresses. *J. Exp. Bot.* 65, 6337–6358. doi: 10.1093/jxb/eru365

Saijo, Y., Loo, E. P., and Yasuda, S. (2018). Pattern recognition receptors and signaling in plant-microbe interactions. *Plant J.* 93, 592–613. doi: 10.1111/tpj.13808

Sakulkoo, W., Osés-Ruiz, M., Garcia, E. O., Soanes, D. M., Littlejohn, G. R., Hacker, C., et al. (2018). A single fungal MAP kinase controls plant cell-to-cell invasion by the rice blast fungus. *Science* 359, 1399–1403. doi: 10.1126/science.aaq0892

Schubert, M., Koteyeva, N. K., Zdyb, A., Santos, P., Voitsekhovskaja, O. V., Demchenko, K. N., et al. (2013). Lignification of cell walls of infected cells in Casuarina glauca nodules that depend on symplastic sugar supply is accompanied by reduction of plasmodesmata number and narrowing of plasmodesmata. *Physiol. Plant* 147, 524–540. doi: 10.1111/j.1399-3054.2012.01685.x

Shemyakina, E. A., Erokhina, T. N., Gorshkova, E. N., Schiemann, J., Solovyev, A. G., and Morozov, S. Y. (2011). Formation of protein complexes containing plant virus movement protein TGBp3 is necessary for its intracellular trafficking. *Biochimie* 93, 742–748. doi: 10.1016/j.biochi.2011.01.002

Shimizu, T., Nakano, T., Takamizawa, D., Desaki, Y., Ishii-Minami, N., Nishizawa, Y., et al. (2010). Two LysM receptor molecules, CEBiP and OsCERK1, cooperatively regulate chitin elicitor signaling in rice. *Plant J.* 64, 204–214. doi: 10.1111/j.1365-313X.2010.04324.x

Simpson, C., Thomas, C., Findlay, K., Bayer, E., and Maule, A. J. (2009). An Arabidopsis GPI-anchor plasmodesmal neck protein with callose binding activity and potential to regulate cell-to-cell trafficking. *Plant Cell* 21, 581–594. doi: 10.1105/tpc.108.060145

Singh, A., Lim, G.-H., and Kachroo, P. (2017). Transport of chemical signals in systemic acquired resistance. *J. Integr. Plant Biol.* 59, 336–344. doi: 10.1111/jipb.12537

Stahl, Y., Grabowski, S., Bleckmann, A., Kuhnemuth, R., Weidtkamp-Peters, S., Pinto, K. G., et al. (2013). Moderation of Arabidopsis root stemness by CLAVATA1 and ARABIDOPSIS CRINKLY4 receptor kinase complexes. *Curr. Biol.* 23, 362–371. doi: 10.1016/j.cub.2013.01.045

Su, S., Liu, Z., Chen, C., Zhang, Y., Wang, X., Zhu, L., et al. (2010). *Cucumber mosaic virus* movement protein severs actin filaments to increase the plasmodesmal size exclusion limit in tobacco. *Plant Cell* 22, 1373–1387. doi: 10.1105/tpc.108.064212

Takeda, R., and Ding, B. (2009). Viroid intercellular trafficking: RNA motifs, cellular factors and broad impacts. *Viruses* 1, 210–221. doi: 10.3390/v1020210

Tamai, A., and Meshi, T. (2001). Cell-to-cell movement of potato virus X: the role of p12 and p8 encoded by the second and third open reading frames of the triple gene block. *Mol. Plant-Microbe Interact.* 14, 1158–1167. doi: 10.1094/MPMI.2001.14.10.1158

Thomas, C. L., Bayer, E. M., Ritzenthaler, C., Fernandez-Calvino, L., and Maule, A. J. (2008). Specific targeting of a plasmodesmal protein affecting cell-to-cell communication. *PLoS Biol.* 6:e7. doi: 10.1371/journal.pbio.0060007

Thomas, C. L., and Maule, A. J. (1995). Identification of structural domains within the cauliflower mosaic virus movement protein by scanning deletion mutagenesis and epitope tagging. *Plant Cell* 7, 561–572. doi: 10.1105/tpc.7.5.561

Tilsner, J., Linnik, O., Louveaux, M., Roberts, I. M., Chapman, S. N., and Oparka, K. J. (2013). Replication and trafficking of a plant virus are coupled at the entrances of plasmodesmata. *J. Cell Biol.* 201, 981–995. doi: 10.1083/jcb.201304003

Tilsner, J., Nicolas, W., Rosado, A., and Bayer, E. M. (2016). Staying tight: plasmodesmal membrane contact sites and the control of cell-to-cell connectivity in plants. *Annu. Rev. Plant Biol.* 67, 337–364. doi: 10.1146/annurev-arplant-043015-111840

Tomczynska, I., Stumpe, M., Doan, T. G., and Mauch, F. (2020). A Phytophthora effector protein promotes symplastic cell-to-cell trafficking by physical interaction with plasmodesmata-localised callose synthases. *New Phytol.* 227, 1467–1478. doi: 10.1111/nph.16653

Toruno, T. Y., Stergiopoulos, I., and Coaker, G. (2016). Plant-pathogen effectors: cellular probes interfering with plant defenses in spatial and temporal manners. *Annu. Rev. Phytopathol.* 54, 419–441. doi: 10.1146/annurev-phyto-080615-100204

Uchiyama, A., Shimada-Beltran, H., Levy, A., Zheng, J. Y., Javia, P. A., and Lazarowitz, S. G. (2014). The Arabidopsis synaptotagmin SYTA regulates the cell-to-cell movement of diverse plant viruses. *Front. Plant Sci.* 5:584. doi: 10.3389/fpls.2014.00584

Vatén, A., Dettmer, J., Wu, S., Stierhof, Y. D., Miyashima, S., Yadav, S. R., et al. (2011). Callose biosynthesis regulates symplastic trafficking during root development. *Dev. Cell* 21, 1144–1155. doi: 10.1016/j.devcel.2011.10.006

Vilar, M., Sauri, A., Monne, M., Marcos, J. F., von Heijne, G., Perez-Paya, E., et al. (2002). Insertion and topology of a plant viral movement protein in the endoplasmic reticulum membrane. *J. Biol. Chem.* 277, 23447–23452. doi: 10.1074/jbc.M202935200

Waigmann, E., Lucas, W. J., Citovsky, V., and Zambryski, P. (1994). Direct functional assay for tobacco mosaic virus cell-to-cell movement protein and identification of a domain involved in increasing plasmodesmal permeability. *Proc. Nati. Acad. Sci. U.S.A.* 91, 1433–1437. doi: 10.1073/pnas.91.4.1433

Waigmann, E., Ueki, S., Trutnyeva, K., and Citovsky, V. (2004). The ins and outs of nondestructive cell-to-cell and systemic movement of plant Viruses. *Critical Rev. Plant Sci.* 23, 195–250. doi: 10.1080/07352680490452807

Wang, X., Sager, R., Cui, W., Zhang, C., Lu, H., and Lee, J.-Y. (2013). Salicylic acid regulates plasmodesmata closure during innate immune responses in *Arabidopsis*. *Plant Cell* 25, 2315–2329. doi: 10.1105/tpc.113.110676

Wendehenne, D., Gao, Q., Kachroo, A., and Kachroo, P. (2014). Free radical-mediated systemic immunity in plants. *Curr. Opin. Plant Biol.* 20 127–134. doi: 10.1016/j.pbi.2014.05.012

Wolf, H., Deom, C. M., Beachy, R. N., and Lucas, W. J. (1989). Movement protein of tobacco mosaic virus modifies plasmodesmatal size exclusion limit. *Science* 246, 377–379. doi: 10.1126/science.246.4928.377

Wright, K. M., Wood, N. T., Roberts, A. G., Chapman, S., Boevink, P., Mackenzie, K. M., et al. (2007). Targeting of TMV movement protein to plasmodesmata requires the actin/ER network: evidence from FRAP. *Traffic* 8, 21–31. doi: 10.1111/j.1600-0854.2006.00510.x

Wu, S., O'lexy, R., Xu, M., Sang, Y., Chen, X., Yu, Q., et al. (2016). Symplastic signaling instructs cell division, cell expansion, and cell polarity in the ground tissue of Arabidopsis thaliana roots. *Proc. Natl. Acad. Sci. U.S.A.* 113, 11621–11626. doi: 10.1073/pnas.1610358113

Wu, S.-W., Kumar, R., Iswanto, A. B. B., and Kim, J.-Y. (2018). Callose balancing at plasmodesmata. *J. Exp. Bot.* 69, 5325–5339. doi: 10.1093/jxb/ery317

Xie, L., Shang, W., Liu, C., Zhang, Q., Sunter, G., Hong, J., et al. (2016). Mutual association of broad bean wilt virus 2 VP37-derived tubules and plasmodesmata obtained from cytological observation. *Sci. Rep.* 6:21552. doi: 10.1038/srep21552

Yan, D., and Liu, Y. (2020). Diverse regulation of plasmodesmal architecture facilitates adaptation to phloem translocation. *J. Exp. Bot.* 71, 2505–2512. doi: 10.1093/jxb/erz567

Yan, D., Yadav, S. R., Paterlini, A., Nicolas, W. J., Petit, J. D., Brocard, L., et al. (2019). Sphingolipid biosynthesis modulates plasmodesmal ultrastructure and phloem unloading. *Nat. Plants* 5, 604–615. doi: 10.1038/41477-019-0429-5

Yang, X., Lu, Y., Wang, F., Chen, Y., Tian, Y., Jiang, L., et al. (2020). Involvement of the chloroplast gene ferredoxin 1 in multiple responses of

Nicotiana benthamiana to *Potato virus X* infection. *J. Exp. Bot*. 71, 2142–2156. doi: 10.1093/jxb/erz565

Yuan, C., Lazarowitz, S. G., and Citovsky, V. (2016). Identification of a functional plasmodesmal localization signal in a plant viral cell-to-cell-movement protein. *mBio* 7, e02052–e02015. doi: 10.1128/mBio.02052-15

Yuan, M., Jiang, Z., Bi, G., Nomura, K., Liu, M., Wang, Y., et al. (2021). Pattern-recognition receptors are required for NLR-mediated plant immunity. *Nature*. 592, 105–109. doi: 10.1038/s41586-021-03316-6

Zambryski, P. (2008). Plasmodesmata. *Curr. Biol*. 18, R324–325. doi: 10.1016/j.cub.2008.01.046

Zambryski, P., and Crawford, K. (2000). PLASMODESMATA: Gatekeepers for cell-to-cell transport of developmental signals in plants. *Annu. Rev. Cell Dev. Biol*. 16, 393–421. doi: 10.1146/annurev.cellbio.16.1.393

Zamyatnin, A. A. Jr., Solovyev, A. G., Savenkov, E. I., Germundsson, A., Sandgren, M., et al. (2004). Transient coexpression of individual genes encoded by the triple gene block of potato mop-top virus reveals requirements for TGBp1 trafficking. *Mol. Plant Microbe Interact*. 17, 921–930. doi: 10.1094/MPMI.2004.17.8.921

Zavaliev, R., Levy, A., Gera, A., and Epel, B. L. (2013). Subcellular dynamics and role of Arabidopsis beta-1,3-glucanases in cell-to-cell movement of tobamoviruses. *Mol. Plant Microbe Interact*. 26, 1016–1030. doi: 10.1094/MPMI-03-13-0062-R

Zavaliev, R., Ueki, S., Epel, B. L., and Citovsky, V. (2011). Biology of callose (beta-1,3-glucan) turnover at plasmodesmata. *Protoplasma* 248, 117–130. doi: 10.1007/s00709-010-0247-0

Zaynab, M., Sharif, Y., Fatima, M., Afzal, M. Z., Aslam, M. M., Raza, M. F., et al. (2020). CRISPR/Cas9 to generate plant immunity against pathogen. *Microb. Pathog*. 141:103996. doi: 10.1016/j.micpath.2020.103996

Zhao, J., Zhang, X., Hong, Y., and Liu, Y. (2016). Chloroplast in plant-virus interaction. *Front. Microbiol*. 7:1566. doi: 10.3389/fmicb.2016.01565

Zhong, X., Archual, A. J., Amin, A. A., and Ding, B. (2008). A genomic map of viroid RNA motifs critical for replication and systemic trafficking. *Plant Cell* 20, 35–47. doi: 10.1105/tpc.107.056606

Conflict of Interest: The authors declare that the research was conducted in the absence of any commercial or financial relationships that could be construed as a potential conflict of interest.

frontiers in Plant Science

ORIGINAL RESEARCH
published: 21 July 2021
doi: 10.3389/fpls.2021.674031

Lipid Body Dynamics in Shoot Meristems: Production, Enlargement, and Putative Organellar Interactions and Plasmodesmal Targeting

*Manikandan Veerabagu[1], Päivi L. H. Rinne[1], Morten Skaugen[2], Laju K. Paul[1] and Christiaan van der Schoot[1]**

[1] Faculty of Biosciences, Department of Plant Sciences, Norwegian University of Life Sciences, Ås, Norway, [2] Faculty of Chemistry, Biotechnology, and Food Science, Norwegian University of Life Sciences, Ås, Norway

Post-embryonic cells contain minute lipid bodies (LBs) that are transient, mobile, engage in organellar interactions, and target plasmodesmata (PD). While LBs can deliver γ-clade 1,3-β-glucanases to PD, the nature of other cargo is elusive. To gain insight into the poorly understood role of LBs in meristems, we investigated their dynamics by microscopy, gene expression analyzes, and proteomics. In developing buds, meristems accumulated LBs, upregulated several LB-specific *OLEOSIN* genes and produced OLEOSINs. During bud maturation, the major gene *OLE6* was strongly downregulated, OLEOSINs disappeared from bud extracts, whereas lipid biosynthesis genes were upregulated, and LBs were enlarged. Proteomic analyses of the LB fraction of dormant buds confirmed that OLEOSINs were no longer present. Instead, we identified the LB-associated proteins CALEOSIN (CLO1), Oil Body Lipase 1 (OBL1), Lipid Droplet Interacting Protein (LDIP), Lipid Droplet Associated Protein1a/b (LDAP1a/b) and LDAP3a/b, and crucial components of the OLEOSIN-deubiquitinating and degradation machinery, such as PUX10 and CDC48A. All mRFP-tagged LDAPs localized to LBs when transiently expressed in *Nicotiana benthamiana*. Together with gene expression analyzes, this suggests that during bud maturation, OLEOSINs were replaced by LDIP/LDAPs at enlarging LBs. The LB fraction contained the meristem-related actin7 (ACT7), "myosin XI tail-binding" RAB GTPase C2A, an LB/PD-associated γ-clade 1,3-β-glucanase, and various organelle- and/or PD-localized proteins. The results are congruent with a model in which LBs, motorized by myosin XI-k/1/2, traffic on F-actin, transiently interact with other organelles, and deliver a diverse cargo to PD.

Keywords: LB/LD proteome, oleosin, LDIP, LDAP, Caleosin, ACT7, Myosin XI-binding Rab C2A, plasmodesmata

OPEN ACCESS

Edited by:
Jung-Youn Lee,
University of Delaware, United States

Reviewed by:
Motoki Tominaga,
Waseda University, Japan
Vivien Rolland,
Commonwealth Scientific and Industrial Research Organisation (CSIRO), Australia

***Correspondence:**
Christiaan van der Schoot
chris.vanderschoot@nmbu.no

Specialty section:
This article was submitted to Plant Cell Biology, a section of the journal Frontiers in Plant Science

Received: *28 February 2021*
Accepted: *14 June 2021*
Published: *21 July 2021*

Citation:
Veerabagu M, Rinne PLH, Skaugen M, Paul LK and van der Schoot C (2021) Lipid Body Dynamics in Shoot Meristems: Production, Enlargement, and Putative Organellar Interactions and Plasmodesmal Targeting. Front. Plant Sci. 12:674031. doi: 10.3389/fpls.2021.674031

INTRODUCTION

Plasmodesmata (PD) are notoriously difficult to investigate, and understanding PD functioning from the composition is fraught with difficulties. Both composition and architecture of PD are subject to regulation by cells that share them. Rather than functioning autonomously, they are subject to control by cells that construct, maintain, and operate them. Consequently, PD composition and function are context-dependent, differing between tissues in dependence on developmental and metabolic cellular states. Filtering out commonalities while recognizing the unique aspects of PD at specific locations and conditions, therefore, remains a challenge.

Information on PD composition and function has been gathered using a variety of plant and tissue systems and approaches. Frequently, investigations are focused on PD (ultra)structure and/or localization of suspected PD proteins by immunochemistry or transgenic expression of fluorescently tagged proteins, microinjection studies, and proteomic and lipidomic studies (reviewed in Faulkner and Maule, 2011; Sager and Lee, 2014; Heinlein, 2015a; Brault et al., 2019; Han et al., 2019; Reagan and Burch-Smith, 2020).

Despite the importance of determining PD composition and architecture, the question remains unanswered of how relevant PD components are delivered to PD and integrated into the functional fabric of the PD channel. The cellular mechanisms that deliver structural PD components also modulate gating events. While the exterior and interior of PD are targeted by distinct mechanisms, PD conductance is also subject to control by physiological processes on both sides of the channels. For example, nuclear-organellar signaling contributes to ROS-mediated plasmodesmal regulation, involving mitochondria and chloroplasts as sensors for cellular homeostasis (Burch-Smith and Zambryski, 2011).

Regarding supply routes, the most frequently studied route is the Brefeldin-sensitive excretion pathway, which delivers proteins to the cell wall (Sager and Lee, 2014; Han et al., 2019; Reagan and Burch-Smith, 2020). Cargos delivered *via* this pathway may include integral membrane proteins and GPI-anchored proteins. The latter can attach to exoplasmic membrane rafts, which move them laterally to the exterior of the PD (Mongrand et al., 2010). With regard to the PD interior, important leads emerged from studies that analyzed how viruses take advantage of existing cellular mechanisms, such as the cortical endoplasmic reticulum (ER) and the cytoskeleton, and how they interact with molecular complexes that control PD gating (reviewed in e.g., Heinlein, 2015b; Reagan and Burch-Smith, 2020). Little explored is the mechanism by which cytoplasmically produced lipid bodies (LBs) target PD to deliver a largely unknown cargo to the channel (Rinne et al., 2011; Veerabagu et al., 2020).

In seeds, LB production requires OLEOSINs (Huang, 1992; Tzen and Huang, 1992; Abell et al., 2002). OLEOSIN proteins are small 15–26 kD proteins that are co-translationally inserted into the bilayer of the ER, guided by an ER-resident signal recognition particle (Abell et al., 2004). The 5–6 nm long hydrophobic hairpin of OLEOSIN is embedded under strain in the bilayer, which facilitates its diffusion into the stable hydrophobic environment of a nascent LB, promoting its eventual release into the cytosol (Abell et al., 2002; Huang and Huang, 2017; Huang, 2018). This budding process is facilitated by a critical imbalance in leaflet surface tensions and involves SEIPIN proteins and interacting lipid biosynthesis genes (Cai et al., 2015; Barbosa and Siniossoglou, 2017). Once formed, OLEOSIN secures the integrity and small size of the LBs by stabilizing the monolayer and preventing coalescence and fusion (Siloto et al., 2006; Shimada et al., 2008; Hsiao and Tzen, 2011). In addition, CALEOSIN and STEROLEOSIN can bind competitively with an expanding monolayer, mediated by short ca. 2 nm hydrophobic hairpins (Huang, 2018).

Like seeds, bud meristems contain LBs, and eight of the nine *Populus OLEOSIN* genes are expressed in apices (Veerabagu et al., 2020). The capacity of LBs to deliver cargos to PD could be important in the shoot apical meristem (SAM), where PD are continuously produced within and between cell lineages (van der Schoot and Rinne, 1999). In the active SAM, individual cells are continuously displaced toward the periphery to be integrated into differentiating tissues. To secure the functional integrity of the SAM, all cells need to continuously update their relative position by exchanging signals, among others, through existing and newly formed PD (Rinne and van der Schoot, 1998). LBs potentially contribute to PD formation, maintenance, and cell-cell signaling by shuttling lipids, enzymes, and signaling molecules to the PD entrance (van der Schoot et al., 2011; Paul et al., 2014a). An LB shuttle function was demonstrated in *N. benthamiana*, where LBs delivered eGFP-tagged 1,3-β-glucanases to PD, identified by TMV MP-mRFP (Rinne et al., 2011). Similarly, transgenic Arabidopsis LBs, tagged with PtOLE6-eGFP, targeted primary and secondary PD in various cell types (Veerabagu et al., 2020). The LBs do not arrive at the PD by bulk cytoplasmic streaming but by processive trafficking on F-actin, mediated by myosin XI-k/1/2 (Veerabagu et al., 2020).

The PD in the SAM of woody perennials are unique in the sense that they are modified during the seasonal cycle. Under short days, the PD are shut down by Dormancy Sphincter Complexes (DSCs). DSCs act as circuit breakers that interrupt the symplasmic circuitry of the SAM, preventing electrical and metabolic coupling and exchange of transcription factors and other regulatory molecules, arresting the SAM in a dormant state (Paul et al., 2014a,b). Unlike classical sphincters where callose is present extracellularly, DSCs contain additional internal deposits that can be targeted by LBs (Rinne et al., 2001; Rinne and van der Schoot, 2003). When recruited to the PD, the LB-associated enzyme 1,3-β-glucanase aligns with its substrate, resulting in callose hydrolysis, restoration of the PD channel, and dormancy release (Rinne et al., 2001; Rinne and van der Schoot, 2003). It is unknown what other cargos LBs can deliver to PD during dormancy release, and to what degree it differs from what is present in active meristems. A consensus view is that cytoplasmic LB motility enriches LB cargos by facilitating organellar interactions and exchange of proteins and lipids (Bartz et al., 2007; Hodges and Wu, 2010; Murphy, 2012; Krahmer et al., 2013; Gao and Goodman, 2015; Zhi et al., 2017). Proteins might also be recruited directly from the cytoplasm, especially when molecular crowding at the monolayer is reduced. These include monolayer-embedded proteins, lipophilic signals, lipid-anchored proteins, electrostatically associated proteins, and molecules that opportunistically hitch a ride on moving LBs (reviewed in van der Schoot et al., 2011; Paul et al., 2014a; Huang, 2018).

As in buds, accumulated LBs constitute a unique proactive dormancy-release and signaling mechanism, LBs may be expected to store proteins related to these functions. LB cargos are likely to include proteins that assist docking at the plasma membrane (PM), possibly proteins that become integrated into the fabric of PD, and non-cell-autonomous signals (van der Schoot et al., 2011; Paul et al., 2014a,b). How the actomyosin system that guides LBs to PD (Veerabagu et al., 2020) connects

to the PD is unknown. Notably, F-actin and myosin VIII have been localized at PD (White et al., 1994; Baluska et al., 2001; Golomb et al., 2008; White and Barton, 2011). In addition, the actin-binding and nucleation complex Arp2/3 was localized at PD (Van Gestel et al., 2003; Deeks and Hussey, 2005; Fiserova et al., 2006), and recently it has been shown that the class I formin FH2 acts as an actin nucleation factor that caps and stabilizes F-actin at PD (Diao et al., 2018). Some plant viruses that move through PD have usurped and hijacked the cytoplasmic actomyosin system to facilitate their cell-to-cell transport (Amari et al., 2011, 2014; Sager and Lee, 2014; Heinlein, 2015b). Although actin can facilitate delivery of viral complexes to the PD entrance, PD-associated actin might restrict the size of the PD channel as virus passage requires severing of this actin (Ding et al., 1996; Su et al., 2010).

While it is unknown how the F-actin on which LBs traffic is anchored to the PD, it is also unknown what enables LBs to dock at PD. Given the difference between LB and PD diameters in dormant meristems, respectively, ca. 1 μm and 60–220 nm (channel and external ring; Rinne and van der Schoot, 2004), it might involve proteins that interact with PD orifices or their immediate surroundings at the PM. Targeting of eGFP-tagged LBs to the PD/PM area yields deflated LBs that appear as juxtaposed fluorescent patches, sandwiching primary and secondary PD (Rinne et al., 2011; Veerabagu et al., 2020). We hypothesized earlier that LBs could dock at remorin-decorated membrane rafts that act as sorting devices (van der Schoot et al., 2011; Paul et al., 2014a) and involve hemifusion between the LB monolayer and the cytoplasmic leaflet of the PM. If so, this might be mediated by SNARE protein complexes, which can localize to LBs (Boström et al., 2007; Sollner, 2007; Murphy et al., 2009; Paul et al., 2014a).

The relation of LBs with PD is virtually unexplored. To gauge how LBs might contribute to cellular homeostasis, organellar interaction, and cargo delivery to PD, we investigated their accumulation and putative composition by microscopy, gene expression analyzes, and proteomics. An important goal was to create an inventory of candidate proteins, such as known LB proteins and proteins that may hitch a ride to the PD. The results indicate that OLEOSIN is responsible for LB accumulation but that at a later stage it is removed and replaced by LDIP/LDAP proteins to allow recruitment of cytoplasmic proteins through reduced molecular crowding at the monolayer. Removal and degradation of OLEOSIN probably involve the action of PUX10, the segregase CDC48A, and the 26S proteasome, all of which were present in the LB fraction. Other identified proteins included CLO1, OBL1, GPAT8, a PD/LB-localized 1,3-β-glucanase, and proteins that likely reflect LB motility, organellar interactions, storage, and docking to PD/PM sites. Confirming LB/PD localization and the role of individual proteins in PD functioning will require future investigations. The current data lay the groundwork for such investigations and expand a model (Veerabagu et al., 2020) in which cargo-enriched LBs are anchored by GTPase RAB-C2A to myosin XI-k/1/2 for actin-guided transport to PD.

RESULTS

LBs in Apices and Developing Buds

Lipid bodies have been detected in meristems previously but their accumulation patterns have not been characterized. In this study, LB production, size, and number were analyzed from transmission electron microscope (TEM) sections of meristems of growing plants (APs), developing terminal buds (DEBs), and dormant terminal buds (DOBs) (**Figures 1A–C**). In all three, LBs were present in the SAM and the subjacent rib meristem/rib zone (RM/RZ) area but their numbers were low in actively growing apices, especially in the RM/RZ area (**Figure 1D**). The low number in this area reflects the high rate of metabolism and cell division related to stem elongation. During bud development, apical stem elongation ceases and LB numbers in the RM/RZ area and the SAM increased significantly, while further increase during dormancy development was minor (**Figure 1D**). Based on LB numbers detected in TEM sections, we approximated their total number for an average cell volume in both the SAM and RM/RZ. The calculation accounted for section thickness (80 nm), LB diameter, and the volume of the nucleus and organelles (**Figure 1E**, **Supplementary Figure 1**). These data showed that all cells contained multiple LBs, even the RM/RZ of actively growing long-day plants. In developing buds, the number of LBs in SAM cells had increased by ca. 25%, while in the RM/RZ it had increased by ca. 50%, corresponding to the cessation of cell division (**Figure 1D**), but beyond that, the increase in number was minor, and only in the SAM by ca. 10%. The increase in LB sizes showed a similar trend. In growing apices, LBs were small (**Figures 1A,E**), but their size had significantly increased in developing buds, both in the SAM and the RM/RZ (**Figures 1B,E**). During dormancy establishment, LB size only increased further in the RM/RZ (**Figures 1C,E**).

OLEOSIN Expression and LB Enlargement

Previously, we showed that very early under dormancy-inducing conditions three of the eight expressed *OLEOSINs* were upregulated (Veerabagu et al., 2020). In this study, we analyzed their expression in growing apices, in developing buds during the LB accumulation phase (**Figure 1D**), and in buds that were developing dormancy (**Figure 2A**). *OLE6* appeared to be the most important of the three *OLEOSINs*, both quantitatively and in its responsiveness to bud development. It was strongly upregulated during the LB accumulation phase and almost completely downregulated during dormancy development. In contrast, the minor genes *OLE3* and *OLE5* were only slightly upregulated during LB production and somewhat downregulated during dormancy development (**Figure 2A**).

To investigate if LB enlargement (**Figures 1C,E**) could be due to increased TAG biosynthesis, which is mediated by DGAT1 (Shockey et al., 2006), we identified two *DGAT1* homologs, *DGAT1a* and *DGAT1b*, in the *Populus trichocarpa* genome (**Supplementary Figure 2**) and analyzed their expression during the same developmental stages. Both *DGAT1a* and *DGAT1b*, but especially *DGAT1a*, were upregulated during bud development and further during dormancy establishment (**Figure 2B**). This suggests that TAG biosynthesis may have increased concomitant

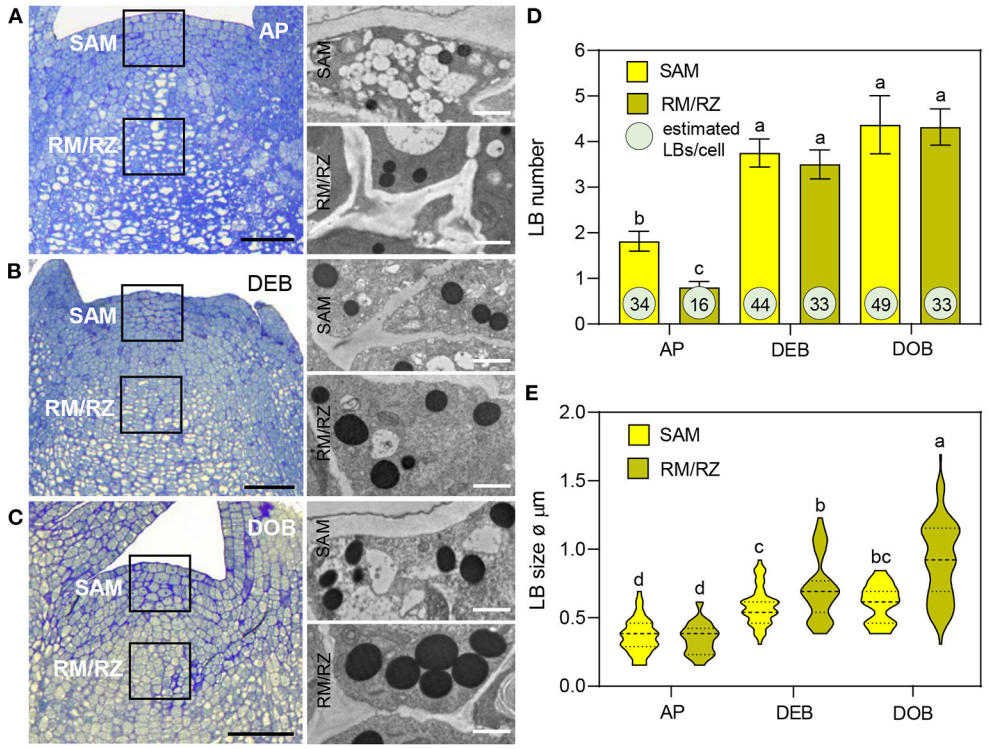

FIGURE 1 | Lipid body (LB) production in the shoot apex of *Populus*. **(A–C)** show apices of **(A)** actively growing plants in long days (APs), **(B)** in short day-induced developing buds (DEBs) and **(C)** dormant buds (DOBs). TEM images **(A–C)** show LBs in the shoot apical meristem (SAM) and the rib meristem/rib zone (RM/RZ) (boxed meristem areas). **(D)** LB numbers were counted and **(E)** LB diameters were measured in successive TEM images. Bar diagram **(D)** shows means ± SD of LB numbers per cell per section. The encircled numbers are calculated LB numbers per cell volume based on average cell sizes, as explained in **Supplementary Figure 1**. **(E)** Violin plots show diameters of LBs including mean-line and quartiles. Different letters indicate statistically significant differences between treatments (one-way ANOVA, Fisher's *post-hoc* analysis $P < 0.05$). Bars are 50 (apices) and 1 µm (LBs).

with LB enlargement (**Figure 1E**). As the expression of lipases might counteract LB enlargement through TAG-hydrolysis, we also analyzed transcript levels of the lipase gene *SUGAR DEPENDENT 1* (*SDP1*) and the mitochondrial gene *SDP6*, which is required for post-germinative seedling growth in *Arabidopsis* (Quettier and Eastmond, 2009). Two isoforms of both *SDP1* and *SDP6* were identified in the *P. trichocarpa* genome (**Supplementary Figure 3**). *SDP1a* and *SDP1b* were upregulated during bud development, whereas *SDP1b* was further upregulated during dormancy establishment. The *SDP6a* expression did not show any change, and *SDP6b* was only slightly upregulated during dormancy establishment (**Figure 2C**). Considering that LBs enlarged, the encoded enzymes might not have targeted the LBs, like in seeds where *SPD1* transcript levels do not correlate with enzyme activity (Eastmond, 2006).

LB-Associated Proteins in Dormant Buds

To identify integral LB proteins (referred to as class I) as well as proteins with amphipathic stretches (class II) and peripherally and transiently associated proteins (Bersuker and Olzmann, 2017; Pyc et al., 2017), we isolated and purified LBs from dormant buds using a protocol modified after Jolivet et al. (2004). Purified LBs were subjected to light and differential interference contrast (DIC) microscopy to confirm the absence of cellular fragments. Total fatty acid methyl ester (FAME) contents were quantified to verify the enrichment of fats in the final LB fraction (**Supplementary Figure 4**). LBs stained with the neutral lipid stain Nile red were further inspected under a confocal laser scanning microscope (CLSM) (Veerabagu et al., 2020). When visible contaminations were completely absent and all LBs were uniform and isodiametric in size, samples were prepared for protein precipitation, and extracted proteins were processed, trypsin-digested, and analyzed by liquid chromatography with tandem mass spectrometry (LC-MS/MS) as described in experimental procedures. MS/MS samples were analyzed using Mascot to search the *P. trichocarpa* database, whereas Scaffold was used to validate MS/MS-based peptide and protein identifications. We analyzed three independent pooled samples, obtained from different sets of plants that were grown at different times, representing biological replicates. To prevent loss of peripherally and transiently associated proteins that might be delivered to PD, such as, for example, the LB- and PD-localized γ-clade 1,3-β-glucanases, we deliberately omitted the commonly used salt step in the final wash of all three samples. However, the third sample received an extra wash, which diminished the number of identified proteins in the LB fraction. All proteins were identified with >99% probability, containing at least two

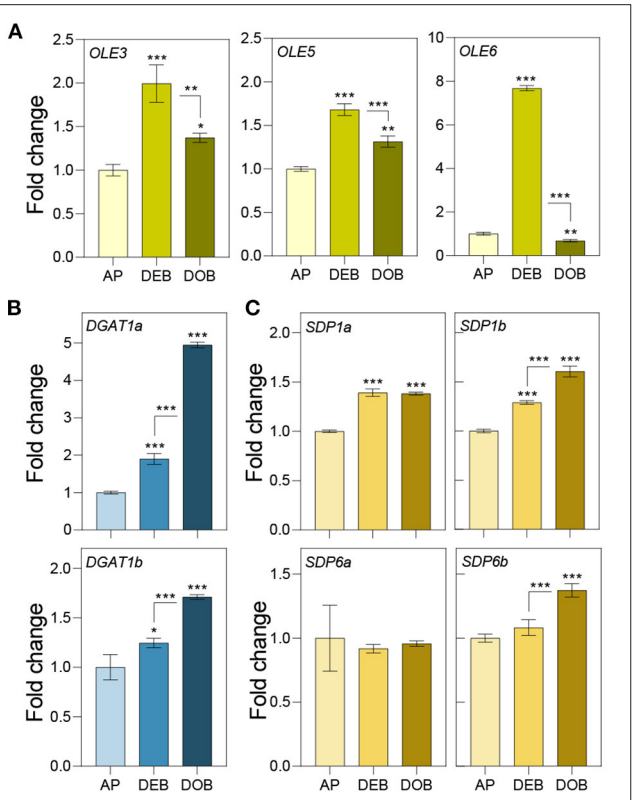

FIGURE 2 | Expression of genes involved in lipid body production and lipid turnover. Relative expression of **(A)** *OLEOSIN* genes *(OLE3*, *OLE5*, and *OLE6)*, **(B)** lipid biosynthesis genes (*DGAT1a,b*), and **(C)** lipase genes (*SDP1a* and b, and *SDP6a* and *b*) in apices under long day (APs), and in developing buds (DEBs), and dormant buds (DOBs) in short days. Values are calculated relative to the control (AP) and represent the means of three technical replicates ± SD of four plants. Asterisk(s) indicate statistical significance between treatments (one-way ANOVA, Tukey analysis; $^{*}P < 0.05$; $^{**}P < 0.01$; and $^{***}P < 0.001$).

unique peptides but often much more. In total, we identified 719 proteins in the LB fraction, of which many were still likely contaminants. To restrict the number of putative candidate proteins, we made a selection based on the previously reported presence of identified proteins at LBs or in LB fractions of plant and non-plant systems, localization at PD, or presence in PD-enriched fractions (**Table 1**).

A striking initial finding was that OLEOSIN proteins were not detected in the LB fraction of dormant buds while eight *OLEOSIN* genes were expressed in developing buds (**Supplementary Table 1**). This was unexpected as we anticipated that OLEOSINs would have remained on the LBs like in desiccated dormant seeds, where they stabilize the monolayer until germination commences (Siloto et al., 2006; Deruyffelaere et al., 2015; Shimada et al., 2018). As OLEOSINs were not detected, they were likely removed from LBs, possibly involving the ubiquitin-mediated 26S degradation system, which removes ubiquitinated OLEOSINs during *Arabidopsis* germination (Deruyffelaere et al., 2015, 2018; Kretzschmar et al., 2018).

To investigate the OLEOSIN disappearance further, we first validated that *Populus* OLEOSINs can be degraded by the ubiquitin-proteasome pathway. For this, we used PtOLE6, as *OLE6* was highly expressed during the LB production phase (**Figure 2A**). Prediction of PtOLE6 ubiquitination sites with Bayesian Discriminant Algorithm Method (BDM-PUB; http://bdmpub.biocuckoo.org/index.php) showed the presence of at least six putative ubiquitination motifs (**Supplementary Figure 5A**). In *Arabidopsis*, OLE1-4 displayed one major and one or two minor ubiquitination sites (Deruyffelaere et al., 2015), and their alignment with PtOLE6 shows that the predicted K130 aligns with the major ubiquitination sites of AtOLE3-K159 and AtOLE4-K144 (**Supplementary Figure 5B**). We next investigated the involvement of the ubiquitin-proteasome-mediated degradation of PtOLE6 by overexpressing *PtOLE6-eGFP* in *Arabidopsis*. While PtOLE6-eGFP was degraded in the controls and the seedlings treated with the vacuolar cysteine protease inhibitor E64d (Deruyffelaere et al., 2015), seedlings treated with the proteasome inhibitor MG132 did not show degradation even after 72 h of imbibition (**Figure 3A**). Additionally, the MG132 treatment increased cytosolic accumulation of PtOLE6-eGFP (**Figure 3B**) in cytosolic aggregates, like in the case of AtOLE1 (Deruyffelaere et al., 2015).

Furthermore, we identified key components of the ubiquitin-mediated 26S degradation system in the LB fraction, such as *Populus* homologs of the *Arabidopsis* "plant UBX-domain-containing protein 10" (PUX10) and the segregase Cell Division Control Protein 48A (CDC48A) (**Table 1**) (Deruyffelaere et al., 2018; Kretzschmar et al., 2018). The bud LB fraction also contained the ubiquitin-activating enzyme UBA1, involved in conjugating ubiquitins to proteins, and several deubiquitinating proteases that prepare the unfolded proteins for degradation by the 20S core protease (Verma et al., 2002) (**Table 1**, **Supplementary Table 1**). In addition, the LB fraction contained multiple subunits of the 26S proteasome, such as the crucial 19S ATPase subunit RPT2A, which is important in meristem development (Lee et al., 2011), and 26S scaffolding components (**Supplementary Table 1**). Although these components are ubiquitous, they are likely to be involved in removing proteins from the LBs, namely, OLEOSINs, as they do so in germinating *Arabidopsis* seeds (Deruyffelaere et al., 2018).

The question remained how LBs retained their structural integrity during their enlargement (**Figure 1**) while OLEOSINs were absent from the LB fraction (**Supplementary Table 1**). A possible contributor to stability is the LB protein CALEOSIN1 (CLO1), which was the only CLO identified in the LB proteome (**Table 1**). However, we identified several other proteins that localize to LBs, such as the recently discovered class II protein Lipid Droplet Interacting Protein (LDIP) (Pyc et al., 2017; Coulon et al., 2020) and the Lipid Droplet Associated Proteins (LDAPs), both of which can contribute to LB stability (Gidda et al., 2016).

Expression of *PUX10*, *CDC48A*, *LDIP*, and *LDAPs*

To assess the possibility that OLEOSINs were replaced by LDAPs/LDIP, we identified by phylogenetic analyses two *P.*

TABLE 1 | Proteins in the LB fraction, identical or similar to described putative LB/PD proteins.

Protein name	*P. trichocarpa* Accession nr	BlastP of *A. thaliana*	Mw kDa	Unique peptides Bio1	Bio2	Bio3
Localized to plant LBs						
LDAP Interacting Protein (LDIP)[1,3,8,27,h]	Potri.004G082300	AT5G16550	24	3	3	4
LD-Associated Protein 3 (LDAP3a)[2,4,5,6,8]	Potri.005G025700	AT3G05500	27	11	11	4
LD-Associated Protein 3 (LDAP3b)[4,5,6,8]	Potri.013G017300	AT3G05500	27	8	10	5
LD-Associated Protein 1 (LDAP1a)[3,5,6,8,27,28]	Potri.003G173100	AT1G67360	25	9	9	8
LD-Associated Protein 1 (LDAP1b)[3,5,6,8,27,28]	Potri.001G055300	AT1G67360	25	7	9	8
Oil body lipase 1 (OBL1a)[8,28,29]	Potri.001G161500	AT3G14360	65	5	8	11
Oil body lipase 1 (OBL1b)[8,28,29]	Potri.003G073800	AT3G14360	63	5	5	6
Caleosin (CLO1)[8]	Potri.010G066600	AT4G26740	27	4	4	2
Plant UBX-domain protein 10 (PUX10)[7,8]	Potri.003G145200	AT4G10790	52	12	13	8
Cell division control protein 48A (CDC48A)[7,8,28]	Potri.012G088200	AT5G03340	90	56	62	7
Beta-1,3-endoglucanase (GH17-44)[9]	Potri.T167100	AT4G16260	35	3	3	4
GPAT8 (redundant with GPAT4)[31,32]	Potri.014G085500	AT4G00400	56	3	8	5
26S Proteasome						
Regulatory particle AAA-ATPase 2A (RPT2A)	Potri.014G194700	AT4G29040	50	18	15	3
26S proteasome, regulatory subunit RPN7	Potri.015G090900	AT4G24820	45	8	8	2
Ubiquitin conjugating enzyme 13A (UBC13A)	Potri.011G111400	AT1G78870	18	4	5	2
Ubiquitin-activating enzyme E1 1 (UBA1)	Potri.009G075700	AT2G30110	121	27	23	6
RAB GTPases—Myosin XI tail binding						
Rab GTPase C2A (RAB-C2A/RAB18)[11,14–16,18,23–26]	Potri.006G121400	AT5G03530	23	4	5	2
Rab GTPase D1 (RAB-D1)	Potri.003G004000	AT3G11730	23	8	7	4
Actin/Microtubule						
Actin 7 (ACT7)[27,b]	Potri.019G010400	AT5G09810	42	23	23	16
V-ATPase B Subunit 2 (VAB2; stabilizes F-actin)	Potri.009G137800	AT4G38510	54	25	24	21
Actin Depolymerizing Factor 4 (ADF4)	Potri.009G028200	AT5G59890	16	6	4	3
PD/PM localized/PD enriched fraction						
Purple acid phosphatase (PAP1)[b,h]	Potri.010G158400	AT1G13750	69	3	3	2
Calreticulin 1A (CRT1 /CRT1A)[b,h]	Potri.005G015100	AT1G56340	48	13	10	4
Calreticulin 1B (CRT2 / CRT1B)[b]	Potri.013G009500	AT1G09210	47	17	13	5
Calnexin 1 (CNX1)[23,24,25,28,a,b]	Potri.012G111100	AT5G61790	61	29	28	14
Zerzaust (ZET), atypical β-1,3 glucanase[b,h]	Potri.019G032900	AT1G64760	53	4	4	2
O-Glycosyl hydrolases family 17 protein[b,h]	Potri.006G080600	AT5G58090	53	5	6	2
O-Glycosyl hydrolases family 17 protein[b,h]	Potri.018G150400	AT5G58090	52	9	8	3
β-1,3-glucanase 1 (BG1) (GH17_37/at PM)	Potri.016G057400	AT3G57270	37	4	5	3
Dehydrin (HIRD11)[c]	Potri.013G062200	AT1G54410	24	11	8	4
Early Responsive to Dehydration 4 (ERD4)[h]	Potri.001G358300	AT1G30360	82	9	5	5
Reticulon like protein B3 (RTN3)[18,b,f,g]	Potri.001G097700	AT1G64090	28	6	7	7
Reticulon like protein B1 (RTN1)[18,b]	Potri.015G027300	AT4G23630	30	3	2	3
Leucine-rich repeat (LRR) family protein[b]	Potri.001G017500	AT3G20820	40	12	13	7
Probable inactive receptor kinase[h]	Potri.018G074300	AT2G26730	71	9	3	2
Reversibly glycosylated polypeptide 3 (RGP3)[h]	Potri.010G156700	AT3G08900	41	36	32	11
Pectinacetylesterase 11 (PAE11/at PD)[TAIR]	Potri.004G233900	AT5G45280	43	14	16	5
Plasma membrane intrinsic protein 1 (PIP1)[h]	Potri.003G128600	AT4G00430	31	6	4	2
Plasma membrane intrinsic protein 3 (PIP3)[b]	Potri.009G136600	AT4G35100	30	4	3	2
Clathrin Heavy Chain 1 (CHC1)[14,18]	Potri.009G073300	AT3G11130	193	55	63	38
SKU5 similar 1 (SKS1)[b,h]	Potri.015G127200	AT4G25240	54	3	2	2
Plant LB fractions						
SecY transport family protein/LB-targeting[28]	Potri.011G107900	AT2G34250	52	8	5	5
Annexin 1 (ANN1)[28,b]	Potri.002G095600	AT1G35720	36	23	22	16

(Continued)

TABLE 1 | Continued

Protein name	*P. trichocarpa* Accession nr	BlastP of *A. thaliana*	Mw kDa	Unique peptides Bio1	Bio2	Bio3
Annexin 2 (ANN2)[20,28]	Potri.005G075900	AT5G65020	36	25	23	9
Early responsive to dehydration 7 (ERD7)[a,28]	Potri.004G174100	AT2G17840	48	12	9	11
Late embryogenesis abundant (LEA26)[28,b]	Potri.007G146300	AT2G44060	35	14	15	11
Late embryogenesis abundant protein (LEA27)[28]	Potri.002G165000	AT2G46140	16	6	4	4
Cytochrome P450 (CYP81K1)[28]	Potri.017G028100	AT5G10610	59	5	8	5
Cytochrome P450 (CYP94B1)[28]	Potri.005G220900	AT5G63450	58	7	6	6
Cytochrome P450 (CYP704A2)[28]	Potri.014G072300	AT2G45510	58	23	19	5
Cytochrome b5 isoform B (CB5-B)[18,28]	Potri.001G314200	AT2G32720	15	5	5	2
Cytochrome b5 isoform E (CB5-E)[18,28]	Potri.012G024600	AT5G53560	15	8	7	3
Alcohol dehydrogenase 1 (ADH1)[14,28]	Potri.002G072100	AT1G77120	41	17	23	15
Alcohol dehydrogenase 2 (ADH2)[14,28]	Potri.014G193800	AT5G43940	23	5	4	3
Alcohol dehydrogenase 2 (ADH2)[14,28]	Potri.002G254900	AT5G43940	41	8	7	3
Sterol methyltransferase 2 (SMT2/CVP1)[8,b]	Potri.002G016300	AT1G20330	41	12	12	2
Embryo-specific protein 3 (ATS3)[8,h]	Potri.015G132700	AT5G62200	21	4	4	3
Tethers/SNARES/Membrane trafficking						
Synaptotagmin 2 (SYTB; SYT2)	Potri.005G241700	AT1G20080	61	7	5	4
Syntaxin of plants 71 (SYP71) (T-SNARE)[b,h]	Potri.016G088200	AT3G09740	30	5	4	2
Secretion 22 (SEC22) (T-SNARE)[25]	Potri.001G165600	AT1G11890	25	8	3	3
ADP-ribosylation factor A1B (ARF1)[14,21]	Potri.002G191400	AT5G14670	21	10	9	9
Small GTP-binding protein (ARA-3/RAB8a)[26,b,h]	Potri.008G051700	AT3G46060	24	10	8	7
Golgi localized small GTPase (RAB-6A)[b]	Potri.003G086700	AT2G44610	23	5	6	4
Suppressor of Variegation 11 (SVR11/RABE1B)[b]	Potri.001G110200	AT4G20360	53	9	12	7
Lipid transfer protein (PR-14)PM[TAIR]	Potri.016G135800	AT5G01870	12	3	2	2
Secretion-associated RAS 1/2 (SAR2/SAR1)[22,30]	Potri.010G141900	AT4G02080	22	20	24	15
COPII vesicle component (Sec24-like)[13]	Potri.005G049100	AT4G32640	111	4	2	2
COPII vesicle component (SAR2)[13]	Potri.010G141900	AT4G02080	22	20	24	15
Coatomer subunit delta (δ-COP/COPI)[13,18,28,b]	Potri.012G125500	AT5G05010	58	14	15	4
Coatomer, alpha subunit-1 (COPI)[13,18,28,b]	Potri.015G069700	AT1G62020	137	48	36	9
Coatomer subunit beta-1 (COPI)[13,18,28,b]	Potri.006G273300	AT4G31480	106	25	19	4
Coatomer subunit gamma (COPI)[13,18,28,b]	Potri.004G153500	AT4G34450	99	30	41	6
Guanine Exchange Protein 5 (GEF)	Potri.006G216900	AT3G43300	198	17	17	3
Protein transport protein SEC31B[28]	Potri.009G055400	AT3G63460	123	17	17	4
Rab1 GTPase subfamily (RAB-1B)	Potri.001G080400	AT1G02130	23	13	14	7
RAB GTPase homolog A1F (RAB-A1F)	Potri.001G374000	AT5G60860	24	21	22	9
RAB GTPase homolog A2A (RAB-A2A)[28]	Potri.003G004100	AT1G09630	24	15	14	10
RAB GTPase homolog A2B (RAB-A2B)	Potri.006G000300	AT1G07410	24	10	8	6
Rab-like GTPase (ARA6/RAB5)[20,23,25]	Potri.010G226300	AT3G54840	22	7	6	2
RAB GTPase homolog G3D (RAB-G3D/RAB7)[10,12]	Potri.003G053400	AT1G52280	23	17	13	2
Organellar						
Mitochondrial Rho GTPase 1 (MIRO1)[b]	Potri.013G023100	AT5G27540	72	26	24	6
Prohibitin 3 (PHB3)-mitochondrial[25,28,b]	Potri.001G335700	AT5G40770	31	17	14	13
Prohibitin 6 (PHB6)-mitochondrial[25,h]	Potri.017G017400	AT2G20530	32	16	16	17
V-type proton ATPase subunit a3 (VHA-a3)[b]	Potri.009G121400	AT4G39080	93	11	7	2
V-ATPase C subunit (DET3)[b]	Potri.017G061100	AT1G12840	43	19	21	7
Vacuolar membrane ATPase 10 (AVMA10)[b]	Potri.008G040300	AT3G01390	12	4	4	2
Vacuolar ATP synthase subunit A (VHA-A)[b]	Potri.010G253500	AT1G78900	69	42	38	24
Vacuolar H+-ATPase subunit E1 (VHAE1)[b]	Potri.013G051500	AT4G11150	26	10	8	7
Heat Shock Proteins/chaperones						
Endoplasmin homolog (Hsp90-7)[24,b]	Potri.005G241100	AT4G24190	94	33	29	18
DNAJ heat shock family protein (ERDJ3B)[14]	Potri.014G122600	AT3G62600	40	5	3	2

(Continued)

TABLE 1 | Continued

Protein name	*P. trichocarpa* Accession nr	BlastP of *A. thaliana*	Mw kDa	Unique peptides Bio1	Bio2	Bio3
Hsp 70 family protein (BIP2)[b]	Potri.001G087500	AT5G42020	74	37	30	19
Hsp; Endoplasmin homolog (Hsp90-6)[b]	Potri.014G164900	AT3G07770	90	18	18	2
Hsp; Endoplasmin homolog (Hsp90-4)[28]	Potri.006G002800	AT5G56000	80	69	61	28
HSP70-10, Heat shock 70 kDa protein 10[23]	Potri.001G285500	AT5G09590	73	27	25	4
cpn60 (TCP-1), CCT8 [STM, KN1 PD-trafficking][d,e]	Potri.019G034200	AT3G03960	59	29	24	4
cpn60 chaperonin (TCP-1)[b]	Potri.008G182300	AT1G24510	59	23	12	5
cpn60 chaperonin (TCP-1)[b]	Potri.009G157400	AT3G11830	60	26	20	7
BAG protein 7 (BAG7) (Bcl-2)[28,b]	Potri.015G126800	AT5G62390	46	3	5	3
Phospolipases-lipases-lipid metabolism						
Phospholipase C (PLC2)[b]	Potri.010G188800	AT3G08510	67	6	6	2
Phospholipase D delta (PLDδ)[b]	Potri.005G105600	AT4G35790	99	2	2	3
Lipase/GDSL-motif esterase (acyltransferase)[b]	Potri.001G342600	AT5G14450	43	9	10	5
Plat domain protein (PLAT2) (lipase)[8]	Potri.005G076900	AT2G22170	19	4	5	5
Sugar dependent 6 (SDP6)	Potri.010G226700	AT3G10370	69	17	14	2
GDSL-motif esterase (GDSL1) (lipase)[b]	Potri.019G008000	AT1G29670	40	6	4	9
GDSL-like Lipase[b]	Potri.018G089300	AT5G45670	28	10	10	6
Lipoxygenase 2, chloroplastic (LOX2)[c]	Potri.001G015500	AT3G45140	103	6	6	4
Dolichyl-diphosphooligosacch. (HAP6/Rpn2)[28]	Potri.005G226100	AT4G21150	75	10	6	10
Dolichyl-diphosphooligosacch. (HAP6/Rpn2)[28]	Potri.002G036600	AT4G21150	75	12	8	13
Glucose 6-phosph. (GPT1) phosphate transl.1[28]	Potri.011G135900	AT5G54800	43	5	3	2
Oxidative stress, antioxidant, histones						
Thioredoxin-dependent peroxidase 1 (TPX1)[h]	Potri.001G423500	AT1G65980	17	9	7	8
Catalase 2 (CAT2)[14,b]	Potri.002G009800	AT4G35090	57	17	14	9
Manganese superoxide dismutase (MSD1)	Potri.013G092600	AT3G10920	25	5	6	4
Peroxidase (PRX36)[b]	Potri.005G195600	AT1G71695	39	15	13	7
Peroxidase (PRX37)[b]	Potri.005G195700	AT1G71695	39	11	9	7
Histone H3 (HTR8, H3.3)[19]	Potri.002G026800	AT5G10980	15	3	2	3
Histone H2A (HTA9, H2A)[19]	Potri.006G249300	AT1G52740	14	3	3	3
Histone H4 (HTA4)[19]	Potri.005G115300	AT5G59970	11	7	5	5

*(1) at LBs or in LB fractions: [1]Pyc et al. (2017); [2]Gidda et al. (2016); [3]Coulon et al. (2020); [4]Horn et al. (2013); [5]Kim et al. (2016); [6]this paper, (**Figure 7**); [7]Deruyffelaere et al. (2018); [8]Kretzschmar et al. (2018); [9]Rinne et al. (2011);[10]Schroeder et al. (2015); [11]Ozeki et al. (2005); [12]Lizaso et al. (2013); [13]Soni et al. (2009); [14]Bartz et al. (2007); [15]Li et al. (2012); [16]Martin et al. (2005); [17]Hodges and Wu (2010); [18]Beller et al. (2008); [19]Cermelli et al. (2006); [20]Fujimoto et al. (2004); [21]Nakamura et al. (2005); [22]Turro et al. (2006); [23]Brasaemle et al. (2004); [24]Umlauf et al. (2004); [25]Liu et al. (2004); [26]Sato et al. (2006); [27]Brocard et al. (2017), [28]Zhi et al. (2017); [29]Müller and Ischbeck (2018); [30]Binns et al. (2006); [31]Fernández-Santaso et al. (2020), [32]Wilfling et al. (2013), (2) at PD or in PD enriched fraction: [a]Liu et al. (2017); [b]Fernandez-Calvino et al. (2011) (blue); [c]Karlson et al. (2003); [d]Xu et al. (2011); [e]Kitagawa and Jackson (2017); [f]Knox et al. (2015); [g]Kriechbaumer et al. (2015); [h]Leijon et al. (2018) (red).*

trichocarpa homologs of PUX10 and CDC48A, six LDAP (LDAP1a, LDAP1b, LDPA2a, LDPA2b, LDAP3a, and LDAP3b), and one LDIP homolog (**Supplementary Figures 6–9**), and studied their expression in apices during bud development and dormancy establishment. Of the two *PUX10* isoforms, *PUX10b* was upregulated during bud development and further during dormancy development (**Figure 4A**). Like in the case of *PUX10a*, the expression of one of the *CDC48A* isoforms, *CDC48A2*, was unaltered while *CDC48A1* was upregulated (**Figure 4B**). The proteins encoded by the upregulated *PUX10b* and *CDC48A1* genes remained present in the LB fraction of dormant buds (**Table 1**), suggesting they might also remove other ubiquitinated LB proteins. The expression patterns of the six *LDAP* genes were not identical, but all were upregulated during dormancy development, relative to expression levels in apices (**Figures 5A–C**). Notably, the major *LDAP1b*, which was upregulated during bud development, and excessively high (160-fold) during dormancy development, was little expressed in apices (**Figures 5A,C**). Also, the genes *LDAP1a* and *LDAP3b* were upregulated during bud development, while *LDAP3a* was not (**Figure 5C**). *LDAP2a* and *LDAP2b* were only slightly upregulated during bud development (**Figure 5B**). At this point, *OLE6* was still very highly expressed (**Figure 2A**). The timeline shows that during dormancy development, when *OLE6* was downregulated below the expression level in apices, all the five *LDAP* genes were strongly upregulated, especially *LDAP1b* (**Figure 5A**). In contrast, the upregulation of *LDIP* (ca. 5-fold; **Figure 5D**) was comparable to that of the other *LDAP*s.

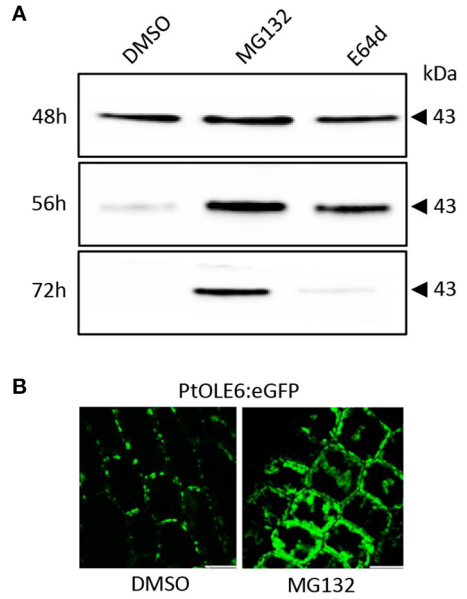

FIGURE 3 | PtOLE6 degradation by the proteasome pathway. **(A)** MG132 inhibits proteasomal degradation of PtOLE6 in germinating *Arabidopsis* seeds. *Arabidopsis* PtOLE6-eGFP overexpressor seeds were germinated in DMSO control, MG132, and E64d for 48–72 h, and immunodetected using an anti-eGFP antibody. **(B)** Treatment with MG132 prevents degradation of PtOLE6-eGFP, resulting in cytosolic accumulation in epidermal cells of the hypocotyl adjacent to the radical. DMSO, control. Bar 50 μm.

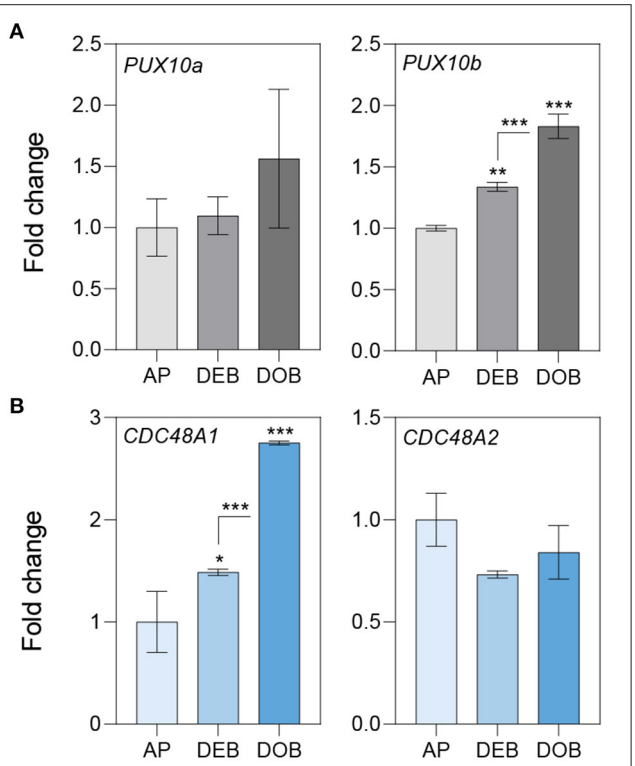

FIGURE 4 | Expression of genes involved in OLEOSIN degradation. Relative expression of genes encoding **(A)** UBX Domain-Containing Proteins (PUX10a, b) and **(B)** Cell Division Control Proteins (CDC48A1,2) in apices (APs) under long day and in developing buds (DEBs) and dormant buds (DOBs) in short days. Values are calculated relative to the control (AP) and represent the means of three technical replicates ± SD of four plants. Asterisk(s) indicate statistical significance between treatments (one-way ANOVA, Tukey analysis; $^{*}P < 0.05$; $^{**}P < 0.01$; and $^{***}P < 0.001$).

Presence of LDAP1 in Maturing Buds and Localization at LBs

In addition to the gene expression studies, we investigated if OLEOSIN and LDAP were present in extracts of buds at different developmental stages during growth and under dormancy-inducing conditions. In growing plants, antibodies detected OLEOSINs in younger developing buds above the bud maturation point (BMP), while LDAP1 was not detected (**Figure 6A**). In contrast, LDAP1 appeared to be abundant in full-grown buds below the BMP, which had ceased development and entered quiescence. Under dormancy-inducing conditions, OLEOSINs could not be detected in any bud, whereas LDAP1 was found in dormant buds and was even increasing over time in dormant buds (**Figure 6B**).

That the *Populus* LDAPs can localize to LBs was demonstrated in leaf epidermal cells of *N. benthamiana* using a binary vector expressing the 35S promotor driven *OLE6-eGFP* fusion protein and binary vectors expressing *LDAP1a-mRFP, LDAP1b-mRFP*, *LDAP2a-mRFP*, *LDAP3a-RFP*, and *LDAP3b-mRFP*. The vectors were transformed into *Agrobacterium tumefaciens* and infiltrated into leaves for 2 days and investigated with CLSM. Captured images (Leica Application Suite X software) showed that all mRFP-tagged LDAPs were exclusively localized to OLE6:eGFP-tagged LBs (**Figure 7**). LDAP1b and LDAP3b did not localize to the smallest LBs, which only contained OLEOSIN. In brief, the upregulation of *LDAPs,* LDAPs presence in the LB fraction, and localization to LBs suggest that they were recruited to the monolayer after OLEOSIN removal. Together, these results suggest that OLEOSINs were degraded and replaced by LDAPs prior to bud completion and the establishment of a quiescent and dormant state.

Candidate LB-Associated Proteins

The proteomic analysis of the bud LB fraction aimed to create an inventory of known and putative LB cargos that may contribute to cellular homeostasis, dormancy release and subsequent intercellular transport, and signaling in meristems. Their detection requires the omission of the salt wash (as shown above) that is commonly used to remove proteins that might associate with the monolayer during LB isolation, or are commonly considered contaminants. As argued above, this would also remove the peripherally associated proteins that hitch a ride to the PD. In buds, cytoplasmic proteins might associate with LBs when molecular crowding is reduced (Kory et al., 2015), and it seems possible that the enlarging LBs recruited a surplus of such proteins. These proteins may be stored at LBs and delivered to the PM and PD during dormancy release, serving membrane repair and renewed cell–cell communication. From the total fraction of 719 proteins, we selected 117 proteins, or ca.

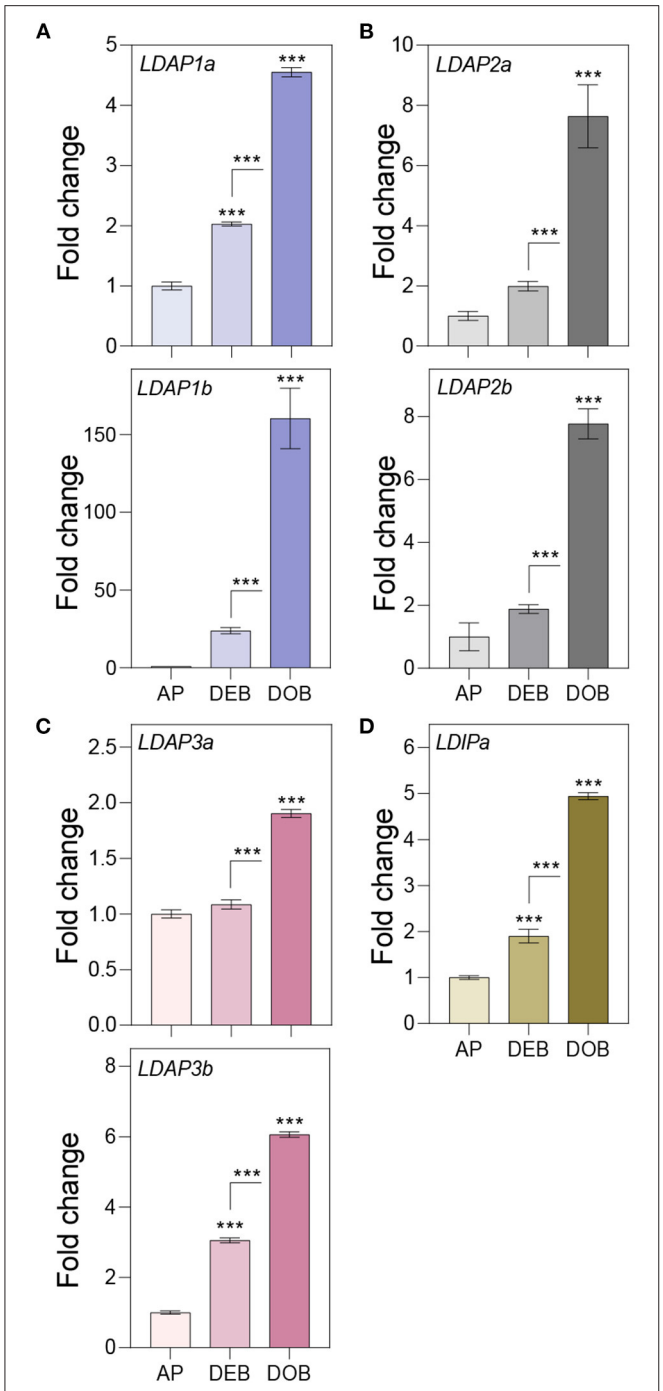

FIGURE 5 | Expression of genes associating with the lipid body monolayer. Relative expression of genes encoding for **(A–C)** LDAPs and **(D)** LDIP in apices (APs) under a long day, and in developing buds (DEBs) and dormant buds (DOBs) in short days. Values are calculated relative to the control (AP) and represent the means of three technical replicates ± SD of four plants. Asterisk(s) indicate statistical significance between treatments (one-way ANOVA, Tukey analysis; ***$P < 0.001$).

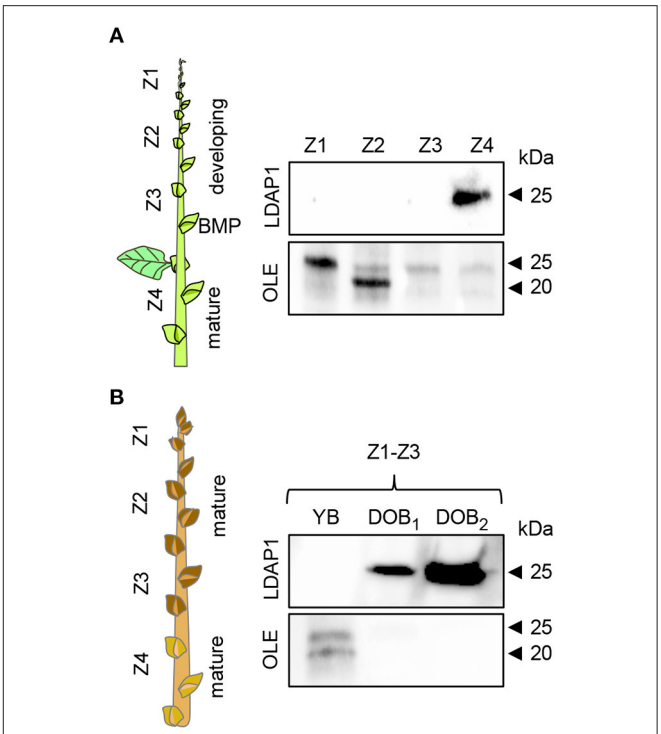

FIGURE 6 | Immunodetection of LDAP1 and OLEOSIN proteins in axillary buds during their maturation under different daylength conditions. **(A)** Developing (zones Z1–Z3) and mature axillary buds (Z4) in reference to the bud maturation point (BMP) in long days. **(B)** Young axillary buds (YB) (Z1–Z3) in long days, and after 6 (DOB_1, dormant buds 1) and 9 weeks (DOB_2, dormant buds 2) in short days. Equal amounts of protein (10 mg) were loaded in wells.

16%, that potentially represent meaningful LB cargos (**Table 1**). As indicated, this selection was based on the reported presence of identical or similar proteins at LBs, in LB fractions, at PD, or in PD-enriched fractions (Fernandez-Calvino et al., 2011; Leijon et al., 2018). Since LBs frequently interact with other cell organelles and PD, we also included proteins that were reported or suggested to assist in LB-organelle-PM tethering, targeting, and hemifusion.

We detected in the LB fraction Caleosin 1 (CLO1), LDPI, LDAP3a, LDAP3b, LDAP1a, LDAP1b, Oil Body Lipase1 (OBL1a,b), GPAT8 (functionally redundant with GPAT4), and the 1,3-β-glucanase enzyme GH17_44 (**Table 1**). Like OLEOSIN, CLO1 has three structural domains, such as a pro-knot motif (Hsieh and Huang, 2004). Its major function is signaling, but at LBs, it contributes to monolayer stability (Chen et al., 1999). LDAPs associate with LB *via* amphipathic helices and similarly provide some structural integrity (Horn et al., 2013; Gidda et al., 2016; Kim et al., 2016). LDIP, which possesses a central hydrophobic sequence and few TMDs (Pyc et al., 2017), interacts with LDAP3 (Pyc et al., 2017) and may associate with nascent LBs (Coulon et al., 2020). OBL1 localizes to LBs in *Arabidopsis* seeds (Eastmond, 2006), and GH17_44 localizes to LBs in *Populus* meristems (Rinne et al., 2011). PUX10 and CDC48A are involved in the degradation of ubiquitinated proteins, such as OLEOSINs and might end up in the LB fraction attached to LB proteins. The LB fraction contained a dozen components of the 26S proteasome (Verma et al., 2002), such as the regulatory

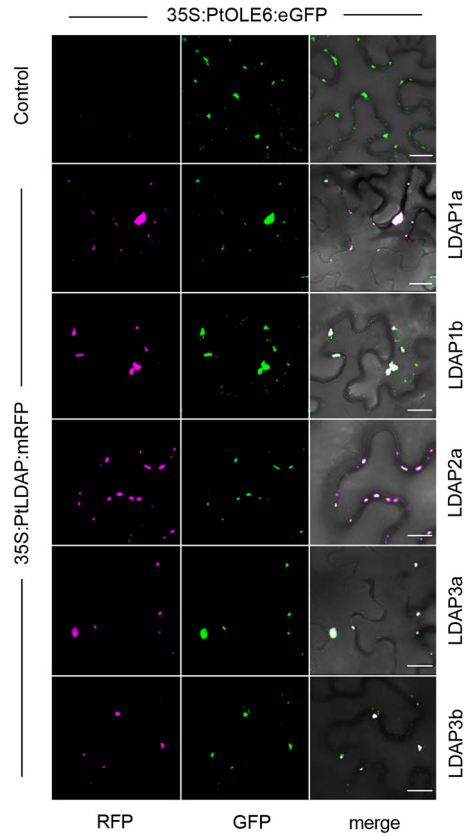

FIGURE 7 | Localization of Lipid Droplet Associated Proteins (LDAPs) at lipid bodies in *N. benthamiana*. Representative confocal laser scanning microscopy images of leaf epidermal cells transiently co-expressing eGFP-tagged OLE6 and corresponding mRFP-tagged LDAPs (magenta). Single optical sections of RFP, GFP, and the merged images are shown for each set of experiments. Bars 50 μm.

particle RPT2A and regulatory subunit RPN7, the ubiquitin-conjugating enzyme 13A (UBC13A), the ubiquitin-activating enzyme E11 (UAB1) (**Table 1**), and other 26S-associated proteins (**Supplementary Table 1**).

As LBs move in the actomyosin system motorized by myosin XI-k/1/2 (Veerabagu et al., 2020), it is of interest that the LB fraction contained two myosin XI tail binding GTPases. RAB-C2a, a homolog of the mammalian RAB18 that localizes to LBs, localizes in plants to peroxisomes that traffic on F-actin, like LBs (Hashimoto et al., 2008). RAB-D1 localizes to Golgi and endosomal vesicles (Pinheiro et al., 2009), which can interact with LBs (see discussion), while ARA6 localizes to LBs (Brasaemle et al., 2004; Fujimoto et al., 2004; Liu et al., 2004). The LB fraction contained only one actin, ACT7. This could be significant as ACT7 is associated with meristematic activity in germination and early plant development (McDowell et al., 1996; Kandasamy et al., 2001, 2009), is required in callus growth and present in PD fractions (Fernandez-Calvino et al., 2011). We also identified proteins that modulate actin dynamics, such as ADF4 and VAB2 (**Table 1**).

Proteins in the LB fraction that localize to PD components or the surrounding PM include, among others, (references in **Table 1**) Purple Acid Phosphatase (PAP1), two calreticulins (CRT1/CRT1A and CRT2/CRTB), two peroxidases (PRX36 and PRX37), the atypical 1,3-β-glucanase Zerzaust (ZET), 1,3-β-glucanase1 (BG1/GH17-37), Dehydrin HIRD11, Reticulon like protein B1 and B3 (RTN3), an inactive receptor kinase, Plasma Membrane Intrinsic Protein 1 and 3 (PIP1 and 3), Calnexin 1 (CNX1), and Bcl-2 Unfolding Protein BAG7 (**Table 1**; **Supplementary Table 1**). Of these, five were present in the *Populus* PD fraction (Leijon et al., 2018) and nine in that of *Arabidopsis* (Fernandez-Calvino et al., 2011). Several of these proteins were also previously localized to LBs, such as CNX1, RTN1, and RTN3 (**Table 1**).

Proteins previously found in LB fractions of plant and non-plant systems included LEA proteins, which protect cellular structure and PD during dehydration stress (Karlson et al., 2003). Among these were ERD7, LEA26, and LEA27 (**Table 1**). Furthermore, we identified alcohol dehydrogenases (ADH1-3), annexins (ANN1,2), transport family protein SecY, sterol methyltransferase (SMT2), embryo-specific protein ATS3, and Cytochrome P450 (**Table 1**).

The LB fraction also contained proteins involved in tethering, membrane trafficking, and membrane fusion, such as the CalB domain Synaptotagmin 2 (SYTB/SYT2), which is a C2 tethering protein, Syntaxins (SYP71) and other SYPs, the vesicle/protein transporter ADP-ribosylation factor 1 (ARF1), and the endosomal protein Guanine Nucleotide-Exchange (GEF), which recruits ARF1 to vesicles (**Table 1**, **Supplementary Table 1**). Moreover, a dozen Rab GTPases were present. These included ARA-3 (RAB8a), Golgi localized RAB-6A, and Suppressor of Variegation 11 (SVR11/RABE1B) (**Table 1**, **Supplementary Table 1**). The presence of CPOII subunits and COPI Coatomer subunits in conjunction with ARF1 is of interest, as they may mediate protein trafficking to and from LBs (Soni et al., 2009) (see discussion).

Other identified proteins potentially reflect organellar interaction, protein folding and unfolding at organelles and PD, lipid metabolism, storage, detoxification, and desiccation stress. Unfolding/folding proteins in the bud LB fraction included the chaperones/Heat Shock proteins Hsp-90-4, Hsp90-6, Hsp90-7, the Hsp70 proteins BIP2 and BIP3, and homologs of the cpn60 chaperonin TCP-1/CCT8. Of the TCP-1 chaperonin family proteins, 10 members were present (**Table 1**, **Supplementary Table 1**). Proteins related to lipid metabolism included Phospholipase C (PLC2), GDSL-motif esterase (acyltransferase), and the lipase Plat Domain Protein 2 (PLAT2). Also identified were three Histones, previously shown to be stored at LBs (Cermelli et al., 2006). The identified antioxidant enzymes may protect stem cells of the embryonic shoot from hypoxia-induced damage in the low-oxygen environment of the bud (Ophir et al., 2009; Meitha et al., 2015). They include Catalase 2 (CAT2), Thioredoxin-dependent peroxidase 1 (TPX1), the peroxidases PRX36 and PRX37, and Manganese Superoxide Dismutase (MSD1).

A direct comparison of the LB fraction of dormant buds and the PD fraction of cell suspension cultures of *P. trichocarpa*

TABLE 2 | Proteins that are shared by the bud LB fraction of *Populus* and the PD-enriched fraction of *Populus trichocarpa* Leijon et al. (2018).

Protein name	*P. trichocarpa* Accession nr	BlastP of *A. thaliana*	Mw	Unique Peptides		
			kDa	Bio 1	Bio 2	Bio 3
LDAP Interacting Protein (LDIP)	Potri.004G082300	AT5G16550	24	3	3	4
CSC1-like protein ERD4 (ERD4) (LEA)	Potri.001G358300	AT1G30360*	82	9	5	5
Syntaxin of plants 71 (SYP71)	Potri.016G088200	AT3G09740*	30	5	4	2
Small GTP-binding protein (ARA-3) (NAC)	Potri.008G051700	AT3G46060*	24	10	8	7
Leucine-rich repeat protein kinase	Potri.018G074300	AT2G26730	71	9	3	2
Calreticulin 1A (CRT1/CRT1A)	Potri.005G015100	AT1G56340*	48	13	10	4
Purple acid phosphatase (PAP1)	Potri.010G158400	AT1G13750*	69	3	3	2
Reversibly glycosylated polypeptide 3 (RGP3)	Potri.010G156700	AT3G08900	41	36	32	11
Zerzaust (ZET), atypical β-1,3 glucanase	Potri.019G032900	AT1G64760*	53	4	4	2
O-Glycosyl hydrolases family 17 protein	Potri.006G080600	AT5G58090*	53	5	6	2
Embryo-specific protein 3 (ATS3)	Potri.015G132700	AT5G62200	21	4	4	3
Plasma membrane intrinsic protein 1 (PIP1)	Potri.003G128600	AT4G00430	31	6	4	2
SKU5 similar 1 (SKS1)	Potri.015G127200	AT4G25240*	66	10	6	4
Thioredoxin-dependent peroxidase 1 (TPX1)	Potri.001G423500	AT1G65980	17	9	7	8
S-formylglutathione hydrolase (SFGH)	Potri.006G047000	AT2G41530	32	6	7	2
Prohibitin 6 (PHB6)	Potri.017G017400	AT2G20530	32	16	16	17
Thioesterase superfamily protein	Potri.003G020300	AT5G10160*	26	5	4	4
Ribosomal protein L10 family protein	Potri.008G066200	AT2G40010*	34	8	9	6
Ribosomal protein L7Ae/L30e/S12e (Gadd45)	Potri.004G196500	AT1G36240	12	4	2	2

Proteins with a star are also present in the PD-enriched fraction of Arabidopsis thaliana (Fernandez-Calvino et al., 2011).*

(Leijon et al., 2018) uncovered 19 identical proteins (**Table 2**). A part of these shared proteins was also identified in the PD fraction of *Arabidopsis* cell suspensions (**Table 2**). The presence of LDIP in the *Populus* PD fraction (Leijon et al., 2018) is of interest because LDIP is a LB protein (Pyc et al., 2017). Of interest is also the syntaxin SYP71, a plant-specific SNARE protein involved in vesicle docking and fusion (Suwastika et al., 2008) that is present in PD fractions of both *Populus* and *Arabidopsis* (**Table 2**). SNAREs can mediate LB tethering to distinct compartments, LB-LB fusion, and hemifusion with bilayer membranes (Boström et al., 2007; Murphy et al., 2009). The GTPase ARA-3 (RAB8a), which mediates vesicle docking, the PD-localized Calreticulin (CRT1/CRT1A) (Baluska et al., 2001), and the LEA protein ERD4 were present in both fractions. Likewise, the following proteins of the bud LB fraction were present in both PD fractions: ZET (Vaddepalli et al., 2017), an O-Glycosyl hydrolases family 17 protein, and the GPI-anchored protein SKU5 similar 1 (SKS1). Some proteins exclusively shared by the LB fraction and the *Populus* PD fraction were the Thioesterase superfamily protein, involved in fatty acid biosynthesis, the seed LB candidate protein Embryo-Specific Protein 3 (ATS3) (Vermachova et al., 2011; Kretzschmar et al., 2020), a leucine-rich receptor kinase (probably inactive), PAP1, the cytoplasmically localized Reversible Glycosylated Polypeptide 3 (RGP3), the aquaporin Plasma Membrane Intrinsic Protein 1 (PIP1), the PHB-domain protein PHB6, the antioxidant TPX1, and the hydrolase S-Formylglutathione Hydrolase (SFGH).

DISCUSSION

Production and Degradation of OLEOSINs

OLEOSINs stabilize the LB monolayer, preventing coalescence and fusion during seed desiccation and dormancy (Siloto et al., 2006; Shimada et al., 2008; Hsiao and Tzen, 2011). Perennial buds also desiccate, albeit partially (Rinne et al., 2015), express *OLEOSIN* genes, produce OLEOSINs, accumulate LBs, and establish dormancy. The major gene *OLE6* was strongly upregulated during bud formation (**Figure 2A**). Given these similarities, it came as a surprise that none of the eight *Populus* OLEOSINs were detected in the LB fraction of dormant buds (**Table 1**; **Supplementary Table 1**). *OLE6* was completely downregulated prior to dormancy establishment (**Figure 2A**), while the minor genes *OLE3* and *OLE5* were expressed very little. The apparent absence of OLEOSINs in the LB fraction of dormant buds suggests they were degraded prior to dormancy establishment, likely by the machinery that also degrades OLEOSINs during seed germination (Deruyffelaere et al., 2018). Core components of this machinery were found in the *Populus* LB fraction, such as the adaptor protein PUX10, the segregase CDC48A (AAA ATPase Cell Division Cycle 48) and various 26S components, the ubiquitin-activating enzyme UBA1, the crucial 19S ATPase subunit RPT2A, and several deubiquitinating proteases, which are required for insertion of proteins into the 20S core (**Table 1**, **Supplementary Table 1**). PUX10 associates with LBs, and interacts with ubiquitin through its UBA domain and with CDC48A through its UBX domain, resulting in the degradation of ubiquitinated OLEOSINs by the

26S proteasome (Hsiao and Tzen, 2011; Deruyffelaere et al., 2015, 2018; Kretzschmar et al., 2018). As AtPUX10 is an integral class I LB protein that binds ubiquitins and recruits CDC48A (Deruyffelaere et al., 2018), it is perhaps not surprising that these components were present in the LB fraction of *Populus* buds. The predicted K130 ubiquitination site of PtOLE6 aligned with the major ubiquitination sites of AtOLE3-K159 and AtOLE4-K144 (**Supplementary Figure 5B**). Moreover, we found that in germinating seeds of an *Arabidopsis*, *PtOLE6* overexpressor PtOLE6 is degraded like AtOLE1-4 (Deruyffelaere et al., 2015), and that degradation is partially inhibited by proteasome inhibitors E64d and blocked by MG132 (**Figure 3**). It seems likely, therefore, that this degradation mechanism is responsible for the early removal of OLEOSINs from LBs of buds, although direct localization of these proteins to the LBs remains to be demonstrated. During bud formation, the major gene *OLE6* was strongly upregulated, producing OLEOSIN protein and many small LBs (**Figures 1**, **2**). During dormancy establishment, *OLE6* was downregulated below the level of growing apices (**Figure 2A**); and while *PUX10b* and *CDC48A1*were upregulated (**Figures 4A,B**), OLEOSINs were no longer detected (**Figure 6B**), and LBs had enlarged (**Figure 1E**). In correspondence with *OLE6* downregulation, *LDIPa*, *LDAP1*, *LDAP2*, and *LDAP3* were upregulated (**Figure 5**); and their encoded proteins, LDIP, LDAP1, and LDAP3, were detected in the bud LB fraction instead of OLEOSINs (**Table 1**). In brief, the data support the hypothesis that OLEOSIN is required for initiation of LB production in buds, but that prior to dormancy establishment OLEOSINs are removed by the PUX10/CDC48a degradation mechanism. PUX10 and CDC48A also likely degrade other LB proteins (Deruyffelaere et al., 2018), as they remain in LBs after OLEOSIN is removed.

Probable Replacement of OLEOSIN by LDIP/LDAPs

That OLEOSINs are replaced by LDAP1 during LB enlargement is supported by the following facts. First, in long-day plants, OLEOSIN was detectable in extracts of developing buds and virtually absent in mature buds, while the reverse was true for LDAP1 (**Figure 6A**). Second, in short-day plants, OLEOSINs could not be detected in dormant buds, while LDAP1 was abundant (**Figure 6B**). Indeed, in general LDAPs might not interact with OLEOSIN-covered LBs, because LDAPs do not possess a hydrophobic hairpin and their relative hydrophilicity allows LB association only in detergent-sensitive manner (Gidda et al., 2016; Kim et al., 2016; Huang and Huang, 2017; Pyc et al., 2017). LDAPs and many of the identified LB fraction proteins might have been recruited to the expanding monolayer surface after OLEOSIN degradation, such as CLO1 (**Table 1**), which binds competitively with the monolayer (Huang, 2018). Noteworthy is that in *N. benthamiana*, the mRFP-tagged LDAP1b and LDAP3b, did not localize to the smallest OLE6-eGFP-tagged LBs (**Figure 7**), suggesting that these two proteins associate only with an expanded monolayer. LDIP anchors itself *via* an amphipathic helix in the monolayer and interacts with LDAP3 (Pyc et al., 2017) but is confined to a small area of the LB while LDAPs cover the entire monolayer (Coulon et al., 2020). LDIP was suggested to facilitate the neo-formation of small LBs (Coulon et al., 2020) in cooperation with SEIPINs (Cai et al., 2015; Barbosa and Siniossoglou, 2017). As *LDIPa* was upregulated during the LB accumulation phase in developing buds (**Figure 5D**), it seems possible that it did assist later LB emergence. LB expansion might be driven by increased TAG biosynthesis (**Figures 1E**, **2B**), possibly involving the ER-localized enzyme GPAT8 (**Table 1**) (Gidda et al., 2009), which functions redundantly with GPAT4 (TAIR). Both localize to LBs in *Arabidopsis* (Fernández-Santaso et al., 2020) and in mammalian and insect cells (Wilfling et al., 2013).

Seed germination involves OLEOSIN degradation, LB enlargement, and recruitment of cytoplasmic proteins that mediate lipolysis and promote seedling growth (Deruyffelaere et al., 2015; Thazar-Poulot et al., 2015; D'Andrea, 2016). Germination cannot occur when the TAG lipase SDP1 is absent (Eastmond, 2006). While in buds *SDP1a* and *SDP1b* were slightly upregulated under short days (**Figure 2C**), the enzymes were absent from the LB fraction (**Supplementary Table 1**), and LB degradation was not observed. Either way, *SPD1* transcript levels might not reflect enzyme activity because it might be post-transcriptionally regulated (Eastmond, 2006), or it is not delivered to LBs by the glyoxysomes that produce them (Thazar-Poulot et al., 2015) but kept in store for later bud activation. Notably, the retromer subunit VPS29 that mediates peroxisome tubulation to deliver SPD1 to the LBs was absent from the LB fraction (**Supplementary Table 1**).

LB Fraction and Putative LB Proteome

LBs function in lipid homeostasis, protein sequestration, and membrane and cargo trafficking (Murphy, 2012). As a result, LB fractions can contain tens or even hundreds of proteins (Bartz et al., 2007; Hodges and Wu, 2010; Brocard et al., 2017; Zhi et al., 2017), most of which lack canonical LB functions. These "refugee" proteins (Hodges and Wu, 2010) are of interest, highlighting the dynamics of protein exchanges. Our proteomic analyzes were aimed at creating an inventory of such transiently associated proteins, as they could be involved in cellular homeostasis, dormancy release, and intercellular transport and signaling. The 719 identified proteins were present in the LB fractions of three independent experiments (**Table 1**, **Supplementary Table 1**), and among these were 117 proteins that included known LB proteins and proteins that were previously identified in LB fractions of various systems (**Table 1**). They relate to the ER, lipid metabolism, cytoskeleton, membrane trafficking, organellar interaction, membrane tethering and fusion, chaperone function, and signaling (Zehmer et al., 2009; Hodges and Wu, 2010; Gao and Goodman, 2015). Some of them might serve the unique needs of dormant bud meristems, which have reduced metabolism, face environmental and endogenous stresses, and maintain a dormancy-release mechanism (Rinne et al., 2001, 2011). In the absence of OLEOSINs, which mitigate desiccation and freezing stress (Siloto et al., 2006; Shimada et al., 2018), LDAPs, CLO1, and hydrophilins, such as LEA proteins (**Table 1**), might confer stability to LBs (Gidda et al., 2016; Kim et al., 2016). The bud, as a survival structure, must protect the

enclosed embryonic shoot and its resident stem cells against environmental and endogenous onslaughts. Considering that the enclosed meristem resides in a hypoxic internal bud environment (Ophir et al., 2009; Meitha et al., 2015), the identified antioxidants might function to protect the stem cells. Notably, the LB fraction contains TPX1, the peroxidases PRX36, PRX37, CAT2, and MSD1 (**Table 1**), which, like in *Drosophila* (Bailey et al., 2015), can mitigate the effects of hypoxia-induced ROS. LBs may also detoxify stem cells by removing cytoplasmic free fatty acids, resulting from membrane degradation and remodeling during desiccation (Listenberger et al., 2003). Given the embryo-like nature of the embryonic shoot, the presence of histones H2A, H3, and H4 in the LB fraction is significant. *Drosophila* stores maternal H2A, H2B, H3, and H4 at LBs in its eggs as a repository for early embryogenesis (Cermelli et al., 2006; Li et al., 2012). Storage at LBs keeps histones available for immediate use while avoiding the cytotoxic effects of free histones (Gunjan and Verreault, 2003). In bud meristems, they could serve a similar purpose.

LB Fraction and LB Trafficking to PD

As shown previously, LBs do not arrive at PD by simple cytoplasmic streaming but by processive trafficking in the actomyosin system, which is severely impaired in an *Arabidopsis* 3KO *myosinxi-k/1/2* mutant (Veerabagu et al., 2020). Myosin XI-K is the most important among the 13 class XI myosins of *Arabidopsis* and is responsible for the movement of mitochondria, peroxisomes, and endomembrane vesicles (Avisar et al., 2008, 2009; Sparkes et al., 2008; Peremyslov et al., 2015). The binding of LBs to myosin XIs, like that of other organelles, might require Rab GTPases. We identified in the LB fraction two "myosin XI tail-binding" proteins, the Rab GTPase homolog C2A (RAB-C2A) and the Rab GTPase homolog D1 (RAB-D1) (**Table 1**). In *Arabidopsis*, these factors interact with the C-terminal tail region of MYA2 (an isoform of myosin XI). While RAB-C2A specifically localizes to peroxisomes (Hashimoto et al., 2008), RAB-D1 associates with the Golgi apparatus (Pinheiro et al., 2009). A recent study on the *Populus* Rab family found that RAB-C2A did not localize at Golgi, TGN, or endosomes but instead at small unidentified vesicles (Zhang et al., 2018), which could have been peroxisomes but possibly also LBs. The presence of RAB-C2A in the LB fraction (**Table 1**) suggests that RAB-C2A is the receptor that anchors LBs to myosin XI-k/1/2, enabling motility, interaction with cell organelles, and targeting of PD. If so, the motility of LBs and peroxisomes on the same RAB-C2A/Myosin XI/actin assembly might explain their frequently observed interaction (Mathur et al., 2002; Hashimoto et al., 2008; Veerabagu et al., 2020). Notably, RAB18, a mammalian homolog of RAB-C2A, is present at LBs and in LB fractions (as shown in references in **Table 1**). The presence of Golgi-related RAB-D1 in the LB fraction (**Table 1**) suggests an interaction between LBs and Golgi- and endosomal vesicles (see below). LBs might move on ACT7, as it is the only actin identified in the bud LB (**Table 1**) and seed LB fractions of Chinese tallow (Zhi et al., 2017). ACT7 is required in seed germination, early plant development, and meristem proliferation (McDowell et al., 1996; Kandasamy et al., 2001, 2009), and it is found in the PD fraction of *Arabidopsis callus* cells (Fernandez-Calvino et al., 2011). The presence of actin-stabilizing VAB2 (Ma et al., 2012) and PD-localized actin-severing ADF4 in the LB fraction (**Table 1**) appears to reflect the dynamics of actin-mediated transport.

Organellar Interactions and Chaperones

As argued by Gao and Goodman (2015), organelle markers, such as ER luminal chaperones and mitochondrial proteins, are so frequently associated with thoroughly purified LBs that it is unlikely that they all represent contaminants. At least some of them might reflect the frequently observed LB-organellar interactions (Murphy et al., 2009; Zehmer et al., 2009), facilitated by their movement on F-actin (Mathur et al., 2002; Van Gestel et al., 2003; Hashimoto et al., 2008; Veerabagu et al., 2020). We identified some mitochondrial proteins, vacuolar proteins, and lipid metabolism proteins, as well as Annexins, Calnexin, LEA proteins, Cytochrome P450s, transport proteins, Alcohol Dehydrogenases, and Embryo-Specific Protein3 (**Table 1**, **Supplementary Table 1**). Several of these are present in seed LB fractions and PD fractions (as shown in references in **Table 1**). The identified annexins putatively link LBs to the PM and PD, as they can bind F-actin, regulate membrane trafficking, bind phospholipids and Ca^{2+}, inhibit callose synthase at PD, act as peroxidases, and induce membrane curvature (Delmer and Potikha, 1997; Clark et al., 2012; Boye et al., 2018).

Organellar interactions involve chaperone-like molecules that mediate membrane and vesicle transport, tethering, and membrane (hemi-)fusion. Chaperones transport, fold and unfold proteins during autophagy, and function at peroxisomes, mitochondria, chloroplasts, and ER (Boston et al., 1996; Kriechbaumer et al., 2012). We identified Synaptotagmin B, various Syntaxins, ARF1 and ARF-related proteins, and transport-related RAB GTPases (**Table 1**). The identified calnexins and several of the chaperones (**Table 1**) were also present in the LB fraction of the Chinese tallow (Zhi et al., 2017). In the SAM, LB-resident chaperones, delivered to PD, could assist in the documented unfolding and refolding of the non-cell-autonomous proteins that move cell-to-cell (Aoki et al., 2002). Essential in SAM function is the intercellular movement of the conserved transcription factor SHOOT MERISTEMLESS (STM) in *Arabidopsis*, and KNOTTED1 (KN1) in maize, which requires chaperon-assisted unfolding in the donor cell and chaperonin-assisted refolding in the destination cell (Kitagawa and Jackson, 2017). The LB fraction contained, among others, the CCT8 subunit of chaperonin CTP-1 (AT3G03960) that refolds STM/KN1 in the destination cell (Xu et al., 2011; Kitagawa and Jackson, 2017). Although CCT8/CTP-1 localization at LBs remains to be shown, LBs that dock at opposite sides of PD (Rinne et al., 2011; Veerabagu et al., 2020) could engage in unfolding proteins for export and refolding incoming proteins in the SAM.

LB Proteins Localized to PD or Present in PD-Enriched Cell Wall Fractions

Lipid bodies can target PD to deliver enzymes that enhance PD conductivity (Rinne et al., 2001, 2011; Veerabagu et al., 2020).

Part of the identified proteins may similarly arrive at the PD interior and surrounding PM *via* the LB shuttle. This seems feasible, as many of the proteins in the LB fraction have been localized to PD, such as acid phosphatases (Esau and Charvat, 1975), calreticulins (Baluska et al., 2001), calnexins (Liu et al., 2017), and reticulon (Knox et al., 2015; Kriechbaumer et al., 2015).

Reticulon, present in the LB fraction of insect cells, adopts a hairpin-like topology in the outer ER leaflet (Beller et al., 2008). It is of interest, therefore, that reticulon3 (RTN3) is present in the bud LB fraction (**Table 1**), and that it is identified in the PD fraction (Fernandez-Calvino et al., 2011) and localized at PD (Knox et al., 2015; Kriechbaumer et al., 2015). This suggests the possibility that in meristems RTN3 could arrive at the desmotubule *via* LBs. The dehydrin HIRD11 (**Table 1**) may protect PM- and PD-localized proteins during winter, such as the PD-localized dehydrin in cold-acclimated tissue of dogwood (Karlson et al., 2003). Similarly, the γ-clade GH17-family protein (**Table 1**) localizes to PD (Rinne et al., 2011). RGP3 might also localize to PD, like RGP2 (Sagi et al., 2005). Proteins in the LB fraction, some of which localized to PD, were also identified in PD fractions of both *Arabidopsis* (Fernandez-Calvino et al., 2011) and *P. trichocarpa* (Leijon et al., 2018), such as ERD4, Syntaxin of Plants 71 (SYP71), small GTP-binding protein ARA-3 (NAC/RAB8a), Calreticulin 1A (CRT1A), PAP1, ZET, O-Glycosyl hydrolases family 17 protein, SKU5 similar 1 (SKS1), and Thioesterase superfamily protein (**Table 2**). The presence of the LB protein LDIP and the candidate LB protein ATS3 (Vermachova et al., 2011; Kretzschmar et al., 2020) in the *Populus* PD proteome (Leijon et al., 2018) and in the LB fraction (**Table 1**) is an independent confirmation that LBs target PD.

The number of proteins in the LB fraction that are destined for PD might be much larger than that which is found in enriched PD fractions of cell cultures because they contain only young primary PD (Fernandez-Calvino et al., 2011; Leijon et al., 2018). In complex three-dimensional tissues, such as bud meristems, LBs dock at both primary and secondary PD (Rinne et al., 2011; Veerabagu et al., 2020). The overlap with available PD proteomes might, therefore, underestimate the LB proteins that are delivered to PD in meristems.

The presence of some ER-luminal proteins and GPI-anchored proteins in the LB fraction appears puzzling. A possible explanation is that they might reside inside a subset of LBs. Most LBs are formed at the cytoplasmic leaflet of the ER, which then determines the composition of the monolayer and its associated proteins (Guo et al., 2009; Walther and Farese, 2009). Alternatively, an entire oil lens may be cut out from the ER, resulting in a bicelle LB, in which the monolayer is derived from both ER leaflets (Ploegh, 2007). Such LBs possess proteins that reside on both sites of the ER membrane and include luminal ER-anchored proteins. In addition, during "vesicular budding" (Walther and Farese, 2009), minute cytoplasmic bilayer vesicles are produced and tethered to ER, while neutral lipids are imported into the bilayer by a lipid shuttle. As a result, the growing LB can contain a minuscule aqueous inclusion inside the remnants of the luminal ER leaflet, as also observed in birch meristems (Rinne and van der Schoot, 2004). In the last two cases, LBs can contain luminal ER proteins, for example, calnexin and BIP (**Table 1**), which are indeed frequently found in LB fractions (Brasaemle et al., 2004; Liu et al., 2004; Umlauf et al., 2004; Ploegh, 2007). LBs might also recruit organellar proteins. For example, LBs interact with ER, the Golgi apparatus, and early and late endosomes (Beller et al., 2010), and the coatomer assemblies SAR1-COPII and GEF-ARF1-COPII are implicated in protein delivery to LBs (Soni et al., 2009). Moreover, Arf1/COP1 locates to LBs, probably directing ER proteins to bridges that connect the ER to LBs (Bartz et al., 2007; Beller et al., 2010; Wilfling et al., 2014; Gao and Goodman, 2015; Brocard et al., 2017; Huang et al., 2019). It is of interest, therefore, that COPII and SAR1/2, as well as COPI, GEF (BIG5), and ARF1, are present in the bud LB fraction (**Table 1**).

The current inventory of putative LB-associated proteins lays out a road map for future investigations into the shuttle function of LBs in plant meristems, serving cellular metabolism, organellar interaction, and uniquely for plants, transport to and through PD.

EXPERIMENTAL PROCEDURES

Plant Materials and Sample Collection

Hybrid aspen (*Populus tremula* × *Populus tremuloides*) clone T89 plants were micro propagated, moved to a glass house, and grown under an 18-h long day (Veerabagu et al., 2020). When the plants reached a height of 80–100 cm, half of them were subjected to 10-h short days to induce dormant buds. We investigated meristems in three distinct phases: actively proliferating apices of growing long-day plants (APs), apices inside developing buds (DEBs, 3–4 weeks old), and dormant apices in completed terminal buds (DOBs, 6–9 weeks old).

P. trichocarpa OLE6-eGFP was overexpressed in *Arabidopsis thaliana* (Col-0), and homozygous lines were obtained as previously described by Veerabagu et al. (2020). Transgenic *Arabidopsis* PtOLE6-eGFP seeds were germinated on Whatman paper, wetted with 2 ml of 0.2% DMSO (control), 200 μM MG132, or 40 μM E64d (Deruyffelaere et al., 2015). Seeds were first subjected to 72 h of stratification at 4°C in the dark and later germinated under continuous light for 48–72 h as indicated at 25°C.

Microscopy of SAMs and LBs

Shoot apices of growing plants (APs), developing buds (DEBs, 4 weeks) and dormant buds (DOBs, 8 weeks) were fixed overnight in 2% (v/v) glutaraldehyde and 3% (v/v) paraformaldehyde at 4°C in 100 mM phosphate citrate buffer (Rinne et al., 2001). Because of the density of the bud tissues, the infiltration into LR white resin (LRW) was done gradually by increasing the LRW concentration stepwise from 30 to 70%, and, finally, incubating 4–7 days in 100% LRW. The resin was polymerized at 55°C for 24 h. Samples were trimmed longitudinally, and 1 μm thick median sections were stained with 1% (w/v) aqueous toluidine blue for light microscopical observation (Leica DM6B, Leica Microsystems, Wetzlar, Germany) and imaging with a digital camera (Leica DMC4500, Leica Microsystems, Wetzlar,

Germany). Subsequently, ultra-thin 80 nm sections were cut from samples and observed with a TEM (FEI Morgagni 268 FEI Company, Eindhoven, The Netherlands), which is electronically set to produce high-contrast LBs.

The number and sizes of LBs were assessed manually in median longitudinal TEM sections, restricted to two areas in the SAM and in the subjacent rib meristem/rib zone region (RM/RZ) (**Figures 1A–C**). Per photoperiod 2–3 replicate apices were used, and LB number and sizes were assessed in two TEM sections. As the chance to section through a LB increases with LB size (diameter), the numbers were corrected relative to DOB. In addition, we calculated the total number of LBs per average cell volume, considering section thickness and LB diameter, as explained in **Supplementary Figure 1**.

RNA Extraction, Quantitative PCR (qPCR), and Cloning

Complementary DNA (cDNA) preparations derived from dormant buds were used as a template to amplify all the LDAPs. The LDAP entry clones were obtained by BP reaction in pDONR207 and verified by sequencing. The binary constructs for mRFP fusion protein expression under the control of the 35S promoter were obtained *via* LR reaction using the respective LDAP entry clones and the destination vector pB7WGR2 (Karimi et al., 2002). For qPCR analyses, we collected apices from growing long-day plants (APs), and from short-day plants with developing buds (DEBs, 3 weeks), and dormant buds (DOBs, 6 weeks). Three biological replicates, each containing pooled samples, were frozen in liquid nitrogen. RNA was extracted from 0.2–0.3 g of frozen samples and analyzed with quantitative qRT-PCR, as described before (Katyayini et al., 2019). All clones were constructed using the Gateway™ technology (Invitrogen, Waltham, MA, United States). The binary vector pK7FWG2 expressing PtOLE6-eGFP fusion protein was constructed as described previously by Veerabagu et al. (2020). cDNA preparations derived from dormant buds were used as a template to amplify all the LDAPs. The LDAP entry clones were obtained by BP reaction in pDONR207 and verified by sequencing. The binary constructs for mRFP fusion protein expression under the control of the 35S promoter were obtained *via* LR reaction using the respective LDAP entry clones and the destination vector pB7WGR2 (Karimi et al., 2002). Gene-specific primer sequences for qPCR analyses were designed using Primer3. The list of primers and genes used for qPCR and cloning are presented in **Supplementary Tables 2, 3**.

Lipid Body Purification

Dormant buds were collected from short-day (9 weeks) exposed plants and used for LB purification and repeated in three independent experiments (Bio 1–3). Freshly harvested buds weighing 5–8 g were kept on ice until all the hard bud scales were carefully removed. The material was rinsed thrice in cold distilled water and then processed for LB extraction and purification. For LB purification, we used a previously described method (Jolivet et al., 2004) with two modifications. First, we deliberately omitted the NaCl ionic elution step to avoid discarding the loosely attached LB-associated proteins, which we aimed to identify. Second, proteins were precipitated using ice-cold methanol instead of hexane. Bio 1–2 received the prescribed 1X Tween20 wash, but Bio 3 was washed once more with Tween20 to increase stringency. The purity of the LB fraction was checked under light and DIC microscope to confirm absence of cellular contaminations. Total FAME measurement was carried out to assess the enrichment of fats in the LB fractions (O'Fallon et al., 2007). A fraction of the floating "fat pads" containing purified LBs was collected and inspected under the confocal microscope to confirm its purity and integrity (**Supplementary Figure 4C**). The fat pad, which was enriched with LBs (**Supplementary Figure 4D**), was further processed for protein precipitation (Veerabagu et al., 2020).

Immunoblotting

To investigate the production of LDAP1 and OLEOSIN in *Populus* buds by immunodetection, axillary buds were obtained from different developmental zones of long and short-day plants, as indicated in **Figure 6**. Proteins were extracted using the 2x Laemmli buffer, and equal amounts of protein (10 mg) were loaded in each well. Western blot analyses were carried out using primary antibodies of *A. thaliana* anti-OLE1 polyclonal antibody (PhytoAB-PHY0954A) at a dilution ratio of 1:2000, *Hevea brasiliensis* anti-SRPP1 (LDAP1) monoclonal antibody (Abcam-ab138711, Abcam, Cambridge, United Kingdom) at a dilution ratio of 1:1000, and anti-eGFP monoclonal antibody (Thermo Fisher-MA1-952, Thermo-Fisher Scientific, Waltham, MA, United States) at a dilution ratio of 1:2000. Goat anti-rabbit IgG H&L (HRP) antibody phytoAB-PHY6000 at a dilution ratio of 1:5000 was used as a secondary antibody for OLE1. Goat anti-mouse IgG H&L (HRP) (Abcam-ab205719) at a dilution ratio of 1:5000 was used as a secondary antibody for both LDAP1 and eGFP antibodies. Immunoblot signals were detected with the Clarity Western ECL kit (Bio-Rad, Hercules, CA, United States) and imaged with a Chemidoc (Bio-Rad, Hercules, CA, United States) digital imager.

Degradation of OLEOSIN and inhibition of degradation were studied in imbibed seeds of transgenic PtOLE6-eGFP-expressing *Arabidopsis* seedlings (**Figure 3**). Proteins were extracted from imbibed PtOLE6-eGFP transgenic seeds and immunoblotted using an anti-eGFP monoclonal antibody (Thermo Fisher-MA1-952, Thermo-Fisher Scientific, Waltham, MA, United States) and detected in Western blots as described above.

Protein Extraction

In short, the LB pellets were rinsed with methanol and air-dried. Subsequently, proteins were extracted in appropriate volumes of 2x Laemmli buffer. The third biological replicate received an additional wash, which further purified the sample. The extracted proteins were loaded on a 10% Bio-Rad mini protein gel (Bio-Rad, Hercules, CA, United States) and allowed to run ∼1.5 cm into the gel. The protein gel was stained with Coomassie Brilliant Blue (MilliporeSigma, Burligton, United States) for an hour and destained overnight. The region of the gel showing stained proteins was isolated and excised into six fractions. The gel pieces were reduced (DTT) and alkylated (iodoacetamide) before overnight digestion with trypsin. After digestion, the

peptides were extracted from the gel by sonication in a 0.1% TFA solution and cleaned up by a reversed-phase (C18) spin-tip procedure. Eluted peptides were dried and re-dissolved in a loading solution (2% acetonitrile, 0.05% TFA in MilliQ water). Samples were analyzed by LC-MS/MS, with Ultimate™ 3000 RSLC nano system coupled with Q Exactive hybrid quadrupole-orbitrap (Thermo-Fisher Scientific, Waltham, MA, United States). Thermo raw files were converted using the msfileconvert module of the Proteowizard (v 3.0.7076) software suite. All MS/MS samples were analyzed using Mascot (Matrix Science, London, UK; version 2.6.1). The mascot was set up to search the *P. trichocarpa* database (txid_3694, 53583 entries). The mascot was searched with a fragment ion mass tolerance of 0.02 Da and a parent ion tolerance of 10.0 PPM. Carbamidomethylation of cysteine was specified in Mascot as a fixed modification. Deamidation of asparagine and glutamine, oxidation of methionine, and acetylation of the n-terminus were specified in the Mascot as variable modifications.

Criteria for Protein Identification

Scaffold (version Scaffold 4.9., Proteome Software Inc., Portland, OR, United States) was used to validate MS/MS-based peptide and protein identifications. Peptide identifications were accepted if they could be established at >95% probability by the Scaffold Local FDR algorithm. Protein identifications were accepted if they could be established at >99% probability and contained at least two identified peptides. Protein probabilities were assigned by the Protein Prophet algorithm (Nesvizhskii et al., 2003). Proteins that contained similar peptides and could not be differentiated based on MS/MS analyses alone were grouped to satisfy the principles of parsimony. Proteins were considered identified only if in all three biological replicates they contained at least two unique peptides. The mass spectrometry proteomics data have been deposited to the ProteomeXchange Consortium *via* the PRIDE* (Perez-Riverol et al., 2019) partner repository with the dataset identifier PXD020099 and 10.6019/PXD020099. Gene ontology information was retrieved using The Arabidopsis Information Resource (TAIR) (Berardini et al., 2015) and The Plant Genome Integrative Explorer Resource (PlantGenIE) (Sundell et al., 2015). The complete list of *Populus* lipid body proteins identified in all the three biological replicates and the proteins identified in individual biological replicates are presented in **Supplementary Table 1**. The *P. trichocarpa* LB proteins identified in this study were checked for their relative protein abundance of different cellular compartments using the Multiple Marker Abundance Profiling (MMAP) tool from the SUBA toolbox and presented in **Supplementary Figure 10**.

Protein *in situ* Localization

The corresponding binary constructs were transformed into the *A. tumefaciens* strain GV3101 pMP90 and further infiltrated into *N. benthamiana* leaves (Schutze et al., 2009) together with the p19 protein from tomato bushy stunt virus cloned in pBIN61 (Voinnet et al., 2000) to suppress gene silencing. After two days of infiltration, tobacco leaf epidermis was investigated with a Leica TCS SP5 CLSM (Leica Microsystems, Wetzlar, Germany), and eGFP (Veerabagu et al., 2020) and mRPF (Van Damme et al., 2004) fluorescence was recorded (eGFP: excitation/emission 488/500–540 nm; mRFP: excitation/emission 561/600–640 nm). The Leica Application Suite X software was used to arrange single optical sections of mRFP (in magenta), eGFP and the corresponding merged images. Degradation of PtOLE6-eGFP and inhibition of degradation were studied in seeds of transgenic PtOLE6-eGFP expressing Arabidopsis seedlings imbibed with 2 ml of.2% DMSO (control), 200 μM MG132, and 40μM E64d, and investigated with CLSM (**Figure 3**).

Statistical Analyses and Bioinformatics

One-way ANOVA followed by Fisher's and Tukey's multiple comparisons tests were performed using GraphPad Prism Version 8.0.0 (www.graphpad.com). The MEGA6 program (http://www.megasoftware.net/) was used for ClustalW multiple sequence alignments and phylogenetic analysis, with maximum likelihood method and Poisson correction model. The *Populus* and *Arabidopsis* proteins of the phylogenetic analyses are presented in **Supplementary Figures 2, 3, 6–9**.

DATA AVAILABILITY STATEMENT

The original contributions presented in the study are publicly available. This data can be found here: https://www.ebi.ac.uk/pride/archive/projects/PXD020099.

AUTHOR CONTRIBUTIONS

MV, PR, LP, and CvdS designed the study. MV, PR, LP, and MS performed the experiments. MV and PR analyzed the data. MV, CvdS, and PR interpreted the data and wrote the manuscript. All authors contributed to the article and approved the submitted version.

FUNDING

The authors acknowledge the financial support of the Norwegian Research Council to CvdS and PR (FRIPRO Grant No: 263117).

ACKNOWLEDGMENTS

The authors are grateful to Professor Klaus Harter, University of Tübingen, for kindly providing them the pB7WGR2 and pBIN61:p19 vectors. The authors thank Lene Cecile Hermansen and Hilde Raanaas Kolstad, Imaging centre, NMBU, for the assistance with the TEM and CLSM, and Ms. Marit Siira for greenhouse assistance.

SUPPLEMENTARY MATERIAL

The Supplementary Material for this article can be found online at: https://www.frontiersin.org/articles/10.3389/fpls.2021.674031/full#supplementary-material

REFERENCES

Abell, B. M., Hahn, M., Holbrook, L. A., and Moloney, M. M. (2004). Membrane topology and sequence requirements for oil body targeting of oleosin. *Plant J.* 37, 461–470. doi: 10.1111/j.1365-313X.2003.01988.x

Abell, B. M., High, S., and Moloney, M. M. (2002). Membrane protein topology of oleosin is constrained by its long hydrophobic domain. *J. Biol. Chem.* 277, 8602–8610. doi: 10.1074/jbc.M103712200

Amari, K., Di Donato, M., Dolja, V. V., and Heinlein, M. (2014). Myosins VIII and XI play distinct roles in reproduction and transport of Tobacco mosaic virus. *PLoS Pathog.* 10:e1004448. doi: 10.1371/journal.ppat.1004448

Amari, K., Lerich, A., Schmitt-Keichinger, C., Dolja, V. V., and Ritzenthaler, C. (2011). Tubule-guided cell-to-cell movement of a plant virus requires class XI myosin motors. *PLoS Pathog.* 7:e1002327. doi: 10.1371/journal.ppat.1002327

Aoki, K., Kragler, F., Xoconostle-Cazares, B., and Lucas, W. J. (2002). A subclass of plant heat shock cognate 70 chaperones carries a motif that facilitates trafficking through plasmodesmata. *Proc. Natl. Acad. Sci. U.S.A.* 99, 16342–16347. doi: 10.1073/pnas.252427999

Avisar, D., Abu-Abied, M., Belausov, E., Sadot, E., Hawes, C., and Sparkes, I. A. (2009). A comparative study of the involvement of 17 Arabidopsis myosin family members on the motility of Golgi and other organelles. *Plant Physiol.* 150, 700–709. doi: 10.1104/pp.109.136853

Avisar, D., Prokhnevsky, A. I., Makarova, K. S., Koonin, E. V., and Dolja, V. V. (2008). Myosin XI-K is required for rapid trafficking of Golgi stacks, peroxisomes, and mitochondria in leaf cells of Nicotiana benthamiana. *Plant Physiol.* 146, 1098–1108. doi: 10.1104/pp.107.113647

Bailey, A. P., Koster, G., Guillermier, C., Hirst, E. M. A., MacRae, J. I., Lechene, C. P., et al. (2015). Antioxidant role for lipid droplets in a stem cell niche of Drosophila. *Cell* 163, 340–353. doi: 10.1016/j.cell.2015.09.020

Baluska, F., Cvrckova, F., Kendrick-Jones, J., and Volkmann, D. (2001). Sink plasmodesmata as gateways for phloem unloading. Myosin VIII and calreticulin as molecular determinants of sink strength? *Plant Physiol.* 126, 39–46. doi: 10.1104/pp.126.1.39

Barbosa, A. D., and Siniossoglou, S. (2017). Function of lipid droplet-organelle interactions in lipid homeostasis. *BBA-Mol. Cell Res.* 1864, 1459–1468. doi: 10.1016/j.bbamcr.2017.04.001

Bartz, R., Zehmer, J. K., Zhu, M. F., Chen, Y., Serrero, G., Zhao, Y. M., et al. (2007). Dynamic activity of lipid droplets: protein phosphorylation and GTP-mediated protein translocation. *J. Proteome Res.* 6, 3256–3265. doi: 10.1021/pr070158j

Beller, M., Sztalryd, C., Southhall, N., Bell, M., Jackle, H., Auld, D. S., et al. (2008). COPI complex is a regulator of lipid homeostasis. *PLoS* 6:e292. doi: 10.1371/journal.pbio.0060292

Beller, M., Thiel, K., Thul, P. J., and Jackle, H. (2010). Lipid droplets: a dynamic organelle moves into focus. *FEBS Lett.* 584, 2176–2182. doi: 10.1016/j.febslet.2010.03.022

Berardini, T. Z., Reiser, L., Li, D. H., Mezheritsky, Y., Muller, R., Strait, E., et al. (2015). The Arabidopsis information resource: making and mining the "gold standard" annotated reference plant genome. *Genesis* 53, 474–485. doi: 10.1002/dvg.22877

Bersuker, K., and Olzmann, J. A. (2017). Establishing the lipid droplet proteome: mechanisms of lipid droplet protein targeting and degradation. *BBA-Mol. Cell Biol. L* 1862, 1166–1177. doi: 10.1016/j.bbalip.2017.06.006

Binns, D., Janusxewski, T., Chen, Y., Hill, J., Larkin, V. S., Zhao, Y., et al. (2006). An intimate collaboration between peroxisomes and lipid bodies. *J. Cell Bio.* 173, 719–731. doi: 10.1083/jcb.200511125

Boston, R. S., Viitanen, P. V., and Vierling, E. (1996). Molecular chaperones and protein folding in plants. *Plant Mol. Biol.* 32, 191–222. doi: 10.1007/BF00039383

Boström, P., Andersson, L., Rutberg, M., Perman, J., Lidberg, U., Johansson, B. R., et al. (2007). SNARE proteins mediate fusion between cytosolic lipid droplets and are implicated in insulin sensitivity. *Nat. Cell Biol.* 9, 1286–1293. doi: 10.1038/ncb1648

Boye, T. L., Jeppesen, J. C., Maeda, K., Pezeshkian, W., Solovyeva, V., Nylandsted, J., et al. (2018). Annexins induce curvature on free-edge membranes displaying distinct morphologies. *Sci. Rep.* 8:10309. doi: 10.1038/s41598-018-28481-z

Brasaemle, D. L., Dolios, G., Shapiro, L., and Wang, R. (2004). Proteomic analysis of proteins associated with lipid droplets of basal and lipolytically stimulated 3T3-L1 adipocytes. *J. Biol. Chem.* 279, 46835–46842. doi: 10.1074/jbc.M409340200

Brault,M. L., Petit, J. D., Immel, F., Nicolas, W. J., Glavier, M., Brocard, L., et al. (2019). Multiple C2 domains and transmembrane region proteins (MCTPs) tether membranes at plasmodesmata. *EMBO Rep.* 20:e47182. doi: 10.15252/embr.201847182

Brocard, L., Immel, F., Coulon, D., Esnay, N., Tuphile, K., Pascal, S., et al. (2017). Proteomic analysis of lipid droplets from Arabidopsis aging leaves brings new insight into their biogenesis and functions. *Front. Plant Sci.* 8:894. doi: 10.3389/fpls.2017.00894

Burch-Smith, T. M., and Zambryski, P. C. (2011). Plasmodesmata paradigm shift: regulation from without versus within. *Annu. Rev. Plant Biol.* 63, 239–260. doi: 10.1146/annurev-arplant-042811-105453

Cai, Y. Q., Goodman, J. M., Pyc, M., Mullen, R. T., Dyer, J. M., and Chapman, K. D. (2015). Arabidopsis SEIPIN proteins modulate triacylglycerol accumulation and influence lipid droplet proliferation. *Plant Cell* 27, 2616–2636. doi: 10.1105/tpc.15.00588

Cermelli, S., Guo, Y., Gross, S. P., and Welte, M. A. (2006). The lipid-droplet proteome reveals that droplets are a protein-storage depot. *Curr. Biol.* 16, 1783–1795. doi: 10.1016/j.cub.2006.07.062

Chen, J. C. F., Tsai, C. C. Y., and Tzen, J. T. C. (1999). Cloning and secondary structure analysis of caleosin, a unique calcium-binding protein in oil bodies of plant seeds. *Plant Cell Physiol.* 40, 1079–1086. doi: 10.1093/oxfordjournals.pcp.a029490

Clark, G. B., Morgan, R. O., Fernandez, M. P., and Roux, S. J. (2012). Evolutionary adaptation of plant annexins has diversified their molecular structures, interactions and functional roles. *New Phytol.* 196, 695–712. doi: 10.1111/j.1469-8137.2012.04308.x

Coulon, D., Brocard, L., Tuphile, K., and Brehelin, C. (2020). Arabidopsis LDIP protein locates at a confined area within the lipid droplet surface and favors lipid droplet formation. *Biochimie* 169, 29–40. doi: 10.1016/j.biochi.2019.09.018

D'Andrea, S. (2016). Lipid droplet mobilization: the different ways to loosen the purse strings. *Biochimie* 120, 17–27. doi: 10.1016/j.biochi.2015.07.010

Deeks, M. J., and Hussey, P. J. (2005). Arp2/3 and scar: plants move to the fore. *Nat. Rev. Mol. Cell Biol.* 6, 954–964. doi: 10.1038/nrm1765

Delmer, D. P., and Potikha, T. S. (1997). Structures and functions of annexins in plants. *Cell. Mol. Life Sci.* 53, 546–553. doi: 10.1007/s000180050070

Deruyffelaere, C., Bouchez, I., Morin, H., Guillot, A., Miquel, M., Froissard, M., et al. (2015). Ubiquitin-mediated proteasomal degradation of oleosins is involved in oil body mobilization during post-germinative seedling growth in Arabidopsis. *Plant Cell Physiol.* 56, 1374–1387. doi: 10.1093/pcp/pcv056

Deruyffelaere, C., Purkrtova, Z., Bouchez, I., Collet, B., Cacas, J. L., Chardot, T., et al. (2018). PUX10 is a CDC48A Adaptor protein that regulates the extraction of ubiquitinated oleosins from seed lipid droplets in Arabidopsis. *Plant Cell* 30, 2116–2136. doi: 10.1105/tpc.18.00275

Diao, M., Ren, S., Wang, Q., Qian, L., Shen, J., Liu, Y., et al. (2018). Arabidopsis formin 2 regulates cell-to-cell trafficking by capping and stabilizing actin filaments at plasmodesmata. *eLife* 7:e36316. doi: 10.7554/eLife.36316

Ding, B., Kwon, M. O., and Warnberg, L. (1996). Evidence that actin filaments are involved in controlling the permeability of plasmodesmata in tobacco mesophyll. *Plant J.* 10, 157–164. doi: 10.1046/j.1365-313X.1996.10010157.x

Eastmond, P. J. (2006). SUGAR-DEPENDENT1 encodes a patatin domain triacylglycerol lipase that initiates storage oil breakdown in germinating Arabidopsis seeds. *Plant Cell* 18, 665–675. doi: 10.1105/tpc.105.040543

Esau, K., and Charvat, I. D. (1975). An ultrastructural study of acid phosphatase localization in cells of Phaseolus vulgaris phloem by the use of the azo dye method. *Tissue Cell,* 7, 619–630. doi: 10.1016/0040-8166(75)90031-2

Faulkner, C., and Maule, A. (2011). Opportunities and successes in the search for plasmodesmal proteins. *Protoplasma* 248, 27–38. doi: 10.1007/s00709-010-0213-x

Fernandez-Calvino, L., Faulkner, C., Walshaw, J., Saalbach, G., Bayer, E., Benitez-Alfonso, Y., et al. (2011). Arabidopsis plasmodesmal proteome. *PLoS ONE* 6:e18880. doi: 10.1371/journal.pone.0018880

Fernández-Santaso, R., Izquierdo, Y., López, A., Muniz, L., Martinez, M., Cascóm, T., et al. (2020). Protein profiles of lipid droplets during the hypersensitive

defense response of Arabidopsis against Pseudomonas infection. *Plant Cell Physiol.* 61, 1144–1157. doi: 10.1093/pcp/pcaa041

Fiserova, J., Schwarzerova, K., Petrasek, J., and Opatrny, Z. (2006). ARP2 and ARP3 are localized to sites of actin filament nucleation in tobacco BY-2 cells. *Protoplasma* 227, 119–128. doi: 10.1007/s00709-006-0146-6

Fujimoto, Y., Itabe, H., Sakai, J., Makita, M., Noda, J., Mori, M., et al. (2004). Identification of major proteins in the lipid droplet fraction isolated from the human hepathocyt cell line HuH7. *Biochim. Biophys. Acta* 1644, 47–59. doi: 10.1016/j.bbamcr.2003.10.018

Gao, Q., and Goodman, J. M. (2015). The lipid droplet-a well-connected organelle. *Front. Cell Devel. Biol.* 3:49. doi: 10.3389/fcell.2015.00049

Gidda, S. K., Park, S., Pyc, M., Yurchenko, O., Cai, Y. Q., Wu, P., et al. (2016). Lipid droplet-associated proteins (LDAPs) are required for the dynamic regulation of neutral lipid compartmentation in plant cells. *Plant Physiol.* 170, 2052–2071. doi: 10.1104/pp.15.01977

Gidda, S. K., Shockey, J. M., Rothstein, S. J., Dyer, J. M., and Mullen, R. T., (2009). *Arabidopsis thaliana*GPAT8 and GPAT9 are localized to the ER and possess distinct ER retrieval signals: functionaldivergence of the dilysine ER retrieval motif in plant cells. *Plant Physiol. Biochem.* 47, 867–879. doi: 10.1016/j.plaphy.2009.05.008

Golomb, L., Abu-Abied, M., Belausov, E., and Sadot, E. (2008). Different subcellular localizations and functions of Arabidopsis myosin VIII. *BMC Plant Biol.* 8:3. doi: 10.1186/1471-2229-8-3

Gunjan, A., and Verreault, A. (2003). A Rad53 kinase-dependent surveillsnce mechanism 3that regulates histone protein levels6 in S. *cerevisiae. Cell* 115, 537–549. doi: 10.1016/S0092-8674(03)00896-1

Guo, Y., Cordes, K. R., Farese, R. V., and Walther, T. C. (2009). Lipid droplets at a glance. *J. Cell Sci.* 122, 749–752. doi: 10.1242/jcs.037630

Han, X., Huang, L.-J., Feng, D., Jiang, W., Miu, W., and Li, N. (2019). Plasmodemata-related structural and functional proteins: the long-sought-after secrets of a cytoplasmic channel in plant cell walls. *Int. J. Mol. Sci.* 20:2946. doi: 10.3390/ijms20122946

Hashimoto, K., Igarashi, H., Mano, S., Takenaka, C., Shiina, T., Yamaguchi, M., et al. (2008). An isoform of Arabidopsis myosin XI interacts with small GTPases in its C-terminal tail region. *J. Exp. Bot.* 59, 3523–3531. doi: 10.1093/jxb/ern202

Heinlein, M. (2015a). "Plasmodesmata," in *Methods and Protocols. Methods in Molecular Biology*, ed. M. Heinlein (New York, NY: Springer), 346. doi: 10.1007/978-1-4939-1523-1

Heinlein, M. (2015b). "Plasmodesmata: channnels for viruses on the move," in *Plasmodesmata. Methods and Protocols. Methods in Molecular Biology*, ed. M. Heinlein (New York, NY: Springer) 25–52. doi: 10.1007/978-1-4939-1523-1_2

Hodges, B. D. M., and Wu, C. C. (2010). Proteomic insights into an expanded cellular role for cytoplasmic lipid droplets. *J. Lipid Res.* 51, 262–273. doi: 10.1194/jlr.R003582

Horn, P. J., James, C. N., Gidda, S. K., Kilaru, A., Dyer, J. M., Mullen, R. T., et al. (2013). Identification of a new class of lipid droplet-associated proteins in plants. *Plant Physiol.* 162, 1926–1936. doi: 10.1104/pp.113.222455

Hsiao, E. S. L., and Tzen, J. T. C. (2011). Ubiquitination of oleosin-H and caleosin in sesame oil bodies after seed germination. *Plant Physiol. Biochem.* 49, 77–81. doi: 10.1016/j.plaphy.2010.10.001

Hsieh, K., and Huang, A. H. C. (2004). Endoplasmic reticulum, oleosins, and oils in seeds and tapetum cells. *Plant Physiol.* 136, 3427–3434. doi: 10.1104/pp.104.051060

Huang, A. H. C. (1992). Oilbodies and oleosins in seeds. *Annu. Rev. Plant Physiol. Plant Mol. Biol.* 43, 177–200. doi: 10.1146/annurev.pp.43.060192.001141

Huang, A. H. C. (2018). Plant lipid droplets and their associated proteins: potential for rapid advances. *Plant Physiol.* 176, 1894–1918. doi: 10.1104/pp.17.01677

Huang, C. Y., and Huang, A. H. C. (2017). Unique motifs and length of hairpin in oleosin target the cytosolic side of endoplasmic reticulum and budding lipid droplet. *Plant Physiol.* 174, 2248–2260. doi: 10.1104/pp.17.00366

Huang, S. X., Jiang, L. W., and Zhuang, X. H. (2019). Possible roles of membrane trafficking components for lipid droplet dynamics in higher plants and green algae. *Front. Plant Sci.* 10:207. doi: 10.3389/fpls.2019.00207

Jolivet, P., Roux, E., d'Andrea, S., Davanture, M., Negroni, L., Zivy, M., et al. (2004). Protein composition of oil bodies in Arabidopsis thaliana ecotype WS. *Plant Physiol. Biochem.* 42, 501–509. doi: 10.1016/j.plaphy.2004.04.006

Kandasamy, M. K., Gilliland, L. U., McKinney, E. C., and Meagher, R. B. (2001). One plant actin isovariant, ACT7, is induced by auxin and required for normal callus formation. *Plant Cell* 13, 1541–1554. doi: 10.1105/TPC.010026

Kandasamy, M. K., McKinney, E. C., and Meagher, R. B. (2009). A Single vegetative actin isovariant overexpressed under the control of multiple regulatory sequences is sufficient for normal Arabidopsis development. *Plant Cell* 21, 701–718. doi: 10.1105/tpc.108.061960

Karimi, M., Inze, D., and Depicker, A. (2002). GATEWAY((TM)) vectors for Agrobacterium-mediated plant transformation. *Trends Plant Sci.* 7, 193–195. doi: 10.1016/S1360-1385(02)02251-3

Karlson, D. T., Fujino, T., Kimura, S., Baba, K., Itoh, T., and Ashworth, E. N. (2003). Novel plasmodesmata association of dehydrin-like proteins in cold-acclimated red-osier dogwood (Cornus sericea). *Tree Physiol.* 23, 759–767. doi: 10.1093/treephys/23.11.759

Katyayini, N. U., Rinne, P. L. H., and van der Schoot, C. (2019). Strigolactone-based node-to-bud signaling may restrain shoot branching in hybrid aspen. *Plant Cell Physiol.* 60, 2797–2811. doi: 10.1093/pcp/pcz170

Kim, E. Y., Park, K. Y., Seo, Y. S., and Kim, W. T. (2016). Arabidopsis small rubber particle protein homolog SRPs play dual roles as positive factors for tissue growth and development and in drought stress responses. *Plant Physiol.* 170, 2494–2510. doi: 10.1104/pp.16.00165

Kitagawa, M., and Jackson, D. (2017). Plasmodesmata-mediated cell-to-cell communication in the shoot apical meristem: how stem cells talk. *Plants* 6:12. doi: 10.3390/plants6010012

Knox, K., Wang, P. W., Kriechbaumer, V., Tilsner, J., Frigerio, L., Sparkes, I., et al. (2015). Putting the squeeze on plasmodesmata: arole for reticulons in primary plasmodesmata formation. *Plant Physiol.* 168, 1563–1572. doi: 10.1104/pp.15.00668

Kory, N., Thiam, A. R., Farese, R. V., and Walther, T. C. (2015). Protein crowding is a determinant of lipid droplet protein composition. *Dev. Cell* 34, 351–363. doi: 10.1016/j.devcel.2015.06.007

Krahmer, N., Hilger, M., Kory, N., Wilfling, F., Stoehr, G., Mann, M., et al. (2013). Protein correlation profiles identify lipid droplet proteins with high confidence. *Mol. Cell. Proteomics* 12, 1115–1126. doi: 10.1074/mcp.M112.020230

Kretzschmar, F. K., Doner, N. M., Krawczyk, H. E., Scholz, P., Schmitt, K., Valerius, O., et al. (2020). Identification of low-abundance lipid droplet proteins in seeds and seedlings. *Plant Physiol.* 182, 1326–1345. doi: 10.1104/pp.19.01255

Kretzschmar, F. K., Mengel, L. A., Muller, A. O., Schmitt, K., Blersch, K. F., Valerius, O., et al. (2018). PUX10 is a lipid droplet-localized scaffold protein that interacts with CELL DIVISION CYCLE48 and is involved in the degradation of lipid droplet proteins. *Plant Cell* 30, 2137–2160. doi: 10.1105/tpc.18.00276

Kriechbaumer, V., Botchway, S. W., Slade, S. E., Knox, K., Frigerio, L., Oparka, K., et al. (2015). Reticulomics: protein-protein interaction studies with two plasmodesmata-localized reticulon family proteins identify binding partners enriched at plasmodesmata, endoplasmic reticulum, and the plasma membrane. *Plant Physiol.* 169, 1933–1945. doi: 10.1104/pp.15.01153

Kriechbaumer, V., von Loffelholz, O., and Abell, B. M. (2012). Chaperone receptors: guiding proteins to intracellular compartments. *Protoplasma* 249, 21–30. doi: 10.1007/s00709-011-0270-9

Lee, K. H., Minami, A., Marshall, R. S., Book, A. J., Farmer, L. M., Walker, J. M., et al. (2011). The RPT2 Subunit of the 26S proteasome directs complex assembly, histone dynamics, and gametophyte and sporophyte development in Arabidopsis. *Plant Cell* 23, 4298–4317. doi: 10.1105/tpc.111.089482

Leijon, F., Melzer, M., Zhou, Q., Srivastava, V., and Bulone, V. (2018). Proteomic analysis of plasmodesmata from Populus cell suspension cultures in relation with callose biosynthesis. *Front. Plant Sci.* 9:1681. doi: 10.3389/fpls.2018.01681

Li, Z. H., Thiel, K., Thul, P. J., Beller, M., Kuhnlein, R. P., and Welte, M. A. (2012). Lipid droplets control the maternal histone supply of Drosophila embryos. *Curr. Biol.* 22, 2104–2113. doi: 10.1016/j.cub.2012.09.018

Listenberger, L. L., Han, X. L., Lewis, S. E., Cases, S., Farese, R. V., Ory, D. S., et al. (2003). Triglyceride accumulation protects against fatty acid-induced lipotoxicity. *Proc. Natl. Acad. Sci. U.S.A.* 100, 3077–3082. doi: 10.1073/pnas.0630588100

Liu, P. S., Ying, Y. S., Zhao, Y. M., Mundy, D. I., Zhu, M. F., and Anderson, R. G. W. (2004). Chinese hamster ovary K2 cell lipid droplets appear to be metabolic organelles involved in membrane traffic. *J. Biol. Chem.* 279, 3787–3792. doi: 10.1074/jbc.M311945200

Liu, Z., Jia, Y., Ding, Y., Shi, Y., Li, Z., Guo, Y., et al. (2017). Plasma membrane CRK1-mediated phosphorylation of 14-3-3 proteins induces their nuclear

import to fine-tune CBF signalling during cold response. *Mol. Cell* 66, 117–128. doi: 10.1016/j.molcel.2017.02.016

Lizaso, A., Tan, K. T., and Lee, Y. H. (2013). Beta-adrenergic receptor-stimulated lipolysis requires the RAB7-mediated autolysosomal lipid degradation. *Autophagy* 9, 1228–1243. doi: 10.4161/auto.24893

Ma, B. Y., Qian, D., Nan, Q., Tan, C., An, L. Z., and Xiang, Y. (2012). Arabidopsis vacuolar H+-ATPase (V-ATPase) B subunits are involved in actin cytoskeleton remodeling via binding to, bundling, and stabilizing F-actin. *J. Biol. Chem.* 287, 19008–19017. doi: 10.1074/jbc.M111.281873

Martin, S., Driessen, K., Nixon, S. J., Zerial, M., and Parton, R. G. (2005). Regulated localization of Rab18 to lipid droplets: effects of lipolytic stimulation and inhibition of lipid droplet catabolism. *J. Biol. Chem.* 280, 42325–42335. doi: 10.1074/jbc.M506651200

Mathur, J., Mathur, N., and Hulskamp, M. (2002). Simultaneous visualization of peroxisomes and cytoskeletal elements reveals actin and not microtubule-based peroxisome motility in plants. *Plant Physiol.* 128, 1031–1045. doi: 10.1104/pp.011018

McDowell, J. M., An, Y. Q., Huang, S. R., McKinney, E. C., and Meagher, R. B. (1996). The Arabidopsis ACT7 actin gene is expressed in rapidly developing tissues and responds to several external stimuli. *Plant Physiol.* 111, 699–711. doi: 10.1104/pp.111.3.699

Meitha, K., Konnerup, D., Colmer, T. D., Considine, J. A., Foyer, C. H., and Considine, M. J. (2015). Spatio-temporal relief from hypoxia and production of reactive oxygen species during bud burst in grapevine (Vitis vinifera). *Ann. Bot.* 116, 703–711. doi: 10.1093/aob/mcv123

Mongrand, S., Stanislas, T., Bayer, E. M. F., Lherminier, J., and Simon-Plas, F. (2010). Membrane rafts in plant cells. *Trends Plant. Sci.* 15, 656–663. doi: 10.1016/j.tplants.2010.09.003

Müller, A. O., and Ischbeck, T. (2018). Characterization of the enzymatic activity and physiological function of the lipid droplet-associated triacylglycerol lipase AtOBL1. *New Phyol.* 217, 1062–1076. doi: 10.1111/nph.14902

Murphy, D. J. (2012). The dynamic roles of intracellular lipid droplets: from archaea to mammals. *Protoplasma* 249, 541–585. doi: 10.1007/s00709-011-0329-7

Murphy, S., Martin, S., and Parton, R. G. (2009). Lipid droplet-organelle interactions; sharing the fats. *BBA-Mol. Cell Biol. L* 1791, 441–447. doi: 10.1016/j.bbalip.2008.07.004

Nakamura, N., Banno, Y., and Tamiya-Koizumi, K. (2005). Arf1-dependent PLD1 is localized to oleic-acid-induced lipid droplets in NIH3T3 cells. *Biochem. Biophys. Res. Commmun.* 335, 117–123. doi: 10.1016/j.bbrc.2005.07.050

Nesvizhskii, A. I., Keller, A., Kolker, E., and Aebersold, R. (2003). A statistical model for identifying proteins by tandem mass spectrometry. *Anal. Chem.* 75, 4646–4658. doi: 10.1021/ac0341261

O'Fallon, J. V. O., Busboom, J. R., Nelson, M. L., and Gaskin, C. T. (2007). A direct method for fatty acid methyl ester synthesis: application to wet meat tissues, oils, and feedstuffs. *J. Anim. Sci.* 85, 1511–1521. doi: 10.2527/jas.2006-491

Ophir, R., Pang, X. Q., Halaly, T., Venkateswari, J., Lavee, S., Galbraith, D., et al. (2009). Gene-expression profiling of grape bud response to two alternative dormancy-release stimuli expose possible links between impaired mitochondrial activity, hypoxia, ethylene-ABA interplay and cell enlargement. *Plant Mol. Biol.* 71, 403–423. doi: 10.1007/s11103-009-9531-9

Ozeki, S., Xheng, J., Tauchi-Satu, K., Hatano, N., Taniguchi, H., and Fujimoto, T. (2005). Rab18 localizes to lipid droplets and induces their close apposition to the endoplasmic reticulum-derived membrane. *J. Cell Sci.* 118, 2601–2611. doi: 10.1242/jcs.02401

Paul, L. K., Rinne, P. L. H., and van der Schoot, C. (2014a). Refurbishing the plasmodesmal chamber: a role for lipid bodies? *Front. Plant Sci.* 5:40. doi: 10.3389/fpls.2014.00040

Paul, L. K., Rinne, P. L. H., and van der Schoot, C. (2014b). Shoot meristems of deciduous woody perennials: self-organization and morphogenetic transitions. *Curr. Opin. Plant Biol.* 17, 86–95. doi: 10.1016/j.pbi.2013.11.009

Peremyslov, V. V., Cole, R. A., Fowler, J. E., and Dolja, V. V. (2015). Myosin-powered membrane compartment drives cytoplasmic streaming, cell expansion and plant development. *PLoS ONE* 10:e0139331. doi: 10.1371/journal.pone.0139331

Perez-Riverol, Y., Csordas, A., Bai, J. W., Bernal-Llinares, M., Hewapathirana, S., Kundu, D. J., et al. (2019). The PRIDE database and related tools and resources in 2019: improving support for quantification data. *Nucleic Acids Res.* 47, D442–D450. doi: 10.1093/nar/gky1106

Pinheiro, H., Samalova, M., Geldner, N., Chory, J., Martinez, A., and Moore, I. (2009). Genetic evidence that the higher plant Rab-D1 and Rab-D2 GTPases exhibit distinct but overlapping interactions in the early secretory pathway. *J. Cell Sci.* 122, 3749–3758. doi: 10.1242/jcs.050625

Ploegh, H. L. (2007). A lipid-based model for the creation of an escape hatch from the endoplasmic reticulum. *Nature* 448, 435–438. doi: 10.1038/nature06004

Pyc, M., Cai, Y. Q., Gidda, S. K., Yurchenko, O., Park, S., Kretzschmar, F. K., et al. (2017). Arabidopsis lipid droplet-associated protein (LDAP) interacting protein (LDIP) influences lipid droplet size and neutral lipid homeostasis in both leaves and seeds. *Plant J.* 92, 1182–1201. doi: 10.1111/tpj.13754

Quettier, A. L., and Eastmond, P. J. (2009). Storage oil hydrolysis during early seedling growth. *Plant Physiol. Biochem.* 47, 485–490. doi: 10.1016/j.plaphy.2008.12.005

Reagan, B. C., and Burch-Smith, T. M. (2020). Viruses reveal the secrets of plasmodesmal cell biology. *Mol. Plant Microb. Int.* 33, 26–39. doi: 10.1094/MPMI-07-19-0212-FI

Rinne, P. L. H., Kaikuranta, P. M., and van der Schoot, C. (2001). The shoot apical meristem restores its symplasmic organization during chilling-induced release from dormancy. *Plant J.* 26, 249–264. doi: 10.1046/j.1365-313X.2001.01022.x

Rinne, P. L. H., Paul, L. K., Vahala, J., Ruonala, R., Kangasjarvi, J., and van der Schoot, C. (2015). Long and short photoperiod buds in hybrid aspen share structural development and expression patterns of marker genes. *J. Exp. Bot.* 66, 6745–6760. doi: 10.1093/jxb/erv380

Rinne, P. L. H., and van der Schoot, C. (1998). Symplasmic fields in the tunica of the shoot apical meristem coordinate morphogenetic events. *Development* 125, 1477–1485. doi: 10.1242/dev.125.8.1477

Rinne, P. L. H., and van der Schoot, C. (2003). Plasmodesmata at the crossroads between development, dormancy, and defense. *Can J. Bot.* 81, 1182–1197. doi: 10.1139/b03-123

Rinne, P. L. H., and van der Schoot, C. (2004). Cell-cell communication as a key factor in dormancy cycling. *J. Crop Improv.* 10, 113–156. doi: 10.1300/J411v10n01_07

Rinne, P. L. H., Welling, A., Vahala, J., Ripel, L., Ruonala, R., Kangasjarvi, J., et al. (2011). Chilling of dormant buds hyperinduces FLOWERING LOCUS T and recruits GA-inducible 1,3-beta-glucanases to reopen signal conduits and release dormancy in Populus. *Plant Cell* 23, 130–146. doi: 10.1105/tpc.110.081307

Sager, R., and Lee, J. Y. (2014). Plasmodesmata in integrated cell signalling: insights from development and environmental signals and stresses. *J. Exp. Bot.* 65, 6337–6358. doi: 10.1093/jxb/eru365

Sagi, G., Katz, A., Guenoune-Gelbart, D., and Epel, B. L. (2005). Class 1 reversibly glycosylated polypeptides are plasmodesmal-associated proteins delivered to plasmodesmata via the Golgi apparatus. *Plant Cell* 17, 1788–1800 doi: 10.1105/tpc.105.031823

Sato, S., Fukasamwa, M., Yamakawa, Y., Natsume, T., Suzuki, T., Shoji, L., et al. (2006). Proteomic profiling of lipid droplet proteins in hepatoma cell lines expressing hepatits C virus core protein. *J. Biochem.* 139, 921–930. doi: 10.1093/jb/mvj104

Schroeder, B.,Schulze, R. J., Weller, S., Sletten, A. C., Casey, C. A., and Mcniven, M. A. (2015). The small GTPase Rab7 as a central regulator of hepatocellular lipophagy. *Hepatology* 61, 1896–1907. doi: 10.1002/hep.27667

Schutze, K., Harter, K., and Chaban, C. (2009). Bimolecular fluorescence complementation (BiFC) to study protein-protein interactions in living plant cells. *Methods Mol. Biol.* 479, 189–202. doi: 10.1007/978-1-59745-289-2_12

Shimada, T. L., Hayashi, M., and Hara-Nishimura, I. (2018). Membrane dynamics and multiple functions of oil bodies in seeds and leaves. *Plant Physiol.* 176, 199–207. doi: 10.1104/pp.17.01522

Shimada, T. L., Shimada, T., Takahashi, H., Fukao, Y., and Hara-Nishimura, I. (2008). A novel role for oleosins in freezing tolerance of oilseeds in Arabidopsis thaliana. *Plant J.* 55, 798–809. doi: 10.1111/j.1365-313X.2008.03553.x

Shockey, J. M., Gidda, S. K., Chapital, D. C., Kuan, J. C., Dhanoa, P. K., Bland, J. M., et al. (2006). Tung tree DGAT1 and DGAT2 have nonredundant functions in triacylglycerol biosynthesis and are localized to different subdomains of the endoplasmic reticulum. *Plant Cell* 18, 2294–2313. doi: 10.1105/tpc.106.043695

Siloto, R. M. P., Findlay, K., Lopez-Villalobos, A., Yeung, E. C., Nykiforuk, C. L., and Moloney, M. M. (2006). The accumulation of oleosins determines

the size of seed oilbodies in Arabidopsis. *Plant Cell* 18, 1961–1974. doi: 10.1105/tpc.106.041269

Sollner, T. H. (2007). Lipid droplets highjack SNAREs. *Nat. Cell Biol.* 9, 1219–1220. doi: 10.1038/ncb1107-1219

Soni, K. G., Mardones, G. A., Sougrat, R., Smirnova, E., Jackson, C. L., and Bonifacino, J. S. (2009). Coatomer-dependent protein delivery to lipid droplets. *J. Cell Sci.* 122, 1834–1841. doi: 10.1242/jcs.045849

Sparkes, I. A., Teanby, N. A., and Hawes, C. (2008). Truncated myosin XI tail fusions inhibit peroxisome, Golgi, and mitochondrial movement in tobacco leaf epidermal cells: a genetic tool for the next generation. *J. Exp. Bot.* 59, 2499–2512. doi: 10.1093/jxb/ern114

Su, S. Z., Liu, Z. H., Chen, C., Zhang, Y., Wang, X., Zhu, L., et al. (2010). Cucumber mosaic virus movement protein severs actin filaments to increase the plasmodesmal size exclusion limit in tobacco. *Plant Cell* 22, 1373–1387. doi: 10.1105/tpc.108.064212

Sundell, D., Mannapperuma, C., Netotea, S., Delhomme, N., Lin, Y. C., Sjodin, A., et al. (2015). The plant genome integrative explorer resource: PlantGenIE.org. *New Phytol.* 208, 1149–1156. doi: 10.1111/nph.13557

Suwastika, I. N., Uemura, T., Shiina, T., Sato, M. H., and Takeyasu, K. (2008). SYP71, a Plant-specific Qc-SNARE protein, reveals dual localization to the plasma membrane and the endoplasmic reticulum in Arabidopsis. *Cell Struct. Funct.* 33, 185–192. doi: 10.1247/csf.08024

Thazar-Poulot, N., Miquel, M., Fobis-Loisy, I., and Gaude, T. (2015). Peroxisome extensions deliver the Arabidopsis SDP1 lipase to oil bodies. *Proc. Natl. Acad. Sci. U.S.A.* 112, 4158–4163. doi: 10.1073/pnas.1403322112

Turro, S., Ingelmo-Torres, M., Estanyol, M., Tebar, F., Fernández, M. A., Albor, C. V., et al. (2006). Identification and characterization of associated with lipid droplet protein 1: a novel membrane assocaiated protein that resids on hepatic lipid droplets. *Traffic* 7, 1254–1269. doi: 10.1111/j.1600-0854.2006.00465.x

Tzen, J. T. C., and Huang, A. H. C. (1992). Surface-structure and properties of plant seed oil bodies. *J. Cell Biol.* 117, 327–335. doi: 10.1083/jcb.117.2.327

Umlauf, E., Csaszar, E., Moertelmaier, M., Schuetz, G. J., Parton, R. G., and Prohaska, R. (2004). Association of stomatin with lipid bodies. *J. Biol. Chem.* 279, 23699–23709. doi: 10.1074/jbc.M310546200

Vaddepalli, P., Fulton, L., Wieland, J., Wassmer, K., Schaeffer, M., Ranf, S., et al. (2017). The cell wall-localized atypical beta-1,3 glucanase ZERZAUST controls tissue morphogenesis in Arabidopsis thaliana. *Development* 144, 2259–2269. doi: 10.1242/dev.152231

Van Damme, D., van Poucke, K., Boutant, E., Ritzenthaler, C., Inz,é, D., and Geelen, D. (2004). *In vivo* dynamics and differential microtubule-binding activities of MAP65 proteins. *Plant Physiol.* 136, 3956–3967. doi: 10.1104/pp.104.051623

van der Schoot, C., Paul, L. K., Paul, S. B., and Rinne, P. L. H. (2011). Plant lipid bodies and cell-cell signaling: a new role for an old organelle? *Plant Signal. Behav.* 6, 1732–1738. doi: 10.4161/psb.6.11.17639

van der Schoot, C., and Rinne, P. (1999). Networks for shoot design. *Trends Plant Sci.* 4, 31–37. doi: 10.1016/S1360-1385(98)01362-4

Van Gestel, K., Slegers, H., von Witsch, M., Samaj, J., Baluska, F., and Verbelen, J. P. (2003). Immunological evidence for the presence of plant homologues of the actin-related protein Arp3 in tobacco and maize: subcellular localization to actin-enriched pit fields and emerging root hairs. *Protoplasma* 222, 45–52. doi: 10.1007/s00709-003-0004-8

Veerabagu, M., Paul, L. K., Rinne, P. L. H., and van der Schoot, C. (2020). Plant lipid bodies traffic on actin to plasmodesmata motorized by myosin XIs. *Int. J. Mol. Sci.* 21:1422. doi: 10.3390/ijms21041422

Verma, R., Aravind, L., Oania, R., McDonald, W. H., Yates, J. R., Koonin, E. V., et al. (2002). Role of Rpn11 metalloprotease in deubiquitination and degradation by the 26S proteasome. *Science* 298, 611–615. doi: 10.1126/science.1075898

Vermachova, M., Purkrtova, Z., Santrucek, J., Jolivet, P., Chardot, T., and Kodicek, M. (2011). New protein isoforms identified within Arabidopsis thaliana seed oil bodies combining chymotrypsin/trypsin digestion and peptide fragmentation analysis. *Proteomics* 11, 3430–3434. doi: 10.1002/pmic.201000603

Voinnet, O., Lederer, C., and Baulcombe, D. C. (2000). A viral movement protein prevents spread of the gene silencing signal in *Nicotiana benthamiana*. *Cell* 103, 157–167. doi: 10.1016/S0092-8674(00)00095-7

Walther, T. C., and Farese, R. V. (2009). The life of lipid droplets. *BBA-Mol. Cell Biol. L* 1791, 459–466. doi: 10.1016/j.bbalip.2008.10.009

White, R. G., Badelt, K., Overall, R. L., and Vesk, M. (1994). Actin associated with plasmodesmata. *Protoplasma* 180, 169–184. doi: 10.1007/BF01507853

White, R. G., and Barton, D. A. (2011). The cytoskeleton in plasmodesmata: a role in intercellular transport? *J. Exp. Bot.* 62, 5249–5266. doi: 10.1093/jxb/err227

Wilfling, F., Thiam, A. R., Olarte, M. J., Wang, J., Beck, R., Gould, T. J., et al. (2014). Arf1/COPI machinery acts directly on lipid droplets and enables their connection to the ER for protein targeting. *Elife* 3:e01607. doi: 10.7554/eLife.01607

Wilfling, F., Wang, H., Haas, J. T., Krahmer, N., Gould, T. J., Uchida, A., et al. (2013). Triacylglycerol synthesis enzymes mediate lipid droplet growth by relocalizing from the ER to lipid droplets. *Dev. Cell.* 24, 384–399. doi: 10.1016/j.devcel.2013.01.013

Xu, X. M., Wang, J., Xuan, Z. Y., Goldshmidt, A., Borrill, P. G. M., Hariharan, N., et al. (2011). Chaperonins Facilitate KNOTTED1 Cell-to-cell trafficking and stem cell function. *Science* 333, 1141–e01144. doi: 10.1126/science.1205727

Zehmer, J. K., Huang, Y. G., Peng, G., Pu, J., Anderson, R. G. W., and Liu, P. S. (2009). A role for lipid droplets in inter-membrane lipid traffic. *Proteomics* 9, 914–921. doi: 10.1002/pmic.200800584

Zhang, J., Li, Y., Liu, B. B., Wang, L. J., Zhang, L., Hu, J. J., et al. (2018). Characterization of the Populus Rab family genes and the function of PtRabE1b in salt tolerance. *BMC Plant Biol.* 18:124. doi: 10.1186/s12870-018-1342-1

Zhi, Y., Taylor, M. C., Campbell, P. M., Warden, A. C., Shrestha, P., El Tahchy, A., et al. (2017). Comparative lipidomics and proteomics of lipid droplets in the mesocarp and seed tissues of Chinese Tallow (*Triadica sebifera*). *Front. Plant Sci.* 8:1339. doi: 10.3389/fpls.2017.01339

Conflict of Interest: The authors declare that the research was conducted in the absence of any commercial or financial relationships that could be construed as a potential conflict of interest.

frontiers in Plant Science

ORIGINAL RESEARCH
published: 29 July 2021
doi: 10.3389/fpls.2021.695415

Leaf Epidermis: The Ambiguous Symplastic Domain

Olga V. Voitsekhovskaja[1,2], Anna N. Melnikova[1,3], Kirill N. Demchenko[1], Alexandra N. Ivanova[1,3], Valeria A. Dmitrieva[1], Anastasiia I. Maksimova[1], Gertrud Lohaus[2,4], A. Deri Tomos[5], Elena V. Tyutereva[1] and Olga A. Koroleva[5]*

[1] Komarov Botanical Institute, Russian Academy of Sciences, Saint Petersburg, Russia, [2] Department of Plant Biochemistry, Albrecht von Haller Institute for Plant Sciences, Göttingen, Germany, [3] Saint Petersburg State University, Saint Petersburg, Russia, [4] Molecular Plant Research/Plant Biochemistry, School of Mathematics and Natural Sciences, University of Wuppertal, Wuppertal, Germany, [5] School of Biological Sciences, Bangor University, Bangor, United Kingdom

OPEN ACCESS

Edited by:
Jung-Youn Lee,
University of Delaware, United States

Reviewed by:
Chul Min Kim,
Wonkwang University, South Korea
John Larkin,
Louisiana State University, United States

***Correspondence:**
Olga V. Voitsekhovskaja
ovoitse@binran.ru

Specialty section:
This article was submitted to Plant Cell Biology, a section of the journal Frontiers in Plant Science

Received: *15 April 2021*
Accepted: *24 June 2021*
Published: *29 July 2021*

Citation:
Voitsekhovskaja OV, Melnikova AN, Demchenko KN, Ivanova AN, Dmitrieva VA, Maksimova AI, Lohaus G, Tomos AD, Tyutereva EV and Koroleva OA (2021) Leaf Epidermis: The Ambiguous Symplastic Domain. Front. Plant Sci. 12:695415. doi: 10.3389/fpls.2021.695415

The ability to develop secondary (post-cytokinetic) plasmodesmata (PD) is an important evolutionary advantage that helps in creating symplastic domains within the plant body. Developmental regulation of secondary PD formation is not completely understood. In flowering plants, secondary PD occur exclusively between cells from different lineages, e.g., at the L1/L2 interface within shoot apices, or between leaf epidermis (L1-derivative), and mesophyll (L2-derivative). However, the highest numbers of secondary PD occur in the minor veins of leaf between bundle sheath cells and phloem companion cells in a group of plant species designated "symplastic" phloem loaders, as opposed to "apoplastic" loaders. This poses a question of whether secondary PD formation is upregulated in general in symplastic loaders. Distribution of PD in leaves and in shoot apices of two symplastic phloem loaders, *Alonsoa meridionalis* and *Asarina barclaiana*, was compared with that in two apoplastic loaders, *Solanum tuberosum* (potato) and *Hordeum vulgare* (barley), using immunolabeling of the PD-specific proteins and transmission electron microscopy (TEM), respectively. Single-cell sampling was performed to correlate sugar allocation between leaf epidermis and mesophyll to PD abundance. Although the distribution of PD in the leaf lamina (except within the vascular tissues) and in the meristem layers was similar in all species examined, far fewer PD were found at the epidermis/epidermis and mesophyll/epidermis boundaries in apoplastic loaders compared to symplastic loaders. In the latter, the leaf epidermis accumulated sugar, suggesting sugar import from the mesophyll *via* PD. Thus, leaf epidermis and mesophyll might represent a single symplastic domain in *Alonsoa meridionalis* and *Asarina barclaiana*.

Keywords: *Alonsoa meridionalis*, *Asarina barclaiana*, *Hordeum vulgare*, *Solanum tuberosum*, leaf epidermis, phloem loading mode, secondary plasmodesmata, single cell sampling

INTRODUCTION

In land plants, cells can be connected by primary and/or secondary plasmodesmata (PD). Primary PD develop during cytokinesis and thus connect "sister cells" of the same cell lineage. In contrast, secondary PD develop *de novo,* i.e., post-cytokinetically, and can occur between "sister cells" as well as between cells which belong to different cell lineages. The ability to specifically enhance the extent of symplastic connectivity at any cell border by means of secondary PD formation represents an important evolutionary advantage, and not all vascular plants are able to develop secondary PD (Evkaikina et al., 2014). The exact mechanisms of the formation of secondary PD and the regulation of this process in different taxa of land plant are far from being completely understood.

In flowering plants, one of the best characterized examples of enhanced secondary PD formation is found in the minor veins of leaf species designated as symplastic phloem loaders (Gamalei, 1991; Van Bel and Gamalei, 1992). In symplastic phloem loaders, transfer of assimilates from the mesophyll into the phloem is assisted by highly developed PD at the boundary between bundle sheath cells and phloem companion cells. As these PD appear during the maturation of the leaf, i.e., after cell divisions have been completed, they represent secondary PD. The number of these PD can be very high in symplastic phloem loaders, especially in species that contain phloem companion cells of the "intermediary cell" and in "intermediary-cell-like" types (Gamalei, 1991; Batashev et al., 2013).

Several studies have suggested that apoplastic phloem loaders represent species with generally low PD frequencies between leaf cells and tissues, while species with generally abundant PD tend to represent symplastic phloem loaders (Gamalei, 1995; Turgeon and Medville, 2004). The overall symplastic connectivity of the cells of the leaf lamina has been proposed to correlate with the number of PD connecting bundle sheath and companion cells in the minor veins of leaf (Gamalei, 1995). This hypothesis was corroborated by the finding that the frequencies of PD between mesophyll cells correlate with the plasmodesmal frequencies at the phloem/mesophyll interface (considered as the indicator of the phloem loading mode, symplastic versus apoplastic) in several species as shown by Turgeon and Medville (2004). However, the question arises whether the high abundance of secondary PD across the mesophyll/phloem boundary of symplastic phloem loaders represents a systemic phenomenon of increased formation of secondary PD. At present, no technique is available to distinguish between secondary and primary PD at the cytological level. Thus, only the PD found between cells derived from different cell lineages, i.e., cells that never had a common division wall, can be safely considered as secondary, while boundaries between the cells of the same lineage are interpreted to contain a mixed population of both primary and secondary PD (Fitzgibbon et al., 2013).

Here, we compared the PD distribution between cells and cell layers in the leaves of four species from the following four different families: barley (*Hordeum vulgare*, Poaceae), potato (*Solanum tuberosum*, Solanaceae), *Alonsoa meridionalis* (Scrophulariaceae), and *Asarina barclaiana* (Plantaginaceae, formerly Scrophulariaceae). Barley and potato represent apoplastic phloem loaders (Riesmeier et al., 1994; Botha and Cross, 1997), while in *A. meridionalis* and *A. barclaiana,* phloem loading has a strong symplastic component (Voitsekhovskaja et al., 2006, 2009). We considered PD between leaf epidermis and mesophyll as secondary because epidermis and mesophyll originate from different cell lineages corresponding to the L1 and L2 layers, respectively in the leaf primordium (Satina and Blakeslee, 1941; Kang and Dengler, 2018). Moreover, in shoot apices of both *A. meridionalis* and *A. barclaiana*, the one-layered tunica of the meristem continuous with the protoderm of leaf primordia can be clearly distinguished, suggesting that like in many other species, cells of this layer represent an independent cell lineage also in *A. meridionalis* and *A. barclaiana* (**Supplementary Figure 1**). The PD between mesophyll cells as well as the PD between epidermal cells were considered as a mixture of primary and secondary PD, although some studies indicated that PD between mesophyll cells are predominantly primary (Oparka et al., 1999). To investigate the distribution of symplastic connections in leaf lamina, we labeled PD with antibodies raised against the PD-specific proteins, such as myosin VIII and calreticulin, respectively (Radford and White, 1998; Baluska et al., 1999; Reichelt et al., 1999; Schubert et al., 2013; Demchenko et al., 2014). We also compared the distribution of PD between cells and cell layers, L1, L2, and L3 in the shoot apical meristems (SAMs) of the same species using TEM. The results showed that the symplastic connectivity between cells of the epidermis, as well as at mesophyll/epidermis boundaries, is higher in the leaves of the symplastic loaders, *A. meridionalis* and *A. barclaiana*, compared to the apoplastic loaders, barley and potato, while no significant differences were detected for other cell boundaries. Moreover, in the species studied, the level of symplastic connectivity between mesophyll and epidermis was correlated with the ability of the latter to serve as a transient storage compartment for soluble sugars. Thus, in *A. meridionalis* and *A. barclaiana,* the leaf epidermis seems to form a symplastic domain together with the mesophyll.

MATERIALS AND METHODS

Plant Material

Alonsoa meridionalis O. Kuntze (Scrophulariaceae) and *Asarina barclaiana* Pennell (Plantaginaceae) were grown on pot soil in a controlled growth chamber (Sanyo Gallenkamp, Loughborough, Leicester UK) at 20°C under a 16 h light/8 h dark cycle and a photon flux of 500 μmol m^{-2} s^{-1} and 0.035% CO_2. Barley (*Hordeum vulgare* L.) was grown hydroponically at similar conditions. Potato plants (*Solanum tuberosum* L. cv. Désirée) were grown in a greenhouse under 12 h of supplemented artificial light of 400 μmol m^{-2} s^{-1} at 26°C and 12 h of dark at 18°C. All studies on whole leaves and on single cell samples were performed using mature fully expanded leaves (usually the third leaf from the top of the shoot). Samples of leaf tissue for immunolocalization studies were taken from the middle parts of the leaves. For TEM analyses of shoot apices, all species were sown from seeds and grown on soil in greenhouse under artificial

light of 150 μmol m^{-2} s^{-1}, at 16 h light/8 h dark cycle, at 21°C in the light and at 19°C in the dark. Apices of 14–30 day-old seedlings were fixed.

Inhibition of Assimilate Export From the Leaves

Leaves of *A. meridionalis* and *A. barclaiana* were detached from the plants 3 h after the beginning of the light period and placed in continuous light conditions with a photon flux of 150 μmol m^{-2} s^{-1} for 24 h, while the petioles were kept in a 2 mM $CaCl_2$ solution to favor the sealing of the phloem with callose (King and Zeevaart, 1974). Sugar concentrations were determined in single cell samples from leaves and in extracts of whole leaves after 24 h of light exposure.

Sampling of Single Cells

Single cell sap was extracted from individual cells from the upper epidermis and palisade mesophyll by glass microcapillary technique (Tomos et al., 1994). Prior to use, a microcapillary was back-filled with low-viscosity water-saturated paraffin oil (Sigma). Ejection of the single cell sample under oil allowed the determination of sugars (glucose, fructose, and sucrose) by an enzymatic assay described by Koroleva et al. (1997, 1998). The measurements were highly reliable in a concentration range between 2 and 200 mM.

Extraction and Analysis of Carbohydrates

Soluble carbohydrates were extracted from leaves with 80% ethanol at 80°C for 1 h. The extraction was repeated two times, and the extracts were combined, vacuum-dried, dissolved in ultra-pure water (Millipore), syringe-filtrated (0.45 μm cellulose-acetate; Schleicher and Schuell, Dassel, Germany), and stored at −80°C. For carbohydrate analysis by high-performance liquid chromatography (HPLC), an anion exchange column (CarboPAC10; Dionex Corp, Sunnyvale, CA, USA) was used. The column was eluted isocratically with 80 mM NaOH (J.T. Baker, England) with a flow rate of 1 ml min^{-1} using the LC-9A pump from Shimadzu (Kyoto, Japan). Sugars were detected by a thin layer of amperometric cell (ESA, Model 5200, Bedford, United States) with a gold electrode and a pulse amperometric detector (Coulochem II, Bedford, USA). The evaluation of chromatograms was performed using the integration program Peaknet 5.1 (Dionex, Idstein, Germany).

Transmission Electron Microscopy of Shoot Apices

Shoot apices were fixed with 2.5% glutaraldehyde in 0.1 M potassium phosphate buffer pH 7.2 and post-fixed in 1% osmium tetroxide in the same buffer. During dehydration in a graded ethanol series followed by a graded acetone series, the material was stained *en bloc* with 1% uranyl acetate in 70% ethanol for 1 h, and then embedded in epon resin (Sigma Aldrich, MO, United States). Ultrathin sections (60–70 nm) were cut with a diamond knife (Diatome, Switzerland) using a Leica EM UC7 ultramicrotome (Leica Microsystems, Wetzlar, Germany), double stained on grids with 1% uranyl acetate and 3% lead citrate, and observed at 120 kV with a Libra 120 Plus electron microscope (Zeiss, Germany). The PD connecting cells of L1, L2, or L3 layers were counted manually in three apices for each species. For each apex, 8–25 cells per cell boundary (L1/L1, L1/L2, L2/L2, L2/L3, and L3/L3, respectively) were analyzed.

Immunolocalization of Myosin VIII and Calreticulin in PD

Fixation, embedding, and sectioning of mature leaves were performed as described by Stumpe et al. (2006). The anti-myosin VIII-antibody (Reichelt et al., 1999) was diluted in the ratio, 1:100 in tris-buffered saline (TBS) containing 1% (w/v) bovine serum albumin (BSA). The anti-calreticulin antibody (Baluska et al., 1999) was diluted in the ratio, 1:200 in the same buffer. In negative controls, the primary antibody was omitted. The secondary antibody, goat anti-rabbit Alexa Fluor 488 (Molecular Probes, Eugene, OR, USA), was diluted in the ratio, 1:500 in TBS with 1% BSA. Semi-thin sections (8–10 μm) were mounted using the ProLong Gold Antifade kit (Molecular Probes, OR, United States). Immunofluorescence was detected using a BX51 microscope (Olympus Deutschland GmbH, Hamburg, Germany). Images were captured with an objective UPlanApo 40×/0.85 ∞/0.11–0.23 using a ColorView II digital camera and Cell F* image analytical software (Olympus Soft Imaging Solutions, Münster, Germany). Images shown in **Figures 1A,B** were obtained using AxioImager.Z1 Microscope (Carl Zeiss, Goettingen, Germany) and UPlanFI 100×/ 1.30 Oil ∞/0.17 C1 objective, an Axiocam 506 color digital camera and ZEN microscope software v. 3.3. **Supplementary Videos 1–8** showing views of different cell junctions in leaves of the species under study were recorded using the same microscope.

Transmission Electron Microscopy of Semi-Thin Sections Used for Immunohistochemistry

Leaf sections (10 μm) were prepared from barley leaf pieces embedded in Steedman's wax as described by Stumpe et al. (2006) using an Automatic rotary microtome Microm HM 360 (Zeiss, Jena, Germany) with the blade lock assembly precooled to +4°C at an ambient temperature below +21°C. Single sections were placed on square coverslips of 1.5 × 1.5 cm size, coated with filtrated egg white (one section per coverslip). Sections were stretched in a drop of distilled water preheated to +40°C pipetted on the coverslips, and dried at +23°C for 2 h. Coverslips with sections were placed in Petri dishes, and dewaxing, rehydration, and blocking were performed as described by Stumpe et al. (2006). A primary anti-calreticulin antibody raised in rabbit (Baluska et al., 1999) was diluted in the ratio, 1:200 in TBS containing 1% (w/v) BSA. An anti-rabbit Alexa Fluor 488-conjugated secondary antibody produced in goat (Molecular Probes, Eugene, OR, USA) was diluted in the ratio, 1:500 in TBS with 10% BSA. In the negative controls, the primary antibody was omitted. The sections were incubated with the primary antibody for 1 h, washed three times with TBS for 15 min, incubated with the secondary antibody for 2 h, and washed three times with TBS for 10 min. After labeling, the coverslips were glued to the bottom of the inner side of Petri dishes of 35 mm diameter using melt

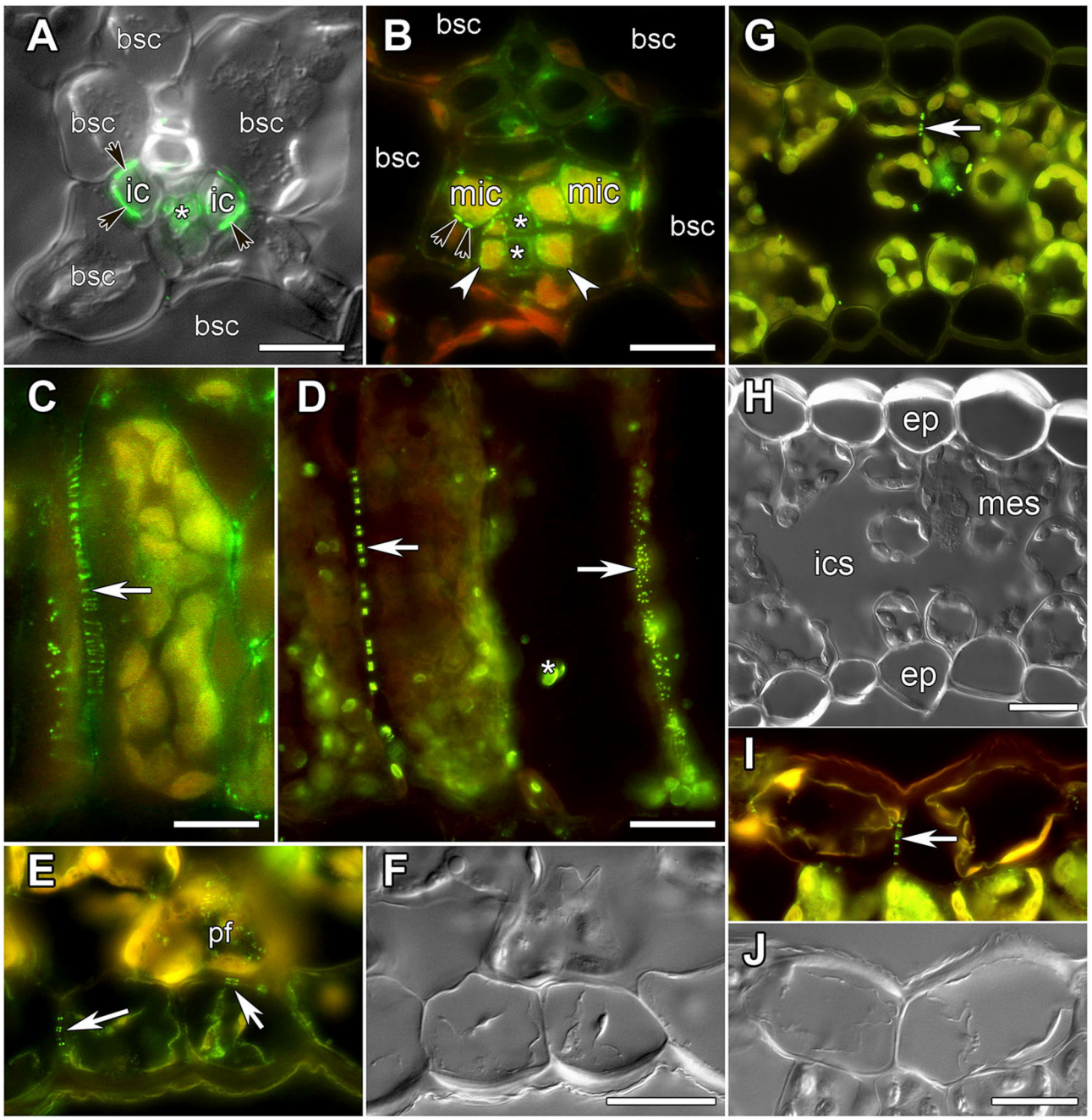

FIGURE 1 | Images of leaf sections obtained using either differential interference contrast **(A,F,H,J)** or epifluorescent microscopy **(A–E,G,I)** showing labeling of PD by immunolocalization of calreticulin **(A–D)** or myosin VIII **(E–J)**, respectively. **(A,C,I,J)** *Alonsoa meridionalis*; **(B,E,F)** *Asarina barclaiana*; **(D)** potato; **(G,H)** barley. **(A,B)** Minor veins. bsc, bundle sheath cell; ic, intermediary companion cells in *A. meridionalis*; mic, modified intermediary cells in *A. barclaiana*; white arrows point to transfer cells in *A. barclaiana*; black arrows point to PD fields between intermediary cells and bundle sheath cells in *A. meridionalis* and between modified intermediary cells and bundle sheath cells in *A. barclaiana*, respectively; asterisks mark sieve elements. **(C,D)** palisade mesophyll cells in *A. meridionalis* **(C)** and potato **(D)**. Arrow points to PD; asterisk marks non-specific chloroplast labeling in potato **(D)**. **(E,F)** Part of an *A. barclaiana* leaf showing the lower epidermis. Arrows point to PD; pf, pitfield. **(G,H)** Transverse section through a barley leaf. ep, epidermal cell; mes, mesophyll cell; ics, intercellular space; arrows point to PD. **(I,J)** Part of an *A. meridionalis* leaf showing the upper epidermis. Arrows point to PD. Size bars: 10 μm **(A,B)**, 20 μm **(C–J)**.

wax as an adhesive. Prior to adhesion of sections, square hollows with a side length of ca. 1.5 cm matching the size of the coverslips had been carved into these Petri dishes with an incandescent spatula. The coverslips were put at the bottom of the Petri dishes using forceps in such a way that the sections in the Petri dish were located above the middle of the hollow. About 1 ml of

glycerin was dropped into the Petri dish to cover the section. Fluorescence of Alexa Fluor 488 was examined with a Laser scanning microscope Leica TCS SP5 using 63× immersion with pZ about 276 nm and XY resolution of 150 nm. The visualization of the whole sections was performed using stereo microscope Leica TCS SP5 MP. Sections were stored at 4°C until they were processed for TEM.

Sections on the coverslips were washed three times for 5 min each in 0.1M phosphate buffer (pH 7.2-7.4) and fixed with 2.5% glutaraldehyde in the same buffer for 20 min on ice, washed again (3 × 5 min) in cold buffer and postfixed in 0.5% OsO_4 for 10 min on ice. Sections were then washed in cold water, dehydrated in a graded ethanol series (50, 70, and 96% for 5 min each) followed by equilibration in 100% acetone, and embedded in Epon EmBed medium grade (Sigma Aldrich, MO, United States). After polymerization, coverslips were detached from the resin blocks by dipping in liquid nitrogen. Outlines of the sections were clearly visible on the surfaces of the blocks. Blocks were trimmed and series of about 140 ultrathin sections were produced. Sections were mounted on formvar coated slot grids and stained with 2% uranyl acetate and 3% lead citrate. Sections were analyzed using JEM Jeol 1400 TEM equipped with Veleta side camera (Olympus Corporation, Tokyo, Japan) at 80 kV.

Quantification of PD and Pitfields Between Cells Using Immunofluorescence

Fluorescent puncta corresponding to single PD or pit fields containing PD-localized calreticulin were counted manually. Altogether, nine types of cell–cell boundaries were analyzed. Numbers of calreticulin-labeled PD/pitfields were counted on the following borders: (1) between anticlinal cell walls of cells of the upper epidermis; (2) between periclinal cell walls of the upper epidermal cells and of palisade parenchyma cells; (3) between anticlinal cell walls of palisade parenchyma cells; (4) between palisade parenchyma and cells of the bundle sheath of minor veins; (5) between periclinal cell walls of palisade parenchyma cells and cell walls of the adjoining spongy parenchyma cells; (6) between spongy parenchyma and cells of the bundle sheath of minor veins; (7) between spongy parenchyma cells; (8) between spongy parenchyma cells and periclinal cell walls of lower epidermis cells; (9) between anticlinal cell walls of cells of the lower epidermis. For barley leaves, mesophyll cells of the adaxial and abaxial halves of the leaf blade were analyzed separately. In all species, only minor veins of higher (4th−5th) orders were analyzed; veins of lower orders ("major" veins) were excluded from the analysis.

Stastistical Treatment of the Data

For statistical verifications, numbers of immunolabeled PD/pitfields were counted on 10 sections per species, all sections originating from different leaves. In every section, analyses were performed in the following manner: within cells of the same tissue, where the stoichiometry of adjoining cells was typically 1:1 (epidermis/epidermis, palisade parenchyma/palisade parenchyma, spongy parenchyma/spongy parenchyma), immunolabeled PD/pitfields were counted for 10 intercellular boundaries per section (which resulted in 100 intercellular boundaries for 10 sections analyzed). Where two different tissues adjoined each other, the stoichiometry was different; e.g., in *A. meridionalis,* usually two or three palisade parenchyma cells bordered one upper epidermal cell. In these cases, the total number of immunolabeled PD/pitfields was counted on the periclinal cell walls of 10 epidermal cells bordering 20–30 parenchyma cells and normalized to one epidermal cell. This resulted in 100 epidermal cells analyzed on 10 sections per species. Similarly, the numbers of immunolabeled PD/pitfields between spongy parenchyma/palisade parenchyma, palisade parenchyma/bundle sheath, and spongy parenchyma/bundle sheath were calculated and normalized to a single cell of spongy parenchyma or palisade parenchyma, respectively. Lengths of cell walls in microns were determined on the same sections.

The significant differences in the numbers of immunolabeled PD/pitfields counted per cell surface unit was analyzed using one-way ANOVA (library "car"; Fox and Weisberg, 2019) with Tukey *post hoc* test, libraries "multcomp" (Hothorn et al., 2008) and "agricolae" (de Mendiburu, 2020). Statistical analysis and data visualization were performed using R 3.6.3 (R Studio Team, 2020) and RStudio (R Studio Team, 2020). R packages "dplyr" (Wickham et al., 2020), "ggplot2" (Wickham, 2016), "readxl" (Wickham and Bryan, 2019) and "knitr" (Xie, 2020) were used as well. For some data sets, log-transformation was applied to satisfy the assumptions of one-way ANOVA; square root transformation was used for countable data sets. The significanct differences in single cell concentrations of sugars were analyzed using Student's t-test.

RESULTS

Visualization of Plasmodesmata (PD) Pitfields in Leaves of *A. barclaiana*, *A. meridionalis*, Barley, and Potato

To analyze the symplastic connections between cells of the leaf lamina in barley, potato, *A. barclaiana,* and *A. meridionalis*, antibodies raised against two PD-associated proteins were used, against myosin VIII (Radford and White, 1998; Reichelt et al., 1999) and calreticulin (Baluska et al., 1999; Schubert et al., 2013; Demchenko et al., 2014). Both antibodies resulted in similar labeling of PD in leaf tissues (**Figure 1**). In the vascular tissues, previous TEM studies had shown the presence of large PD fields at the intermediary cell/bundle sheath cell boundary in the minor veins of *A. meridionalis* leaves, and also smaller PD fields between modified intermediary cells and bundle sheath cells in the minor veins of *A. barclaiana* (Voitsekhovskaja et al., 2006). These PD fields were detected by immunofluorescence staining of calreticulin as shown in **Figures 1A,B** for *A. meridionalis* and *A. barclaiana*, respectively, as well as by myosin labeling (data not shown), but single PD within these fields could not be distinguished due to the small size of the cells and extremely high density of PD (Gamalei, 1991). In the parenchymatous tissues, however, PD were clearly recognized as multiple fluorescent puncta in cell walls that were sometimes seen as threads penetrating the cell walls, depending on the angle of the section (**Figures 1C,D**). In all the species

studied, immunofluorescence revealed multiple PD between mesophyll cells (shown in **Figures 1C,D** for *A. meridionalis* and potato, respectively). In potato, but not in the other species, some non-specific binding of the antibodies to structures within chloroplasts occurred as can be seen in **Figure 1D**. This was the only non-specific labeling observed; except for this, the immunofluorescence patterns were similar to the PD-specific patterns reported in other studies with the same antibodies (Radford and White, 1998; Baluska et al., 1999; Reichelt et al., 1999; Schubert et al., 2013; Demchenko et al., 2014). Fields of fluorescent puncta like those found in the cell walls of mesophyll cells were also found between cells of neighboring epidermal cells and at the mesophyll/epidermis interface (shown in **Figures 1E,F** for *A. barclaiana*, **Figures 1G,H** for barley, **Figures 1I,J** for *A. meridionalis*; see also **Supplementary Videos 1–8**).

As the resolution limit of light microscopy is ca. 200 nm, and the diameter of PD is in the range of several tenths of nanometers (Robards, 1976), several closely adjoining PD in a pitfield would be detected as a single immunolabeled fluorescent punctum. Moreover, it has been reported that in certain plant tissues, PD do not contain calreticulin (Demchenko et al., 2014). In order to address the question whether punctate pattern of immunofluorescence staining of calreticulin was associated exclusively with PD, we performed TEM analysis of immunolabeled leaf sections as shown in **Figure 2** for a barley leaf. A series of ultrathin sections (70 nm) were cut through the whole depth of a semi-thin (10 μm) section which had been imaged with the confocal laser scanning microscopy (CLSM) prior to TEM (a single scan; **Figures 2B,C**) to visualize fluorescent puncta corresponding to PD-localized calreticulin. A cell selected for TEM analysis is marked with an asterisk in **Figures 2A–D**. TEM analyses revealed single, twinned, and Y-shaped PD (**Figure 2**, TEM images 1–9) which were grouped in pitfields containing 3–7 PD (**Figure 2**, arrows 1, 2, 4, 5, 7–9), or present as single PD (**Figure 2**, arrow 6). In the upper part of the analyzed cell, four fluorescent puncta in the cell wall (arrows 1, 2, 4, 5) corresponded to pitfields with 3–7 PD, while no PD were detected by TEM in the cell wall site without immunolabeling (arrow 3). In the lower part of the same cell, TEM study revealed a single PD (arrow 6) and three pitfields (arrows 7–9) while only sites 6 and 8 showed some immunolabeling (**Figure 2C**). This could be explained by a slight bending of the section that probably resulted in the lower part of the cell which is out of the CLSM focal plane. Altogether, we concluded that immunolabeled calreticulin was confined to PD in the cell walls, and that immunohistochemistry was a reliable method to detect sites of symplastic connections between leaf cells.

Distribution of Immunolabeled PD/pitfields Between Cells and Tissues in the Leaves of *A. barclaiana*, *A. meridionalis*, Barley, and Potato

In order to provide a quantitative estimate of the abundance of sites of symplastic contacts between various types of cells and tissues of leaves of the four species under study, the numbers of fluorescent puncta (representing immunolabeled PD/pitfields) per length of the cell wall in microns were counted at the boundaries between all cell types except for vascular tissues. An example of a transverse section used for counting is shown in **Figure 1D** for the palisade cells on the left. For this procedure, we used the anti-calreticulin antibody for immunolabeling. Altogether, nine types of intercellular boundaries were analyzed. In the leaves of all species, we distinguished between upper and lower epidermis, palisade and spongy mesophyll, and cells of the bundle sheath around minor veins (major veins were excluded from the analyses). In barley leaves where only one type of mesophyll cells is present, "upper" (adaxial) and "lower" (abaxial) layers of the mesophyll were analyzed separately and are designated here as "palisade" and "spongy" to simplify the comparison with the other species. Based on leaf development, secondary PD are exclusively expected to be found at epidermis/mesophyll boundaries, while other boundaries analyzed in this study are expected to be connected by both primary and secondary PD (Satina and Blakeslee, 1941; Poethig, 1987). The numbers of immunolabeled PD/pitfields and the length of the cell walls for all cell types examined in this study are shown in **Table 1**.

In the three dicot species analyzed, the highest numbers of fluorescent puncta per cell–cell boundary (corresponding to immunolabeled PD/pitfields) were found in the palisade mesophyll. Here, the average numbers ranged from 14 puncta per cell–cell boundary in *A. meridionalis* to 38 in potato (**Table 1**). A somewhat lower abundance of symplastic connections was observed for spongy parenchyma cells and between palisade and spongy parenchyma (**Table 1**). In the monocot barley, the highest numbers (17 puncta per cell boundary) were observed between the mesophyll cells of the abaxial part of the blade, which significantly differed from the numbers for the adaxial blade part (**Table 1**). In all the four species, mesophyll cells were symplastically connected to each other to the highest extent as compared to other tissues, while the lowest numbers (0.2–1.5 puncta per cell boundary) were found in leaves of barley and potato for epidermis/epidermis (upper and lower) and upper epidermis/palisade parenchyma boundaries (**Table 1**).

When the lengths of the cell walls were taken into account, the highest values (1–2 fluorescent puncta corresponding to immunolabeled PD/pitfields per micron of cell wall length) were observed between cells of the spongy parenchyma in all species (**Figure 3A**). A cross-section of the leaf of *A. barclaiana* indicating the position of the analyzed cell types within the leaf lamina is shown in **Figure 3B**. The values of other cell types were much lower (0.25–0.60 immunolabeled PD/pitfields μm^{-1} CW length). Strikingly low symplastic connectivity (0.02–0.10 immunolabeled PD/pitfields μm^{-1} CW length) was found for upper epidermis/upper epidermis and upper epidermis/palisade mesophyll boundaries in barley and potato, as well as for lower epidermis/lower epidermis and lower epidermis/spongy mesophyll boundaries in barley. At the same time, values for boundaries of epidermal cells in *A. meridionalis* and *A. barclaiana* did not differ from those for other cell types, being in the range of 0.3–0.6 immunolabeled PD/pitfields μm^{-1} CW length (**Figure 3A**).

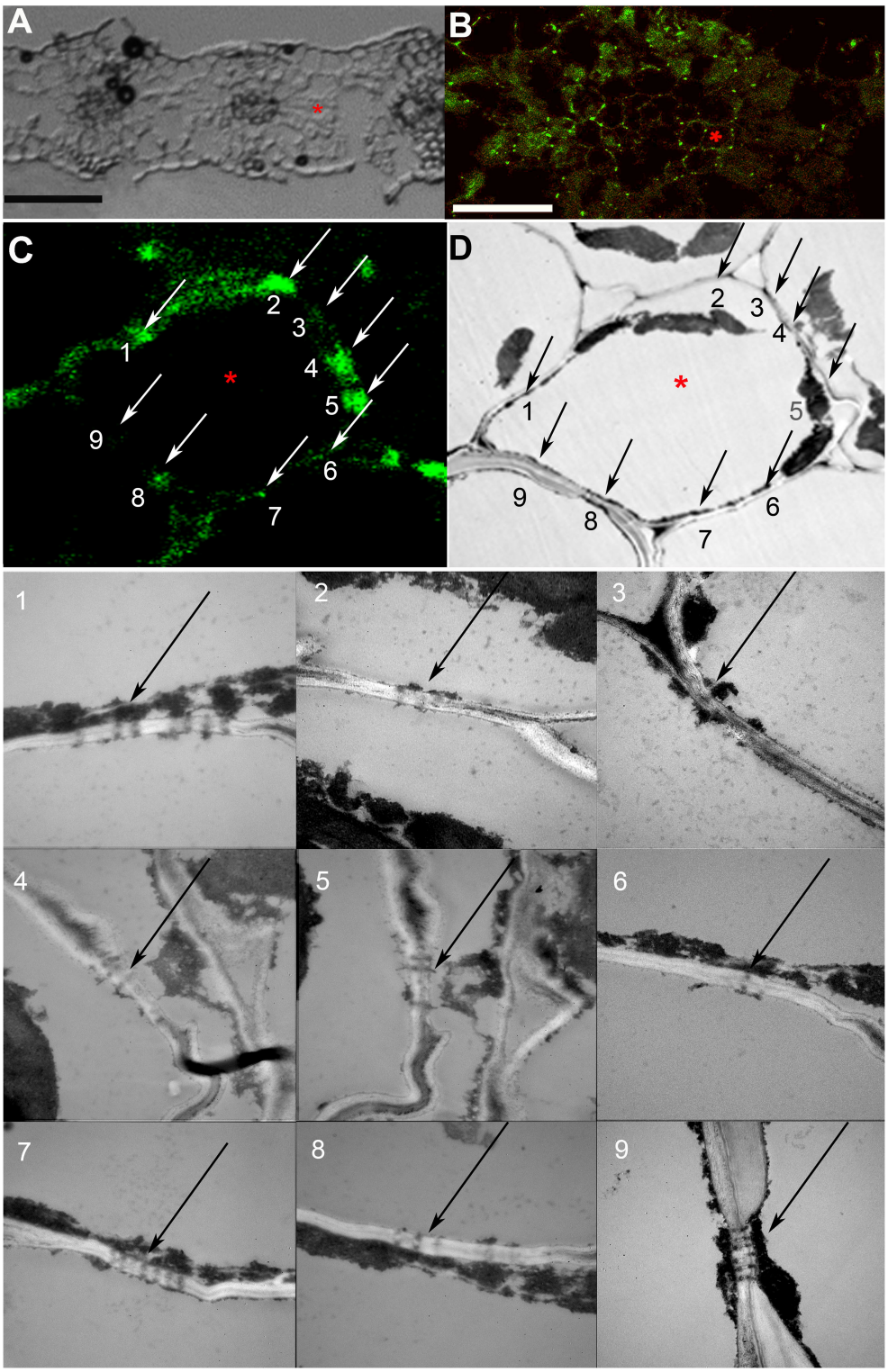

FIGURE 2 | Co-localization study of immunolabeled calreticulin and of plasmodesmata (PD). **(A)** A section of a barley leaf, an asterisk marks a mesophyll cell selected for further analysis. **(B)** A single confocal laser scanning microscopy (CLSM) image of the same section, the asterisk marks the same cell as in **(A)**. **(C,D)** Immunolabeled punctate pattern in the cell walls **(C)** and TEM image **(D)** of the cell marked with asterisk in **(A)** and **(B)**. Numbered arrows **(C,D)** point at sites of the cell wall that were examined by TEM as shown in TEM images with the same numbering; black arrows point to PD and pitfields. Size bars: 50 μm **(A)**, 30 μm **(B)**.

TABLE 1 | Numbers of fluorescent puncta per cell wall corresponding to anti-calreticulin-labeled PD/pitfields, and the mean lengths of shared cell walls between abutting specified cell types expressed on a per cell basis (in μm), as determined for nine types of cell/cell boundaries in leaves of *A. barclaiana*, *A. meridionalis*, barley, and potato.

Type of the cell border	*Asarina barclaiana*		*Alonsoa meridionalis*		Potato		Barley	
	Number of PD/pitfields per cell wall	Length of the shared cell wall (μm)	Number of PD/pitfields per cell wall	Length of the shared cell wall (μm)	Number of PD/pitfields per cell wall	Length of the shared cell wall (μm)	Number of PD/pitfields per cell wall l	Length of the cell wall [μm]
UE/UE	**4.4 ± 0.5a**	7.5 ± 1.5^{A}	**4.0 ± 0.7a**	9.2 ± 3.0^{B}	**0.4 ± 0.2b**	$8.9 \pm 2.2A^{B}$	**0.2 ± 0.1b**	10.7 ± 2.8^{B}
UE/PM	**4.8 ± 0.7a**	13.8 ± 3.3^{A}	**4.0 ± 0.5b**	13.8 ± 4.5^{A}	**0.4 ± 0.2c**	18.6 ± 6.5^{B}	**0.8 ± 0.2d**	7.3 ± 1.6^{C}
PM/PM	**24.2 ± 0.9a**	31.0 ± 2.9^{A}	**14.4 ± 1.5b**	43.2 ± 12.6^{B}	**37.9 ± 0.5c**	86.1 ± 9.4^{C}	**11.1 ± 0.5d**	21.0 ± 6.9^{D}
PM/BS	**3.8 ± 0.4a**	12.8 ± 3.3^{AB}	**3.2 ± 0.2b**	9.9 ± 2.9^{AC}	**4.0 ± 0.3a**	15.5 ± 4.5^{B}	**3.5 ± 0.3b**	8.1 ± 2.5^{C}
PM/SM	**5.9 ± 0.7a**	11.1 ± 2.9^{A}	**4.1 ± 0.3b**	10.9 ± 2.8^{A}	**7.1 ± 0.4c**	15.3 ± 3.5^{B}	**5.5 ± 0.4a**	8.8 ± 2.5^{A}
SM/BS	**4.0 ± 0.3a**	12.8 ± 4.7^{AB}	**3.3 ± 0.2b**	9.3 ± 2.4^{AC}	**4.0 ± 0.3a**	14.5 ± 6.3^{B}	**4.3 ± 0.3a**	8.5 ± 1.4^{B}
SM/SM	**14.0 ± 0.5a**	11.3 ± 6.7^{A}	**10.9 ± 0.5b**	8.0 ± 3.5^{A}	**10.6 ± 0.4b**	11.0 ± 5.8^{A}	**17.3 ± 0.6c**	7.9 ± 3.0^{A}
SM/LE	**3.3 ± 0.3a**	11.2 ± 4.4^{A}	**4.2 ± 0.3b**	10.6 ± 2.7^{A}	**3.1 ± 0.5a**	11.1 ± 2.5^{A}	**1.3 ± 0.3c**	11.0 ± 2.7^{A}
LE/LE	**4.3 ± 0.2a**	7.1 ± 2.3^{AB}	**4.2 ± 0.4a**	8.4 ± 1.4^{AC}	**1.5 ± 0.3b**	6.3 ± 1.7^{B}	**1.4 ± 0.3b**	9.8 ± 1.6^{B}

Data are average values for n = 10 ± SD.

UE, upper epidermis; PM, palisade mesophyll; BS, bundle sheath; SM, spongy mesophyll; LE, lower epidermis. Different letters indicate significant differences between species for given type of the cell border at p-value < 0.05 or less as analyzed by one-way ANOVA; lowercase letters show differences for PD/pitfields numbers per cell wall and uppercase letters for cell wall length, respectively.

Distribution of PD in Shoot Apical Meristems of *A. barclaiana*, *A. meridionalis*, Barley, and Potato

In angiosperms, shoot apical meristems (SAMs) are organized in distinct cell layers originating from the initial cells. Cells of the L1 and sometimes L2 layers, forming the tunica, undergo anticlinal divisions while cells of the L3 layer do not show a distinct pattern of divisions (see also **Supplementary Figure 1** for L1 in *A. barclaiana* and *A. meridionalis* SAMs). Based on this model, it is easy to conclude that secondary PD are present at L1/L2 and at L2/L3 boundaries, and primary PD connect cells of the same layer (although the formation of secondary PD between cells derived from the same layer is possible; Fitzgibbon et al., 2013). PD at the borders of cells belonging to L1 and L2 layers, as well as at L1/L2 and L2/L3 boundaries, were quantified in SAMs of *A. barclaiana*, *A. meridionalis*, barley, and potato by means of TEM, because the small size of the SAM cells would not allow reliable determinations using immunohistochemistry as was performed for leaves. The patterns of PD distribution and their frequencies were generally similar in the SAMs of all species studied (**Figure 4**). The frequencies of PD between cells of the L1 layer (designated as primary PD) were significantly lower than the frequencies of PD between cells of L1 and L2 (secondary PD) in potato and barley, but not in the other species, at the level of $p < 0.05$. A general tendency to form more secondary PD than primary PD per cell wall length unit was apparent for all species.

Concentrations of Sucrose and Hexoses in Epidermal and Mesophyll Cells of *A. meridionalis* and *A. barclaiana*

The level of symplastic connectivity between epidermis and mesophyll in *A. meridionalis* and *A. barclaiana* was similar to that between mesophyll cells, in contrast to barley and potato, where symplastic connectivity was higher within the mesophyll than between the epidermis and mesophyll (**Figure 3A**). Thus, the question arose whether symplastic exchange of sugars between epidermis and mesophyll might occur in *A. meridionalis* and *A. barclaiana*. We therefore analyzed the concentrations of sucrose and hexoses in single epidermal and mesophyll cells in *A. meridionalis* and *A. barclaiana* during the day and during forced accumulation of sugars in leaves due to blockage of export *via* the phloem.

First, the levels of non-structural carbohydrates were measured in the whole leaves of *A. barclaiana* and *A. meridionalis*, and no pronounced changes were observed over the diurnal rhythm (**Figures 5A,B**). In order to cause the accumulation of soluble carbohydrates in the leaves, leaves were detached from the plants after 3 h of the light period and placed in continuous light for 24 h, while the petioles were kept in a 2 mM $CaCl_2$ solution to favor sealing of the phloem with callose (King and Zeevaart, 1974). This treatment disrupted sugar export from the leaves while photosynthesis continued. At the end of the light exposure period, concentrations of sucrose, glucose, and fructose had increased significantly in the detached leaves from *A. barclaiana* and *A. meridionalis*, as compared to their levels at the end of the day in normally functioning attached leaves (**Figures 5A,B**). Another major carbohydrate-conjugated compound, the iridoid glucoside antirrhinoside, found in *A. barclaiana* (Voitsekhovskaja et al., 2006), showed no significant accumulation upon export blockage from the leaves (**Figure 5A**); neither did mannitol, myo-inositol, galactinol, raffinose, and stachyose in leaves of both species (data not shown).

The concentrations of glucose, fructose, and sucrose in the epidermal cells of *A. meridionalis* and *A. barclaiana* were compared with those in mesophyll cells in the morning (after 3 h of illumination) and in the evening (after 11 h of illumination) at the single-cell level in plants growing under a 16 h light/8 h

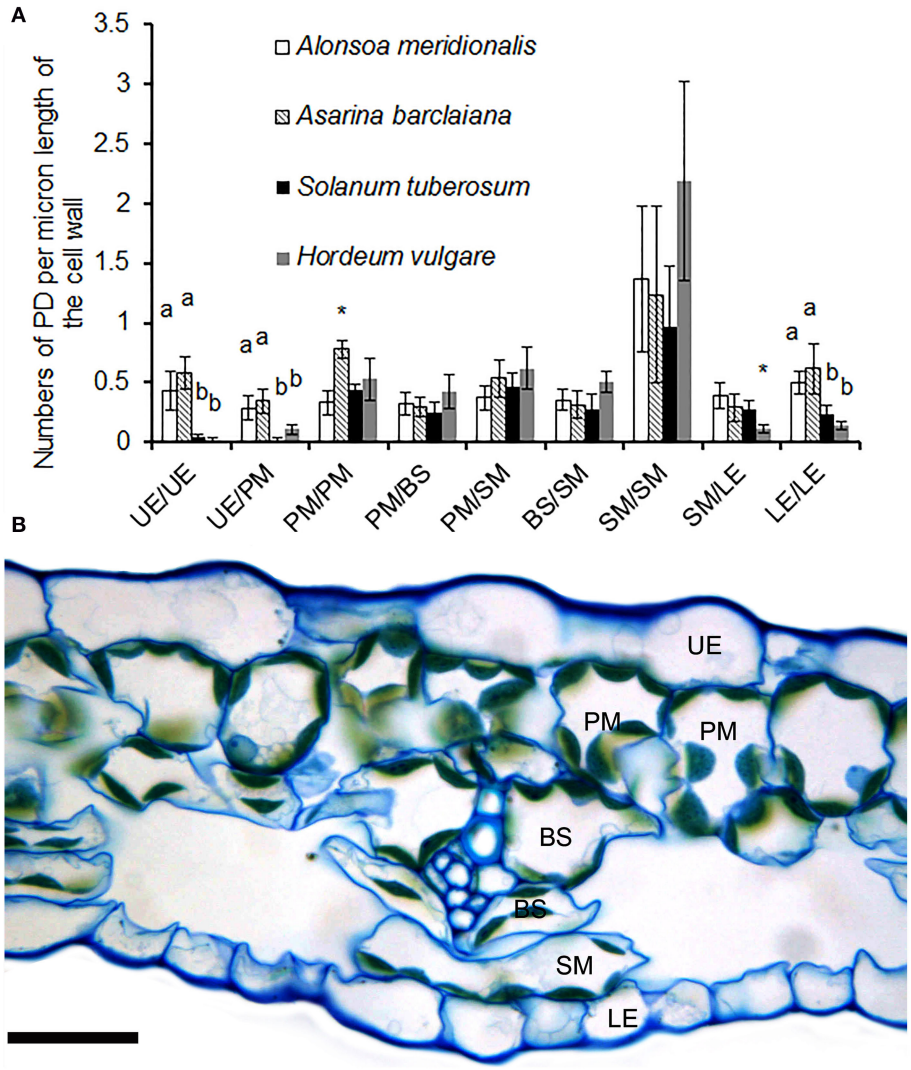

FIGURE 3 | (A) Counts of immunolabeled PD/pitfields between different cells/tissues per μm length of cell wall as found on transverse sections through the cell wall in leaves of *A. meridionalis*, *A. barclaiana*, potato (*Solanum tuberosum*), and barley (*Hordeum vulgare*). Data represent average values for 10 cell borders ± SD. UE, upper epidermis; PM, palisade mesophyll; BS, bundle sheath; SM, spongy mesophyll; LE, lower epidermis. Different letters indicate significant differences between species for a boundary type at least at the level of $p < 0.01$, * stands for significant differences at the level of $p < 0.05$, according to one-way ANOVA with *post hoc* Tukey's test. **(B)** Cross-section of a leaf of *A. barclaiana* showing the position of the analyzed cell types within the leaf lamina. Size bar: 20 μm.

dark regime. The results are shown in **Figures 5C,D**. At both "morning" and "evening" time points, the levels of these sugars were in a similar range for epidermis and mesophyll cells in both species, except for the accumulation of glucose in mesophyll cells of *A. barclaiana* in the "evening". When expressed on the basis of total hexose units, the "morning" concentrations of soluble sugars in mesophyll cells did not differ significantly from those in epidermal cells in these species and were in the range between 20 and 70 mM (**Figures 5E,F**). At the "evening" time points, sugar concentrations in mesophyll cells of both species were in the range between 20 and 100 mM and thus were significantly higher than those in epidermal cells (20–70 mM) at the level of $p < 0.05$ (**Figures 5E,F**).

When the assimilate export from the leaves was blocked by the detachment of the leaves, the epidermal cells in both plants accumulated soluble carbohydrates up to the levels measured in mesophyll cells as shown by the concentrations of sucrose and hexoses measured in the single cells of detached leaves after 24 h of illumination (**Figures 5E,F**). In *A. barclaiana*, the single-cell total sugar concentrations (calculated as a sum of hexoses and sucrose, expressed in hexose units) were 157 ± 40 mM in the epidermal cells and 175 ± 50 mM in the mesophyll cells. In *A. meridionalis*, these values were 126 ± 50 mM in epidermal cells and 113 ± 40 mM in mesophyll cells. These data indicate that in *A. meridionalis* and *A. barclaiana* leaves, the epidermis is able to accumulate soluble sugars.

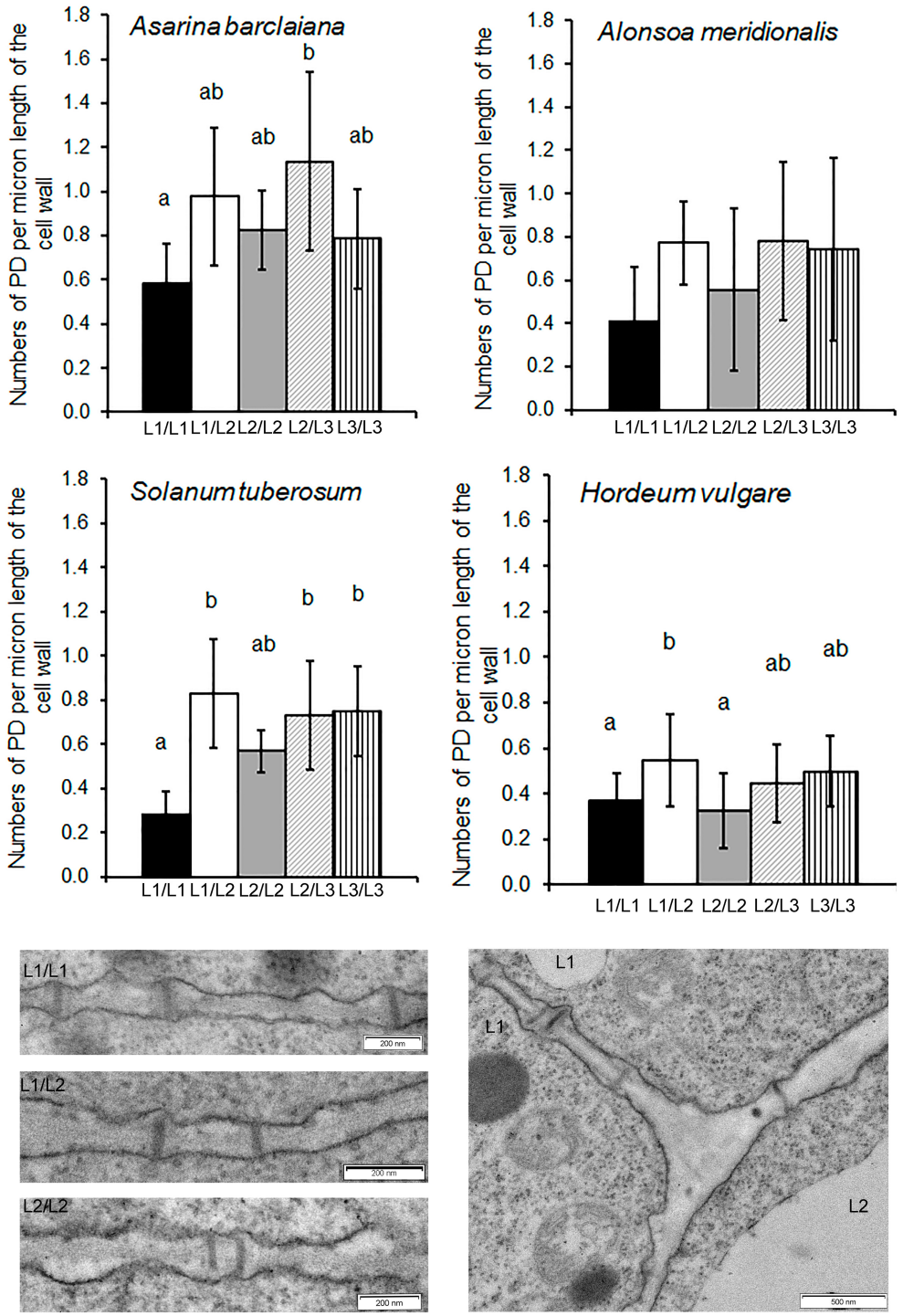

FIGURE 4 | Quantitative estimates for PD between different cells/layers in shoot apical meristems of *A. meridionalis*, *A. barclaiana*, potato, and barley. PD frequencies are expressed as numbers of PD per μm length of cell wall as found on transverse sections through the cell wall. Data represent average values for 6–25 cells ± SE. Different letters indicate significant differences at $p < 0.05$ according to one-way ANOVA with *post hoc* Tukey's test. Data for barley are reproduced from Dmitrieva et al. (2017). Micrographs show PD in one of the *Solanum tuberosum* apices examined. L1 and L2 mark cells of the corresponding cell layers.

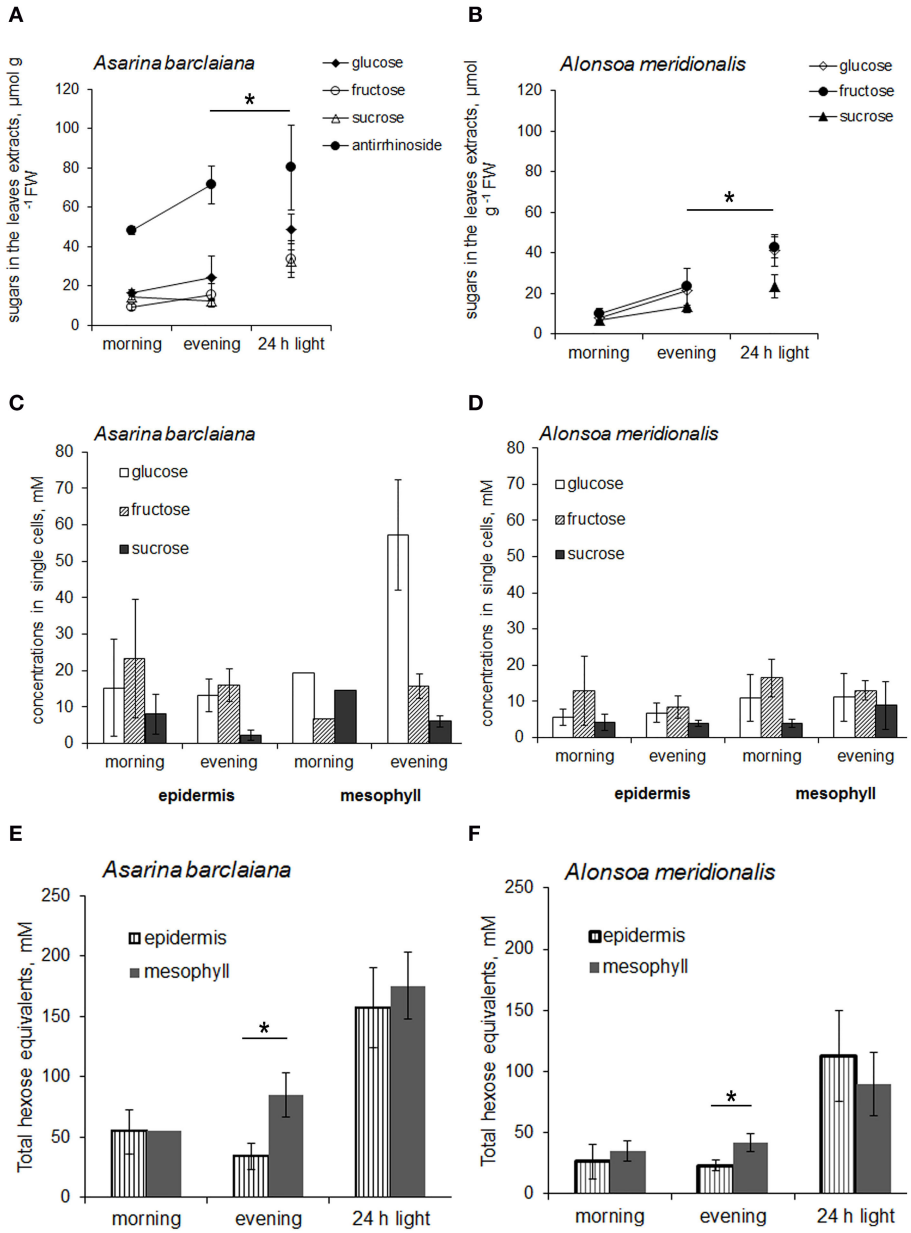

FIGURE 5 | Sugar concentrations in leaves **(A,B)** and in single cells samples obtained from the epidermis and mesophyll **(C–F)** of *A. barclaiana* **(A,C,E)** and *A. meridionalis* **(B,D,F)** at the beginning of the light period after 3 h of illumination ("morning"), at the end of the light period after 11 h illumination ("evening"), and after 24 h exposure of detached leaves to continuous light, respectively. **(A,B)** Open triangles stand for glucose, closed triangles for fructose, open circles for sucrose, and closed circles for antirrhinoside, respectively. Mean values of 3–5 independent measurements ± SE are shown except for the "morning" time points in **(C)** and **(E)** which represent the values from a single measurement. Data in **(E)** and **(F)** are expressed on the basis of hexose equivalents for total amounts of glucose, fructose, and sucrose. Asterisks indicate significant different values at least at the $p < 0.05$ level according to Student's *t*-test, except for antirrhinoside contents **(A)** where differences between "evening" and "24 h light" points were non-significant.

DISCUSSION

Determination of cell fate and specification of cell layers in SAMs as well as in leaves during their development requires precise regulation of symplastic exchange between cells. A whole orchestra of regulators, such as transcription factors, RNA, and small molecules like hormones move through PD enabling SAM functioning as well as proper development of leaves from leaf primordia (Kitagawa and Jackson, 2017; Liu and Chen, 2018; Bhatia et al., 2021; Maksimova et al., 2021;

Romanova et al., 2021). Moreover, also in the mature leaves, exchange of regulatory molecules as well as assimilates between cells and tissues *via* PD is a highly important and finely tuned process (Cui et al., 2014; Liu and Chen, 2018; Dmitrieva et al., 2021). Recent studies further reveal the role of metabolite networks in the regulation of the development (Omidbakhshfard et al., 2020). To understand the whole-leaf compartmentation of developmental regulators as well as metabolites, mapping of symplastic connections and domains within plant organs, and our understanding of how they emerge and change during development, is of high importance.

The establishment of primary PD during leaf development occurs between cells of the same lineage, that is, cells that are derived from a single mother cell and share a common division cell wall. Such lineages can be easily observed, and the fate of their cells traced, within SAMs; in angiosperms, they include the superficial cell layer L1, the subsuperficial layer L2, and the bulk of meristematic cells in the center of SAMs designated as layer L3 (Kang and Dengler, 2018). PD at L1/L2 and L2/L3 boundaries are obligatorily secondary (Evkaikina et al., 2014). Similarly, leaf primordia in angiosperms include layers, L1, L2, and L3 that produce the epidermis, the leaf parenchyma, and the central vascular bundle, respectively (Satina and Blakeslee, 1941; Sharman, 1945; Poethig, 1987; Alvarez et al., 2016; Du et al., 2018). However, as a leaf develops *via* the action of marginal and plate meristems, tracing cell lineages originating from these layers becomes challenging (Poethig, 1987; Alvarez et al., 2016; Du et al., 2018). Nevertheless, studies on periclinal chlorophyll chimeras and colchicine-induced cytochimeras performed on the monocot and dicot species revealed that the leaf epidermis always originates from L1, the palisade mesophyll is produced by L2, the spongy mesophyll (including the leaf minor veins) originates from L2 and/or L3, and the main conducting bundle of the leaf is produced by L3 (Dermen, 1947, 1953; Stewart and Burk, 1970; Poethig, 1987). Within L2-derivatives, minor veins and bundle sheath cells originate from a different cell lineage than the mesophyll in the C4 grass, *Stenotaphrum secundatum* (Sud and Dengler, 2000), while in barley, bundle sheath cells and mesophylls originate from another lineage than mestome sheath and vascular tissues (both major and minor veins) (Trivett and Evert, 1998). In dicots, the minor veins originate from the same cell lineage as the spongy mesophyll (Dermen, 1947, 1951).

In this study, the question was asked whether in plants with highly developed secondary PD at the mesophyll/phloem interface, such as the symplastic phloem loaders, *Asarina barclaiana* and *Alonsoa meridionalis*, secondary PD formation is generally enhanced at other boundaries, contrary to apoplastic phloem loaders which in our study were represented by potato and barley. According to the above mentioned studies, secondary PD are present at L1/L2 and L2/L3 boundaries in SAMs, at the epidermis/mesophyll interface in leaves, and they can be expected to occur in leaves between palisade mesophyll and spongy mesophyll, and between palisade mesophyll and the bundle sheath of minor veins. The TEM of SAMs did not reveal any differences in the secondary PD formation between the species under examination (**Figure 4**); rather, a general tendency to form more secondary PD than primary PD was apparent for all species. To obtain a quantitative estimation of the distribution of PD between different cell types within leaf laminae, immunostaining with antibodies against a PD-specific protein was used (Danila et al., 2016). We applied an antibody raised against calreticulin, which is a major chaperone protein in the lumen of the endoplasmic reticulum (ER); however, it is also shown to represent a reliable PD marker in different plant species and tissues, such as maize root apices (Baluska et al., 1999) and symbiotic root nodules of *Casuarina glauca* (Demchenko et al., 2014), respectively. Baluska et al. (1999) showed that calreticulin is located at the ER domain of the PD, and not at other ER compartments. This is in contrast to another ER-specific protein, calnexin, which was found both in ER strands located in the cytoplasm and in PD in Arabidopsis (Liu et al., 2015).

In our study, in the leaves of the four species, labeling was highly specific to immunolabeled PD/pitfields in the cell walls (**Figure 1**; **Supplementary Videos 1–8**). This specificity was further confirmed by TEM studies of immunolabeled leaf sections (**Figure 2**); this approach was taken as a substitute for correlation light electron microscopy (CLEM) (Brault et al., 2019; Modla et al., 2020), because the latter is based on the expression of genes encoding PD-targeted fluorescent proteins that was not possible for the species used in this study. Interestingly, although the data confirmed that a single fluorescent punctum corresponded in most cases to pitfields with multiple PD (**Figure 2**), estimates of the numbers of puncta for barley and potato were similar to or slightly higher than those determined using TEM analyses at the same tissue boundaries which confidently distinguished separate PD (**Table 2**). Thus, PD labeling by means of calreticulin antibodies seems to produce reliable estimates of the numbers of sites of symplastic connections within the leaf epidermis and parenchyma, although it cannot be applied to tissues where PD numbers are much higher, but to the smaller cells, than parenchyma cells, e.g., to the phloem (**Figures 1A,B**).

In both symplastic and apoplastic phloem loaders analyzed in the present study, numbers of immunolabeled PD/pitfields at cell boundaries other than bundle sheath/phloem companion cells did not show any correlation with the loading mode, independent of whether the boundaries contained primary or secondary PD. This was observed for both leaves and SAMs (**Figures 3**, **4**), with only one exception found in leaf laminae. The numbers of immunolabeled PD/pitfields at the epidermis/epidermis and epidermis/mesophyll boundaries were strikingly low in the apoplastic loaders, potato and barley, while in the symplastic loaders, *A. meridionalis* and *A. barclaiana,* these numbers did not differ much from those between mesophyll cells (**Figure 3**).

Remarkably, the numbers of immunolabeled PD/pitfieldsper length unit of cell walls between spongy parenchyma cells in the dicot species, *A. meridionalis*, *A. barclaiana,* and potato, as well as between mesophyll cells of the abaxial part of the leaf blade in the monocot barley, were significantly higher than those numbers at other interfaces in leaf laminae (**Figure 3**). In dicot leaves, spongy mesophyll cells are surrounded by large intercellular spaces due to the abaxial position of the stomata, so that the metabolite exchange *via* apoplastic water phase is probably restricted, necessitating the compensatory enhancement of symplastic

TABLE 2 | Comparison of the numbers of immunolabeled PD/pitfields with PD frequencies (PD μm^{-1} length CW) determined in leaves of several species by means of immunolabeling (this study) and TEM (literature data), respectively.

Cell boundary	*Coleus blumei*[A] (TEM)	*Alonsoa meridionalis*[B] (Immunolabeling)	*Hordeum vulgare* (TEM and immunolabeling)		*Solanum tuberosum* (TEM and immunolabeling)	
			TEM	Immuno-labeling	TEM[D]	Immuno-labeling[B]
UE/UE	0.19	0.43	–	–	–	–
UE/PM	–	–	0.05[E]	–	0.01	0.02
PM/PM	0.19	0.33	0.13[E]	0.1[E]	0.05	0.44
PM/BS	0.12	0.32	0.25[C]	0.42[B]	0.09	0.26
PM/SM	0.10	0.37	–	–	–	–
SM/BS	0.18	0.35	–	–	0.13	0.28
SM/SM	0.26	1.37	–	–	0.15	0.96
LE/SM	–	–	–	–	0.05	0.28

UE, upper epidermis; PM, palisade mesophyll; BS, bundle sheath; SM, spongy mesophyll; LE, lower epidermis. "-" stands for variants where no TEM data are available for comparison.
[A]Data from Fisher (1986). Coleus blumei belongs to the Lamiaceae family and is a close relative of A. meridionalis from the Scrophulariaceae family, both from the order Lamiales. Both species possess phloem companion cells of the intermediary cell type with similar abundance of secondary PD.
[B]This study.
[C]Data from Evert et al. (1996).
[D]Data from McCauley and Evert (1989).
[E]Data from Dmitrieva et al. (2017).

traffic. However, stomata and intercellular spaces are located at both abaxial and adaxial sides in barley leaves. Therefore, a more plausible explanation for the increase in PD frequencies in the abaxial mesophyll might be the proximity of the cells to the phloem part of the leaf veins which are abaxially positioned in dicots as well as monocots. Movement of sugars from the mesophyll to the phloem occurs *via* the symplast through PD in the leaf lamina. The reason for this is probably the necessity to compartmentalize the sugar flux in order not to be perturbed by the transpiration water flow, which has the opposite direction and is compartmentalized to the apoplast. Thus an increase of PD frequency on the abaxial side of the leaf lamina might reflect the intensification of symplastic transport near the phloem. However, more studies are required to confirm this interpretation.

It is well known that the vacuoles of mesophyll cells can serve as a temporary storage compartment for sucrose and sucrose-derived hexoses, in order to avoid their accumulation in the cytosol which could cause osmotic swelling of the cytoplasm and lead to disturbances in cytosolic metabolism (Heber and Kaiser, 1984). Usually, the cells with the strongest vacuolization are those of the leaf epidermis (Winter et al., 1993, 1994; Leidreiter et al., 1995), which theoretically could provide an additional temporal sink for an excess of soluble sugars in leaves. However, earlier studies on barley and potato, where sugar contents were measured in individual mesophyll and epidermal cells, led to the conclusion that the epidermis does not take part in the partitioning of soluble sugars within leaves. In barley, the levels of sucrose and hexoses in the epidermal cells were negligible throughout the day as well as under conditions of inhibited export of assimilates from the leaves, when malate is known to accumulate in the epidermis (Koroleva et al., 1997, 1998, 2000). In wild-type potato plants, the levels of soluble sugars in the epidermis were very low as compared to the mesophyll, although high amounts of sucrose and hexoses accumulated in epidermal cells of transgenic plants with severely impaired phloem loading (Kehr et al., 1998, 1999). Yet, in the symplastic loaders, such as *Asarina barclaiana* and *Alonsoa meridionalis,* the epidermal cells of leaf accumulated soluble sugars up to levels similar to those of mesophyll cells. We assume that these sugars entered the epidermis *via* the PD connecting both tissues.

Accumulation of sugars in the leaf epidermis of symplastic loaders as found in the present study might have consequences for the regulation of guard cells by apoplastic sucrose. In apoplastic phloem loaders, apoplastic sucrose supplied to guard cells together with abscisic acid (ABA) from transpiration stream promoted guard cell closure (Kang et al., 2007a; Daloso et al., 2016; Antunes et al., 2017). It was hypothesized that the apoplastic sucrose concentration around guard cells represents an integrating signal allowing guard cells to keep pace with transpiration, photosynthesis, and phloem translocation rates. However, this regulation of stomata by apoplastic sucrose levels was lacking in symplastic loaders (Kang et al., 2007b). Accumulation of sucrose in the epidermis of the leaves of symplastic phloem loaders as shown in the present study might provide an alternative mechanism of the regulation of stomata in the absence of the necessary levels of apoplastic sucrose, not related to the uptake of sucrose from the apoplast into guard cells (Antunes et al., 2017).

In conclusion, the estimation of symplastic connectivity in leaf laminae, as well as between cells in SAMs, analyzed in this study for four species differing in their phloem loading mode, did not reveal a general increase of the formation of secondary PD in symplastic relative to apoplastic phloem loaders. In the two symplastic loaders, the leaf epidermis was shown to be able to accumulate sugars to levels similar to those found in mesophyll cells. The species, *A. barclaiana* and *A. meridionalis*, contained

on average from 3 to 15 times more immunolabeled PD/pitfields per length cell wall between epidermal and mesophyll cells than barley and potato which do not accumulate sugars in the epidermis. This suggests that in the symplastic phloem loaders, the exchange of sugars between the mesophyll and the epidermis can occur *via* the symplastic pathway, rather than the apoplastic pathway, and that in these species, the leaf epidermis forms a symplastic domain together with the mesophyll. This is a novel role of the leaf epidermis, and it would be interesting to gain more information on the occurrence of this phenomenon as well as on how it might influence other functions of the epidermis, such as its roles as barrier for pathogens and in the regulation of stomatal closure.

DATA AVAILABILITY STATEMENT

The raw data supporting the conclusions of this article will be made available by the authors, without undue reservation.

AUTHOR CONTRIBUTIONS

OV and OK conceptualized the research and performed single cell sampling. AT and GL supervised the research. OV performed sugar analyses and wrote the manuscript. ANM and AIM performed morphometric analyses. KD performed immunolocalization of myosin VIII and calreticulin in PD. VD performed immunolocalization of calreticulin on leaf sections used for TEM. AI performed TEM studies. ET and OV analyzed TEM data. All authors analyzed and discussed the data including the production of figures. All authors read and approved the final version of the article.

FUNDING

This project was partially supported by the Russian Foundation for Basic Research (#07-04-0170 to OV). Analyses of plasmodesmata in barley were supported by the Russian Science Foundation (#14-16-00120-P to OV). The visit of OV to the University of Bangor was financed by the University of Göttingen. The German Academic Exchange Service (DAAD) is gratefully acknowledged for a fellowship to OV and for the generous donation of a fluorescent microscope to the Komarov Botanical Institute of RAS.

ACKNOWLEDGMENTS

We are grateful to František Baluška (University of Bonn, Germany), Richard Napier (University of Warwick, UK) and Marta Lenartowska (Nicolaus Copernicus University, Torun, Poland) for the generous gift of the anti-myosin VIII and anti-calreticulin antibodies, respectively, to Marian Płaszczyca (Biostat, Rybnik, Poland) and Valentina Domashkina (Komarov Botanical Institute of RAS) for help with statistics, to Denis Batashev (Komarov Botanical Institute of RAS, Saint. Petersburg, Russia) for providing an overview image of *Asarina barclaiana* leaf, and to Katharina Pawlowski (Stockholm University, Stockholm, Sweden) for the critical reading of the manuscript. The Core Facilities Centre "Cell and Molecular Technologies in Plant Science" at the Komarov Botanical Institute RAS and the Research Resource Centre "Molecular and Cell Technologies" at Saint Petersburg State University, are gratefully acknowledged for technical support. We gratefully dedicate this study to the memory of Prof. Hans-Walter Heldt (1934-2019), the Head of Plant Biochemistry at Göttingen University, who made this work possible.

SUPPLEMENTARY MATERIAL

The Supplementary Material for this article can be found online at: https://www.frontiersin.org/articles/10.3389/fpls.2021.695415/full#supplementary-material

Supplementary Figure 1 | Sections of shoot apices of *Asarina barclaiana* **(A)** and *Alonsoa meridionalis* **(B)**. Within the shoot apical meristems, the tunica consists of the L1 layer which is continuous with the protoderm layer of leaf primordia (P) as outlined in red. Arrows point on glandular hairs. Shoot apices were embedded in epon resin and semi-thin sections were produced as described in Materials and Methods. The sections were stained with toluidine blue (0.05%). Scale bar: 20 μm.

Supplementary Video 1 | Plasmodesmata (PD) between cells of the palisade parenchyma in leaves of *Asarina barclaiana* (arrows point at selected face-on views) as visualized by means of immunohistochemistry using calreticulin-specific antibodies.

Supplementary Video 2 | Plasmodesmata (PD) between cells of the spongy parenchyma in leaves of *Asarina barclaiana* (arrows point at selected face-on views) as visualized by means of immunohistochemistry using calreticulin-specific antibodies.

Supplementary Video 3 | Plasmodesmata (PD) between cells of the palisade parenchyma in leaves of *Alonsoa meridionalis* (arrows point at selected face-on views) as visualized by means of immunohistochemistry using calreticulin-specific antibodies.

Supplementary Video 4 | Plasmodesmata (PD) between cells of the palisade parenchyma in leaves of *Alonsoa meridionalis* (arrows point at selected face-on views) as visualized by means of immunohistochemistry using calreticulin-specific antibodies.

Supplementary Video 5 | Plasmodesmata (PD) between cells of the palisade parenchyma in leaves of *Solanum tuberosum* (arrows point at selected face-on views) as visualized by means of immunohistochemistry using calreticulin-specific antibodies.

Supplementary Video 6 | Plasmodesmata (PD) between cells of the spongy parenchyma (top; arrows point at selected face-on views) and between the cells of the palisade parenchyma and the bundle sheath (a single arrow; bottom) in leaves of *Solanum tuberosum*. In the center, a xylem ending surrounded by bundle sheath cells is shown. The PD were visualized by means of immunohistochemistry using calreticulin-specific antibodies; note unspecific staining of starch grains in this species.

Supplementary Video 7 | A section through a leaf of *Hordeum vulgare* showing plasmodesmata (PD) between mesophyll cells in the adaxial and abaxial parts of the leaf (arrows). The PD were visualized by means of immunohistochemistry using calreticulin-specific antibodies.

Supplementary Video 8 | Plasmodesmata (PD) between cells of the spongy parenchyma in leaves of *Hordeum vulgare* (arrow points at face-on view) as visualized by means of immunohistochemistry using calreticulin-specific antibodies.

REFERENCES

Alvarez, J. P., Furumizu, C., Efroni, I., Eshed, Y., and Bowman, J. L. (2016). Active suppression of a leaf meristem orchestrates determinate leaf growth. *eLife* 5:e15023. doi: 10.7554/eLife.15023

Antunes, W. C., Daloso, D. M., Pinheiro, D. P., Williams, T. C. R., and Loureiro, M. E. (2017). Guard cell-specific down-regulation of the sucrose transporter SUT1 leads to improved water use efficiency and reveals the interplay between carbohydrate metabolism and K+ accumulation in the regulation of stomatal opening. *Environ. Exp. Bot.* 135, 73–85. doi: 10.1016/j.envexpbot.2016.12.004

Baluska, F., Samaj, J., Napier, R., and Volkmann, D. (1999). Maize calreticulin localizes preferentially to plasmodesmata in root apex. *Plant J.* 19, 481–488. doi: 10.1046/j.1365-313X.1999.00530.x

Batashev, D. R., Pakhomova, M. V., Razumovskaya, A. V., Voitsekhovskaja, O. V., and Gamalei, Y. V. (2013). Cytology of the minor-vein phloem in 320 species from the subclass Asteridae suggests a high diversity of phloem-loading modes. *Front. Plant Sci.* 4:312. doi: 10.3389/fpls.2013.00312

Bhatia, S., Kumar, H., Mahajan, M., Yadav, S., Saini, P., Yadav, S., et al. (2021). A cellular expression map of epidermal and subepidermal cell layer-enriched transcription factor genes integrated with the regulatory network in Arabidopsis shoot apical meristem. *Plant Direct*. 5:e00306. doi: 10.1002/pld3.306

Botha, C. E. J., and Cross, R. H. M. (1997).Plasmodesmatal frequency in relation to short-distance transport and phloem loading in leaves of barley (*Hordeum vulgare*). Phloem is not loaded directly from the symplast. *Physiol. Plant.* 99, 355–362. doi: 10.1034/j.1399-3054.1997.990301.x

Brault, M. L., Petit, J. D., Immel, F., Nicolas, W. J., Glavier, M., Brocard, L., et al. (2019). Multiple C2 domains and transmembrane region proteins (MCTPs) tether membranes at plasmodesmata. *EMBO Rep*. 20:e47182. doi: 10.15252/embr.201847182

Cui, H., Kong, D., Liu, X., and Hao, Y. (2014). SCARECROW, SCR-LIKE 23 and SHORT-ROOT control bundle sheath cell fate and function in *Arabidopsis thaliana*. *Plant J.* 78, 319–327. doi: 10.1111/tpj.12470

Daloso, D. M., dos Anjos, L., and Fernie, A. R. (2016). Roles of sucrose in guard cell regulation. *New Phytol.* 211, 809–818. doi: 10.1111/nph.13950

Danila, F. R., Quick, W. P., White, R. G., Furbank, R. T., and von Caemmerer, S. (2016). The metabolite pathway between bundle sheath and mesophyll: quantification of plasmodesmata in leaves of C3 and C4 monocots. *Plant Cell* 28, 1461–1471. doi: 10.1105/tpc.16.00155

de Mendiburu, F. (2020). agricolae: Statistical Procedures for Agricultural Research. R package version 1.3-3. Available online at: https://CRAN.R-project.org/package=agricolae (accessed March 29, 2021).

Demchenko, K. N., Voitsekhovskaja, O. V., and Pawlowski, K. (2014). Plasmodesmata without callose and calreticulin in higher plants—open channels for fast symplastic transport? *Front. Plant Sci.* 5:74. doi: 10.3389/fpls.2014.00074

Dermen, H. (1947). Periclinal cytochimeras and histogenesis in cranberry. *Am. J. Bot.* 34, 32–43. doi: 10.1002/j.1537-2197.1947.tb12955.x

Dermen, H. (1951). Ontogeny of tissues in stem and leaf of cytochimeral apples. *Am. J. Bot.* 38, 753–760. doi: 10.1002/j.1537-2197.1951.tb14888.x

Dermen, H. (1953). Periclinal cytochimeras and origin of tissues in stem and leaf of peach. *Am. J. Bot.* 40, 154–168. doi: 10.1002/j.1537-2197.1953.tb06463.x

Dmitrieva, V. A., Domashkina, V. V., Ivanova, A. N., Sukhov, V. S., Tyutereva, E. V., and Voitsekhovskaja, O. V. (2021). Regulation of plasmodesmata in leaves of *Arabidopsis*: ATP, NADPH and chlorophyll *b* levels matter. *J. Exp. Bot.* (inpress). doi: 10.1093/jxb/erab205

Dmitrieva, V. A., Ivanova, A. N., Tyutereva, E. V., Evkaikina, A. I., Klimova, E. A., and Voitsekhovskaja, O. V. (2017). Chlorophyllide-a-Oxygenase (CAO) deficiency affects the levels of singlet oxygen and formation of plasmodesmata in leaves and shoot apical meristems of barley. *Plant Signal. Behav.* 12:e1300732. doi: 10.1080/15592324.2017.1300732

Du, F., Guan, C., and Jiao, Y. (2018). Molecular mechanisms of leaf morphogenesis. *Mol. Plant* 11, 1117–1134. doi: 10.1016/j.molp.2018.06.006

Evert, R. F., Russin, W. A., and Botha, C. E. J. (1996). Distribution and frequency of plasmodesmata in relation to photoassimilate pathway and phloem loading in the barley leaf. *Planta* 198, 572–579. doi: 10.1007/BF00262644

Evkaikina, A. I., Romanova, M. A., and Voitsekhovskaja, O. V. (2014). Evolutionary aspects of non-cell-autonomous regulation in vascular plants: structural background and models to study. *Front. Plant Sci.* 5:31. doi: 10.3389/fpls.2014.00031

Fisher, D. G. (1986). Ultrastructure, plasmodesmatal frequency, and solute concentration in green areas of variegated *Coleus blumei* Benth. leaves. *Planta* 169, 141–152. doi: 10.1007/BF00392308

Fitzgibbon, J., Beck, M., Zhou, J., Faulkner, C., Robatzek, S., and Oparka, K. (2013). A developmental framework for complex plasmodesmata formation revealed by large-scale imaging of the Arabidopsis leaf epidermis. *Plant Cell* 21, 57–70. doi: 10.1105/tpc.112.105890

Fox, J., and Weisberg, S. (2019). *An R Companion to Applied Regression, Third Edition*. Thousand Oaks, CA: Sage.

Gamalei, Y. V. (1991). Phloem loading and its development related to plant evolution from trees to herbs. *Trees* 5, 50–64. doi: 10.1007/BF00225335

Gamalei, Y. V. (1995). "Comparative biology of trees and herbs: intercellular communication," in *L'Arbre. Biologie et Development - 3ème colloque*, ed C. Edelin (Montpellier), 1–11.

Heber, U., and Kaiser, G. (1984). Sucrose transport into vacuoles isolated from barley mesophyll protoplasts. *Planta* 161, 562–568. doi: 10.1007/BF00407090

Hothorn, T., Bretz, F., and Westfall, P. (2008). Simultaneous inference in general parametric models. *Biomet. J.* 50, 346–363. doi: 10.1002/bimj.200810425

Kang, J., and Dengler, N. G. (2018). "Leaf architecture: regulation of leaf position, shape and internal structure," in *Annual Plant Reviews Online*, eds J. A. Roberts. doi: 10.1002/9781119312994.apr0164

Kang, Y., Outlaw W. H. Jr., Andersen, P. C., and Fiore, G. B. (2007a). Guard cell apoplastic sucrose concentration—a link between leaf photosynthesis and stomatal aperture size in the apoplastic phloem loader *Vicia faba* L. *Plant Cell Environ.* 30, 551–558. doi: 10.1111/j.1365-3040.2007.01635.x

Kang, Y., Outlaw W. H. Jr., Fiore, G. B., and Riddle, K. A. (2007b). Guard cell apoplastic photosynthate accumulation corresponds to a phloem-loading mechanism. *J. Exp. Bot.* 58, 4061–4070. doi: 10.1093/jxb/erm262

Kehr, J., Hustiak, F., Walz, C., Willmitzer, L., and Fisahn, J. (1998). Transgenic plants changed in carbon allocation pattern display a shift in diurnal growth pattern. *Plant J.* 16, 497–503. doi: 10.1046/j.1365-313x.1998.00318.x

Kehr, J., Wagner, U., Willmitzer, L., and Fisahn, J. (1999). Effect of modified carbon allocation on turgor, osmolality, sugar and potassium content, and membrane potential in the epidermis of transgenic potato (*Solanum tuberosum* L.) plants. *J. Exp. Bot.* 50, 565–571. doi: 10.1093/jxb/50.334.565

King, R. W., and Zeevaart, J. A. D. (1974). Enhancement of phloem exudation from cut petioles by chelating agents. *Plant Physiol.* 53, 96–103. doi: 10.1104/pp.53.1.96

Kitagawa, M., and Jackson, D. (2017). Plasmodesmata-mediated cell-to-cell communication in the shoot apical meristem: how stem cells talk. *Plants* 6:12. doi: 10.3390/plants6010012

Koroleva, O. A., Farrar, J. F., Tomos, A. D., and Pollock, C. J. (1997). Patterns of solute in individual mesophyll, bundle sheath and epidermal cells of barley leaves induced to accumulate carbohydrate. *New Phytol.* 136, 97–104. doi: 10.1111/j.1469-8137.1997.tb04735.x

Koroleva, O. A., Farrar, J. F., Tomos, A. D., and Pollock, C. J. (1998). Carbohydrates in individual cells of epidermis, mesophyll, and bundle sheath in barley leaves with changed export or photosynthetic rate. *Plant Physiol.* 118, 1525–1532. doi: 10.1104/pp.118.4.1525

Koroleva, O. A., Tomos, A. D., Farrar, J. F., Roberts, P., and Pollock, C. J. (2000). Tissue distribution of primary metabolism between epidermal, mesophyll and parenchymatous bundle sheath cells in barley leaves. *Aust. J. Plant Physiol.* 27, 747–755. doi: 10.1071/PP99156

Leidreiter, K., Kruse, A., Heineke, D., Robinson, D. G., and Heldt, H. W. (1995). Subcellular volumes and metabolite concentrations in potato (*Solanum tuberosum* cv. Désirée) leaves. *Bot. Acta* 108, 439–444. doi: 10.1111/j.1438-8677.1995.tb00518.x

Liu, D. Y. T., Smith, P. M. C., Barton, D. A., Day, D. A., and Overall, R. L. (2015). Characterisation of Arabidopsis calnexin 1 and calnexin 2 in the endoplasmic reticulum and at plasmodesmata. *Protoplasma* 254, 125–136. doi: 10.1007/s00709-015-0921-3

Liu, L., and Chen, X. (2018).Intercellular and systemic trafficking of RNAsin plants. *Nat. Plants* 4, 869–878. doi: 10.1038/s41477-018-0288-5

Maksimova, A. I., Berke, L., Salgado, M. G., Klimova, E. A., Romanova, M. A., Pawlowski, K., et al. (2021). What can the phylogeny of class I KNOX genes and their expression patterns in land plants tell us about the evolution of shoot development? *Bot. J. Linn. Soc.* 195, 254–280. doi: 10.1093/botlinnean/boaa088

McCauley, M. M., and Evert, R. F. (1989). Minor veins of the potato (*Solanum tuberosum* L.) leaf: ultrastructure and plasmodesmatal frequency. *Bot. Gazette* 150: 351–368. doi: 10.1086/337781

Modla, S., Caplan, J. L., Czymmek, K. J., and Lee, J.-Y. (2020). "Localization of fluorescently tagged protein to plasmodesmata by Correlative Light and Electron Microscopy," in *Plasmodesmata: Methods and Protocols, Methods in Molecular Biology*, *vol. 1217*, eds M. Heinlein, 121–133.

Omidbakhshfard, M. A., Sokolowska, E. M., Di Vittori, V., de Souza, L.P., Kuhalskaya, A., Brotman, Y., et al. (2020). Multi-omics analysis of earlyleaf development in *Arabidopsis thaliana*. *Patterns* 2:100235. doi: 10.1016/j.patter.2021.100235

Oparka, K. J., Roberts, A. G., Boevink, P., Santa Cruz, S., Roberts, I., Pradel, K. S., et al. (1999). Simple, but not branched, plasmodesmata allow the non-specific trafficking of protein in developing tobacco leaves. *Cell* 97, 743–754. doi: 10.1016/S0092-8674(00)80786-2

Poethig, W. S. (1987). Clonal analysis of cell lineage patterns in plant development. *Am. J. Bot.* 74, 581–594. doi: 10.1002/j.1537-2197.1987.tb08679.x

R Core Team (2020). *R: A Language and Environment for Statistical Computing. Vienna: R Foundation for Statistical Computing.* Available online at: https://www.R-project.org/

Radford, J. E., and White, R. G. (1998). Localization of a myosin-like protein to plasmodesmata. *Plant J.* 14, 743–750. doi: 10.1046/j.1365-313x.1998.00162.x

Reichelt, S., Knight, A. E., Hodge, T. P., Baluska, F., Samaj, J., Volkmann, D., et al. (1999). Characterization of the unconventional myosin VIII in plant cells and its localization at the post-cytokinetic cell wall. *Plant J.* 19, 555–567. doi: 10.1046/j.1365-313X.1999.00553.x

Riesmeier, J. W., Willmitzer, L., and Frommer, W. B. (1994). Evidence for an essential role of the sucrose transporter in phloem loading and assimilate partitioning. *EMBO J.* 13, 1–7. doi: 10.1002/j.1460-2075.1994.tb06229.x

Robards, A. W. (1976). "Plasmodesmata in higher plants," in *Intercellular Communication in Plants: Studies on Plasmodesmata*, eds B. E. S. Gunning and A. W. Robards (Berlin; Heidelberg: Springer). doi: 10.1007/978-3-642-66294-2_2

Romanova, M. A., Maksimova, A. I., Pawlowski, K., and Voitsekhovskaja, O. V. (2021). YABBY genes in the development and evolution of land plants. *Int. J. Mol. Sci.* 22:4139. doi: 10.3390/ijms22084139

Satina, S., and Blakeslee, A. F. (1941). Periclinal chimeras in *Datura stramonium* in relation to development of leaf and flower. Amer. Jour. *Bot.* 28, 862–871. doi: 10.1002/j.1537-2197.1941.tb11017.x

Schubert, M., Koteyeva, N. K., Zdyb, A., Santos, P., Voitsekhovskaja, O. V., Demchenko, K. N., et al. (2013). Lignification of cell walls of infected cells in *Casuarina glauca* nodules that depend on symplastic sugar supply is accompanied by reduction of plasmodesmata number and narrowing of plasmodesmata. *Physiol. Plant.* 147, 524–540. doi: 10.1111/j.1399-3054.2012.01685.x

Sharman, B. C. (1945). Leaf and bud initiation in the Gramineae. *Bot. Gaz.* 106, 269–289. doi: 10.1086/335298

Stewart, R. N., and Burk, L. G. (1970). Independence of tissues derived from apical layers in ontogeny of the tobacco leaf and ovary. *Am. J. Bot.* 57, 1010–1016. doi: 10.1002/j.1537-2197.1970.tb09902.x

Stumpe, M., Göbel, C., Demchenko, K., Hoffmann, M., Klösgen, R. B., Pawlowski, K., et al. (2006). Identification of an allene oxide synthase (CYP74C) that leads to formation of α-ketols from 9-hydroperoxides of linoleic and linolenic acid in below-ground organs of potato. *Plant J.* 47, 883–896. doi: 10.1111/j.1365-313X.2006.02843.x

Sud, R. M., and Dengler, N. G. (2000). Cell lineage of vein formation in variegated leaves of the C4 grass *Stenotaphrum secundatum*. *Ann. Bot.* 86, 99–112. doi: 10.1006/anbo.2000.1165

Tomos, A. D., Hinde, P., Richardson, P., Pritchard, J., and Fricke, W. (1994). "Microsampling and measurement of solutes in single cells," in *Plant Cell Biology—A Practical Approach*, eds N. Harris, K. J. Oparka (Oxford: IRL Press), 297–314.

Trivett, C. L., and Evert, R. F. (1998). Ontogeny of the vascular bundles and contiguous tissues in the barley leaf blade. *Int. J. Plant Sci.* 159, 716–723. doi: 10.1086/297589

Turgeon, R., and Medville, R. (2004). Phloem loading: a revaluation of the relationship between plasmodesmatal frequencies and loading strategies. *Plant Physiol.* 136, 3795–3803. doi: 10.1104/pp.104.042036

Van Bel, A. J. E., and Gamalei, V. Y. (1992). Ecophysiology of phloem loading in source leaves. *Plant Cell Environ.* 15, 265–270. doi: 10.1111/j.1365-3040.1992.tb00973.x

Voitsekhovskaja, O. V., Koroleva, O. A., Batashev, D. R., Knop, C., Tomos, A. D., Gamalei Y. V., et al. (2006). Phloem loading in two Scrophulariaceae species. What can drive symplastic flow via plasmodesmata? *Plant Physiol.* 140, 383–395. doi: 10.1104/pp.105.068312

Voitsekhovskaja, O. V., Rudashevskaya, E. L., Demchenko, K. N., Pakhomova, M. V., Batashev, D. R., Gamalei Y. V., et al. (2009). Evidence for functional heterogeneity of sieve element-companion cell complexes in minor vein phloem of *Alonsoameridionalis*. *J. Exp. Bot.* 60, 1873–1883. doi: 10.1093/jxb/erp074

Wickham, H. (2016). *ggplot2: Elegant Graphics for Data Analysis*. New York, NY: Springer. doi: 10.1007/978-3-319-24277-4_9

Wickham, H., Francois, R., Henry, L., and Muller, K. (2020). dplyr: A Grammar of Data Manipulation. R package version. 1.0.2. Available online at: https://CRAN.R-project.org/package=dplyr

Wickham, H., and Bryan, J. (2019). readxl: Read Excel Files. R package version 1.3.1. Available online at: https://CRAN.R-project.org/package=readxl (accessed March 29, 2021).

Winter, H., Robinson, D. G., and Heldt, H. W. (1993). Subcellular volumes and metabolite concentrations in barley leaves. *Planta* 191, 180–190. doi: 10.1007/BF00199748

Winter, H., Robinson, D. G., and Heldt, H. W. (1994). Subcellular concentrations and metabolite concentrations in spinach leaves. *Planta* 193, 530–535. doi: 10.1007/BF02411558

Xie, Y. (2020). knitr: A General-Purpose Package for Dynamic Report Generation in R. R package version 1.30.

Conflict of Interest: The authors declare that the research was conducted in the absence of any commercial or financial relationships that could be construed as a potential conflict of interest.

Publisher's Note: All claims expressed in this article are solely those of the authors and do not necessarily represent those of their affiliated organizations, or those of the publisher, the editors and the reviewers. Any product that may be evaluated in this article, or claim that may be made by its manufacturer, is not guaranteed or endorsed by the publisher.

Advantages of publishing in Frontiers

OPEN ACCESS
Articles are free to read for greatest visibility and readership

FAST PUBLICATION
Around 90 days from submission to decision

HIGH QUALITY PEER-REVIEW
Rigorous, collaborative, and constructive peer-review

TRANSPARENT PEER-REVIEW
Editors and reviewers acknowledged by name on published articles

Frontiers
Avenue du Tribunal-Fédéral 34
1005 Lausanne | Switzerland

Visit us: www.frontiersin.org
Contact us: frontiersin.org/about/contact

REPRODUCIBILITY OF RESEARCH
Support open data and methods to enhance research reproducibility

DIGITAL PUBLISHING
Articles designed for optimal readership across devices

FOLLOW US
@frontiersin

IMPACT METRICS
Advanced article metrics track visibility across digital media

EXTENSIVE PROMOTION
Marketing and promotion of impactful research

LOOP RESEARCH NETWORK
Our network increases your article's readership